Fall 2010

The patterning and determinants of craniofacial robusticity in extant Homo sapiens

Steven Frederick Miller
University of Iowa

THE PATTERNING AND DETERMINANTS OF CRANIOFACIAL ROBUSTICITY IN EXTANT *HOMO SAPIENS*

by

Steven Frederick Miller

An Abstract

Of a thesis submitted in partial fulfillment
of the requirements for the Doctor of
Philosophy degree in Anthropology
in the Graduate College of
The University of Iowa

December 2010

Thesis Supervisor: Associate Professor Robert G. Franciscus

ABSTRACT

Skeletal superstructure characteristics such as thick cranial vaults and well-developed supraorbital, infraorbital, zygomatic, temporal, and nuchal regions in hominins are collectively referred to as aspects of craniofacial robusticity. A better understanding of craniofacial robusticity is important because these features are regularly employed as individual traits in circumscribing fossil hominins as a means to separate other taxonomic groups from modern *Homo sapiens* even though the developmental and functional underpinnings of such traits are incompletely understood. The work of some researchers suggests that these features may be tied to a broader "robusticity complex", in which the expression of all the classically "robust" characteristics of the hominin cranium are intercorrelated and intrinsically linked. If true, then previous studies that have focused on characteristics of craniofacial robusticity as individual characters could be flawed.

This study tests for the presence of an intercorrelated craniofacial robusticity complex in a geographically diverse sample of recent *Homo sapiens* using a morphological integration framework. Within this framework, significant levels of correlation between features of craniofacial robusticity are demonstrative of integration and thus a "robusticity complex", while non-significant levels of correlation provide evidence for modularity and therefore an independent expression of these traits. Craniofacial robusticity is examined among four anatomical areas of the human cranium including the frontal, zygomaxillary, temporal, and occipital regions. The expression of robusticity among these anatomical regions is quantified using three-dimensional coordinate landmark data in addition to classical discrete measures and is analyzed via two-block partial least squares regression analysis.

The results show that levels of interaction between these major anatomical units are characterized by a range of correlation values with most obtaining statistical significance. These results frequently provide evidence for integration between subunits

demonstrating at least partial evidence for a “robusticity complex” in the craniofacial skeleton of extant humans.

Abstract Approved: _____
Thesis Supervisor

_____
Title and Department

_____
Date

THE PATTERNING AND DETERMINANTS OF CRANIOFACIAL ROBUSTICITY IN EXTANT *HOMO SAPIENS*

by

Steven Frederick Miller

A thesis submitted in partial fulfillment
of the requirements for the Doctor of
Philosophy degree in Anthropology
in the Graduate College of
The University of Iowa

December 2010

Thesis Supervisor: Associate Professor Robert G. Franciscus

Graduate College
The University of Iowa
Iowa City, Iowa

CERTIFICATE OF APPROVAL

_____

PH.D. THESIS

_____

This is to certify that the Ph.D. thesis of

Steven Frederick Miller

has been approved by the Examining Committee
for the thesis requirement for the Doctor of Philosophy
degree in Anthropology at the December 2010 graduation.

Thesis Committee: _____
Robert G. Franciscus, Thesis Supervisor

_____
Russell L. Ciochon

_____
James G. Enloe

_____
Thomas E. Southard

_____
Dennis E. Slice

In loving memory of my Grandmother, Lucy Miley

ACKNOWLEDGMENTS

I would like to thank my Ph.D. committee members for their participation, resources and insights: Robert G. Franciscus (Ph.D. committee chair), Russell L. Ciochon, James G. Enloe, Thomas E. Southard, and Dennis E. Slice. I also would like to thank Ian Tattersall and Gary J. Sawyer at the American Museum of Natural History for access to their Felix von Luschan skeletal collection, which provided the cranial sample used in this study.

Special thanks to my parents: Dan and Gail Miller, as well as my sister Katie, who, without their love and support, I would have never made it to this point. I also would like to thank my colleague and friend, Josh Polanski, for all his help, support, and guidance as we worked our way through graduate school together. I would also like to acknowledge the support of many of my friends over the years from the University of Iowa: Alex Woods, Grant McCall, and Jessica White, as well as my friends from back home in Pennsylvania: Greg Miller, Jason Spearly, Justin Bregar, and Mike Surfin. Finally, I thank my fiancé, Christina Nicholas, whose encouragement, love, and guidance has given me the strength to get through the final, and most challenging stages of my dissertation work.

ABSTRACT

Skeletal superstructure characteristics such as thick cranial vaults and well-developed supraorbital, infraorbital, zygomatic, temporal, and nuchal regions in hominins are collectively referred to as aspects of craniofacial robusticity. A better understanding of craniofacial robusticity is important because these features are regularly employed as individual traits in circumscribing fossil hominins as a means to separate other taxonomic groups from modern *Homo sapiens* even though the developmental and functional underpinnings of such traits are incompletely understood. The work of some researchers suggests that these features may be tied to a broader "robusticity complex", in which the expression of all the classically "robust" characteristics of the hominin cranium are intercorrelated and intrinsically linked. If true, then previous studies that have focused on characteristics of craniofacial robusticity as individual characters could be flawed.

This study tests for the presence of an intercorrelated craniofacial robusticity complex in a geographically diverse sample of recent *Homo sapiens* using a morphological integration framework. Within this framework, significant levels of correlation between features of craniofacial robusticity are demonstrative of integration and thus a "robusticity complex", while non-significant levels of correlation provide evidence for modularity and therefore an independent expression of these traits. Craniofacial robusticity is examined among four anatomical areas of the human cranium including the frontal, zygomaxillary, temporal, and occipital regions. The expression of robusticity among these anatomical regions is quantified using three-dimensional coordinate landmark data in addition to classical discrete measures and is analyzed via two-block partial least squares regression analysis.

The results show that levels of interaction between these major anatomical units are characterized by a range of correlation values with most obtaining statistical significance. These results frequently provide evidence for integration between subunits

demonstrating at least partial evidence for a “robusticity complex” in the craniofacial skeleton of extant humans

TABLE OF CONTENTS

LIST OF TABLES

LIST OF FIGURES

CHAPTER 1. INTRODUCTION

Ever since the earliest fossil hominin discoveries of the 19th century, biological anthropologists have focused on understanding how these fossil forms are related to ourselves. While we have many characteristics in common, extant *Homo sapiens* and pre-modern[1] fossil hominin forms display a great deal of diversity in craniofacial anatomy. It is these differences, more so than postcranial features, that have served as the baseline for understanding hominin phylogeny and variability throughout the millions of years of our evolutionary history (Pearson, 2008). While the features that have been cited in segregating out modern *Homo sapiens* from pre-modern fossils are numerous, several key characteristics are recurrent in these attempts. Large and prominent supraorbital and nuchal tori, inflated or expanded infraorbital regions, thick cranial vaults, increased mandibular thickness and size, enlarged dentition, the presence of occipital bunning and angular tori, and aspects of cranial vault shape (such as low, sloping frontal regions) are just a few of the many characteristics that have been employed in essentially every study of fossil hominin craniofacial anatomy and phylogeny over the last five decades (Brace, 1963; 1995; Smith & Ranyard, 1980; Trinkaus & LeMay, 1982; Russell, 1985; Frayer et al., 1993; Gauld, 1996; Lieberman, 1996; Antón, 1997; Antón and Franzen, 1997; Bookstein et al., 1999; Antón, 1999; Wolpoff, 1999; Lieberman et al., 2000a, etc.). The unifying factor that all of these features of cranial anatomy have in common is that they can be classified under the more encompassing character set of "craniofacial robusticity". Given the universal inclusion of these features in studies of hominin phylogeny and evolution, it is important that those seeking to employ these characteristics fully understand their expression and distribution.

---

[1] Terms such as pre-modern and modern are used here as convenient descriptors for differentiating between recent *Homo sapiens* and earlier fossil forms. While a more precise meaning of "modernity" is a current topic of debate among paleoanthropologists, it is beyond the scope of the present study.

Despite its overarching usage, many questions remain unanswered about the patterning and determinants of craniofacial robusticity in studies of hominin evolution. What characteristics can reliably and accurately be considered to be features of craniofacial robusticity and precisely how are they defined? What is the overall range of variation for these features? What, if any, is their functional or evolutionary significance? How can these features be used to fully understand other aspects of craniofacial variation throughout the history of the hominin clade (such as encephalization and sexual dimorphism)? While there are many questions regarding the importance of craniofacial robusticity, perhaps the most salient of these asks: Is there a craniofacial "robusticity complex" in hominin evolution, and if so, what is its nature? Several researchers have, in fact, hinted that these robusticity features may be related (Gauld, 1996; Lahr and Wright, 1996; Hublin, 1992), and the work of Lahr (1996) has brought this question to the forefront. Through her work, Lahr has examined features of craniofacial robusticity in light of the modern human origins debate with respect to regional continuity (particularly in Asia), based on their shared distribution and apparent relationship to craniofacial size (Lahr, 1994; Lahr, 1996; Lahr and Wright, 1996). In addition to the substantial contribution that this work has already provided for the field of modern human origins, it is argued here that the question of a "robusticity complex" has an even more important aspect to it. If craniofacial robusticity characteristics, such as supraorbital tori, aspects of zygomaxillary and temporal robusticity, and nuchal tori do, in fact, exist within a greater complex, where their expression is intrinsically linked, then any study that has focused primarily on the usage of one or more of these features in trait lists must be reconsidered based on a lack of character independence (Frayer et al., 1993, Lieberman, 1995). Given that such "robusticity" features are frequently included in the suite of characteristics used to separate modern *Homo sapiens* from all other hominin forms, the far reaching implications of the assumption of "robusticity" character independence are apparent. Additionally, if these craniofacial robusticity features do

array themselves within an intercorrelated complex, what is the evolutionary significance of that complex? Perhaps it would not be the expression of the features as isolated characters which is the usual explicit or implicit assumption, but rather the patterning of covariation between these features that can be used to segregate fossil hominin taxa from modern humans? *It is the primary goal of this study to test the validity of a "robusticity complex" within a large, geographically diverse sample of extant*[2] Homo sapiens.

With the primary question of the study highlighted, how then will the actual presence or absence of a "robusticity complex" be tested? To answer this question, we must turn to the concept of evolvability within evolutionary biology (Wagner & Altenberg, 1996; Kirschner & Gerhart, 1998; Ancel & Fontana, 2000; Raff and Raff, 2000; Yang, 2001; Ebner et al, 2002; Hansen, 2003; Hansen et al, 2003; Gardner & Zuidema, 2003; Pepper, 2003). Evolvability is concerned with the process of how functional and developmental complexes arise within taxa, as well as how these complexes impact the expression and distribution of traits across an organism. There are two primary classifications within evolvability: integration and modularity. Traits that are integrated share a high degree of joint covariation, with lower levels of covariation being present between other characters. Integration can therefore serve as a hypothesis for testing the presence or absence of trait complexes and can provide evidence for a functional or developmental pathway of the proposed complex (Zelditch & Carmichael, 1989; Zelditch et al, 1992; Strait, 2001; Hallgrimsson et al, 2002). Modularity, on the other hand, is used to classify characters that display a lack of covariation between each other. Features that are modularized display a high degree of autonomy within a larger system of traits. Because modularized features are expressed independently, evolutionary

---

[2] This study focuses on variation within extant (or recent) *Homo sapiens* populations to obtain a baseline pattern of craniofacial robusticity expression within our species. Fossil forms of *Homo sapiens* (as well as other extinct hominin taxa) are not considered here, but will be the focus of future research.

forces are free to act on their phenotype without causing systemic, large scale, evolutionary change across the entire organism. Given this, modularity can act as a buffer against environmental and genetic perturbations that could otherwise pose dire consequences for the organism and is accomplished through the process of canalization (Hallgrimsson et al, 2002). This present study will investigate the presence or absence of a robusticity complex using the framework of evolvability.

In order to examine the integrative or modularized nature of craniofacial robusticity, it is necessary to employ data that captures the complex expression of these features. One of the most difficult challenges inherent to studying craniofacial robusticity is that these features display a wide range of subtle variation between forms. Unlike postcranial robusticity, which has a longer and more explicitly developed history of inquiry (Ruff et al., 1993; Trinkaus, 2000a; Trinkaus, 2000b), definitions and characterizations of craniofacial robusticity in the literature are more nebulous. This is most likely due to a lack of easily repeatable and standardized measurements for most of the features that are encompassed within craniofacial robusticity. These features (referred to as *superstructures* in the literature, Lahr and Wright, 1996; Anton and Franzen, 1997; Anton, 1999, Churchill, 1997) often demonstrate a complete lack of standard landmarks that are typically employed in other linear metric analyses. While attempts have been made to circumvent these shortcomings via the usage of discrete coding systems (Lahr, 1994; 1996) or via modified metrical analyses of size and projection (for example, refer to Vinyard & Smith, 2001; Smith & Ranyard, 1980 for an operationalized scheme of measurement for the supraorbital region), previous methods for quantifying the *shape* of these superstructures have been limited by the nature of their data collection.

In order to deal effectively with the challenge of shape quantification in studying craniofacial robusticity, a relatively new methodology that has rapidly become the standard for studying shape will be employed. Referred to collectively as geometric

morphometrics, this methodology provides a means to accurately quantify shape within two-dimensional or (in the case of the present study) three-dimensional space (Adams et al, 2004; Richtsmeier et al, 2002). The use of geometric morphometrics (GM) accomplishes this by providing mathematical and visual information with respect to how forms differ in shape. This information is manifested within the two- or three-dimensional positioning of landmarks along any structure under study. Coordinate landmark data has proved to be highly versatile in that landmarks can be taken at discrete points (or even continuous points which are in turn allowed to slide) along a surface of any feature or structure. While GM has its roots in the work of D'Arcy Thompson at the beginning of the 20th century, a modern revival of the field came about in the early 1990s through the efforts of researchers such as Bookstein and Rohlf (Bookstein, 1991; Rohlf and Marcus, 1993). Progress in the theoretical underpinnings of geometric morphometrics as well as the computational power of computers, has allowed the field of GM to move from Thompson's hand drawn transformational grids to a highly structured and repeatable means of demonstrating and quantifying shape change between different forms (Adams et al, 2004).

The present study melds previous studies of craniofacial robusticity, which rely on the collection of discrete data, with a more modern geometric morphometric approach. Features of robusticity across four major anatomical regions of the hominin cranium are examined in detail, including the frontal, zygomaxillary, temporal, and occipital region. The features and superstructures under study across these anatomical regions include the superciliary arch/supraorbital torus, facial massiveness and projection, mastoid expression, and external occipital protuberance/nuchal torus. The study is conducted using a large, geographically diverse sample of complete and well preserved recent *Homo sapiens* crania (n=140), in order to address the following specific questions: 1) How is craniofacial robusticity manifested in *Homo sapiens*? 2) How do these features vary across a global sample with respect to sex and geographic region? 3) What is the nature

of craniofacial robusticity expression in *Homo sapiens* with respect to a proposed "robusticity complex"? Relative warps analyses (RWA) is employed to address the expression and variability of craniofacial robusticity in detail across the global sample, while Two-block Partial Least Squares (PLS) analyses is used to test hypotheses of superstructure integration in a pairwise manner. These hypotheses therefore involve comparisons of: 1) Frontal vs. Zygomaxillary robusticity, 2) Frontal vs. Temporal robusticity, 3) Frontal vs. Occipital robusticity, 4) Zygomaxillary vs. Temporal robusticity, 5) Zygomaxillary vs. Occipital robusticity, and finally 6) Temporal vs. Occipital robusticity. If significant levels of covariation exist between *all* of these anatomical regions of craniofacial robusticity, then evidence for integration is present and support is lent to the proposition of a "robusticity complex" within the extant hominin cranium. If non-significant levels of covariation exist among all of these comparisons, then support for a modularized nature of craniofacial robusticity is demonstrated. In the event that the results provide mixed signals of integration and modularity, further hypotheses are provided and tested to explain the patterns evident in the data.

This thesis provides a multifaceted approach to the study of craniofacial robusticity that incorporates anthropological and biological theory, current methodological techniques (as well as previously used and standardized measures) for the quantification and examination of robusticity characteristics, and a detailed discussion of the pattering of craniofacial robusticity within our species. Chapter 2 reviews current and past ideas on the nature of craniofacial robusticity within genus *Homo*, which serves as a baseline for understanding how craniofacial robusticity develops and manifests in the skull, as well as hypotheses for explaining why having low or high levels of craniofacial robusticity could be biologically, ecologically, or technologically relevant. Chapter 3 provides a discussion of evolvability, the framework through which craniofacial robusticity is considered in the present study. This chapter provides an in-depth review and discussion of morphological integration and modularity from a biological standpoint

and how these concepts apply to the study of craniofacial morphology. Chapter 4 outlines the materials and methods employed in the study as well as a detailed consideration of why these methods were chosen over others. Chapter 4 also provides a list of specific hypotheses to be examined throughout the course of the thesis and some discussion into what these hypotheses mean with regard to the patterning of robusticity in the cranium. Chapter 5 (results) provides a detailed examination of the expression of craniofacial robusticity through the usage of Relative Warps Analysis (RWA) as well as the patterning of craniofacial robusticity across the skull following a morphological integration framework via Partial Least Squares Analysis (PLS). The results are discussed in detail in chapter 6, with consideration given to other recent studies that examine the relationship of craniofacial and postcranial robusticity to other factors (such as subsistence and activity patterns) as well as how the present study can augment our current understanding of these characters. Finally, chapter 7 provides summary conclusions for this study as well as directions for future research.

CHAPTER 2. CRANIAL ROBUSTICITY

Introduction

The study of hominin cranial robusticity in one of the oldest areas of inquiry in the field of Biological Anthropology, with its origins dating back to the earliest fossil hominin descriptions. Ever since the discovery and recognition of fossil hominin forms, researchers have sought to understand the nature of skeletal robusticity in the cranium. Central to these interpretations is the notion that cranial robusticity can be used in classifying hominins as either "archaic" or "pre-modern" in comparison to ourselves. Moreover, it is the observed pattern of cranial robusticity reduction throughout the evolution of genus *Homo*, especially in the latter stages associated with the Upper Paleolithic "transition", that has frequently been cited as the definition for what can be considered anatomically (and by extension, behaviorally) modern *Homo sapiens* (e.g., Brace, 1963; Frayer, 1984; Trinkaus, 1986; 2000a; 2005; McBrearty & Brooks, 2000; Pearson, 2000; Thompson & Nelson, 2000; Shea, 2003a; 2003b; 2007; 2008).

Given that "gracility", or the loss of both cranial and post-cranial robusticity, has been viewed as a key defining character of our species, many researchers have posited explanatory models for the cause of this apparent pattern of morphological change in genus *Homo*. Some have cited the importance of cultural advancement, indicative of the latter stages of hominin evolution, as a possible cause in robusticity reduction (Trinkaus, 2000a; Smith, 1983; Frayer, 1984; Brace, 1963; 1995; Holt & Formicola, 2008). Others have focused on changes in the timing and pace of growth and development as a consequence of environment pressures (Brothwell, 1975; Green and Smith, 1990, Smith and Green, 1991; Thompson and Nelson, 2000). In reality, it is almost certainly the interplay of these two factors, as well as the possibility of non-adaptive processes, that has most likely shaped the trends we observe in the hominin fossil record.

The question that follows this is: To what extent is robusticity (or the loss thereof) an adaptive strategy in hominin evolution? The two adaptive models briefly highlighted above operate under the idea that skeletal robusticity must have been either selected for or against in hominin evolution, and that the nature of this selection mechanism is what is biologically relevant. A distinction must be made here between "grade" (or "anageneisis") and "clade" (or "cladogenesis") interpretations of cranial robusticity. Arguments that cite robusticity as following a "Robusticity Transition" (Trinkaus, 1984; 1986; 2000a), posit that this associated change from archaic to modern anatomy follows a grade process. Thus, it is assumed that the evolution of genus *Homo*, from the earliest forms of *Homo habilis*, through *Homo erectus* and "archaic" *Homo sapiens*, and up to present day modern *Homo sapiens*, is associated with changes in selective pressures in the environment. While many of these changes are biological, and can be considered as evolutionary adaptations, of primary interest here is how cultural responses may have developed to alleviate the effect of these selective pressures. If this means of addressing cranial robusticity is correct, then a better understanding of the evolution of gracility may be tied to behavioral changes that arise with increasingly sophisticated culture and technology, especially during the Upper Paleolithic (Frayer, 1984; Trinkaus, 2000a; McBrearty & Brooks, 2000; Pearson, 2000; Shea, 2003a; 2003b; 2007; 2008). In this case, craniofacial robusticity could be considered a homoiology (a characteristic that is tied to phenotypic plasticity) that is expressed as a result of non-genetic behavioral patterns seen throughout the lifetime of an individual (Collard & Wood, 2007; Cramon-Taubadel, 2009). As a result, similarities in craniofacial robusticity between taxa might not be phylogenetically informative. Additionally, continuous change from archaic to modern anatomy would indicate that cranial robusticity is not useful for making species level distinctions since specific states of robusticity expression can not be defined (Lieberman, 1995).

Conversely, if the evolution of robusticity occurred in the process of cladogenesis, this would indicate that certain features of robusticity may be important for cladistic analyses. Craniofacial robusticity need not be adaptive in this case, allowing for the possibility of neutral or non-adaptive explanations for its expression. Here, the expression of robusticity features is considered to be discrete and biologically meaningful for making species level distinctions. In order for this to be the case, cranial robusticity features 1) must be homologous across all hominin taxa, 2) have clearly defined character state polarity, and 3) must be observable in all represented taxa (Lieberman, 1995). Given that the features commonly indicated in cranial robusticity follow these criteria, as argued by some researchers, (e.g. Lahr, 1995; Rightmire, 1995; Trinkaus, 1995, Wolpoff & Crummett, 1995) it is the task of the researcher to clearly lay out definitions for robusticity features, and to explain their occurrence in hominin evolution. Some researchers have questioned the use of cranial robusticity characters in human evolution arguing that they are primitive features that do not meet the criteria laid out above (see Lieberman, 1995; 1996; 1999). It is possible, however, that if certain aspects of cranial robusticity are not meaningful in terms of trait assumption for cladistic analysis, the overall expression of the complex of robusticity may in fact shed light on this question (Gauld, 1996; Lahr, 1996).

In order to address these debates pertaining to the evolutionary significance of robusticity in the cranium, a more basic question must first be asked: How do we define cranial robusticity, and what is the nature of its expression in the hominin skull? Features of craniofacial robusticity are expressed across the entire cranium, from the supraorbital tori, occipital tori and cranial vault thickness, to mastoid and zygomaxillary prominence, and aspects of facial projection and massiveness (Antón, 1997; Gauld, 1996; Lahr, 1996; Lieberman, 1996; Smith & Ranyard, 1980; Trinkaus & LeMay, 1982). While these features have been studied almost exclusively in isolation, some research has indicated that these aspects of robusticity should in fact be studied as a related (intercorrelated)

complex (Lahr, 1996; Lahr & Wright, 1996). The significance of this possibility would be that robusticity features are uninformative (or redundant) taken in isolation, but when considered as a whole, this complex of features may enable researchers to better delineate differences between hominin taxa irrespective of the precise phylogenetic method. This hypothesis of a cranial "robusticity complex" has been only recently explicitly addressed (Baab et al., 2010) and is thoroughly and independently tested in this dissertation.

Defining Cranial Robusticity

An important step in building a more comprehensive understanding of the nature of cranial robusticity expression in the skull is to lay out a clear definition of what is meant by a "robust" cranium. While studies relating to cranial robusticity often highlight key areas of the cranium as being large and heavily built, there has been no systematic definition of cranial robusticity explicated to date. Postcranial robusticity, on the other hand, has been more thoroughly standardized (Ruff et al., 1993; Ruff, 2000; Trinkaus et al., 1991; Trinkaus, 1997; 2000a; 2000b). A review of the relevant postcranial literature in this regard is therefore useful prior to focusing on cranial robusticity.

Defining Postcranial Robusticity – A Brief Digression

Postcranial robusticity is most generally defined as a measure of bone strength or buttressing as a response to mechanical loads placed upon it (Ruff et al., 1993; Trinkaus et al., 1994; Ruff, 2000; Ruff et al., 2006; Stock & Shaw, 2007; Shackelford, 2007; Shaw & Stock, 2009a; 2009b). This buttressing can be in response to either infrequent high loadings placed on the bone, or lower levels of loading that occur much more frequently. In addressing levels of postcranial robusticity between taxonomic groups, it is important that allometric scaling is accounted for. Therefore, a more concise definition of postcranial robusticity would be a measure of bone resistance to loads placed upon it, scaled to a relative measure of bone length or overall body size (Ruff et al., 1993;

Trinkaus et al., 1994; Ruff, 2000; Trinkaus, 2000a; Holliday, 2002; Carlson et al., 2007; Cowgill & Hager, 2007).

Given that postcranial robusticity involves some measure of bone strength against loadings placed upon it, how do we quantify this property of bone? One way to approach this problem is by examining the cross-sectional geometry of long bones (Ruff et al., 1993; Trinkaus et al., 1994; Trinkaus, 1997, Ruff, 2000; Holliday, 2002; Pearson & Lieberman, 2004; Carlson et al., 2007; Holt & Formicola, 2008; Cowgill, 2010; Cowgill et al., 2010). The cross-sectional area of long bones relates to the ability of the structure to withstand compressive and torsional stresses. Another way to address this property of bone is to study relative cortical area, a measure of robusticity that deals with the relationship of cortical bone thickness relative to medullary cavity breadth or area (Ruff et al., 1993; Ruff et al., 1994; Trinkaus et al., 1994; Holliday, 2002; Cowgill & Hager, 2007). More specifically, a measure of percent cortical area index (%CA) can be utilized to quantify long bone robusticity. %CA can be calculated as (cortical area ÷ periosteal area) × 100 (Ruff et al., 1993; Ruff et al., 1994; Holliday, 2002; Shackelford, 2007; Carlson et al, 2007; Shaw & Stock, 2009a; 2009b).

In addition to methods of standardizing cortical bone thickness to the total area of cross-sectional bone, secondary moments of area (SMA) are also employed. SMA provides a measure of bone strength to bending and torsion (Ruff et al., 1993; Ruff et al., 1994; Trinkaus et al., 1994; Trinkaus, 2000a). Secondary moments of area are analogous to polar moments of area as they both provide information on bending and torsonal strength (Ruff, 2000; Ruff et al., 2006; Carlson et al., 2007; Cowgill & Hager, 2007; Shaw & Stock, 2009a; 2009b; Cowgill, 2010). This measure of robusticity differs from those highlighted above in that SMA scales the unit area of a bone cross-section to a standardized measure of bone size. This can be accomplished by either calculating the product of the unit area and the squared distance from the axis through the section of bone for a measure of bending strength, or by calculating the product of unit area and the

squared distance from the section centroid in order to measure torsional strength (Ruff et al., 1993; Ruff et al., 1994; Trinkaus et al., 1994, Ruff, 2000).

In addition to the cross-sectional properties of long bones, information on bone articular surfaces also serves as an appropriate indicator of bone robusticity (Ruff et al., 1993; Trinkaus et al., 1994; Trinkaus, 2000a; Trinkaus, 2000b; Lieberman et al., 2001; Carlson et al., 2007). Forces that are experienced by bones during loading are transmitted through the joints where two bones articulate, and therefore, information relating to the overall size of this articular area can be incorporated into a quantification of robusticity. As an example of how this can be measured, femur articular surface area is often comprised of three variables: articular breadth, medial facet breadth, and lateral facet breadth (Ruff et al., 1993; Trinkaus et al., 1994; Trinkaus, 2000b; Ruff, 2002; Ruff, 2003). Closely related to this measure is articular volume, or the measure of the trabecular bone that underlies the joint articular surface (Ruff et al., 1993).

General Overview of Cranial Robusticity Concepts

Unfortunately, simply applying the measures of postcranial robusticity highlighted above to the question of how to quantify cranial robusticity is not possible. While these measures work well in postcranial elements, the complex shape of the splanchnocranium and neurocranium prevent simple application of these methods to defining cranial robusticity. In some cases, researchers have turned to finite element analysis, a method that simplifies a complex morphological structure, such as the splanchnocranium, by reducing its complex shape into a series of finite simple shapes (such as triangles or squares, a process known as descritizing) that can be modeled more easily and then combined to provide an approximation of forces and stress throughout the entire structure (Korioth et al., 1992; Korioth, 1997; Grine et al., 2010). Finite element analysis, however, is constrained by computational power and limited in scope to developing and testing biomechanical hypotheses in functional systems (Grine et al.,

2010). In order to accurately quantify shape as well as focus on the interactions between anatomical subunits, others have turned to geometric morphometrics (GM). GM is a method that captures the complex shape of an object as discrete landmarks that can be examined in two- or three-dimensions to provide information on shape similarities and differences. This methodology has been recently incorporated as part of investigations into the complex nature of craniofacial robusticity (Baab et al., 2010). Methodologies such as these are useful for obtaining information regarding external morphology as well as cross-sectional properties of the cranium, and this knowledge is necessary for developing a universal definition of craniofacial robusticity.

When dealing with describing robusticity in the cranium we can subdivide features into two broad classes: cranial vault thickness and cranial superstructures (Lahr, 1996; Lahr and Wright, 1996; Lieberman et al., 2000a; Bookstein et al., 1999; Antón, 1999; Antón and Franzen, 1997). Cranial vault thickness simply refers to the thickness of bone in any given region along the cranial vault, and is commonly done via the use of radiographs or CT scans (Antón and Franzen, 1997; Bookstein, et al, 1999; Lieberman, 1996). This class of robusticity is tied to the second, cranial superstructures, in that the latter is essentially the outward expansion of the external table of the former in various regions of the cranium (Antón, 1999; Antón and Franzen, 1997). Cranial superstructures have been analyzed in more ways then cranial vault thickness has, and this is most likely due to the inherent complexity of form that many of these structures possess. Some studies have employed discrete character analyses in order to analyze the robusticity of these cranial superstructures (Lahr, 1994; Lahr, 1996; Lahr & Wright, 1996; Lieberman et al, 2002). Others have employed metrics to assess the overall massiveness as well as projection of these structures (Smith and Ranyard, 1980; Smith, 1984).

It has also been argued that cranial robustness (with respect to cranial superstructures) is closely correlated to overall craniofacial size, where highly robust crania are often very large crania (Lahr, 1996; Lahr & Wright, 1996). Cranial shape also

relates to the expression of robusticity, but to a lesser extent. Here, robust crania tend to be long narrow skulls with broad upper faces and large palates and teeth, while gracile crania tend to have broad frontal and parietal bones and narrow faces with small teeth (Lahr & Wright, 1996). Similar results have been noted for non-human primates as well, such as the large bodied dental apes (or primates that have "ape-like" dental anatomy) (Ravosa, 2000). Other measures of size are also closely correlated with measures of cranial robusticity. Overall body size for example may also serve as a strong correlate to cranial vault thickness, and therefore a possible factor that is driving the increased expression of robusticity in large bodied hominins (Gauld, 1996). In addition to general aspects of cranial robusticity, a more detailed discussion of the specific features of robusticity in warranted. These features can be subdivided into zygomaxillary (facial) robusticity, frontal (brow ridge) robusticity, occipital (nuchal torus) robusticity, temporal (mastoid) robusticity, and finally, cranial vault thickness.

Zygomaxillary Robusticity

Robusticity of the zygomaxillary or midfacial region has been quantified in several different ways. Measurements of overall cranial massiveness have been implicated in robusticity expression, and this is true of the facial region as well. As noted above, it has been demonstrated using the standard Howells measurements (see Howells, 1973) that facial size is tied very closely to craniofacial robusticity (Lahr, 1996, Lahr & Wright, 1996). Trends in facial and dental reduction throughout hominin evolution have been also tied to a loss of robusticity in the modern "gracilized" form (Brace, 1963; 1995; Wolpoff, 1999). It is therefore important that information on the dimensionality of the face be retained in any analysis of cranial robusticity, given these observations.

Many superstructures reside within the zygomaxillary region that can provide important information regarding the robusticity of the splanchnocranium. The zygomatic and maxillary bones have processes that articulate with the frontal bone (White, 2000)

and several aspects of the morphology of these bones share a special relationship to the supraorbital torus (brow ridge). The zygomatic trigone is an expansion of bone on the frontal process of the zygomatic (as well as the zygomatic process of the frontal) and is one such superstructure that characterizes this anatomical region (Lahr, 1996). Another, the zygomaxillary tubercle, may be found on the body of the zygomatic bone, and is related to expression of the masseter muscle which has its origin on the lower margin of the zygomatic (Lahr, 1996, White, 2000). Finally, a characterization of the infraglabellar notch (which is comprised of both the maxillary and nasal bones and their articulation to the frontal) is closely tied to supraorbital morphology, and can also be scored in its relation to cranial robusticity (Lahr, 1996).

Biomechanical studies of this anatomical region have also been used to address the ability of the facial skeleton to withstand strains and stresses placed upon it (Antón, 1994; 1996; Spencer and Demes, 1993; Rak, 1986; Demes, 1987; Trinkaus, 1987; Carlson and Van Gerven, 1977; Smith, 1983). These studies cite aspects of facial shape that serve to better buttress the splanchnocranium from excessive loadings placed on it through mastication and paramastication. Using the definition of postcranial robusticity as a beginning framework, it is possible to model robusticity of the face as the ability to resist torsional, tensile, and compressive forces. Several different models have been proposed, such as the "zygomatic retreat model" (Trinkaus, 1987), the "infraorbital plate model" (Rak, 1986), and the "shell model" (Demes, 1987), but all address the shape of this anatomical region as a means of alleviating stresses placed upon it. Recently, workers have employed finite element analysis as a more complex means of modeling stress and strain within the facial skeleton (Lieberman et al., 2004; Wang et al., 2006; Strait et al., 2007; Grine et al., 2010). Studies of this nature have provided useful insight into many aspects of hominin evolution, such as the morphological and biomechanical diversity of the facial form across *Australopithecus* and *Paranthropus* (Strait et al., 2007; Grine et al., 2010). The biomechanical and behavioral implications for these arguments

with respect to their relationship with paramasticatory behavior, as well as other aspects of cultural change in hominin evolution, will be addressed in detail later.

Frontal Robusticity

Perhaps one of the most prominent cranial superstructures that can be studied is the supraorbital torus, more commonly referred to as the brow ridge. Several studies have provided means to quantify this structure (Vinyard and Smith, 1997; 2001; Smith & Ranyard, 1980; Smith, 1984) as well as provide morphological interpretations for its expression (Endo, 1966; Russell, 1985, Ravosa, 1991, Hylander et al., 1991; Moss and Young, 1960). The supraorbital torus can span the entire breadth of the inferior portion of the frontal bone, just superior to the eye orbits. It is generally composed of several portions of the frontal, a projection at glabella, the projection of the superciliary ridges above each (left and right) orbit, and the expansion of the supraorbital trigones on the zygomatic process of the frontal (Vinyard & Smith, 2001; Smith & Ranyard, 1980, Lahr, 1996). It also has close associations with the infraglabellar notch and the zygomatic trigone which provide inferior and lateral margins for this structure respectively (Lahr, 1996). Researchers have observed that the expression of this anatomical region is closely correlated to the frontal angle (defined as the angle formed between metopion, nasion, and prosthion) and the neuro-orbital angle (defined as the angle formed between a line following the contour of the cranial vault and a line following the axis of the orbit) (Ravosa, 1991, Wolpoff, 1999). Measurements of the supraorbital torus have been operationalized, with measurements of torus thickness and projection often taken at given intervals along the structure (such as medial supraorbital height and projection, midorbital supraorbital projection, and lateral supraorbital height, see Vinyard & Smith, 2001; Smith & Ranyard, 1980).

As with facial robusticity, arguments over the biomechanical significance of the supraorbital torus during mastication and paramastication have also been posited (Endo,

1966; Russell, 1985, Hylander et al., 1991; Moss and Young, 1960). These studies generally address the relevance of modeling the supraorbital torus as a "bent beam" which serves to dissipate forces transmitted through this anatomical region (Wolpoff, 1999; Hylander et al, 1991; Daegling and Hylander, 2000). The "spatial hypothesis" originally proposed by Moss and Young (1960) offers an alternative explanation for this anatomical region: the brow ridge functions primarily to maintain spatial continuity between the facial and neurocranial regions of the skull. These arguments are relevant to discussions of cultural and behavioral determinants of robusticity and will be expanded upon later.

Occipital Robusticity

Robusticity of the occipital region of the skull is generally characterized by the size and expression of an occipital (or nuchal) torus (Lahr, 1996; Lahr & Wright, 1996; Trinkaus & LeMay, 1982; Lieberman et al, 2000a). In general, the occipital torus can be defined as a bony projection from the occipital squama that is formed between the superior and supreme nuchal lines which provide attachment regions for many of the nuchal muscles (Lahr, 1996). The morphology of this anatomical region can be quite variable, ranging from faint or non-existent nuchal lines, to a projecting continuous torus or large nuchal bun. Nuchal bunning is a variant that has been described in several different forms of fossil hominins such as Neandertals and early modern humans (Trinkaus & LeMay, 1982; Churchill & Smith, 2000; Gunz & Harvati, 2007; Bastir et al., 2010). Nuchal buns are similar to nuchal tori in that they represent a posterior projection of the occipital, with the difference being that nuchal buns can be characterized as an overall inflation of the occipital squama from lambda (as its superior boundary) to the internal occipital protuberance (its inferior boundary). Not only is the thickness of the occipital bone greater in this region, but also there is a marked increase in surface area related to the expression of nuchal buns (Trinkaus & LeMay, 1982; Bastir et al., 2010).

These structures are also characterized by a depression above inion, called the suprainiac fossa (Smith, 1983; Lieberman, 1995; Bastir et al., 2010).

Since this region is in close association with the musculature of the neck, some have speculated the association of this morphology with masticatory and paramasticatory behavior (Brose & Wolpoff, 1971; Wolpoff, 1999). As an alternative hypothesis, researchers have proposed that brain growth and overall cranial shape may be the causal mechanism for the expression of this morphology in hominins (Trinkaus & LeMay, 1982; Lieberman et al, 2000a; Gunz & Harvati, 2007). This relationship will be further expanded upon in the developmental and behavioral implications of cranial robusticity below.

Temporal Robusticity

Robusticity of the temporal region of the skull is most often characterized by the mastoid and juxtamastoid regions. The mastoid process (and associated surrounding anatomy) provides muscle attachment for several muscles involved in both mastication and movement of the neck. Several bony landmarks that have been attributed as superstructures of this anatomical region include: the supramastoid crest, retromastoid process, supramastoid tubercles, as well as the mastoid process proper (Lahr & Wright, 1996). Quantification of these structures often entails measurement of mastoid height and width (see Howells, 1973), with larger dimensions indicating a greater degree of bony expansion, and therefore higher levels of robusticity. Researchers have noted that while Neandertals (and early modern *Homo* sapiens) tend to have higher levels of robusticity in other regions of the cranium, they often exhibit diminished mastoid regions (Churchill & Smith, 2000; Wolpoff et al., 2000; Balzeau & Radovcic, 2008). While this may be the case, Neandertals are also characterized by having expanded juxtamastoid regions (on the inferior surface of the temporal and occipital) and it is this expansion that may be masking the overall size of the mastoid process (Santa Luca, 1978, Duarte et al,

1999). More recent studies of temporal bone morphology using geometric morphometrics have further elucidated these differences between fossil hominin forms, such as Neandertals and modern humans (Harvati, 2002; 2003a).

Cranial Vault Thickness

Having surveyed the major superstructures associated with robusticity throughout the cranium, it is appropriate to provide a discussion of cranial vault thickness and how it relates to robusticity expression in the skull. Cranial vault thickness (CVT) is a measure characterized by three cross-sectional components: the external table, the diplöe, and the internal table (Antón & Franzen, 1997; Antón, 1999; Peterson & Dechow, 2002; Tobias, 2006). CVT is often taken in midline at set cranial landmarks, like bregma (Lieberman, 1996; Bookstein et al, 2003; Caspari & Radovcic, 2006), but it may also be evaluated in other regions of the cranial vault as well (Gauld, 1996; Peterson & Dechow, 2002; 2003; Balzeau & Grimaud-Herve, 2006; Wang & Dechow, 2006; Dechow et al., 2010). Recall that the external table of the cranial vault is what forms the basis for the bony expansion of the cranial superstructures, and it therefore has a close association with expression of external robusticity features. Studies of morphological differences between the internal and external tables have shown that while the external table has undergone significant morphological changes throughout hominin evolution, the internal table has remained relatively constant. The conservative nature of this relationship may have implications for brain evolution across genus *Homo* (Bookstein et al, 1999). Expansion of the cranial vault may not always be a good indicator of robusticity however. Antón (1997) has shown that in the case of some fossil hominins (Sangiran 2, Gibraltar 1, and Shanidar 5), a pathology called *Hyperostosis Calvariae Interna* which involves the thickening of the internal table of the frontal and parietal regions can be noted. This pathology makes these specimens seem more robust in CVT then their normal anatomy would indicate, and as a result care must be taken when addressing CVT in fossil hominin studies (Antón,

1997). When studies of cranial vault thickness are considered outside the context of pathology, they are typically biomechanical in nature. Systemic or hormonal responses to increased activity patterns (Lieberman, 1996; Copes, 2009) and CVT expansion due to masticatory loading and stress tied to diet (Menegaz et al., 2010) both offer testable hypotheses for evolutionary trends in cranial vault thickness across genus *Homo*.

Developmental Mechanisms for the Evolution of Cranial Robusticity

Having addressed the aspects of morphology that constitute a "robust" cranium, we may now move on to explanations of the evolutionary significance of this anatomy in genus *Homo* evolution. There are two broader areas of research that have addressed aspects of robusticity evolution in the cranium, the first dealing with developmental timing and change in hominin evolution, and the second dealing with behavioral and cultural influences on this anatomy. Since developmental mechanisms deal with underlying growth and development, while behavioral mechanisms are a more secondary consequence of *in vivo* activity patterns, development will be considered first.

Review of Growth and Development

Before addressing some of the research that has been done regarding the evolution of robusticity from a developmental perspective, a discussion of some of the terminology and theory behind growth and development is warranted. In general, research into the evolution of development deals broadly with changes in the timing of growth as well as the rate of growth in an individual organism (Gould, 1977; Alberch et al, 1979; McKinney & McNamara, 1991, Godfrey & Sutherland, 1995). This is referred to as heterochrony in the literature and is defined as changes in the rate of development for a particular stage of growth relative to that of the ancestor (McKinney & McNamara, 1991; Williams & Krovitz, 2004; Rosas et al., 2006; Zollikofer & Ponce de Leon, 2006).

Gould's (1977) clock model provides a general outline through which studies in growth and development may be conducted. This model approaches the change in form tied to growth and development from two aspects: change in size versus change in shape. Change in size is tied closely to the growth of an organism, while change in shape is related to differences in development (Gould, 1977; Godfrey & Sutherland, 1995; Williams & Orban, 2007). With this dichotomy in mind, the clock model provides a number of outcomes in the evolution of growth and development within a species. It is important to remember that studies regarding evolutionary development consider changes in the timing of aspects of growth and development from the ancestor to the descendent. Therefore, if an organism reaches its juvenile shape at a later stage of growth (or larger body size) *relative* to its ancestor, then the organism has undergone "retardation" or "neoteny". Conversely, the organism has undergone "acceleration" *relative* to its ancestor if the juvenile shape is attained at an earlier stage of growth (Gould, 1977).

While this model addresses the rate of developmental change witnessed in a descendant relative to its ancestor, it does not address change in the onset or offset of growth in an organism. This concept is equally important and must be expanded upon. If an organism undergoes a shift in the timing of growth, so that it begins growing at an earlier stage (again, relative to the ancestor), this is referred to as "pre-displacement". "Post-displacement", therefore refers to onset of growth at a later developmental stage (Alberch et al, 1979). It is also possible that changes to the offset of growth may occur in the evolution of an organism. If growth changes stop at an earlier stage than the ancestor (i.e. it has an early offset of growth), then the organism has undergone "progenesis". Counter to this, if an organism has a later offset of growth (it continues growth into a later stage then the ancestor), then it has undergone "hypermorphosis" (Alberch et al, 1979; for a review see Godfrey and Sutherland, 1995).

The sum of these changes in growth and development can be described in one of two ways. If an organism evolves in a manner that maintains juvenile features into

adulthood, then it is considered to have undergone *paedomorphosis*. In the case where a descendant develops beyond the range of the ancestor, this is termed *peramorphosis* (Churchill, 1998; Williams, 2002; Ponce de Leon & Zollikofer, 2006). More specifically, paedomorphosis and peramorphosis are the resultant manifestations of the processes outlined above. Therefore, the evolution of a paedomorphic descendent can involve either neoteny (also referred to as retardation), a late onset of development (post-displacement), early offset of development (progenesis), or a combination of any of these processes. Peramorphosis, then is the result of acceleration, an early onset of development (pre-displacement), a late offset of development (hypermorphosis), or any different combinations of these (Godfrey and Sutherland, 1995; Ponce de Leon & Zollikofer, 2001; Ponce de Leon & Zollikofer, 2006).

Genetics of Craniofacial Development

Given that growth and development are largely under the influence of genetic control, a brief review of this literature will be provided here. While research in genetics and craniofacial development is not a new area of research, some of the most interesting developments in this field have only come about over the past ten to fifteen years. With an increase in our knowledge of craniofacial genetics, come more questions that researchers must address. It has become increasingly difficult to draw the line between genetic and behavioral influences on cranial robusticity and cranial growth. As some of the studies (see Lieberman, 1996) have shown, genetics may not have a measurable effect on robusticity in certain parts of the cranium. However, genetics do play a role in the timing and expression of traits during and after ontogeny and they also affect cranial morphology in different anatomical regions (such as the face).

The roots of modern research in craniofacial genetics can be traced back to 1984, when the existence of homeotic genes (referred to as HOX genes), was discovered in fruit flies and mice. HOX genes are a group of genes that control the "geometry of the body

form" (Slavkin, 2000). The discovery of HOX genes in human craniofacial development has opened up new areas of research in genetics. Geneticists now know that homeotic genes control segmentation in embryos along an anteroposterior axis, which separates areas of the forebrain, midbrain, hindbrain, and spinal cord (Slavkin, 2000). Morphoregulatory genes have been discovered that code for dorsal-ventral development of the maxilla, mandible, tongue and dentition (called the first branchial arch) and other aspects of morphogenesis. The morphoregulatory genes of the first branchial arch have been found to be highly conserved throughout evolution (Slavkin, 2000). This should come as no surprise considering that the maxilla, mandible, and dentition play a key role in both mastication and respiration, and are therefore vital to an organism's survival. Due to the interaction of this functional complex with the environment, the genes controlling the morphogenesis of this area would have been under the direct influence of selection throughout hominin evolution.

Over the past few years, many studies (see Vieille-Grosjean et al., 1997; Barni et al., 1998; Schumacher, 1999; Zhang et al., 2000) have been conducted in an attempt to reveal which genes are involved in human craniofacial morphogenesis and how those genes affect the development of craniofacial features. As we have already seen, research being conducted in the genetics of human facial growth is of particular importance to human evolution. In one such study, eight HOX genes were isolated and studied with respect to human craniofacial morphogenesis. Interestingly, the results of this study show that research conducted on the same area for mice may also be relevant to the study of the genetics of human craniofacial growth (Vieille-Grosjean et al., 1997). Through a close examination of the genes involved, light has been shed on the timing and expression of some of the branchial HOX genes involved in the process of facial development. While, to date, there have been few loci in this gene complex that have been implicated for craniofacial abnormalities, further research in this area will

undoubtedly highlight areas where mutations have had an effect on facial form (Vieille-Grosjean et al., 1997).

Another study in the genetics of human craniofacial morphogenesis focused in on the role of genes in the expression of endothelins, which can be defined as "peptides that are involved in various biological functions in many tissues and organs" (Barni et al., 1998:183). Endothelin-1 (ET-1) and its associated receptors (ETA and ETB) play a key role in the development and osteogenesis of the human mandible (Barni et al., 1998). Understanding the influences of genes on the development of the hominin jaw is of vital importance due to the relationship of this complex to craniofacial biomechanics and future studies in this area of genetics will provide greater insight into the evolution of modern human craniofacial form.

In light of these developmental and possible underlying genetic controls, how would craniofacial robusticity variation evolve? If we hypothesize that cranial robusticity features are the result of peramorphosis, or any suite of developmental changes that cause the descendant to undergo "overdevelopment", then the evolution of gracility, that is commonly attributed to *Homo sapiens*, is a result of paedomorphic change in our lineage (see Churchill, 1998; Brothwell, 1975; Green and Smith, 1990). Two specific models have been proposed to explain the evolution of these different resultant morphologies: the Endocrine-Shift Model (Brothwell, 1975) and the Accelerated Endochondral Growth Model (Green & Smith, 1990; Smith & Green, 1991).

Endocrine-Shift Model

The Endocrine-Shift Model, proposed originally by Brothwell (1975), serves as a possible explanation for the robust anatomy of fossil hominins. Brothwell hypothesizes that given the cold temperate environments that the Neandertals and other later archaic populations would have encountered in Europe; these fossil groups would have needed to obtain larger levels of skeletal robusticity and muscularity (the latter being closely

associated with the former) as a means to increase overall body mass relative to surface area at a much earlier stage of development. This would have been achieved by shifting the onset of growth hormone (GH) release and sex steroid production to an earlier stage development. The resulting pre-displacement would have caused the Neandertals to have a much earlier growth spurt, which would have then been followed by a longer adolescent period, where the individuals would continue to grow (producing a peramorphic anatomy) until reaching the levels of robusticity characteristic of the taxonomic group (Brothwell, 1975).

Another side effect of this pattern of growth would be a premature closure of the epiphyseal lines, producing shorter limbs in the adult Neandertal, relative to earlier ancestral forms (Brothwell, 1975). As noted above, shifts in the timing of GH release would have also provided the stimulus needed to grow much larger bones and muscles. When these two factors are considered together (limb foreshortening due to premature closure of the epiphyseal lines as well as large increases in lean body mass as a result of increased muscular growth), this model provides a framework for explaining how Neandertal morphology (with respect to proportionality and robusticity) arose in response to Allen's and Bergmann's Rules, given their cold climate (Churchill, 1998; Churchill, 2006).

Accelerated Endochondral Growth Model

A second model proposed originally by Green & Smith (1990) falls along the same lines as the Endocrine-Shift Model above, in that like the previous model, the Accelerated Endochondral Growth Model attributes higher levels of robusticity in fossil hominins to peramorphosis. The key difference here is that while the previous model posits an earlier onset of development via the premature release of GH, this model predicts that the overall growth rate of fossil hominin groups was accelerated relative to modern *Homo sapiens* and as a result fossil hominins would have developed a

peramorphic (or hyper-robust anatomy) within the same growth period (Green & Smith, 1990; Smith & Green, 1991; Ponce de Leon & Zollikofer, 2001; Rosas et al., 2006).

Again, given the cold temperate climate that these hominins would have inhabited during the coldest stages of the Pleistocene, we would expect to see adaptive changes in the postcranial and cranial skeleton in these fossil hominins that would have produced an appropriate body form for their environment. While the Endocrine-Shift Model states that this could be achieved by having an earlier onset of growth, it would actually take longer for the individual to develop a properly cold adapted body form and therefore place the individual at greater risk during infancy – the time of highest vulnerability in growth and development. By positing acceleration as the mechanism for obtaining a peramorphic (or robust) form, infants would have developed an appropriate cold adapted anatomy earlier, which would place them at risk for a shorter period of time (Smith & Green, 1991; Churchill, 1998). Another benefit that this model has over the Endocrine-Shift Model is that it can be more readily tested in the fossil record by examining difference in developmental stages between archaic and modern populations (Churchill, 1998).

It should be noted that while the above models provide provocative arguments for changes in developmental timing throughout human evolution, these models have been questioned elsewhere (Churchill, 1998). The Endocrine-Shift Model often fails to address the full range of variation seen in the fossil record, and as a result, it does not find large support. The Accelerated Endochondral Growth Model fairs better, in that it is narrower in scope and can be tested by comparing differences in juvenile developmental stages between modern and archaic populations (Churchill, 1998). More recently, there has been a shift from models that stress differences in the timing, rate, and onset/offset of ontogenetic trajectories to models that provide a more systems-based approach (following morphological integration) to understanding Neandertal and early modern *Homo sapiens* cranial form (Rosas et al., 2006; Pearson, 2008; Lieberman, 2008). It is argued by these

studies that there are only a few actual developmental shifts involved in the evolution of a derived modern *Homo sapiens* craniofacial form, and that most of the characters used to define *Homo sapiens* actually form an integrated craniofacial complex (Lieberman, 2008; Pearson, 2008).

Ecological Responses and Trends in Hominin / non-Hominin Evolution

As noted earlier, the general trend of the expression of robusticity in hominins declined throughout the course of the Pleistocene. We know from numerous studies that the climate throughout the Pleistocene was variable, with times of glacial advances and retreats (see Anklin et al., 1993; Dansgaard et al., 1993; Taylor et al., 1993). This environmental variability has been central to many ideas on hominin evolutionary trends, such as Endocrine-shift Model and Accelerated Endochondral Growth Model surveyed above. Perhaps the best place to start examining this question is not with hominin morphology however (which, especially in later times, would have been under the influence of external factors of increasing complexity, like culture), but with faunal morphology. Churchill (et al. 2000, for a general discussion see Churchill, 1998) notes that with black wildebeest, *Connochaetes gnou*, a trend toward decreasing body mass occurs throughout the Pleistocene. With this reduction in mass, a reduction in metapodial robusticity has been noted as well. It is interesting to note, however, that measures of reduction in black wildebeest postcranial robusticity are equal to that of hominin postcranial reduction (Churchill et al., 2000). Although not many studies of this nature have been carried out in this area of faunal robusticity patterning, others have noted similar trends (Weaver and Ingram, 1969; Sterns, 1982).

Studies involving the trends of hominin body mass throughout the Pleistocene also aid in better understanding the accompanying trends in cranial robusticity reduction. With an overall decline in global temperatures and with more and more hominins

migrating north into cooler latitudes, a trend in the increase of body mass can be noted (following Bergman's Rule). Three trajectories in the relation of brain mass or encephalization to body mass (referred to as the encephalization quotient, or EQ) have been noted (see Ruff et al., 1997). They are an Early to middle Middle Pleistocene trajectory (body mass stays relatively stable), a late Middle to early Late Pleistocene to late archaic *Homo sapiens* trajectory (body mass increases, which is also related to more fossils being found in higher latitudes), and a trajectory including early and recent modern *Homo sapiens* (body mass decreases) (Ruff et al., 1997). The late Middle to early Late Pleistocene trajectory is of prime importance because it is transitional between the early Pleistocene and early/recent modern human samples. Interestingly, with recent modern humans, a decline in absolute brain size can be observed, and this ties in directly with a decrease in body mass since around 50 kya BP (Ruff et al., 1997). Although studies such as Ruff et al. (1997) are concerned with trends in body mass and brain size throughout the Pleistocene, these trends may also mirror evolutionary change in cranial/postcranial robusticity.

Research pertaining to the evolutionary trajectory of long bone robusticity has highlighted a near linear decline in cortical area at femoral midshaft throughout the past 1.8 my, along with a slight increase in polar second moment of area (a measure related to bending and torsional rigidity of bones) between earlier *Homo erectus* and later archaic *Homo sapiens* (Ruff et al., 1993). A steep drop off in robusticity occurs within the last 50,000 years, which also seems to fit with Ruff et al. (1997). It has already been demonstrated by Ruff et al. (1993) that an inverse relationship between postcranial robusticity and brain size exists, in that as cranial capacity increases, femoral robusticity decreases.

Although a dietary shift may be seen as a cultural factor relating to trends in robusticity, a shift of this nature can also relate to community ecology. As a result, diet will be briefly examined here. Bone robusticity can be related to protein intake in that an

increased intake of protein, relative to fat intake, can cause an increase of urinary calcium output (calciuria). This causes bone resorption and a decline in overall bone robusticity (Cachel, 1997). Pre-modern hominins that would have had a high protein diet (such as those hominins living in more northern latitudes) would have also had to increase their intake of fat (whether it be through bone marrow or fatty meat) in order to maintain higher levels of bone robusticity. It has been argued that in the Late Upper Paleolithic, population expansion among humans would have decreased individual workloads, which would have had a similar effect on skeletal robusticity. This decline would have made it possible for humans to consume less fat relative to protein, since calciuria would have been lessened to tolerable levels. This would, in turn, further the decline of skeletal robusticity until it had reached modern day levels (Cachel, 1997). Also, with the diversification and of subsistence strategies and technological advances during the Upper Paleolithic, this would have given humans a great deal of breadth with respect to their dietary regimes (Holt & Formicola, 2008). Again, this trend can be seen as part of an overall ecological trend toward skeletal gracilization. These changes can also be tied into cooking and other applications of technology. This relationship between culture and robusticity will be further explored in the following section.

Behavioral Mechanisms for the Evolution of Cranial Robusticity

The second class of mechanisms that can be implicated in the development of robust craniofacial anatomy relates to idiosyncratic behavior and how the cranium serves as an interface between the individual and the environment. The previous section on developmental mechanisms attributed the adaptive significance of robusticity as a secondary result of peramorphic growth in order to achieve a body form that would be best suited for colder climates. These explanations do not address how behavior may

further shape the phenotype of an individual, and therefore a discussion of this mechanism and how it relates to the evolution of robusticity is also necessary.

Craniofacial Biomechanics

As reviewed above, biomechanical forces can have a drastic effect on postcranial robusticity. Biomechanics can also aid in our understanding of the functional significance of cranial robusticity. What makes biomechanical studies of the cranium distinct from postcranial biomechanics is that the bones of the cranium are non-weight bearing. Nonetheless, since the mandible, dentition, and to a lesser extent, the facial skeleton are all involved in the process of mastication, studies can be conducting in these areas to gain a better understanding on how forces produced during food processing and paramasticatory behavior can be modeled and understood. This information can then be applied to studies of craniofacial robusticity. As a departure from the previous sections on craniofacial development and genetics (which are based in the human genome), biomechanics influences the development of epigenetic traits. Since these traits are commonly cited in studies of robusticity, it is important that they be addressed here. Before examining literature pertaining to the hominin fossil record, let us first turn to our closest anthropoid relatives.

There is a substantial amount of literature dedicated to the biomechanics of the primate mastication. It is important to stress that the primate masticatory system is exactly that: a system. Most of the studies in this area model only one aspect of this functional unit, and as we gain insight into how biomechanics can be modeled in the dental arcade, the mandible, the maxilla, or the facial skeleton, it is of prime importance that we do not lose site of this area as a functional complex (O'Conner et al., 2005). As has been stated above, research in craniofacial robusticity must be approached in this manner, and as a result we must also approach the biomechanics of mastication in the same way.

Several studies have been conducted on the biomechanics of hominoid species (Spears and Crompton, 1996; Chen and Chen, 1998, Taylor, 2002; 2006; Daegling, 2007) and non-hominoid primates (Hylander et al., 1991; Daegling, 1992; Anapol and Lee, 1994; Ravosa et al., 2000a; Wright, 2005; Wang & Dechow, 2006; Daegling & McGraw, 2007; Rae & Koppe, 2008; Kupczik et al., 2009; Koyabu & Endo, 2009; Wang et al., 2010). These studies provide a good starting point for reviewing the biomechanics of the hominin facial skeleton. One such study of masticatory biomechanics in genus *Cebus* has been conducted in an attempt to establish the factors involved in the expression of jaw robusticity among two different species: *Cebus apella* and *Cebus capucinus*. These two species were chosen because they both demonstrate similar body size (Daegling, 1992). As we have already seen, robusticity is highly correlated with body size, so by comparing two different species with similar body sizes, this variable is controlled for, which allows for more accurate observations on mandibular shape and robusticity to be made. In many cases, mandibular robusticity can be tied to loading regimes found at the mandibular symphysis (the midline portion of the mandibular corpus which can be diagnostic of the level of robusticity in the mandible). "Wishboning", the primary source of stress at the symphysis, is described as a bending moment, which bends the mandible along its plane of curvature (Daegling, 1992). Keeping this in mind, it is possible to model the mandible as a "curved beam" in line with beam theory (Daegling, 1992). This study shows that *C. apella* mandibles are more robust than *C. capucinus*. This can be observed in CT images of the mandibular symphysis. In *C. apella*, the configuration of the mandibular corpus appears to be optimized (by being more robust) for torsion at the symphysis, presumably as a result of a more frequent processing of hard foods compared to *C. capucinus* (Daegling, 1992). Daegling also notes that since the shape of the mandibular corpus is similar between these two species, this indicates that the mandibles are most likely being subjected to similar patterns of bending regimes between the two species, with absolute magnitudes of these forces being markedly higher in *C. apella*.

Related to the above study of genus *Cebus*, the degrees of certain robust features that were expressed between eight different platyrrhine species (among those examined was *C. apella*) have been analyzed (Anapol and Lee, 1994). By examining the differences in diet among these species of platyrrhines, researchers have been able to draw some conclusions regarding the effect of diet on mandibular and dental morphology. Some of these findings show that incisor row/length is highly correlated with frugivory and faunivory, while it is inversely correlated with folivory (Anapol and Lee, 1994). Also, mandibular robusticity at the symphysis is highly correlated with seed predation, while it is inversely correlated with frugivory. It is interesting to note, that while primates are commonly seen as having generalized dentition compared to other mammalian orders, the expressed variability in dental and mandibular structure (as seen in varying degrees of robusticity) demonstrate that a relatively high degree of food resource specialization can be observed when conducting cross species studies (Anapol and Lee, 1994).

Studies of primate mandibular corpus cross-sectional geometry have also been very useful in correlating mandibular form with mechanical loading patterns. Chen and Chen (1998) have conducted a study on a gorilla mandibular cross-section using finite elements analysis to test the usefulness of several proposed models of torsional properties. Among the models tested in the study were the "robusticity index" (corporeal breadth/depth) and Bredt's formula which proposes the following relationship: relative strength=A t min, "where A is the area bounded by the median line of the external and internal perimeters of the section, and t min is the minimal thickness of the section" (Chen and Chen, 1998:612). Through an analysis using the gorilla mandibular cross-section, it has been found that there is a significant correlation between mandibular cortical thickness and maximum shear strains on the periosteal aspect of the cortex. This means that Bredt's formula, which takes this into account, should accurately characterize torsional properties of the mandible (Chen and Chen, 1998). Note that the application of

Bredt's formula (in which the cross-sectional area of corpus bone is standardized to a measure of size such as minimal thickness) in the mandible is very similar to the application of measures of robusticity to long bones discussed earlier (refer to Ruff et al., 1993).

A study conducted on molar occlusal morphology has made several observations on the significance of mechanical processes employed during food breakdown in great apes and humans (Spears and Crompton, 1996). Here, a stress model has been created to show what forces are used to break down food particles according to the morphology of the occlusal surface of the molars. Among the great apes, genus *Pan*, *Gorilla*, and *Homo* are more likely to employ shear to break down food particles, while *Pongo* is more likely to use simple stress, or "crush" (Spears and Crompton, 1996). These results can be observed by examining molar cusp relief. Molar relief of *Pan* and *Homo* may be more adaptive for diets that require a wider range of mechanical properties to process the various foods exploited, whereas the simple stress model employed by *Pongo* is the most efficient for breaking down food particles found specifically in "hard/brittle" diets (Spears and Crompton, 1996).

While much work has been conducted on primate masticatory biomechanics, several researchers (see Osborn, 1996; Daegling and Hylander, 1998; Spencer, 1998; Tsunori et al., 1998) have conducted similar studies with respect to human masticatory biomechanics. Osborn (1996) created a model to study ways in which maximum bite force (MBF) can be optimized in the human jaw. The largest bite forces recorded for anterior dentition (incisors) range from 200 N (Osborn and Mao, 1993) to 300 N (Dahlstrom et al., 1988). The largest bite forces recorded in the posterior dentition (molars) range anywhere from 600 N to 700 N (Carlsson, 1974; Hagberg et al., 1985). Narrowing of the jaws was found to increase MBF in humans. Therefore, by having a more parabolic arch (in which the anterior teeth are more medially located), human mandibles and maxillae are capable of generating greater anterior MBF than mandibles

and maxillae that do not follow this pattern. Also, the articular eminence (located above the condyle of the mandible and unique to humans) serves the purpose of increasing MBF in the human jaw.

A complex relationship can be shown to exist between mandibular robusticity and facial type. Buccal cortical bone thickness (as opposed to lingual or basal cortical bone thickness) is strongly correlated with facial type, in that an increase of robusticity in this area yields smaller gonial angles and flatter mandibular planes, larger posterior facial height, and shorter anterior facial height (Tsunori et al., 1998). It is important to incorporate many different structures into an analysis of craniofacial biomechanics because many separate features of the facial skeleton can act as a single functional unit when producing bite forces. The expression of certain features usually has a complex relationship with other expressed features of the facial skeleton, and studies that seek to further elucidate models of craniofacial biomechanics must take this into account.

Now that we have identified some of the specifics of craniofacial biomechanics, we can now turn to the fossil records and see how these studies can advance our understanding of biomechanics and robusticity throughout the evolution of genus *Homo*. Several interesting studies of biomechanics have been applied to the Neandertal facial skeleton (see Spencer and Demes, 1993; Antón, 1994; Antón, 1996). In a study of Neandertal craniofacial morphology, Antón (1994) notes that many features of the Neandertal face, such as "the relatively posterior positioning of the lateral relative to medial facial (particularly orbital) components, the strongly anteroposteriorly oriented zygomatic processes and the more sagittally oriented infraorbital plates" are a result of the long and low cranial vault and base observed in Neandertal skulls (Antón, 1994:692). Recall that Lahr and Wright (1996) have indicated the significance of long narrow cranial vaults in the expression of craniofacial robusticity. Studies pertaining to the significance of craniofacial biomechanics of mastication and paramastication in hominin evolution will be examined in further detail below.

Anterior Dental Loading and the Evolution of Facial Robusticity

The fundamental behavior that is associated with the cranium is mastication and paramastication. As a result, any behavioral mechanism that addresses the evolution of cranial robusticity must take this into account. Recall back to our previous discussion of the definition of robusticity in the postcranium which serves to relate the ability of a bone to withstand the force of loads placed upon it. This same principle can be invoked here, where buttressing of craniofacial morphology can be seen as a response to increased masticatory and paramasticatory loadings. This has been an area of intense research, and a brief review of the literature is provided here.

Several aspects of Neandertal craniofacial form and robusticity have been cited as possible adaptations that increase the efficiency or strength of bite force production in fossil hominin forms, as well as buttress their crania from heavy or cyclical loadings placed upon them. The Anterior Dental Loading Hypothesis argues that Neandertal craniofacial morphology would have been highly adaptive for placing heavy loads on the front teeth (Smith, 1983; for an alternative view see Antón, 1994). This hypothesis is based on both dental and facial observations. The relatively large proportions of the anterior dentition have often been cites as possible evidence for an increased use of the anterior teeth (Brace, 1995; Frayer, 1984). In this case, having larger dentition is beneficial because it increases the longevity of the teeth in response to greater loads placed upon them (essentially making the dentition more robust) (Demes & Creel, 1988). Others have noted that higher levels of midfacial prognathism would also be required to accommodate the spatial requirements of a large set of anterior teeth (Smith, 1983; Trinkaus, 1987).

While it is important that the dentition be both resistant to wear and have increased longevity, others have argued that structural modifications of the face would also be needed to cope with the stresses placed upon it. Rak (1986) has proposed a model

(termed the "Infraorbital Plate Model" by Trinkaus, 1987), which argues that the zygomatic bones (the infraorbital plate) were re-oriented into a parasagittal plane in Neandertals to increased resistance to transversely oriented forces in the midface. The "Zygomatic Retreat" model originally proposed by Trinkaus (1987) claims that this re-orientation of the zygomatics is not a response to biomechanical loading, but rather, it is a means to maintain structural continuity of a prognathic face with the rest of the cranium. Finally, Demes' Shell Model (1987) states that the rounded infraorbital regions of the midface may have been adopted as a means to decrease the occurrence of edges along the bony articulations of the midface where stresses could build and ultimately cause the system to fail. A more recent study conducted by Spencer and Demes (1993) has further supported these ideas of craniofacial adaptation to high bite force loadings by noting similarities in craniofacial biomechanics between Neandertals and the modern day Inuit, a group that has been shown to regularly undertake in anterior dental loading (Hylander, 1977).

These studies have been called into question by some (Antón, 1994; 1996, O'Connor, et al, 2005) stating that these early archaic forms were not capable of producing absolutely higher bite forces (which in turn would require a stronger apparatus through which forces could be transmitted and dissipated). Even though Neandertals and other archaic hominins with these craniofacial features would have had powerful masseter and temporalis muscles (employed in mastication), this would have been offset by the fact that these muscles would have been posteriorly placed with respect to the anterior dental arcade, and thus would have been less efficient for mastication (Antón, 1996). The end result is that Neandertals would have required larger muscles in order to generate bite forces of the same magnitude as modern humans (Antón, 1994). Given this argument, the Neandertal face would *not* have had to cope with large mechanical loads, in fact it would have been quite the opposite – Neandertal facial anatomy would have had to work harder in order to produce similar levels of bite force seen in modern humans.

Similar conclusions lending further support to this argument (that Neandertals were less efficient in overall bit force production then *Homo sapiens*) have been reached more recently by O'Connor, et al. (2005).

Biomechanical and non-Biomechanical Interpretations of the Supraorbital Torus

Of all the characters that can be described as being "robust" in the evolution of genus *Homo*, one of the most well known and readily identifiable is the supraorbital torus (or browridge). Many studies have examined the role of browridges in the biomechanics of mastication. Early work in this area sought to model the browridge as a beam, in a similar manner that long bones have been modeled, for gaining insight into the stresses placed upon this region during mastication (Endo, 1966; Russell, 1985). These early studies in browridge biomechanics posited that: 1) during mastication, the lower third of the frontal bone (the region in which the browridge is located) undergoes the most stress, 2) only anterior loading during mastication places stress on the supraorbital region, whereas posterior loading does not, and 3) the center of the browridge (at glabella) and the lateral aspect of the orbits encounter the greatest amount of stress in mastication (Endo, 1966). Later studies within this paradigm also showed a correlation between muscle force (calculated by using a standardized measure such as cross-sectional area of the temporal fossa to gain information about temporalis muscle size and therefore muscle force) and browridge size and development (Russell, 1985).

The degree to which browridges are expressed in the cranium can be shown to be correlated with the frontal angle (defined as the angle formed between metopion, nasion, and prosthion) and the neuro-orbital angle (defined as the angle formed between a line following the contour of the cranial vault and a line following the axis of the orbit) (Ravosa, 1991). While these early studies proposed that these angles had an influence on browridge biomechanics, it has been shown more recently that these measures are more

closely related to the spatial placement of the splanchnocranium relative to the neurocranium (Vinyard and Smith, 2001).

In an attempt to test the masticatory stress models proposed above, researchers (Ravosa, 1991; Hylander et al., 1991) have used strain gauges and other measures of muscle forces to show that the browridge region in fact does not encounter much stress during dental loading. If researchers reject biomechanical models for this anatomical region, then an alternative hypothesis for browridges is required.

The "Spatial Hypothesis" (counter to hypotheses dealing with masticatory stress as the main force behind browridge expression) states that the development of the supraorbital region is a secondary result of the development of superior portion of the frontal and the development of roof of the orbits inferiorly. During ontogeny, these two fields separate spatially, and the roof of the orbits become thicker and more pnuematized, which result in the development of the supraorbital region (Moss and Young, 1960). Other more recent studies have provided further support for this hypothesis (Vinyard, 1994; Bookstein et al., 1999; Vinyard and Smith, 2001). As noted above the two facial angles that were originally employed to better understand craniofacial biomechanics, actually prove to be more useful when applied to the spatial hypothesis. In this model, the disjunction between the braincase and midface can be demonstrated by the craniofacial angle, while the neuro-orbital angle is limited to demonstrating disjunction between the orbits and the braincase (Ravosa, 1991).

In addition to the spatial hypothesis, models that incorporate allometry also apply to browridge morphology. Allometry has been shown to play a key role in the expression of many features of robusticity in the cranium, including the browridges (Simmons et al., 1991; Lahr and Wright, 1996; Vinyard and Smith, 2001). Determinants of craniofacial size are strongly correlated with measures of browridge size, in that as craniofacial size increases, so does browridge size. Other studies have shown that body mass (in addition to cranial size) is also important in the scaling of the supraorbital region (Tarricone,

2000). It is important that researchers incorporate aspects of overall size and spatial considerations when characterizing browridges as a feature of robusticity.

PME and the Expensive Tissue Hypothesis

While the association of craniofacial and dental aspects and masticatory and paramasticatory behavior is important for understanding the expression of robusticity in the cranium, it is equally as important to address issues of structural reduction and the possible causal factors behind them. Brace (1963) has long been an advocate of the "Probable Mutation Effect" (PME) as a mechanism for the evolution of gracility. This model states that as natural selection is relaxed from maintaining a robust structure (such as large dentition), accumulations of mutations that can alter the structure in question will not be selected against, and over time, the robust structure will be lost (Brace, 1963; 1967; 1995). Although this model does provide an explanation for the apparent loss of robusticity that can be observed in the fossil record, it does not provide a positive adaptive mechanism through which selection would operate (since the proposed mechanism is essentially modeling genetic drift).

A solution to this can be seen in Aiello and Wheeler's (1995) "Expensive Tissue Hypothesis" (also referred to as the Metabolic Load Effect, see Churchill, 1997). The Expensive Tissue Hypothesis has much in common with PME, except it provides a selective mechanism through which adaptive variants can have higher fitness. At the core of its thesis, the Expensive Tissue Hypothesis states that metabolically expensive tissues such as bone will not be maintained if not directly selected for and that these structures will be lost in favor of others, such as brain expansion (Aiello & Wheeler, 1995). But, in order for this mechanism to work with cranial robusticity, natural selection must have been relaxed so that large robust cranial elements would not be necessary. The explanation for this shift in selective pressure can be closely tied to increases in cultural sophistication, such as cooking and hunting that would have allowed

hominins to obtain and process food without relying as heavily on their own skeletal structure (Brace, 1963; 1967; 1995; Wrangham et al., 1999; Wrangham & Conklin-Brittain, 2003; Wrangham, 2009).

Upper Paleolithic Culture and the Robusticity Transition

Ideas of cultural advancement and increases in behavioral sophistication have also been proposed as a means of addressing trends in robusticity change though time. At the center of these is the notion of a "Robusticity Transition" (Trinkaus, 1983; 1984; 1986; 2000a). It has been well documented that the Upper Paleolithic was a time of great cultural and morphological change in hominin evolution (Frayer, 1984; Trinkaus, 1984; 1986; 2000a; Churchill & Smith, 2000). The association of cultural sophistication with trends of gracilization in the hominin skeleton through the Late Paleolithic is very apparent, and this has lead researchers to conclude that the loss of robusticity in the skeleton relates to the cultural and behavioral advancements characteristic of modern *Homo sapiens* (Trinkaus, 1984; 1986; 2000a, Churchill, 1996).

On the Pleisiomorphic Status of Cranial Robusticity Features

While many researchers have sought to explain the adaptive significance of cranial robusticity evolution in genus *Homo*, the utility of these characters for phylogenetic analyses have been called into question (Lieberman, 1995; 1996; 1999). There are difficulties in assigning phylogenetic weight to both cranial superstructures and cranial vault thickness. It has been argued that these features are pleisiomorphic retentions and are therefore inappropriate in any type of taxonomic analysis (Lieberman, 1995).

In order for a trait to be phylogenetically relevant, it must fulfill three criteria: 1) it must demonstrate clear homology, meaning that the same structure found in one taxonomic group must also be found in another, 2) it must have definable character-state

polarity, and therefore a distinction between primitive and derived states must exist, and finally 3) it must be observable in all taxa under study (Lieberman, 1995). Supraorbital tori, nuchal tori/buns, the size and shape of the zygomaxillary region, and cranial vault thickness are noted as not fulfilling several of the criteria listed above (Lieberman, 1995). While supraorbital tori can be noted in all taxa, the developmental trajectory of this feature may be different between different hominin groups, and as a result this feature may not be a homologous trait (Lieberman, 1995). The size of the zygomatic region (i.e. large zygomatics being a robusticity trait based on massiveness) is interpreted as a primitive trait without clear character-state polarity, as well as being under the influence of epigenetic (behavioral) factors which further serve to alter the structure and cause superficial similarities, or homoiologies, to arise between taxa (Lieberman, 1995; Collard & Wood, 2007; Cramon-Taubadel, 2009). The nuchal region (more specifically nuchal buns) is argued to be a convergent trait that is a result of large brained dolichocephalic (long narrow crania) individuals, and is therefore not a derived character, but rather, its expression is dependent on overall cranial shape (see Lieberman et al, 2000a). Cranial vault thickness at bregma exceeding 9 mm is considered to be robust, but this value of CVT can be observed across several taxa indicating that it is a primitive character (Lieberman, 1995). CVT has also been shown to vary according to systemic changes brought on by excessive exercise, meaning that this trait may also be epigenetic in nature (Lieberman, 1996).

These assertions have not gone unchallenged. Lahr (1995) and Rightmire (1995) have both argued that aspects of these features such as the supraorbital tori and the nuchal tori are still useful for understanding diversity and hominin evolution, but they agree with Lieberman that careful analysis of these traits must be undertaken in order to identify relevant biological factors. Trinkaus (1995) has addressed these critiques from a broader level by pointing out that the use of cladistics may not always be capable of addressing questions that deal with shifts in the patterning of variation from one fossil form to the

next (along such lines as adaptive significance within taxonomic units). The work of other researchers have also shown that rather then examining the basis of variation between taxonomic groups on a character by character basis, it may be the covariation of these structures that is important (Lahr, 1996, Gauld, 1996). The expression of cranial superstructures has a strong relationship with both cranial size and cranial shape, and it is the nature of this expression that is important, prompting some to suggest robusticity as a "complex" throughout the cranium (Lahr, 1996; Lahr & Wright, 1996). Others have addressed the nature of robusticity variation in the cranial vault, showing that when CVT is measured in several areas of the vault, the variation in thickness between these different regions serve as accurate taxonomic indicators (Gauld, 1996). The nature of the relationship between the variable expression of cranial vault thickness and cranial superstructures is not well understood, and as a result, more work must be conducted in this area.

CHAPTER 3. EVOLVABILITY AS A THEORETICAL FRAMEWORK

Introduction

In order to test the hypothesis that cranial robusticity is expressed as a complex (see Lahr, 1996; Lahr & Wright, 1996; Gauld, 1996), a method through which we can evaluate trait complexes or trait independence must be adopted. The larger framework for this area of research has gained increasing attention in the field of evolutionary biology and has been classified as "evolvability" (Wagner & Altenberg, 1996; Kirschner & Gerhart, 1998; Ancel & Fontana, 2000; Raff and Raff, 2000; Yang, 2001; Ebner et al, 2002; Hansen, 2003; Hansen et al, 2003; Gardner & Zuidema, 2003; Pepper, 2003).

The area of evolvability has its roots in the work of Olson & Miller (1951). In their work, Olson & Miller (1951, 1958) developed a methodology through which to examine and understand patterns of covariation in the morphology of organisms. This contribution was only marginally recognized at the time, and employed in only a few early studies (see Van Valen, 1965). These early studies in morphological integration would serve as the basis for a modern revival of the subject by Cheverud (1982; 1984; 1995; 1996). Highlighted in these studies are the processes through which functional and developmental complexes evolve, and the effect that this evolution has on the expression of traits within the individual.

Defining Evolvability

Evolvability has been defined in several ways. Kirschner & Gerhart (1998) define evolvability as the ability of an organism to produce new phenotypic variation. Hansen (2003) states that the evolvability of an organism can be defined as its ability to respond to selective pressures, while Yang (2001) notes that evolvability is the intrinsic capacity of an organism for evolutionary change. This concept can be further elaborated through conditional evolvability, or the ability of a character to undergo directional selection, while other characters undergo stabilizing selection (Hansen, 2003; Hansen et

al, 2003). All of these definitions essentially share one aspect in common: they all underscore the necessity of phenotypic variation as a response to evolutionary change, with evolvability being the mechanism through which that change may be realized (Raff and Raff, 2000; Hansen, 2003; Kirschner and Gerhart, 1998).

Defining Integration

Studies into the evolvability of an organism generally fall within two categories: integration and modularity. Morphological integration can be defined as the complex patterns of correlation and covariation that serve to demonstrate a lack of independence among variables (Lieberman et al, 2000a, b; Cheverud, 1996). Bookstein et al. (2003) further elaborate on this by stating that integration can be assessed by examining the patterns of phenotypic association among traits. According to Wagner and Altenberg (1996), integration refers to the selective acquisition of pleiotropy among characters in the same group. Pleiotropy serves as a key component of morphological integration and is implicated in two patterns through which morphological integration may evolve (Ehrich et al, 2003). The first pattern is that pleiotropic effects of genes will affect the distinct modules of developmentally and functionally related traits. The second pattern is that given a balance of positive and negative pleiotropy, this will result in lower levels of correlation among unrelated traits (Ehrich et al, 2003, see also Cheverud et al, 1997).

Integration can also be defined as the association between how the co-inheritance of traits reflects the degree to which the inherited traits *develop* and *function* together (Ehrich et al, 2003). Given this definition, it is important to make a distinction between developmental and functional integration (Hallgrimsson et al, 2002; Strait, 2001; Zelditch & Carmichael, 1989; Zelditch et al, 1992). Developmental integration refers to the covariation among morphological structures via the common developmental processes that are indicated in their expression (Klingenberg & Zaklan, 2000) or the degree to which interaction among components during the process of ontogeny, serves to create a

larger system (McShea, 2000). Functional integration on the other hand addresses the covariation among structures that is the result of serving a common functional role (Beldade & Brakefield, 2003; Zelditch & Carmichael, 1989; Zelditch et al, 1992).

Defining Modularity

Given the high intercorrelation of traits in an integrated complex, this can sometimes lead to maladaptive conditions arising from a mutation in one character which in turn alters the entire trait complex. A way to minimize and lessen the effects of mutation on the entire character complex is to adopt a modularized pattern of character expression (Hansen, 2003). Modularity therefore, essentially refers to a division of a biological structure (or module), that is its development and physiology, into smaller standardized and repeatable units (Winther, 2001). Modules can be further classified as a subset of characters with a high level of internal interactions and sparse interaction to the rest of the complex of characters (von Dassow and Munro, 1999).

In reality, modularity lacks a single unified definition because this concept is based on a hierarchical organization of features (Raff & Raff, 2000). Put another way, a suite of characters may serve as a module, but the characters that comprise the module are actually integrated among one another. As a result, all modules are integrated in nature, but if modules can be identified in a larger system, then the system is modularized, rather then integrated (Raff and Raff, 2000; Bolker, 2000; Winther, 2001). In order to define a module for a given aspect of morphology, it must: 1) work across several different taxa, 2) have more internal integration then external integration; 3) be possible to differentiate the module from the its surroundings, 4) be able to be delineated from other modules which share interactions with it, and 5) be applicable at different hierarchical levels (Bolker, 2000). It is important to understand the underlying causal factors for modules, and not just which characters can be expressed as separate modules (von Dassow and Munro, 1999).

Plesiomorphy, Apomorphy, and the evolution of Modularity

Given that a modular organization of structures has been noted in many organisms, such as arthropod limb evolution (Carroll, 2001, Williams & Nagy, 2001, Bolker, 2000), fin development in some groups of fish (Mabee et al, 2002), aspects of brain growth and development (Redies & Puelles, 2001), and even bumble bee wings (Klingenberg et al, 2001), this has prompted researchers to address the question: what is the nature of modularity in biological evolution, and what are the possible phylogenetic interpretations that accompany its expression? It has been argued that modularity is an evolved property that is derived in nature (Wagner & Altenberg, 1996). As one character undergoes directional selection (in a modularized system), other characters are allowed to remain under the control of stabilizing selection. This allows for new phenotypic variation to arise creating a derived condition separate from the ancestral integrated condition.

The process through which new derived modules can evolve is referred to as parcellation (Wagner, 1996). This process works via alternating patterns of directional and stabilizing selection. The evolutionary significance of modularization is that when systems become decoupled (or show a loss of integration), then directional selection can act on one module, while stabilizing selection can keep other modules fixed (Wagner, 1996). Parcellation can lead to a suppression of pleiotropic genes that act on characters that are not selected for in unison, while favoring pleiotropy in genes that control the expression of functionally related traits (Hansen et al, 2003). Researchers that follow this view find support for this claim in noting that patterns of modularity evolve as organisms become more specialized (Winther, 2001). This has been noted, for example, in arthropod limb development (Williams & Nagy, 2001) as well as some flowers (Hansen et al., 2003).

On the other hand, modularity can be considered the primitive condition given that early organisms had differentiated organelles and genes that over time became further modularized and more distinct (Winther, 2001). The best way to test if modularity of a given suite of characters is derived or primitive is to examine patterns of covariation through time. If modularity of a character set appears later in the evolution of an organism, then it can be seen as a derived character, whereas if this condition had always existed in the lineage in question, then it can be viewed as a primitive character (Winther, 2001). These different viewpoints allow for a test of hypotheses related to the primitive or derived status of craniofacial robusticity.

Canalization and the Adaptive Significance of Modularity

Defining Canalization

Having discussed the theory behind integration and modularity, a final question must be addressed: what is the adaptive significance of modularity in evolutionary biology? In order to answer this, we must consider the process of canalization (Amzallag, 2000; Ancel & Fontana, 2000; Wagner & Altenberg, 1996; Wagner et al, 1997; Arjan et al, 2003; Gibson & Wagner, 2000; Hallgrimsson et al, 2002; Kawecki, 2000; Lipson et al, 2002). Canalization (also referred to as "robustness" see Arjan et al, 2003) can be generally defined as the ability of an organism to buffer itself from perturbations experienced in development (Amzallag, 2000; Hallgrimsson et al, 2002; Wagner & Altenberg, 1996). This concept can also be applied to population genetics as well, through the lessening of the effects of mutation or environmental instability on phenotypic change (Wagner et al, 1997).

The term "canalization" was coined by Waddington in 1942 (1942, 1957), but was independently arrived at by Schmalhausen (1949). Waddington proposed canalization as a concept in evolutionary biology to deal with the observations that 1) organisms are made up of a finite number of discrete cells and that because of this, the

processes that create this variation must be discrete as well, with set endpoints in development; and, 2) in many cases, the processes of growth and development will form a normal adult phenotype, even in the face of extreme perturbations. As this appears to be the case in many organisms, this implies that there must also be a genetic basis for the resistance to of an individual to insults during development (Waddington 1942, 1957; for a review, see also Hallgrimsson et al, 2002).

Environmental and Genetic Canalization

There are two different types of canalization: environmental and genetic canalization (Ancel & Fontana, 2000; Arjan et al, 2003; Wagner et al, 1997). Environmental canalization refers to the reduction of the impact of the environment throughout development. Organisms that show marked levels of environmental canalization are able to withstand large levels of non-heritable perturbations (Arjan et al, 2003). Experimental studies have shown that plants grown in salt treated conditions will produce normal phenotypic variation within two generations of adapting to these conditions, indicating that these traits are highly conserved (Amzallag, 2000).

Genetic canalization, on the other hand, refers to the ability of an organism to withstand genetic perturbations (i.e. mutations) throughout the course of development. This concept is often seen as a byproduct of environmental canalization, and not as a unique adaptive response (Ancel & Fontana, 2000). Genetic canalization can further be described as selection for the average effect of mutations on a given genetic locus (for a discussion of canalization and population genetics, see Wagner et al, 1997). Here, genetic canalization is seen as a response to genetic variability, in that the greater the degree of variability seen in a given population, the stronger the effects of canalization (Wagner et al, 1997).

Genetic canalization is closely tied to (but not congruent with) developmental stability, or the suppression of phenotypic variability within individuals (Hallgrimsson et

al, 2002). Developmental stability is best understood when addressing the concept of developmental noise. Early attempts to define developmental noise (see Waddington, 1957) attribute this phenomenon to imperfections in the processes of development. This has been recently refined to incorporate our increased knowledge of genotype/phenotype interactions. The processes of gene transcription and translation have been documented to show complex random fluctuations that act to increase variation (McAdams and Arkin, 1997, 1999; Ozbudak et al, 2002). These fluctuations are the causal factors of developmental noise. Developmental stability therefore refers to a lack of developmental noise within the interaction between genes and an organism's phenotype (Hallgrimsson et al, 2002).

Fluctuating Asymmetry

The best way to examine developmental stability is to employ an analysis of asymmetry. Given that developmental noise is attributed to random variations in the expression of genes, then one of the best (and most often used) means to examine variations is by examining the left and right side of a symmetrical organism. Since both halves of an organism grow and adapt to a set environment via the same genetic controls, then any fluctuations in symmetry can be attributed to developmental noise (Hallgrimsson et al, 2002).

There are three types of asymmetry: the first, directional asymmetry, accounts for asymmetry that is biased to either the right or left side of an organism. The second, antisymmetry, refers to a negative correlation between sides, or as one side becomes asymmetrical in a given way, the other side will become asymmetrical in the exact opposite way. Both of these types explain predictable patterns in asymmetry. This is not the case in the third type, *fluctuating asymmetry* (FA), which accounts for random fluctuations between two symmetrical halves. Because the probability distribution of this final form of asymmetry has a mean of 0 (and therefore is non-predictive), it follows that

fluctuating asymmetry is the best test for developmental noise in an organism (Van Valen, 1962).

The Relationship of Canalization to Variability

Canalization is characterized as a loss of plasticity, which means that phenotypic changes are resisted in this process (Ancel & Fontana, 2000). Following this is the notion of plastogenetic congruence, or simply, low plasticity which implies low levels of variability and vice versa (Ancel & Fontana, 2000). Canalization then ultimately leads to a loss of variability in a population, which, given standard evolutionary theory, is detrimental to the adaptive health of a population. While this appears to be the case superficially, canalization is often a better evolutionary strategy because it is less costly to maintain low levels of variability in a population (Ancel & Fontana, 2000). Schmalhausen (1949), one of the first scholars to address canalization did not see the interaction of canalization and plasticity as opposing concepts. In this light, canalization is seen as a means through which natural selection produces the mechanisms needed to resist perturbation, and as a result, increases the amount of variation in a population (Schmalhausen, 1949, see also Hallgrimsson et al, 2002).

A distinction between variability and variation can further clarify this concept. Variation represents the total amount of differences that exist within a population. Variability, on the other hand, refers to the propensity of a character to vary within a population (Wagner et al, 1997). Given that these two concepts are distinct, it is possible to maintain high levels of variation, even in the event of low variability. This is accomplished through the evolution of modularity (Wagner et al, 1997; Wagner & Altenberg, 1996; Ancel & Fontana, 2000; Arjan et al, 2003). Modules are highly conserved (i.e. they are resistant to plasticity), but they are also independent, which allows them to be reorganized in many novel ways that serve to increase variation (Ancel & Fontana, 2000). The adaptive advantage of modularity can be seen in the fact that

even though modules are robust to change, their organization allows for large numbers of variations to exist.

Case Studies in Evolvability Research

Before addressing how evolvability can be an integral part in understanding the evolution of cranial robusticity in the hominin crania, it is relevant to discuss some other research areas that have employed this theoretical framework in order to gain a better understanding of its usefulness in evolutionary biology. Three areas of research will be considered here: tetrapod limb development and evolution, insect wing development and evolution, and anthropological studies of anthropoid limb development and hominin craniofacial evolution. While these three areas have some overlap (dealing with the evolution of appendages) it would be problematic to consider them in unison. To do so, would introduce complications in interpretation based on convergence in evolution, given that vertebrates and invertebrates do not share a recent common ancestry.

Tetrapod Limb Development and Evolution

The vertebrate limb has been an area of interest in studies of modularity and integration over the years. Many scholars have done work in this area and this body of literature will be surveyed here (Chui & Hamrick, 2002; Hanken et al, 2001; Capdevila & Izpisua Belmonte, 2000; von Dassow & Munro, 1999; Hallgrimsson et al, 2002; Carroll, 2001; Bolker, 2000). Since modularity refers to subunits of an organism, whose expression is standardized and repeatable in nature (see Winther, 2001), vertebrate limbs serve as an excellent starting point for a discussion of how modularity can be used to address issues in evolutionary biology. Limb buds are recognizable early in embryonic development, are under the control of known HOX genes in many cases, and directly relate to the adult form (Bolker, 2000; Carroll, 2001; Capdevila & Izpisua Belmonte, 2000). Another added benefit to looking at limb evolution is that it is often identified as homologous across many different taxonomic groups (Bolker, 2000).

There are two ways to look at limb growth in vertebrates. The first is to take a more classical embryonic approach and look at specific regions within the limb bud, such as the zone of polarizing activity (ZPA) or the apical ectodermal ridge (AER). The other way to approach limb growth is to treat genes as units that control developmental function. This second means of study is mostly interested in looking at gene complexes, like Hox genes, or genetic products, such as Sonic Hedgehog (Shh) (von Dassow & Munro, 1999). These discoveries are relatively recent, and have brought studies of modularity in limb evolution to the foreground of evolutionary biology (Hanken et al, 2001).

Most of our knowledge pertaining to these two modalities for limb growth span from studies regarding two classic laboratory species: the chicken and the mouse. Within these two groups, limb bud evolution is considered to be highly conserved in evolution (Shubin et al., 1997; Martin, 1998). As a result, limb bud evolution is hypothesized to be conserved throughout all vertebrates (Hanken et al, 2001). In a study of frog limb development (specifically, the development of *Eleutherodactylus coqui*, the Puerto Rican tree frog), Hanken et al, 2001 address the question of conservation in limb morphogenesis. This research examines the expression of the Distal-less gene family (Dlx) in *E. coqui*. Dlx is similar to Sonic Hedgehog (Shh) but rather than being expressed in the ZPA, like Shh is, Dlx is expressed in the distal limb bud ectoderm, known as the apical ectodermal ridge (AER) (Hanken et al, 2001).

The results of this study find that with respect to *E. coqui*, there are both conserved *and* novel (non-conserved) elements in limb morphogenesis. It confirms that Shh and Dlx (much like in other more well non taxa) are highly conserved, providing further support to the notion of conservation in the limb bud module. On the other hand, novel features, like the absence of a distinct AER or the ability of a limb bud to continue growth even after removal of the distal ectoderm, show that conservation in limb bud modules may not always be the case. It is noted that this example pertains solely to

frogs, and that it is unclear how widespread this exception may be. This result therefore does not deny the validity of a tetrapod limb bud module. It does highlight that limb bud modules are not static in their expression, meaning that they are subject to evolutionary change (Hanken et al, 2001).

While the ZPA and AER are at the center of debates involving the modularity of tetrapod limbs, it is important to note several other issues in this discussion. One such issue is that in the growth of the tetrapod limb, these two regions are dependant on each other for morphogenesis. Given this, it is impossible to change one area without affecting the other. As a result, the tetrapod limb represents a sort of "epigenetic trap" where these two aspects of the module are constrained to work together to form the limb, or not produce anything at all (von Dassow & Munro, 1999 quoting G. Wagner in discussion).

Also, following along lines noted above, the tetrapod limb is not always homologous, which can serve to complicate the hypothesis that tetrapod limb bud evolution acts as a conserved module. Among three groups of tetrapods, the urodele (salamanders and newts), the anuran (frogs and toads), and the amniote (mammals, reptiles, birds), the process through which fingers develop is non-homologous. In urodele development, fingers grow out of the from the developing limb bud, while in the anuran and amniote hand, fingers are formed by the remodeling of the paddle-shaped limb bud (von Dassow & Munro, 1999; Hanken et al, 2001). These differences serve to complicate the universal homology of tetrapod limb development, calling for a more careful consideration of how modules form within this group of organisms.

In a similar discussion of the evolution of bird limbs, scholars have attributed dissociability as a possible underlying mechanism that works to shape the tetrapod limb (Wagner & Gauthier, 1999). Bird limbs maintain the 1^{st}, 2^{nd}, and 3^{rd}, digits of the reptilian hand, but this is not homologous to what happens with all other amniotes, where the 1^{st} and 5^{th} digit are lost first in evolution (von Dassow & Munro, 1999). Why did the

birds maintain digits 1, 2, and 3 when the amniote pattern is to maintain digits 2, 3, and 4? A possible explanation for this is that through dissociability of the digits, the ancestors of the birds where able to keep their 1st digit due to selective pressures to maintain a thumb, even though digit reduction invariability starts with the 1st and then the 5th digits (Wagner & Gauthier, 1999). These cases highlight the need to understand concepts of dissociability and modularity in limb bud evolution in order to explain the differences seen in the growth of this region.

Insect Wing Development and Evolution

Another area where evolvability has illuminated our understanding of the evolution of animal form is the insect wing. Many workers have employed this theoretical framework in this line of research (Beldade and Brakefield, 2003; Klingenberg & Zaklan, 2000; Klingenberg et al, 2001; Brakefield, 2001; Klingenberg, 2002). While the tetrapod limb serves as an excellent example of modularity, (given that limbs serve as standardized, repeatable units) insect wings can show patterns of both modularity and integration. The literature highlights these relationships in butterfly, fruit fly, and bumble bee wing morphology (Beldade and Brakefield, 2003; Klingenberg & Zaklan, 2000; Klingenberg et al, 2001).

A study on a species of African butterfly, *Bicyclus anynana*, serves as a good starting point for examining this literature (Beldade & Brakefield, 2003; Brakefield, 2001). Butterfly wing patterning has been classically described as being a repeated homologous series (Nijhout, 1991). This description falls right in line with our definition of modularity, and bears resemblance to what has been seen thus far in tetrapod limb evolution. This patterning has been looked at more recently and research now shows that while different pattern elements are independent of each other, there is a degree of correlation that can be seen between homologous elements, indicating that integration

may also characterize butterfly wing patterns (Brakefield, 1984; Paulsen and Nijhout, 1993; Monteiro et al, 1994; Paulsen, 1994; Nijhout, 2001).

B. anynana is characterized by having "eyespots" (circular markings) on both the dorsal and ventral surfaces of the wing. These markings are typically similar in color but show marked variation in size. While these eyespots vary morphologically, all eyespots respond similarly to artificial selection. This interaction is based on the hypothesis that eyespots are derived from the same developmental basis (Beldade & Brakefield, 2003).

In their study Beldade & Brakefield (2003) test this hypothesis of eyespot development in order to determine the extent to which these patterns are hierarchically organized into modules. This was done by examining changes in eyespot size, number, color, and position brought on by artificial selection across many generations. Their findings show that while eyespots act as modules (in that they are serial repeats), they do show a degree of coupling (integration) in their patterning. This is interpreted as an evolutionary pathway leading to genetic integration in eyespot patterning but still maintaining individuality in eyespot morphology (Beldade & Brakefield, 2003). This result falls in line with the theoretical assertion that in cases where traits serve a common functional role, morphological integration is expected to evolve and maintain the system (Cheverud, 1996; Wagner, 1996). In the case of *B. anynana*, eyespots are used in visual communication between butterflies, and this may serve as an explanation for the integration of these spots on the dorsal and ventral wing surfaces. This coupling has been documented elsewhere, and the argument has been made to treat eyespot expression as a single character due to this pattern of integration (at least on the dorsal and ventral wing surfaces, where integration is apparent) (Brakefield, 2001). Conversely, if the ancestral pattern of eyespots follows morphological integration, then subsequent evolution would have favored a decoupling (modularity) of these characters. This second explanation is favored by Beldade and colleagues (Beldade & Brakefield, 2003; Beldade et al, 2002).

Another area where insect wing morphology has been aided by the theoretical framework of evolvability is that of the fruit fly, *Drosophila melanogaster* (Klingenberg & Zaklan, 2000; Klingenberg, 2002). The wing veins of *D. melanogaster* serve as an excellent study sample because they provide easily recognized and recordable landmarks, and wing development in this species is understood well (Klingenberg, 2002). *D. melanogaster* wings are separated into anterior and posterior compartments and this is of particular interest because each of these compartments is under the control of known genetic expression. Because of this fact, they have been treated as candidates for examples of individual developmental modules (Klingenberg & Zaklan, 2000).

The question here is, to what extent are the wings of *D. melanogaster* modularized or integrated? Hypotheses that have been proposed to address this question involve a hierarchical explanation of integration. That is, while each of the wing compartments may form an integrated whole, there is a very low level of integration between compartments, hence modularization of the *D. melanogaster* wing. Klingenberg & Zaklan (2000) set out to test this hypothesis using geometric morphometrics.

The results of this study highlight and overall covariation of landmark position between both wing compartments, demonstrating a marked level of integration within the *D. melanogaster* wing (Klingenberg & Zaklan, 2000). The first line of evidence in landmark covariation is that the dominant pattern is for narrow, pointed wing tips, or for rounded, broader wing tips. This variation simultaneously effects both the anterior and posterior wing compartments and is contributed to patterns of growth in the pupal stage, where wing tips become more pointed and narrower. Other axes of variation show a correlation between the positions of the crossveins with respect to the longitudinal veins that they are adjacent too. Similar shits in the crossvein positions also occurred in both the anterior and posterior wing compartments (Klingenberg & Zaklan, 2000).

Previous studied that concluded in favor of modularity between anterior and posterior wing compartments were conducted using standard linear metrics. While the

results of these studies are valid, they do not take into account the *multivariate nature* of the data, a property that is better explored using geometric morphometrics and examining variation in overall landmark positioning. Landmark positions co-vary across both compartments of the *D. melanogaster* wing, but the degree to which these landmark positions change differ, as well as the direction in which they change (Klingenberg & Zaklan, 2000). While previous studies documented these patterns as being demonstrative of modularity in the wing, the application of geometric morphometric techniques in this study have showed that the overarching patterns in vein expression do, in fact, show a marked level of morphological integration.

Given that *D. melanogaster* wing shows a marked level of integration between compartments, is this true in other insect groups as well? Studies have been undertaken to examine this in *Bombus empatiens*, the bumble bee (Klingenberg et al, 2001). The fore- and hindwing of *B. empatiens* develop from separate imaginal discs, and as a result, they can be hypothesized to be developmental modules. Three predictions pertaining to this statement are tested by Klingenberg et al, (2001): 1) if each wing is a developmental module, then the parts within each wing should co-vary together; 2) since each module is under the control of distinct developmental pathways, patterns within individuals should be similar to patterns of fluctuating asymmetry within fore- and hindwing configurations; 3) if these wings act as separate modules, then individual variation will follow similar patterns of covariation, but fluctuating asymmetry will be independent between wings.

Again, using geometric morphometrics, Klingenberg et al, (2001) find no evidence for parcellation in *B. empatiens* wing morphology (i.e., there are no smaller integrated units within each wing that are expressed independently of one another). Any perturbations that cause fluctuating asymmetry between wings are not regionalized, but rather, are expressed across the entire fore- or hindwing. Given this level of interaction, it is argued that the fore- and hindwings of bumble bees are examples of developmental modules. While each of these modules shows high levels of internal interaction, they

also show evidence of covariation between fore- and hindwing compartments. This result falls in line with what has been concluded for *D. melanogaster* above, indicating that while organisms are made up of distinct modules; these modules interact in ways that are indicative of integration at the organismal level (Klingenberg et al, 2001).

Application of Evolvability to Studies of Hominin Evolution

While the above studies have demonstrated how an evolvability framework can be applied to non-anthropoid systems, how has this framework been employed in studies of anthropoid (and ultimately, hominoid) evolution? A surprising number of studies in anthropology have used this approach in addressing these sorts of questions (Bookstein et al, 2003; Hallgrimsson et al, 2002; Marroig & Cheverud, 2001; Chui & Hamrick, 2002; Ackermann, 2002; Strait, 2001; Cheverud, 1996; Ackermann & Cheverud, 2000; Ackermann & Cheverud, 2002; Polanski and Franciscus, 2006). These studies range from the evolution of the primate limb, to the hominin cranial base, craniofacial skeleton and cranial vault. Some landmark articles will be briefly surveyed here.

Much like studies of the tetrapod limb (highlighted above), the primate limb has been used as an example for the evolution of modularity (Hallgrimsson et al, 2002; Chui & Hamrick, 2002). Following the work of others in the area of mammalian limb development (Rodriguez-Esteban et al, 1999; Ahn et al, 2002; Logan & Tabin, 1999; Martin, 2001; Capdevila and Izpisua Belmonte, 2001), Hallgrimsson et al, 2002 set out to examine the patterning of variability in the mammalian limb. They examine three hypotheses regarding this topic: 1) since limb growth follows a proximo-distal trajectory, than any sort of environmental and fluctuating asymmetry variation should be manifest along this vector; 2) environmental and fluctuating asymmetry variation will not be correlated across traits if the mechanisms that reduce variation are not the same (or at least closely related); 3) the limb is comprised of a hierarchical arrangement of modules,

which are arranged in an integrated pattern (linking structures within each limb, and between the fore- and hindlimb, recall that this final hypothesis has also been examined in bumble bee wings, see Klingenberg et al, 2001 above). These hypotheses are tested with respect to mice limb organization (serving as the generalized mammalian pattern) and *Macaca mulatta*, the Rhesus macaque (as a proxy for primate patterning).

Hallgrimsson et al (2002) find that with respect to the first hypothesis, mice limbs do not show any sort of proximo-distal variability due to FA or environmental factors. This however is not the case in the macaque sample. Here, both FA and environmental factors increase as you move distally along the limb. It is not parsimonious to explain this difference in limb bud developmental trajectories as a result of genetic interaction, since both mice and primate limb growth is under the influence of the same gene complexes. This difference in results is best explained as a result of epigenetic mechanical responses of the macaque limb to the environment (Hallgrimsson et al, 2002).

With respect to the second hypothesis, results show that traits that are under weak genetic control showed higher levels of fluctuating asymmetry. This highlights a possible relationship of environmental canalization and developmental stability, which is interpreted by Hallgrimsson and colleagues as evidence for similarity in the processes that buffer against environmental effects among and within individuals (Hallgrimsson et al, 2002).

Finally, results of a test of morphological integration (hypothesis #3) in both mice and macaques show that there is evidence (albeit not conclusive) for interaction between homologous limb components between fore- and hindlimb. This interaction is greater than what is noted within each limb element. As a result, this shows that limb growth and development follows an integrated pattern. If this is the case in mammalian (and primate) evolution, then any differences in the evolution of fore- and hindlimb morphology must get around this developmental linkage. A way to look at this is to examine two closely related groups with different fore- and hindlimb morphologies (such

as a human and a bat). In these cases, we can hypothesize that there are relatively stronger levels of with-limb interaction then among limb interaction – a suggestion that falls directly in line with modularization of the limb. This has been shown to be the case in other organisms such as birds (see Van Valen, 1965) where both forelimb and hindlimb serve completely different functions. Since the results of Hallgrimsson and colleagues does not note this to be the case in primates, then natural selection would have to overcome this mechanism of integration in order to alter one pair of limbs without drastically changing the other (Hallgrimsson et al, 2002). This sets up an interesting question regarding the strength of the selective pressures needed to influence the divergence in fore- and hindlimb morphology in the hominoids. In order to break this level of integration between forelimb and hindlimb in the case of hominin evolution, a very strong selective pressure would have been needed indeed. With respect to the hand and foot, other research has shown that there is a submodule (exhibiting a degree of developmental autonomy) that may provide an explanatory basis for how selection might have circumvented the high level of interaction between fore- and hindlimb elements (Chui and Hamrick, 2002).

Another area where evolvability has furthered our understanding of hominin evolution is that of the hominin cranial base (Strait, 2001; Lieberman et al, 2000a). Given that basicranial characters are important for cladistic analyses in hominin evolution (see Lieberman et al, 2000a), the relationship of these characteristics to one another must be understood before they can be safely used in a cladistic analysis. Since cladistics assumes that characters must be independent of one another (Lieberman, 1995), if hypotheses of integration can not be falsified, then these characters must be rejected from cladistic analysis. Strait (2001) examines the hypothesis of integration in the primate and hominin cranial base in order to determine the relevance of basicranial characters in phylogenetic analyses.

Morphological integration can be studied at five distinct levels, the genetic level, the cellular level, the individual level, the populational (or intraspecific) level, and finally, the interspecific level. Strait (2001) focuses on integration at the interspecific level since the questions being asked pertain to a phylogenetic analysis (as opposed to studies highlighted above which work at levels lower then the populational level, such as the genetic or individual level). It is assumed that demonstrating levels of interspecific integration would indicate that integration would be present at all lower levels (individual and below) (Strait, 2001).

The results of this study show that while characters of the basicranium are largely independent (given functional and structural hypotheses), this independence is not universal and that low levels of integration can be noted in the hominin cranial base. Even this low level of integration was significant enough to affect the outcomes of parsimony analyses when producing phylogenies based on these basicranial characters. This study serves as a cautionary tale, highlighting the importance of understanding hypotheses of integration in phylogenetic analyses (Strait, 2001).

An additional anthropological study which employs an integration framework to further aid in our understanding of hominin evolution is that of Bookstein and colleagues (2003). This study uses geometric morphometrics to compare levels of correlation between anatomical regions of the cranium. These regions of interest (the cranial vault, cranial base, and face) have been cited in other works on morphological integration as well (see Cheverud, 1996). Here, singular warps analysis – the application of Partial Least Squares (PLS) analysis in morphometrics, is used to determine the levels of interaction between the face, cranial base, and cranial vault (Bookstein et al, 2003).

Results of this analysis show that with respect to the two patterns of integration: evolutionary integration and ontogenetic integration, the face and cranial vault show similar patterns of integration. This is the not the case, however, for the cranial base. Bookstein et al (2003) find that there are marked differences in covariation between the

face and vault with the cranial base particularly with respect to relative clivus length and anterior cranial base orientation, as well as cranial vault length, and the posterior cranial vault.

Polanski and Franciscus (2006) shed further light on this subject through an investigation of craniofacial integration within *Pan*, *Gorilla*, and recent *Homo sapiens*, but with an emphasis on conditional independence modeling rather than geometric morphometrics. The results of their study show that across all samples, there is an overall level of non-integration between the face and neurocranium. There is, however, a high level of integration within the face of both *Pan* and *Gorilla*, especially with measurements of facial prognathism. The opposite result is seen in *Homo sapiens*, where there is an overall pattern of non-integration with respect to facial prognathism. It is argued that this result is due to a de-emphasis of facial projection over the course of genus *Homo* evolution. Neurocranially, there are high levels of integration within the sagittal plane of both the African apes and recent humans, but *Homo sapiens* also demonstrate high levels of cranial breadth integration as well. This is most likely due to the increased importance of neurocranial globularity (and as a result, brain size increase) within the evolution of our genus (Polanski and Franciscus, 2006).

Hypotheses of Integration and Modularity in genus *Homo* Evolution

Examining Hypotheses in a Morphological Integration Framework

When developing a plan of study for the morphological interaction of traits, and whether they can be characterized by integration or not, it is important to start with a set of potential causal factors, be they developmental, functional, or environmental, for the evolution of integration (or conversely modularization) in the character complex (Strait, 2001). Once a modality for a possible evolution of integration is set, the next step is to

determine the traits that should be incorporated in the study. In his work on craniofacial integration in tamarins, Cheverud (see Cheverud, 1996) defined 6 anatomical regions of skull whose development may be tied together: the cranial vault, cranial base, oral apparatus, nasal region, orbital region, and zygomatic region. After the traits of the study have been identified, patterns of observed character correlation are then compared to hypothesized relationships of integration between characters. If the observed patterns meet the criteria for the hypothesis of integration, they are then said to be morphologically integrated (see Cheverud, 1996; Ackermann & Cheverud, 2000; Ackermann & Cheverud, 2002, Polanski & Francsicus, 2006).

This approach is not always directly applicable, however. When it is unclear what relationships (developmental, functional, or environmental) may be driving selection for integration, it is often best to start with the assumption that *all* the characters in the study are integrated and then narrow this hypothesis to a set of possible integration outcomes that can be examined individually. This functional/structural analysis has been employed in phylogenetic examinations of morphological integration (Strait, 2001).

Integration, Modularity, and the Evolution of Cranial Robusticity

While we have gained insight into how robusticity can be expressed throughout the cranium, little is understood about how cranial superstructures (the foundation for cranial robusticity) co-vary with one another. Some studies have suggested that cranial robusticity should be viewed and understood as a complex (Lahr, 1994; 1996; Lahr and Wright, 1996; Gauld, 1996), but no work has yet been undertaken to specifically test the nature of robusticity expression across the entire cranium with respect to *all* aspects of craniofacial robusticity indicated in the previous chapter. These aspects of robusticity will be addressed with respect to modularity and integration. It is through this framework that we can test the nature of robusticity expression in the cranium throughout hominin

evolution, and begin to gain a comprehensive understanding of its relevance in origin of modern *Homo sapiens*.

If cranial superstructures are shown to be integrated, this could support claims of structural reduction as a result of changing selective pressures due to biocultural interaction within modern *H. sapiens*, causing a cascade effect that it would have affected all the integrated components of craniofacial robusticity (Brace, 1963; 1967; 1995, Trinkaus, 1983; 1984; 1986; 2000a). This hypothesis falls in line with a *functional hypothesis* for the integration of cranial superstructures, highlighting the need for a robusticity complex in hominin evolution as a result of mechanical pressures on mastication and paramastication in the environment. Integration of cranial superstructures would also highlight the need to rethink how these characters should be used in studies that attempt to ascribe fossil forms to modern or pre-modern taxonomic groups.

Modularity of these features would indicate separate trajectories of development for these features, supporting a *developmental hypothesis* for craniofacial robusticity (Brothwell, 1975; Green & Smith, 1990; Smith & Green, 1991). Additionally, if cranial robusticity follows a modularized pattern in *Homo*, this could indicate that while individual robusticity elements (modules) are conserved in hominin evolution, their organization between taxonomic groups may not, and as a result this could serve as a means of differentiation of groups on the basis of cranial robusticity. While the work of some researchers (Lieberman, 1995; 1996; 1999, refer to chapter 2 for a discussion) have pointed out potential pitfalls in using *individual* cranial robusticity features as a phylogenetic concept, these criticisms have not been applied to addressing cranial robusticity as an integral complex in hominin evolution.

CHAPTER 4. MATERIALS AND METHODS

Introduction

The primary goal of the present study is to provide a more complete understanding of cranial robusticity expression in genus *Homo* by examining the patterns of covariation, if any exist, among superstructures within the hominin cranium, in order to evaluate the likelihood of a "robusticity complex" in hominin evolution (Lahr, 1996; Lahr & Wright, 1996). Given that this is a novel approach for research into cranial robusticity, the scope of this study is to examine patterns of cranial robusticity variation in extant *Homo sapiens* populations only. While the ultimate goal of this line of research is to address these same issues in the fossil record, that goal is currently hindered by the paucity of sufficiently complete crania. A full understanding of the variation in modern *Homo sapiens* at this juncture serves as a useful comparative baseline and starting point.

By limiting the research question to extant *Homo sapiens*, problems with incompleteness of specimens, as well as issues of capturing adequate levels of populational variation can be nullified (for a similar discussion of these constraints pertaining to the taxonomic position of Neandertals, see Ackermann 2005; Ahern et al, 2005; Harvati et al, 2005). Since the present project's scope does not include fossil samples, a review of the methods for superimposing known levels of variation in an extant species onto extinct ones is not required. It should be noted, however, that this is an extremely important area of human paleontological research, one that must be addressed critically (Ackermann, 2002; Ackermann, 2003).

Quantifying robusticity in the cranium is a difficult proposition because the features of interest do not conform to uniform shapes and their anatomy is quite complex, making their interpretation through the use of linear measurement difficult. Over the past two decades, a new technique through which morphology can be studied, called "geometric morphometrics", has been developed and employed to address a wide range

of evolutionary questions such as phylogeny (Harvati, 2002; Harvati 2003a; Harvati, 2003b; Strait, 2001), ontogeny (Berge and Penin, 2004; Penin et al, 2002; Marroig and Cheverud, 2001; Ponce de Leon and Zollikofer, 2001; Zelditch et al, 1992), allometry (Frost et al, 2003; Larson, 2002; Loy et al, 1998; Rosas and Bastir, 2002), and integration (Bookstein et al, 2003; Klingenberg, 2002; Klingenberg and Zaklan, 2000; Strait, 2001). Geometric morphometrics (also called "3D or three-dimensional morphometrics") examines the relationships of digitized coordinate landmarks in either two or three dimensions in order to address levels of similarity or difference between forms (Adams et al, 2004). The nature of shape change between different forms can be fully explored through geometric morphometrics, and both multivariate tests and complex visualizations provide the tools through which biological inferences can be made.

Size and shape are the components that come together to make up form, and geometric morphometrics acts to separate these two in order to allow an examination of residual shape. While shape often provides an excellent quantity through which researchers can formulate hypotheses and examine biology, the effects of size on shape (allometry) is also important and must also be considered. Since it is the role of geometric morphometrics to separate out these quantities, it also provides a powerful tool through which these relationships can be further explored (see Frost et al, 2003; Larson, 2002; Rosas and Bastir, 2002).

Sampling Criteria

In order to understand the patterning of cranial robusticity in *Homo sapiens*, a large and diverse sample is required. Small and regionally restricted samples risk mischaracterizing our species' full range and modal patterning in this regard. While levels of intra- and interpopulational cranial variation in modern *Homo sapiens* has been examined on large global samples previously (most notably by W. W. Howells, 1973, 1989), such studies have only employed the use of standard cranial osteometrics, and

have not dealt specifically with questions relating to cranial robusticity expression. To overcome this knowledge gap, the present study employs coordinate landmark data collection on a geographically diverse sample of modern *Homo sapiens* crania.

The samples used in this study are derived from the western Old World and encompass variation in *Homo sapiens* across the continents of Africa, Eurasia, and Australia. All samples are from the Felix von Luschan collection at the American Museum of Natural History, in New York. While the population samples were selected *a priori* in order to guarantee adequate representation of *Homo sapiens* throughout the Old World, additional considerations also had to be taken into account for sex composition, attaining a reasonable range in robusticity level expression throughout the sample, and an adequate representation of all 72 landmarks across each skull included in the study.

Sex

Sexual dimorphism in hominin crania has been well documented (Kjellstrom, 2004; Ricklan & Tobias, 1986; Konigsberg & Hens, 1998; Baughan & Demirjian, 1978). Studies of cranial form in *Homo sapiens* must deal with this fact when selecting an appropriate study sample. Often, studies will only focus on one sex (typically male). This is not the case with the present study. The reasoning behind using males *and* females in the study is threefold. First, by including both males and females for each population, extremely gracile forms (which tend to be female) or extremely robust forms (which tend to be male) were not precluded from the analysis and thus the largest possible range of robusticity could be examined. Second, the incorporation of males and females allows the present study to explore questions pertaining to possible differences in the level and the patterning of cranial robusticity in the sexes. Finally, by including both males and females, patterns of robusticity in both sexes could be explored and the option to pool the data to increase samples sizes, if warranted, would be possible.

Cranial Robusticity Scoring

Given that this analysis is aimed at understanding the expression of cranial robusticity across *Homo sapiens*, it is important to make certain that appropriate levels of variation across the supraorbital region, zygomaxillary region, occipital region, and mastoid region be represented. In order to ensure this, skulls from each sample were visually inspected (see below for details) across these anatomical regions for completeness of cranial superstructures. Individuals with damaged or pathological superstructural elements were not included. Steps were taken to maximize cranial robusticity variation in each population by using a maximum variation sampling approach in the selection of individuals (Patton, 1990). Also, attempts were made to find maximal and minimal robusticity expression among superstructure elements in each sample. In some populations, as elaborated below, it was possible to sample the entire range of robusticity expression across one element. Finally, it bears mentioning that mandibles were excluded from this study because they are frequently missing from cranial collections and thus their inclusion would have adversely affected both population representation and sample sizes overall.

Coordinate Landmark Data

As part of this study, three-dimensional coordinate landmark data was collected on all skulls analyzed. As its basis, geometric morphometric analyses require two-dimensional or three-dimensional coordinate landmark data (for geometric morphometric theory, see below). This also serves as a limitation for which cranial material could be used within each sample. The landmarks and structures to be digitized must be clear and visible on each specimen. In cases where anatomy was missing or unclear, the individual was not included in the study sample. As with the visual determination and scoring of robusticity, attempts were made to maximize the variation of landmark configurations within each sample.

Sex Determination

Given that the sex of individuals contained within the Felix von Luschan collection is largely undocumented, sexing was required before commencing data collection. Ultimately, the pelvis serves as the best indicator for sex in a skeleton, but in cases where the postcrania are not available (such as with the present study sample) cranial material can be used with reasonable success. The basis of sex determination in the skull is built around the assumption that male crania are larger and more robust than female crania with respect to certain characteristics, such as supraorbital development and mastoid process size (White, 2000).

It is important to note that the primary criteria for determining sex in virtually all discrete or metric sexing schemes for the cranium is based on sexual dimorphism in the size and shape of the cranium, particularly with respect to features that are typically considered "robust" (White, 2000). Since cranial shape and size demonstrate moderate to very strong correlations with cranial robusticity (Lahr, 1996; Lahr and Wright, 1996) this poses a unique methodological consideration to the present study since its goal lies in the patterning and determination of robusticity in the hominin cranium (for further discussion see the last section of Chapter 5).

Ideally, sex determination for this study would be independent of the features being used to analyze cranial robusticity, but given the lack of postcrania, this recourse was not possible. Instead, levels of robusticity are measured using alternative means (see below). Even though the structures under consideration are the same as those being employed in the sex determination analysis, a separate scoring system (following Lahr, 1996) was adopted to measure discrete levels of robusticity in the cranium. This provides the present study with two data sets, based on different scoring criteria, and with different purposes (sex determination vs. robusticity scoring), that are methodologically independent of one another.

For each of the individuals in the sample, sex was determined using Walker's discrete scoring system (Buikstra and Ubelaker, 1994). This readily accessible and widely used system focuses on the expression of five separate anatomical regions of the skull: (1) the nuchal crest, (2) the mastoid process, (3) the supraorbital margin, (4) supraorbital projection in the glabellar region, and (5) the mental eminence. For each characteristic, a five-point scale is used to determine the degree of expression (compared against a series of line drawings) with more gracile, "female" characteristics scoring 1 or 2, while more robust "male" characteristics are scored as 3 and higher (see Figure B1). An average of the five anatomical regions was calculated per skull and used to determine male vs. female (with an average above 2.5 indicating male and an average below 2.5 indicating female).

It is often difficult to sex an individual skull without first considering variability in the entire population, since different populations display different patterns of sexual dimorphism (White, 2000). Every attempt was made to understand variation in the subsamples before final sexing was determined. For each population in the study sample, two rounds of sex determination were undertaken. Sex for each skull was considered before data collection, and then after the population was studied in more detailed, individual sex determinations were reconsidered following observations pertaining to the variability of each sample (such as placing a greater emphasis on the mastoid region in the Sub-Saharan Bantu sample, since most of the other features under consideration did not vary much between males and females, except under extreme circumstances).

Visually Assessing Levels of Cranial Robusticity

In order to ensure that adequate levels of cranial robusticity are being represented in the study sample, a means for visually assessing cranial robusticity is required. Lahr's (1996) scoring system is adopted to meet this requirement. Lahr (1994; 1996) originally designed the use of her discrete scoring system to measure 'regional continuity traits' in

her analysis of the Multiregional Hypothesis in modern human origins, particularly to test for the continuity between Australian and South East Asian populations with *Homo erectus*. She uses many of these characteristics to measure cranial robusticity in the skull as well.

The characters that Lahr's coding system employs are the (1) infraglabella notch, (2) supraorbital ridge/torus, (3) zygomatic trigone, (4) zygomaxillary (malar) tuberosity, (5) occipital crest, and (6) occipital torus. Each of these characteristics have 3, 4, 5, or 7 discrete codes to measure the degree of robusticity expression, with higher codings representing sequentially higher levels of robusticity (see Figure B2). In cases where more than one aspect of a superstructure was being coded with separate coding criteria (such as the supraorbital torus, which consists of characteristics 1 – 3 above) the scores were averaged together to produce a robusticity score for that anatomical region.

The goals of visually assessing cranial robusticity in the study sample are twofold. First, as mentioned above, this was a necessary step in the selection of crania to be employed in the study, ensuring that adequate levels of cranial robusticity variation were being sampled from each population. A second goal of this step is to provide a means of comparison between a previous documented method for assessing cranial robusticity, with the present study's novel approach to this problem using geometric morphometrics (see below).

Sample

The present study sample consists of a total of n=140 extant *Homo sapiens* crania from eight geographic regions of the Western Old World (Table 1). These regions are: (1) North Africa, (2) Sub-Saharan Africa, (3) Western Europe, (4) Central Europe, (5) Mediterranean/Near East, (6) Asia, (7) South East Asia, and (8) Australia. All crania included in the present study are from the Felix von Luschan collection at the American Museum of Natural History, in New York. There is a total of n=91 males and n=49

females in the study sample, representing a large range of regional variation in size, shape, and cranial robusticity expression across extant *Homo sapiens*.

Table 1. Listing of all the samples used in the present study.

Sample	Males	Females	Total
North Africa	6	3	9
Sub-Saharan Africa – Bantu	10	8	18
Sub-Saharan Africa – Khoisan	2	3	5
Western Europe	12	5	17
Central Europe	13	6	19
Mediterranean/Near East	13	8	21
Asia – India	8	4	12
Asia – China	8	3	11
S.E. Asia – Malay Peninsula	4	2	6
S.E. Asia – New Guinea	3	2	5
Australia	12	5	17
Totals	91	49	140

North Africa

The North African sample is comprised of specimens from Libya and includes males and females (sex is documented on four of these individuals; the sex of the remaining five is estimated). This population demonstrates low to moderate levels of cranial robusticity using Lahr's system (1996) with respect to all anatomical regions included in the study, with the exception of mastoid massiveness, which tends to fall toward a higher level robusticity expression.

Sub-Saharan Africa

The Sub-Saharan African sample is divided into two subsets: the Bantu sample and the Khoisan sample. The Bantu sample derives mainly from Cameroon and consists

of both males and females; sex had to be estimated for each. This sample shows relatively low levels of supraorbital robusticity and especially low levels of occipital robusticity throughout based on Lahr's system. As with the North African sample, this sample also demonstrates a degree of mastoid robusticity variation that is higher than average.

The smaller Khoisan sample is made up of males and females (of which the sex was documented on two specimens). This sample is relative gracile throughout the anatomical regions studied, showing remarkably low levels of zygomaxillary and mastoid robusticity.

Western Europe

A total of skulls where studied for the Western European sample, consisting of males and females from Germany (sex was estimated for each). While these skulls demonstrate moderate levels of cranial robusticity using Lahr's system throughout the sample, there is a marked level of variation (particularly in the male subset).

Central Europe

The Central European sample derives from Hungary, Austria, and the Czech Republic and consists of crania (subdivided into male and female skulls, all skulls required sexing). This sample demonstrates moderate to low levels of cranial robusticity across all regions studied using Lahr's system, with marked levels of intrapopulational variation noted throughout.

Mediterranean/Near East

The Mediterranean/Near East sample is comprised of individuals from Greece and Syria. This sample consists of both males and females (all of which sex had to be determined). Overall, this population is rather moderate in superstructure expression,

with notable levels of gracility in the supraorbital region following Lahr's (1996) scoring system.

Asia

The Asian sample consists of individuals from India and China. The Indian subset is comprised of both male and female crania (five of the twelve crania were labeled male or female, the rest required sexing). All individuals from this sample come from Bengali, India. This subset shows remarkable levels of gracility in all regions surveyed except the mastoid region, which demonstrates moderate levels of robusticity.

The Chinese subset represents individuals from the Canton and Tientsin regions of China. There was no documentation on the sex of any of the individuals in this sample, and as a result, sex was estimated for the entire subset. This sample demonstrates a rather unique pattern of cranial robusticity in terms of Lahr's system. Robusticity levels for the supraorbital and zygomaxillary region are among the lowest in the entire study sample, mastoid robusticity is slightly above average and occipital robusticity levels are markedly high (with only the Australian sample having higher levels of robusticity in this anatomical region).

South East Asia

This sample is made up of two small subsets, a sample from the Malay Peninsula, and a sample from New Guinea. The Malay Peninsula sample consists of individuals from Singapore, of which both males and females are represented (sex was estimated for all individuals in this set). This sample is moderately robust in all anatomical areas (following Lahr's system) with the exception of the supraorbital region which is rather gracile and the mastoid region, which is characterized by excessively high levels of robusticity.

The New Guinea subset (from Humboldt Bay) contains both males and females, of which two of the five individuals had sex labeled, while the others required sexing.

This sample demonstrates moderate to low levels of robusticity throughout, with the exception of one individual, who demonstrated the highest level of robusticity seen in any of the crania studied. This individual could not be included in the analysis, however, due to extreme intentional cranial deformation.

Australia

The final geographic region surveyed is Australia. This sample is made up of Australian Aborigines. Males and females are both represented in the sample, all of which (except one single individual, who was estimated) documentation of sex was provided. Australian Aborigines serve as a unique group because they show marked levels of superstructure development, while simultaneously having relatively small crania (Lahr, 1996). This pattern is noted here as well, with moderate to high levels of supraorbital robusticity and the highest level of occipital robusticity for the entire sample. Facial dimensions (as noted by the zygomaxillary region scores) are among the smallest in the sample.

Coordinate Landmark Data Collection

Landmark Types

The present study employs a total of n=72 three-dimensional coordinate landmarks per cranium (Table 2). These landmarks are a combination of Bookstein's Type I, II, and III landmarks (Bookstein, 1991; Slice et al, 1996). Type I landmarks contain the highest level of homology between forms since they are both geometrically and developmentally homologous (O'Higgins, 2000). These landmarks are collected at the boundary of a given structure, which can be easily delimited by the juxtaposition of 3 or more different structures to the one in question (Penin et al, 2002; MacLeod, 2002). Bregma is a classic example of a Type I landmark, since it lies at the intersection of the

coronal and sagittal sutures of a skull (which serve as the articulation for three cranial bones: the frontal, left, and right parietals).

Table 2. Coodinate landmark data.

No.	Landmark[1]	Region	Type	Description
1	Bregma	Frontal	I	Standard landmark
2	Nasion	Frontal	I	Standard landmark
3	Maxillofrontale	Frontal	II	Standard landmark
4	Frontomalare Anterior	Frontal	II	Standard landmark
5-7	Midline Frontal Line (3)	Frontal	III	Line from Bregma to Nasion
8-10	Medial Supraorbital Line (3)	Frontal	III	Line tracing the medial supraorbital region
11-13	Lateral Supraorbital Line (3)	Frontal	III	Line tracing the lateral supraorbital region
14-16	Midorbit Supraorbital Line (3)	Frontal	III	Line tracing the midorbit supraorbital region
17-21	Superior Supraorbital Line (5)	Frontal	III	Line tracing the top of the supraorbital ridge
22-24	Inferior Supraorbital Line (3)	Frontal	III	Line tracing the top of the orbit
25	Zygomaxillare	Zygomax.	I	Standard landmark
26	Zygoorbitale	Zygomax.	I	Standard landmark
27	Jugale	Zygomax.	II	Standard landmark
28	Alare	Zygomax.	II	Standard landmark
29-34	Zygomatic Line (6)	Zygomax.	III	Line tracing the zygomatic bone
35-44	Maxillary Line (10)	Zygomax.	III	Line tracing the Maxilla
45	Jugale/Zygomaxillare Midpoint	Zygomax.	III	Midpoint between Jugale and Zygomaxillare
46	Alare/Zygomaxillare Midpoint	Zygomax.	III	Midpoint between Alare and Zygomaxillare
47	Porion	Temporal	II	Standard landmark
48-51	Antero-Posterior Mastoid Line (4)	Temporal	III	Line tracing the a-p mastoid margin
52-56	Medio-Lateral Mastoid Line (5)	Temporal	III	Line tracing the m-l mastoid margin
57	Opisthion	Occipital	II	Standard landmark
58	Lambda	Occipital	I	Standard landmark
59-61	Midline Occipital Line (3)	Occipital	III	Line from Lambda to Opisthion
62-64	Midline Parietal Line (3)	Occipital	III	Line from Bregma to Lambda
65-69	Superior Nuchal Line (5)	Occipital	III	Line tracing the superior nuchal line
70-72	Supreme Nuchal Line (3)	Occipital	III	Line tracing the supreme nuchal line

[1]All type III landmarks are resampled from a continuous landmark line traced across the identified structure.

Type II landmarks maintain homology in overall geometric relationships, but not necessarily in developmental ones (O'Higgins, 2000). These landmarks are points that lie on the extremes of a structure, and are therefore defined by the maximum of curvature

for the given object (MacLeod, 2002). Points such as glabella (the maximum projection of the glabellar region, when the skull is oriented in the Frankfurt Horizontal) or alare (the most lateral point on the nasal aperture) are examples of type II landmarks. It is important to note that even though these landmarks may not necessarily be developmentally homologous (such as type I landmarks described above), they still maintain a level of homology and are also often used in studies of shape in geometric morphometrics (for example, Harvati 2002; 2003a; 2003b).

Type III landmarks maintain the lowest level of homology between forms. This is because they often have at least one inaccurate coordinate, meaning that their placement can be accurately attributed to an outline or surface of an object, but their exact location can not be repeated (O'Higgins, 2000). These landmarks are often referred to as "semilandmarks" or "sliding landmarks", because their position is not fixed on a single object, but rather, it is allowed to move with respect to the reference form (Bookstein, 1997; Adams et al, 2004). In order to decrease the effects of non-homology between points (given that the only homology that these points can share is that they lie on the surface of the same object, but their exact placement with respect to one another is not homologous) is to lessen the effects of landmark variation between forms by relaxing the bending energy reflected by the large distances between points (attributed to non-homology) so that the residual patterns reflect some aspect of homology across the surface of the structure in question (Bookstein et al, 2003).

Landmark Acquisition

All crania in the study sample were digitized using a Microscribe 3DX digitizer (Immersion Corp.). In order to ensure accurate data collection, the Microscribe was calibrated before data collection, using the Microscribe Utility Software (MUS). Coordinate landmark data collection focuses on the major anatomical regions of the study: (1) the frontal region, (2) the zygomaxillary region, (3) the temporal region, and

(4) the occipital region. For each of these regions, landmarks were collected on and around the superstructures in question. While coordinate data were collected for both sides of the cranium, only the left side of the cranium was included in the landmark analysis in order to maximize sample size and minimize the effects of correlation between bilateral elements when examining the patterns of covariation between superstructures.

Frontal Region

The coordinate landmarks of this region are designed to capture supraorbital ridge (or in extreme cases, torus) development. Data were also collected on the curvature of the frontal bone in order to allow examination into the slope of the frontal region. Nasion, Bregma, Maxillofrontale, and Frontomalare Anterior all serve as type I anchor landmarks for this region. Glabella (type II landmark) served as the endpoint for one of several type III semilandmark lines used to capture the shape of the supraorbital ridge. Semilandmark lines at the medial, lateral, and mid-orbital region of the supraorbital ridge (based on Smith & Ranyard, 1980; Vinyard & Smith, 2001) are used to provide information on the projection of the supraorbital ridge. Refer to figure B3 for a representation of the supraorbital landmark wireframe.

Zygomaxillary Region

Landmarks of the zygomaxillary region are used to capture overall levels of facial massiveness, facial prognathism, and the shape of the infraorbital region. Here, Zygomaxillare and Zygomaxillare Orbitale are used as type I anchor points for semilandmark lines that trace the outer contour of the zygomatic bones and the maxillae. Alare and Jugale are type II landmarks used to form two semilandmark lines from Zygomaxillare that provide information on the depression or inflation of the maxillary and zygomatic regions of the face. Figure B4 demonstrates the wireframe for the zygomaxillary region landmarks.

Temporal Region

The overall massiveness and shape of the mastoid process serves as the primary focus of landmarks in this region of the cranium. Two semilandmark lines were used to capture the shape of the mastoid in antero-posterior and medio-lateral planes. Porion (type II) serves as the starting point for the antero-posterior line tracing the mastoid process in this plane. A second semilandmark line was taken from the medial mastoid base to the lateral mastoid base in order to obtain information on overall projection in the medio-lateral plane. Both semilandmark lines are traced through the tip of the mastoid process (Mastoidale) in order to record information on the degree of mastoid projection inferiorly. The mastoid landmark wireframe is shown in figure B5.

Occipital Region

The last of the four regions examined in the present study is the occipital region. Landmarks here focus on capturing the overall size, shape, and projection of the occipital/nuchal torus. While a full torus configuration is rare in most cases (with the exception of the Australian sample), all crania displayed superior and supreme nuchal lines (forming a torus configuration in their greatest degree of robusticity expression) which were traced via two semilandmark lines. Lambda (type I) and Opisthion (type II) serve as endpoints for a semilandmark line that traces the occipital in midline, thus capturing information on the projection of this region out from midline. An additional semilandmark line was traced from Bregma to Lambda to provide information on overall angulation of the rear cranial vault. A wireframe of the nuchal region landmarks is shown in figure B6.

The Utility of Geometric Morphometrics in the Present Study

Geometric morphometrics can be characterized as the combination of geometry and biology to examine size and shape in both two- and three-dimensional space

(Richtsmeier et al, 2002). Coordinate landmark based approaches to biological questions have become common over the past few years, and this is due (at least in part) to some of the benefits that this method of quantification has over more traditional linear metric based methods. One of the benefits associated with this method is its versatility. By collecting coordinate landmark data in two- or three-dimensions, the researcher can conduct any geometric morphometric analysis necessary *or* the coordinate data can be used to collect standard Euclidean distances between landmarks to obtain linear metric data. This latter point is quite common in the literature, and it shows that coordinate landmark approaches can be employed in non-geometric morphometric analyses as well (see Ackermann and Cheverud, 2000; Birch, 1999; Cheverud, 1996; Larson, 2002).

Another added benefit of using coordinate data is that it maintains the true dimensionality of a given form, rather then compressing it down into linear measurements or angles (Rohlf and Marcus, 1993, Richtsmeier et al, 2002; Hennessy and Stringer, 2002). By maintaining coordinate information in two- or three-dimensional space, geometric relationships can be examined much more readily across the entire form of an object (Richtsmeier et al, 2002). Geometric morphometrics is also capable of delimiting very subtle changes in form via coordinate landmarks, since it is highly sensitive to differences in landmark data (Klingenberg, 2002).

In addition to quantitatively demonstrating subtle differences in form between objects, geometric morphometrics provides researchers with a powerful visualization tool to observe how these form changes manifest (Harvati, 2002). Geometric morphometrics further augments the visualization of form difference between objects by quantifying size and shape differences in objects that calipers alone have difficulty doing. This is possible because coordinate landmarks can be collected along the surface of any object (Harvati, 2002). This last point is very important for the present study, given that almost all features of cranial robusticity fall into this class of objects that can not be easily quantified with calipers or discrete character states.

Specific Geometric Morphometric Approaches Used in the Present Study

Generalized Procrustes Analysis (GPA) is the most commonly employed approach to studying form differences in geometric morphometrics and will be used here. Since GPA is a coordinate based approach, it uses the relationships of landmarks within a common coordinate system to show similarities or differences in form. In order to align all the coordinate landmarks for each form into a single coordinate landmark system, GPA has to register the coordinate data. To do this, GPA must rotate, translate, and scale the data, so that all objects are superimposed on one another in the same coordinate system. Rotation refers to reorientation of a form around an axis, while translation refers to movement of a form in any direction without causing any changes in orientation along a rotational axis (Richtsmeier et al, 2002). GPA accomplishes these tasks by minimizing *d*, known as the "procrustes distance". The procrustes distance is simply the square root of the sum of squared differences between the corresponding landmarks between each form (Rohlf, 1999). Once rotation and translation have been accomplished, GPA scales the data in order to compare differences in residual shape between forms. In order to remove size, GPA scales all coordinate landmarks to the "centroid size", which is calculated as the square root of the sum of all the squared coordinate distances to the centroid, or center of mass of an object (Rohlf, 1999).

Once all of these adjustments have been made, the coordinates exist in what is called Kendall's shape space (Kendall, 1984). Kendall's shape space is non-Euclidean in nature, and therefore care must be taken when using multivariate statistics in this shape space (Rohlf, 1999; Richtsmeier et al, 2002; Slice, 2001). It has been demonstrated, however, that when shape differences between forms are small, then multivariate techniques can be used in Kendall's shape space (Harvati, 2002, Slice, 2001). Given that biological data is often restricted in its variation between forms, this shape space is generally appropriate for statistical testing (Harvati, 2002). This assumption must be

tested however. If the procrustes distances are not equal to the Euclidean distances between landmarks, then further statistical testing *can not* be conducted in shape space (Harvati, 2002; Hennessy and Stringer, 2002; Singleton, 2002). Instead, all shape coordinates from Kendall's shape space must be orthogonally projected into Kent's tangent space (Frost et al, 2003; Pan et al, 2003; Rohlf, 1999; 2003; Richtsmeier et al, 2002). This space is Euclidean, and therefore multivariate statistics can be carried out on the coordinate data once it has been projected into this shape space (Rohlf 1999, 2003).

One of the principle other approaches to the coordinate based method of GPA is a Euclidean Distance Matrix Analysis (or EDMA, see Richtsmeier et al, 2002; Richtsmeier et al, 1992; Lele and Richtsmeier, 1991; Lele, 1993; Richtsmeier and Walker, 1993). EDMA does not employ a registration routine to bring all coordinate landmarks into a common coordinate system. Instead, this method uses a matrix which is comprised of the Euclidean distances from each landmark to every other landmark in the coordinate data set (Lele, 1993; Richtsmeier et al, 2002; Cole III and Richtsmeier, 1998).

The present study adopts a coordinate based (GPA) method for analyzing coordinate landmark data rather than EDMA. The reasons for this are two-fold. Firstly, coordinate based methods are at an advantage when it comes to visualization of shape differences. A large portion of the analysis of shape in this study relies on demonstrating and interpreting the complex patterns of shape change both between and within individuals. This is most readily accomplished by employing plots of coordinate landmark data with superimposed wireframes which aid in visually assessing these patterns. While a methodology for visualization of shape differences has been proposed for EDMA (Cole and Richtsmeier, 1998), it lacks the ability to visually demonstrate shape differences in a nature that can be readily tied back to the shape of the actual object. This aspect of the analysis is important because the present study combines shape data from coordinate landmarks with discrete coding data that is based on the visual assessment of the structures in question. While the nature of these two datasets is

different (discrete data vs. coordinate landmarks) they both provide information that applies directly into the visualization of the object.

Secondly, many of the analyses employed in this study, such as Partial Least Squares (PLS) analysis (see below), have been demonstrated and adopted with a coordinate based approach in mind (Bookstein et al., 2003). Analyses of this nature benefit from coordinate based approaches because of the versatility of the data used. The positioning of each coordinate landmark in two-dimensional or three-dimensional space provides information that pertains to both the shape and size of an object. While coordinate landmark data can be transformed and analyzed as alternative forms of shape data, such as partial warp scores, this transformation is not necessary for the approaches used here. An EDMA based approach would require transforming the coordinate data into a matrix of linear shapes which would then serve as the basis for analyses such as PLS. Using an approach of this nature, the resulting output would be one step removed from the actual raw data. Due to this fact, a coordinate based approach is favored for the methods employed here. For further discussion on the utility of this method to quantifying shape, refer to Rohlf (2000; 2003).

Specific Applications of Coordinate Based Geometric Morphometrics in the Present Study

Two of the most common way to demonstrate shape differences between forms is through the use of thin-plate spline analysis (TPS) and relative warps analysis (RWA). The roots of TPS date back to D'Arcy Thompson, the father of modern day geometric morphometrics (Richtsmeier et al, 2002). Thompson's 1917 work, *On Growth and Form*, highlights a method where a Cartesian grid is superimposed over one form (the target form) and serves to illustrate degree of shape difference with respect to a reference form by deforming the grid in order to make the target form match with a reference (Cerney et al, 2003). By studying the degree to which the Cartesian grid (or spline) is

deformed, researchers can demonstrate the degree to which forms differ in shape between one another (see Bookstein et al, 1999; Bookstein et al, 2003; O'Higgins and Jones, 1998; Yaroch, 1996; Monteiro and Abe, 1999; Rosas and Bastir, 2002; Zelditch et al, 1992).

While the grid deformations in a TPS analysis can be visually inspected in order to understand which areas differ from one form to another in shape, more powerful statistical analyses based on the bending energy matrix of the spline can be conducted (Larson, 2002; Monteiro and Abe, 1999). This type of analysis falls under the category or relative warps analysis (RWA), which is the primary analytical tool of the present study. The values that constitute the eigenvectors of the bending energy matrix of a spline are called the *principle warps*, which serve as the basic unit of observation in TPS (Larson, 2002). Principle warps do not contain information regarding the differences in shape between forms directly, but rather they must be projected onto the coordinate system of the object in order to be related to shape within a given form (Monteiro and Abe, 1999). This projection produces *partial warps*, which do contain information regarding shape difference between forms. A standard principal components analysis can be conducted on the partial warp scores in order to produce *relative warps*, which serve as the unit of analysis for describing biologically relevant differences in shape between 2 objects (Bookstein et al, 1999; Bookstein et al, 2003; Guy et al, 2003; Larson, 2002; Monteiro and Abe, 1999).

Geometric morphometrics can also be applied to studies of the allometric influence of size on shape within organisms. Recall that "centroid size" is the scaling factor employed in GPA in order to remove size from the coordinate data. While this serves as a necessary aspect of any procrustes fit routine, it also provides workers with an excellent measure of over all size for the form (given that it is the factor by which all forms in the analysis are scaled). In order to test for allometric effects of size on shape, the centroid size (the measure of overall size of the object, which serves as the

independent variable) can be regressed against the PC scores of the procrustes residuals (or shape coordinates, which serve as the dependent variables) to look for significant correlations of size with aspects of shape variation (Klingenberg and Zaklan, 2000; Klingenberg et al, 2001; Penin et al, 2002; Rosas and Bastir, 2002; Singleton, 2002).

Specific Hypotheses and Analyses in the Present Study

The present study tests several hypotheses regarding the nature and expression of craniofacial robusticity in modern *H. sapiens* using the specific methodology elaborated below. The hypotheses are modeled after Platt's strong inference (Platt, 1964). First, variation in the shape of craniofacial robusticity is examined within the large and geographically diverse sample of modern human crania described above in order to determine the overall pattern of phenotypic variation within modern *H. sapiens*. Secondly, patterns of allometry are tested in order to determine whether cranial robusticity is largely a factor of size (Lahr, 1996; Lahr and Wright, 1996). Hypotheses regarding the nature of cranial superstructure robusticity in modern *Homo sapiens* are tested in the framework of morphological integration and finally, implications for research into the evolution of modern cranial robusticity form will are highlighted. If robusticity is expressed as a complex, in that all the features of robusticity are integrated, then the assertions of Lahr (1996) and Gauld (1996) are supported and the use of isolated robusticity characters in analyses should be avoided. Conversely, if each of the robusticity features identified can be characterized as a separate module (i.e. modularity more accurately characterizes robusticity in the cranium), then studies of these features in isolation (following, Trinkaus and LeMay, 1982; Smith and Ranyard, 1980, Lieberman, 1996) are supported.

Relative Warps Analysis

All collected coordinate landmark data is subjected to a Relative Warps Analysis (RWA, also called a Principle Components of Shape Analysis, or PCs, Polly, 2001) using

the software package Morphologika (O'Higgins and Jones, 2006). Given that any geometric morphometric analysis often involves large amounts of coordinate data, it is difficult to interpret changes in each coordinate landmark with respect to one another. Employing a relative warps analysis for coordinate landmark data is analogous to using a standard PCA analysis on linear measurements in that it reduces the variation in the scaled coordinate landmarks to a set of component axes, which explain overall differences in shape variation. RWA allows the researcher to isolate the components that explain the greatest proportion of the variance in the data set (by examining the eigenvalues for each component, a process that is identical to standard PCA) and then run further tests on those components (Berge and Penin, 2004).

The present study provides an extensive RWA to illustrate the complex patterns of variation in cranial robusticity across modern humans. For this section, RWA will be conducted on the entire craniofacial landmark dataset as well as many subdivisions of the primary dataset to highlight universal patterns of robusticity variation as well as how this variation breaks down regionally.

First, RWA is carried out on the entire n=140 craniofacial dataset, for all 72 landmarks, in order to demonstrate global patterns of variation for all anatomical regions of cranial robusticity studied in the human skull because a secondary goal is to show how shape variation is expressed between the frontal, zygomaxillary, mastoid, and occipital regions for the global sample. This analysis will be broken down further to assess how cranial robusticity features interact between males and females, as well as within each of the n=11 subpopulations in the study.

Second, the total n=72 landmark coordinate dataset is broken down into 4 subsets, each corresponding to one of the four anatomical regions of the skull (frontal, zygomaxillary, mastoid, and occipital) for the entire global sample. The goal of this analysis is to illustrate variation in each of the primary anatomical regions of study and highlight any patterns of global variation seen in robusticity features (such as the

supraorbital torus or nuchal torus). A further extension of this analysis is carried out for males and females for the global dataset and across each of the 11 subpopulations with the goal of demonstrating how shape in the four primary anatomical regions of study varies within these groups.

For each RWA (across all of the subdivisions of the data highlighted above), the percent variation explained for each component of the RWA is defined, as well as a description of the variation noted along each relative warp axis. Additionally, the degree of morphological variation across each of the relative warps axes is documented visually in plots of landmark data demonstrating variation in the spatial relationships of the coordinates across each RW axis.

Testing for Allometry

While there is great utility in conducting shape analyses on the coordinate data to explore the patterns of expression of cranial robusticity in *H. sapiens*, it is equally important to examine the role of size and its possible allometric effects. Lahr and Wright (1996) have noted the substantial influence of cranial size on levels of robusticity expression, and this relationship is further explored in the present study.

As part of its algorithm, GPA uses centroid size to scale all the coordinate data (Rohlf, 1999). So while the final result of GPA is a scaled coordinate system, it also provides information on the size of each form through scaling. While there are several ways to examine the possible effects of allometry in a coordinate data set (Klingenberg and Zaklan, 2000; Klingenberg et al, 2001; Birch, 1999; Larson, 2002; Loy et al, 1998; Rosas and Bastir, 2002), an approach similar to the one adopted by Zelditch and colleagues, (Fink & Zelditch, 1995; Zelditch et al, 1998) is used in the present study. This method was chosen over others because it uses the PC scores from the RWA as the shape variables which are then regressed onto centroid size rather then relying on the

actual shape coordinate values, which can carry redundant information (Rohlf, 1998; Bookstein, 1991).

The statistical package NCSS (Hintze, 2000) is used to conduct the regression analysis of PC scores (the shape variables) onto centroid size. PC scores and centroid size data are obtained from the coordinate landmark data using the software package Morphologika (O'Higgins and Jones, 2006). Output for the association between size and shape will be given in the form or correlation (R^2) values for each of the anatomical regions involved in the study: 1) Frontal, 2) Zygomaxillary, 3) Mastoid, and 4) Occipital.

While this study provides the first large scale, systematic investigation of cranial robusticity using coordinate based methods, other works based on linear metrics and discrete codings precede this one (Lahr, 1994; Lahr, 1996; Lahr & Wright, 1996; Lieberman et al, 2002). In order to provide some continuity between these earlier approaches with the coordinate approach provided here, discrete codings for each of the superstructures in the anatomical regions in question (following Lahr, 1996 and highlighted in chapter 4) are compared via regression analysis (using NCSS) with the provided relative warp scores and centroid sizes obtained from the coordinate landmark data. Summarized below are hypotheses[3] pertaining to allometric considerations of craniofacial robusticity throughout the present study.

H_1: The relationship of shape (relative warp scores) to size (centroid size) in the frontal region (supraorbital) landmark dataset follows an allometric pattern (i.e. shape is related to size).

H_2: The relationship of shape (relative warp scores) to size (centroid size) in the zygomaxillary region (facial) landmark dataset follows an allometric pattern (i.e. shape is related to size).

---

[3] These hypotheses will be tested across three different datasets: 1) the complete sample (n=140), 2) the male sub-sample (n=91), and 3) the female sub-sample (n=49).

H_3: The relationship of shape (relative warp scores) to size (centroid size) in the temporal region (mastoid) landmark dataset follows an allometric pattern (i.e. shape is related to size).

H_4: The relationship of shape (relative warp scores) to size (centroid size) in the occipital region (nuchal) landmark dataset follows an allometric pattern (i.e. shape is related to size).

H_5: Following Lahr's (1996) observation that discrete measures of craniofacial robusticity are related to overall craniofacial size, it is hypothesized that centroid size (a GM measure of size) of the complete 72 landmark dataset is correlated with all discrete measures of craniofacial robusticity.

H_6: Centroid size of the frontal region landmark dataset is correlated with Lahr's (1996) discrete measures of supraorbital robusticity.

H_7: Centroid size of the zygomaxillary region landmark dataset is correlated with Lahr's (1996) discrete measures of supraorbital robusticity.

H_8: Centroid size of the temporal region landmark dataset is correlated with discrete measures of supraorbital robusticity.

H_9: Centroid size of the occipital region landmark dataset is correlated with Lahr's (1996) discrete measures of nuchal robusticity.

Two-Block Partial Least Squares Analysis (2B-PLS)

Two-Block Partial Least Squares Analysis (2B-PLS), also referred to as singular warps by Bookstein et al (2003) provides a powerful tool for investigating the patterns of interaction between two separate collections (or "blocks") of data (Zelditch et al, 2004). Because of this, 2B-PLS serves as a strong candidate for analyzing patterns of modularity and integration with a dataset, and as such is used in the present study to test the hypotheses elaborated above.

It should be noted that PLS analyses are not useful for defining discrete blocks of data, because this method requires that the data to be partitioned *a priori* into blocks. This is useful, however, when testing hypotheses about interactions between well defined subunits (Zelditch et al, 2004). In the case of the present study, interactions between well defined (but not well understood) biological units of craniofacial robusticity serve as the definitions for the blocks of data to be used.

PLS is based on singular value decomposition (SVD), a technique that is very similar to the extraction of principle components via eigenanalysis. The prime difference here is that the PCs are extracted from a variance-covariance matrix, while PLS is extracted from an interblock variance-covariance matrix. The results are then ordered by the amount of covariance explained *between* the two blocks, as opposed to total variance explained in a PCA. SVD is the mathematical method by which the amount of between covariance is determined. This method is used (as opposed to eigenanalysis) because the covariance matrix between the two blocks of data does not have to be square (like it is in PCA). This is a beneficial aspect of the method, since it allows for the comparison of an unequal number of landmarks between blocks. Given that most blocks of data (including all of the blocks employed in the present study) are not comprised of the same number of variables, SVD provides a means for highlighting levels of interaction between different groups of data (Zelditch et al, 2004).

This study uses PLS to determine the level of covariance between the four anatomical regions of cranial robusticity highlighted previously: frontal, zygomaxillary, temporal, and occipital robusticity. Given its two block nature, these comparisons will be carried out in a pairwise fashion. While methodologies exist for carrying out multi-block (more than two blocks) PLS analyses, these methods require a great deal of mathematical manipulation and at present are largely experimental (Bookstein et al, 2003; Klingenberg, 2009).

The Partial Least Squares analysis employed in the present study is carried out using the software package MorphoJ (Klingenberg, 2008). Coordinate landmark data are separated into the blocks relevant to the study (frontal, zygomaxillary, temporal, and occipital robusticity landmarks) and then subjected to pairwise PLS analyses. These pairwise comparisons are as follows: 1) Frontal block vs. Zygomaxillary block, 2) Frontal block vs. Mastoid block, 3) Frontal block vs. Occipital block, 4) Mastoid block vs. Zygomaxillary block, 5) Mastoid block vs. Occipital block, and finally 6) Occipital block vs. Zygomaxillary block. The 2B-PLS for each comparison is broken down into two separate analyses, one with the centroid sizes of the blocks (used to determine if the *size* of the two anatomical regions show any degree of association) and one with the procrustes fitted coordinates (with size removed in order to determine if there is any relationship between the *shape* of the two blocks of data). MorphoJ provides an RV coefficient (Robert & Escoufier, 1976) as a measure of similarity between two matrices (or blocks) of coordinate landmark data. Additionally, wireframes for this second set of pairwise comparisons is provided in order to highlight the patterns of covariation between the separate blocks. Below are the specific hypotheses[4] of integration to be tested using two-block partial least squares analysis.

H_{10}: Supraorbital-Zygomaxillary integration – Integration of the supraorbital and zygomaxillary region will be tested to determine if robusticity in the frontal region is tied to the facial region and additionally, hypotheses arguing for a spatial relationship between these two regions would be supported (Moss and Young, 1960).

H_{11}: Supraorbital-Mastoid Integration – This hypothesis tests integration between the supraorbital region and the mastoid region. This could lead to implications that

[4] These hypotheses will be tested across three different datasets: 1) the complete sample (n=140), 2) the male sub-sample (n=91), and 3) the female sub-sample (n=49).

robusticity expression in the frontal region may be tied to aspects of robusticity in the anterior cranial base.

H_{12}: Supraorbital-Occipital Integration – Similar to H2 above, with the focus shifted to the integration of frontal robusticity and robusticity in the posterior cranial base via the external occipital protuberance and superior/supreme nuchal lines.

H_{13}: Mastoid-Zygomaxillary Integration – This hypothesis tests the interaction of robusticity between the facial region and aspects of anterior cranial base robusticity.

H_{14}: Mastoid-Occipital Integration – If integration is shown to be the pattern of interaction between the mastoid region (anterior cranial base) and the nuchal region (posterior cranial base), this would imply that basicranial robusticity should be treated as a singular entity.

H_{21}: Occipital-Zygomaxillary Integration – Similar to H4 above, this interaction would provide evidence for a facial-posterior cranial base vector of morphological integration.

CHAPTER 5. RESULTS

Introduction

The purpose of this chapter is to present a comprehensive analysis of the size and shape information pertaining to the current dataset. The results from analyses undertaken on the global sample coordinate landmark dataset will be broken down into the following sections: 1) An analysis of Allometry, with respect to centroid size and 2 types of shape data – procrustes coordinate data and discrete coded data, 2) A comprehensive Relative Warps Analysis, highlighting shape variation across the global sample with respect to total global robusticity variation, as well as a breakdown of male vs. female and regional robusticity variation, and finally 3) A Two-Block Partial Least Squares Analysis of the coordinate data to highlight how each of the cranial superstructures covary with respect to one another in both size and shape.

The goal of these analyses is to provide a complete analysis of size and shape in an attempt to capture variation in cranial robusticity at a global level, as well as provide the data to formulate an understanding of the nature of robusticity expression in the cranium of *Homo sapiens*. This is accomplished through analyses regarding both discrete coding and coordinate landmark data. Size is examined with respect to each of the anatomical regions and superstructures in question via the use of established coding methodologies, as well as the calculation of centroid size through coordinate landmark based techniques. Shape analyses are presented both visually, and numerically through the use of geometric morphometrics (refer to Chapter 4 – Materials and Methods for a discussion of these techniques), and the aim of these analyses to provide an understanding of the variation in cranial superstructures and cranial robusticity with in our species. While some discussion is provided throughout the sections of this chapter, the following chapter (Chapter 6 – Discussion) will combine all these results into an all-encompassing framework through which cranial robusticity expression in *Homo sapiens*

can be understood as well as provide avenues of research for highlighting overall patterns of craniofacial variation throughout the evolution of the Homininae.

Relative Warps Analysis (RWA)

This section provides results for the Relative Warps Analysis (RWA) for all the coordinate landmark data in the study. Results will be broken down into four separate groups: 1) Overall Global Variation: a RWA of all 72 coordinate landmarks in the study with all individuals included in order to asses levels of total cranial variation in the entire sample, 2) Overall Male/Female Variation: a series of RWA conducted on the entire 72 coordinate dataset between males and females to highlight variability between the sexes (also, refer to Appendix A for overall variation within each of the 11 geographical populations), 3) Global Robusticity Variation: RWA of each of the 4 cranial robusticity regions (frontal, zygomaxillary, temporal, and occipital) to asses overall variation in cranial superstructures across the entire global sample, 4) Male/Female Robusticity Variation: and finally, a series of RWA of the 4 cranial robusticity regions between males and females which examines variation between male and female superstructures (refer to Appendix A for robusticity variation within each of the 11 populations which highlights variation in the expression of robusticity characters between geographic regions).

Overall Global Variation

The RWA for all landmarks in the global sample provides a total of 139 relative warps, with the first 9 relative warps accounting for about 2/3 (66.63%) of the total variation in the dataset. As a result, these first 9 relative warps are examined individually and described below (refer to figure C1 for a scree plot of all the relative warps).

The first relative warp (RW1) for the global sample accounts for 15.76% of the total variation in the dataset. Examining the range of shape variation along RW1 shows that most of this variation involves the shape of the occipital region, specifically, the placement and shape of the nuchal lines (refer to figure C2). Here, the component

contrasts an occipital torus configuration with an external occipital protuberance shape in the occipital region. There is also a degree of flattening of the occipital plane associated with a more torus-like configuration of the nuchal lines.

RW1 also contains a component of overall cranial shape (albeit to a much lesser degree than that of the occipital region) in that it contrasts antero-posteriorly longer cranial vaults with vaults that are shorter in this plane. There is also some variation in the frontal region as well (specifically in the supraorbital region) that shows a degree of supero-inferior elongation. It is interesting to note that here, the morphology of the supraorbital region and the occipital region are tied together in that an expansion of the supraorbital region is associated with an occipital torus like configuration (both are markers of cranial robusticity).

RW2 explains 13.56% of the variation in the dataset and deals mostly with cranial vault shape and mastoid shape (figure C3). This component contrasts low and high cranial vaults (along the supero-inferior axis). High cranial vaults are also associated with an expansion of the mastoid process as well as a relatively orthognathic facial configuration. Lower cranial vaults are associated with smaller mastoids and a pronounced degree of facial prognathism. Facial dimensions are also reduced in the supero-inferior plane in conjunction with higher degrees of facial prognathism. There is also a degree of variation along the nuchal lines (mostly in the spacing between the superior and supreme nuchal lines) in this component as well, but to a much lesser extent that RW1.

Variation along RW3 deals mostly with the orientation of the cranial vault and face and accounts for an additional 8.55% of the variance (figure C4). This component deals primarily with an expansion of the frontal and occipital regions of the cranial vault, contrasting flat frontal and occipital regions with more rounded configurations. Along with the more rounded frontal configurations, there is an associated increase in the projection of the supraorbital region (although there is not an increase in the overall size

of the supraorbital region). The configuration of the face also changes along this axis, in that the more flattened frontal/occipital regions are associated with a relative elongation of the face, while the more rounded cranial vault configuration is associated with a relative shortening of the face in the supero-inferior plane.

While the first 3 relative warp axes dealt primarily with shape variation in the supero-inferior plane, RW4 (accounting for 7.46% of the variance) addresses variation in the medio-lateral plane (figure C5). More specifically, the component shows an overall widening of the face (especially in the zygomatic region) as well as an increase in the medio-lateral portion of the mastoid. RW4 also attributes variation to the relative placement of the nuchal lines in the supero-inferior plane, with high nuchal lines being associated with the narrower facial and temporal breadths. Lower nuchal lines are also associated with a more rounded posterior aspect of the cranial vault (around the parietals and occipital).

RW5 explains another 6.64% of the variance and accounts for overall facial massiveness (refer to figure C6). Here we see an expansion of the face in all planes and this expansion is accompanied by an increase in the cranial vault around the region of vertex. The smaller facial configurations are in association with a slight expansion of the occipital region. It is important to note that unlike previous components, this one does not address any sort of variation in the nuchal lines (only the curvature of the occipital planum).

RW6 deals mostly with the mastoid process (figure C7). This component explains 4.38% of the variance and contrasts the placement of the mastoid in the antero-posterior plane. More posterior placed mastoid processes are associated with a slight expansion in the face, as well as an increase in the height and massiveness of the supraorbital region. The more anteriorly oriented mastoid process configuration is associated with an expansion of the occipital region, especially in the shape of the supreme nuchal line and the overall rounding of the occipital plane.

RW7 is addresses an additional height component in the variation of the cranial vault and accounts for 3.78% of the variance (figure C8). Here, high cranial vaults (with the most superior point being more anterior placed, around bregma) are associated with high supreme nuchal lines and a slight decrease in the massiveness of the mastoid process and supraorbital region. Lower cranial vaults are associated with lower supreme nuchal lines and a relatively small but present increase in the massiveness of the supraorbital and mastoid regions.

RW8 (figure C9) deals mostly with the facial region and highlights variation in both the height and breadth of this area. It accounts for an additional 3.50% of the variance. Most of the variation in the height component of this relative warp is attributed to the orientation of landmarks along the medial aspect of the maxilla, which define the nasal aperture. As a result, this component contrasts tall and short nasal apertures, and this variation is also associated with breadth of the face. Slightly broader faces are associated with shorter nasal apertures and slightly narrower faces are associated with taller nasal apertures. In addition to variation in the face, RW8 also shows variation in the mastoid. More massive mastoids (in both A-P and S-I planes) accompany the shorter nasal length configurations.

RW9 accounts for almost 3% (2.99% exactly) of the total variance and is the final relative warp to be examined here (refer to figure C10). The majority of the landmark variation along this component is in the orientation of the superior nuchal line. The superior nuchal line has an inferior orientation at one extent of the variation of the RW axis and a more superior orientation at the other extent. This superior orientation of the nuchal line is also associated with a degree of alveolar prognathism in the face, while the more inferior orientation is associated with a more orthognathic face. There is also a slight degree of supraorbital expansion with the more inferior orientation of the superior nuchal line.

Given that the sample of *H. sapiens* included in this study is geographically diverse, it is also useful to examine variation within and between these geographical groups in the complete 72 landmark cranial dataset. Below are a series of relative warps plots (RW plots) that demonstrate how the 11 groups included in the study compare to one another in multivariate space.

Throughout the RW plots for the complete cranial landmark dataset, most of the geographical groups plot in close relationship to one another. This is not surprising since all individuals are recent *H. sapiens* and share overall patterns of craniofacial shape. That is not to say, however, that examining variation amongst groups is a fruitless effort. There are some interesting patterns that emerge from these plots which will be examined below.

A plot of RW1 and RW2, which counts for a total of nearly 30% of the total variance (29.32% exactly), shows a relatively tight clustering of the Australian aboriginal population on both RW1 and RW2 (figure C11). This group is characterized along these components by demonstrating high levels of occipital morphology consistent with an occipital torus and relatively diminutive faces with elevated levels of alveolar prognathism. The Chinese population clusters tightly on RW1 but spans nearly the entire range of variation on RW2. This means that the population is relatively diverse in cranial vault shape from high rounded vault to a low and more swept back vault but maintains continuity in other areas such as occipital and temporal robusticity. The North African sample also groups together showing expanded mastoid regions.

Plotting RW2 and RW3, which accounts for a total of 22.11% of the total variation in the dataset, shows a relative wide scatter of all geographic samples along RW3 while most groups maintain some degree of continuity along the 2nd relative warp (figure C12). Recall that RW3 addresses variation in the face (more specifically supero-inferior elongation) as well as cranial vault shape consistent with more rounded and expanded frontal and occipital areas. Given the high degree of scatter on this component

(compared to RW2), we can infer that there is a fair degree of facial variation among all groups studied.

An additional 16.01% of the variance in the global sample can be observed in a plot of RW3 and RW4 (figure C13). This plot shows a high degree of intrapopulational variation amongst both components. This makes interpretations difficult, however, this plot does not account for much of the total variance. There is a considerable amount of inter-populational overlap in on these two components however, demonstrating that with respect to aspects of facial shape and craniofacial breadth (as noted on these components above) there is considerable overlap in all populations studied.

Plotting RW1 and RW3 (a total of 24.31% variance explained) together provides a better picture for understanding the global variation of the sample than the above plot of RW3 and RW4 (refer to figure C14). The geographic populations group more tightly in this plot showing relative similarity in morphology between Mediterranean/Near East samples, the Chinese samples, and the Singapore samples. Most of the other groups display consistent levels of overlap across both components, with the Sub-Saharan Bantu population showing the highest level of intrapopulational diversity.

Overall Male/Female Variation

This section examines cranial variation seen within the male (*n*=91) and female (*n*=49) subsamples of the entire *Homo sapiens* global sample. Both the male and female subsets possess the full suite of 72 landmark coordinates and the results of the relative warps analysis for these data are discussed below.

Males. The total variation for the male subsample for the full 72 landmark coordinate dataset is summarized in 90 non-zero relative warps. A scree plot of these 90 relative warps (figure D1) demonstrates that the first 5 relative warps explain the majority of overall landmark variation. These relative warps address a total of 53.24% of the total variance explained.

The first relative warp, RW1, accounts for 17.78% of the total variance in the male full coordinate landmark dataset. This component contrasts large facial morphology, expanded mastoids, and larger nuchal lines with reduced faces, mastoids, and nuchal lines (figure D2). Variation in overall cranial shape also makes up a large portion of this relative warp. Here, long and low cranial vaults are contrasted with high cranial vaults with decreased antero-posterior dimensions. In the former, there is an associated expansion of the supraorbital region as well as an expansion of the occipital region in the area of lambda. The latter shows a relatively globular overall profile with slightly decreased supraorbitals and a more rounded occipital.

Relative warp 2 addresses 11.29% of the total variance and this component highlights variation in facial size and shape, as well as nuchal morphology. Also seen along this component is a degree of mastoid shape change and an expansion/reduction of the supraorbital region (figure D3). Expanded zygomaxillary regions are seen in association with an expansion of the mastoid but a notable reduction in both supraorbital morphology as well as supreme nuchal line height. The opposite is true of the smaller and more anteriorly oriented (i.e. prognathic) zygomaxillary morphology.

RW3 accounts for another 9.03% of the variance and can be visualized in figure D4. This component demonstrates variation primarily in the maxillary region as well as in overall nuchal line height. An expansion in the maxillary region is associated with a increase in nuchal line height. Along with this morphology, there is also a slight reduction in supraorbital morphology both in anterior projection and medio-lateral length. At the opposite end of variation for this component, reduced maxillary regions are seen in conjunction with and expansion of the supraorbital region and a more inferior placement of the superior and supreme nuchal lines. Reduced facial configurations are also associated with a more globular cranial configuration along this component.

Relative warp 4 highlights variation primarily in mastoid and nuchal configurations (figure D5). This component addresses another 7.87% of the total

variance. Reduced mastoid dimensions accompany and expansion of the supreme nuchal line along RW4, while the opposite is true of expanded mastoid configurations. There is little variation in supraorbital morphology here, but a change in the orientation of the zygomaxillary region, with slightly more inflated maxillae being associated with increased mastoids, can be observed.

The final relative warp to be examined here, RW5, addresses 7.27% of the variance (figure D6). This component displays variation primarily in the zygomaxillary and supraorbital regions, along with a degree of vault shape change as well. Expansion of the zygomaxillary region (in overall size, but especially in alveolar prognathism) is seen in conjunction with a reduction supraorbital size. There is also an increase in parietal expansion as well as a more posterior orientation of the parietal region and a flattening of the occipital region that accompanies the expanded zygomaxillary region morphology. The alternative zygomaxillary morphology (reduced in overall appearance) is seen with a concurrent expansion of the supraorbital region (primarily in anterior projection) as well as a more globular cranial vault.

Females. The complete 72 coordinate landmark relative warps analysis of the female subset provides a total of 48 non-zero relative warps. Plotting the eigenvalues of these relative warps in a scree plot (figure D7) shows that the first 3 relative warps make up a large proportion of the overall variance. These three relative warps combined account for 45.30% of the variation in the female complete coordinate landmark dataset and as such, will be examined in further detail below.

RW1 accounts for 23.10% of the total variance in the female complete landmark dataset and this component highlights variation in mastoid size, nuchal morphology, and facial orientation (figure D8). As mastoid size increases along this component, the size of the supreme nuchal line decreases (forming a small external occipital protuberance) and the facial configuration becomes more orthognathic. A decrease in mastoid expression shows an opposite trend with faces becoming more prognathic and the

supreme nuchal line increasing in size and more “torus-like”. Interestingly, there is very little, if any, variation in cranial vault shape along this first component, in contrast to what can be seen above in male variation along RW1.

The second relative warp addresses 12.11% of the variation in the dataset and focuses primarily on cranial vault shape variation (figure D9). Here, high foreheads and rounded cranial vaults contrast with lower and longer cranial vault configurations. The latter configuration is associated with an increase in supraorbital robusticity as well as a decrease in mastoid and zygomaxillary expression. The former is associated with an increase in mastoid length and breadth and also a slight increase in overall facial massiveness. The more rounded cranial vault configuration also demonstrates a decrease in supraorbital morphology, which is most likely tied to an increase in frontal height.

RW3 is the final relative warp to be examined in detail here, and this component addresses 10.17% of the variation in the female subset. Variation along this final component is characterized primarily by cranial vault shape (although in a different manner from RW2) as well as zygomaxillary size and orientation, supraorbital morphology and supreme nuchal line size (figure D10). Cranial vaults vary from a more rounded, globular shape along this component to a form that demonstrates both parietal expansion and occipital flattening. The more rounded vault configuration is tied to an increase in superciliary arch height and a more orthognathic facial configuration. The more angular vault configuration, on the other hand, shows a simultaneous increase in supraorbital projection and alveolar prognathism.

Global Robusticity Variation

In this section of the relative warps analysis, we will examine the levels variation in each of the four anatomical regions of the skull tied to cranial robusticity (the frontal, facial, temporal, and occipital regions) for the entire global sample of 140 individuals. The goal of this section is to provide a more specific examination of how each

superstructure, such as the brow ridge, or external occipital protuberance/occipital torus, varies in its shape and expression across the entire dataset to provide some insights into how these features are expressed on a global level.

Frontal Robusticity. Frontal robusticity is examined in the supraorbital region with a focus placed on the overall sized and projection of the superciliary arch. A relative warps analysis of the landmarks along the supraorbital region provides a total of 53 components, accounting for all the variation in the dataset. Of these 53 components, the first 5 account for a total of 72.75% of the variance and are addressed in further detail below (see figure E1 for a scree plot of the relative warps).

RW1 accounts for the largest proportion of the variation in the supraorbital dataset (33.62%) and can be examined visually in figure E2. This component summarizes variation in the overall length of the superciliary arch, contrasting superstructures with more laterally placed medial and midorbital semilandmark lines with ones that are much more medially oriented. This means that medio-lateral length of the superciliary arch is the most variable component in the dataset.

RW2 accounts for an additional 16.10% of the variance and contrasts supero-inferiorly elongated superciliary arches with more diminutive ones (figure E3). There is also a component of antero-posterior projection along this component but this is to a lesser degree. Superciliary arches that are expanded in the S-I plane also project more in the A-P plane. Finally, there is also variation in M-L placement of the medial semilandmark line, demonstrating an overall expansion of the glabellar and medial components of the superciliary arch that accompanies the increase in supraorbital projection.

RW3 summarizes variation in lateral trigone size as well as superciliary arch projection and supero-inferior expansion of the arch. This component addresses 12.50% of the variance and can be seen in figure E4. Supero-inferiorly compressed supraorbital regions are also associated with increased levels of anterior projection as well as a drastic

increase in the size of the lateral trigone. As the S-I dimensions of the superciliary arch increase, they become less projecting and the trigone becomes less massive (this is contrary to the variation that was summarized in RW2).

RW4 addresses 5.50% of the variation in the supraorbital landmark dataset and accounts for variation in the lateral trigone and glabellar regions (figure E5). As the lateral trigone along this component increases in size, there is a concurrent increase in the expression of the glabellar region. We can also note a degree of supraorbital projection (in the A-P plane) along with an increase in the size of both glabella and the lateral trigone. The exact opposite is true for supraorbital forms with diminished lateral trigones and reduced glabellar regions.

Finally, RW5 summarized variation primarily in the anterior projection of the supraorbital region and accounts for 5.08% of the variance in the dataset (figure E6). Here, superciliary arches that have higher levels of anterior projection are also expanded in the supero-inferior plane. There is also a slight increase in the size of the lateral trigone with these expanded superciliary archers. As the levels of anterior projection drop off along this component, we see a decrease in both the size of the lateral trigone as well as a decrease in the S-I dimensionality of the supraorbital region.

A scatter plot of RW1 and RW2, accounting for nearly half of the variation in the dataset (a total of 49.72%) for all individuals in the study provides some insights into how geographic variation in supraorbital robusticity is manifested (see figure E7). There is considerable overlap in supraorbital morphology among all the groups included in the study along RW1 and RW2. Along RW1 Central and Western Europe tend to group toward the range of variation characterized by laterally expanded brow ridges. The New Guinea sample also has a tendency to group here as well. The North African sample is found at the opposite end of the range of variation, while all other groups can be found across the entirety of RW1. Lower values along RW2 are indicative of expansion and projection of the glabella and medial aspect of the supraorbital region, while higher

values are diagnostic of a decrease in the medial morphology of the supraorbital region. Here, the Central European population once again shows an affinity toward having a more robust supraorbital morphology, as well as several individuals from the Mediterranean/Near East sample.

Plotting out the RW scores for components RW1 and RW3 addresses an additional 46.12% of the total variance in supraorbital morphology (figure E8). Most of the individuals in the study again group toward the middle of the plot but there are some notable outliers along both components. RW1 again shows a similar pattern of the European samples being more indicative of laterally expanded supraorbitals while RW3 (contrasting more projecting supraorbitals that are supero-inferiorly compressed with flatter more S-I expanded supraorbitals) highlights a degree of variation in the Sub-Saharan Bantu population which ranges from average values to values that denote elevated levels of supraorbital projection. There are also low values for some of the Central and Western European and Australian Aboriginal populations as well. Some groups with the highest values along RW3 (again, meaning flatter but supero-inferiorly expanded supraorbitals) are the Chinese and North African datasets.

Finally, a plot of RW2 and RW3, accounting for 28.60% of the variance, shows a tendency for all individuals in the dataset to have relatively reduced glabellar regions as well as more S-I expanded and flatter supraorbitals (figure E9). There are no individuals that have simultaneously low values for both of these components (indicative of a robust supraorbital morphology that has high levels of projection with an expanded glabellar region). There are, however, some individuals from the European populations, as well as the Bantu and Mediterranean/Near East samples that come close to this robust supraorbital morphology.

Zygomaxillary Robusticity. Robusticity in the facial region of the cranium (characterized by the morphology of the zygomaxillary region) is examined in the section below. Robusticity in this anatomical region is often characterized by having more

massive faces or larger superstructures, such as the zygomaxillary tubercle (Lahr, 1996). An overall assessment of shape variability within the global sample will highlight patterns in zygomaxillary expression across the entire dataset.

The RWA of the zygomaxillary landmark subset provides a total of 59 non-zero components. Of these 59 components, the first 6 account for over 2/3 of the total variation (69.13%) and will be examined individually to elucidate patterns of variation in this anatomical region across the global sample (figure F1 provides a scree plot for zygomaxillary region relative warps) .

RW1 accounts for 27.61% of the variance and deals mostly with variation in the shape of the nasal aperture, as well as an overall elongation of the zygomaxillary region (figure F2). This component contrasts more superiorly placed nasal apertures more inferiorly placed nasal apertures. The latter condition is accompanied by an increase in alveolar prognathism. The other major axis of variation along this component deals with the overall A-P length of the zygomaxillary region, as well as its overall massiveness (particularly in cheek height). At one end of the range of variation, there is a significant level of antero-posterior elongation (particularly involving the zygomatic), which is accompanied by a drastic reduction in facial and cheek height. This configuration is hype-gracilized compared to the other extreme along this component which is very robust. This second condition is marked by greatly expanded maxillary and cheek heights, as well as having a more 'swept-back' zygomatic morphology.

RW2 also deals with nasal aperture morphology, as well as zygomatic A-P elongation, but does not show as great a level of variation in zygomaxillary height and massiveness as did the first relative warp. This component accounts for 15.11% of the total variance and can be examined visually in figure F3. Variation in the morphology of the nasal aperture is characterized primarily in nasal breadth along this component (as opposed to nasal height in RW1) but there is also a degree of variation in height of the aperture as well. Antero-posterior length of the zygomatic bone varies greatly along this

component as well, but unlike the previous component, RW2 also highlights variation in the width of the frontal process of the zygomatic (which at its most superior extent helps to form the trigone, which is part of the of supraorbital region, discussed above).

Unlike the previous components, RW3 shows almost no variation in the anterior nasal aperture or the zygomatic region. This component, highlights variation in orbital shape as well as expansion of the inferior aspect of the maxilla (particularly in the alveolar region, see figure F4). Accounting for an additional 9.25% of the variance, RW3 contrasts maxillae that are supero-inferiorly elongated with expanded alveolar regions with ones that are compressed in this plane and also have reduced cheek heights and are wider in the medio-lateral plane. The orbits are wider with the more broad facial configurations, while in the more narrow facial configurations, the orbits tend to be narrower as well.

RW4 contrasts overall expansion of the zygomatic bone with the expansion of the maxilla, and addresses 6.80% of the variance in the zygomaxillary landmark dataset (figure F5). The zygomatic and maxilla have an inverse relationship along this component: as the zygomatic bone increases in overall massiveness, the maxilla decreases, and vice versa. There is also a significant degree of facial breadth variation along this component, with very wide faces being associated with an expansion of the zygomatic bone, and not the maxilla.

RW5 shows variation in facial breadth as well as the orientation of the zygomatic bone and accounts for 5.73% of the variance (figure F6). Along this component there is considerable variation in facial breadth (again, tied to the expression of the zygomatic). More ‘swept back’ zygomatics are associated with an increase in facial breadth, while the orthogonally oriented zygomatic bones are associated with reduced facial breadths.

Finally, RW6 accounts 4.63% of the variance and highlights a great deal of variation in the orbits (figure F7). This final component contrasts expanded orbits (in all planes) with orbits that are reduced in size. Along with this increase in orbital size, we

see a concurrent decrease in the size of the frontal process of the zygomatic (which forms the lateral wall of the orbit).

A graphical representation of the variation in zygomaxillary morphology, provided by a scatter plot of RW1 and RW2 (figure F8), accounts for a total of 42.72% of the variance in dataset. Low values along RW1 are indicative of an expanded nasal aperture as well as a reduction in the size and shape of the face, where higher values are indicative of the opposite morphology. Along RW2, lower values are associated with expanded zygomatics and reduced maxillae. Given this summation of the variation in the plot, individuals with lower RW1 and RW2 values have more reduced faces. The Australian and Sub-Saharan Bantu populations are mostly characterized by this morphology. The opposite is true for the Central and Western European populations as well as the Mediterranean/Near East population. These three groups show the highest values in both RW1 and RW2 meaning that they tend to have larger facial configurations.

Figure F9 shows a plot of RW1 and RW3 accounting for an additional 36.86% of the variation in the zygomaxillary dataset. Once again low values along these two components are indicative of having more reduced facial morphologies, while higher values indicate expansion in the zygomaxillary region. As in figure F8, the Australian population shows the lowest values along these components implying that they have the most reduced faces of the global dataset. The Sub-Saharan Bantu and interestingly the Sub-Saharan Khoisan populations also both tend to demonstrate this facial reduction as well (although not to the extent of the Australian subset). The Western European and Mediterranean/Near East samples tend to group toward the edge of the plot that is indicative of facial expansion.

Finally, plotting RW2 and RW3 (addressing an additional 24.36% of the total variance, see figure F10) shows a rather tight grouping of all the sub-samples toward the center of the plot. The same patterns that have been highlighted above appear to be the case for this plot as well, only with less separation between groups with larger more

robust faces and the ones with smaller more gracile ones. This lack of distinction in credited to the fact that this plot represents a lower percentage of the total variance and therefore clear morphological signals in the data are more difficult to ascertain.

Mastoid Robusticity. The mastoid process is the focus of robusticity in the temporal region of the cranium. A RWA of the mastoid landmarks provides a total of 23 individual components accounting for the total amount of variance the mastoid region. Of these 23 components, the first 5 address the majority of the variation (77.12%) and are examined in closer detail below (refer to figure G1 for a scree plot).

RW1 accounts for 35.65% of the variance and addresses the overall level of projection from the cranial base (figure G2). There is a great deal of inferior projection seen in the inferior landmarks of the mastoid (especially at the tip of the mastoid) at one end of the range of variation along this component, while the other extreme shows a greatly reduced level of mastoid projection from the cranial base. In addition to this, there is also variation in the orientation of the mastoid. As the level of inferior projection in the mastoid increases, the overall orientation of the mastoid is moved posteriorly. The mastoid becomes more anteriorly oriented as the level of mastoid projection diminishes.

RW2 displays a similar pattern to RW1 in morphological variation and addresses 15.08% of the variance in the dataset (figure G3). As with the first component, RW2 contrasts more projecting mastoids (in the supero-inferior plane) with more reduced ones, as well as the overall antero-posterior orientation of the structure. Unlike RW1, however, this second component shows that mastoids that are more projecting are also more anteriorly oriented. Finally, this component highlights variation in overall mastoid breadth (medio-lateral), with increased mastoid breadth being associated with an overall increase in mastoid projection.

RW3 accounts for variation in the antero-posterior length of the mastoid as well as medio-lateral breadth. This component addresses and additional 14.17% of the variance and can be visualized in figure G4. Here, the overall pattern demonstrates that

as the mastoid increases in massiveness in the medio-lateral plane (or mastoid width) it becomes dramatically longer in A-P dimensionality also. The exact opposite is true for medio-laterally reduced mastoids, which show a great deal of gracilization in length, but also tend to project slightly more than the more robust mastoid condition.

RW4 highlights variation in the orientation medial portion of the mastoid and accounts for 7.38% of the variance (figure G5). While most of the mastoid landmarks show little change in location along this component, the medial aspect of the mastoid changes drastically. This line is indicative of mastoid breadth and well as projection, and variation along this aspect of the mastoid shows that as mastoid breadth increases, the structure becomes far less projecting. A subsequent decrease in breadth sees a concurrent increase in mastoid projection from the base of the cranium.

Finally, RW5 also highlights variation in mastoid width and accounts for an additional 4.85% of the variance (figure G6). While previous components that dealt with mastoid width focused primarily on the inferior portion of the structure, RW5 accounts for changes in M-L width primarily in the mastoid base (near the base of the cranium). While this is the case, there is also a level of variation in width near the tip of the mastoid as well, with wider tips being associated with wider bases as well.

A plot of RW1 and RW2 for the mastoid RWA accounts for just over half the variation in the subset (50.73% exactly, see figure G7). Lower RW values along both RW1 and RW2 are indicative of more reduced mastoids both antero-posterior (RW1) and medio-lateral (RW1 and RW2) dimensions. Groups such as the Sub-Saharan Khoisan and Australian Aborigines tend to show more reduced mastoid processes while the European samples (Central and West Europe) and Chinese and Indian sample show more expanded mastoid processes along these components. The other groups in the sample cluster in the middle of these two axes.

Plotting out RW1 and RW3 again show a similar distribution of the modern human groups (figure G8). Accounting for 49.82% of the variance, this plot highlights

variation in A-P length (as seen in RW1) and a component of mastoid height, as noted in RW3. Again, the Australian and Khoisan populations are arrayed toward the more reduced end of the range of variation (meaning that they have less projecting mastoids), while groups such as the two European samples, the Chinese sample, and the Indian sample, again tend to plot toward the more projecting and A-P elongated side of the range of variation.

Finally, plotting out RW2 and RW3 (accounting for an additional 29.25% of the variance in the dataset) shows most of the populations grouping together in the center of the graph with only a few outliers from the Australian population (figure G9). Aside from a small proportion of the Australian subset (which spans most of the variation along these two relative warps) the rest of the samples demonstrate rather average mastoid morphology along these components (which account for variation in both M-L and S-I planes).

Occipital Robusticity. The anatomical final region of the cranium to be examined for the global dataset is the occipital region. The superstructure of interest here is the occipital/nuchal torus. Given that this superstructure is formed by the superior and supreme nuchal lines, variation in the semilandmarks that make up these lines are examined below.

Unlike the other areas of the cranium examined above, a RWA of the occipital region shows a significant proportion of the variance in the dataset occurring in the first 3 relative warps. Out of a total of 17 relative warps, which account for the full amount of the variance in the dataset, relative warps 1-3 account for a combined 91.46%. As a result, it is only necessary to provide a discussion of the 3 relative warps in the following section (see figure H1 for the relevant scree plot).

RW1 accounts for a very large proportion of landmark variance (73.76%) and is represented visually in figure H2. This component deals specifically with the morphology of the supreme nuchal line and contrasts a diminished supreme nuchal line

(with a morphology indicative of an external occipital protuberance) with an expanded one. Expansion of the supreme nuchal line in both medio-lateral and supero-inferior plans is indicative of an occipital torus, and therefore this component shows the full range of occipital morphology (from external occipital protuberance to occipital torus) in the global dataset.

RW2 covers 11.60% of the variance (signifying a large drop off from RW1) and this component addresses variation in supreme nuchal line height (figure H3). At one end of the range of variation along RW2, the supreme nuchal line is extremely low on the occipital (practically overlapping with the superior nuchal line) while at the other extreme, the supreme nuchal line is placed far superior to the superior nuchal line, high up on the occipital bone. This superior orientation of the supreme nuchal line also is associated with a slight reduction in the length of the superior nuchal line, while the more inferiorly placed supreme nuchal line is expressed in tandem with an increased length in the superior nuchal line.

RW3 is the final component to be examined here, and addresses the orientation of the supreme nuchal line. This component covers an additional 6.10% of the variance and can be seen in figure H4. The supreme nuchal line varies in its orientation from an infero-medial position to a supero-lateral position at one end of the range of variation along RW1 to a more supero-medial to infero-lateral orientation at the other extreme in the range of variation. This means that there is an expansion of the medial component of the supreme nuchal line at one extreme, while the other shows an expansion in the lateral component of the supreme nuchal line. As with the prior 2 components, variation in the expression of the superior nuchal line is marginal.

RW plots (see figure H5) of the occipital landmark dataset will help gain an understanding of which groups in the global sample overlap in relation to the morphology of this anatomical region (i.e. whether or not groups tend to be more indicative of an external occipital protuberance or, if they show morphologies more in line with an

occipital torus). A plot of RW1 and RW2 shows considerable separation of groups along both axes to a degree that has not been seen in the previous RW plots. This plot, accounting for 85.36% of the variance, addresses variation in supreme nuchal line. RW1 accounts for change in the M-L length of the nuchal line, while RW2 describes variation in the S-I placement of the supreme nuchal line relative to the superior nuchal line. A 'torus-like' configuration is indicated by lower values along both RW1 and especially along RW2. The Australian sample almost entirely occupies the shape space indicative of a torus configuration, with only a few outliers from the New Guinean and Khoisan populations in this space. The Sub-Saharan Bantu population is the most gracile with respect to occipital robusticity according to the graph, along with the Western and Central European populations and the North African population (although the North African and Central European groups are encroaching on the shape space that is diagnostic of expanded occipital robusticity. Other groups such as the Mediterranean/Near East sample are highly variable with respect to these aspects of occipital morphology.

Plotting out RW1 and RW3, accounting for 79.86% of the variance, also shows considerable separation amongst many of the sub-samples in the global dataset (figure H6). As with the plot above, most of the variation is along RW1 with only a few groups showing significant separation along RW3 (due to the fact that RW3 only describes 6.10% of the variance). Both components again deal with variation in the orientation of the supreme nuchal line, with groups such as the Singapore and Chinese samples showing greatly expanded M-L lengths in the supreme nuchal line. In contrast, the Sub-Saharan Bantu group and the Western European group, show morphology indicative of an external occipital protuberance.

In contrast to the two plots described above, the plot of RW2 vs. RW3 shows a considerable deal of grouping around the average form for these two components (figure H7). This is most likely due to the fact that this plot only describes 17.70% of the remaining morphological variation. While most populations tend to plot near the center

of these two components, the Australian and New Guinea samples display some degree of separation from the rest of the samples. The Australian morphology along these components shows a high degree of S-I separation between the superior and supreme nuchal lines. The New Guinea sample shows less separation in the aspect but does display morphology that is more robust than the average form along RW3.

Male/Female Robusticity Variation

In order to gain a more complete understanding in superstructure morphological variability between males and females, separate RWAs are presented below for each of the four anatomical regions under study: the frontal region, zygomaxillary region, mastoid region, and occipital region.

Males, Frontal Region. A RWA of the 20 landmark frontal region coordinate data in the male subsample provides a total of 53 non-zero relative warps, of which the first 3 demonstrate the largest amount of variance explained (totaling 62.71% total variance, a scree plot is provided in figure I1). These relative warps will be explored in further detail below.

RW1 accounts for 34.50% of the total variance and highlights variation in superciliary arch length and projection (figure I2). Superciliary arches that are medio-laterally shortened show a decrease in antero-posterior projection, while the oppose range of variation highlights a medio-laterally expanded and much more anteriorly projecting supraorbital configuration. The later is consistent with a supraorbital torus configuration.

RW2 addresses another 16.21% of the variation in the male supraorbital dataset, and this second relative warp deals primarily with superciliary height variation (figure I3). As superciliary arches expand in the supero-inferior plane along this component, there is a consecutive decrease in the size and projection of the lateral trigone. More supero-inferiorly compressed superciliary arches demonstrate a more expanded trigone region.

The final relative warp to be examined here, RW3, accounts for 11.99% of the overall variance and is illustrated in figure I4. This last component also addresses variation in trigone size and overall supraorbital height and projection. As the supraorbital region decreases in overall height, there is a simultaneous increase in trigone size, as well as anterior projection of the superciliary arch. Arches that are expanded in the supero-inferior plane, conversely, show a decrease in both anterior projection and lateral trigone dimensionality.

Males, Zygomaxillary Region. The 22 coordinate landmark zygomaxillary region dataset for the male subsample provides a total of 59 non-zero relative warps. Of these 59 warps, a scree plot shows that the first 3 warps account for the majority (52.58%) of the facial variation seen in this subsample (figure J1).

RW1 addresses 27.91% of the zygomaxillary variation seen in the male subset, and this warp can be visualized in figure J2. This component highlights variation in overall zygomaxillary size, specifically in maxillary massiveness and aspects of zygomatic dimensionality. As overall facial massiveness increases (primarily in the maxillae), zygomatic region tends to become less posteriorly oriented and slightly less prominent. An increase in zygomatic expression is coupled with a decrease in maxillary dimensions as well as a slight increase in alveolar prognathism.

RW2 accounts for another 14.61% of the variance, and this component shows variation in a similar manner to RW1 above (figure J3). Here, variation in maxillary size is again tied to zygomatic size and facial projection. As the maxillary region increases in massiveness, there is a subsequent decrease in zygomaxillary expression, primarily seen in a decrease in frontal process width and the posterior extent of the zygomatic. Unlike RW1, however, there is also an increase in facial prognathism with the larger, more robust maxillary configurations. The opposite condition is true for decreased maxillae.

Finally, RW3 accounts for 10.05% of the total variance in the male subsample. This component shows variation in cheek height (figure J4). Greater cheek heights are

seen in individuals with fuller, more heavily built maxillae, while the opposite condition is true for reduced maxillae.

Males, Mastoid Region. A relative warps analysis of the mastoid region in males provides a total of 23 non-zero relative warps (from 10 coordinate landmarks), and of these warps, the first 4 address the largest portion of variability in the dataset (refer to scree plot, figure K1). These first four warps cover a total of 71.42% of the variance and are detailed below.

RW1 demonstrates variation in antero-posterior width, as well as overall mastoid height (figure K2). This component accounts for 34.82% of the total variance, which is almost as much as the next 3 warps combined. Along this axis of variation, a-p widened mastoids are contrasted with mastoids that have increased mastoid heights, that is to say, as mastoids get wider, they also get shorter at the same time. Increased mastoid height is seen with low mastoid widths.

RW2 covers another 14.97% of the total variance and this component deals almost exclusively with mastoid medio-lateral breadth (figure K3). This axis also shows some variation in mastoid a-p width, but to a lesser degree than breath variation. As the mastoid increase in overall breadth, there is a simultaneous increase in antero-posterior width as well, providing the more robust configuration for the mastoid. The more gracile form along this axis has both diminished a-p widths and m-l breadths.

RW3 shows a similar pattern of variation to RW2 – variation in mastoid breadth tied to width, but here there is an additional aspect of mastoid orientation (either more anteriorly oriented or posteriorly oriented). This component accounts for 12.94% of the variance and is illustrated in figure K4. As with RW2, there is a similar link between width and breadth (as one increases, so does the other) but in addition to this pattern, there is a slight tendency for mastoids to be oriented more anteriorly when in the more gracile form and more posteriorly as mastoid robusticity increases.

RW4 addresses another 8.70% of the overall variation, and this final component highlights variation almost exclusively in mastoid breadth (figure K5). While this component addresses extreme levels of breath variation, there is also some variation in mastoid width to be accounted for. Interestingly, this component shows that mastoid breadth increases with a decrease in mastoid width (counter to what has been shown in the previous relative warps).

Males, Occipital Region. The final anatomical region to be considered for the male dataset is the occipital region. Here, 8 occipital landmarks provide a total of 17 non-zero relative warps. Of these 17, RW1 covers the vast majority of the variation in the dataset at 72.40%. Upon further examination of the scree plot for this RWA, the first 3 warps cover almost all of the variation in the dataset (totaling 90.91%, see figure L1). These warps are addressed in further detail below.

RW1 of the occipital region dataset accounts for 72.40% and addresses variation primarily between a small external occipital protuberance and a large, robust occipital torus (figure L2). There is a large degree of projection seen between the supreme and superior nuchal lines in conjunction with the torus configuration, while overall superior and supreme nuchal line length is decreased in the external occipital protuberance configuration.

RW2 addresses variation primarily in spacing between the superior and supreme nuchal lines, and this component accounts for another 11.88% of the overall variance (figure L3). There's also a degree of posterior projection of the nuchal lines (primarily the supreme nuchal line) along this axis. This projection increases as supero-inferior distance between the superior and supreme nuchal lines increases.

RW3, the final component to be discussed, accounts for 6.63% of the total variance and this last component deals primarily with the orientation of the supreme nuchal line (figure L4). Variation in this orientation ranges from a supreme nuchal line

that runs supero-medially to infero-laterally to the opposite morphology of running infero-medially to supero-laterally.

Females, Frontal Region. The female subset contains 49 individuals and the supraorbital region coordinate landmark dataset is comprised of 20 landmarks. A relative warps analysis of this dataset provides a total of 48 non-zero RWs and of these, the first 3 RWs cover the largest portion of the overall variation (figure M1).

RW1 accounts for 33.73% of the variation in the supraorbital dataset. This component addresses variation in lateral extent of the superciliary arch as well as lateral trigone robusticity (figure M2). Along this component, there is an association with an increase in lateral trigone robusticity as the superciliary arch becomes more laterally extended. The opposite, more gracile form, displays both reduced superciliary arch lengths and diminished trigone regions.

RW2 addresses an additional 19.76% of the total variance and this second component covers variation in glabellar projection and overall superciliary arch height (figure M3). As glabellar projection increases along this axis, there is a simultaneous increase in overall superciliary arch height and a slight decrease in superciliary arch length. Reduction in glabellar robusticity comes with a decrease in supraorbital height and a slight increase in length.

RW3, the final component to be discussed here, covers 12.00% of the overall variance, and it covers variation primarily in supraorbital projection (figure M4). As overall anterior supraorbital projection increases, there is a decrease in glabellar size and a major increase in trigone robusticity. Increase in the glabellar region along this axis also demonstrates a decrease in trigone size and superciliary arch projection.

Females, Zygomaxillary Region. The zygomaxillary coordinate landmark dataset for the female subset is comprised of a 22 landmarks, which yield a total of 48 non-zero RWs from a relative warps analysis. A scree plot of the eigenvalues for this RWA shows that the first 3 components address the majority of the overall dataset variation,

accounting for a total of 57.68% (figure N1). These three RWs will be examined in further detail below.

RW1, covering 29.67% of the overall variation, contrasts zygomaxillary regions that are expanded and inflated with faces that are more reduced in this aspect. There is also a degree of facial prognathism observed along this component also (figure N2). As faces become more inflated and expanded in the zygomaxillary region along this component, there is a concurrent decrease in overall facial projection, yielding a more orthognathic face. Decrease in overall zygomaxillary robusticity is coupled with an increase in facial projection along this component.

RW2 addresses variation in the maxillae morphology (particularly in overall depth of the maxilla) as well as expansion of the zygomatic and this component accounts for 17.80% of the total variance (figure N3). Expansion of the maxillary region is inversely proportional to zygomatic expression along this component. As the maxilla increases in antero-posterior breadth, there is a simultaneous decrease in overall zygomatic size and robusticity.

RW3 is the last component to be discussed here, and this relative warp accounts for 10.20% of the total variance (figure N4). The majority of variation along this warp is demonstrated in overall facial height. Faces that are supero-inferiorly taller tend to be more medio-laterally wide. The opposite condition is seen with supero-inferiorly diminished zygomaxillary regions.

Females, Mastoid Region. The 10 coordinate landmark mastoid dataset for the female mastoid data provides a total of 23 non-zero relative warps accounting for the entire range of variation in the subsample. A scree plot of the eigenvalues for these relative warps demonstrates that the first 3 components explain the largest portion (totaling 68.92%) of the overall variation (figure O1).

RW1 covers a similar pattern of mastoid variation seen above in the male subsample. Here, mastoid antero-posterior width and supero-inferior height vary the

most along this axis (which covers 39.87% of the total variance, see figure O2). As with the males, the pattern of variation in the female mastoid sample shows that as antero-posterior widths increase, there is a decrease in supero-inferior height. The opposite is true for mastoids that are narrower in the a-p plane.

RW2 addresses variation in mastoid height and mastoid orientation, and this second component covers an additional 14.88% of the total variance (figure O3). As mastoid height increases along this axis, there is a tendency for the mastoid tip to become more anteriorly oriented. The mastoid tip moves to a more posterior position as mastoid height decreases.

RW3 covers 14.18% of the variance (almost as much as the percent variance explained in RW2) and this final component demonstrates variation in a-p width and mastoid height (figure O4). Although this component shows variation in a manner similar to RW1, the degree of the variation is more extreme here. Very wide mastoids are shown to be very short, while a marked increase in mastoid height is seen in conjunction with a large decrease in mastoid width.

Females, Occipital Region. The final anatomical region to be examined for the female subset is the occipital region. A RWA of the 8 coordinate landmark occipital dataset provides a total of 17 non-zero RWs. Of these, the first 3 warps cover a large majority of the overall variation (totaling 92.44%, refer to figure P1). These 3 warps will be examined in further detail below.

RW1 accounts for the majority of the dataset variation at 76.14% and this component addresses variation ranging from an external occipital protuberance to a full occipital torus (figure P2). Superior and supreme nuchal line projection increases medially in conjunction with the more "torus-like" occipital configuration, while there is a slight increase in lateral superior nuchal line projection with the external occipital protuberance.

RW2 covers an additional 10.22% of the variance and this component describes variation primarily in supreme nuchal height (figure P3). As distance between the superior and supreme nuchal line increases, (i.e. the supreme nuchal line is more superiorly oriented) there is a slight change in supreme nuchal line shape from a parabolic shape to a more linear shape. On the other end of the range of variation, the supreme nuchal line is placed much closer to the superior nuchal line and its shape in this orientation is more parabolic.

RW3 shows a similar pattern of variation seen in the male subsample for the occipital region. This final component accounts for 6.08% of the variance and it addresses variation in supreme nuchal line orientation (figure P4). Along this last component, the supreme nuchal line runs supero-medially to infero-laterally at one end of the range of variation, while at the opposite end of the range of variation, it runs infero-medially to supero-laterally.

Allometry

Centroid Sizes and Superstructure Expression

Given that centroid size is a geometric morphometric proxy for overall massiveness of a coordinate dataset (in a multi-dimensional sense), this measure will be used to compare measures of size across the entire n=140 dataset, with respect to geographical differences in the following categories: 1) Overall centroid size, 2) Supraorbital centroid size, 3) Zygomaxillary centroid size, 4) Mastoid centroid size, and finally 5) Nuchal region centroid size.

Overall Centroid Size. Overall centroid size is based on the entire 72 landmark dataset (across the entire cranium) and serves as a measure of cranial massiveness. Centroid sizes for all of the groups in the present study are summarized in Table 3. The global average for centroid size across the entire cranium is 627.56mm. When comparing geographical differences in centroid size, the global average is useful for

determining which groups are larger or smaller given the global mean. The Sub-Saharan Khoisan group demonstrates the lowest overall centroid size (607.35mm), while Sub-Saharan Bantu group is the largest overall at 647.00mm. Most of the other groups center around the mean, with the Australian Aborigines (615.95mm) and the Mediterranean/Near East (623.35mm) being on the smaller than average, while the North African (631.12mm) and Singapore 638.56mm) being larger than average.

Table 3. Overall centroid size.

Population	CS (mm)
Australian	615.94589
C. Europe	624.306442
China	627.831677
India	627.771222
Medit/Near E.	623.352847
New Guinea	625.328795
North Africa	631.116544
Singapore	638.56185
Sub-Sahar Bantu	647.002415
Sub-Sahar Khoisan	607.34549
W. Europe	627.971055
MEAN	627.564702

Supraorbital Centroid Size. When comparing just the supraorbital coordinate landmark data, the overall centroid size for the global sample is 80.45mm (refer to Table 4). The New Guinea sample demonstrates the lowest supraorbital centroid size at 75.52mm, with the Sub-Saharan Khoisan also being rather small at 77.29mm. At the other end of the range of size variation, the Sub-Saharan Bantu provide the overall largest centroid size at 83.82mm, followed closely by Singapore (82.42mm), the Australian Aborigines (81.28mm), and Western Europeans (81.26mm). When comparing the

proportion of supraorbital centroid size to overall centroid size, the group with the largest supraorbital region relative to overall size is the Australian Aborigines (13.2% of the overall centroid size), while the New Guinea population has the smallest supraorbital region relative to overall size (12.1%).

Table 4. Frontal Region (Supraorbital) Centroid Size

Population	CS (mm)	% Total CS
Australian	81.2809186	0.13196113
C. Europe	79.4980022	0.12733811
China	80.7682948	0.12864642
India	78.7205095	0.12539681
Medit/Near E.	79.6978906	0.12785358
New Guinea	75.5170293	0.12076372
North Africa	79.4852321	0.12594383
Singapore	82.4184126	0.1290688
Sub-Sahar Bantu	83.8174298	0.12954732
Sub-Sahar Khoisan	77.2892608	0.12725749
W. Europe	81.2599465	0.12940078
MEAN	80.4502326	0.12819432

Zygomaxillary Centroid Size. The zygomaxillary region is the largest subdivision in the overall dataset because it encompasses essentially the entire face. The global average for the zygomaxillary region is 137.42mm (see Table 5). The smallest zygomaxillary centroid size can be seen with the Sub-Saharan Khoisan (130.92mm) while the largest group with respect to this metric is the Singapore sample at 145.31mm. With respect to proportionality of the face relative to the entire cranium both the Indian and North African (both populations are at 21.4%) have the lowest zygomaxillary centroid sizes given cranial size, while the Singapore sample has the largest zygomaxillary size relative to the rest of the cranium at 22.7%.

Table 5. Zygomaxillary Region Centroid Size.

Population	CS (mm)	% Total CS
Australian	135.366329	0.219769839
C. Europe	135.6782105	0.217326302
China	141.1176379	0.224769859
India	134.4530587	0.21417525
Medit/Near E.	136.9313207	0.219669039
New Guinea	134.864436	0.21566964
North Africa	135.2278765	0.214267678
Singapore	145.3059955	0.227551952
Sub-Sahar Bantu	143.094187	0.221164842
Sub-Sahar Khoisan	130.9190456	0.215559426
W. Europe	136.7377011	0.217745229
MEAN	137.4174472	0.21896937

Mastoid Centroid Size. With respect to mastoid centroid size, the global average is 45.33mm with a large amount of geographical variation in centroid size values (Table 6). Following the regional breakdown, the smallest mastoid centroid sizes can be found within the Australian Aborigine population at 38.84mm, while the largest centroid sizes are observed within the Singapore population (49.52mm). China (48.16mm) and Western Europe (47.29mm) both demonstrate large mastoid regions, while the Sub-Saharan Khoisan (40.17mm) have the second smallest mastoid centroid size values in the global sample. With respect to mastoid size relative to the entire cranium, the Australian (6.3%) and Sub-Saharan Khoisan (6.6%) populations have the smallest proportional mastoid centroid sizes, while the largest mastoids, given cranial size, belong to the Singapore sample (7.8%).

Table 6. Temporal Region (Mastoid) Centroid Size.

Population	CS (mm)	% Total CS
Australian	38.843591	0.06306332
C. Europe	44.2203957	0.07083123
China	48.1568405	0.07670343
India	46.9549029	0.0747962
Medit/Near E.	46.7287758	0.0749636
New Guinea	45.3410467	0.07250753
North Africa	46.0240144	0.07292475
Singapore	49.5169723	0.07754452
Sub-Sahar Bantu	46.0337244	0.07114923
Sub-Sahar Khoisan	40.1659025	0.06613353
W. Europe	47.2854477	0.07529877
MEAN	45.3309235	0.07223307

Nuchal Region Centroid Size. The final subset of data pertains to the nuchal region and the overall global mean for centroid sizes here is 59.23mm (refer to Table 7). The largest centroid size in this dataset can be found in the Western European sample (63.28mm), while the smallest centroid size is present in the Australian population (56.38mm). Comparing nuchal region size to overall cranial size, the Sub-Saharan Bantu population has the smallest proportional nuchal value at 8.8%, while the Western European population has the largest proportional nuchal region (10.1%).

Table 7. Occipital Region (EOP/Occ. Torus) Centroid Size.

Population	CS (mm)	% Total CS
Australian	56.3805641	0.09153493
C. Europe	60.0505916	0.09618769
China	57.3835364	0.09139956
India	57.0520555	0.09088033
Medit/Near E.	60.1248802	0.09645401
New Guinea	61.9737984	0.09910594
North Africa	59.8492797	0.09483079
Singapore	62.04101	0.0971574
Sub-Sahar Bantu	56.8775808	0.08790938
Sub-Sahar Khoisan	58.8677591	0.09692631
W. Europe	63.2865419	0.10077939
MEAN	59.2332994	0.09438596

Regression Analysis on Centroid Size vs. Shape Data

(Complete Dataset)

In this section, centroid size is regressed against shape data to examine the overall level of correlation between the shape variables and a geometric morphometric proxy for overall size. Regressions are carried out for the 4 anatomical regions of the study, 1) Supraorbital region, 2) Zygomaxillary region, 3) Mastoid region, and 4) the Occipital Region. All results are summarized in Table 8.

Table 8. Relationship of shape to size (RW vs. CS).

Region	R^2	p-value
Frontal (Supraorbital)	0.6018	0.0001
Zygomaxillary	0.6055	0.0012
Temporal (Mastoid)	0.4841	< 0.0001
Occipital (EOP/Torus)	0.2227	0.0128

Supraorbital Region. The supraorbital region shape data demonstrates the second highest correlation with centroid size amongst all the anatomical regions with an R^2 value of 0.6018. This value is highly significant with a p-value of 0.0001.

Zygomaxillary Region. Demonstrating the highest relationship between size and shape, the zygomaxillary region shape data correlates with centroid size with an R^2 value of 0.6055. This relationship is also significant with p-value of 0.0012.

Mastoid Region. The mastoid region demonstrates a moderate degree of allometry with a R^2 of 0.4841 between the shape data and centroid size. Although the correlation is moderate in strength, the p-value for this relationship is the strongest in this analysis at $p < 0.0001$.

Nuchal Region. Finally, the occipital region provides the weakest relationship between centroid size and shape data, with an R^2 value of 0.2227. This result is also significant with a p-value of 0.0128.

Regression Analysis on Centroid Size vs. Shape Data (Male/Female Datasets)

Similar to the section above, here a regression analysis of centroid size and the relative warps (shape data) for both the male and female subsets are reported. This data for the four anatomical regions of the study is summarized in table 9.

Table 9. Relationshiup of shape to size (RW vs. CS) for Males/Females.

Region	Sex	R^2	p-value
Frontal (Supraorbital)	Male	0.7639	0.0052
	Female	N/A	N/A
Zygomaxillary	Male	0.7832	0.0274
	Female	N/A	N/A
Temporal (Mastoid)	Male	0.5359	0.0001
	Female	0.6526	0.0422
Occipital (EOP/Torus)	Male	0.2694	0.0911
	Female	0.4358	0.1985

Supraorbital Region. Similar to the complete dataset above, the frontal region dataset for the males provides the second highest correlation between size and shape with a significant R^2 value of 0.7639. While this result is significant in males, the test was not possible with the female subset due to lack of samples.

Zygomaxillary Region. The zygomaxillary region provides the highest R^2 value across all the relative warp and centroid size regressions for the male subset. The male dataset provides an R^2 value of 0.7632 for the regression and this result is significant (p-value = 0.0274). The female subset did not have the requisite sample size in order to conduct this test.

Mastoid Region. A regression of shape and size variables for the mastoid region between males and females yield significant results for both subsets. In males, there is an R^2 value of 0.5359. Females demonstrate a stronger relationship with an $R^2 = 0.6526$. Both of these results are significant (male p-value = 0.0001, female p-value = 0.0422).

Nuchal Region. The final region to be examined between males and females is the occipital region. Similar to the above results for the complete global dataset, this region provides the lowest correlations between size and shape for both males and females. Not only are these values the lowest for all anatomical regions studied (male R^2

= 0.2694, female R^2 = 0.4358), neither the male of female results provided are significant at the .05 level (male p = 0.0911, female p = 0.1985).

Regression Analysis on Relative Warps/Centroid Size vs. Coded Data (Complete Dataset)

To serve as an alternative to the large coordinate landmark dataset employed in the analyses in this chapter, discrete coding data for all the anatomical regions in question is provided in this section. Discrete data for each of the anatomical regions of the study is compared (via regression analysis) with both centroid size and relative warp data. The goal of this is two-fold: 1) Determine the level of similarity between discrete data and coordinate landmark data with regard to overall shape for each anatomical region in question, and 2) Provide an analysis to show the relationship between discrete measures of shape for each anatomical region with centroid size.

Table 10. Relationship of shape to size (RW vs. Discrete Codings).

Region	**R^2**	**p-value**
Frontal (Supraorbital)		
IN	0.8012	< 0.0001
ST	0.7733	< 0.0001
TR	0.7303	< 0.0001
Zygomaxillary		
ZT	0.5876	0.0031
ZM	0.6551	< 0.0001
Temporal (Mastoid)		
MS	0.3189	0.0015
Occipital (EOP/Torus)		
OT	0.6543	< 0.0001
OCR	0.2402	0.0054

Supraorbital Region Discrete Data. The discrete codings used to quantify the supraorbital region are: infraglabellar notch (IN), supraorbital ridge/torus (ST), and zygomatic trigone (TR) (Lahr, 1996; refer to Chapter 4 – Materials and Methods for more details). A regression analysis involving these 3 discrete codings and the relative warp scores from the geometric morphometric data demonstrate high levels of correlation between the two measures (Table 10). The correlation between IN and the supraorbital relative warp data give an R^2 value of 0.8012 (the highest in the sample) with a highly significant p-value < 0.0001. ST correlates to the shape data with an R^2 of 0.7733 (p-value < 0.0001) and the relationship between TR and the relative warp data provides an R^2 of 0.7303 (p-value < 0.0001). Overall, these correlations between the discrete codings and the geometric morphometric data show that the discrete codings are a good proxy for the landmark data.

When comparing size (using the measure of centroid size) to the discrete coding data, we find a low (but significant) correlation between the two measures. The R^2 between IN, ST, TR and centroid size is 0.2179 with a p-value < 0.0001 (see Table 11).

Table 11. Relationship of shape to size (CS vs. Discrete Codings).

Region	**R^2**	**p-value**
Frontal (Supraorbital)		
IN, ST, TR	0.2179	< 0.0001
Zygomaxillary		
ZT, ZM	0.4584	< 0.0001
Temporal (Mastoid)		
MS	0.502	< 0.0001
Occipital (EOP/Torus)		
OT, OCR	0.0039	0.7639
Complete Cranium		
IN, ST, TR, ZT, ZM, MS, OT, OCR	0.9633	< 0.0001

Zygomaxillary Region Discrete Data. Discrete coding of the zygomaxillary region uses zygomaxillary tuberosity (ZT) (Lahr, 1996, Chapter 4) and zygomaxillary massiveness (ZM). Both discrete measures demonstrate moderate levels of correlation with the geometric morphometric data (Table 10). ZT correlates with the zygomaxillary relative warp data with an R^2 of 0.5876 (p-value 0.0031). ZM has a higher R^2 value at 0.6551 (p-value < 0.001) with the zygomaxillary geometric morphometric data. These results also demonstrate that the discrete data and geometric morphometric data share an overall similarity and can be used as proxies for one another.

Zygomaxillary discrete codings also show a moderately strong relationship to overall size. The R^2 value of the regression analysis between the zygomaxillary discrete data and centroid size is 0.4584 (p-value < 0.0001). This result is the second highest among the discrete coding data (Table 11).

Mastoid Region Discrete Data. The mastoid discrete coding used in this analysis is mastoid size (MS). This discrete measure demonstrates a moderately low correlation with the geometric morphometric data with an R^2 of 0.3189 (Table 10). This result is highly significant, nonetheless, with a p-value of 0.0015.

While MS demonstrates a weak correlation with the coordinate landmark data, comparing MS to centroid size provides the strongest R^2 amongst all of the discrete variables. The R^2 value of this regression is 0.5020, with a p-value < 0.001 (Table 11).

Occipital Region Discrete Data. The two discrete measures for the occipital region are both derived from Lahr, 1996 and are occipital crest (OCR), and occipital torus (OT) (for further discussion, see Chapter 4). Regression analysis between these two variables and the geometric morphometric data give differing results (Table 10). In the other anatomical regions where more than one discrete variable is used, all the variables in question demonstrate similar levels of correlation with the coordinate data. Here, however, OT demonstrates a relatively high degree of similarity (R^2 = 0.6543, p-value < 0.001), while OCR shows little relationship with an R^2 of 0.2402 (p-value = 0.0054).

A comparison of the discrete values for occipital superstructure expression with centroid size demonstrates a near-zero relationship (in this case, a non-relationship, see Table 11). The R^2 for the occipital region analysis is 0.0039 and this result is non-significant (p-value = 0.7639). Unlike all of the discrete measures highlighted above, the values for the occipital region do not show a relationship between shape and size.

Complete Cranium Discrete Data. Finally, a regression of overall cranial size (in the form of centroid size calculated for the entire 72 coordinate landmark dataset) against all of the discrete measures used in the study provides evidence for a strong correlation between size and cranial robusticity (table 11). The R^2 value of this correlation is 0.9633, with a p-value < 0.0001. This result confirms the assertions of Lahr (1996), that cranial size (in this case size is provided as the GM metric, centroid size) is related to overall cranial robusticity.

Regression Analysis on Relative Warps/Centroid Size vs. Coded Data (Male/Female Datasets)

The following section highlights the relationships of both centroid size and GM measures of shape (relative warps) and size (centroid size) to the discrete coded data used by Lahr, 1996. Results are broken down by anatomical region, with particular attention paid to each of the discrete measures employed in this study.

Supraorbital Region Discrete Data (Male subsample). Within the male subsample, there are strong correlations between the discrete measures of robusticity (IN, ST, TR) and geometric morphometric measures of shape (relative warps, table 12). All correlations for this analysis demonstrate R^2 values at or above 0.7682 (ST showing the lowest correlation with the RW scores). All correlations for the supraorbital shape region are also highly significant with p-values at or near 0.0001. This pattern in the male subset is very similar to the global dataset discussed above.

Table 12. RW Scores and Discrete Codings in Male/Female subsets.

Region	Sex	R^2	p-value
Frontal (Supraorbital)			
IN	Male	0.8606	< 0.0001
ST	Male	0.7682	0.0042
TR	Male	0.8353	0.0001
IN	Female	N/A	N/A
ST	Female	N/A	N/A
TR	Female	N/A	N/A
Zygomaxillary			
ZT	Male	0.7071	0.2386
ZM	Male	0.8171	0.0058
ZT	Female	N/A	N/A
ZM	Female	N/A	N/A
Temporal (Mastoid)			
MS	Male	0.4360	0.0053
MS	Female	0.6610	0.0348
Occipital (EOP/Torus)			
OT	Male	0.6369	< 0.0001
OCR	Male	0.3002	0.0384
OT	Female	0.8699	< 0.0001
OCR	Female	0.4726	0.1147

A comparison of centroid size with discrete measures of supraorbital robusticity displays a different pattern, however (table 13). Here, males show a very low (R^2 = 0.0800) correlation with centroid size. This result is also non-significant with a p-value of 0.0630. While there is a weaker relationship between centroid size and discrete measures of supraorbital robusticity in the global dataset as well, the global sample does highlight a significant relationship between the two.

Table 13. Centroid Size and Discrete Codings in Male/Female subsets.

Region	Sex	R^2	p-value
Frontal (Supraorbital)			
IN, ST, TR	Male	0.0800	0.0630
IN, ST, TR	Female	0.1600	0.0474
Zygomaxillary			
ZT, ZM	Male	0.4207	< 0.0001
ZT, ZM	Female	0.4089	< 0.0001
Temporal (Mastoid)			
MS	Male	0.4552	< 0.0001
MS	Female	0.4089	< 0.0001
Occipital (EOP/Torus)			
OT, OCR	Male	0.0261	0.3118
OT, OCR	Female	0.0162	0.6861
Complete Cranium			
IN, ST, TR, ZT, ZM, MS, OT, OCR	Male	0.9782	< 0.0001
IN, ST, TR, ZT, ZM, MS, OT, OCR	Female	0.9776	< 0.0001

Supraorbital Region Discrete Data (Female subsample). Due to limitations in the size of the female dataset (n=49) and the large amount of relative warps needed to characterize shape in the supraorbital region (53 total), no reliable results can be provided (table 12).

As far as comparing centroid size with the discrete supraorbital robusticity scores, females show a weak correlation with size to the discrete codings of the region with an R^2 value of 0.1600 (table 13). This result is significant at the .05 level ($p = 0.0474$), which is not the case in the male subsample. Overall, females demonstrate a stronger relationship between centroid size with the discrete robusticity scores for the supraorbital region when compared to the male subsample.

Zygomaxillary Region Discrete Data (Male subsample). The male dataset shows that once again GM measures of shape correlate strongly with discrete measures of facial robusticity (table 12). While both ZT and ZM show strong correlation values with the

relative warp scores ($R^2 = 0.7071$ and $R^2 = 0.8171$ respectively), only the ZM correlation is significant ($p = 0.0058$). These correlations are higher then the combined global dataset.

A comparison of centroid size with the discrete measures of facial robusticity demonstrates moderately strong correlation values (table 13). In males, this relationship is highlighted by an R^2 value of 0.4207. This result is also very significant (p-value < 0.0001) and is right in line with the global sample comparison above.

Zygomaxillary Region Discrete Data (Female subsample). As with the supraorbital dataset above, the female subsample is not large enough to allow a reliable comparison of the 59 relative warps needed to characterize the zygomaxillary region (table 12).

Examining the relationship of centroid size to the discrete measures of facial robusticity, however, provides a moderately strong correlation ($R^2 = 0.4089$) that is highly significant ($p < 0.0001$, see table 13). This result is very close to the male result provided above, which demonstrates that there is a similar relationship of size to robusticity in both the male and female subsamples.

Mastoid Region Discrete Data (Male subsample). Within the male subsample, there is a moderately strong relationship between GM and discrete measures of mastoid robusticity (table 12). A correlation of MS with the 23 relative warp scores provides a R^2 value of 0.4360. This value is also very significant (p-value = 0.0053). Compared to the global sample, the males show a slightly higher correlation between these two values.

Comparing centroid size with MS shows an equally strong correlation between the two ($R^2 = 0.4552$) as is seen above with the relative warp scores (table 13). This result is also significant but is slightly lower in the strength of the correlation compared to the entire global sample.

Mastoid Region Discrete Data (Female subsample). The female subsample highlights a rather strong correlation between the relative warp scores associated with the

mastoid region and a discrete measure of mastoid robusticity (MS). The R^2 value for this correlation is 0.6610 (p-value = 0.0348), a value that is higher than both the male and the global samples provided above (table 12).

The correlation between centroid size and MS is not as strong as the shape correlation within the female subsample, and this relationship is also not as strong as it is in males but it is stronger than that of the global dataset (R^2 = 0.4089, see table 13). This correlation is also significant with a p-value < 0.0001.

Occipital Region Discrete Data (Male subsample). The last of the anatomical regions to be examined with the male and female subsets is the occipital region. As with the global comparison above, the shape data for the occipital region in males provides a strong correlation with OT, but fairly weak correlation with OCR (table 12). Both of these relationships are significant at the .05 level, however.

Comparing centroid size with discrete measures of occipital robusticity shows a different pattern (table 13). Here, there is a near-zero correlation (R^2 = 0.0261) between size and both OT and OCR, and this result is not significant with a p-value of 0.3118. The global comparison examined above displays a similar pattern.

Occipital Region Discrete Data (Female subsample). Correlations among shape with discrete measures of occipital robusticity in the female subset provide higher R^2 values than the male subset. Here, OT is strongly correlated with shape (R^2 = 0.8699, the strongest correlation in both the male and female subsets), while OCR is moderately correlated with shape (R^2 = 0.4762, see table 12). The OT correlation is significant (p < 0.0001) in this comparison, as it was with the males above, but the correlation between OCR and shape is not (p = 0.1147).

Similar to the male comparison of size with occipital robusticity, the female subsample displays a near-zero correlation amongst these two variables (R^2 = 0.0162, table 13). Additionally, this result is not significant at the .05 level (p-value = 0.6861) mirroring both the male and global patterns for the occipital region.

Complete Cranium Discrete Data (Male subsample). A final comparison conducted between overall centroid size of the entire cranium with the discrete measures of cranial robusticity within the male subsample shows a very strong correlation between these variables. The male R^2 value for this correlation is 0.9782 (table 13). This result is has a p-value < 0.0001, and illustrates the strong connection between size in shape in the male sample.

Complete Cranium Discrete Data (Female subsample). The female results for the overall centroid size/discrete robusticity scoring regression analysis provide equally strong correlations as the male subsample and complete n=140 cranial dataset. Here, R^2 = 0.9776, a result that is highly significant at the .05 level (p-value < 0.0001, see table 13). Once again, these values confirm the assertion or Lahr (1996) that cranial size is related to cranial robusticity, not only across the entire sample, but also within both the male and female subsamples.

Two-Block Partial Least Squares Analysis (2B-PLS)

The following section provides an in-depth examination of the patterns of covariation between the cranial superstructures in the present study. A series of Two-Block Partial Least Squares (2B-PLS) analyses are used to test the null hypothesis of independence (with a significant p-value providing evidence for integration) between blocks and highlight the strength of the correlations amongst the pairwise comparisons for each of the four superstructures and anatomical regions highlighted above in the RWA. Given the relevance of size in an understanding of cranial robusticity, pairwise comparisons of superstructure data (referred to from here on as "blocks") will be carried out with centroid size data (size data) as well as procrustes coordinate data (shape data). Within the shape data, patterns of coordinate landmark variation between two blocks of data can also be interpreted much like a standard RWA and as such will be discussed below also. The breakdown of the results for the 2B-PLS section are as follows (with

separate sections for size and shape comparison): 1) Comparison of the Frontal Block and Zygomaxillary Block, 2) Comparison of the Frontal Block and Mastoid Block, 3) Comparison of the Frontal Block and Occipital Block, 4) Comparison of the Zygomaxillary Block and Mastoid Block, 5) Comparison of the Zygomaxillary Block and Occipital Block, 6) Comparison of the Mastoid Block and Occipital Block. For the following sections, refer to table 14 for a summary of the findings for the PLS analysis.

Table 14. PLS Results Summary for the Present Study.

PLS (Centroid Size)	**Global**	**Male**	**Female**
Frontal-Zygomaxillary	Integration	Integration	Integration
Frontal-Mastoid	Integration	Modularized	Modularized
Frontal-Occipital	Modularized	Modularized	Modularized
Mastoid-Zygomaxillary	Integration	Integration	Modularized
Mastoid-Occipital	Integration	Modularized	Modularized
Occipital-Zygomaxillary	Modularized	Modularized	Modularized
PLS (Relative Warps)			
Frontal-Zygomaxillary	Integration	Integration	Modularized
Frontal-Mastoid	Integration	Modularized	Integrated
Frontal-Occipital	Integration	Integration	Modularized
Mastoid-Zygomaxillary	Integration	Integration	Modularized
Mastoid-Occipital	Integration	Integration	Modularized
Occipital-Zygomaxillary	Integration	Modularized	Modularized

PLS Analyses for the Global sample based on Size

(Centroid Size)

Frontal Block and Zygomaxillary Block Size Comparison. The 2B-PLS analysis undertaken for centroid sizes of both the frontal and zygomaxillary blocks provides insight into how the expression of these two anatomical regions covary with respect to one another. The overall strength of association between these two blocks of data is

0.4986, with a significance of <.0001, indicating that there is an association between these two blocks. This provides evidence for a moderately strong association of the size of the frontal (i.e. supraorbital) and zygomaxillary regions.

Frontal Block and Mastoid Block Size Comparison. Results for the 2B-PLS comparison of the supraorbital and mastoid regions also reject the null hypothesis of independence with highly significant p-value of 0.0001, but provide evidence for a very weak correlation between the sizes of the two blocks with an RV coefficient (Robert & Escoufier, 1976) of 0.0935. This result provides strong evidence that the size of the frontal and mastoid regions can be considered to be integrated, but the strength of this relationship is very weak.

Frontal Block and Occipital Block Size Comparison. The 2B-PLS comparison of the supraorbital and nuchal regions of the skull demonstrate almost no association (RV = 0.0002) and the permutation test of these data provides an insignificant p-value (p = 0.8823) failing to reject the null hypothesis of complete independence. These results show that there is no association between the size of the frontal (supraorbital area) and the size of the occipital (nuchal torus/external occipital protuberance area) and that these two anatomical regions are modularized with respect to one another.

Mastoid Block and Zygomaxillary Block Size Comparison. For this test, the size of the mastoid region was compared with the zygomaxillary region to determine the strength and significance of their relationship. The 2B-PLS results for this section demonstrate integration ($p < .0001$) and the strength of association between these two blocks is rather low relative to some of the other blocks highlighted (RV = 0.2162). These data provide evidence for integration in the sizes of these two blocks, although the strength of that association is rather weak.

Mastoid Block and Occipital Block Size Comparison. This 2B-PLS analysis shows a significant (p = 0.0138) relationship, once again rejecting the null hypothesis of independence between the sizes of the mastoid and occipital blocks with an extremely

low RV coefficient (0.0423). Much like the mastoid – frontal comparison above, this means that while these two blocks provide evidence for integration, the strength of the association between the size of these two anatomical regions is very weak.

Occipital Block and Zygomaxillary Block Size Comparison. The final 2B-PLS comparison to be carried out for the size data between the occipital and zygomaxillary datasets. As seen in the comparison of the size of the frontal and occipital regions above, there is an insignificant relationship in the size of these two blocks of data ($p = 0.1268$) with an RV coefficient of 0.0170. This means that as far as size is considered, the occipital and zygomaxillary blocks are modularized with respect to one another.

PLS Analyses for the Global sample based on Shape

(Procrustes Coordinate Data)

Frontal Block and Zygomaxillary Block Shape Comparison. The 2B-PLS output for the comparison of shape (based on the procrustes coordinates) between the frontal and zygomaxillary regions provides an RV coefficient of 0.1182 with an associated p-value = 0.0001. The level of covariation between the shape coordinates of these two structures is much lower than the covariation of centroid size, but this relationship, nonetheless, rejects the null hypothesis of complete independence.

The covariation in shape between these two structures can be demonstrated visually in a series of graphs, similar to what has been presented above in the RWA section. For each of these PLS axes, the scaling factor used was -0.2 to accentuate change from the consensus form. If a scaling factor of 0.2 is used, the same relationship between these two structures still holds true, but the expression of the landmarks will be flipped. The first PLS axis (figure Q1) accounts for 65.13% of the covariance between the supraorbital and facial regions. Here, we can see that the expansion of the medial region of the superciliary arch is correlated with an expansion of the lateral maxilla and zygomatic region of the face (and vice versa). Along the next axis, PLS2 (which

accounts for another 12.21% of the covariance, see figure Q2), there is an expansion of the frontal process of the maxilla, and an expansion of the frontal process of the zygomatic in conjunction with an expansion of the glabellar area of the supraorbital region and an overall increase in the lateral extent of the superciliary arch. Finally, PLS3 (figure Q3) accounts for 10.23% of the covariation between these two structures which can be summarized as an overall reduction in the supraorbital region (especially in the glabellar area and lateral trigone) occurring in conjunction with an overall decrease in the zygomaxillary region except in the area of premaxilla and anterior nasal aperture.

Frontal Block and Mastoid Block Shape Comparison. The PLS comparison of the frontal block and mastoid block provide a RV coefficient of 0.0804 with a respective p-value of 0.0033. While this correlation once again is low, the result indicates integration through rejecting the null hypothesis of independence.

Along PLS1 (66.58% of the covariance explained, figure Q4), the relationship of the supraorbital region and the mastoid region can best be defined as an increase in supraorbital massiveness concurrent with a widening and more squared off expression of the inferior aspect of the mastoid near the tip. PLS2 accounts for a total of 13.49% covariance explained and this component shows an inverse relationship between mastoid and supraorbital expression (figure Q5). Here, as the superciliary arch becomes more medio-laterally compressed with a slightly expanded glabellar region, there is a simultaneous inflation of the mastoid in the antero-posterior plane. Finally, PLS3 accounts for another 9.24% of the covariance explained, and this PLS component once again demonstrates a relationship of superciliary arch length to mastoid antero-posterior length. This time however, the resulting graphs show an increase in superciliary arch M-L length concurrent with an A-P compression of the mastoid closer to the mastoid tip (figure Q6).

Frontal Block and Occipital Block Shape Comparison. The final PLS shape comparison with the frontal block data involves the occipital region. Here, the shape of

the supraorbital region is compared to that of the nuchal region, with focus on the superior and supreme nuchal lines. The RV coefficient of this comparison is 0.0435, with a p-value of 0.0469, once again indicating a relationship of interdependence between the blocks.

PLS1 accounts for a large portion of the total variance at 81.16%, and this PLS demonstrates an overall relationship of supraorbital massiveness, particularly in the glabellar and medial aspect of the supraorbital region with a medio-lateral elongation (and to a lesser degree supero-inferior expansion) of the nuchal superstructures (figure Q7). PLS2, on the other hand, demonstrates an overall increase in the expression of the nuchal region, particularly in the more medial aspect of the structure, concurrent with a decrease of the more lateral aspect of the supraorbital region (from mid-orbit to the area of the lateral trigone, figure Q8). PLS2 accounts for an additional 12.45% of the covariance explained in the PLS analysis. All subsequent PLS axes cover 2% or less of the overall covariance and therefore do not cover a large enough potion of this variation to be covered here.

Mastoid Block and Zygomaxillary Block Shape Comparison. PLS results from the mastoid – zygomaxillary region comparison demonstrate a highly significant relationship between these two anatomical regions with a p-value of 0.0001. While the relationship provides evidence for integration, the RV coefficient between the mastoid and zygomaxillary region is rather low at 0.1098.

Between these two anatomical regions, PLS1 accounts for a total of 73.88% of the variance. This PLS accounts for variation in mastoid A-P width in relation to overall cheek height and facial breadth (figure Q9). As mastoid width increases, there is a concurrent increase in cheek (as well as overall facial) height and a decrease in facial breadth. The opposite is true for a decrease in mastoid width. PLS2 accounts for an additional 11.10% of the variance between these two structures. Here, mastoid A-P width (and to a lesser extent, mastoid height) is correlated with the shape of the maxilla

(figure Q10). As the mastoid ranges from very narrow in the A-P plane to being very wide, there is an inverse relationship of the maxilla ranging from expanded (particularly toward the medial aspect of the face near the nasal aperture) to reduced in its configuration. Accounting for only 4.73% of the variance (all subsequent PLS components cover 3% or less of the total variance) PLS3 demonstrates a weak relationship between mastoid width and mastoid breadth with the overall expansion of the zygomatic bone (figure Q11). Expansion of the zygomatic bone (as well as the lateral portion of the maxilla) occurs concurrently with a decrease in mastoid width, as well as slight increase in mastoid breadth.

Mastoid Block and Occipital Block Shape Comparison. The results from the PLS analysis of the mastoid and occipital regions provide a low RV coefficient of 0.0597, with an associated p-value of 0.0086, rejecting the null hypothesis of complete independence. This demonstrates another case of integration, but with a near-zero correlation in shape between the two anatomical regions.

Given that the first two PLS axes combined account for over 95% of the total variance in this comparison, only PLS1 and PLS2 will be examined here. PLS1 accounts for 85.51% of the variance between these two datasets, and demonstrates a relationship between mastoid A-P width and expansion in the nuchal region with regard to the expansion of the supreme and superior nuchal lines (figure Q12). As mastoid with decreases, there is an overall increase in the expansion of the nuchal lines (particularly in the supero-inferior plane), highlighting an inverse relationship between robusticity of these two structures. PLS2 accounts for another 10.59% of the variance present in this dataset, and this component addresses variation in mastoid width and breadth relative to the overall expansion (both in supero-inferior dimensions, as well as posterior projection) of the nuchal region (figure Q13). As the mastoid increases in both the M-L and A-P planes, there is a correlated increase in nuchal superstructure projection (expansion of the

nuchal lines into a nuchal torus-like configuration) as well as an increase in the supero-inferior dimensionality of this region.

Occipital Block and Zygomaxillary Block Shape Comparison. The final pairwise shape comparison conducted for the PLS results is between the occipital and zygomaxillary blocks. The RV coefficient of this PLS is higher than most of the coefficients determined thus far, but is still incredibly low at 0.1626. This result rejects the null hypothesis of independence with a p-value of 0.0363.

The first 3 PLS components account for a total of almost 95% (94.991%) of the total overall variance between these two structures. PLS1 covers 58.26% of the variance and this component associates expanded nuchal regions with diminished facial regions (figure Q14). With a reduction in zygomaxillary expression (particularly in check height, massiveness of the zygomatic body, and thickness of the frontal process of the zygomatic) there is a connection to the expansion of the nuchal lines (particularly in the medial aspect of the occipital) in both supero-inferior spacing, as well as projection. PLS2 accounts for another large portion of the variance at 31.72% and this component addresses expansion of the nuchal lines in length and spacing in association with an increase in facial breadth (figure Q15). As the nuchal region expands, as denoted by an increase in the length and spacing of the superior and supreme nuchal lines, there is an increase in facial breadth as well as an expansion of the premaxillary region resulting in an increase in alveolar prognathism. Finally PLS3 ties nuchal expression with the overall massiveness of the lateral face (particularly in the region of the zygomatic bone) and this component accounts for another 4.993% of the variance (figure Q16). An expansion of the zygomatic region of the face is associated with an overall increase in the size of expression of the medial aspect of the nuchal lines as well as an increase in the curvature of both the superior and supreme nuchal lines.

PLS Analyses for the Male/Female subsamples based on

Size (Centroid Size)

Frontal Block and Zygomaxillary Block Size Comparison. Size comparisons between the frontal and zygomaxillary blocks in the male and female subsets both yield moderate and high RV coefficients. The male subsample shows an RV coefficient of 0.3824 (p-value < 0.0001) and the female subsample shows an RV coefficient of 0.5028 (p-value < 0.0001). Both of these results indicate a pattern of integration (similar to the global sample discussed above) and demonstrate the highest level of covariation in size between any of the male/female 2-block comparisons, implying that the size of both of these anatomical regions share a similar pattern of covariation between males and females.

Frontal Block and Mastoid Block Size Comparison. The level of covariation between the frontal and mastoid block is very low compared to the frontal/zygomaxillary comparison above. Here, there is a low RV coefficient of 0.0419 between these two blocks in the male subsample and an even lower RV of 0.0079 in females. Both of these results fail to reject the null hypothesis of complete independence (p = 0.0526 for the male comparison and p = 0.5394 for the females) but the male result is nearly significant at the .05 level.

Frontal Block and Occipital Block Size Comparison. As with the global sample above, this comparison among the male and female subsamples provide evidence for a modularized nature of the frontal and occipital blocks. RV coefficients for both comparisons demonstrate near zero-level correlations (males = 0.00190, females = 0.01080) and these results are highly non-significant (a male p-value = 0.6760, the highest all 2-block size comparisons, and a female p-value = 0.4810) indicating that they are not independent units.

Mastoid Block and Zygomaxillary Block Size Comparison. The mastoid/zygomaxillary block comparison demonstrates another highly significant

correlation for the male subsample. Here, males have the second highest RV coefficient of 0.1967 for the entire set of 2-block comparisons, second only to the level of covariation between the frontal and zygomaxillary blocks. This result is highly significant with a p-value < 0.0001. The female comparison, on the other hand, provides a much lower RV = 0.0558, and this result is not significant (p-value = 0.1058). This shows that there is a relationship between the size of the facial and mastoid regions in males, but such a relationship does not appear to exist in females.

Occipital Block and Zygomaxillary Block Size Comparison. As with the frontal/occipital block comparison above, there is little evidence for size correlation between occipital and zygomaxillary blocks. Males and females show extremely low RV coefficients (0.0044 and 0.0079 respectively) with non-significant p-values (0.5301 for males and 0.5463 for females). This result is also similar to that of the global dataset for these two block, indicating a pattern of modularity in the occipital block.

Mastoid Block and Occipital Block Size Comparison. The last comparison to be conducted here is between the mastoid and occipital blocks. While both the males and females demonstrate low RV coefficients (males = 0.0114 and females = 0.0791) the female relationship provides a near-significant p-value of 0.0525, which almost provides evidence for integration between these two anatomical regions. The p-value for the male comparison, however, is non-significant at 0.3112. This implies that while there is no evidence for integration between these two blocks for the males, there is much more relevant connection between the mastoid and occipital in females.

PLS Analyses for the Male/Female subsamples based on Shape (Procrustes Coordinate Data)

Frontal Block and Zygomaxillary Block Shape Comparison (Male subsample). PLS results for the frontal and zygomaxillary block comparison of shape show a RV coefficient of 0.1618 with a highly significant p-value of 0.0002. This implies that while

there is a low correlation between the shapes of these two anatomical regions, the nature of the co-expression (i.e. integration) between the frontal and zygomaxillary regions is highly significant. The bulk of variation between these two blocks is covered in the first three PLS axes, accounting for a combined total of 86.08% of the total variance.

PLS 1 accounts for 57.13% of the total variation between the supraorbital and zygomaxillary region (figure R1). Along this axis, expansion of the face, especially the maxillary region of the face, is closely tied to a supero-inferior expansion of the supraorbital region in males. Smaller maxillary regions are seen in conjunction with a reduction in supero-inferior dimensionality and a substantial increase in anterior projection of the supraorbital region. PL2, addressing an additional 18.28% of the total variation, highlights variation between the glabellar and lateral trigone regions of the supraorbital area with aspects of zygomatic and maxillary expansion (figure R2). Increases in the both the glabellar and lateral trigone portions of the supraorbital region are seen in conjunction with an increase in the maxillary region of the facial skeleton. There is also a medio-lateral expansion of the frontal process of the maxilla tied to the glabellar/lateral trigone expansion of the supraorbital region. Finally, PLS 3 accounts for 10.67% of the variance between these two anatomical regions and this variation is characterized by expansion of the supraorbital region with changes in orbital size and shape (figure R3). Along this axis, an increase in supraorbital region robusticity (particularly anterior projection and overall expansion of the midorbital aspect of the supraorbital region) is related to an overall expansion of orbital size. Orbital expansion is indicated by an increase in the distance between the frontal process of the maxilla and the frontal process of the zygomatic. There is also an increase in the zygomatic region of the face as a response to increased levels of robusticity in the supraorbital region.

Frontal Block and Zygomaxillary Block Shape Comparison (Female subsample). The PLS results for the female subsample with regard to the frontal and zygomaxillary comparison show a low correlation and non-significant p-value between the two blocks.

The RV coefficient for this comparison is 0.1446, with a p-value of 0.2384. The first four PLS axes cover a total of 81.28% of the variance and are covered in greater detail below.

PLS 1 explains 50.29% of the variance and this component defines a relationship between zygomaxillary massiveness and supraorbital projection (figure R4). Much like the male comparison discussed above, the greatest amount of variation between these two regions in females can be summed up as follows: supero-inferiorly reduced but more anteriorly projecting supraorbital regions are expressed simultaneously with an overall reduction in zygomaxillary architecture. Increases in supero-inferior height of the supraorbital region are related to an overall expansion of the face (particularly in lateral aspect). PLS 2 addresses expansion in the glabellar region along with an increase in the zygomatic region, and this second component addresses another 14.67% of the total variance (figure R5). Along this component, glabellar expression is tied to maxillary and zygomatic expression, with larger glabellar regions being tied to expansion of the maxillary region (particularly in maxillary projection) and reduced glabellar regions being tied to an increase in zygomatic expression. This component is also similar its patterning to the male comparison highlighted above. The third component, PLS3, addresses 9.685% of the variance and shows a relationship between a reduction of supraorbital projection with an expansion of the lateral portion of the face (figure R6). A flattening of the supraorbital region (which occurs simultaneously with an expansion of supraorbital height, particularly at glabella) appears to be accompanied by an increase in both zygomatic size as well as an increase in the massiveness of the frontal process of the zygomatic. An increase in supraorbital (particularly midorbit) anterior projection is seen in conjunction with an increase in the medial aspect of the face (with an expanded maxilla and in increase in the massiveness of the frontal process of the maxilla). Finally, PLS 4, accounting for 6.64% of the remaining variance, addresses variation in a reduction of the lateral aspect of the supraorbital region and a reduction in the width but increase in

the length of the frontal process of the zygomatic (figure R7). Along this component, a decrease in the robusticity of the later porion of the supraorbital region (at the location of the lateral trigone) is tied to a decrease in the massiveness of the frontal process of the zygomatic. These two anatomical regions combined demonstrate that PLS 4 highlights the relationship between the lateral trigone and the lateral portion of the face defined by the zygomatic bone. An increase in the projection and massiveness of the lateral trigone is tied to an increase in width, but a reduction in height of the frontal process of the zygomatic.

Frontal Block and Mastoid Block Shape Comparison (Male subsample). A comparison of the frontal block data with the mastoid block in males yield a very low RV coefficient of 0.0663 with a non-significant p-value (0.3872). The first 3 PLS components address the majority of the variation in the subsample, accounting for a combined total of 82.32% of the variance.

PLS 1 accounts for 50.26% of the total variance and this component addresses variation in supraorbital height and projection with mastoid antero-posterior width (figure R8). Less projecting but more supero-inferiorly expanded supraorbital regions are seen in conjunction with an increase in mastoid width, particularly more inferiorly along the mastoid near the mastoid tip. A more reduced mastoid (particularly in width) is tied to a smaller but more anteriorly projecting supraorbital region. PLS 2 (accounting for another 18.56% of the variance) demonstrates a link between the massiveness of glabella and mastoid robusticity (figure R9). As glabellar massiveness in both supero-inferior and anterior projection increases, there is a subsequent increase in mastoid medio-lateral breadth. Reduction of the glabellar region coincides with a reduction in the mastoid region as well. PLS 3 addresses 13.50% of the total variance, and this final component demonstrates a relationship between supraorbital projection and mastoid height and width (figure R10). An increase in supraorbital projection and supero-inferior height (particularly at the midorbit region) is associated with an increase in mastoid height but a

reduction in mastoid antero-posterior width. A more reduced supraorbital region is tied to a decrease in mastoid height, but a noticeable increase in mastoid width.

Frontal Block and Mastoid Block Shape Comparison (Female subsample). The female subsample PLS for the frontal and mastoid block comparison provides the highest RV coefficient (0.1659) for all the female block comparisons. The relationship between these two blocks is verified by a significant p-value of 0.0296. Unlike the male comparison between these two blocks discussed above, the female sample demonstrates a pattern of integration between these two components. The first three PLS components summarize 89.97% of the total variance, and these components will be addressed in further detail below.

PLS 1 accounts for 69.39% of the total variance and this component addresses variation in supraorbital height and mastoid a-p breadth (figure R11). An increase in supraorbital height, along PLS 1, is accompanied by an increase in mastoid a-p width (particularly near the mastoid tip). A decrease in the expression of the supraorbital region, therefore, yields a less robust mastoid process. PLS 2 (11.20% variance explained) contrasts glabellar and lateral trigone robusticity with mastoid height and medio-lateral breadth (figure R12). Expansion of the glabellar and midorbit aspects of the supraorbital region coincide with an increase in mastoid height and breadth. A decrease in mastoid robusticity (marked by a decrease in height and breadth) is associated with an increase in lateral trigone size. Finally, PLS 3 addresses another 9.38% of the variance and this last component again contrasts glabellar and lateral trigone robusticity with aspects of mastoid height and breadth (figure R13). Along PLS 3, an increase in glabellar height and anterior projection is associated with an increase in mastoid antero-posterior width. At the other end of the range of variation, an increase in lateral trigone size (following a decrease in massiveness of glabella) is accompanied by an increase in mastoid medio-lateral breadth.

Frontal Block and Occipital Block Shape Comparison (Male subsample). A PLS comparison of the frontal and occipital blocks in the male subsample provides a low correlation with evidence of integration (RV = 0.0721, p-value = 0.0319). While there are a total of 17 PLS components generated from these two blocks, only the first two components account for any significant portion of the variation. PLS 1 and PLS 2 combined explain 94.38% of the total variance, and as a result, these are the only components to be considered below.

PLS 1 accounts for 81.81% of the total variance, and this component contrasts robust and gracile supraorbital regions with occipital morphology that varies between an external occipital protuberance and a occipital torus configuration (figure R14). Along this component, an overall decrease in supraorbital massiveness (both in height and lateral projection, with the exception of having a slightly more projecting glabellar region) is tied to a more gracile external occipital protuberance with diminished superior and supreme nuchal lines. An increase in supraorbital robusticity, however, is accompanied by a substantial increase in the expression of the superior and supreme nuchal lines, forming a torus-like configuration. PLS 2 (12.52% variance explained) demonstrates a connection between supraorbital projection and an increase in the spacing between the superior and supreme nuchal lines (figure R15). Supraorbital configurations that have increased height dimensions are correlated with superior and supreme nuchal lines that have very little spacing in between, while increased supraorbital projection is accompanied by a greater supero-inferior spacing of the nuchal lines.

Frontal Block and Occipital Block Shape Comparison (Female subsample). As with the male subsample above, the female subsample demonstrates an equally low level of correlation (RV = 0.0733) between these two blocks. Unlike the male subset above, however, the female relationship in non-significant (p-value = 0.2928). The first two PLS axes cover 93.14% of the total variance, and thus are the focus of this comparison.

PLS 1 accounts for 81.50% of the total variance across this comparison, and it provides evidence for a link between robust supraorbital morphology and an expansion of nuchal morphology (figure R16). As supraorbital robusticity increases along this component (particularly in supraorbital height and projection, especially at glabella), there is an increase in the length of the supreme nuchal line (although its morphology is not increased to the point of forming a torus). A reduction in supraorbital robusticity is seen with an overall decrease in the length of the supreme nuchal line. PLS 2 (addressing an additional 11.63% of the total variance) compares supraorbital height with aspects of nuchal line spacing (figure R17). Here, supraorbital height dimensionality shows an inverse relationship with the distance between the superior and supreme nuchal lines. Therefore, closely spaced nuchal lines are seen in conjunction with an expanded supero-inferior supraorbital morphology, while in increase in the spacing between the superior and supreme nuchal lines is associated with diminished supraorbital heights.

Mastoid Block and Zygomaxillary Block Shape Comparison (Male subsample). A comparison of the zygomaxillary and mastoid blocks within the male subsample provides second highest correlation (with the highest being seen between the supraorbital and zygomaxillary blocks) and a significant relationship, with an RV coefficient = 0.1385 and a p-value = 0.0023. The first three PLS components explain a combined 87.05% of the variance, and are expanded upon below.

PLS 1 addresses 70.03% of the total variance and this component shows a relationship between overall facial size with mastoid antero-posterior width (figure R18). A decrease in mastoid width (accompanied with a slight increase in mastoid height) is associated with an overall decrease of the zygomaxillary complex, yielding reduced facial morphologies. As mastoid width increases (followed by a decrease in mastoid height), there is a concurrent increase in overall facial massiveness. PLS 2 also compares aspects of mastoid height and width with facial massiveness (as in PLS 1), and this component explains another 9.55% of the variance in the dataset (figure R19). Here, and increase in

overall maxillary mass, particularly in the frontal process of the maxilla, is associated with mastoids that have increased antero-posterior width dimensions as well as decrease heights. An increase in the size of the zygomatic portion of the facial complex as well as the frontal process of the zygomatic is accompanied by an increase in mastoid height and a decrease in mastoid width. Finally, PLS 3 addresses the covariation of mastoid width and breadth with a marked increase or decrease in zygomaxillary expression, and this last component addresses 7.48% of the remaining variance (figure R20). As with the other components discussed in this section, PLS 3 compares overall zygomaxillary massiveness with mastoid width. Larger and more robust zygomaxillary regions are seen in conjunction with wider (in the a-p plane) mastoids that have decreased m-l breadths. As the zygomaxillary region becomes more gracile, there is a decrease in mastoid width, but an increase in mastoid breadth.

Mastoid Block and Zygomaxillary Block Shape Comparison (Female subsample). The female subsample provides a similarly high correlation value to the males between the mastoid and zygomaxillary regions (RV = 0.1340), but unlike the male subsample, this relationship is non-significant (p-value = 0.2365). The results for this comparison provide a total of 23 PLS axes, with the first two components addressing the largest amount of the variance (77.56%).

PLS 1 explains 50.86% of the total variance across this mastoid-zygomaxillary block comparison (figure R21). Along this component, expansion of the mastoid region in antero-posterior width (most noticeably near the mastoid tip) is accompanied by an overall expansion of the zygomaxillary region. More diminished zygomaxillary regions (particularly in cheek height) are seen with a more gracile mastoid process that is considerably reduced in antero-posterior dimensions. PLS 2, the final component to be examined here highlights variation between the expansion of either the lateral or medial portion of the zygomaxillary complex with changes in both mastoid height and width (figure R22). This component covers an additional 26.70% of the variance, which is a

rather high value given the other two block PLS analyses discussed thus far. Expansion of the medial portion of the face (particularly around the maxillary region) is seen in conjunction with mastoid processes that are both supero-inferiorly elongated and have a larger medio-lateral breadth component. Reduction in the height and breadth of the mastoid is seen with faces that have reduced maxillae but more prominent zygomatic regions. Mastoids that are tied to this second facial configuration type display an increased antero-posterior width component.

Occipital Block and Zygomaxillary Block Shape Comparison (Male subset). The PLS comparison of the occipital and zygomaxillary blocks yields a low RV coefficient of 0.0526 with a non-significant p-value = 0.2210. This analysis provides a total of 17 components; with only the first two covering any significant amount of variation (the total variance explained between PLS 1 and PLS 2 is 89.11%). These two components will be discussed in further detail below.

This first PLS component for the occipital/zygomaxillary block comparison addresses 70.49% of the total variance, and this component demonstrates an association between nuchal line morphology and an overall expansion or reduction of the zygomaxillary region (figure R23). An overall decrease in facial morphology, denoted by smaller cheek heights and an overall more gracile appearance of the zygomaxillary region, is related to a more inferiorly placed superior nuchal line and a reduced supreme nuchal line. As zygomaxillary size and robusticity increase, there is a simultaneous increase in the length of the supreme nuchal line with the superior nuchal line being placed much higher on the occipital so that the nuchal lines as spaced closely together. PLS 2 (explaining another 18.62% of the total variation) addresses variation in the size and spacing of the nuchal lines with changes in medial and lateral zygomaxillary morphology (figure R24). Expansion in the both the lengths of, and spacing between the superior and supreme nuchal lines is seen in conjunction with an increase in medial facial expression. This nuchal morphology is tied to an increase in the size of the maxilla and

a slight decrease in the massiveness of the zygomatic. An overall decrease in the size and spacing of the nuchal lines is related to an expansion of the frontal processes of the zygomatic and maxillary bones.

Occipital Block and Zygomaxillary Block Shape Comparison (Female subset). A PLS comparison of the occipital and zygomaxillary blocks yields an RV = 0.1122, that indicates a modularized nature between these two blocks with a p-value = 0.0802 (although this value is close to significance at the .05 level). The first two PLS components address the majority of the variance between these two blocks at 92.95%.

PLS 1 accounts for 82.27% of the total variance and this variation in manifested as inverse relationship between facial and occipital robusticity (figure R25). A more gracile zygomaxillary configuration is associated with larger superior and supreme nuchal lines, while a decrease in nuchal line expression (especially supreme nuchal line length) is associated with an increase in zygomaxillary robusticity (particularly in respect to the maxillary region). PLS 2 highlights variation in the orientation and projection of the zygomatic with aspects of supreme nuchal line morphology, and this second component addresses another 10.68% of the dataset variance (figure R26). Zygomatics that are more posteriorly projecting and slightly superiorly oriented are associated with superior and supreme nuchal lines that are spaced farther apart. As the nuchal lines become more closely aligned, there is a reduction in the projection of the zygomatic and the posterior portion of this region is more inferiorly oriented.

Mastoid Block and Occipital Block Shape Comparison (Male subsample). The final PLS shape comparison to be discussed here is between the mastoid and occipital blocks. In males, this comparison yields a low (although relatively moderate compared to the other block comparisons above) RV = 0.1100, which rejects of null hypothesis of complete independence (p-value = 0.0021). Interestingly, the first PLS component addresses the vast majority of the dataset variance at 92.44%, with all subsequent

components accounting for 2% or less of the dataset variance. As a result, only PLS 1 will be covered in detail here.

PLS 1 shows a relationship between mastoid robusticity and the presence of a 'torus-like' occipital configuration (figure R27). An increase in the length and massiveness of both the superior and supreme nuchal lines is accompanied by an increase in mastoid antero-posterior width, but a slight decrease in mastoid height and breadth. A much more gracile occipital configuration, demonstrated by a decreased length of the superior and especially the supreme nuchal lines (forming an external occipital protuberance in this case) is associated with increased breadth and height dimensions for the mastoid process.

Mastoid Block and Occipital Block Shape Comparison (Female subsample). The female results for the mastoid/occipital block shape comparison provide a lower RV coefficient than the males (RV = 0.0836) with a non-significant p-value = 0.1468. The first two components address a combined 94.57% of the variance, with all of the other components addressing only 2% or less of the variance.

PLS 1 demonstrates a link between mastoid and occipital robusticity, and this component addresses 69.53% of the variance between these two blocks (figure R28). An increase in mastoid robusticity, particularly in width and breadth, is seen in conjunction with a sizeable increase in the length and spacing of the superior and supreme nuchal lines. Mastoids that have reduced width and breadth dimensions are associated with decreased occipital morphology, particularly in the length of the supreme nuchal line. PLS 2 (25.04% variance explained) shows an inverse relationship between the robusticity of the mastoid and occipital regions (figure R29). An increase in mastoid width along this component is tied to a decrease in the spacing of the superior and supreme nuchal lines. As mastoid width decreases, however, the superior and supreme nuchal lines become more prominent in their spacing, but there is a slight decrease in the length of the supreme nuchal line as a result.

A Note on Sample Composition and Analysis

The analyses included in this study have been presented for the global sample and for the male and female subsamples (this chapter), as well as across all 11 geographical subsamples (Appendix A). As noted in Chapter 4, the focus of this investigation is to understand the patterning and variation of craniofacial robusticity in a large, diverse, sample of recent *Homo sapiens*. While a discussion is provided for subsample comparisons in the next chapter, as well as in Appendix A, primary consideration is given to the global results throughout the rest of this dissertation. As noted previously, sex was estimated for most of the individuals included in the study. Given the general lack of documentation for sex across all samples studied, and the added concern of using robusticity characteristics to determine sex, it is argued here that the global sample provides the most conservative unit of analysis for the remainder of the thesis. The rationale for pooling the subsamples is twofold. First, while males and females show some differences in overall craniofacial robusticity with respect to size, both subsamples are rather similar in overall shape. Given that extant *Homo sapiens* is not a very sexually dimorphic species compared to fossil hominins or the great apes (Shea, 1985; O'Higgins & Dryden, 1993; Richmond & Jungers, 1995; Kelley, 1995), combining these subsamples maximizes variation and removes the concern of under or over representing gracile or robust craniofacial morphology. Secondly, combining samples avoids the conundrum of analyzing robusticity features between subsamples defined primarily by craniofacial robusticity. Steps were taken to maximize accuracy in sex determination (see Chapter 4), but, as with any study that must estimate sex from craniofacial skeletal markers, misclassification is possible. For example, as noted recently by Maddux and Franciscus (2009), a recent independent corroborative study using standard osteological variables in a contemporary regionally specific sample from the Balkans (Đurić et al., 2005) documented a drop from near 100% accuracy based on aggregate pelvic traits to only ca. 70% when using aggregate skull features. Additionally, mandibular robustness

was by far the single best indicator among skull features. Therefore, skulls lacking mandibles, as in the present study, would be even more difficult to sex accurately. Interestingly, the determination of sex based on isolated fossil hominin crania is even more difficult (Genovés, 1954; Armelagos and Van Gerven, 1980; Sládek et al., 2001; Brůžek et al., 2006). By pooling the samples, this negates the possibility of errors where gracile males are misclassified as females and robust females are classified as males. Finally, it should be noted that Baab et al. (2010) also use a combined sex sample in their recent work in craniofacial robusticity in order to maximize sample sizes and to maximize variability in their dataset.

CHAPTER 6. DISCUSSION

The Relationship of Shape to Cranial Robusticity

Discrete Data and Relative Warps: Comparing the present study with past research

Overall, the shape variation captured by both discrete measures of craniofacial robusticity and the coordinate based approach employed in this study demonstrate relative close affinities to one another. This implies that the novel approach used here is compatible with previous studies of robusticity while providing greater analytical detail and more vigorous quantification of robusticity size and shape. Because of this, coordinate based methods are favored by the present study. However, in order to maintain continuity with the recent work of other researchers (such as Baab et al., 2010) discrete methods of quantifying craniofacial robusticity are discussed as well.

Shape Variation in the Global Sample

The following section will discuss shape within each of the anatomical regions studied.

Frontal Region Variability and Supraorbital Robusticity. The frontal region, encompassing the superciliary arches (or in the most extreme cases, a supraorbital torus) demonstrates variation in several key aspects of morphology. Across the global sample, the aspect of the supraorbital region that accounts for the greatest amount of variation (and therefore is a key factor in defining the superstructure in *Homo sapiens*) is medio-lateral length. This aspect, which accounts for 33.6% of the variation explained, is the primary factor in highlighting a difference between a weakly defined superciliary arch (if one is even present) and a hyper-robust fully expressed supraorbital torus along a scale appropriate to recent *Homo sapiens*. Given this result, a robust supraorbital region in extant humans is in great measure a mediolaterally expanded region.

The second largest component of variation is found in supero-inferior height with robust supraorbital regions being rather expansive in the S-I plane. This aspect of variation has been documented in other works that consider fossil hominins in addition to extant *Homo sapiens* (see Vinyard and Smith, 1997; 2001; Smith & Ranyard, 1980), and is also noted as an important aspect of variation here.

Surprisingly, when the entire global sample is considered, anterior projection of the supraorbital region is only weakly expressed on the first two components. Given the results of the relative warps analysis, the variability in projection across the supraorbital region is tied primarily to lateral trigone size and variation in supero-inferior height. It is likely that anterior projection may play a larger role in the variability encompassing pre-modern and modern populations, and that this aspect of supraorbital morphology may be more important in considerations of defining the supraorbital region for those groups.

Across extant *Homo sapiens* therefore, the most important aspects of supraorbital robusticity variability encompass the expansion of supraorbital length and supraorbital height.

Zygomaxillary Region Variability and Facial Robusticity. Unlike the supraorbital region, the zygomaxillary region displays a wider and more complex pattern of variability with respect to extant facial robusticity. Along the primary axis of variation, three modes of variation can be identified: 1) variability in facial massiveness and projection, 2) antero-posterior expansion of the zygomatic region, and 3) an increase (or decrease) in cheek height. The interplay of these three factors is rather complex, with an increase in facial projection (seen primarily as alveolar prognathism) being tied to A-P expanded zygomatics that also display reduced cheek heights. Given that facial robusticity has a relatively high correlation with size (see below) it would be expected that an increase in the expression of each of these areas would result in a robust facial configuration. The data presented here demonstrate a more complex and nuanced relationship, however.

Across the components explaining the greatest amount of variation for the facial region, the zygomatic appears to play a primary role in the morphological variability of robusticity. Aspects of facial variation that interface with the frontal (and therefore the supraorbital region) are highlighted on the second relative warp component. A primary aspect of variability involves the frontal process of the zygomatic. Here, larger frontal processes (particularly in antero-posterior width as the specific shape aspect) are contrasted with smaller ones. Given that this area also encompasses the lateral trigone (which is typically considered to be a supraorbital feature); this result provides further support for the idea of considering aspects of zygomaxillary and supraorbital robusticity in unison (see Endo, 1966; Russell, 1985, Hylander et al., 1991; Moss and Young, 1960).

Apart from the alveolar region, the maxilla does not play as large a role in facial robusticity variability as the zygomatic bone in extant humans, but some notable aspects exist. Supero-inferiorly expanded maxillae accompany elevated levels of alveolar expansion, while a decrease in this aspect of morphology accompanies an increase in the width component of the facial region (see also Maddux & Franciscus, 2009).

In light of this, a consistent definition of extant facial robusticity proves to be more complicated than the other anatomical regions studied. Variability in zygomatic antero-posterior length, alveolar projection, and maxillary height all appear to be primary factors, and size must also be factored in characterizing robusticity for this region as well (see below). Increase in the expression of these three key factors of facial variability (along with overall zygomaxillary massiveness) collectively constitute a robust facial region. A discussion of the PLS results between the frontal and zygomaxillary data proves to be more enlightening on this topic and will be considered in further detail below.

Temporal Region Variability and Mastoid Robusticity. As opposed to the zygomaxillary region, characterizing variability in mastoid robusticity is more straightforward. Across the global dataset, the primary factor reflective of mastoid

robusticity is inferior projection. Robust mastoids are characterized by a high degree of projection beyond the basicranial plane. Mastoids that demonstrate high levels of inferior projection also tend to have a rather large medio-lateral breadth and antero-posterior length components to their morphology. Mastoid medio-lateral breadth on the other hand, plays a smaller role in robusticity variation. The addition of the latter aspect thus is important in overall mastoid shape characterization.

Another large component of mastoid shape variation involves the anterior versus posterior orientation of the mastoid tip. However, depending on the relative warp axis, larger more robust mastoids can be shown to either be anteriorly oriented, or posteriorly oriented, indicating that while orientation is a factor in mastoid variability, its relationship to mastoid robusticity is highly variable and does not reflect robusticity per se.

Across the global dataset, the most reliable indicator of mastoid robusticity involves mastoid inferior projection and mastoid antero-posterior length. A-P elongated and more inferiorly projecting mastoids in extant humans constitute the robust condition for this feature, while a more gracile mastoid is characterized by decreased projection and antero-posterior length. An increase in mastoid medio-lateral breadth also tends to accompany an increase in mastoid projection and overall robusticity.

Occipital Region Variability and Nuchal Robusticity. Variability in nuchal robusticity appears to be the most straightforward and tractable throughout the global dataset. The primary distinction made in past studies of occipital robusticity in recent *Homo sapiens* and pre-modern hominin fossils involves the degree of expression of a nuchal torus (Lahr, 1996, Trinkaus & LeMay, 1982; Lieberman et al, 2000a). A nuchal torus constitutes an extreme in the morphology of the superior and supreme nuchal lines. An increase in the size, length, and projection of these morphological features are thus used to describe a hyper-robust torus configuration. While this condition has been noted in pre-modern hominin fossils (primarily in *Homo erectus*, see Anton, 2002; Wood,

1991), the global dataset provided here also demonstrates that some variability along this component exists in recent *Homo sapiens* as well.

The more common condition in the present study is for a reduced superior nuchal line (both in length and projection) coupled with a very diminutive supreme nuchal line (which in these cases forms the external occipital protuberance). This structure is highly variable, however, constituting 73.8% of the total variance for the occipital region dataset. The robust configuration for this region in extant humans involves a large expansion of the superior and supreme nuchal lines, encompassing a medio-lateral length component, as well as supero-inferior height component, but, importantly, not an A-P projection element.

It should be noted that while the more robust torus-like configuration is not very common in recent *Homo sapiens*, this morphology does appear in some of the populations studied (primarily the Australian subsample, but single outliers in the Central Europe, Chinese, and Mediterranean subsamples were observed as well), albeit to a much lesser extent than observed in non-human fossil hominin groups.

The Relationship of Size to Cranial Robusticity

Discrete Data and Centroid Size: Comparing the present study with past research

While many studies agree that size has a considerable influence on cranial robusticity (Lahr, 1996; Lahr & Wright, 1996; Gauld, 1996; Ravosa, 2000), this has been called into question more recently (Baab et al, 2006). This disagreement regarding the relationship of overall size to craniofacial robusticity warrants closer attention. Most previous studies have used employed Lahr's (1994, 1996) coding criteria for craniofacial superstructures in order to understand the relationship of this discretely coded data with some overall measure of size. This study has also used this approach (in addition to the geometric morphometric approach) in order to compare results with previous studies.

Where this study differs from previous studies that have set out to address the relationship of size in robusticity is how "size" is defined. Here, size is considered as the centroid size of the anatomical region in question. Given that centroid size is the square root of the sum squared distances of each landmark in the dataset to the centroid (the mean of all landmarks), and that this measure is calculated as part of Procrustes superimposition, it serves as a useful, convenient, and objective measure of size (Bookstein, 1989, Guy et al., 2003).

For the complete n=140 extant global sample, the mean centroid size for the supraorbital region as calculated is 80.5mm. This superstructure encompasses 12.8% of the overall centroid size of the craniofacial landmark dataset. When comparing the data derived using Lahr's (1994, 1996) coding scheme with supraorbital centroid size, the results show a rather low association of these two measures ($R^2 = 0.2179$, $p < 0.0001$). While this result is statistically significant, it demonstrates a rather low association between discrete coding values and overall centroid size for the supraorbital region. This implies that while size does have an effect on the expression of the supraorbital region as defined in discrete values (i.e. demarcating a weak superciliary arch versus a heavily built supraorbital torus) its effect is rather small. When the relationship of centroid size and discrete robusticity scores for the supraorbital region is considered with respect to sex, this association is even weaker. Both males and females demonstrate low level correlations (male $R^2 = 0.0800$, $p = 0.0630$, female $R^2 = 0.1600$, $p = 0.0474$) with the male sample result being non-significant at the .05 level.

The zygomaxillary region is the largest studied within the global dataset. With an average centroid size of 137.4mm, this region encompasses 21.9% of the size for the entire landmark dataset. There is a rather moderate correlation of overall zygomaxillary size to discrete codings of robusticity for this region demonstrated by an R^2 value of 0.4584 and this result is highly significant ($p < 0.0001$). While not the highest correlation of size to discrete measures of robusticity, the zygomaxillary subset does provide

evidence for a moderate degree of size related shape variability in the discrete data. This result implies that size does play a role in previously employed definitions of facial robusticity. Males and females both follow the trends seen in the global sample, with moderately high R^2 values of 0.4207 and 0.4089, respectively. Both of these results are significant and suggest that in both males and females, the size of the zygomaxillary region is tied to robusticity expression.

With respect to the mastoid region, the mean centroid size across the global sample is 45.3mm. This is the smallest anatomical region in the present study and only encompasses 7.2% of the overall craniofacial coordinate landmark dataset. Interestingly, the mastoid centroid size data shows the highest correlations with discrete measures of overall mastoid robusticity ($R^2 = 0.5020$, p-value < 0.0001). This highly significant result demonstrates that like the zygomaxillary subset, the mastoid subset also provides a rather strong support for the influence of size on overall superstructure robusticity. The male and female datasets also mirror this result with R^2 values slightly below the global dataset.

For the final region, the occipital area, which focuses primarily on the expression of nuchal robusticity by means of the superior and supreme nuchal lines, the mean centroid size across the entire sample is 59.2mm, which encompasses 9.4% of the entire craniofacial coordinate landmark dataset. Unlike the previous anatomical regions, the occipital data shows no association of size to shape. Here occipital size is correlated with the discrete data with a near zero R^2 value of 0.0039, and this result is not significant ($p = 0.7639$). Results for the male and female correlations between occipital centroid size and occipital robusticity scores are equally non-significant with near-zero level correlations for each subset.

The relationship of size with discrete measures of robusticity within the four anatomical regions highlighted in the study provides an unclear picture as to the importance of this metric for understanding craniofacial robusticity. This relationship is

clarified, when centroid size (calculated for the full 72 coordinate landmark dataset) for the entire cranium is compared simultaneously to all discrete measures of craniofacial robusticity. When this is done, results indicate a very strong relationship within the global sample ($R^2 = 0.9633$, $p < 0.0001$). This correlation is slightly higher within the male and female subsets ($R^2 = 0.9782$ and $R^2 = 0.9776$, respectively) and between males and females the relationship of size to levels of craniofacial robusticity is nearly identical.

Provided the information above on size and discrete measures of robusticity, further evidence is provided for a relationship between the two (as has been put forward in other work, primarily Lahr, 1996; Lahr & Wright, 1996). It is important to note that, at least with respect to previously employed discrete measures of robusticity, size is not always the major determining factor in robusticity expression when considerations across each individual anatomical region is concerned (for example, the supraorbital and occipital regions). However, given the data provided here, support for claims (e.g. Baab et al., 2010) that size plays only a minor role (if any) in craniofacial robusticity expression is unfounded, and therefore removing size metrics from considerations of craniofacial robusticity is, depending on the specific research objective, not necessarily informative.

Size and Allometric Considerations

It is important to remember that while the previous section considers the relationship of size to more classically employed measures of robusticity in the literature, a potentially more useful metric of this association lies in the relationship of centroid size with geometric morphometric measures of superstructure shape. This novel approach is the focus of the present section. Here, size (again defined as centroid size for the superstructure region in question) is compared with a GM definition of shape following the usage of relative warp scores for each of the four anatomical regions examined in the study.

For the global dataset, measures of size demonstrate a slightly higher affinity to superstructure shape as defined by relative warps scores as opposed to the discrete coding data highlighted in the previous section. This relationship proves to be more complex, however. All correlations between shape variables and centroid size are significant, with the highest p-value (for the occipital region) still maintaining a level of significance at 0.0128. With this data, centroid size still correlates moderately with the zygomaxillary shape data with an R^2 value of 0.6055. This correlation is the highest of the centroid size to relative warp comparisons and seems to follow the same pattern as with the discrete data discussed above. Interestingly, the supraorbital relative warp data also correlates closely to the RW scores with an R^2 value of 0.6018. This result is in contrast to the lower affinity of size to the discrete data. The mastoid region and occipital region have lower R^2 values (0.4841 and 0.2227 respectively), with the occipital region once again showing the lowest correlation with size.

Examining the relationships of centroid size to the relative warp scores in males and females provides greater insight into this relationship. Within the males, size and shape (as defined using geometric morphometric measures) show a strong relationship for the frontal and zygomaxillary region. These correlations are, in fact, higher than those observed in the entire global dataset. With a sample size of n=49, the female subsample is not large enough to allow similar correlations between centroid size and the many relative warp scores which combine to quantify shape for the frontal and zygomaxillary regions. This is not the case with the mastoid and occipital regions, however, since the shape of these areas are defined by fewer relative warps. Females show a stronger relationship between size and shape within the mastoid region (R^2 = 0.6536) than the males (R^2 = 0.5359). Females also show a much stronger relationship between centroid size and RW scores for the occipital region, with an R^2 = 0.4348, although this relationship provides a non-significant p-value of 0.1985. These results may provide evidence that, at least in some cases, males and females differ in patterns of

allometry with respect to shape within the anatomical regions of craniofacial robusticity examined.

The present study supports a more detailed definition of craniofacial robusticity with respect to measures of size. It is argued here that while size should be considered as a *potential* factor in the influence of robusticity expression (as defined in previous studies of craniofacial variation) but not as the sole causal factor of its expression. While overall craniofacial size correlates strongly with overall craniofacial robusticity (following Lahr, 1996), the influence of size on robusticity also appears to be superstructure independent with the supraorbital and zygomaxillary regions showing higher affinities to size variation with the relative warp data. Mastoid shape variability is moderately influenced by size while the nuchal region has the lowest affinity to size given both the coordinate landmark and discrete datasets.

The Patterning of Robusticity in the Cranium

Having considered craniofacial robusticity within the context of a definition involving size and shape, as well as how features of robusticity vary within *Homo sapiens*, a discussion with respect to the patterning of these features can now be presented. The primary goal of this study is to examine the validity of a "robusticity complex" that has been put forward by other researchers (Lahr, 1996; Lahr and Wright, 1996; Hublin, 1992; Gauld, 1996). If interactions exist between the four different anatomical regions of craniofacial robusticity examined in the present study, then support for the claim of integration among features and therefore an existence of a trait complex is confirmed. As described in Chapter 5, hypotheses of complete independence (the null hypothesis for all 2-block partial least squares analyses) are falsified for most comparisons based on centroid size and *every* comparison based on shape for the global sample. Comparisons within the male and female subsamples show more variability in which blocks are integrated and which are modularized, but these results still agree with

the overall assertion that at least some of the cranial robusticity features in the study show clear patterns of integration. *Given these observations, the present study lends support (at least partially) to the hypothesis of integration and the existence of a "robusticity complex" within recent* Homo sapiens. While this is the case, the strength of interaction between the four anatomical regions of craniofacial robusticity are relatively low, providing evidence for a more complicated patterning of robusticity across the cranium. These interactions will be discussed more closely in this section.

Interpretating Patterns of Integartion in the Cranium

Frontal Robusticity and Zygomaxillary Robusticity. Perhaps one of the more widely expressed ideas with respect to frontal robusticity, and particularly supraorbital morphology, is that the presence or absence of a large supraorbital torus, superciliary arch, or any configuration in between, is due in some part to the interaction of the frontal bone with the zygomaxillary (facial) complex. Ideas that supraorbital morphology serves a biomechanical role in the face, as a 'bent beam' for example, to dissipate stresses incurred during mastication (Endo, 1966; Russell, 1985, Hylander et al., 1991; Moss and Young, 1960), or that this region of the cranium acts as a zone of continuity between the splanchno- and neuro-cranium and is therefore dependent on the expression of these two regions for a 'spatial hypothesis' (Moss and Young, 1960) both require that these two portions of the cranium must be correlated in some way.

It is interesting that within the present study, the sizes of the frontal and zygomaxillary regions display the highest level of interaction across all anatomical regions studied with an RV[5] $= 0.4986$ ($p<0.0001$, providing evidence for integration of these two regions). With respect to all comparisons studied across all of the anatomical

---

[5] The reader is reminded that the RV coefficient is a measure of similarity between two data matrices (Robert & Escoufier, 1976), and is used by two-block partial least squares analyses to show the strength of correlation between two blocks of coordinate landmark data.

regions highlighted for craniofacial robusticity (and between shape and size), this first interaction serves as the closest possible evidence for integration between two features. The shape data PLS between these two features provides only very weak evidence of interaction (although still integrated) between the facial and frontal zones (RV = 0.1182, p=0.0001). The shape of the medial supraorbital region appears to be tied closely to the lateral expression of the maxilla and zygomatic bones and, perhaps more interestingly, the expansion of the frontal process of the maxilla is tied in part to the expansion of the glabellar region, while the expansion of the frontal process of the zygomatic is tied to increases in the lateral extent of the supraorbital region.

Given that support for integration is found in both the size and shape data, but higher correlations exist among the size data between the frontal and zygomaxillary regions while weaker correlations are noted in the shape data, the spatial hypothesis (Moss and Young, 1960) is partially supported. This support is based on the fact that the size of these two anatomical regions is closely related, and that the points of connection between the zygomaxillary and frontal regions (i.e. the frontal process of the maxilla and the glabellar region of the frontal, the frontal process of the zygomatic and the lateral expression of the superciliary arch) demonstrate a weak but integrated level of interaction. With regard to size, both the male and female subsamples also provide clear evidence of integration of these anatomical regions, but differences arise in how shape integration in manifested between these groups. Like the global sample, males are also integrated in the shape of the frontal and zygomaxillary regions, while females are not. This provides evidence that there is a stronger link between the expression of the supraorbital region and the zygomaxillary region within males, than in females.

Frontal Robusticity and Mastoid Robusticity. Integration within aspects of robusticity for the frontal and mastoid regions of the cranium may provide evidence, in part, for a greater neurocranial robusticity component that may be evident across the entire cranial vault. In this case, integration would mean a proposed relationship between

the frontal and temporal bones. While not often as closely studied as the other anatomical regions of the cranium, the shape of the temporal region has been implicated in studies of hominin morphology and taxonomy (specifically with respect to the Neandertals see Harvati, 2002; 2003a; 2003b; Harvati et al, 2005).

If evidence for integration were to be found between the supraorbital and mastoid regions, then studies that attempt to examine temporal morphology (e.g., Harvati, 2002; 2003a; 2003b) with respect to taxonomic questions would need to consider the morphology of the frontal region as well. The PLS analyses for the size and shape data of the frontal and mastoid blocks do support the hypothesis of integration between these two anatomical regions in extant humans (*size* PLS RV = 0.0935, p=0.0001; *shape* PLS RV = 0.0804, p=0.0033) although the level of interaction between these two anatomical regions is low.

While this is the case for the global sample, the male and female subsamples show that these two anatomical regions are largely modularized between the sexes. Only the female shape comparison provides clear support for the hypothesis of integration between the supraorbital and mastoid regions. Given these results, studies that examine extant *Homo sapiens* temporal morphology in isolation are supported, although further research is needed to test this in other pre-modern hominin groups, such as the Neandertals.

Frontal Robusticity and Occipital Robusticity. Another hypothesis with respect to an overall neurocranial robusticity component involves the possible integration of the frontal and occipital regions and the superstructures contained therein. Robust configurations for both of these anatomical regions involve a 'torus-like' morphology and this relationship could be supported in the comparisons of shape for both of these regions. On the other hand, the size of these two regions are most likely implicated in completely different roles (such as a connection for neck musculature for the occipital, or a spatial connection of the frontal and zygomaxillary regions).

The size comparison PLS between the frontal and occipital regions demonstrates an RV = 0.0002 with a non-significant p-value of 0.8783, indicating modularity between these two blocks. This result is not seen in the shape data, however, which does provide a significant p-value indicating non-independence (shape PLS RV = 0.0435, p=0.0469). Therefore, evidence for a modularized nature between the frontal and occipital features of craniofacial robusticity is only *partially* supported if size and shape are considered equally important.

As with the frontal-mastoid comparison highlighted above, the majority of evidence within the male and female subsets points to a more modularized pattern within these two anatomical regions. The only comparison between these two regions that supports integration is within the male shape PLS. Perhaps this result is to be expected given a higher frequency of 'torus-like' supraorbital and nuchal structures in some of the male subsamples.

Mastoid Robusticity and Zygomaxillary Robusticity. Both the zygomatic/maxilla and mastoid bones give rise to attachments sites for muscles involved in mastication such as the masseter and digastric muscles (Williams et al, 1999) and therefore might be expected to demonstrate a level of integration based on their robusticity. If this were the case, it would lend support for the integration of anatomical regions based on aspects related to biomechanical function.

Within the present extant human dataset, the interaction between these two regions provides evidence for the second highest relationship between size, with a PLS RV = 0.2162 which statistically confirms integration ($p<0.0001$). While this correlation is weak, it does show some possible evidence for a zygomaxillary/temporal robusticity complex. It is argued here that interaction between these two anatomical regions could be tied to a common function: mastication. With respect to shape, the mastoid and zygomaxillary data share an RV = 0.1098 (p=0.0001). This correlation, while supporting the hypothesis of integration, is very weak but given the *relatively* high correlation in size

with respect to the other block comparisons, further discussion on shape interactions are warranted. Increases in mastoid A-P width are shown to be tied to increases in overall cheek height, with a secondary (and weaker) association of mastoid massiveness being tied to the overall expression of the zygomatic bone. This interaction is rather complex, but it is argued that these data provide a weak but definite signal of integration between these two features based on their important shared biomechanical function.

The results for the male subset mirror those of the global sample for the integration of both the zygomaxillary and mastoid region. The female sample, however, appears to be modularized. This further complicates the proposed connection between these two regions. Given the sexual dimorphic nature of these anatomical regions, it is possible that while there is a common required function in both males and females (i.e. mastication) for the mastoid and zygomaxillary complex, the exact nature of this relationship may be rooted in size differences between males and females.

Mastoid Robusticity and Occipital Robusticity. The temporal and occipital bones combine to form the basicranium of the skull, which is derived from cartilaginous ossification (Lieberman et al., 2000a; 2000b; Williams et al, 1999). Based on the common developmental vectors of the petromastoid part of the temporal and the non-squamosal portion of the occipital (anything below and including the nuchal lines, see Williams et al, 1999; White, 2000), this could serve as potential evidence for development integration between aspects of craniofacial/basicranial robusticity.

Evidence from the PLS analysis of size between these two anatomical regions provides a very low RV = 0.0423, which is significant (p=0.0138). Based on this result and the equally low but significant shape PLS results (RV = 0.0597, p=0.0086), evidence for basicranial superstructure developmental integration is present. Nonetheless, while statistical support for integration is evident between these two superstructures, their overall level of interaction is actually quite low.

Once again, males and females show a more complicated pattern when examined separately. Males provide partial evidence for integration, especially in the shape of these two anatomical regions, but females indicate a more modularized nature for the occipital and mastoid regions.

Occipital Robusticity and Zygomaxillary Robusticity. The final comparison to be discussed involves a potential correlation between occipital and zygomaxillary determinants of craniofacial robusticity. A relationship between these two components would again provide evidence for a biomechanical role for craniofacial robusticity. This proposition is based on importance of these two anatomical regions for muscle attachment cites for head and neck movement as well as mastication (Caspari, 1991; Williams et al, 1999; White, 2000).

Given the results of the PLS analysis, there is possible (although weak) evidence for a degree of integration between these two anatomical regions based on shape. With the shape PLS RV = 0.1596 (significant at p = 0.0363), this provides the strongest level of shape correlation across all of the pairwise correlations. Shape variability between these two anatomical regions involves an inverse relationship between cheek height and the expansion of the nuchal lines. There is a direct relationship between components of facial breadth and premaxillary expression (alveolar prognathism) with occipital robusticity, meaning that as nuchal line expression increases, so does facial breath and alveolar prognathism. The size PLS results provided do not demonstrate any reliable relationship between these two regions, however. With a near-zero and non-significant coefficient of variation (RV = 0.0170, p=0.1268), there is no evidence for size integration between these two regions. These results combined with the results of the mastoid vs. zygomaxillary interactions highlighted above provide partial evidence for a biomechanical vector for some aspects of craniofacial robusticity. It should be noted, however, that this interaction appears to be rather complex, involving differing levels of size and shape integration between the structures studied.

When considered separately, males and females both highlight a more modularized expression for the occipital and zygomaxillary regions. It is suggested here, that given the majority of signals pointing to modularity within both the male and female subsets, as well as partial modularity in the global dataset, the most likely pattern is an overall modularized relationship between these two regions. The only caveat to this observation is that shape (again possibly tied to the biomechanics of these anatomical regions) does show some potential evidence for integration.

The Biological Relevance of Craniofacial Robusticity

While the above discussion has focused primarily on characterizing craniofacial robusticity and addressing the patterning of robusticity in *Homo sapiens*, this final section turns to the question of biological relevance. To what extent are the documented interactions between craniofacial superstructures derived from this study important and useful? What information does this study provide that may be useful in future studies of hominin craniofacial robusticity? What is the importance of a mixed pattern of integration and modularity in craniofacial robusticity expression? How can this information impact the question of craniofacial robusticity in the field of biological anthropology more generally?

On the Integrated and Modularized Nature of Craniofacial Robusticity in extant *Homo sapiens*

Most formal definitions of integration are based on patterns of correlation and covariation that demonstrate a lack of independence among variables (Lieberman et al, 2000a, 2000b; Cheverud, 1996). Modules, on the other hand, are defined by the existence of high levels of internal interactions and low levels of external interactions with other characters (von Dassow and Munro, 1999; Raff & Raff, 2000; Winther, 2001; Bastir & Rosas, 2005). It is perhaps the most important finding of the present study that as a whole, craniofacial robusticity expression follows a largely but not completely

integrated pattern. While tests for independence between the anatomical regions studied are largely falsified (lending credence to the claim of a "robusticity complex"), the fact that there are very sparse levels of interaction between frontal, zygomaxillary, temporal, and occipital robusticity characters, suggests that these features are not strongly integrated. In some comparisons, higher than average levels of shape integration such as the frontal and zygomaxillary comparison, the temporal and zygomaxillary comparison, or the occipital and zygomaxillary comparison, provide stronger support for an integrated robusticity complex. Occipital robusticity demonstrates a modularized pattern in overall size, however, as denoted by the PLS analysis of centroid size in the frontal-occipital comparison and the occipital-zygomaxillary comparison (refer to table 14). Recent work by others (Baab et al., 2010) independently confirms these findings by demonstrating that most features of craniofacial robusticity are integrated, with the exception of occipital robusticity, which appears to be modularized.

The evolution of modularity in a system has been argued to be either a derived property (Wagner & Altenberg, 1996), or a primitive property (Winther, 2001). The distinction to be made here is at what point in the evolutionary history of an organism does modularity occur? While the present study only considers recent *Homo sapiens*, testing patterns of modularity and integration in pre-modern hominins would provide insight into this question. Given recent studies that highlight a more modularized pattern of craniofacial interaction within modern humans as compared to pre-modern fossil groups and non-human primate species, it can be inferred that craniofacial modularity (at least to some extent) may be a derived condition of *Homo sapiens* (Polanski and Franciscus, 2006; Bastir and Rosas, 2005; Bookstein et al, 2003; Lieberman et al, 2000a) although all studies incorporating fossil hominins face significant sampling problems (Ackermann, 2002). If patterns in craniofacial robusticity are to be considered derived in recent *Homo sapiens*, then this would allow robusticity characters to have loose interactions with one another, allowing selection to act on characters individually without

causing a complete shift in an entire suite of craniofacial robusticity traits (Wagner & Altenberg, 1996).

Given an integrated pattern of craniofacial robusticity (but with some signals of modularity throughout the cranium), what implications does this have for the evolutionary significance of these characters, if any? At least with respect to modularity in evolution this question can be answered in terms of canalization (see Chapter 3). Canalization allows organisms to buffer themselves from perturbations in growth and development that might be caused through either environmental or genetic pathways (Amzallag, 2000; Hallgrimsson et al, 2002; Wagner & Altenberg, 1996; Ancel & Fontana, 2000; Arjan et al, 2003; Wagner et al, 1997). In circumstances where craniofacial robusticity follows a modularized pattern, e.g., the frontal-occipital and occipital-zygomaxillary block comparisons, canalization could act as a buffer against large scale changes in robusticity across these regions. Given this, evolutionary changes in occipital robusticity could occur in isolation without having a larger impact on the robusticity of the facial skeleton. Further research could provide insights into the potential causes (biocultural, environmental, or ontogenetic) of occipital robusticity modularity.

Future Considerations in Craniofacial Robusticity Research

This research serves as a starting point for a more detailed research program into the expression, functionality, and origins of craniofacial robusticity in genus *Homo* and other closely related taxa. While this study has provided insight into the integrated nature of the craniofacial robusticity complex in an adult sample of recent *Homo sapiens*, little is known about the developmental trajectories of these characters. Questions to be asked within this framework are: when is the earliest onset of craniofacial robusticity in the growth of recent *Homo sapiens*, and what is the rate at which these features develop? While many studies have proposed endocrine models for potential changes in the onset

and rate of growth of robusticity features (Brothwell, 1975; Green & Smith, 1990; Smith & Green, 1991; Ponce de Leon & Zollikofer, 2001; Rosas et al., 2006; Bernal et al., 2006), there has been no morphometric investigation into the actual timing of craniofacial robusticity expression across a longitudinal sample of recent *Homo sapiens*. Longitudinal data based on craniofacial radiographs are widely available and can provide metric and coordinate landmark data on craniofacial superstructures as well as cranial vault thickness. Investigation along these lines may provide new hypotheses regarding the growth and development of robusticity in *Homo sapiens* generally, as well as between males and females, and possibly across different geographic populations.

In addition to developmental considerations of craniofacial robusticity in recent *Homo sapiens*, a more detailed investigation into hypotheses relating to behavioral and ecological factors potentially governing craniofacial robusticity is warranted. Preliminary analyses of craniofacial robusticity in different recent *Homo sapiens* populations in this study indicate that variation in robusticity may be tied to subsistence patterns and activity levels. This observation is based on similarities noted between the Australian aboriginal sample and the Sub-Saharan Khoisan sample (Appendix A). While these results are preliminary and based on small sample sizes, there is tentative agreement with previous research regarding systemic models for cranial robusticity (Lieberman, 1996). This relationship between subsistence patterns and robusticity may be more complex, however, based on recent observations that hunter-gatherer groups are not always more robust than non hunter-gatherer groups (Baab et al., 2010). Little evidence is found to support hypotheses relating craniofacial robusticity to climatic variability and latitude in this study, and this observation has also been noted elsewhere (Baab et al, 2010). Nonetheless, other researchers have found evidence for a relationship between both postcranial robusticity and body size (Houghton, 1990) and cranial robusticity (Bernal et al., 2006; Perez et al., 2007) with climate. Clearly, further research on this topic is needed.

While this study has focused on craniofacial robusticity in recent *Homo sapiens*, the essential questions that have been addressed must eventually be applied to the hominin fossil record. We require a much better understanding of the differences in robusticity levels noted between *Homo sapiens* and pre-modern fossil hominins such as *Homo erectus* (Lahr, 1996; Antón, 1997; Antón & Franzen, 1997; Antón, 2002) for example, and this extends, in fact, to the need for a better understanding of robusticity variation among all pre-modern *Homo* lineages. The primary questions that have been raised from the present work revolve around the sequence of evolutionary events leading up to an integrated pattern of craniofacial robusticity that is apparent in recent *Homo sapiens* with some exceptions where modularity is present. If morphological integration in craniofacial robusticity is a derived pattern in *Homo sapiens*, then this would imply that modularity of these features must be present in pre-modern fossil hominin forms. Moreover, this begs the question of how developmental patterns might have been altered in this process, as well as the possible evolutionary causes (i.e., whether they were genetic, environmental, or biocultural).

In addition to these considerations, it is important to determine if craniofacial robusticity (as defined in *Homo sapiens*) can be applied to members of our own lineage outside of genus *Homo*. Most research conducted on craniofacial variation in *Australopithecus* and *Paranthropus* has highlighted differences in craniofacial form, including some aspects of robusticity between these two groups, primarily with respect to the masticatory complex (Rak, 1983; Demes and Creel, 1988; Hylander, 1988; Daegling, 1989; Constantino and Wood, 2007; Menegaz et al., 2009). While such differences in craniofacial robusticity exist, it is interesting to note that overall levels of cranial vault thickness are similarly thin between both *Australopithecus* and *Paranthropus* (Menegaz et al., 2010). This observation may suggests that levels of robusticity in cranial vault thickness could be modularized with respect to facial robusticity (since facial robusticity appears to be independent of cranial vault thickness), and that this pattern may be

different from other members of the hominin lineage, such as early members of genus *Homo* (e.g., *Homo habilis*). Further investigation into these differences might help identify when the patterns of craniofacial robusticity seen in genus *Homo* may have originally evolved.

At present, there has been no thorough investigation into the integrated or modularized nature of craniofacial robusticity in pre-modern fossil hominins. Unfortunately, sample size issues abound with present fossil samples (Ackermann, 2002), and this explains a large part of the current knowledge gap. There are methodologies available for reconstructing damaged fossils that could act to increase sample sizes in some cases (e.g., Ponce de Leon and Zollikofer, 2001; Gunz et al, 2003), as well as continuing technical refinement in morphometric methodologies . Nonetheless, a fragmentary fossil record will likely remain a significant constraining factor for the foreseeable future.

A final question worth considering is the degree to which craniofacial robusticity, as approached in the present work, can be applied to other closely related non-human primate groups, such as *Pan* and *Gorilla*. While much work has been conducted on primate craniofacial biomechanics and its relationship to levels of mandibular robusticity (Spears and Crompton, 1996; Chen and Chen, 1998, Taylor, 2002; 2006; Daegling, 2007), as well as robusticity of the supraorbital (Ravosa et al., 2000b) and zygomaxillary regions (Hylander and Johnson, 1997), the linkage of these studies to questions of craniofacial robusticity in genus *Homo* has not been sufficiently explicated and examined. Is craniofacial robusticity variation in non-human primate groups homologous to that found in *Homo sapiens*? If the concept of craniofacial robusticity can be applied to non-human primate groups, like it is in genus *Homo*, how would robusticity features vary between these two groups? If morphological integration defines recent *Homo sapiens* craniofacial robusticity, should we expect a pattern of modularity in non-human

primates? Clearly, despite the myriad difficulties involved, the questions raised here are worth continued exploration.

CHAPTER 7. CONCLUSIONS

The primary goal of this study has been to test the presence or absence of a "robusticity complex" within recent *Homo sapiens*, as proposed by previous researchers (Lahr, 1996; Lahr and Wright, 1996; Gauld, 1996; Baab et al., 2010). It has also aimed, via the incorporation of a novel means of quantifying robusticity expression through the use of geometric morphometrics, as well as classic (discrete coding) measures of craniofacial robusticity, to provide insights into how craniofacial robusticity should be characterized within our species. Here, I briefly summarize the main findings and address the next logical steps in this area of research.

It has been proposed by Lahr and others (Lahr, 1996; Lahr and Wright, 1996; Hublin, 1992; Gauld, 1996) that the cranial features often highlighted as being features of craniofacial robusticity within our species, as well as our fossil ancestors, may act together to form a craniofacial "robusticity complex" rather than a suite of individual traits. The importance of this possibility is evident in the fact that these features have frequently been cited in past works (Smith & Ranyard, 1980; Trinkaus & LeMay, 1982; Brace, 1963; 1995; Russell, 1985) and very recent works (Smith and Grine, 2008; Bruner and Manzi, 2007; Baab, 2008a; Baab, 2008b; Spoor et al, 2008), with respect to debates over hominin anatomical variation and phylogeny. Studies such as these have largely focused on aspects of craniofacial robusticity in isolation, highlighting only supraorbital morphology, or only nuchal morphology, for example, or examining trait lists in order to gain insights into patterns of craniofacial variability throughout our genus. While informative, these studies may be only providing a portion of the picture if such a proposed complex of robusticity traits does exist within *Homo sapiens* and closely related hominins.

The results of this study do, in fact, find evidence for a "robusticity complex" within modern *Homo sapiens*. Given the results of the two-block partial least squares

analyses, most of the hypotheses for pairwise integration across the robusticity regions studied in the modern human skull are accepted with only a few instances where modularity is evident. While there is evidence for an associated complex of robusticity traits, the level of interaction between these anatomical regions, while statistically significant, is rather weak. The moderately higher than average PLS correlation results between the supraorbital and zygomaxillary regions with respect to size supports the "spatial hypothesis", originally proposed by Moss and Young (1960). The fact that the zygomaxillary region also has slightly higher than average levels of correlation with the mastoid, and nuchal regions may provide evidence for a shared degree of robusticity variation deriving from biomechanical functions of the skull through masticatory and paramasticatory actions.

Previous considerations of cranial robusticity have tended to center on aspects of size, and one goal of this study has been to address both size and shape in a more comprehensive treatment of these traits. With respect to measures of size, this study illustrates the need for a more nuanced consideration of the interactions of size on a superstructure-by-superstructure basis. Assertions that size is the *most* important factor in craniofacial robusticity expression (Lahr, 1996; Lahr and Wright, 1996) can be questioned, since in the present dataset, only the zygomaxillary and mastoid regions demonstrate high associations with size. The supraorbital and nuchal regions, however, provide a more complicated picture between the interactions of size and shape. Size appears to have little effect on the expression of robusticity in the nuchal region, while the supraorbital region displays varying levels of size dependent variation in the coordinate landmark and discrete datasets.

The findings of this study support the idea that shape variation is on par with size variation in the importance of craniofacial robusticity expression within recent *Homo sapiens*. Shape variation in the supraorbital region is driven primarily by variability in the medio-lateral expansion of the superciliary arch, as well as supero-inferior expansion,

with "robust" supraorbital regions displaying a marked increase in massiveness in both of these planes. On the whole, supraorbital projection is less important because not all subsamples studied display marked levels of variability in this aspect.

Zygomaxillary shape variability across the global sample appears to be characterized primarily by 1) variability in alveolar prognathism, 2) antero-posterior expansion of the zygomatic region, and 3) an increase (or decrease) in cheek height. These factors, as well as the shared co-variability of the zygomaxillary and frontal regions indicated above, highlight the importance of the zygomatic bone (and to a lesser extent, the maxilla) in characterizing facial robusticity.

Robusticity in the temporal region is manifested primarily as an inferior expansion of the mastoid process beyond the basicranial plane. More projecting mastoids are often associated with an increase in antero-posterior length. Interestingly, the orientation of the mastoid tip (ranging from an anterior to posterior position) is also highly variable, but this variation is not strongly tied to variation in mastoid robusticity.

Finally, the nuchal region appears to manifest in robusticity primarily as a function of supreme nuchal line expansion. Variation in this structure can lead to either an external occipital protuberance (which is the more gracilized form) or a full nuchal torus (the robust form). It should be noted that the latter configuration is observed occasionally in some recent human populations (particularly Australian aboriginals), indicating that the full range of robusticity variation in this trait is evident across the global sample.

This study serves as an initial step along with Baab et al., 2010, into a much larger examination of craniofacial robusticity within the Homininae. While the pattern of craniofacial robusticity in recent *Homo sapiens* appears to be integrated, little is known about the patterning of robusticity in fossil hominin forms. While other studies have addressed larger questions of modularity and integration in craniofacial form throughout hominin evolution (Bookstein et al., 2003), or have investigated patterns of robusticity

expression in recent *Homo sapiens* (Baab et al., 2010) questions pertaining to the integration or modularity of craniofacial robusticity in fossil hominin forms have yet to be answered. If differences in the patterning of robusticity exist between recent *Homo sapiens* and earlier forms, then such craniofacial robusticity patterning may prove to be a reliable and important factor in questions pertaining to the phylogeny or our species and closely related taxa. Further investigation of these questions is the next logical step in the continuing investigation of the evolutionary significance of craniofacial robusticity throughout our lineage.

APPENDIX A. REGIONAL SUBSAMPLE DATA

Regional Relative Warps Analysis

Appendix A contains the results for the regional subsample RWA. These data are presented in an appendix rather than in Chapter 5: Results because of an issue with intrapopulational sample sizes. Recall that while the global sample size for the present study n=140, with n=91 males and n=49 females, the intrapopulational sample sizes on average are much smaller, ranging from the Mediterranean/Near East sample (n=21) to the Sub-Saharan Khoisan (n=5) (refer to Table 1). While these data may not be as robust as data from the larger global sample and male/female subsamples, they provide interesting insight into craniofacial robusticity variation in recent *Homo sapiens*. These data are also relevant for providing future hypotheses for potential interactions and relationships between craniofacial robusticity and different geographical regions, climatic zones, and subsistence/activity patterns. For these reasons, the results of this analysis are presented below.

Overall Regional Variation

Australian Aborigines. A RWA of the Australian Aborigine population (n=17) with the entire 72 landmark dataset provides a total of 16 relative warps accounting for the total variation in the sub-sample. Of these 16 relative warps, the first 5 account for a total of 2/3 (66.65%) of the variance and are examined below.

RW1, accounting for 20.40% of the variance in the sample, deals largely with the morphology of the nuchal plane (as it did with the global sample above), and more specifically with the shape and expression of an external occipital protuberance versus a full occipital torus (figure S1). This is evidenced by the shape change observed by the supreme nuchal line. There is also a slight degree of facial expansion in the medio-lateral plane as well as well as a reorientation of the maxilla from a more forward, anterior position to a more swept back, posterior position. Narrower craniofacial breadths and a

more swept back maxilla are associated with the expansion of the occipital torus while the exact opposite is true for the occipital landmark configurations resulting in an external occipital protuberance.

RW2 addresses variation between the supraorbital region, the position of the occipital torus, and the shape of the frontal process of the maxilla (as well as nasal aperture shape). This component accounts for another 14.48% of the variation (see figure S2). Here, a more superior positioning of the occipital torus is associated with a slightly diminished supraorbital region and a higher more, projecting frontal process of the maxilla. Recall from the RW plots above that the Australian population has a tendency to display a reduced facial morphology combined with a more pronounced level of supraorbital and occipital robusticity. It is important to note that along this component, the expansion of the supraorbital region is associated with a relatively inferior placement of the occipital torus.

RW3 accounts for 13.14% of the total variance and again deals with orientation of the supreme nuchal line in the supero-inferior plane (figure S3). Here the overall shape of the nuchal lines is diagnostic of an occipital torus, but the placement of the supreme nuchal line along RW3 indicates the overall expansion of the torus supero-inferiorly. Interestingly, this component associates S-I expanded occipital tori with diminished mastoids and supraorbital morphology, while a smaller more S-I compressed occipital torus is associated with increased levels of robusticity in the mastoid and supraorbital region.

RW4 is the first component to deal mostly with cranial vault morphology (figure S4). It covers an additional 10.37% of the variance. The majority of variation along the cranial vault landmarks occurs more posteriorly on the parietals near the region of vertex. However, this variation is also tied to the medio-lateral length of the superciliary arches, with more elongated (especially at the medial and midorbital positions, refer to Vinyard

& Smith, 2001; Smith & Ranyard, 1980) arches being associated with lower cranial vaults around the region of vertex.

Finally, RW5 accounts for 8.27% of the variance and this component covers overall medio-lateral length of the occipital torus as well as changes in the degree of alveolar prognathism in the sub-sample (figure S5). Higher levels of alveolar prognathism are associated with more M-L compressed toral configurations. To a lesser extent, RW5 also deals with a reorientation of the mastoid process from a supero-posterior orientation (accompanying an increase in alveolar prognathism) to a more infero-anterior orientation (in tandem with a decrease in alveolar prognathism).

Central Europe. The Central European sub-sample of the complete 72 landmark dataset consists of 19 individuals and 18 relative warps accounting for the entire range of variation in the sub-set. Of the 18 relative warps, the first 5 account for 68.16% of the variation and are examined in detail below.

RW1 accounts for 24.74% of the variation in the analysis and can be seen visually in figure S6. This first component addresses variation in both occipital and frontal robusticity as well as cranial vault height. At one end of the range of variation, RW1 shows an expansion of the supraorbital region (with significant superciliary arch development) along with a torus configuration for the superior and supreme nuchal lines. The increase in robusticity is accompanied by a decrease in the height of the cranial vault, with a low sloping shape in the frontal region. Overall gracilization of the frontal and occipital regions is associated with a high cranial vault and more vertically oriented frontal. There is also a component of facial shape along this component with more expanded and massive faces being associated with the more robust configuration of the nuchal and supraorbital regions, while a more diminished facial configuration is seen with the more gracilized overall craniofacial form. Interestingly, an increase in mastoid breadth (which would be also considered a marker for robusticity) is associated with the gracile configuration.

RW2 addresses variation in cranial breadth as well as mastoid expression and the length of the supreme nuchal line. This component accounts for an additional 15.63% of the variance explained and can be seen visually in figure S7. Increase in mastoid size (both in M-L and S-I dimensions) is associated with an increase in cranial breadth along this component. There is also an elongation of the supreme nuchal line along with the increase in mastoid size.

Accounting for 11.39% variance in the Central European sub-sample, RW3 highlights variation in supraorbital morphology, occipital shape and a degree facial elongation in the supero-inferior plane (figure S8). Here, an elongated facial form is associated with an increase in superciliary arch height (with no increase in projection) and an angular occipital region. A more rounded occipital is seen with smaller faces and diminished supraorbital heights. There is also a degree of variation in the placement of the superior nuchal line in the A-P plane. Posteriorly oriented nuchal lines are associated with the more angular occipital form, while the opposite is true of the anteriorly positioned nuchal lines.

RW4 (figure S9) addresses variation in the anterior projection of the nasal aperture (and midfacial prognathism) as well as an increase in the mastoid region. This component accounts for an additional 9.26% of the variance in the set. There is an aspect of cranial vault shape along this component also. Interestingly, it also describes variation in the angulation of the occipital, but here, a more angled occipital form is associated with larger mastoids and more projecting midfaces (as opposed to being associated with more elongated faces and higher superciliary arches seen in RW3).

RW5, the final component to be examined here in the Central European sub-sample, accounts for 7.15% of the variance (figure S10). Variation in facial massiveness is the primary focus of this relative warp. Here, more massive facial expression is tied to a more posteriorly oriented frontal and more rounded parietal and occipital regions, while

smaller faces can be seen with more anteriorly oriented frontals and flatter parietal/occipital regions.

China. The Chinese sub-sample for the complete 72 landmark dataset encompasses a total of 11 individuals and is provides 10 total relative warps equaling 100% of the total variance. Of these 10 relative warps, the first 4 components account for 72% of the overall variation in the dataset and are examined in further detail below.

RW1 accounts for 23.10% of the variance and this variation can be observed in figure S11. This component summarizes variation in several aspects of craniofacial anatomy. It accounts for variation in cranial vault height, mastoid size, facial size and prognathism, and occipital torus/external occipital protuberance morphology. Large mastoid processes are associated with large (albeit orthognathic) faces and high cranial vaults, while reduced mastoids are associated with a reduction in both cranial vault height and facial dimensions with a degree of alveolar prognathism. The nuchal lines are more pronounced and projecting (and higher up on the occipital) in conjunction with the smaller face/vault/mastoid morphologies, while they are lower and less projecting with the more massive craniofacial forms. This shows that there is an inverse relationship in this sub-sample between occipital robusticity and levels of robusticity across the rest of the cranium.

The second relative warp explains almost as much variation as the first relative warp (21.10% of the total variance) and is primarily involved with facial breadth (figure S12). Here, increased facial breadth dimensions are associated with elevated levels of alveolar prognathism, more medially placed superciliary arches, and reduced supreme nuchal lines. Decreased facial breadths are in turn associated with a slight degree of midfacial prognathism, drastically increased supreme nuchal lines (almost as long as the superior nuchal line) and longer, more laterally expanded superciliary arches.

RW3 also deals with facial breadth and frontal robusticity and accounts for an additional 17.62% of the variance (figure S13). This component shows variation in brow

morphology from diminutive superciliary arches to expanded (in all aspects) and robust brow ridges. The more robust brow morphology is associated with an increase in facial breadth, while reduction in this region shows a decrease in facial breadths as well. There is also a degree of variation in the orientation of the supreme nuchal line. More superiorly oriented nuchal lines are seen with the reduced facial morphologies, while inferiorly oriented supreme nuchal line is associated with the more robust facial morphologies.

Unlike the first three components, RW4 does not address much variation in the face (figure S14). This component accounts for 10.21% of the variance (as significant drop from RW3 in variance explained) and deals mostly with the cranial vault and the mastoid process. Expanded mastoid processes (in both A-P and M-L planes) are associated with higher cranial vaults around the region of bregma, while reduced mastoids are seen with lower vaults. This component still addresses alveolar prognathism to some degree, with slightly more prognathic faces being associated with larger mastoids and higher cranial vaults, but this aspect of the variation is minor compared to the above components.

The final component examined here (RW5) accounts for 7.31% of the variance and can be seen visually in figure S15. This component addresses variation mostly in the face with specific attention to the zygomatic and nasal regions. Here, increased zygomatics are associated with an increase in nasal projection and a decreased nuchal morphology. A decrease in the zygomatic region, however, is accompanied by a significant increase in size and projection of the nuchal region (approaching morphologies that are very 'torus-like' in expression).

India. The Indian sub-sample consists of 12 individuals and 11 relative warps that summarize the total amount of morphological variation in the data set. Out of these 11 relative warps, the first 5 components account for a total of 80.98% of the variance and are examined in detail below.

RW1 of the Indian sub-sample accounts for a fair majority of the overall variation in the dataset (31.03%) and is summarized in figure S16. The shape and expression of the superciliary arches as well as the supreme nuchal line drive the variation along this relative warp axis. Expansion of the glabellar area of the supraorbital region can be seen here in conjunction with an expansion of the supreme nuchal line (superiorly and laterally along the occipital). There are slight variations in facial breadth along this component with slightly wider faces in the zygomaxillary region associated with larger brow ridge configurations.

RW2 explains variance in overall craniofacial height, as well as mastoid expression nuchal morphology. This component covers an additional 19.10% and can be seen visually in figure S17. The major focus of RW2 is variation along the supero-inferior plan with S-I compressed faces and cranial vaults being contrasted with taller faces and cranial vaults. There is also a drastic amount of variation in mastoid robusticity along this component, with larger mastoid processes (primarily in supero-inferior and anterior-posterior dimensionality) being associated with expanded faces and cranial vaults. The nuchal lines demonstrate an inverse relationship with the mastoid process and craniofacial dimensions. Expression of the supreme nuchal line (and to a lesser extent the superior nuchal line) is reduced in the more robust mastoid and craniofacial configurations.

The third relative warp (12.31% variance explained) accounts for variation in the parietal and occipital portions of the cranial vault as well as the mastoid process and facial breadth (figure S18). As mastoid length (A-P) decreases along this axis, there is a concurrent flattening of the posterior parietal and occipital regions of the vault as well as slight decrease facial breath. Interestingly, with this decrease in facial breadth, there is also an increase in the breadth (and robusticity) of the lateral trigone of the supraorbital region.

RW4 accounts for an additional 10.70% of the variance and the vast majority of this variation occurs in the cranial vault (figure S19). This axis contrasts a cranial vault with flat frontal regions and high and rounded parietals with a lower overall cranial vault displaying a more rounded frontal and flattened occipital. There is an expansion of the nuchal region, antero-posterior dimension of the mastoid and maxillary region with the former cranial vault configuration while the latter cranial vault morphology is associated with decreases in these regions.

RW5 is the last component to be examined here and accounts for 7.87% of the remaining variation in the dataset (figure S20). This component addresses variation in mastoid process height and width, supreme nuchal line orientation, superciliary arch height, and cranial vault height (to a slight degree). Of further interest is variation seen in the occipital region near the foramen magnum (at the point of opisthion). Along this component, there is a large degree in variation in the projection of the inferior portion of the cranial base, with more projecting cranial bases being associated with smaller mastoid processes (in height and width) as well as a lower cranial vault and decreased superciliary arch height. Flatter cranial bases are associated with a more 'torus-like' nuchal line configuration and expanded mastoids and cranial vault heights.

Mediterranean and Near East. This sub-sample contains 21 individuals from Western Asia (primarily Greece and Syria) and provides a total of 20 relative warps from the RWA. Of these 20 components, the first 5 relative warp axes account for slightly over 2/3 of the total variation in the landmark dataset of this sub-sample and are explored in further detail below.

RW1 primarily addresses variation in nuchal morphology and accounts for 22.65% of the variation in this sub-sample (figure S21). Here, the supreme nuchal line demonstrates a high degree of variation in its expression, ranging from a diminutive external occipital protuberance to an expanded 'torus-like' morphology. There is also a slight degree of variation in both cranial height and facial breadth along this component,

but this variation is subdued compared to the variation of the nuchal region. Slightly increased facial breadths are associated with more expanded supreme nuchal lines, while an increase in cranial height accompanies the expression of an external occipital protuberance.

RW2 shows a higher degree of variation in landmark positioning than RW1 and explains an additional 17.62% of the variation (figure S22). This component addresses variation in supraorbital morphology, mastoid expression, nuchal morphology, and cranial height. Low cranial vault heights are associated with reduced mastoids, smaller superciliary arches, and an increase in projection and height along the occipital, but not the overall size of the nuchal lines. Conversely, high cranial vaults are accompanied by increased mastoid, supraorbital, and nuchal line morphology, with the nuchal lines occurring low on the occipital.

RW3 accounts for 13.50% of the variation and can be visualized in figure S23. This component shows a degree of variation in cranial antero-posterior length, as well as facial supero-inferior length and superciliary arch projection. Compressed A-P dimensions of the cranial vault are concurrent with and increase in facial S-I length. As cranial vault length increases along this component, there is a supraorbital projection and a more superior placement of the supreme nuchal line on the occipital.

RW4 demonstrates variation in zygomaxillary size and superciliary arch expression (especially around glabella). There is also a degree of variation in the orientation of the cranial base. This component accounts for an additional 7.78% and can be seen in figure S24. Here, there is an association of zygomaxillary expansion and superciliary arch expansion. This component displays a significant amount of variation in the size and projection of glabella also. More flat and angular cranial bases are also seen along with the increases in facial morphology noted above. This component also highlights variation in mastoid breadth, with increased mastoid breadths being associated with the more gracile facial and brow ridge forms.

RW5, the last component examined for the Mediterranean and Near East sample accounts for 6.00% of the remaining variation in the dataset (figure S25). This component also demonstrates variation in facial breadth and zygomaxillary size, along with mastoid size. Expanded facial dimensions are associated with a dramatic increase in mastoid expression along RW5. The cranial vault takes on a more rounded shape (especially in the frontal and occipital regions) with the more gracile facial and mastoid forms, while the vault is more angular in these regions as temporal and facial robusticity increases.

New Guinea. The New Guinea sub-sample is a small sample of 5 individuals representing a part of the greater South Eastern Asia sample (with Singapore representing the other component of the sample, see below). The RWA of this sub-sample provides 4 relative warps accounting for 100% of the variation. Given that this set has so few relative warps axes to explain (with each representing a significant portion of the total variance), all four will be examined below.

Unlike the previous sub-samples studied, the percent variance explained of the first relative warp component is very high (56.90%). This is due to the fact that the New Guinea sub-sample only contains 5 individuals (refer to figure S26). This component summarizes variation in craniofacial robusticity in all the regions studied. Large facial lengths and breadths as well as an increase in the zygomaxillary size are associated with an expansion of the mastoid, supraorbital, and nuchal regions (in this last case, a 'torus-like' configuration). At the other end of the variation of this component, there is an expansion of the cranial vault along with a complete gracilization of all the other robusticity components studied. The nuchal region is characterized by an external occipital protuberance at this end of the range of variation also.

RW2 accounts for 21.40% of the variation in the sub-sample and addresses variation in cranial vault shape and facial shape (figure S27). Increases in zygomaxillary size (but not facial breadth) are associated with an overall flattening of the occipital and

frontal regions of the cranial vault. This component addresses a significant amount of supreme nuchal line variation also, ranging from diminutive (in association with increased zygomaxillary size) to a larger more expanded morphology. There are also slight variations in mastoid A-P length along this component as well as an increase in M-L length of the superciliary arches.

RW3 deals with variation in supraorbital morphology, mastoid orientation, and nuchal line morphology and accounts for an additional 12.71% (figure S28). An increase in brow ridge height and glabellar size and projection is associated with a more posterior oriented mastoid processes, while a decrease in supraorbital expression is associated with a more anterior orientation of the mastoid process. The third relative warp also demonstrates variation in the supreme nuchal line height on the occipital as well as the orientation of superior nuchal line.

RW4 accounts for the final 9.00% of the variation and can be visualized in figure S29. This final component also contrasts variation in supraorbital morphology and mastoid morphology as well as levels of alveolar prognathism. Here, expansion of the medial aspect of the superciliary arch is inversely related to expansion of the trigone (or the lateral part of the superciliary arch). This expansion of the lateral part of the supraorbital region is also associated with an increase in alveolar prognathism. Finally, this component contrasts length in the mastoid along the supero-inferior plane.

North Africa. The North African sub-sample derives from Libya and is made up of 9 individuals. A relative warps analysis of this sub-sample provides a total of 8 components with the first 5 components covering a cumulative 81.76% of the variance and is examined in further detail in the following section.

RW1 accounts for 26.73% of the variance in the sub-sample and can be visualized in figure S30. This component addresses variation in cranial vault height (contrasting low sloping vaults with high vertical vaults) as well as an expansion of the supraorbital region. There is also variation in the mastoid and nuchal regions, although this variation

is lesser in extent. Here, expanded brow ridges (particularly in the area of glabella) are associated with sloping frontals and low cranial vault heights. We also see a degree of variation in midfacial prognathism along this component, with higher levels of prognathism associated with expanded supraorbitals and low cranial vaults. Finally, while there is a slight amount of variation of mastoid morphology in the S-I and A-P plains, there is a significant degree in M-L (breadth) dimensions.

RW2 explains variation in occipital, frontal, and facial morphology and accounts for an additional 16.75% of the variance (figure S31). Variation in the maxillary region, mostly around the anterior nasal aperture contrasts longer supero-inferior apertures with shorter supero-inferior apertures. There is also in increase in the length of the glabellar region associated with longer nasal apertures. RW2 also contrasts occipital shape and nuchal morphology, with more rounded occipitals being associated with elongated supreme nuchal lines. Flattened occipitals are associated with a decrease in the expression of nuchal morphology, which is more diagnostic of an external occipital protuberance.

RW3 again highlights variation in the nasal region as well as the mastoids and facial breadth. This component explains almost as much variation as RW2 (15.60%) and is represented visually in figure S32. Mastoid morphology varies considerably in all planes along this component with larger more robust mastoids being associated with wider faces having more expanded zygomatics as well as shorter more narrow anterior nasal apertures. The opposite is true of reduced mastoids, which accompany a narrower facial form and broad nasal apertures. There is also a degree of parietal/occipital flattening in the posterior aspect of the cranial vault and this flattening accompanies an external occipital protuberance morphology of the supreme nuchal line, while the more rounded vault form is associated with an expansion of the nuchal lines.

RW4 shows a high degree of variation in supraorbital robusticity and facial and frontal region morphology and accounts for 12.11% of the variance (figure S33). Across

this component, supraorbital morphology ranges from being diminutive in all aspects (superciliary height, length, and projection) to having very pronounced brow ridges. Interestingly, increased supraorbital robusticity is associated with a decrease in facial massiveness along RW4. Finally, this component also demonstrates variation in the A-P placement of the mastoid process, with more posteriorly oriented (and slightly more massive) mastoids being associated with the expanded supraorbitals.

The final component examined for the North African sample, RW5, accounts for 10.57% of the variance (figure S34). As with most of the components discussed above, this RW5 also addresses variation in supraorbital morphology (contrasting higher, more massive superciliary arches and reduced trigones with reduced superciliary arches and expanded trigones) as well as a degree of variation in mastoid expression and the placement of the nuchal lines. Increased mastoid breadth along this component is associated with higher nuchal line placement along the occipital.

Singapore. Rounding out the South East Asian sample, the Singapore sub-sample from the Malay Peninsula consists of 6 individuals. The RWA of this sub-sample provides 5 relative warps covering the total amount of variation in the dataset. Given the low number of relative warps, all 5 will be addressed below.

RW1 explains 39.70% of the variance in the Singapore sub-sample and can be visualized in figure S35. This component summarizes variation in the nuchal and supraorbital region. There is also a degree of maxillary inflation along this component as well. Interestingly the inflated maxillary form is associated with a reduced superciliary region and diminished nuchal lines. Expansion of the nuchal lines (especially the size and shape of the supreme nuchal line) is associated along this component with larger superciliary arches. These robusticity features are associated with a reduced and deflated maxillary region, however.

RW2 covers variation in the facial region and accounts for an additional 21.89% of the variance (figure S36). There is a large degree of variation in alveolar prognathism

summarized along this component, with high degrees of alveolar prognathism being associated with reduced mastoids in the S-I plane but with increased breadths (M-L plane). Also associated with this alveolar prognathism is a projection on the superior nuchal line, as well as a slight degree of occipital flattening. Reduction of the face is seen in tandem with an increase in mastoid S-I length, as well as a slight increase in superciliary arch height and projection.

RW3 deals mostly with variation in the facial and frontal regions and accounts for 16.60% of the variance (figure S37). This component contrasts expanded brow ridges (especially in height and projection) with reduced ones. This variation in supraorbital morphology is connected to variation in the zygomaxillary region as well, with larger brow ridges being associated with an overall reduction of the maxillae, but an expansion of the zygomatic region. Low sloping frontals are associated with an increase in supraorbital expression as well. In addition to this variation, RW3 also contrasts the placement of the mastoid as well as the size of the superior nuchal line. Increased superior nuchal lines are seen in tandem with a more anteriorly placed mastoid process, while the exact is true for reduction nuchal line morphology.

RW4 explains almost as much variation as RW3 (15.80%) and this component addresses overall cranial vault shape as well as zygomaxillary and frontal morphology (figure S38). Low sloping frontal bones with the greatest height of the vault placed more posteriorly on the parietal bones are contrasted with a more rounded frontal and parietal cranial vault form. Interestingly, the variation in supraorbital morphology along this component is opposite what would be typically expected, with more massive supraorbitals being associated with the a much more rounded vault, while reduction in this region is seen with the low sloping vault configuration. There is also some degree of variation in zygomaxillary breadth along this component, as well as changes in the orientation of the supreme nuchal line (ranging from an arching configuration to a rather flat and linear configuration).

RW5 addresses the final 6.01% of the variance and can be examined in figure S39. This final component addresses only slight levels of morphological variation (given its small portion of the variance explained) and focuses mostly on nuchal line morphology. The supreme and superior nuchal lines range from being close together to rather far apart highlighting variation in the size of the nuchal region. This component also explains some variation in the alveolar region of the maxilla, contrasting larger and more projecting alveolar bones with more reduced ones.

Sub-Saharan Africa – Bantu Population. This sub-set of the Sub-Saharan African sample consists of 18 individuals and provides 17 distinct components of variation from the RWA (addressing 100% of the variance in the dataset). This dataset is analyzed separately from the smaller Khoisan sub-set from Sub-Saharan Africa. The Khoisan dataset will be addressed in the following section. The first 6 components account for a combined 71.90% of the variance and will be addressed in more detail below.

RW1 addresses a great deal of variation in cranial vault form and accounts for 21.02% of the variance (figure S40). Dolichocephalic cranial forms are contrasted with more brachycephalic forms along this component. There is also a significant amount of facial reduction (in all planes) in association with the narrower cranial vault morphologies along with an expansion of the supraorbital region and nuchal region. The opposite is true of the more rounded vault form, with the exception of this form being associated with a larger mastoid process.

RW2 accounts for an additional 18.82% of the variance (figure S41). This component summarizes variation in the facial region as well as the mastoid region of the cranium. Here, crania with overall larger faces (particularly in facial breadth, but also showing a degree of maxillary inflation) are contrasted with smaller faces. Expansion in the facial region is also accompanied by an increase in superciliary arch expression, as well as increase in the size and shape of the mastoid processes. The smaller, more gracile facial configurations are associated with an overall gracilization of these regions, with the

exception of the nuchal region. There is an expansion of both the superior and supreme nuchal lines (forming a torus configuration) in association with the gracilized face.

RW3 addresses variation in a manner similar to RW2 and accounts for 10.03% of the variance (figure S42). Facial form varies from larger to more gracile forms with the larger forms demonstrating increased size in both breadth and midfacial projection. An increase in mastoid size (primarily in mastoid height) accompanies the more reduced facial forms while the opposite is true for the smaller mastoid variations. There is also a slight degree of frontal bone flattening with smaller faces along this component. Finally, RW3 addresses variation in supreme nuchal line expression moving from an external occipital protuberance (as seen with the expanded facial forms) to a more 'torus-like' configuration (associated with the reduced facial forms).

RW4 addresses variation in the midfacial region of the cranium and accounts for 8.73% of the variance explained in the sub-set (figure S43). This component highlights variation in the landmarks around the anterior nasal aperture contrasting wider noses with more narrow noses. Larger frontal processes of the maxilla are associated with the narrow nasal forms while the opposite is true of the wider nasal forms. Narrower nasal configurations are also seen in conjunction with an increase in alveolar projection. Finally this component deals with a degree of flattening on the posterior portion of the frontal bone (where it articulates with the parietals) and this vault configuration is associated with the narrower nasal forms.

RW5 primarily deals with variation in supraorbital and mastoid robusticity and accounts for 7.02% of the variance (figure S44). Here, larger supraorbital configurations (resulting in the expression of a brow ridge) are associated with greatly increased mastoid processes (in all planes). Interestingly, the increase in robusticity in these areas is associated with an overall reduction in facial breadth as well as facial (specifically alveolar) projection. The inverse is true for more robust facial forms along this component.

Finally, RW6 covers 6.30% of the variance explained and again addresses variation in the face as well as the mastoid region (with some other notable areas being covered along this component as well, see figure S45). Larger more robust mastoids are associated with more inflated and projecting maxillae, while reduced mastoids and maxillae are accompanied by an increase in the level of alveolar prognathism. More vertically oriented frontal bones are seen with the reduced facial form and this configuration also demonstrates a reduction in the superior nuchal line (with little variation occurring with the supreme nuchal line along this component).

Sub-Saharan Africa – Khoisan Population. Rounding out the Sub-Saharan sample is a subset of 5 Khoisan individuals. Though small, this subset provides us with some interesting details regarding craniofacial variation. A RWA of this subset provides 4 relative warps accounting for the total amount of variance, and therefore all 4 components will be examined in detail below.

RW1 for the Khoisan sample resembles that of the first axis of variation in the Bantu sample. This component again contrasts elongated, dolichocephalic crania with more rounded, brachycephalic ones and accounts for 38.03% of the variance (figure S46). The longer cranial forms are associated with reduced maxillae, mastoids, and supreme nuchal lines. This cranial form is associated with increased supraorbitals, zygomatics, and superior nuchal lines however. The more brachycephalic cranial forms also show a significant increase in nuchal line size and as well as an increase in the size of the mastoids in length and width.

RW2 deals primarily with maxillary and nuchal variation and accounts for 30.10% of the variance in the dataset (figure S47). Most of the landmark variation here can be seen in the positioning and size of the supreme nuchal line, contrasting high elongated supreme nuchal lines (that form a torus configuration) with low and reduced lines (forming an external occipital protuberance). RW2 shows variation in the maxillary landmarks as well. Landmarks along the maxilla (and also the zygomatics) range from

being more vertically oriented to a swept back configuration. Finally, there is variation in cranial vault shape along this component. At one end of the range of variation, there is distinct occipital flattening, while at the other end of the range of variation, parietal flattening (near the articulation with the frontal bone) can be observed.

RW3 accounts for an additional 21.82% of the variance and can be visualized in figure S48. This component primarily contrasts the projection and length of the superciliary arches. There is also variation in the cranial base along RW3. This variation can be summarized as a degree of flattening in the inferior portion of the occipital (near the foramen magnum). Finally, like RW2, this component also demonstrates flattening of the occipital near lambda and this superior occipital flattening coincides with the inferior flattening described above, creating an angled occipital.

RW4 again demonstrates variation in the supraorbital region and mastoid region and accounts for the final 10.06% of the variation in the Khoisan sub-set (figure S49). Increased supraorbital morphology (in both superciliary height and projection) is seen in tandem with an increase in the mastoid region but a decrease in the size of the orbits. This last component also demonstrates a level of variation in the orientation of the supreme nuchal line ranging from an external occipital protuberance to a diminutive (but present) toral configuration.

Western Europe. The Western European sub-sample contains 17 individuals from Germany and provides 16 non-zero relative warps from a RWA. The first 5 relative warps cover 73.80% of the total variance and will be examined below.

RW1 covers 32.04% of the variance and addresses all areas of robusticity highlighted in the study (figure S50). Increased size and projection of the supraorbital region is seen in tandem with an increase in length and breadth of the mastoid and an increase in the length and expression of the supreme nuchal line (forming a more 'torus-like' configuration). There is also an increase in facial breadth, but not facial length with the more robust supraorbital, mastoid, and nuchal regions. Finally, there is a level of

frontal sloping with the increase in supraorbital robusticity. The more gracile end of the range of the variation along this component (with reduced supraorbital, mastoid and nuchal regions) shows an increase in facial length as well as a flattening of the inferior portion of the occipital at the cranial base.

RW2 again addresses supraorbital variation and accounts for an additional 17.42% of the variance (figure S51). This component addresses variation in superciliary arch projection and length (to a slighter degree). Increases in supraorbital projection are associated with an increase in the height and expression of the supreme nuchal line, again forming a more pronounced torus configuration. The more reduced supraorbital forms are associated with a slight increase in length and breadth of the mastoid process, as well as a greatly diminished supreme nuchal line (although it is important to not that along this component, the supreme nuchal line does not form an external occipital protuberance).

RW3 shows a great deal of variation in the cranial vault as well as facial breadth and nuchal morphology, covering 10.67% of the variance (figure S52). At one end of the range of variation along this component, we see a significant increase in supraorbital projection, as well as an increase in cranial vault size relative to the rest of the cranium. There is also an increase in mastoid breadth (but not length) associated with the expansion of the vault and supraorbital projection. Finally, at this extreme of the range of variation along RW3, there is an increase in the expression of the nuchal lines as well as more inferior placement of them along the occipital. At the other end of the variation along this component, we see a decrease in supraorbital projection, as well as more diminished, and superior placed nuchal lines. Additionally, there is a degree of reduction in the overall size of the cranial vault.

RW4 accounts for 7.67% of the variance in the Western European sub-set and again addresses variation in the supraorbital and nuchal regions (figure S53). Unlike previous components, however, this component focuses mainly on superciliary arch height, rather than projection. Superciliary arch height has an inverse relationship with

nuchal morphology, meaning that as the height of these superstructures increase, there is a subsequent decrease in the expression of the nuchal lines (specifically the supreme nuchal line). Expanded nuchal lines are associated with the lower and more reduced supraorbital region.

RW5 is the last component to be examined in this sub-set and accounts for an additional 6.00% of the variance (figure S54). This component addresses cranial vault shape; especially variation in the rounding of the occipital, where more rounded occipitals are associated with more inferiorly placed nuchal lines, with the opposite being true of the more flattened occipital cranial forms. This occipital rounding also is associated with an increase in mastoid breadth as well as overall decrease in facial breadth and supraorbital projection (especially at glabella). Increased levels of facial and supraorbital robusticity are associated with the more flattened occipital forms.

Regional Robusticity Variation

Australian Aborigines, Frontal Region. While the Australian subsample tends to be on the smaller range of the variation throughout the entire dataset (with an average cranial centroid size of 615.95, the only smaller group in the study is the Khoisan subset), they often demonstrate high levels of cranial robusticity in the supraorbital region. A RWA of the supraorbital landmarks for the Australian subset provides 16 relative warps accounting for the entire range of variation in the supraorbital landmarks. The first 3 RWs account for a cumulative 68.90% (over 2/3) of the variance and will be examined in further detail below.

Accounting for a total of 47.36% of the variance, RW1 highlights variation in superciliary arch length along the medio-lateral axis and also superciliary arch projection in the antero-posterior plane (figure T1). As superciliary arch length increases, there is also an increase in projection. RW2 (accounting for 13.38% of the variance, and highlighted in figure T2) addresses variation in superciliary arch height, especially at

glabella (in the supero-inferior plane) as well as trigone width, with these expression of these two features being tied together (increase in one shows a similar increase in the other). Finally, RW3 (much like RW2) shows variation in medial supraorbital height as well as trigone width, and accounts for 8.15% of the variance in the dataset (figure T3).

Australian Aborigines, Zygomaxillary Region. A RWA of the zygomaxillary region of for the Australian subset provides a total of 16 relative warps account for the total amount of variation in the dataset. Out of those 16 RWs, the first 4 account for a majority of the total variation (69.90%) and will be examined below.

RW1 addresses variation primarily in cheek height (although, recall that the Australian population has smaller zygomaxillary regions compared to the rest of the sample as seen above) as well as the nasal aperture landmarks. This component accounts for 34.63% of the variance (see figure T4) and contrasts greater cheek heights, with lower ones. RW2, accounting for an additional 17.45% of the variance (figure T5) highlights variation in the zygomatic, specifically the width of the frontal process of the zygomatic. Here larger frontal process widths are associated with more massive maxillae, while the reduced frontal processes are associated with reduced maxillae. RW3 highlights variation mostly in the orbital landmarks, but also addresses a degree of variation in zygomatic. This component addresses an additional 8.82% of the variance and can be visualized in figure T6. Finally, figure T7 shows the variation of zygomaxillary landmarks along RW4, which accounts for 8.34% of the variance. This last component demonstrates a slight degree of variation in zygomatic and maxillary massiveness as well as a degree of variation in the frontal process of the zygomatic. The greatest degree of variation seen here is with the anterior projection of the cheek landmarks.

Australian Aborigines, Mastoid Region. Out of the 16 relative warps that make up the RWA for the Australian subset, the first 3 account for 72.35% of the total variance and as a result, will be examined in further detail.

The first relative warp accounts for 35.16% of the variance and addresses variation mainly in mastoid breadth, but it also deals with some variation in length as well (figure T8). RW1 contrasts medio-laterally wide mastoids that are less projecting with mastoids that are very narrow but project more from the base of the skull. RW2 accounts for a relatively high proportion on the variance (23.62%) and accounts for variation in mastoid antero-posterior width, with a degree in variation in the orientation of the mastoid tip (ranging from anteriorly oriented to posteriorly oriented, see figure T9). Finally, RW3 accounts for 13.57% of the variance and highlights variation in mastoid antero-posterior width as well as supero-inferior length (figure T10). Here, wider mastoids tend to be less projecting, while narrower ones have a greater degree projection in the supero-inferior plane.

Australian Aborigines, Occipital Region. The final region to be examined for the Australian population is the occipital region. It has been noted that this population has a high incidence of occipital morphology that in consistent with an occipital torus (Lahr, 1996), and the landmark data in the present study support this observation as well. There are a total of 16 relative warps for the occipital subset of the Australian dataset, with the first 3 accounting for a large proportion of the total variance (88.76%).

RW1 shows a high degree of variation in the supreme nuchal line, ranging from a hyper-robust torus-like configuration, to a reduced external occipital protuberance configuration (figure T11). This component accounts for over half of the entire morphological variation in the Australian dataset (55.64% of the variance explained). RW2 (23.14% variance explained), contrasts the height of the supreme nuchal line with respect to the superior nuchal line, implying variation in the overall size of the occipital torus for individuals in this dataset that demonstrate this morphology (figure T12). RW3 addresses the orientation of the supreme and superior nuchal line and accounts for 9.98% of the variance (figure T13). This final component contrasts curved superior nuchal lines and infero-medial to supero-laterally oriented supreme nuchal lines with a morphology

that is indicative of rather flat superior nuchal lines and supero-medial to infero-laterally oriented supreme nuchal lines.

Sub-Saharan Africa Bantu, Frontal Region. The RWA for the Sub-Saharan African Bantu population dataset (n=18) provides a total of 17 non-zero RWs, accounting for the total variation in the frontal region landmarks. Out of these 17 RWs, the first 4 account for three quarters of the variance (75.00%) and will be addressed here.

RW1 (figure T14) accounts for a grand total of 35.48% of the variance and describes variation in the length and height of the supraorbital region. Here, length and height have an inverse relationship, so as the lateral extent of the superstructure increases, the overall height decreases, particularly around the glabellar region. There is little variation in supraorbital projection along this component, but there is a degree of variation in the lateral trigone. As the lateral extent of the supraorbital region increases, there is also an increase in trigone size. RW2 on the other hand deals strictly with the medial orbital landmarks (refer to figure T15). Variation along this axis covers the medial or lateral placement of the medial orbital landmarks, meaning that there is significant lateral variation in the location of the highest point on the superciliary arch. This component addresses an additional 21.15% if the variance. The third RW covers an additional 11.20% of the variance and can be visualized in figure T16. This axis of variation addresses superciliary height, showing a large degree in the maximum superior extent of the superstructure, particularly at the medial orbital, and glabellar region landmarks. Finally, RW4 (figure T17, accounting for 7.17% of the variation) deals with a slight degree of projection, but mostly with the expression of the lateral trigone. There is also some variation with the orientation of the superior orbital rim. The orbital rim ranges from a more anteriorly projecting orientation to a more posteriorly receding (or inward pointing) orientation. Surprisingly, there is very little evidence for any major degree of variation in the anterior projection of the superciliary arch along all RWs examined (with the exception of RW4, which provides slight evidence at best of this),

suggesting that the Bantu population provides little evidence for projecting supraorbital regions.

Sub-Saharan Africa Bantu, Zygomaxillary Region. The first 4 RW of the 22 zygomaxillary landmarks for the Bantu dataset cover a total of 70.67% of the variance and are highlighted here. RW1 accounts for 29.38% of the variance and addresses variation in the zygomatic and anterior nasal aperture regions (figure T18). Here, a lower nasal breadth is associated with a flatter, more vertical maxilla and a reduced zygomatic region. RW2 deals mostly with variation in the frontal process of the zygomatic, and accounts for an additional 17.67% of the variance (figure T19). While there is a slight degree in alveolar projection along this component also, the bulk of the variation seen in the coordinate landmarks is along the frontal process of the zygomatic. Landmarks vary from a rather narrow and reduced frontal process to a greatly expanded one. There is also a degree of zygomatic expansion that accompanies the increase in the frontal process of this bone. RW3 addresses cheek height, alveolar (particularly premaxillary) prognathism, and the orientation of the zygomaxillary region in the antero-posterior plane ("swept-back" versus an orthographic orientation). This component accounts for almost 14% (13.99% to be exact) of the variance and can be visualized in figure T20). Here, a swept-back zygomaxillary orientation is coupled with a drastic increase in alveolar prognathism, as well as a decrease in cheek height, while the opposite is true for the more vertical orientation of the zygomaxillary region. Finally, RW4, which accounts for 9.65% of the variance (figure T21) deals mostly with overall facial height. Posterior expansion of the zygomatic bone accompanies an overall decrease in facial height, while the opposite is true for the reduction of the zygomatic.

Sub-Saharan Africa Bantu, Mastoid Region. The mastoid region of the Bantu dataset encompasses 10 landmarks and a RWA of these landmarks provides us with a total of 17 RWs, out of which the first 4 cover three quarters of the total variation (75.52% exactly). These four RWs will be examined in the space below.

RW1 accounts for 38.32% of the variance explained and can be seen graphically in figure T22. This component addresses variation in the antero-posterior plane, contrasting wider mastoid processes with much narrower ones. Wider mastoids also tend to be less projecting inferiorly, and are expanded in breadth (medio-lateral plane) while the opposite is true for the more narrow mastoid configuration. RW2 on the other hand addresses variation in the anterior border of the mastoid process, as well as variation in the tip of the structure (figure T23). The second relative warp covers an additional 15.84% of the variation in the dataset contrasts a more pointed mastoid tip, with a more rounded one. There is also variation in the orientation of the anterior border of the mastoid ranging from a more anteriorly placed point of porion, to a more posteriorly oriented location for this landmark. RW3 accounts for 12.13% of the variance and deals only with landmark variation in the medio-lateral plane. Here, variation in mastoid breadth is highlighted for the data set without being tied to any other form of landmark variation (figure T24). Finally, RW4 (figure T25) addresses 9.22% of the variation in the dataset, and this component highlights variation in the projection of the mastoid tip inferiorly from the cranial base.

Sub-Saharan Africa Bantu, Occipital Region. The last morphological area to be examined within the Sub-Saharan Bantu population is the occipital region. This region is comprised of 8 landmarks, and provides a total of 17 relative warps, of which the first 3 RWs account for over 90% of the variance (90.53%). These three relative warps will be described below.

RW1 accounts for a great deal of the morphological variation in the dataset (71.54%) and can be seen in figure T26. Here there is a large degree of variation in the supreme nuchal line landmarks, raging from a diminutive external occipital protuberance to a laterally expanded supreme nuchal line that gives the appearance of a “torus-like” configuration. In comparison to RW1, the second relative warp explains a much smaller percentage of the variance in this dataset (only, 13.96%) and this component deals with

the height of the supreme nuchal line. There is variation in the superior placement of the supreme nuchal line along the occipital bone, ranging from a position that is only slightly above the superior nuchal line, to one that is placed much more superiorly on the occipital (see figure T27). RW3 addresses the curvature of the superior nuchal line, with little variation in the supreme nuchal line (which has been the focus for the previous two components) and this final relative warp accounts for only 5.03% of the variation (figure T28). This component contrasts a flatter, more superior nuchal line, particularly in the 3 most medial semilandmarks, with a configuration that is much more curved and superiorly placed in the more medial aspect of the structure.

Central Europe, Frontal Region. The Central European sub-sample is composed of 19 individuals and therefore provides 18 non-zero relative warps from the RWA. Of these 18 relative warps, the first 4 RWs account for almost 80% of the total variance (79.88%) and will be examined in greater detail in the following section.

RW1 accounts for 38.19% of the variance in this sub-sample and can be examined visually in figure T29. This component (like most other first relative warps that have been examined so far) addresses variation in the medio-lateral length of the superciliary arch. There is also a large degree of anterior projection of the supraorbital region along this component, which is also associated with the increase in length. In addition to this, there is also expansion of the lateral trigone in association with the more robust supraorbital configuration. RW2 also deals with variation in the expression of the lateral trigone, but here this variation is tied to expansion, both in supero-inferior length, as well as antero-posterior projection, of the glabellar region and medial aspect of the superciliary arch. This component accounts for an additional 24.67% of the variance in the dataset (figure T30). There is slight variation in the lateral extent of the superstructure, but most of this variation is not due to the high degree of variability in the super-inferior expression of the medial supraorbital semilandmark line, but rather its medio-lateral placement. While the first two RWs account to over half the total variance,

the next two deal with much smaller levels of variation. RW3 only accounts for 9.52% of the variance, and this variation can be summed up as uniform variation in supero-inferior height (figure T31). This component contrasts a superiorly expanded supraorbital region with a more S-I compressed supraorbital region. There is no medio-lateral or antero-posterior variation along this axis. Finally, RW4 addresses variation mostly in the placement of supraglabella (the landmark superior to glabella that marks the edge of the projection of the glabellar region), and accounts for a total of 7.51% of the variance (figure T32). Here, a larger (i.e. expansion in the supero-inferior plane) glabellar region is also tied to expansion of the lateral aspect of the superciliary arch as well as the lateral trigone.

Central Europe, Zygomaxillary Region. The zygomaxillary region of the Central European dataset provides a total of 18 relative warps, with the first 4 addressing the majority of the overall variance (68.99%). These 4 RWs will be examined in detail below.

RW1 accounts for a substantial majority of the overall dataset variance at 37.14%, which is greater than RWs 2-4 combined, and can be see graphically in figure T33. This component addresses variation in the anterior nasal aperture landmarks, as well as the zygomatic region of the face. Here, more posteriorly elongated zygomatic bones are associated with a wider frontal process of the zygomatic as well as a more projecting alveolar process and lower maximum nasal breadth. The opposite is true for the smaller, more gracile zygomatic configuration. RW2 summarizes variation in overall facial breadth and height, and accounts for an additional 12.92% of the variance (figure T34). As the face tends to become wider along this component, it also tends to get shorter, while elongated faces also tend to be narrower in breadth. RW3 explains another 10.88% of the variance and addresses variation mostly in the zygomatic region (figure T35). This component contrasts small, gracile zygomatics with narrower frontal processes, with more robust ones. There is little other variation in landmark placement along this

component. Finally, RW4 appears to also deal with facial breadth but along this component, variation in breadth is tied to variation in the alveolar region of the maxilla (figure T36). This relative warp axis accounts for 8.05% of the variance and shows an association between wider faces and a more reduced alveolar region while the opposite is true of narrower faces.

Central Europe, Mastoid Region. There are a total of 18 relative warps for the Central Europe mastoid RWA, of which the first 3 relative warps account for a majority of the overall variation. The combined variance explained for these first 3 RWs is 74.19% and will be addressed more closely in the following section.

RW1 for the mastoid coordinate data subset accounts for the majority of the variance at 41.27% (figure T37). This relative warp addresses variation in mastoid height and projection from the base of the skull contrasting long projecting mastoid processes with shorter ones. RW2 accounts for another 19.21% of the variation and deals mostly in breadth variation (figure T38). Along with this variation in medio-lateral breadth, there is an inverse associated change in mastoid antero-posterior width. Mastoids that have greater M-L dimensions also have lower A-P widths, and vice versa. Finally, RW3 deals with mastoid width and orientation and this component accounts for 13.71% of the total variation (figure T39). Wider mastoids tend to have a mastoid tip that is more anteriorly oriented, while narrower M-L mastoids tend to have more posteriorly oriented mastoids tips.

Central Europe, Occipital Region. The last morphological region in the Central European dataset is the occipital region, which consists of 17 relative warps. The first three RWs account for over 90% of the total variation (91.37%). These 3 relative warps are addressed in further detail below.

RW1 explains the majority of the dataset's occipital variation (76.01%) and demonstrates a similar pattern to what has been seen thus far in other samples. Along this component, there is a contrast between the expression of a small external occipital

protuberance (where the supreme nuchal line only extends slightly laterally beyond the midline) and an expanded, laterally elongated supreme nuchal line (figure T40). RW2 encapsulates variation in the height of the supreme nuchal line relative to the superior nuchal line, and explains an additional 10.31% of the variation (figure T41). This pattern has also been highlighted in other regional datasets (such as the Bantu population discussed above). Finally, RW3 accounts for 5.05% of the coordinate landmark variation and this component deals with the orientation of the supreme nuchal line (figure T42). This component contrasts supreme nuchal lines that follow a supero-medial to infero-lateral orientation with supreme nuchal lines that run infero-medially to supero-laterally. It should be noted that among these three components, there is very little shape difference along the superior nuchal line, showing that the form of this structure is more conserved then some of the other populations studied.

China, Frontal Region. A relative warps analysis of the Chinese sub-sample provides a total of 10 non-zero relative warps for the 20 landmark supraorbital region. Of these, the first four relative warps account for a total of 80.08% of the total dataset variance. These relative warps will be examined in further detail below.

The first relative warp addresses 42.64% of the variance and summarizes variation in supraorbital medio-lateral length and lateral trigone size (figure T43). As has been seen in previous sub-samples, this component contrasts superciliary arches that are larger and extend further laterally over the orbit with ones that are more diminished. More laterally extending superciliary arches are seen in conjunction with an increase in trigone size showing further evidence for an association between these two structures. RW2 accounts for overall supero-inferior height of the supraorbital region and accounts for 15.33% of the variance (figure T44). As superciliary height increases there is a concurrent increase in lateral extent of the arch, while a decrease in height is accompanied by a decrease in the lateral extent of the arch. RW3, accounting for an additional 12.58% of the variance, summarizes variation in the expression of the lateral

trigone (figure T45). There is also a degree of anterior projection summarized in this component, but interestingly, there is an inverse relationship between trigone size and overall anterior projection of the superciliary arch. So, as trigone size increases, supraorbital projection decreases. Finally, RW4 contrasts projecting superciliary arches with flatter ones and accounts for 9.53% of the variance (figure T46). Along this component, there is also a rather drastic increase in glabellar region size and the medial orbital section of the superciliary arch.

China, Zygomaxillary Region. RWA of the facial region of the Chinese sub-set provides a total of 10 relative warps accounting for all the variation in this region of the skull. Of these relative warps, the first 4 account for nearly 3/4 of the variation (74.91%) in the entire dataset and will be discussed in the following section.

RW1 summarizes variation in overall facial height as well as zygomatic size and accounts for the majority of the variation in the dataset at 35.46% (figure T47). Along this component, and increase in facial height as accompanied be a drastic decrease in zygomatic size. A decrease in facial height, on the other hand, is associated with an increase in the size of the frontal process of the zygomatic as well as an overall increase in zygomatic A-P length. RW2 show a great degree of variation in alveolar prognathism (particularly in the pre-maxillary region) as well as variation once again in zygomatic expression. This component accounts for an additional 17.07% of the variance and can be seen graphically in figure T48. There is also variation in anterior nasal aperture along RW2 contrasting a more laterally extending position of alare with a more medial placement of this landmark as well as variation in the overall height of the anterior nasal aperture. The configuration with the less projecting alveolar process also is associated with an increase in overall zygomatic massiveness. RW3 accounts for 12.44% of the variation (figure T49) and addresses variation mostly in the posterior aspect of the alveolar region of the maxilla, which impacts overall maxillary height. Faces with slightly lesser maxillary height also tend to be broader (medio-laterally) along this

component. Lastly, RW4 addresses significant change in the overall expansion, and particularly the projection of the zygomatic region. This final component addresses nearly 10% of the variance (9.94%) and can be visualized in figure T50.

China, Mastoid Region. These first 3 relative warps of the mastoid landmark dataset in the Chinese sub-sample accounts for over 80% of the variation (82.88%) in the mastoid region. RW1 addresses variation in overall mastoid length and projection, and accounts for the majority of variation in the mastoid coordinate landmark dataset (45.87%, see figure T51). As has been seen in other groups, more projecting mastoid processes are associated with a decrease in overall mastoid A-P length, while the opposite is true of a decrease in mastoid projection. RW2, on the other hand, addresses variation in the orientation of the mastoid process, and accounts for an additional 24.05% (figure T52). Along this component, the mastoid processes ranges from having a very anteriorly oriented mastoid tip, to being more symmetrical in the antero-posterior plan. More anteriorly oriented mastoids also tend to be narrower than the more symmetrical forms. RW3, accounting for 12.95% of the variance, once again shows variation in antero-posterior length (figure T53). Interestingly, there is little variation in mastoid medio-lateral breadth amongst these first three components, meaning that variation in this axis (which has been common in the other groups studied thus far) is fairly absent here.

China, Occipital Region. The final region under study in the Chinese sub-set is the occipital region. A relative warps analysis for this area of study provides us with a total of 10 warps, of which the first 3 account for a vast majority of the dataset's variation (94.42%). RW1, contributing to 3/4 (75.32%) of the variation in this sub-set, addresses variation in the overall length of the supreme nuchal line (figure T54). Here the supreme nuchal line ranges in variation from about 1/3 the length of the superior nuchal line all the way to being equivalent in length to the superior nuchal line. Thus far, no other dataset has shown this level of length variation for the supreme nuchal line (including the Australian subset, which is largely characterized by 'torus-like' occipital regions). There

is also a deal of arching of the both nuchal lines along this axis of variation. RW2, accounting an additional 12.47% toward the overall variation in occipital morphology, continues this trend in increased length of the supreme nuchal line (figure T55). Along this component, the supreme nuchal line runs almost the entire length of the superior nuchal line, and displays variation in overall orientation (with an inverse relationship of medial supreme nuchal line height to lateral nuchal line height). This type of nuchal line variation has been seen in other groups as well in the present study. Finally, RW3 accounts for 6.64% of the variation, and accounts for variation almost exclusively in the medial aspect of the superior nuchal line (figure T56). Here, the landmarks that make up the medial aspect of the superior nuchal line are placed much further inferiorly on the occipital bone, accentuating the 'arch-like; configuration of both the superior and supreme nuchal lines. The supreme nuchal line along this component still runs for almost the entire length of the superior nuchal line (again, a phenomenon which has not been documented in the population sub-sets studied above). Overall, the Chinese occipital landmark dataset provides some interesting departures from typical patterns in the variation in the region documented thus far.

India, Frontal Region. Switching focus now to the Indian sub-sample, a relative warps analysis of the supraorbital data, provides a total of 11 non-zero components for the 21 coordinate landmarks that comprise this set. The first relative warps cover 75.58% of the data and will be examined in further detail below.

RW1 provides a similar pattern that has been seen in every other group so far with variation being summarized mostly in the lateral length of the superciliary arch, as well as an increase in superciliary height and lateral trigone size. This component covers 27.55% of the overall supraorbital landmark variation and is represented graphically in figure T57. As the superciliary arch increases in M-L length, it increases in both supero-inferior dimensionality as well as lateral trigone size. These three factors of supraorbital variation appear tied to one another across the entire global dataset. RW2, on the other

hand, addresses variation mostly in the medial orbital landmark line (near the glabellar region) and accounts for another 18.63% of the variation (figure T58). An increase in glabellar region size is associated with a more medially occurring medial orbital landmark line, providing evidence that this component contrasts expanded medial supraorbital forms with rather gracilized ones. The other extreme form along this axis of variation shows a slightly expanded lateral trigone area while the medial component of the superstructure is reduced. RW3 addresses variation in superciliary arch height and covers 17.32% of the variation in the dataset (figure T59). Here, an increase in supraorbital height is associated with a very slight increase in supraorbital projection in the A-P plane, but this projection is very minimal. Finally, RW4 addresses variation almost solely in lateral trigone size as well as a degree of A-P projection in the medial aspect of the superciliary arch. This final component addresses 12.09% of the variance and is represented in figure T60. It is interesting to note that A-P projection is inversely related to trigone size along this component, meaning that a drastic increase in trigone size is associated with a decrease in supraorbital projection. Across all the components studied for this superstructure in the Indian coordinate landmark dataset, there has been little to no variation in supraorbital projection, in contrast to several of the groups highlighted above.

India, Zygomaxillary Region. The zygomaxillary landmark dataset for the Indian sub-sample provides a total of 11 relative warps covering the entire amount of variation for this region. Of these, the first 4 account for over 3/4 (76.10%) of the total variation, and will be analyzed to provide insight in this region.

RW1 provides an inverse relationship between maxillary and zygomatic size and expression, and this first component addresses the greatest amount of variation in the dataset (30.71%, see figure T61). Facial forms with larger zygomatics tend to have a diminished maxillary region, while the opposite is true for reduced zygomatics. Increases in maxillary expression focus on the projection alveolar region, while larger zygomatic

forms show increase in the frontal process and the length of the zygomatic body. RW2 accounts for 20.95% of the variation and highlights variation the anterior nasal aperture (figure T62). The shape of the anterior nasal aperture varies from being rather wide at alare, and narrowing as you move superiorly to the opposite form (a wider aperture superiorly, with lower widths inferiorly, around the position of alare). Narrower apertures also appear to be associated with an increase in pre-maxillary projection. RW3 accounts for another 14.58% of the variation in the dataset, and this variation is manifest in cheek height and maxillary expression (figure T63). Decreased cheek heights are associated with a decrease in both maxillary and zygomatic expression, and overall facial height is loosely associated with this variation in cheek height as well. Finally, RW4 addresses variation in facial breadth (particularly in the zygomatic region) and accounts for 9.87% of the variance in the dataset (figure T64). Most of the variation in breadth seems tied to variation width and height in the zygomatic region.

India, Mastoid Region. Explaining variance for over 80% of the entire data, the first 3 relative warps for the mastoid landmark dataset will be covered in this section. RW1 accounting for just over half (52.55%) of the total variance, summarizes both antero-posterior and supero-inferior variation in the dataset (figure T65). As the mastoid process becomes more supero-inferiorly elongated (and more projecting for the cranial base) it tends to become more A-P compressed. Larger A-P dimensions, on the other hand, are associated with a less projecting mastoid process. RW2 also deals with mastoid projection from the cranial base, but along this component, the majority of the landmark variation is associated with the anterior border of the mastoid. This second component accounts for an additional 17.59% of the variance (figure T66). Reduced and less projecting mastoids are seen in conjunction with a more ‘concave-like’ appearance of the anterior border, while the opposite is true for a ‘convex-like’ anterior border shape. Finally, RW3 addresses variation in both M-L breadth of the mastoid as well as the orientation of the mastoid tip (14.47% variance explained, see figure T67). Here, a more

anteriorly oriented mastoid tip is associated with a narrower mastoid breadth, while wider mastoid breadths are seen with a less anteriorly oriented mastoid tip.

India, Occipital Region. The final set of data to be examined for the Indian sub-sample is from the occipital region. A RWA of this coordinate landmark dataset provides a total of 11 non-zero relative warps, with the first 3 accounting for nearly all the variation in the dataset (95.59% total variance explained). As such, these relative warps will be examined below.

RW1 accounts for a total of 84.16% of the variance and can be viewed in figure T68. This relative warp addresses variation in the external occipital protuberance (formed by the supreme nuchal line). Along this first component, the supreme nuchal line ranges in expression from a diminutive external occipital protuberance with very limited lateral extension to a greatly expanded form which runs the entire length of the superior nuchal line. RW2, accounting for another 6.98% of the variance, addressed the supero-inferior placement of the supreme nuchal line in relation to the superior nuchal line (with little to no variation in medio-lateral length, see figure T69). A higher placement of the supreme nuchal line is associated with a slight decrease in the size of the superior nuchal line, with the superior nuchal line expanding in M-L length as the supreme nuchal line moves inferiorly along the occipital. Unlike the first two relative warps, which show patterns of variation seen elsewhere in the other regional datasets, RW3 (accounting for another 4.44% of the variance) summarizes an aspect of variation unique to the Indian sub-sample (figure T70). Along this final component, the supreme nuchal line ranges from being level with the superior nuchal line to having a sharply inferiorly oriented lateral aspect. In turn, the superior nuchal line ranges from being rather flat to having a sharp curvature, with a greater degree of superior nuchal line curvature being associated with the flatter supreme nuchal line form.

Sub-Saharan Africa Khoisan, Frontal Region. Although it is a small dataset, the African Khoisan sub-sample provides us with some interesting insights into the variation

of people in the Sub-Saharan region. There are a total of 4 relative warps in the Khoisan sub-sample with the first 3 making up a total of 91.30% of the total variation. As a result, these relative warps axes will be examined in further detail.

RW1 accounts for 43.43% of the supraorbital variance in the Khoisan sub-sample and is graphically represented in figure T71. This axis summarizes variation in superciliary arch projection as well as lateral trigone size and positioning of medial orbital landmarks. An increase in supraorbital anterior projection is accompanied by a likewise increase in lateral trigone size and a more medial (i.e. closer to glabella) placement of the medial orbital landmarks. As the projection of the superciliary region decreases, there is also a decrease in lateral trigone expression and a more lateral placement of the medial orbital landmarks. RW2 accounts for an additional 26.61% of the variation in the dataset and this component deals with variation in superciliary arch height and projection (figure T72). An increase in arch height along this component is tied to a decrease in supraorbital projection, while the opposite is true of more anteriorly projecting supraorbital regions. Finally, RW3 accounts for 21.25% of the variance and this component addresses variation in the lateral expression of the superciliary arch as well as (once again) lateral trigone size (figure T73). Interestingly, as superciliary arch length increases there is a concurrent decrease in the size of the lateral trigone region.

Sub-Saharan Africa Khoisan, Zygomaxillary Region. The zygomaxillary region RWA once again provides us with 4 non-zero relative warps, of which the first 3 account for a total of 88.13% of the variance in the dataset. RW1 summarizes 48.51% of the total variance and addresses variation in maxillary and zygomatic bone massiveness (figure T74). As the maxilla increases in size and expression (with a larger alveolar region, and more massive frontal process and a slightly larger anterior nasal aperture), there is a decrease in the size (especially in antero-posterior length) of the zygomatic region. RW2 shows variation in the orientation of the zygomatics and maxillae, and this component accounts for an additional 24.53% of the variation (figure T75). Here, as the anterior

portion of the maxilla is rotated superiorly, there is a consequent inferior rotation of the zygomatic region, as well as an increase in projection of the body of the zygomatic. RW3 accounts for another 15.08% of the variance, and it addresses variation in maxillary size (figure T76). This component simply contrasts larger maxillae with smaller ones. Along this last component, there is a slight increase in nasal breadth associated with the smaller maxillary configuration, but it is interesting to note that there has been little variation in the anterior nasal aperture landmarks for this regional subset compared to other groups.

Sub-Saharan Africa Khoisan, Mastoid Region. The coordinate landmark dataset for the Khoisan mastoid region once again provides a total of 4 relative warps, of which the first 3 (accounting for a total of 95.96% of the variance) are summarized in this section. RW1 contrasts variation in mastoids with large A-P widths and minimal projection beyond the cranial base, with very narrow A-P widths and drastically increased M-L breadths as well as a greater degree of projection beyond the cranial base. This component accounts for 54.46% of the total variance in the dataset, and the patterns of mastoid variation along RW1 can be viewed in figure T77. RW2 also deals with variation in mastoid A-P width and accounts for 31.64% of the variation (figure T78). The variation in this component, however, is far less drastic than what has been seen in the first relative warp. A slight increase in A-P width of the mastoid along RW2 is also associated with a slight decrease in mastoid projection, while the opposite is true of decreased A-P widths. RW3 follows this same trend and also describes variation in A-P width, although along this component the greatest change in width is not at the base of the mastoid, but closer to the tip (figure T79). This component accounts for 9.86% of the remaining variation in the mastoid dataset.

Sub-Saharan Africa Khoisan, Occipital Region. A RWA of the occipital region presents us with a total of 4 relative warps accounting for the total variation in the

dataset. The first 3 relative warps summarize almost all of the variation (98.14%) in this dataset and will be examined in detail below.

RW1 covers over 3/4 (75.68%) of the total variation in the dataset and this first component addresses variation in the supreme nuchal line (figure T80). Along this first component, the supreme nuchal line ranges from a minor external occipital protuberance, to a greatly expanded (in both medio-lateral and supero-inferior dimensions) line almost indicative of a nuchal torus-like configuration. The expanded supreme nuchal line also is associated with a slight decrease in the expression of the superior nuchal line. RW2 addresses another 16.02% of the variance (figure T81) and this component shows variation in the positioning of the supreme nuchal line. Supreme nuchal line placement along RW2 ranges from a medial starting position to a more lateral starting position. This form of supreme nuchal line variation has not been seen in the other sub-samples studied above. Finally, RW3 addresses curvature of the superior nuchal line, as well as the lateral positioning of the supreme nuchal line, and this component accounts for 6.44% of the variance (figure T82). As superior nuchal line curvature increases along this component, the lateral aspect of the supreme nuchal line becomes more inferiorly oriented. Less curvature in the superior nuchal line is associated with a superiorly oriented lateral supreme nuchal line.

Mediterranean and Near East, Frontal Region. For the Mediterranean and Near East sub-sample, the RWA provides a total of 20 non-zero components, accounting for the entire range of variation in the dataset. Components 1-4 account for nearly 4/5 (79.41%) of the total range of variation in this geographical region, and as a result, these 4 components will be examined in greater detail below.

RW1 accounts for 44.14% of the total variance in the dataset and addresses variation (similar to many of the other samples studied) superciliary arch length, as well as lateral trigone size and supraorbital projection (figure T83). Along this first component, as the length of the superciliary arch increases, there is also a noted increase

in the anterior projection of the superciliary arch as well an increase in the massiveness of the lateral trigone. RW2 also shows variation in the projection of the supraorbital region, but this time, variation in projection is tied to overall height of the superciliary arch, as well as the M-L placement of the medial orbital semilandmark line (figure T84). This component addresses another 17.94% of the variation in the dataset. Increase in the height of the superciliary arch occurs in conjunction with an expansion of the glabellar region (as well as a more medial placement of the medial orbital semilandmark line). Also tied to this is an increase in the anterior projection of the supraorbital region as well as a slight expansion of the lateral trigone. RW3 deals with superciliary height and projection and accounts for another 10.61% of the variance explained (figure T85). Interestingly, this component shows an association of greater supraorbital projection with a more compressed (supero-inferiorly) superciliary arch. An increase in height of the superciliary arch along RW3 is associated with a decrease (contrary to RW2) in anterior projection. Finally, RW4 addresses superciliary height and medial expansion of the glabellar region (as well as some additional variation in the lateral trigone size) and accounts for 6.72% of the variation in the dataset (figure T86). Expansion of the entire glabellar region (identified here as an increase in superciliary arch height medially, as well as a more lateral placement and expansion of the medial orbital semilandmark line) is associated again with an increase in the massiveness of the lateral trigone.

Mediterranean and Near East, Zygomaxillary Region. The zygomaxillary landmark dataset for the Mediterranean and Near East sample consists of 22 landmarks, with a RWA providing a total of 20 non-zero relative warps. Of the total 20 relative warps, the first 4 account for a majority of the variance in the dataset (69.08%) and are examined in further detail below.

RW1 for the zygomaxillary landmark dataset accounts for a total of 24.05% of the overall variation (figure T87). This component contrasts expanded zygomatic regions (particularly in the area of the frontal process) with more reduced zygomatics, as well as

a high degree of facial prognathism contrasted with a more orthognathic face. A reduced zygomatic region is coupled with a more projecting face along this component while the opposite is true of the expanded zygomatic form. Variation in anterior nasal aperture breadth (at alare) is also present along this component. RW2 once again contrasts differences in zygomatic shape as well as an overall level of facial height. This component accounts for another large portion of the variance (22.90%) and can be observed in figure T88. More elongated facial forms along this component have larger zygomatic regions and a greater degree of lower facial prognathism, while the more antero-posterior reduced facial form also tends to be associated with a greater supero-inferior height. RW3, accounting for another 15.00% of the variance, addresses variation almost exclusively in the supero-inferior plane (figure T89). This component contrasts faces with greater height dimensions with one with reduced facial heights. There is also a degree of variation in orbital shape along this component. The final relative warp to be examined, RW4 (7.14% variance explained, see figure T90), addresses a slight degree of variation in both zygomatic expression as well as facial prognathism. While the overall level of variation in this component is reduced, it shows a similar pattern to that seen in the first relative warp: reduced zygomatics are associated with an increase in lower facial prognathism, and vice versa.

Mediterranean and Near East, Mastoid Region. A relative warps analysis for the mastoid coordinate landmark data provides 20 components, of which the first 4 account for over 3/4 (76.53%) of the overall variation in the dataset. RW1 (accounting for 41.50% of the overall variance) demonstrates variation in mastoid projection (figure T91). This component contrasts mastoids that have higher degrees of inferior projection beyond the cranial base with ones that are much more reduced in this dimension. There is also variation in the orientation of the mastoid tip, ranging from a more anteriorly oriented tip (found in conjunction with decreased mastoid projection) to a relatively more posterior orientation (as the mastoid becomes more projecting). RW2 covers an

additional 18.10% of the variation in the dataset, and this component also addresses mastoid orientation and projection, although the pattern that this component displays is opposite that of RW1 (figure T92). Here, more anteriorly oriented mastoids tend to be more projecting, while more posteriorly oriented mastoids tend to be less projecting. This 2nd component also shows a slight degree of variation in mastoid breadth, with more projecting mastoids tending to be slightly broader in the medio-lateral plane. RW3 addresses variation in mastoid height and A-P width, and accounts for another 9.60% of the overall variance (figure T93). The pattern displayed in this component has been seen in previous datasets as well: mastoids with wider A-P widths tend to have decreased height dimensions, while narrower mastoids also tend to have higher mastoid heights. Finally, RW4 covers variation almost completely in the medio-lateral plane. This component accounts for 7.34% of the remaining variation and can be seen graphically in figure T94. While almost no landmark variation occurs in either the A-P or S-I planes, there is a considerable amount of M-L variation along this RW axis (variation that is either missing entirely or is greatly subdued in previous relative warps) indicating that there is little variation mastoid breadth in this population.

Mediterranean and Near East, Occipital Region. As has been the case in all of the previous groups examined thus far, the first 3 relative warps for the occipital region RWA explain nearly all of the variation seen in the dataset (93.73%). These three components, therefore, will be examined in further detail below.

RW1 accounts for the vast majority of the variation in the dataset at 78.08% and is represented in figure T95. This component (like most other RW1s for the other groups studied) addresses variation in supreme nuchal line expression. Along RW1, the supreme nuchal line varies in expression from a diminutive external occipital protuberance, to an extremely elongated and prominent supreme nuchal line. There is also a slight degree in variation in the length and curvature of the superior nuchal line (although no where near as evident as the supreme nuchal line) with longer superior nuchal lines with greater

curvature being associated with the external occipital protuberance-like expression of the supreme nuchal line. RW2 addresses variation in the height of the supreme nuchal line from the superior nuchal line, and accounts for an additional 8.94% of the variance in the dataset (figure T96). In configurations that place the supreme nuchal line closer to the superior nuchal line (that is to say, where the supreme nuchal line is lower on the occipital), there is an expansion of the superior nuchal line in overall size. As the supreme nuchal line increases in distance superiorly from the superior nuchal line, the overall size of the superior nuchal line decreases. Finally, RW3 addresses variation almost completely in the medial aspect of the supreme nuchal line. This component addresses an additional 6.71% of the variance (figure T97). Here, the medial-most landmark on the supreme nuchal line varies from being close to the superior nuchal line, to being placed further superior along the midline of the occipital.

New Guinea, Frontal Region. While the New Guinea sample is one of the smallest sub-samples in the present study (n=5), it nonetheless demonstrates a large degree of variation in cranial robusticity features. Due to this fact, the New Guinea sample will be analyzed in the following section. An RWA of the coordinate landmark data provide only 4 non-zero relative warps, of which the first 3 account for 94.05% of the variance explained.

RW1 in the New Guinea sample provides a remarkable range of variation in supraorbital expression, ranging from a diminutive superciliary arch, to a massive supraorbital torus. This component accounts for over half the variation in the dataset (58.60%) and can be viewed in figure T98. The superciliary arch configuration is characterized by a reduced medial orbital region, including glabella, a more medially placed arch that does not extend laterally over the orbit, and a reduced lateral trigone. Also, this form shows almost no anterior projection. The torus configuration, on the other, extends the entire length of the orbit, with greatly expanded lateral trigone and glabellar region. This robust configuration also shows a large degree of anterior

projection. RW2 shows variation in supraorbital height and projection, and this component accounts for an additional 19.54% of the variance explained (figure T99). Here, an increase in the supero-inferior dimensionality of the supraorbital region is coupled with an increase in anterior projection, while reduction in the S-I dimension of the region also results in a reduction in supraorbital projection. Finally, RW3 accounts for 15.91% of the variance in the dataset and demonstrates variation in the placement medial orbital semilandmark line (figure T100). Placement of this structure ranges from a more medial position, seen in tandem with an overall reduction in the S-I dimensionality of the supraorbital region (particularly on the more lateral aspect) to a more lateral position (which in concurrent with an overall expansion of the lateral supraorbital region).

New Guinea, Zygomaxillary Region. The RWA for the zygomaxillary region of the New Guinea sample provides a total of 4 non-zero relative warps (again, due to the small size of this sub-sample). Of these, the first 3 account for a total of 91.47% and are covered in further detail here. RW1 covers 48.90% of the variance and demonstrates a rather complex pattern of variation (figure T101). This component addresses variation in zygomatic and maxillary projection in a manner similar to what has been seen above: as the zygomatic increases in massiveness, particularly in the size and prominence of the zygomatic body, the level of maxillary projection (specifically alveolar prognathism) decreases, and vice versa. In addition to this variation, there is also a component of zygomatic orientation to this component. The posterior aspect of the zygomatic becomes more superiorly oriented (so that it appears to rotate in a counter-clockwise manner when viewed from the lateral side) as the level of alveolar prognathism increases. In all morphs of the facial region along this component, there is a high degree of overall prognathism, with midfacial prognathism being maintained throughout both extremes of the variation. RW2 shows a pattern similar to RW1, albeit with a much reduced level of landmark variation, but the main focus of the variation along this axis can been seen in

the midfacial region. This component accounts for an additional 31.84% of the variation and can be visualized in figure T102. The anterior nasal aperture points range from a marked degree of midfacial prognathism to a much lower degree of prognathism. There is also level of variation seen in the frontal process of the zygomatic, where variation ranges from a tall and more pronounced frontal process to a more reduced one. Finally, RW3 addresses variation in the alveolar region of the maxilla, and accounts for 10.73% of the variance explained (figure T103). An expansion of the alveolar region of the maxilla is concurrent with an overall decrease in mid-facial prognathism, while the opposite is true of a more reduced alveolar region.

New Guinea, Mastoid Region. A RWA for the mastoid coordinate landmark data provides a total of 4 relative warps, with the first 3 accounting for 97.05% of the total variance in the dataset. The first relative warp, accounting for just over half (50.81%) of the total variance demonstrates variation in the M-L breadth of the mastoid process, as well as the amount of projection and orientation of the tip of the mastoid (figure T104). More anteriorly placed mastoid tips tend to also have greater M-L breadths as well as a slightly higher degree of projection from cranial base. The opposite is true of mastoid processes that are more posteriorly oriented. This latter case is far more gracile than the former anteriorly oriented mastoid form. RW2 demonstrates variation once again in M-L breadth, but in this case, variation of this nature is tied to the A-P width of the mastoid (as well as a slight component of mastoid projection as well). This second component accounts for 31.51% of the variance and is depicted graphically in figure T105. As A-P width increases along RW2, there is a concurrent decrease in both M-L breadth, and inferior projection of the mastoid tip, while a decrease in A-P width shows both an increase in these other two dimensions. RW3 deals solely with mastoid breadth, and this final relative warp accounts for an additional 14.73% of the variance in the dataset (figure T106). Breadth variation is far greater along this component than what has been seen in

the previous two components, while the rest of the landmarks show almost no variation in positioning whatsoever.

New Guinea, Occipital Region. As with all the other superstructures for the New Guinea sample, the entire range of variation in the landmark dataset is summarized by 4 relative warps, with the first 3 accounting for almost all the variation present (99.58%). Of these first three RWs, the first relative warp accounts for the vast majority of the dataset variation at 88.73% (figure T107). RW1 demonstrates variation ranging from a gracile external occipital protuberance to a full 'torus-like' configuration. In the later form, there is a considerable degree of separation between the superior and supreme nuchal line demonstrating an extremely robust nuchal region at the far end of the range of variation. RW2 accounts for a much smaller portion of the dataset variation (7.66%) and this component demonstrates variation in the height of the supreme nuchal line (figure T108). Here, the supreme nuchal line remains small in M-L length, but its position along the occipital varies from an inferior position, close to the superior nuchal line, to a much more superior position. Finally, RW3 accounts for an additional 3.19% of the variation, and this component also deals with variation in the expression of the supreme nuchal line (figure T109). Much like RW2, this component also deals with variation in the supreme nuchal line in the supero-inferior plane, but only with respect to the middle landmark. The endpoints of the supreme nuchal line remain fixed along RW3 (which is the opposite of what can be seen in RW2).

North Africa, Frontal Region. The North African coordinate landmark dataset is comprised of 9 individuals primarily from Libya. The RWA of this sub-set provides a total of 8 relative warps, with the first 3 relative warps totaling just over 80% (80.24%) of the entire range of variation in the dataset. These 3 RWs will be examined in further detail in the following section.

RW1 shows a pattern of variation seen in many samples already studied. Along this component, there is variation in the overall lateral extent of the superciliary arch, and

this variation accounts for most (i.e. 44.52%) of this dataset's variation (figure T110). The superciliary arch ranges from being more reduced and medially oriented, to a configuration that is more laterally expanded. The more laterally expanded supraorbital region also has a tendency to be slightly more projecting anteriorly, also. RW2 provides information on supraorbital height variation, and this component accounts for an additional 21.23% of the total variance (figure T111). While there is little variation in the length of the superciliary arch in this component, there is a marked level of supero-inferior height variation in this superstructure, with higher superciliary arches proving to also be more projecting, while the more reduced variants are both smaller and less projecting. RW3 provides information on medial semilandmark line positioning as well as lateral trigone size, and this final component accounts for another 14.48% of the total landmark variation (figure T112). This type of variation has also been seen previously, where the medial semilandmark line varies from a more medial position (closer to glabella), resulting in a more reduced medial portion of the superstructure, to a more lateral position. This component also provides information on lateral trigone variation, with larger, more prominent trigones being associated with a more medial (and, interestingly, a more reduced) superciliary arch.

North Africa, Zygomaxillary Region. A relative warps analysis of the zygomaxillary region provides a total of 8 RW scores, accounting for 100% of the variation in this dataset. Of these 8 RWs, the first 4 account for 85.84% of the total variance and will be examined in further detail below.

RW1 accounts for a total of 44.84% of the total zygomaxillary landmark variance and this component can be seen graphically in figure T113. The majority of the variation along this axis can be observed along the anterior nasal aperture and pre-maxillary region. Facial form ranges from very orthognathic (with an extended frontal process of the maxilla and an almost recessed prosthion resulting in a very vertical pre-maxillary region) to a much more prognathic configuration with a much smaller frontal process.

RW2 shows variation mostly in the size and orientation of the zygomatic region and accounts for another 21.35% of the total dataset variance (figure T114). The smaller zygomatic form also has a more counter-clockwise rotated orientation (where the posterior aspect of the bone is more superiorly oriented) while the larger form also tends to be more A-P oriented and also more prominent in relation to its projection. RW3, accounting for 11.78% of the variance, addresses variation in the posterior border of the zygomatic bone (specifically along the frontal process, see figure T115). At one extent of the range of variation along this component, the posterior border of the zygomatic is more anteriorly oriented, causing an overall shift in the placement of the frontal process of the zygomatic to a more anterior position. The other end of the range variation places the frontal process of the zygomatic more posteriorly. Associated with the anterior movement of this region is an increase in the projection (and overall massiveness) of the zygomatic body. Finally, RW4 accounts for 7.86% of the variation, and this component addresses a small degree of variation once again in the zygomatic bone (figure T116). Here, there is variation in the morphology of the posterior border of the zygomatic around the position of jugale, ranging from a very concave shape of the posterior border, to an almost convex shape (where jugale is placed in a more posterior position).

North Africa, Mastoid Region. The results of the mastoid region RWA are similar to those seen in the zygomaxillary region above. Of the 8 total components, the first 4 in the mastoid dataset account for the majority (85.96%) of the variation. These 4 components will be examined in further detail in this section.

RW1 addresses variation in the height of the mastoid process, and accounts for 38.18% of the total variation (figure T117). An increase in mastoid height along this axis, equates to an increase in the projection of the mastoid tip beyond the basicranial plane. There is also a slight degree of variation in the orientation of the mastoid process (from a more anterior to more posterior positioning of the mastoid tip) along this component. As mastoid height increases, the mastoid tip tends to be positioned more

posteriorly, and vice versa. RW2 deals almost entirely with the anterior or posterior placement of the mastoid tip (similar to what was seen in RW1) and accounts for a total of 20.27% of the total variance (figure T118). This variation in orientation is tied to a slight degree of variation in mastoid breadth (in the M-L plane), where more posteriorly oriented mastoid processes tend to have higher M-L dimensions, than the more anteriorly oriented mastoid processes. RW3 covers variation in the M-L breadth of the mastoid, and accounts for an additional 16.07% of the variation (figure T119). Breadth dimensions for the mastoid process range from reduced, to rather high along this axis of variation. RW4 deals primarily with the A-P width of the mastoid process and this final component covers 11.44% of the variation (figure T120). Mastoid width demonstrates an association with mastoid height along this component. Wider mastoids also tend to have shorter height dimensions, while narrower mastoids are also taller.

North Africa, Occipital Region. The following section provides a relative warps analysis of occipital region coordinate landmark data for North African sample. Of the 8 total relative warps provided in this analysis, the first 3 cover the majority (totaling 91.00%) of the variance. RW1 accounts for 60.51% of the total variance and this component addresses variation in the supreme nuchal line (figure T121). Along this first axis of variation, the supreme nuchal line ranges from a more reduced and flat variant (nearly resembling the typical external occipital protuberance form) to a more expanded and arching variant (which is larger, but not necessarily 'torus-like'). RW2 provides information on supreme nuchal line height, and this component accounts for an additional 18.79% of the total variance (figure T122). Here, the supreme nuchal line varies from occupying a position close to the superior nuchal line to being represented more superiorly along the occipital. As the overall height of the supreme nuchal line increases, there is also a trend for the lateral aspect of the supreme nuchal line to become more superiorly oriented relative to the medial aspect of the line. RW3, the final relative warp to be examined here, accounts for 11.71% of the total variance, and can be viewed in

figure T123. This component covers variation in both the supreme and superior nuchal line. As the superior nuchal line becomes more curved, there is a concurrent lengthening of the supreme nuchal line, while a decrease in superior nuchal line curvature (i.e. the superior nuchal line becomes more flat and more medial-laterally oriented) there is a reduction in the expression of the supreme nuchal line.

Singapore, Frontal Region. Individuals from Singapore (in addition to the New Guinea sample discussed above) provide us with a picture of craniofacial variation in the Southeast Asian region. This sample consists of n=6 individuals, with a total of 5 non-zero relative warps. Of these 5 total RWs, the first 3 components account for the overall majority of variation in the sample (totaling 87.74%).

RW1, which addresses 45.81% of the total variance in the dataset, contrasts very robust supraorbital regions with very gracile ones (figure T124). Along this component, the supraorbital region ranges from only slightly projecting, with a reduced lateral trigone and reduced superciliary arch height (especially as you move laterally along the superstructure) to a fully represented 'orbital torus-like' structure, which spans almost the entire supraorbital area, with increased anterior projection, a greatly increased lateral trigone region, and an expanded height and medio-lateral length. RW2 (30.91% variance explained), on the other hand, deals primarily with superciliary arch height, with only minimal variation in the medial or lateral aspect of the structure (figure T125). Superciliary arch height varies from small, to rather large, particularly in the medial orbital region. There is also a slight degree of variation in trigone size (not to the extent seen in RW1, however), where slightly larger trigones are associated with reduced superciliary arch heights. Finally, RW3 accounts for 11.02% of the total variance, and this component summarizes variation in supraorbital projection, and to a lesser extent, trigone size and glabellar height (figure T126). As supraorbital projection increases along this axis of variation, there is a subsequent reduction in lateral trigone and glabellar size, while the opposite is true of less projection supraorbital regions.

Singapore, Zygomaxillary Region. The RWA on the zygomaxillary coordinate landmark dataset for the Singapore sample provides us with a total of 5 relative warp scores, of which the first 3 account for 84.67% of the total variation. These 3 RWs will be examined in further detail here. RW1 accounts for the largest portion of variation in the dataset at 46.04% and this component explains variation in alveolar prognathism, orbital size, and, to a lesser extent, zygomatic size (figure T127). As lower facial prognathism (at the point of prosthion) increases, there is a concurrent decrease in both orbital size and zygomatic size. The opposite is true of the more orthognathic facial from, where noticeably increased orbital size and zygomatic massiveness can be observed. RW2 highlights variation mostly in the zygomatic region, with some secondary increases in alveolar region as well. This component describes another 26.71% of the variance in the dataset and can be visualized in figure T128. Variation in the zygomatic can be seen in both the frontal and temporal processes of the zygomatic, where at one extreme of the range of variation, both of these processes are expanded posteriorly to provide greater widths in these processes, while they are reduced at the other extreme (however, at this other end of the range of variation, there is a slight increase in the projection of the zygomatic body). Decreases in zygomatic size occur concurrently with an increase in the size of the alveolar region (although this increase is not necessarily tied to an increase in lower facial prognathism). Finally, RW3 describes 11.92% of the variation and this component demonstrates low levels of landmark variation across the component (figure T129). Observing discernable trends in landmark variation along RW3 is difficult given the low level of variation explained, however, like in the previous 2 RWs, there seems to be variation in the alveolar landmarks as well as some variation in the zygomatic landmarks. Once again, the A-P length of the zygomatic bone varies along this component, as well as the placement of some of the alveolar landmarks.

Singapore, Mastoid Region. There are a total of 5 relative warp axes generated from the RWA for the mastoid coordinate landmark dataset in the Singapore sample. Of these 5, the first 3 summarize a total of 94.82% of the variation observed. These 3 components will be examined in further detail below.

RW1 accounts for almost 48% (47.99%) of the total variance, and this component summarizes variation in mastoid height and width (figure T130). As with most of the datasets observed in this section, the primary mode of variation here is supero-inferior height, coupled with the degree of projection of the mastoid tip beyond the basicranium. More projecting mastoids also tend to be narrower in the antero-posterior dimension, while mastoids that barely project beyond the base of the skull are much wider. RW2 highlights variation in mastoid M-L breadth, as well as an overall anterior vs. posterior orientation of the mastoid, and this component addresses 31.43% of the total dataset variance (figure T131). As M-L breadth increases along RW2, the mastoid process becomes more anteriorly oriented (as far as placement of the mastoid tip is concerned). This orientation changes to a more posterior placed position as the breadth decreases. Finally, RW3 accounts for 15.40% of the total variance, and this component also deals with mastoid breadth, only along this component, breadth is tied to the shape of the anterior border of the mastoid (figure T132). An increase in M-L breadth along this component occurs in unison with a more concavely shaped anterior mastoid border (which, like RW1, provides decreased mastoid widths). As the M-L dimension of the mastoid is reduced, the anterior border of the mastoid becomes more convex (as shape tied to wider mastoid dimensions).

Singapore, Occipital Region. A RWA of the occipital superstructure region provides a total of 5 relative warps, with the first 3 accounting for nearly all (97.36%) of the variation in the dataset. These 3 components will be examined in this section. RW1 accounts for the vast majority of variation in this dataset at 85.67% (figure T133). The mean shape for the superior and supreme nuchal lines shows a rather large expansion of

the supreme nuchal line (more so than most of the populations examined previously). Along RW1, the supreme nuchal line ranges from a diminutive external occipital protuberance, to providing a much more prominent and almost 'torus-like' configuration. As the length of the supreme nuchal line increases there is a slight be noticeable decrease in the length of the superior nuchal line as well. RW2 accounts for an additional 7.03% of the variance for the occipital dataset, and this component primarily addresses the height of the supreme nuchal line in relation to the superior nuchal line (figure T134). While the most lateral point of the supreme nuchal line stays rather fixed in space, the medial and middle semilandmarks range from a position close to the superior nuchal line to a position (especially with regard to the middle semilandmark) that is much more superior along the occipital. This increase in supreme nuchal line height is accompanied by an overall increase in the curvature of the superior nuchal line. Finally, RW3 accounts for 4.67% of the variation, and this component displays another rather common form of variation in the supreme nuchal line (figure T135). Here, the supreme nuchal line varies from an infero-medial to supero-lateral orientation to an orientation that runs supero-medial to infero-lateral. As the supreme nuchal line approaches a more infero-medial to supero-lateral orientation, the curvature of the superior nuchal line increases rather drastically, while the opposite is true of the other supreme nuchal line configuration.

Western Europe, Frontal Region. The Western European sample consists of n=17 individuals, and provides a total of 16 non-zero relative warps for the frontal region RWA. Of these 16 RWs, the first 4 account for over 3/4 of the total variation (77.82%), and these components will be examined in further detail in the following section.

RW1 accounts for a total of 32.44% of the overall variation in the dataset (figure T136. This component addresses variation primarily in the placement of the medial orbital semilandmark line. Along RW1, the placement of this line ranges from a more medial position (in closer proximity to the glabellar region) to a more lateral position (closer to the mid-orbital semilandmark line). Also, as the medial orbital line becomes

more laterally oriented, there is a slight increase in the supero-inferior height of the superciliary arch as well, demonstrating once again the relationship of higher degrees of supraorbital robusticity with a more lateral placement of the medial orbital semilandmark line. RW2 accounts for another significant portion of the overall variance at 24.61%, and this component demonstrates a marked level of variation in supraorbital (anterior) projection (figure T137). The amount of variation seen in supraorbital projection along this component is among the most notable in the entire global dataset. Once again, this aspect of supraorbital robusticity (supraorbital projection) is tied to a more laterally elongated superciliary arch. It is interesting to note, that along this axis of variation, a more reduced glabellar region is tied to an increase supraorbital projection, and not vice versa. RW3 addresses variation primarily in the shape of the superior orbital rim as well the expression of the lateral trigone, and this component accounts for another 11.68% of the variation explained (figure T138). As the lateral trigone expands in size along this component, the superior orbital rim tends to become flatter and more medio-laterally oriented. The opposite (a more curved superior orbital rim) is associated with a decrease in the expression of the lateral trigone. Finally, RW4 once again demonstrates variation in supraorbital projection (although not as marked as RW2) as well as variation in the medial and mid-orbital semilandmark lines. This component accounts for another 9.08% of the variation explained, and can be visualized graphically in figure T139. Along this component supraorbital projection appears to be tied to a decrease in the medio-lateral length of the superciliary arch. The M-L length of this region, however, is determined by a more complex relationship of the supraorbital semilandmark lines. In most circumstances seen above, an increase in supraorbital length was shown by a more lateral placement of both the medial and mid-orbital semilandmark lines. Along this component, an increase in the lateral length of the supraorbital region is shown by a more medial positioning of the medial orbital semilandmark line and a more lateral placement of the mid-orbital semilandmark line (i.e. The two semilandmark lines are further apart

from each other). The opposite extreme along this component shows a laterally shortened superciliary arch where the medial and mid-orbital semilandmark lines are in close proximity to each other.

Western Europe, Zygomaxillary Region. The RWA for the Western European zygomaxillary region provides a total of 16 non-zero RWs, which account for 100% of the variation in the sample. Variation in region is rather complex compared to many of the samples studied previously, in that it requires 5 RWs to explain just over 75% of the variation in the dataset – most of the previous datasets accomplish this in 2 or 3 relative warps. As a result the first 5 RWs will be examined in greater detail below.

RW1 accounts for 27.09% of the variation in the Western European dataset and variation along this component can be visualized in figure T140. RW1 describes variation primarily in zygomatic expression and the shape of the anterior nasal aperture. At one extreme, the anterior nasal aperture points and the landmarks defining the midline of the face are elongated supero-inferiorly, resulting in a very superiorly placed nasion (indicating an elongated frontal process of the maxilla) and a more inferiorly elongated prosthion and alveolar process. This configuration also demonstrates a very narrow nasal breadth (alare to midline). This increased elongation of the anterior portion of the face is associated with a reduced zygomatic. Enlarged zygomatic regions along RW1 are associated with a reduction in the anterior face. RW2 accounts for variation in the form of the orbit, as well as the zygomatic, and addresses another 19.91% of the variance in the dataset (figure T141). Here, there is a marked increase in the size (particularly the A-P width) of the frontal process of the zygomatic, which defines the lateral border of the orbit. The orbit, itself, ranges from a larger (particularly in the supero-inferior aspect, but with an increase in M-L width as well) form to a more reduced form. The size of the zygomatic body as well as the frontal process of the zygomatic is associated with an increase in the dimensionality of the orbit. As opposed to the previous components, RW3 addresses a more narrowly defined axis of variation (accounting for 15.53% of the

variation explained). Along the 3rd component, shape variation is manifested in the posterior aspect of the zygomatic, primarily in the elongation of the temporal process of the zygomatic (figure T142). A marked degree of variation in the posterior zygomatic is noted here as well as variation in the size of the alveolar region of the maxilla. A decreased alveolar region is associated with an increase in posterior zygomatic length, while the opposite is true for a reduced alveolar region. RW4 accounts for 7.48% of the variation (figure T143) and this component addresses overall variation in facial A-P length. An increase in zygomatic A-P length (as particularly noted in the frontal process of the zygomatic) is associated with an increase in anterior projection of the alveolar region causing the face to range from a more elongated antero-posterior form to a more reduced antero-posterior form. Finally, RW5 accounts for an additional 6.89% of the variance and can be visualized in figure T144. This component addresses variation primarily in the positioning of jugale as well as inferior aspect of the maxilla (again, around the alveolar region). A more deeply positioned jugale (resulting in a reduction of both A-P widths for the frontal process as well as S-I height of the temporal process) coincides with a decrease in the expression of the inferior aspect of the maxilla, particularly with respect to the alveolar process. This form also shows a marked increase in the anterior projection of the anterior nasal aperture and nasal bones.

Western Europe, Mastoid Region. The mastoid region RWA provides a total of 16 RWs with the first 4 explaining the majority of the overall variation in the dataset (81.75%). These 4 relative warps will be analyzed in the following section.

RW1 accounts for 36.54% of the overall variation in the mastoid RWA and this component summarizes variation in mastoid supero-inferior height and antero-posterior length (figure T145). This pattern of morphological variation has been common amongst all populations studied and is by no surprise the primary mode of variation here as well. As mastoid height increases along this component, there is a subsequent decrease in mastoid length, while the opposite is true for decreases in the height component. Also, as

mastoid height increases, there is a concurrent increase in mastoid projection beyond the occipital plane. RW2 primarily summarizes mastoid medio-lateral breadth, and this component accounts for an additional 21.86% of the variation explained (figure T146). While breadth variation along this component is considerable, there is little other noteworthy variation present. RW3 summarizes a less common but still present form of shape variation in the mastoid. Here, morphological variation is manifest in the anterior vs. posterior orientation of the mastoid process. That is to say, at one extreme of the range of variation, the mastoid tip is more anteriorly oriented causing the overall height axis of the mastoid to slant in a supero-posterior to infero-anterior way. The other extreme shows the mastoid in a more vertical supero-inferior orientation. This 3rd component addresses 13.54% of the variation in the dataset and can be seen graphically in figure T147). Finally, RW4 accounts for 9.80% of the variation and this component accounts primarily for mastoid projection beyond the occipital plane (figure T148). While this accounts for most of the variation along RW4, there is a degree of variation in mastoid A-P length as well. As mastoid projection increases there is also an increase in the A-P length of the mastoid as well.

Western Europe, Occipital Region. The final section of the Western European regional robusticity variation RWA provides a total of 16 RWs with the first 3 accounting for the vast majority of the overall variation in both supreme and superior nuchal line expression. These 3 components address a total of 94.67% of the variation and will be addressed in the next section.

RW1 for the occipital region RWA (as has been the case in most samples studied thus far) accounts for a very high percentage of the overall shape variation in the sample at 83.72% (figure T149). This variation can be summarized as an increase or decrease in the lateral extension of the supreme nuchal line. At one extreme of the range of variation, the supreme nuchal line forms a small external occipital protuberance, while at the other extreme; it is laterally expanded to an almost ‘torus-like’ expression. The external

occipital protuberance form demonstrates marked curvature of the superior nuchal line, while the more 'torus-like' configuration is accompanied by a more laterally expanded and more linear superior nuchal line. RW2 accounts for variation in supreme nuchal line height, and this component addresses another 7.05% of the variation (figure T150). Here, there supreme nuchal line ranges from being in contact with the superior nuchal line to the other extreme which places it at a more superior location along the occipital above the superior nuchal line. Finally, RW3 accounts for 3.90% of the total variation and this component demonstrates shape variation in the orientation of the supreme nuchal line (figure T151). Along this axis of variation, the supreme nuchal line ranges from an orientation that is best described as infero-medial to supero-lateral, to an orientation that is supero-medial to infero-lateral (while this second orientation is more exaggerated than the first orientation). There is also a slight degree of variation in the curvature of the superior nuchal line as well along this axis of variation.

Regional Dataset Cluster Analysis

In order to examine the nature of robusticity variation across the 11 regional samples, a hierarchical cluster analysis is provided. A dendrogram based on the GM shape data for each regional sample (based on the average relative warps scores within each region) demonstrates clear affinities among sub-Saharan African groups and the Australian subsample, as well as some affinities among the south east Asian groups (figure T152). The Singapore and China subsamples are clustered together and are separate from the rest of the global subsamples. The Central and Western Europe subsample cluster closely together with close affinities to the Mediterranean/Near east subsample, as well as the N. African subsample. Finally, both sub-Saharan African groups (the Bantu and Khoisan subsamples) cluster closely together, and both of these groups demonstrate a close relationship to the Australian subsample.

Populational Variability and Craniofacial Robusticity

While defining robusticity in the cranium across the global sample serves as the primary focus of this dissertation, understanding variability in aspects of robusticity between the regional populations can provide a more in-depth look at how craniofacial robusticity varies with other variables (such as subsistence patterns). It is the goal of this section to highlight variability between the 11 sub-samples studied across 8 regions of the Old World and to provide a discussion of factors that may be indicated in the expression of craniofacial robusticity.

Variability in Size

With respect to overall cranial size, the two smallest groups studied are the Sub-Saharan Khoisan and Australian Aborigines. These two groups have followed hunter-gatherer subsistence patterns up until relatively recently and are often used as proxies for hunter-gatherer populations with respect to lifeways (Carlson et al, 2007; Gilligan and Bulbeck, 2007). The Sub-Saharan Bantu population demonstrates the largest average centroid size across the entire cranial landmark dataset with the North African and Singapore (Malay Peninsula) samples also demonstrating greater centroid sizes than the global mean. The mean centroid size for the global dataset is 627.56mm and many sub-samples, including the Asian populations (India and China) as well as the Western European sample fall very near the global mean (see Table 3).

Patterns in craniofacial centroid size variation in the dataset appear to separate non-hunter-gatherer populations from the hunter-gatherer populations. Geographic location plays a smaller role in cranial size variability in the present dataset, but it is recognized that across more expansive datasets, cranial size is affected by factors such as climate and Bergmann's Rule (Beals et al, 1984). The primary importance of mean cranial centroid size data is to serve as a scaling factor in highlighting variation in size differences between the cranial superstructures studied. Given that cranial size is

variable across the dataset, scaling is required in order to facilitate direct comparisons of supraorbital, facial, mastoid, and nuchal region size. These data will be considered with respect to geographic location and subsistence patterns below.

With respect to the frontal region, the present data provides insight into global variability in supraorbital size. Within the sample, the most gracile supraorbital region is found within the New Guinea sample with respect to both absolute size and size relative to the overall craniofacial centroid size. The largest supraorbital region, on the other hand, is found within the Australian sample. It should be noted that with respect to absolute size, the Australian sample is not the largest (the Sub-Saharan Bantu population demonstrates the largest supraorbital region with respect to absolute centroid size), but given the smaller craniofacial size of the Australian population, when scaled, this sample contains largest supraorbital regions. Other populations that contain relatively small supraorbital regions consist of the Indian and Sub-Saharan Khoisan populations. In addition to the Australian sample, the Western Europe, Singapore, and Sub-Saharan Bantu populations demonstrate the largest supraorbital regions (both in relative and absolute size).

Zygomaxillary centroid size is used as a proxy for overall facial massiveness, and given the results of the centroid size data, the Indian sample contains the smallest zygomaxillary region relative to craniofacial size, but it is not the smallest absolute size. The Sub-Saharan Khoisan demonstrates the smallest overall facial sizes, and this is again due to their rather small craniofacial dimensions with respect to the rest of the global sample. The Sub-Saharan Khoisan as well as the North African and New Guinea populations demonstrate the lowest zygomaxillary sizes with respect of overall craniofacial size, while the largest relative (and absolute) zygomaxillary size is found within the Singapore population. The Chinese, Sub-Saharan Bantu, and Australian Aborigine samples also demonstrate larger than average zygomaxillary regions. With respect to the Australian sample, absolute facial sizes are on the small end, but when

scaled to overall craniofacial size, they are among the largest in the dataset. The Western European, Central European, and Mediterranean/Near East sample all demonstrate remarkably similar absolute and scaled zygomaxillary sizes (which fall around the mean zygomaxillary size). This is an interesting result give the close geographical proximity of these three populations.

Within the mastoid region dataset, the largest overall (and scaled) centroid sizes are seen within the Singapore and Chinese populations. Recall that these populations also share relatively, and absolutely larger zygomaxillary sizes as well. The Australian and Sub-Saharan Khoisan contain the smallest overall mastoid regions, which again, is due to their recorded lower craniofacial centroid sizes. However, these two populations also demonstrate the lowest relative mastoid sizes with respect to overall craniofacial size, which may be in relation to subsistence patterns. The rest of the populations in the global dataset fall right around the mean, with the Mediterranean/Near East and Western European samples demonstrating relatively larger than average mastoids, and the Central European and Sub-Saharan Bantu populations demonstrating relatively smaller than average mastoids.

The occipital region dataset provides some interesting insights into the interplay between size and shape across the global sample. While the Australian Aborigine population has been shown in past research to display nuchal tori (see Lahr, 1996), a result that is confirmed in the discussion of shape below, with respect to absolute and relative nuchal region centroid size, this population falls within the low end of global sample. This result, coupled with the lack of correlation between size and discrete measures of occipital robusticity, is used as evidence that while size may be a factor in nuchal torus expression, it is not the primary factor. It is argued here that shape expression is the primary factor in nuchal torus morphology. The smallest nuchal region centroid sizes are found within the Sub-Saharan Bantu, Indian, and Chinese samples, while the largest nuchal regions are found within the Western Europe, Singapore, and

New Guinea samples. The similarity in centroid size numbers between the Singapore and New Guinea samples is interesting given their close geographic location.

Variability in Shape

Shape expression within the frontal region across the regional dataset highlights three components of shape that are variable for supraorbital morphology. These components are: 1) the lateral extent of the superciliary arch, 2) projection of the supraorbital region, 3) lateral trigone size. Note that while projection and trigone size may be a factor in inter-populational variability, when considered across the entire dataset, variation in these aspects across *all* populations is relatively small and does not account for the levels of variability seen in supraorbital M-L length or S-I height. All populations demonstrate a strong lateral component to the shape of the supraorbital region (discussed above for the entire dataset) once again demonstrating that variability medio-lateral length is the primary indicator of supraorbital robusticity. While this is the case, there is variability in how medio-lateral length of the supraorbital region relates to other aspect of supraorbital morphology. The Australian, Sub-Saharan Khoisan, and North African populations all demonstrate a degree of anterior projection of the supraorbital region coupled with increases in the lateral extent of the superciliary arch. On the other hand, the Chinese and Indian samples highlight variability in lateral trigone expression as well as medio-lateral length. The majority of the samples, however, highlight variability in all three of these aspects, contrasting gracile supraorbital regions (with a reduced M-L component, slight or non-existent anterior projection, and reduced lateral trigone) with a more torus-like configuration (consisting of an expanded M-L component, increased supraorbital projection, and an enlarged trigone).

When considering inter-populational variability in the zygomaxillary region, height and projection play a role in demarcating populations. Most populations demonstrate high levels of variability in zygomatic size (either in cheek height, or overall

massiveness) with respect to maxillary size or, in some cases, anterior nasal aperture shape. While this is the case, there is a degree of lower facial prognathism that also factors into variability across many of the regional samples, including the Central European, Indian, Mediterranean/Near East, New Guinea, North African, and Singapore samples.

While there are differences in both absolute and relative size of the mastoid region between the 11 sub-samples, shape variability across the entire dataset is rather uniform. All samples studied highlight a strong component of mastoid projection, where projecting mastoids are contrasted with much smaller configurations. Differences arise across the geographic populations with respect to what aspect(s) of mastoid morphology vary with mastoid projection. In some populations, such as the Mediterranean/Near East, New Guinea, and North African samples, the orientation of the mastoid tip (either being more anteriorly or posteriorly placed) factors into the variability of mastoid projection. However, across the majority of the samples studied, anterior-posterior width factors into mastoid projection. As mastoid projection increases (a configuration that is often accompanied by increased M-L breadth), A-P width decreases. Less projecting mastoids tend to have lager A-P widths.

Variation in the occipital region primarily involves the expression of the supreme nuchal line. While most samples studied provide evidence for an external occipital protuberance (based on the size and shape of the supreme nuchal line in comparison to the superior nuchal line) there is a high degree of variability seen in this structure. While configurations that highlight a more nuchal torus-like morphology can be seen primarily in the Australian sample, examples of this morphology occur across many of the sub-samples in the global dataset, including the Sub-Saharan Bantu, Sub-Saharan Khoisan, New Guinea, Singapore, and Western European samples. While torus configurations are rare in all of the other samples, evidence for variability in supreme nuchal line length (which is the key aspect in nuchal torus expression) is apparent.

Global Patterns and Trends in Craniofacial Robusticity

As has been discussed above, there are many similarities with respect to size and shape across the regions of craniofacial robusticity studied in the regional subsamples. These patterns, such as variability in M-L supraorbital length, size and expression of the zygomatic bone, projection of the mastoid beyond the occipital plane, and the contrasting morphologies of an external occipital protuberance and (in some cases) a fully expressed nuchal torus, appear to be present across all regions. It is argued here that these features may be indicative of patterns of craniofacial robusticity within *Homo sapiens*. While this is the case, there are some slight differences that appear between many of the populations that might be indicative of geographical variability or subsistence patterns.

With respect to aspects of absolute size, the Australian and Sub-Saharan Khoisan populations tend to demonstrate smaller craniofacial *and* superstructure dimensions. Given relative size, however, these populations display a more complex pattern of expression in craniofacial robusticity. The Australian population, for example, highlights relatively large supraorbital and zygomaxillary configurations, but smaller nuchal region size. When shape of the nuchal region is considered, this population also displays a high frequency of torus-like nuchal morphology. A higher than average degree of supraorbital projection is consistent with both the Khoisan and Australian populations even though the Khoisan demonstrates a decreased centroid size of the supraorbital region. It is possible that aspects of morphology such as these may be tied to a primarily (up until recently) hunter-gatherer style of subsistence. Previous arguments based on post-cranial anatomy have also indicated subsistence, and more specifically, mobility, as a primary cause in the expression of robusticity (Carlson et al, 2007; Cowgill and Hager, 2007; Cowgill, 2009; Shackelford, 2007; Holt and Formicola, 2008; Maggiano et al, 2008). A similar, albeit indirect, relationship may exist between mobility and activity patterns with craniofacial robusticity as well. This could be tied to arguments of systemic robusticity responses to external stimuli (Lieberman, 1996).

While not common in the present dataset, some populations that are geographically close to one another demonstrate similar affinities in aspects of craniofacial robusticity. Similar supraorbital sizes indicated in the European and Mediterranean/Near East populations, as well as the diminished nuchal regions of the New Guinea and Singapore populations may serve as evidence that craniofacial robusticity has a geographic component to it as well. Likewise, similarities such as the shape of the supraorbital region of the Indian and Chinese samples with respect to trigone expression may also be indicative of geographical location to a minor extent. A cluster analysis of the regional dataset relative warp scores provides further evidence for a relationship between shape-related measures of cranial robusticity and global proximity, by grouping most subsamples based on geographic location. Close geographical location may imply that similar climates or a possible presence of gene flow may also contribute to the expression of craniofacial robusticity. Questions such as these could serve as grounds for future research regarding the global distribution of features indicated in craniofacial robusticity.

APPENDIX B. DISCRETE CODING AND COORDINATE LANDMARK DATA COLLECTION

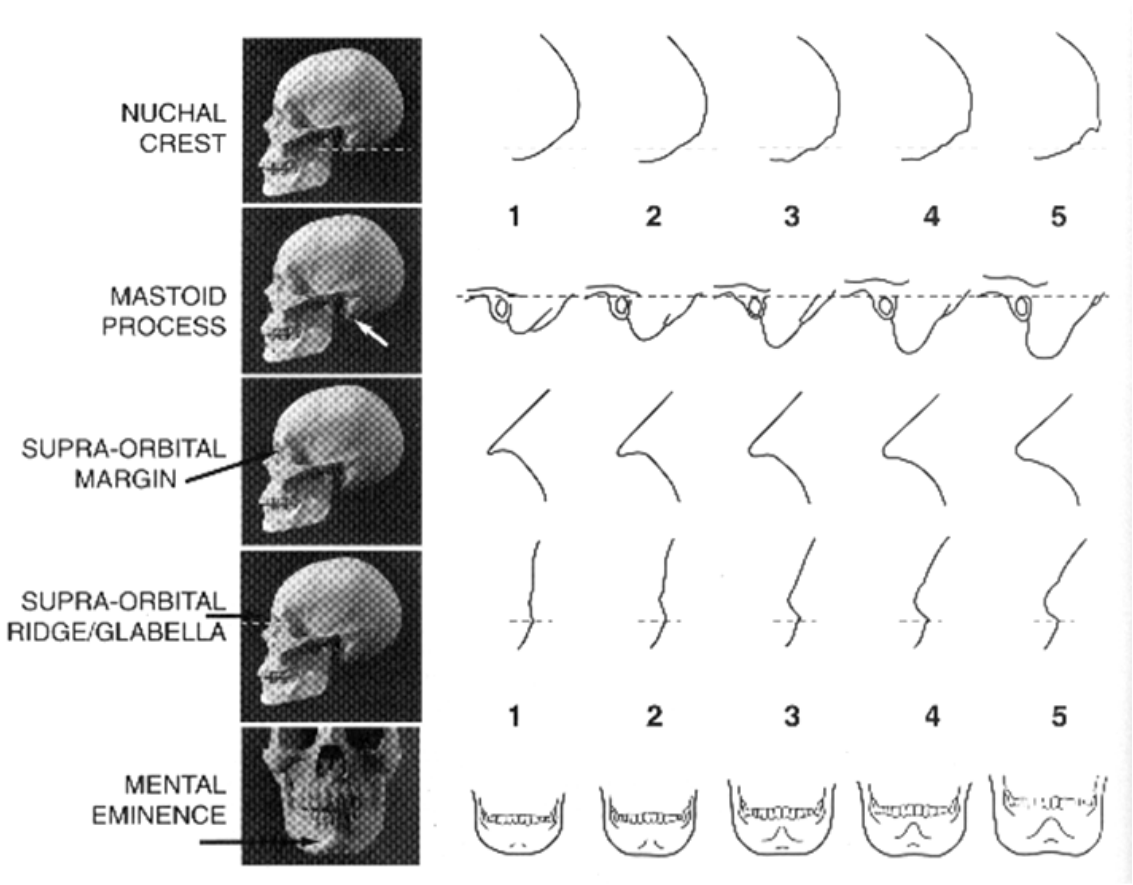

Figure B1. Discrete coding of sexually dimorphic characters for use in sex determination based on cranial anatomy (from Walker in Buikstra and Ubelaker, 1994). Image taken from White, 2000.

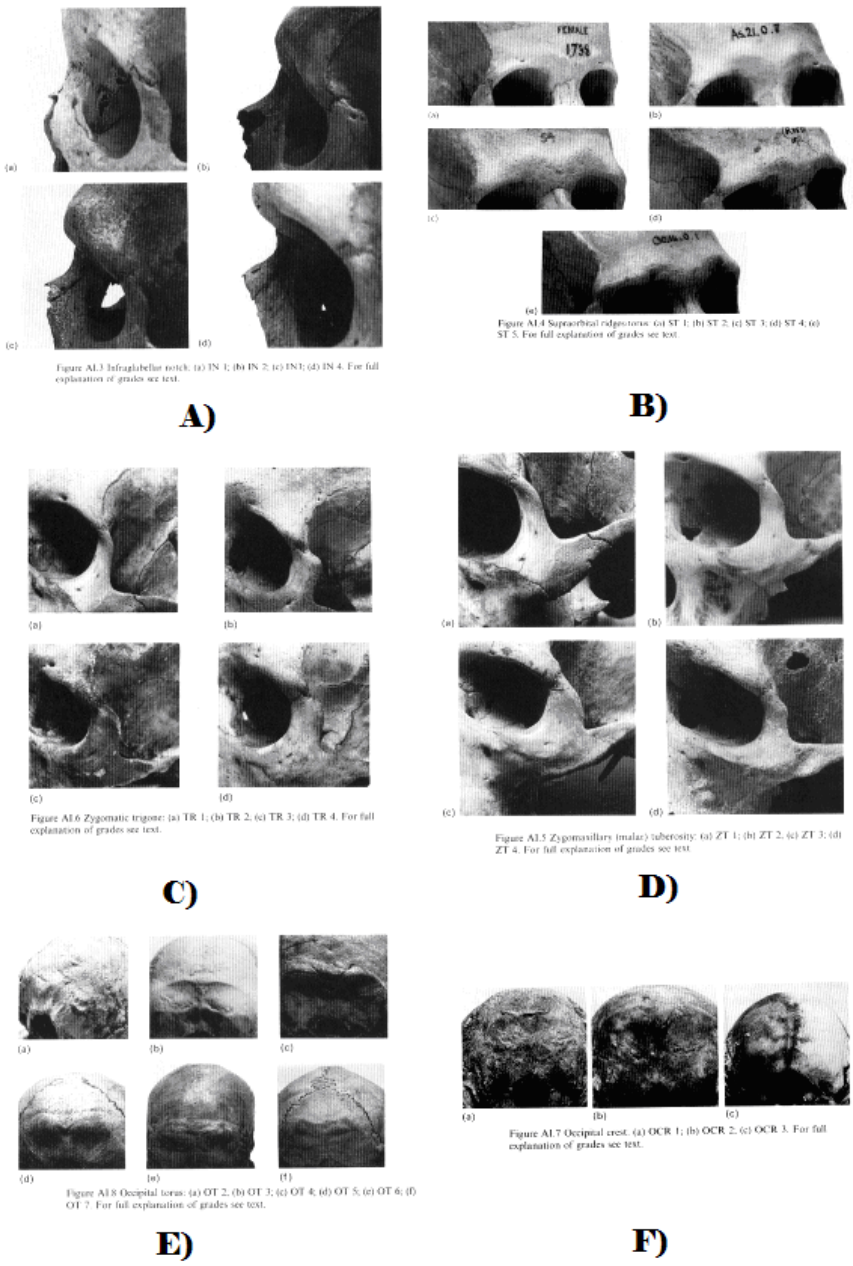

Figure B2. Robusticity coding following Lahr (1996) for the Infraglabellar Notch (A), Supraorbital Ridge/Torus (B), Zygomatic Trigone (C), Zygomaxillary Tuberosity (D), Occipital Torus (E), and Occipital Crest (F). Images taken from Lahr (1996).

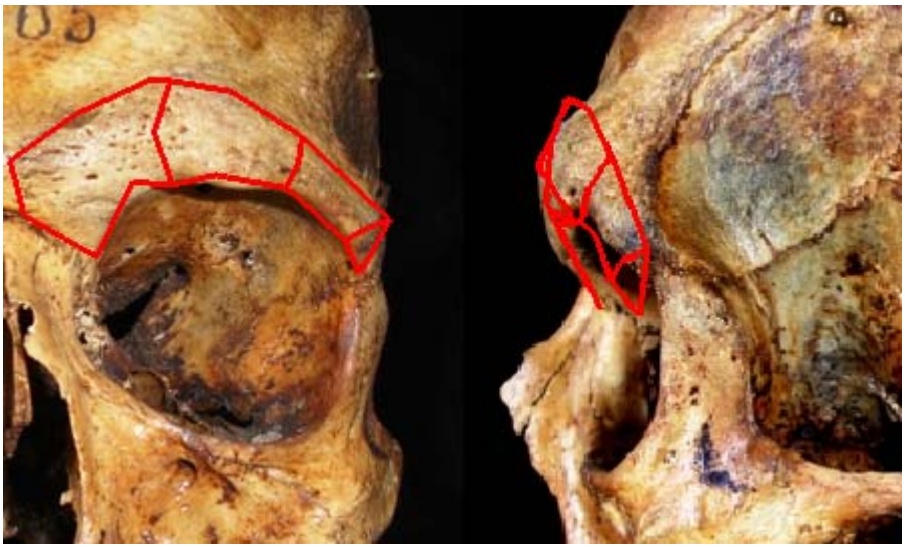

Figure B3. Coordinate landmark wireframe for Supraorbital landmark dataset superimposed on cranium (wireframes produced from the cranium shown in photo using Morphologika for illustrative purposes; mapping from 3-D landmarks onto 2-D photo image format is approximate).

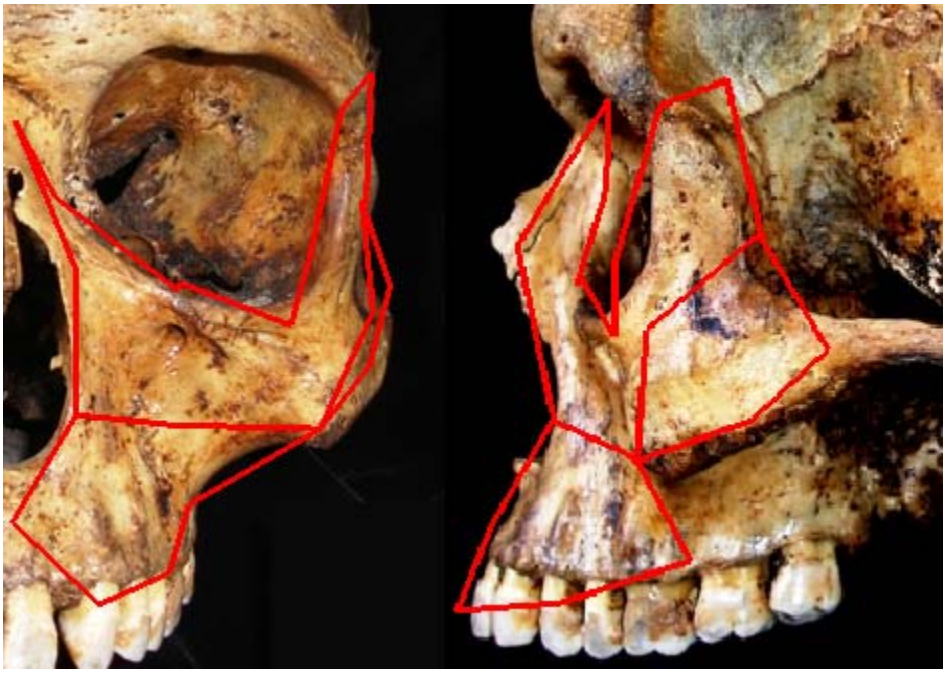

Figure B4. Coordinate landmark wireframe for Zygomaxillary landmark dataset superimposed on cranium (see Fig. B3 for notes on wireframe mapping).

Figure B5. Coordinate landmark wireframe for Mastoid landmark dataset superimposed on cranium. Lines represent resampled data from the original digitized line (see methodology, Chapter 4).

Figure B6. Coordinate landmark wireframe for Nuchal landmark dataset superimposed on cranium. Lines represent resampled data from the original digitized line (see Fig. B5).

APPENDIX C. MORPHOLOGICAL VARIATION IN COMPLETE LANDMARK DATASET FOR GLOBAL SAMPLE

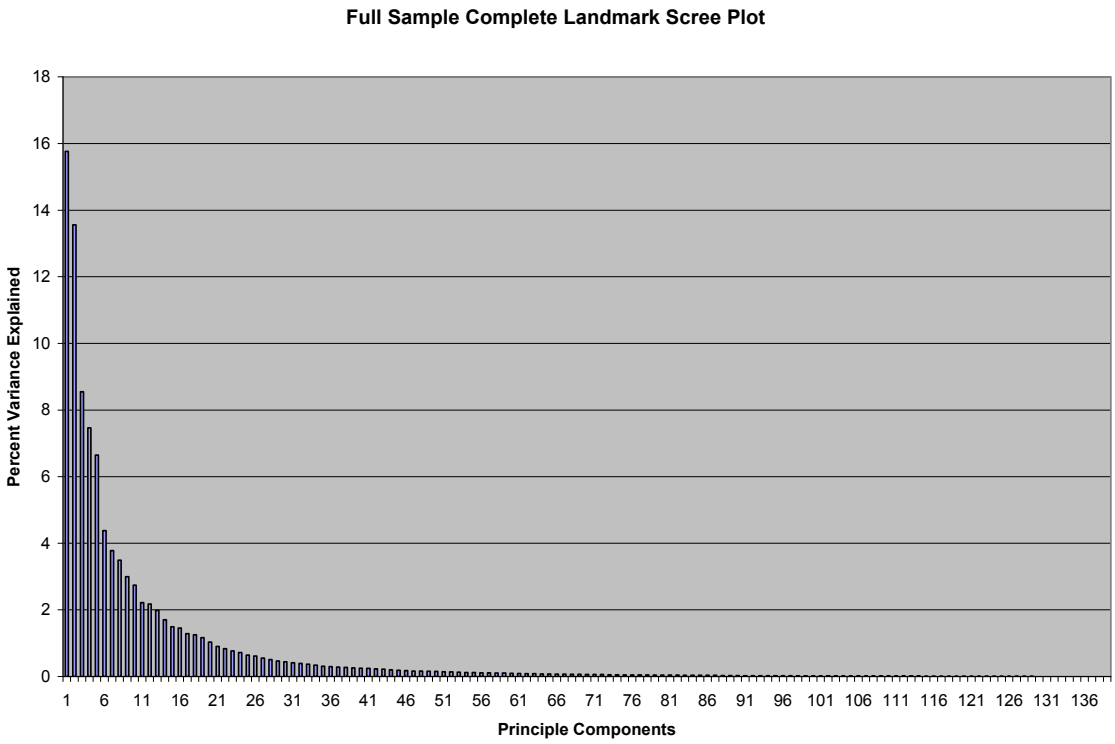

Figure C1. Scree plot of the 139 relative warps for the full 72 coordinate landmark dataset of the global sample. Warps 1-9 were selected for subsequent analyses.

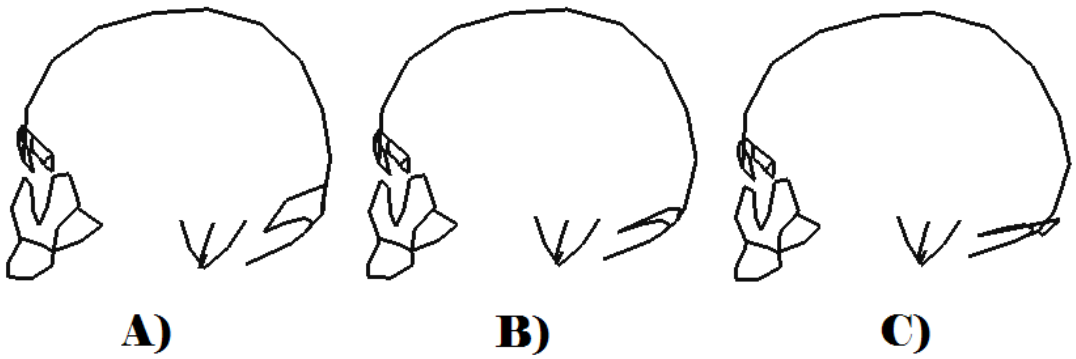

Figure C2. Morphological variation along RW1 for the overall global dataset: A) Lower extreme of variation, B) Consensus form, C) Upper extreme of variation.

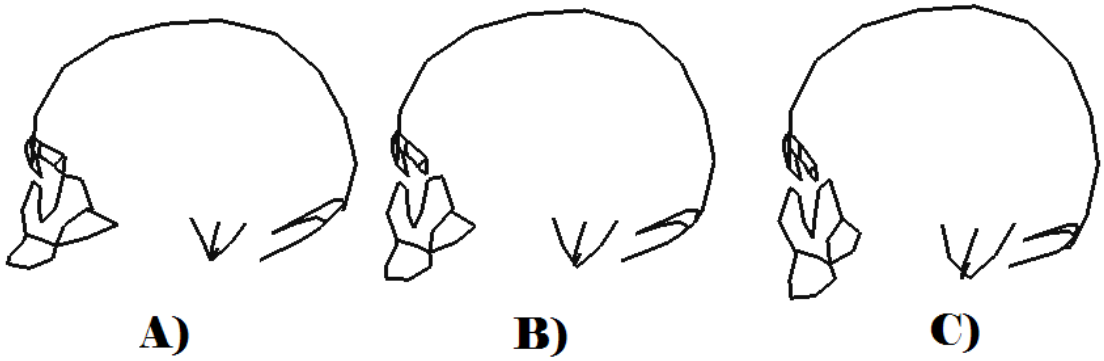

Figure C3. Morphological variation along RW2 for the overall global dataset: A) Lower extreme of variation, B) Consensus form, C) Upper extreme of variation.

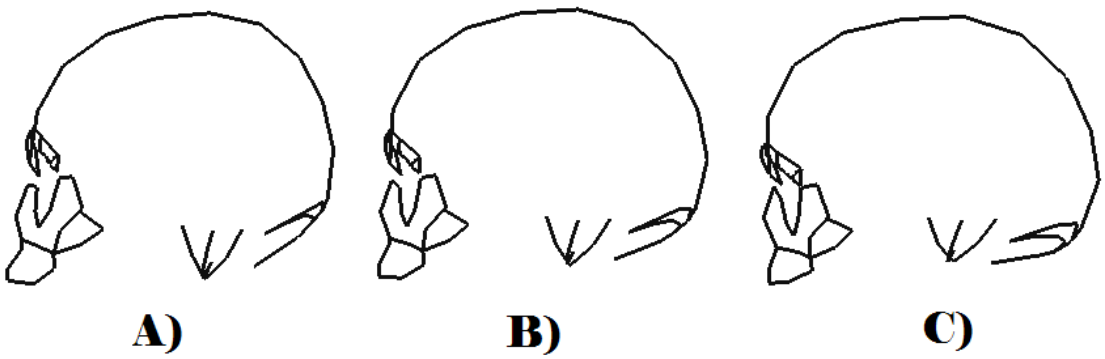

Figure C4. Morphological variation along RW3 for the overall global dataset: A) Lower extreme of variation, B) Consensus form, C) Upper extreme of variation.

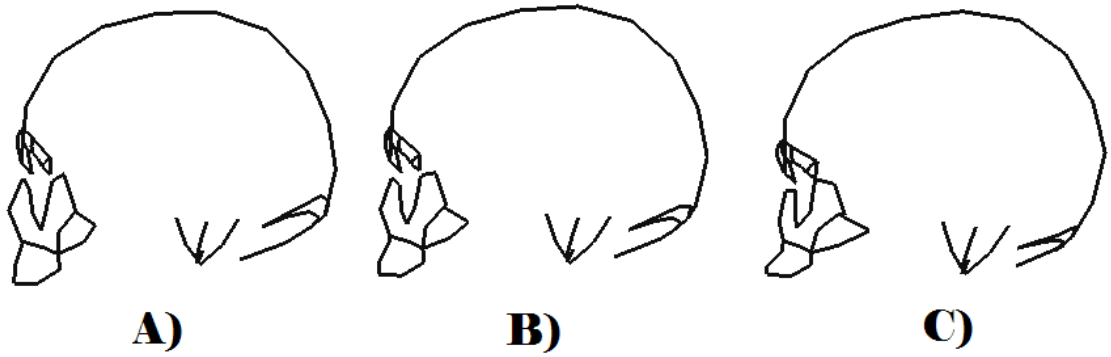

Figure C5. Morphological variation along RW4 for the overall global dataset: A) Lower extreme of variation, B) Consensus form, C) Upper extreme of variation.

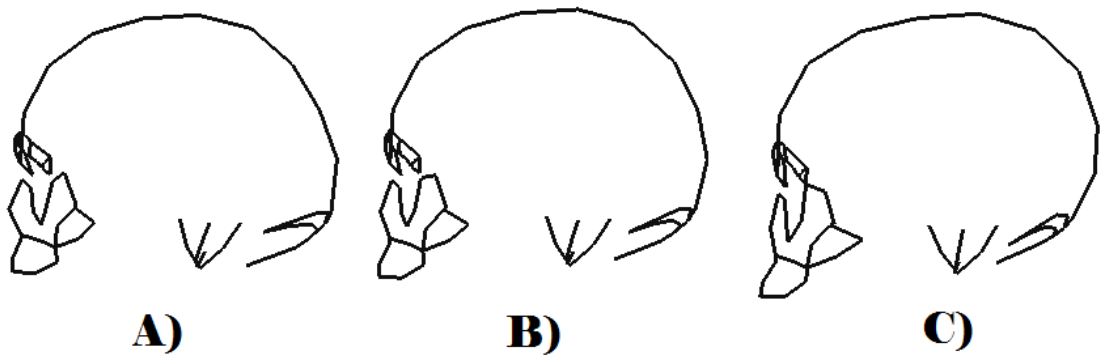

Figure C6. Morphological variation along RW5 for the overall global dataset: A) Lower extreme of variation, B) Consensus form, C) Upper extreme of variation.

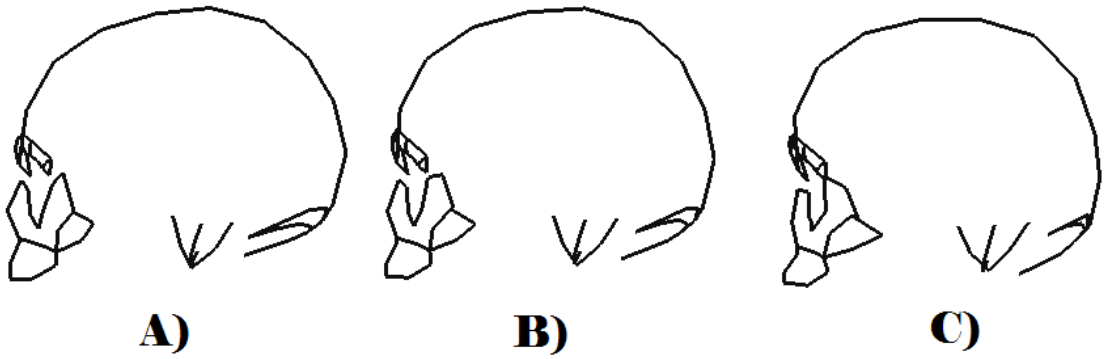

Figure C7. Morphological variation along RW6 for the overall global dataset: A) Lower extreme of variation, B) Consensus form, C) Upper extreme of variation.

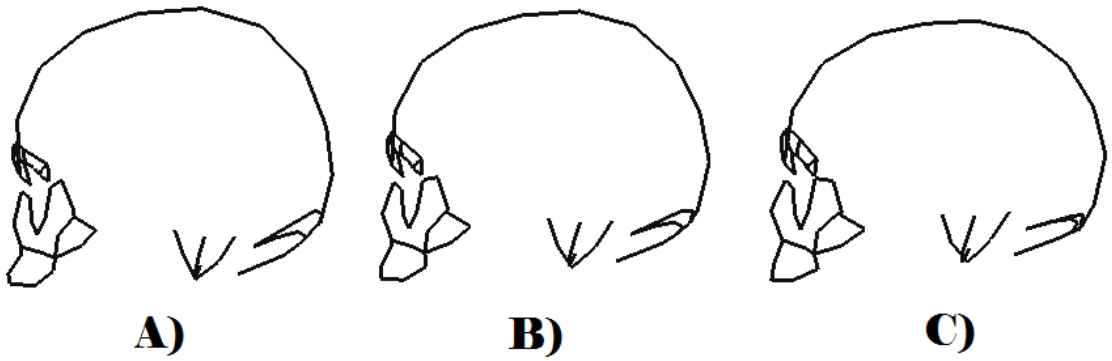

Figure C8. Morphological variation along RW7 for the overall global dataset: A) Lower extreme of variation, B) Consensus form, C) Upper extreme of variation.

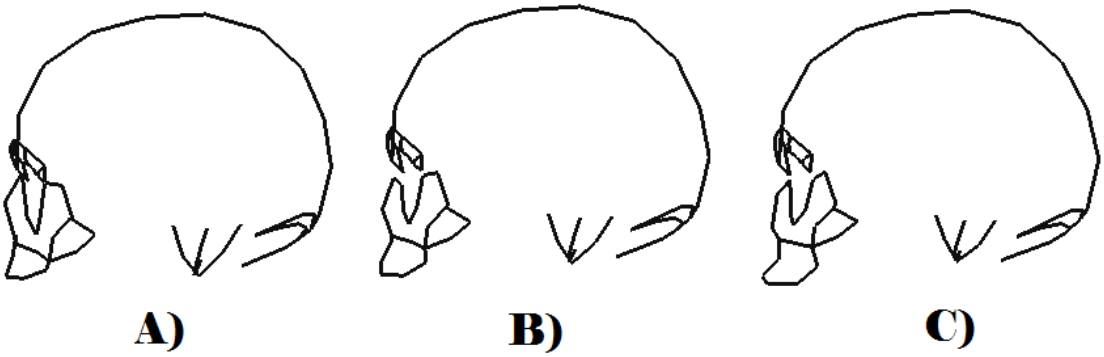

Figure C9. Morphological variation along RW8 for the overall global dataset: A) Lower extreme of variation, B) Consensus form, C) Upper extreme of variation.

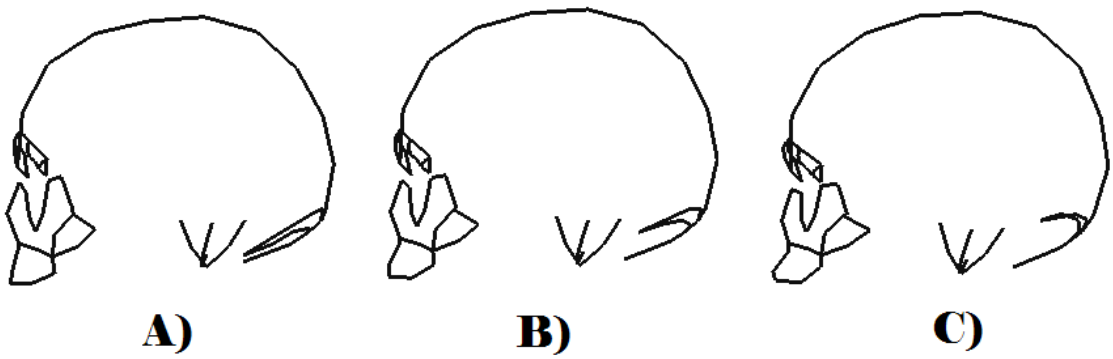

Figure C10. Morphological variation along RW9 for the overall global dataset: A) Lower extreme of variation, B) Consensus form, C) Upper extreme of variation.

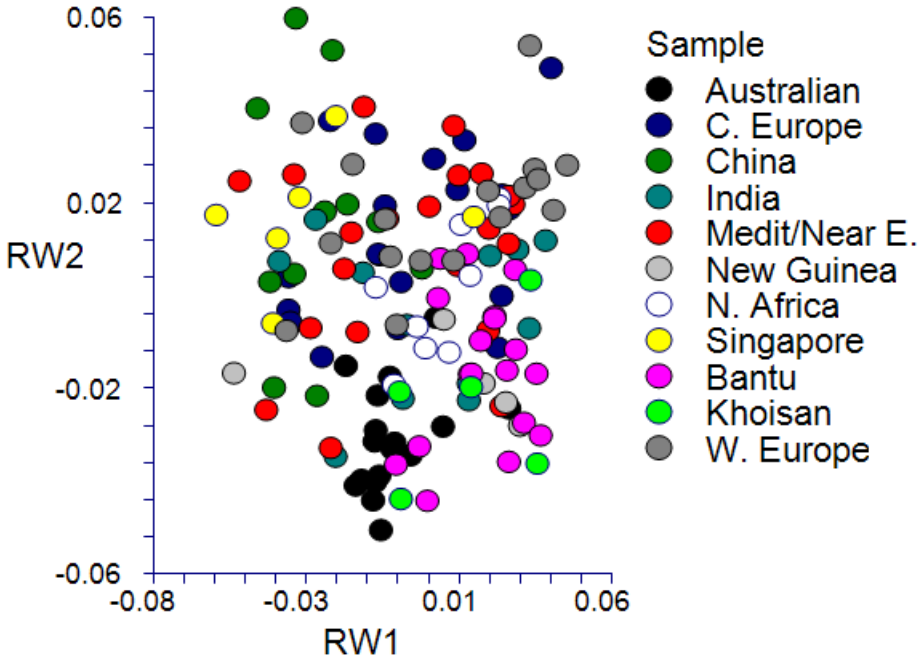

Figure C11. Plot of RW1 (15.76% variance explained) and RW2 (13.56% variance explained) for the full 72 coordinate landmark dataset across the global sample.

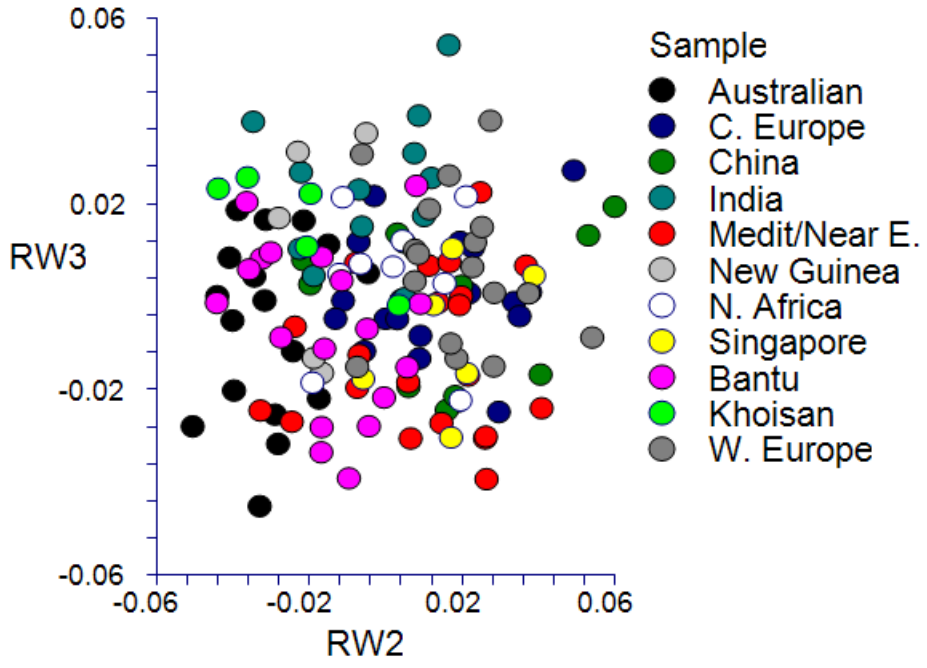

Figure C12. Plot of RW2 (13.56% variance explained) and RW3 (8.55% variance explained) for the full 72 coordinate landmark dataset across the global sample.

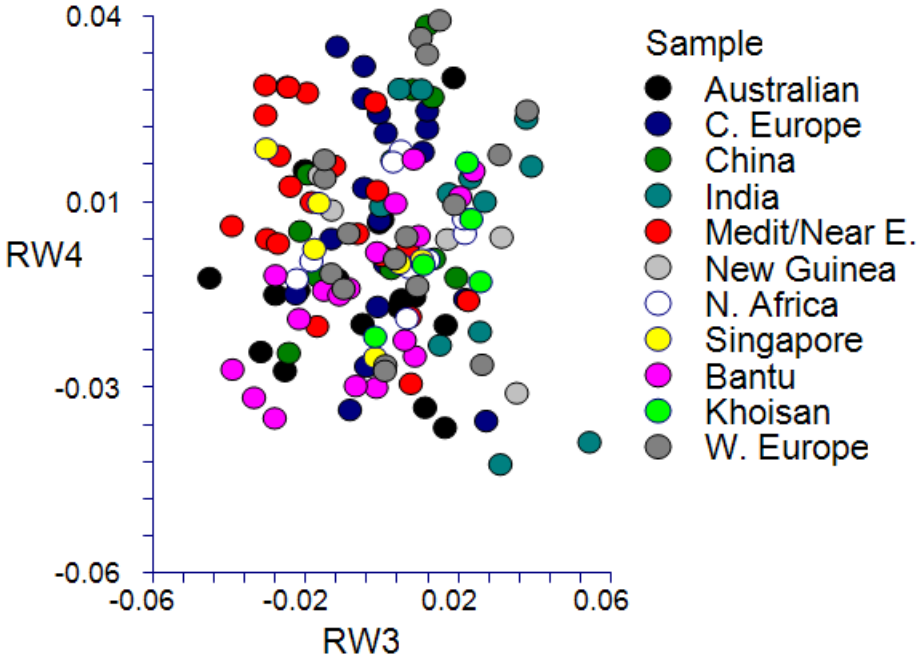

Figure C13. Plot of RW3 (8.55% variance explained) and RW4 (7.46% variance explained) for the full 72 coordinate landmark dataset across the global sample.

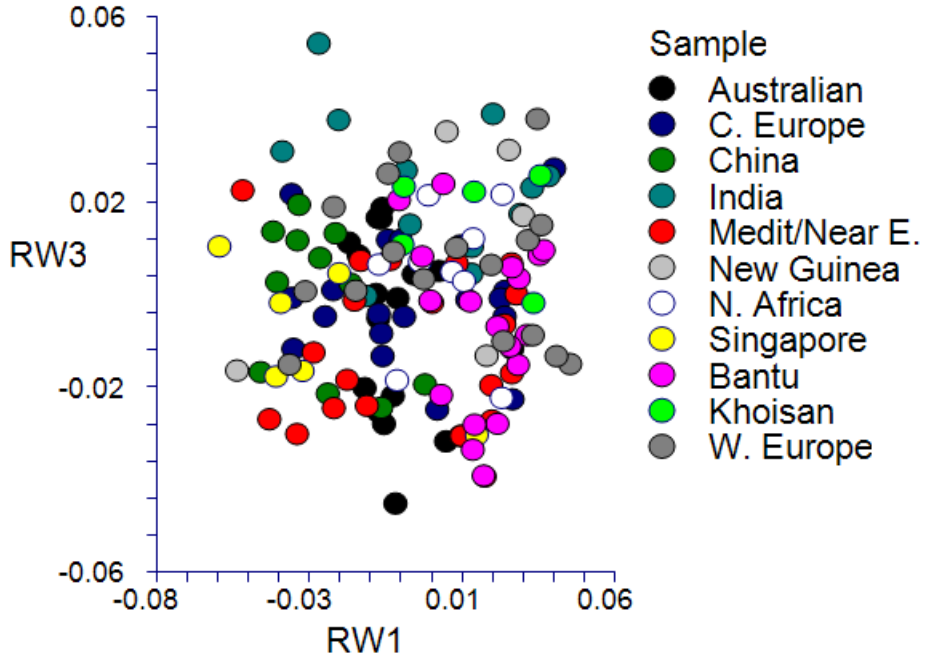

Figure C14. Plot of RW1 (15.76% variance explained) and RW3 (8.55% variance explained) for the full 72 coordinate landmark dataset across the global sample.

APPENDIX D. MORPHOLOGICAL VARIATION IN COMPLETE LANDMARK DATASET FOR MALE/FEMALE SUBSAMPLES

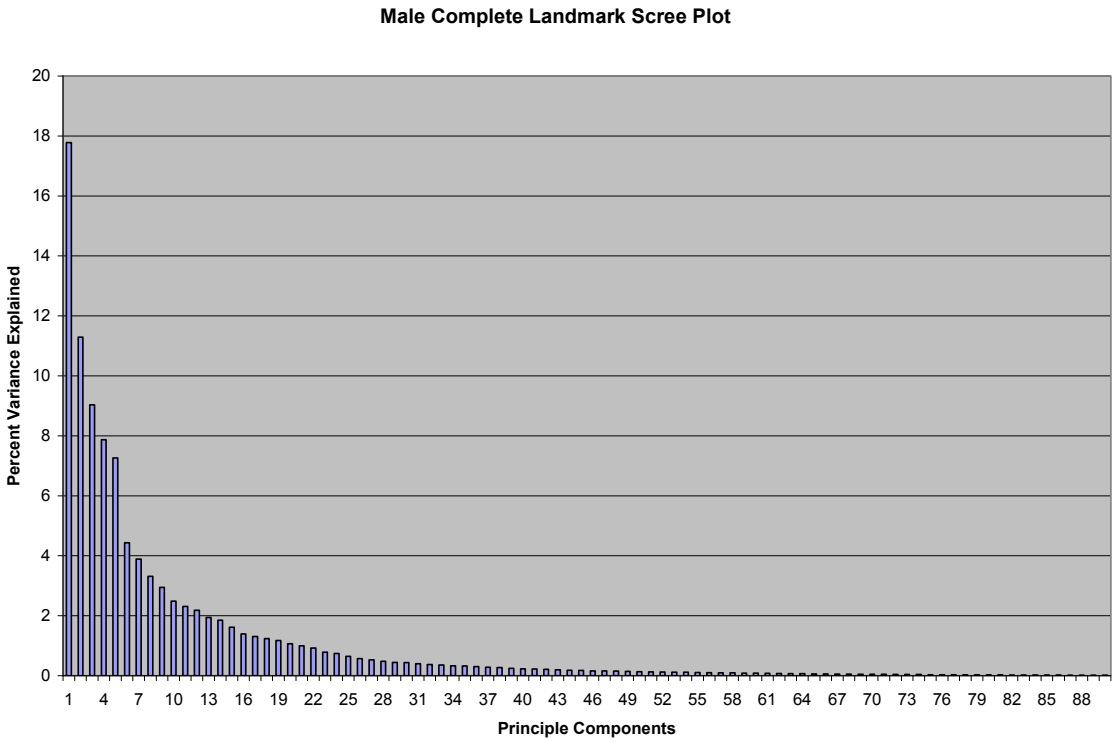

Figure D1. Scree plot of the 90 relative warps for the full 72 coordinate landmark dataset of the male subsample. Warps 1-4 were selected for subsequent analyses.

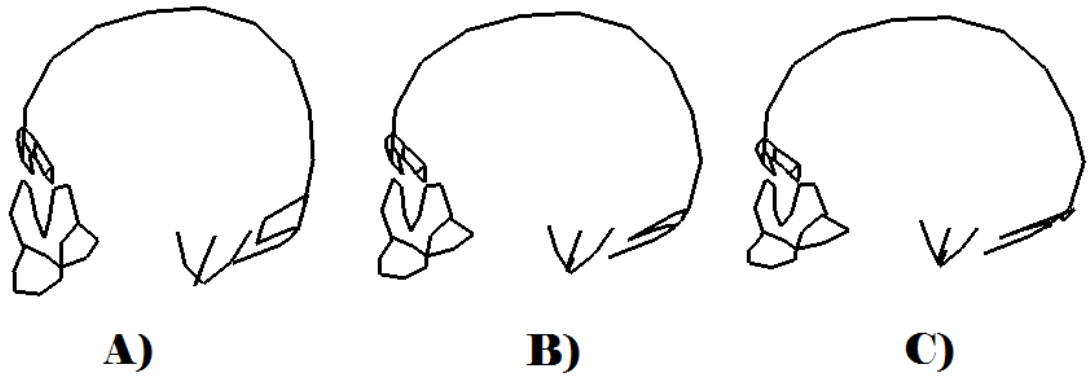

Figure D2. Morphological variation along RW1 for the male subsample: A) Lower extreme of variation, B) Consensus form, C) Upper extreme of variation.

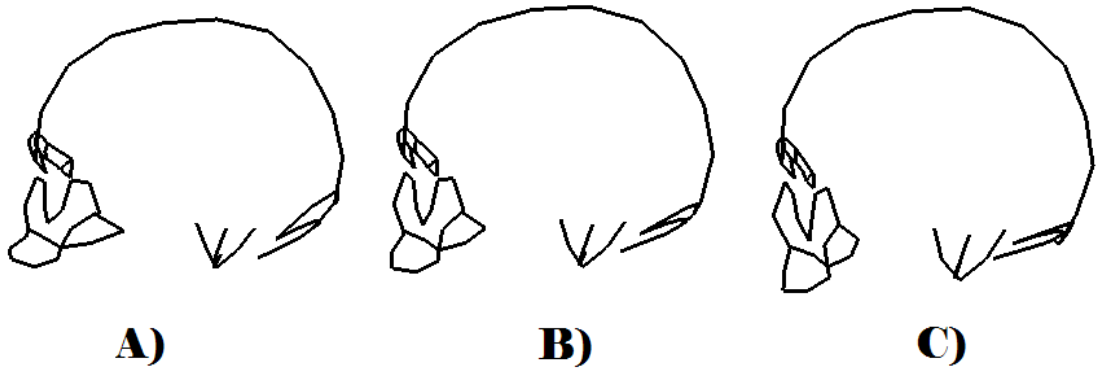

Figure D3. Morphological variation along RW2 for the male subsample: A) Lower extreme of variation, B) Consensus form, C) Upper extreme of variation.

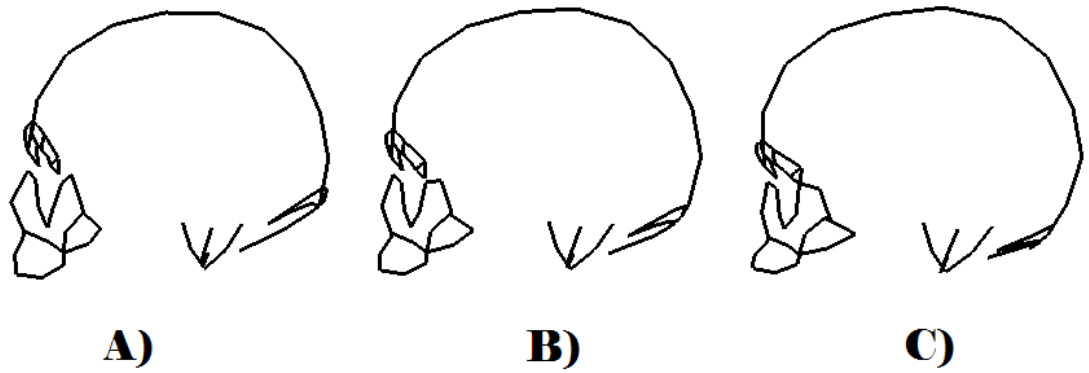

Figure D4. Morphological variation along RW3 for the male subsample: A) Lower extreme of variation, B) Consensus form, C) Upper extreme of variation.

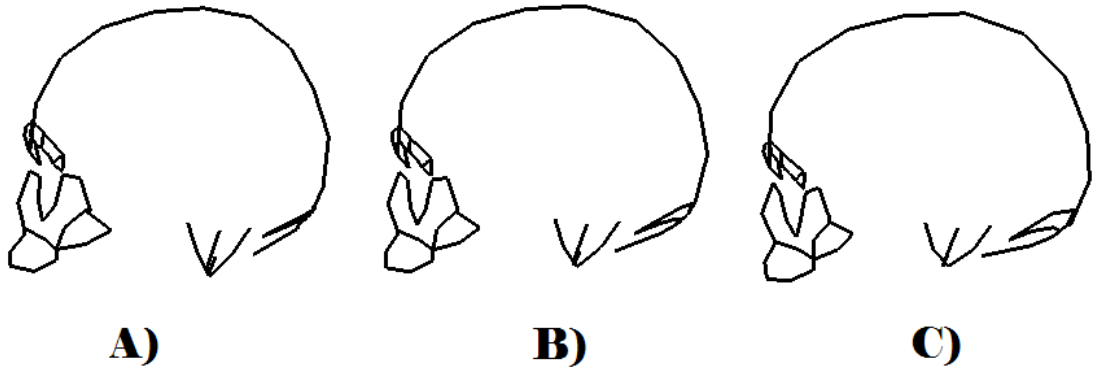

Figure D5. Morphological variation along RW4 for the male subsample: A) Lower extreme of variation, B) Consensus form, C) Upper extreme of variation.

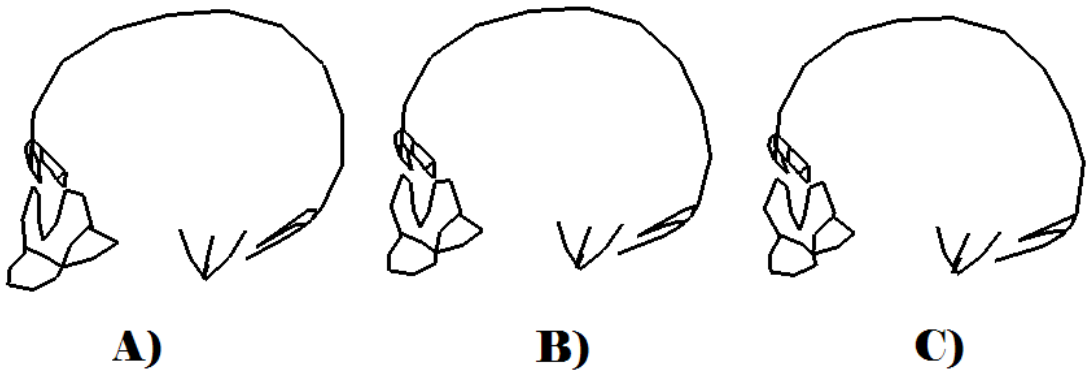

Figure D6. Morphological variation along RW5 for the male subsample: A) Lower extreme of variation, B) Consensus form, C) Upper extreme of variation.

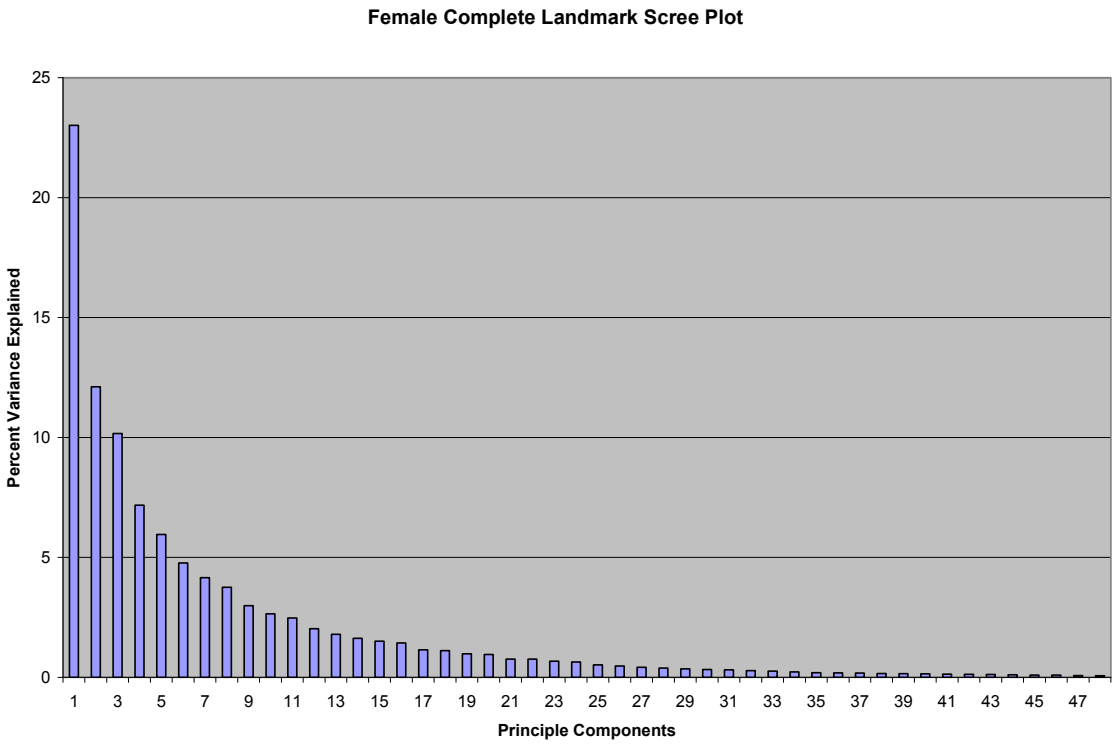

Figure D7. Scree plot of the 48 relative warps for the full 72 coordinate landmark dataset of the female subsample. Warps 1-3 were selected for subsequent analyses.

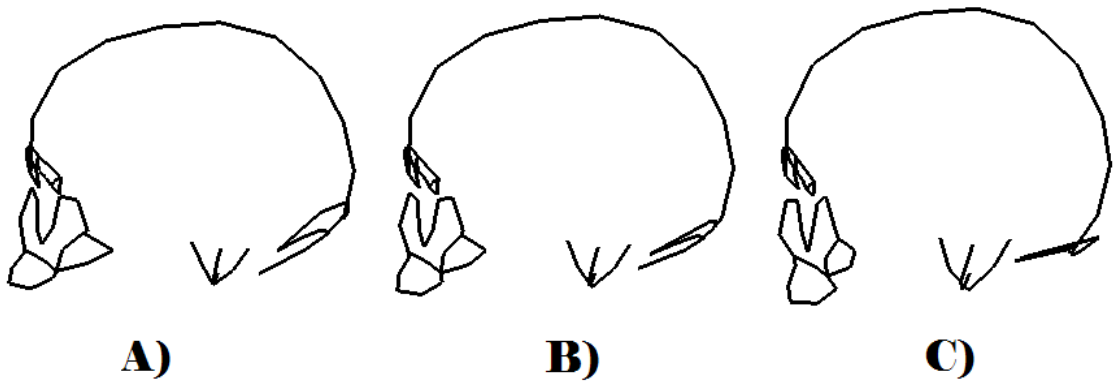

Figure D8. Morphological variation along RW1 for the female subsample: A) Lower extreme of variation, B) Consensus form, C) Upper extreme of variation.

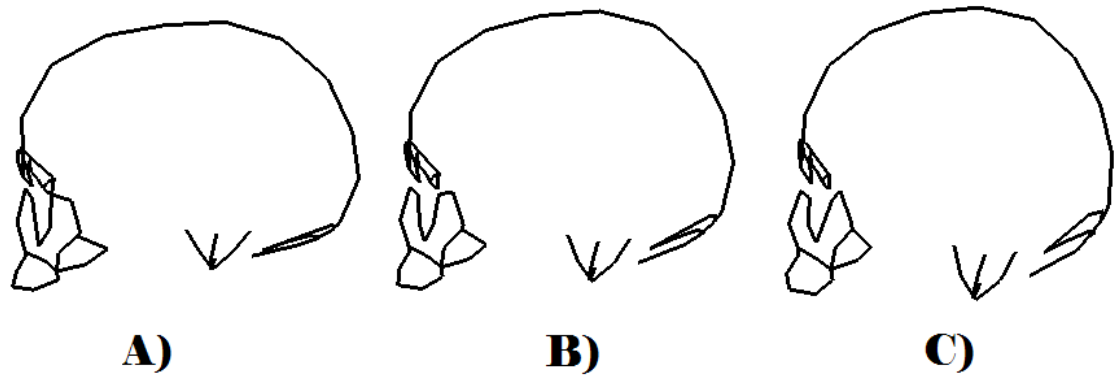

Figure D9. Morphological variation along RW2 for the female subsample: A) Lower extreme of variation, B) Consensus form, C) Upper extreme of variation.

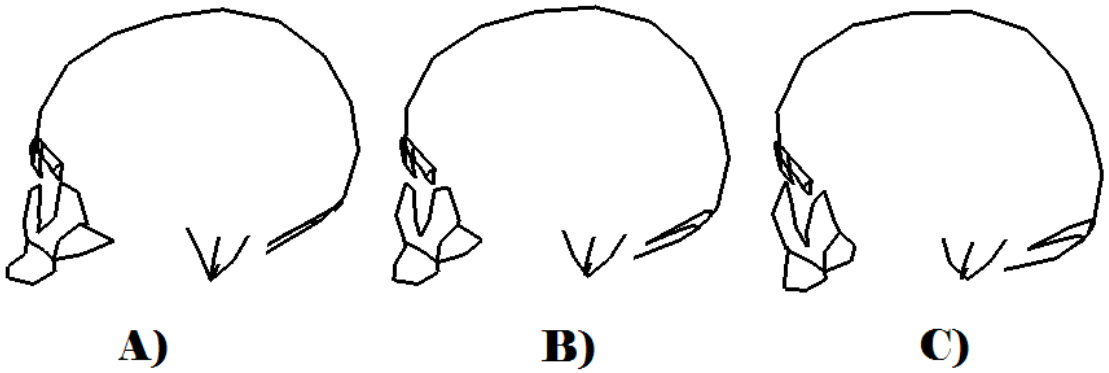

Figure D10. Morphological variation along RW3 for the female subsample: A) Lower extreme of variation, B) Consensus form, C) Upper extreme of variation.

APPENDIX E. MORPHOLOGICAL VARIATION IN SUPRAORBITAL LANDMARK DATASET FOR GLOBAL SAMPLE

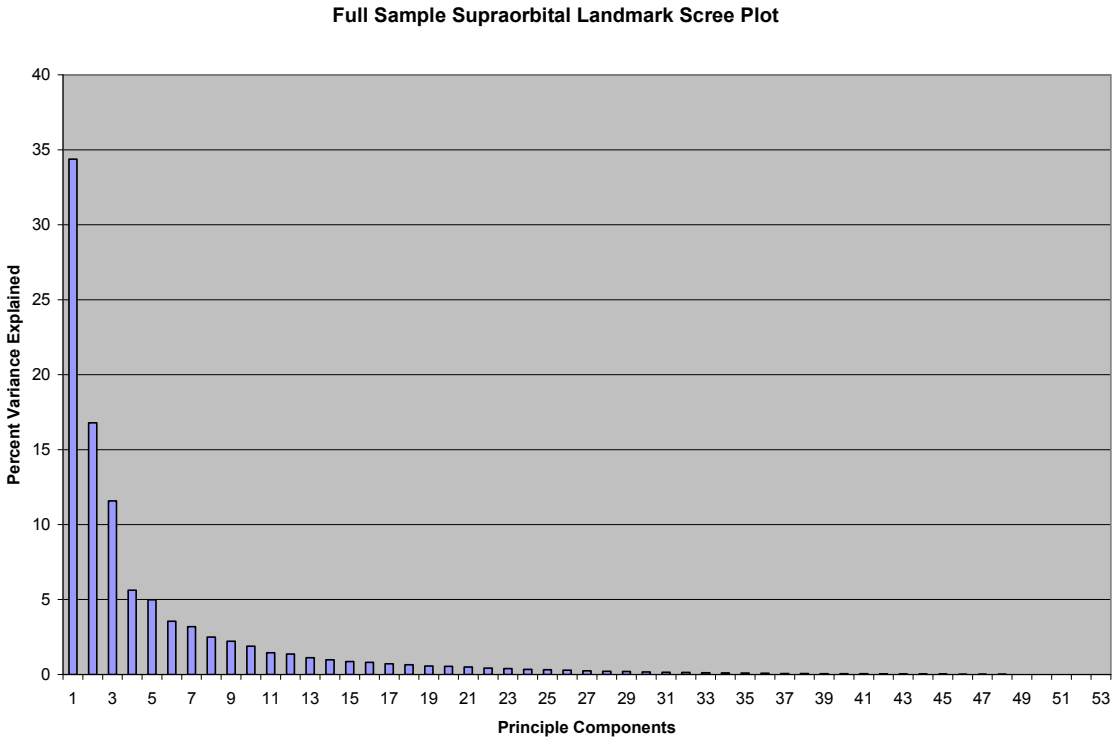

Figure E1. Scree plot of the 53 relative warps for the frontal region coordinate landmark dataset of the global sample. Warps 1-5 were selected for subsequent analyses.

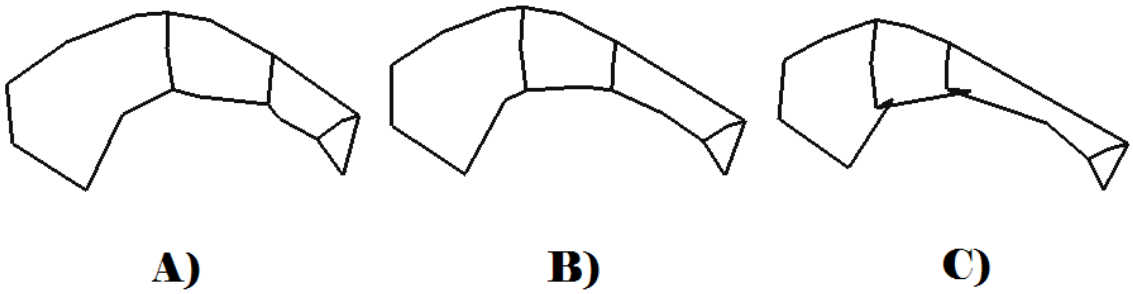

Figure E2. Variation in Supraorbital Landmarks along RW1 for the complete sample: A) Lower extreme of variation, B) Consensus form, C) Upper extreme of variation.

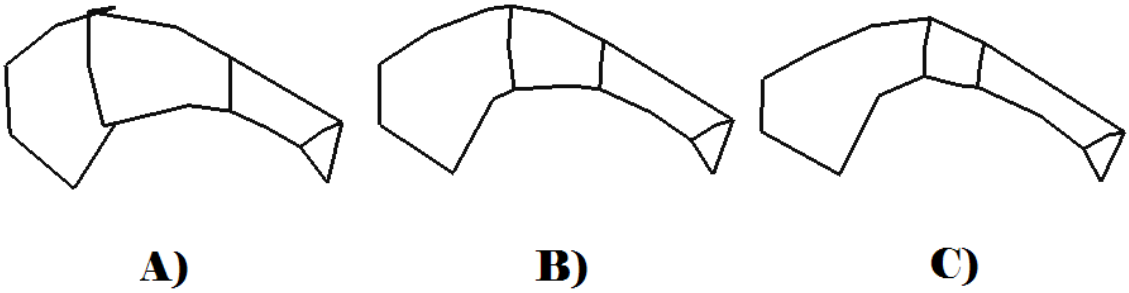

Figure E3. Variation in Supraorbital Landmarks along RW2 for the complete sample: A) Lower extreme of variation, B) Consensus form, C) Upper extreme of variation.

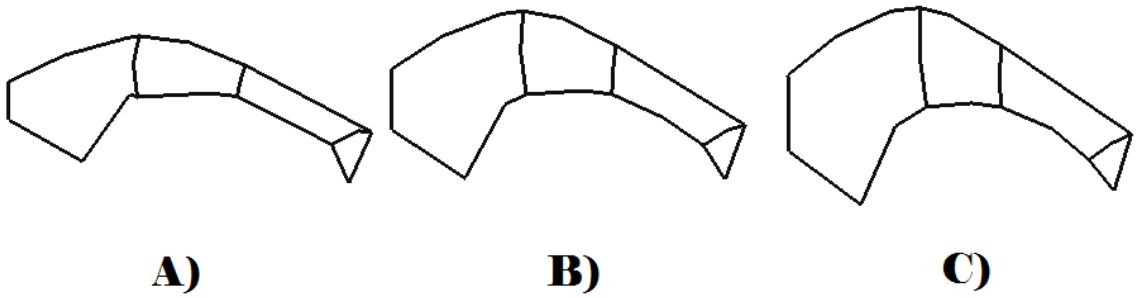

Figure E4. Variation in Supraorbital Landmarks along RW3 for the complete sample: A) Lower extreme of variation, B) Consensus form, C) Upper extreme of variation.

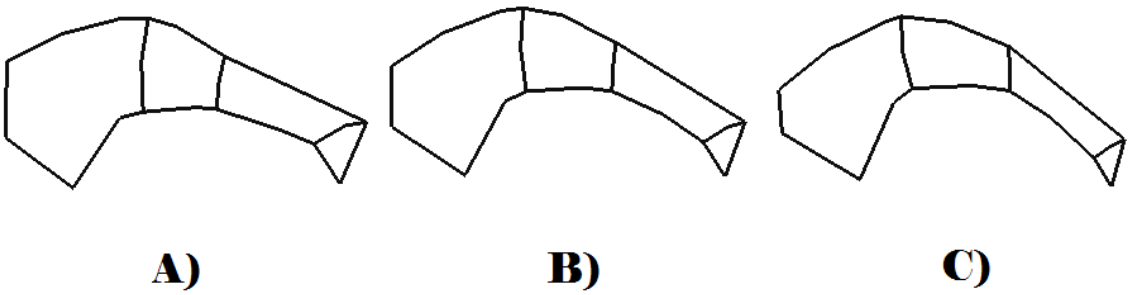

Figure E5. Variation in Supraorbital Landmarks along RW4 for the complete sample: A) Lower extreme of variation, B) Consensus form, C) Upper extreme of variation.

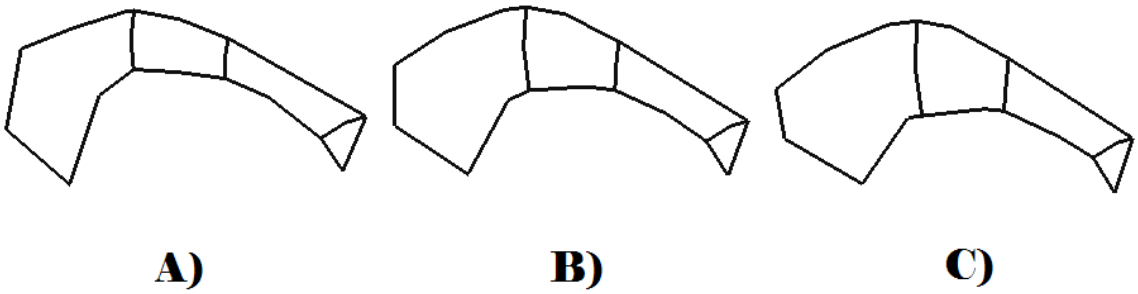

Figure E6. Variation in Supraorbital Landmarks along RW5 for the complete sample: A) Lower extreme of variation, B) Consensus form, C) Upper extreme of variation.

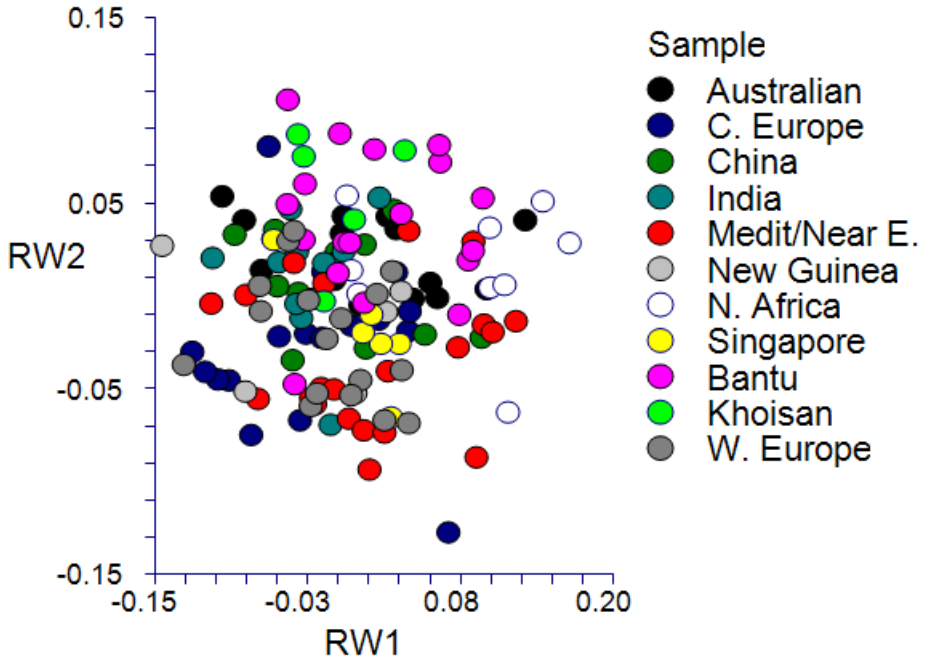

Figure E7. Plot of RW1 (33.62% variance explained) and RW2 (16.10% variance explained) of the Supraorbital landmark dataset across the global sample.

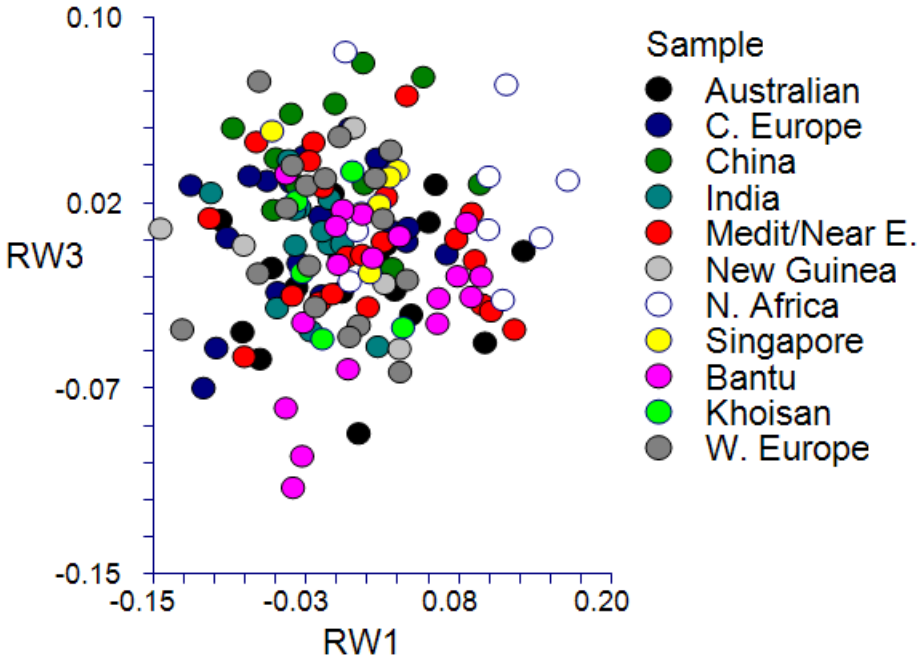

Figure E8. Plot of RW1 (33.62% variance explained) and RW3 (12.50% variance explained) of the Supraorbital landmark dataset across the global sample.

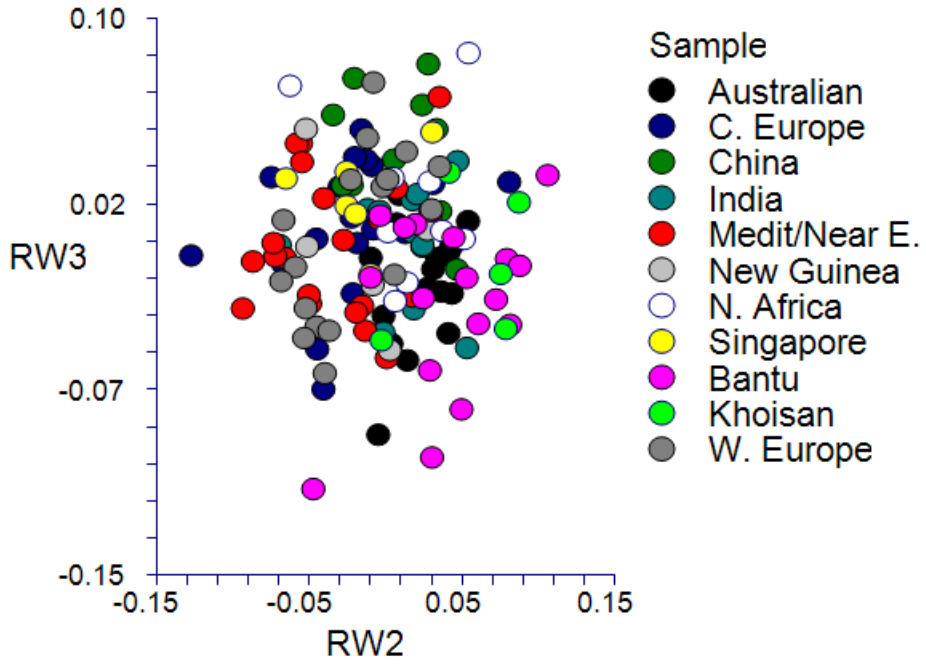

Figure E9. Plot of RW2 (16.10% variance explained) and RW3 (12.50% variance explained) of the Supraorbital landmark dataset across the global sample.

APPENDIX F. MORPHOLOGICAL VARIATION IN ZYGOMAXILLARY LANDMARK DATASET FOR GLOBAL SAMPLE

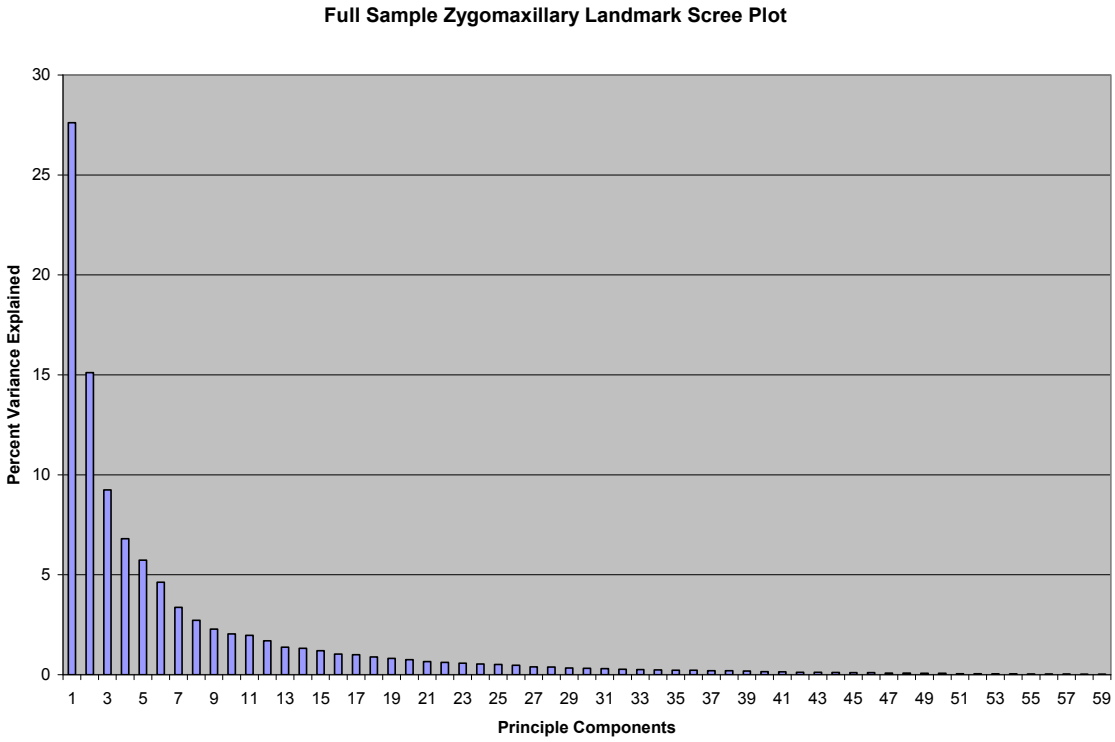

Figure F1. Scree plot of the 59 relative warps for the zygomaxillary region coordinate landmark dataset of the global sample. Warps 1-6 were selected for subsequent analyses.

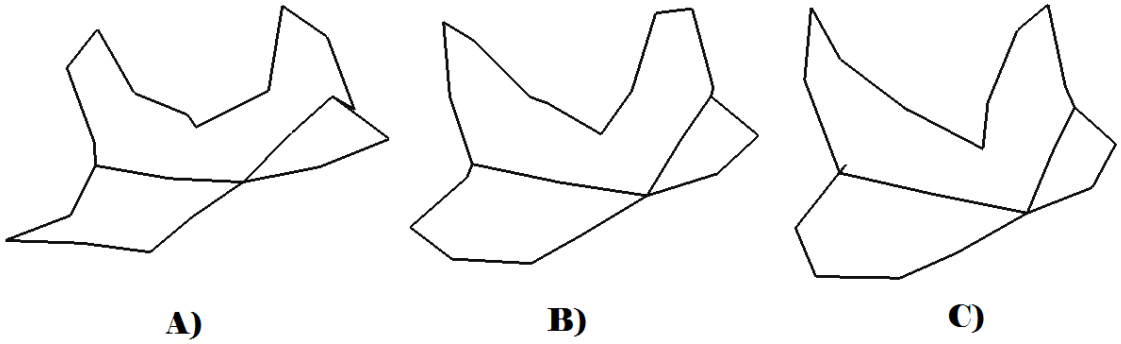

Figure F2. Variation in Zygomaxillary Landmarks along RW1 for the complete sample: A) Lower extreme of variation, B) Consensus form, C) Upper extreme of variation.

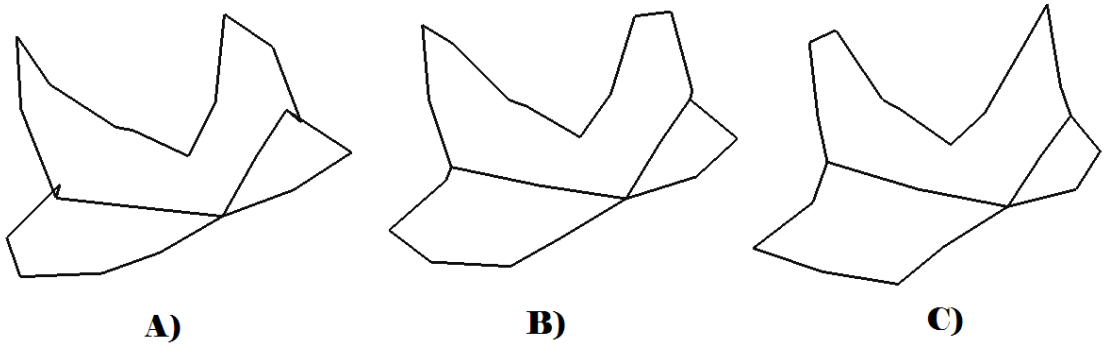

Figure F3. Variation in Zygomaxillary Landmarks along RW2 for the complete sample: A) Lower extreme of variation, B) Consensus form, C) Upper extreme of variation.

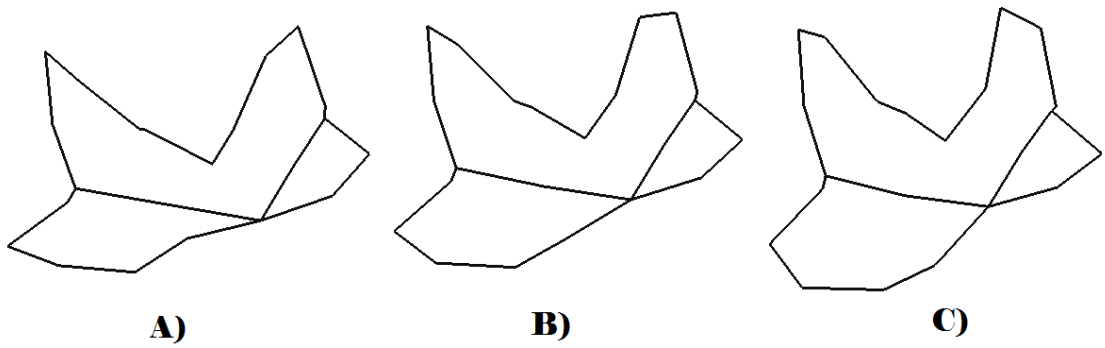

Figure F4. Variation in Zygomaxillary Landmarks along RW3 for the complete sample: A) Lower extreme of variation, B) Consensus form, C) Upper extreme of variation.

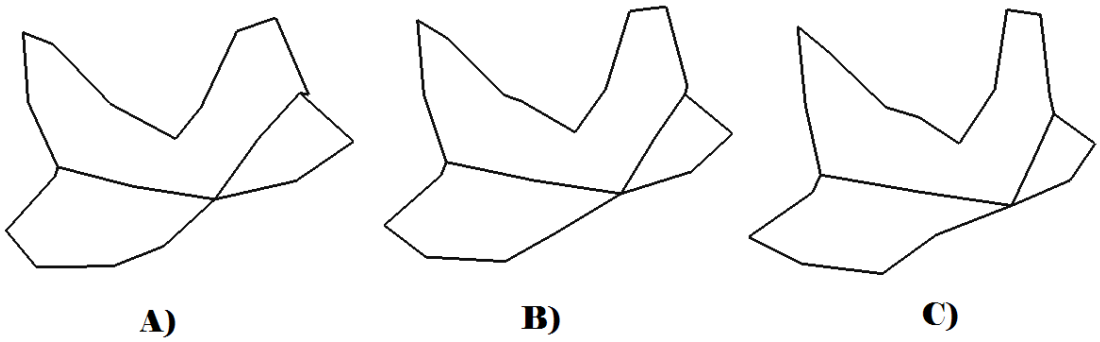

Figure F5. Variation in Zygomaxillary Landmarks along RW4 for the complete sample: A) Lower extreme of variation, B) Consensus form, C) Upper extreme of variation.

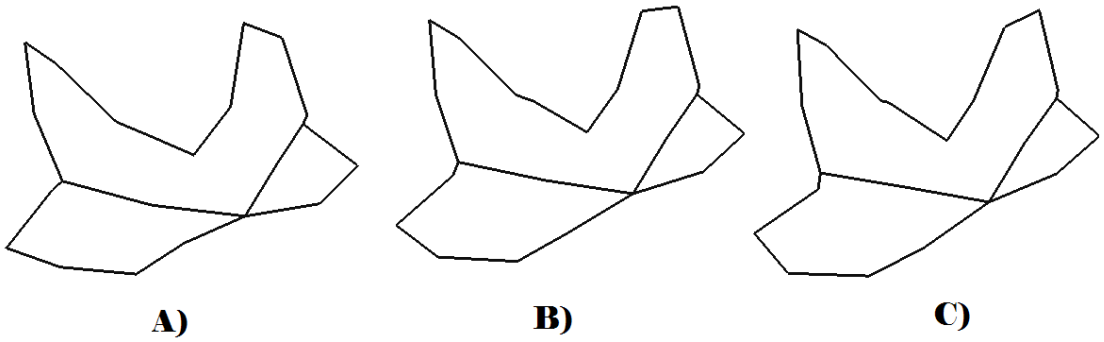

Figure F6. Variation in Zygomaxillary Landmarks along RW5 for the complete sample: A) Lower extreme of variation, B) Consensus form, C) Upper extreme of variation.

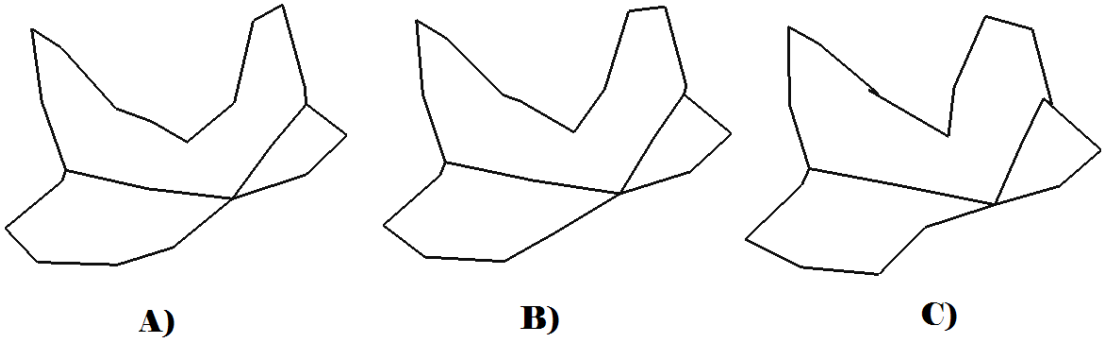

Figure F7. Variation in Zygomaxillary Landmarks along RW6 for the complete sample: A) Lower extreme of variation, B) Consensus form, C) Upper extreme of variation.

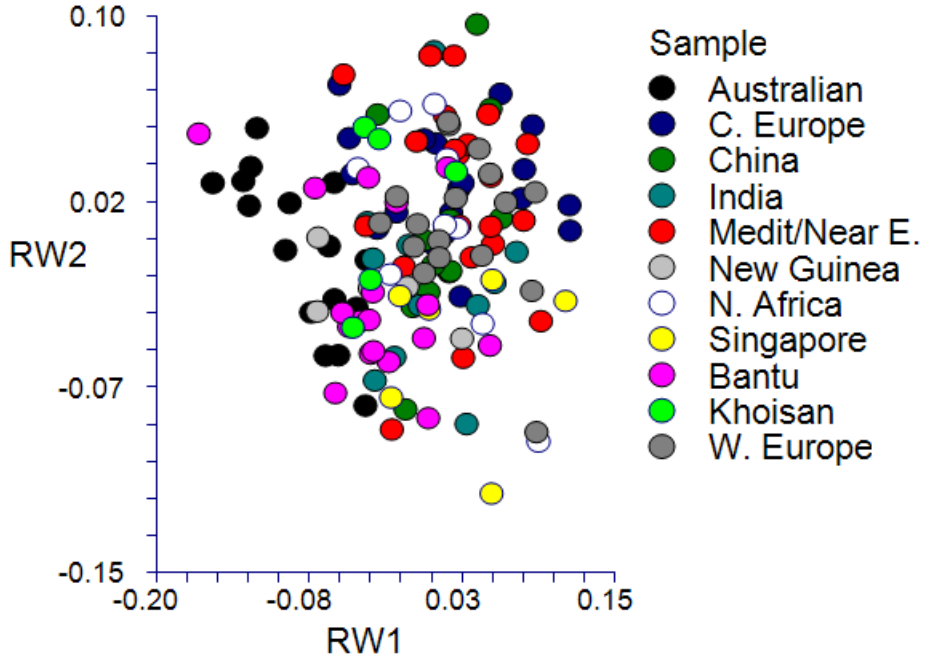

Figure F8. Plot of RW1 (27.61% variance explained) and RW2 (15.11% variance explained) of the Zygomaxillary landmark dataset across the global sample.

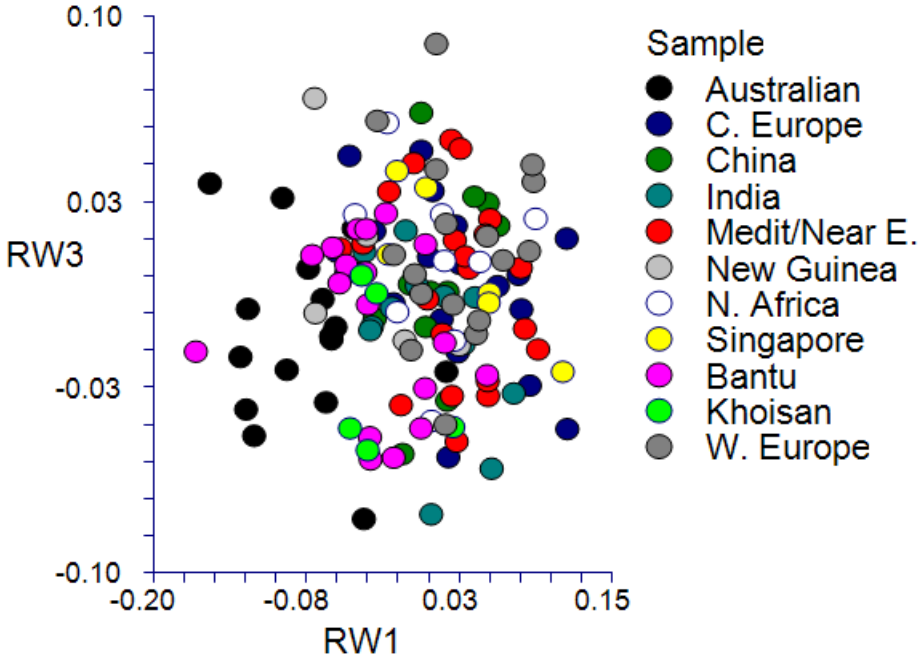

Figure F9. Plot of RW1 (27.61% variance explained) and RW3 (9.25% variance explained) of the Zygomaxillary landmark dataset across the global sample.

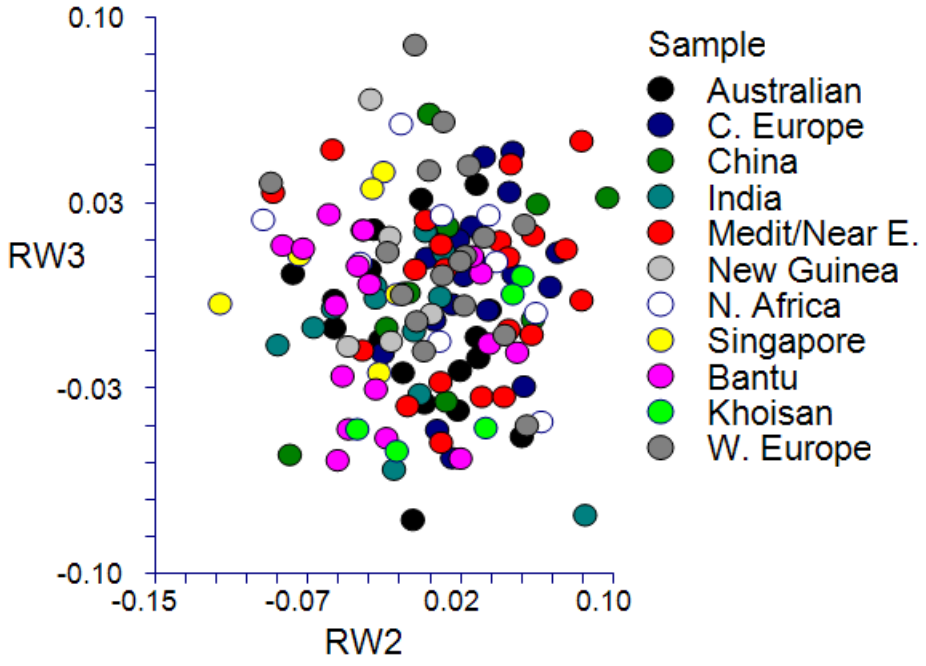

Figure F10. Plot of RW2 (15.11% variance explained) and RW3 (9.25% variance explained) of the Zygomaxillary landmark dataset across the global sample.

APPENDIX G. MORPHOLOGICAL VARIATION IN MASTOID LANDMARK DATASET FOR GLOBAL SAMPLE

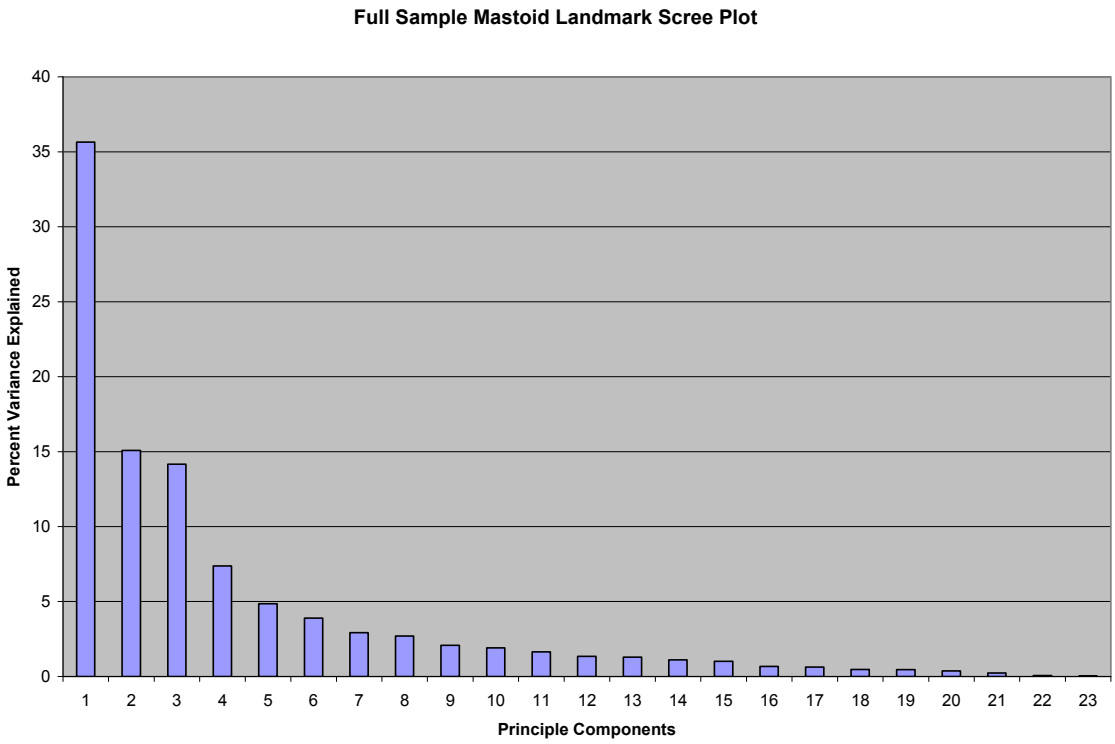

Figure G1. Scree plot of the 23 relative warps for the mastoid region coordinate landmark dataset of the global sample. Warps 1-5 were selected for subsequent analyses.

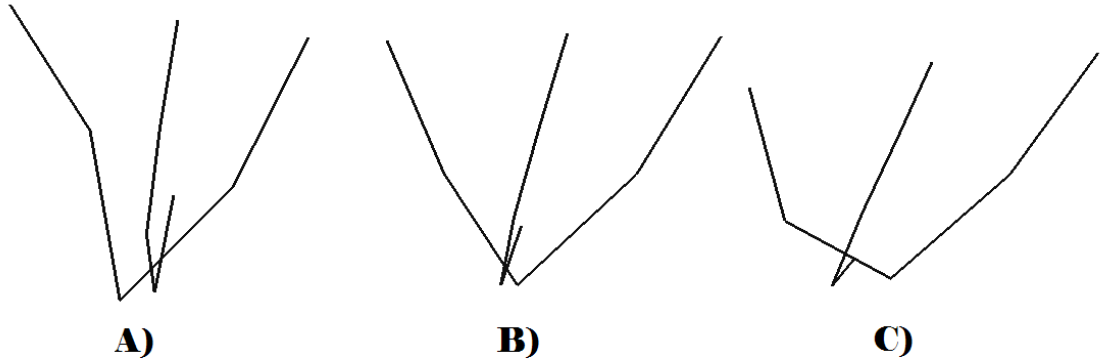

Figure G2. Variation in Mastoid Landmarks along RW1 for the complete sample: A) Lower extreme of variation, B) Consensus form, C) Upper extreme of variation.

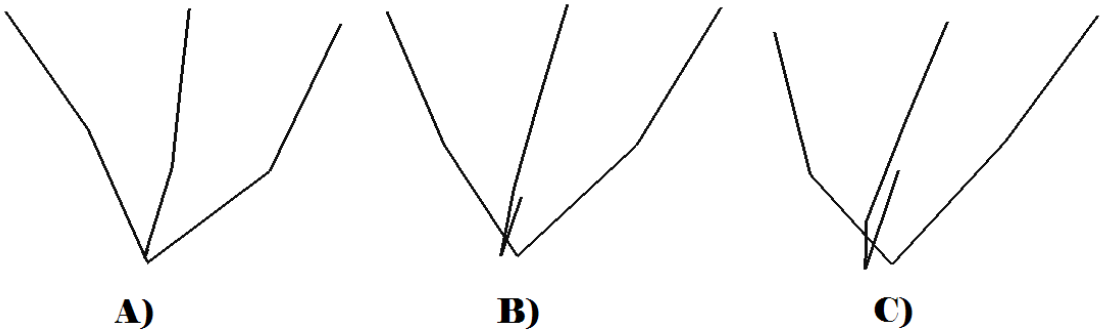

Figure G3. Variation in Mastoid Landmarks along RW2 for the complete sample: A) Lower extreme of variation, B) Consensus form, C) Upper extreme of variation.

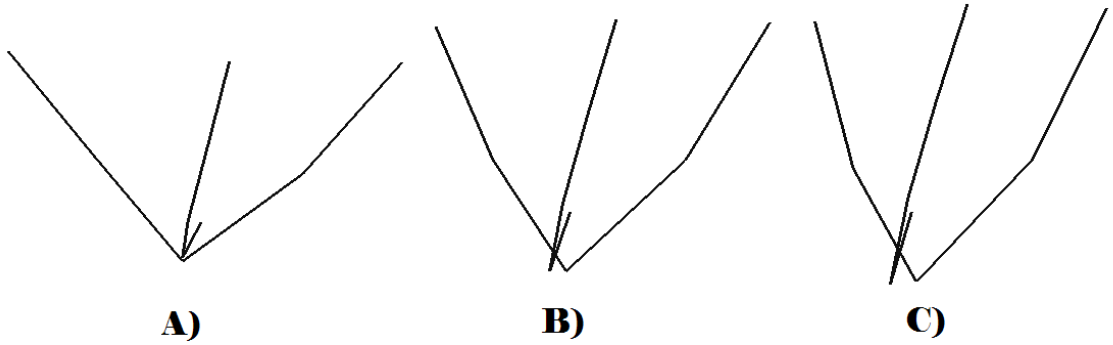

Figure G4. Variation in Mastoid Landmarks along RW3 for the complete sample: A) Lower extreme of variation, B) Consensus form, C) Upper extreme of variation.

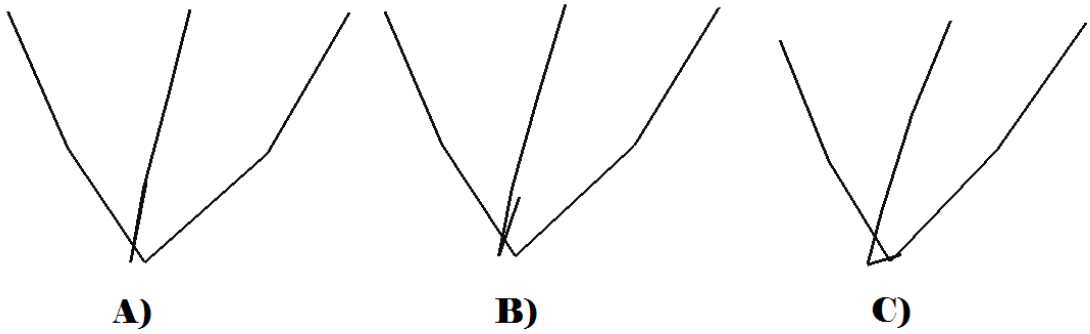

Figure G5. Variation in Mastoid Landmarks along RW4 for the complete sample: A) Lower extreme of variation, B) Consensus form, C) Upper extreme of variation.

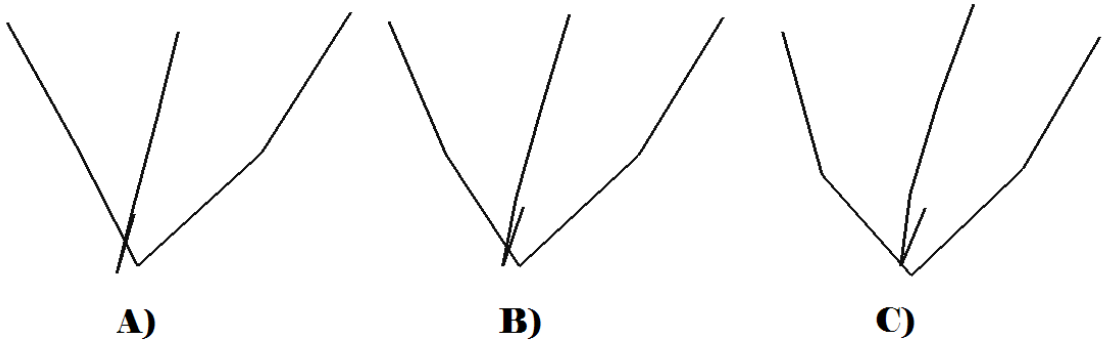

Figure G6. Variation in Mastoid Landmarks along RW5 for the complete sample: A) Lower extreme of variation, B) Consensus form, C) Upper extreme of variation.

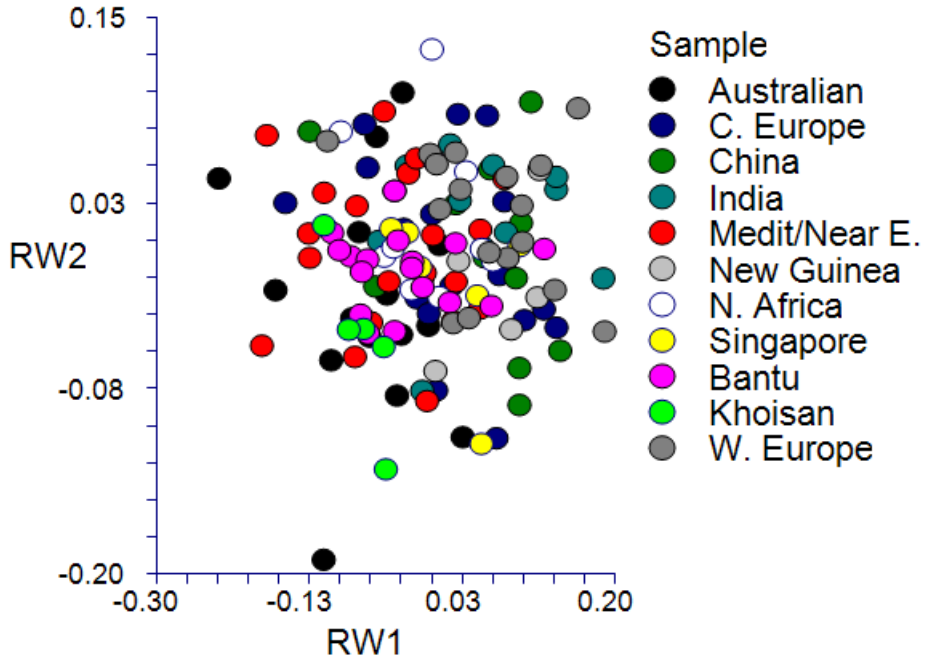

Figure G7. Plot of RW1 (35.65% variance explained) and RW2 (15.08% variance explained) of the Mastoid landmark dataset across the global sample.

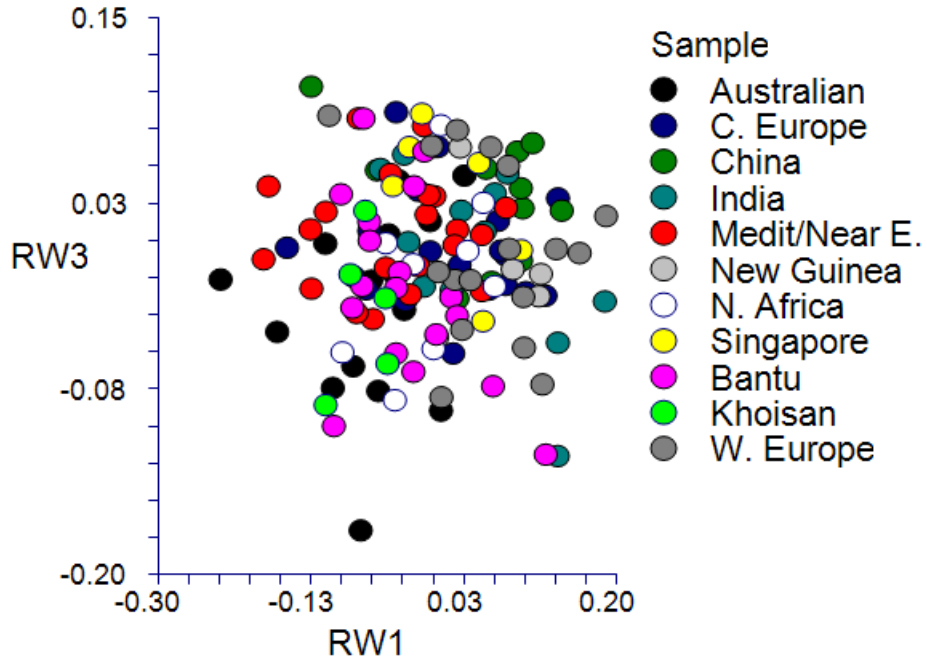

Figure G8. Plot of RW1 (35.65% variance explained) and RW3 (14.17% variance explained) of the Mastoid landmark dataset across the global sample.

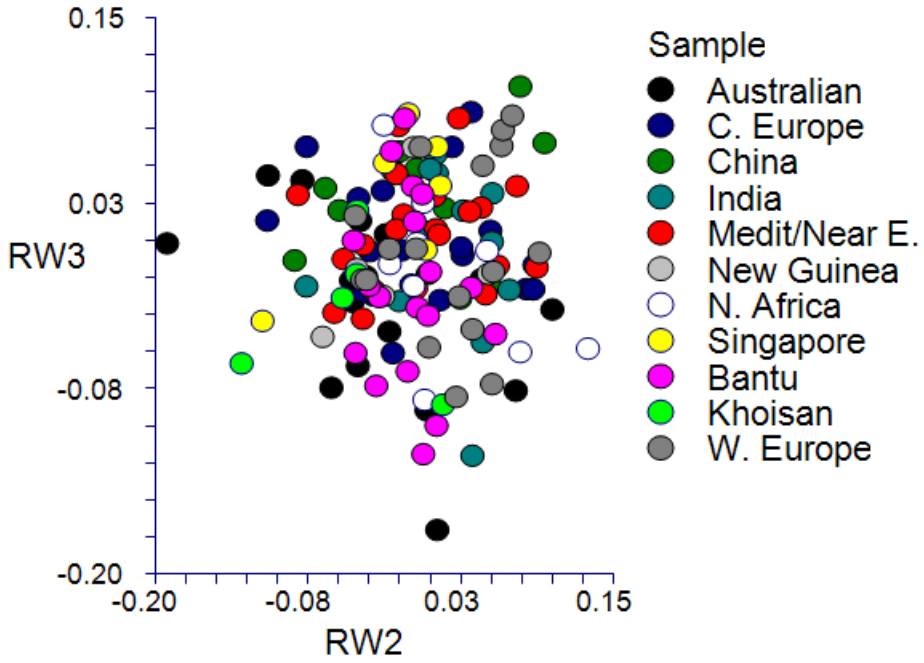

Figure G9. Plot of RW2 (15.08% variance explained) and RW3 (14.17% variance explained) of the Mastoid landmark dataset across the global sample.

APPENDIX H. MORPHOLOGICAL VARIATION IN OCCIPITAL LANDMARK DATASET FOR GLOBAL SAMPLE

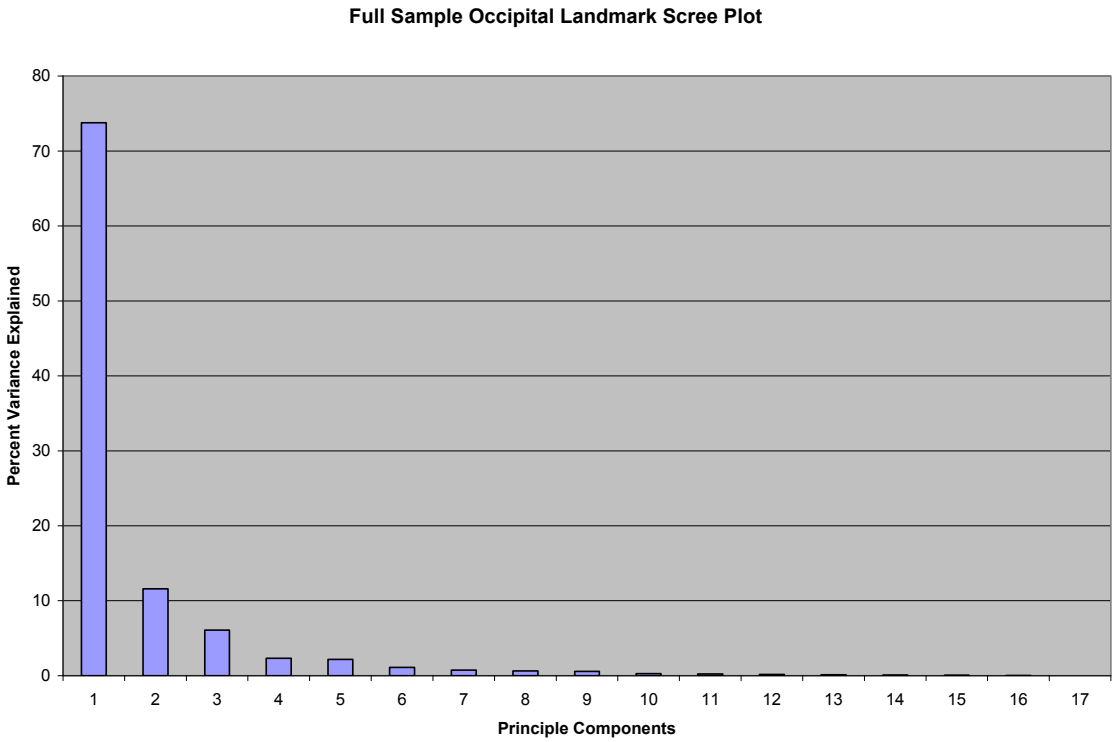

Figure H1. Scree plot of the 17 relative warps for the occipital region coordinate landmark dataset of the global sample. Warps 1-3 were selected for subsequent analyses.

Figure H2. Variation in Occipital Landmarks along RW1 for the complete sample: A) Lower extreme of variation, B) Consensus form, C) Upper extreme of variation.

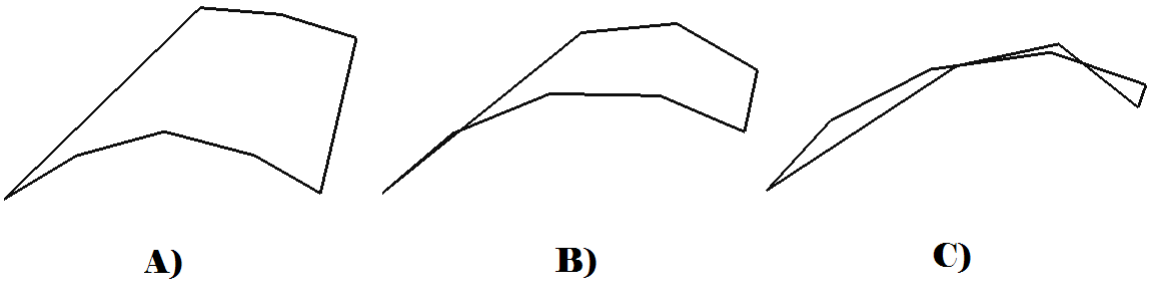

Figure H3. Variation in Occipital Landmarks along RW2 for the complete sample: A) Lower extreme of variation, B) Consensus form, C) Upper extreme of variation.

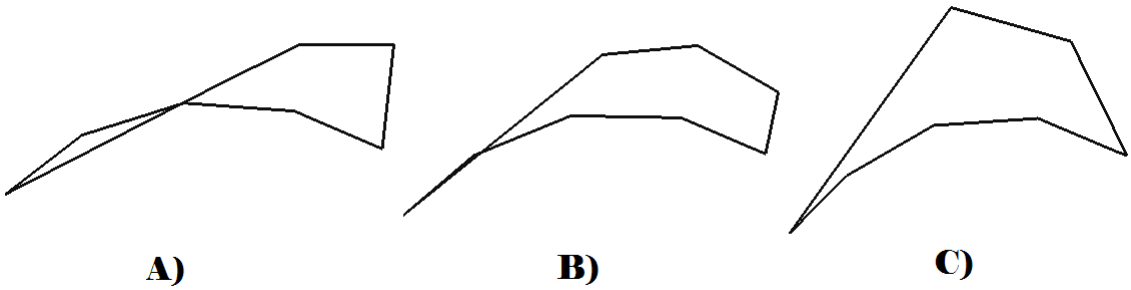

Figure H4. Variation in Occipital Landmarks along RW3 for the complete sample: A) Lower extreme of variation, B) Consensus form, C) Upper extreme of variation.

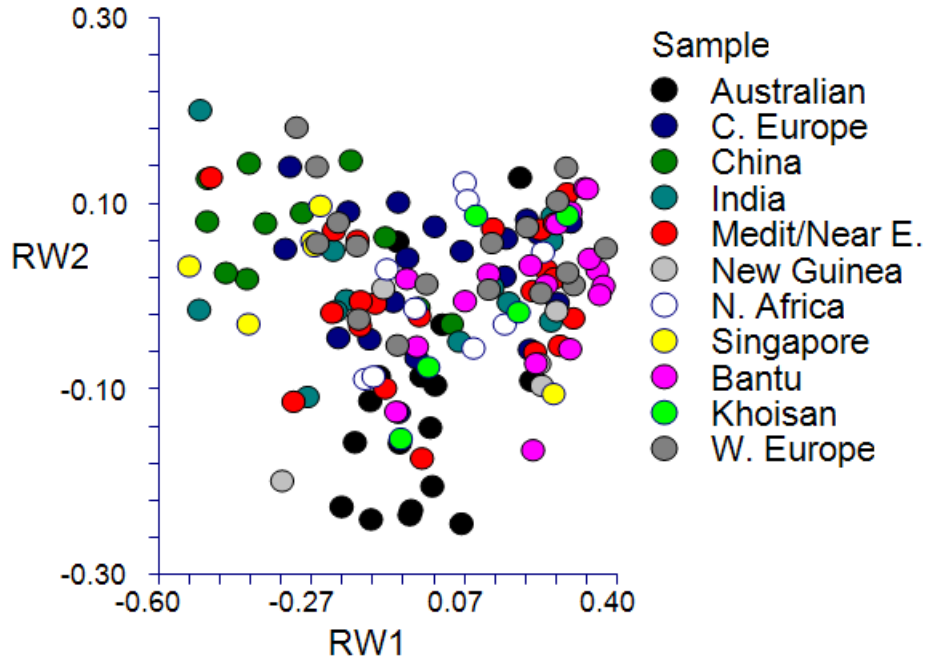

Figure H5. Plot of RW1 (73.76% variance explained) and RW2 (11.60% variance explained) of the Occipital landmark dataset across the global sample.

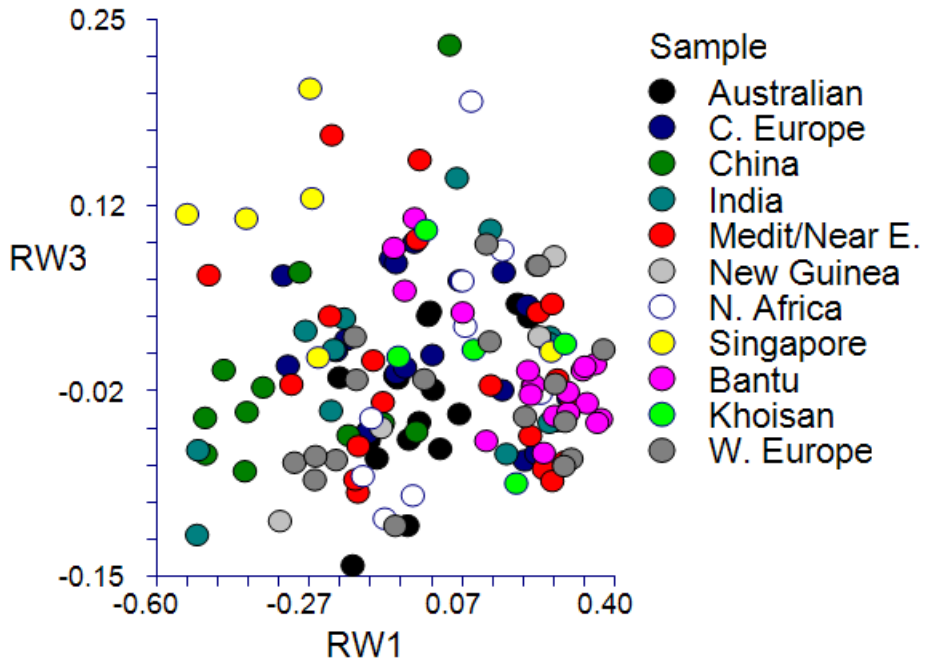

Figure H6. Plot of RW1 (73.76% variance explained) and RW3 (6.10% variance explained) of the Occipital landmark dataset across the global sample.

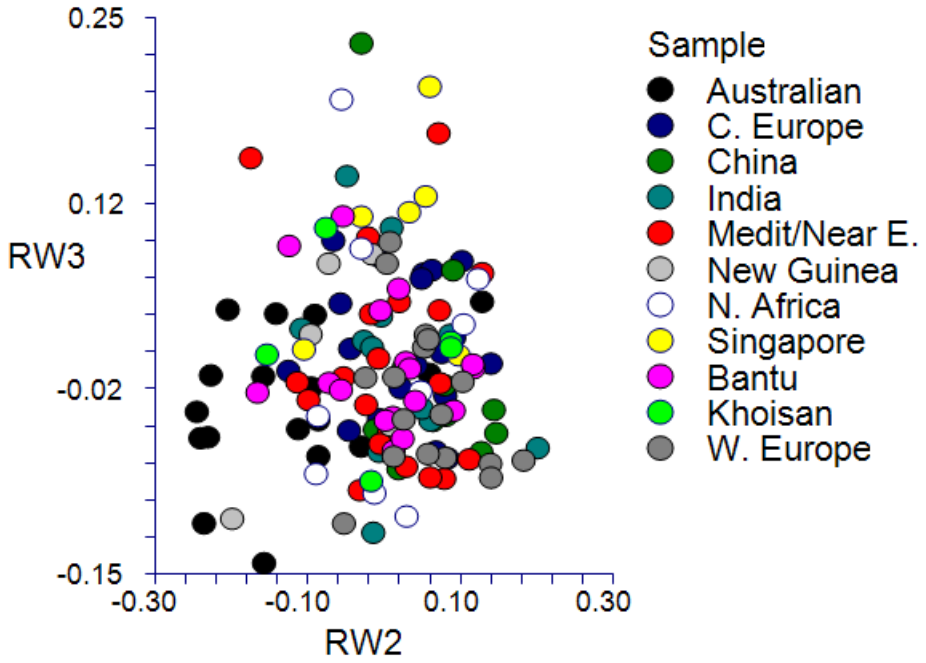

Figure H7. Plot of RW2 (11.60% variance explained) and RW3 (6.10% variance explained) of the Occipital landmark dataset across the global sample.

APPENDIX I. MORPHOLOGICAL VARIATION IN SUPRAORBITAL LANDMARK DATASET FOR MALE SUBSAMPLE

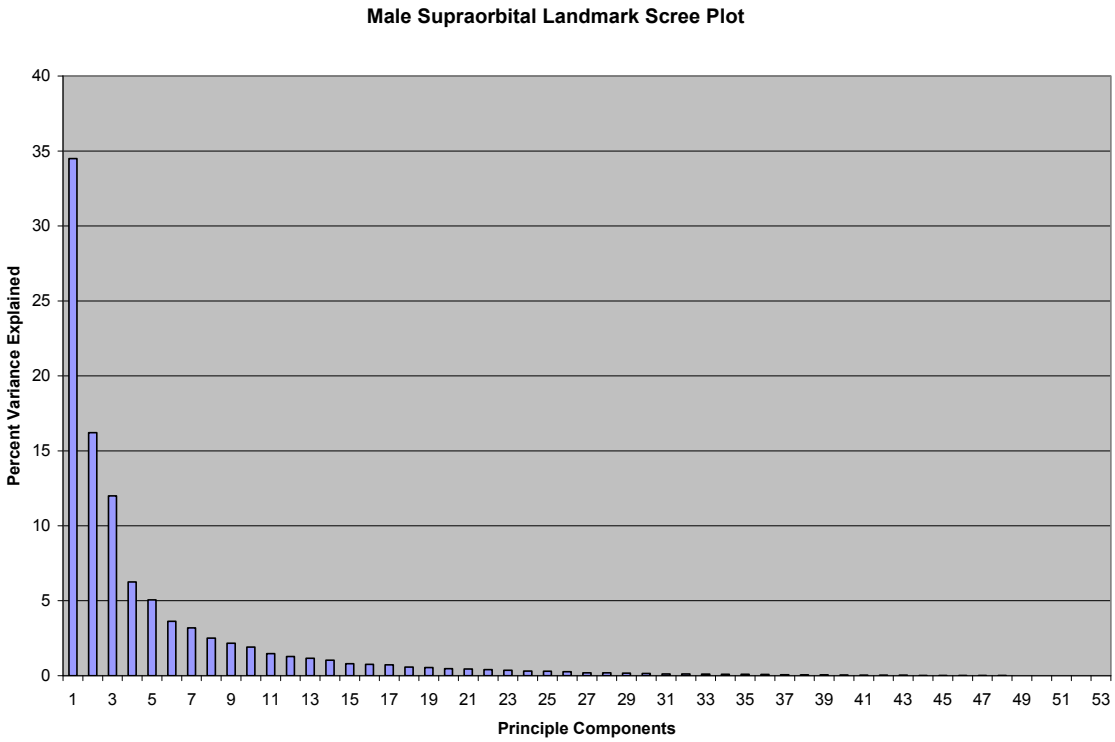

Figure I1. Scree plot of the 53 relative warps for the frontal region coordinate landmark dataset of the male subsample. Warps 1-3 were selected for subsequent analyses.

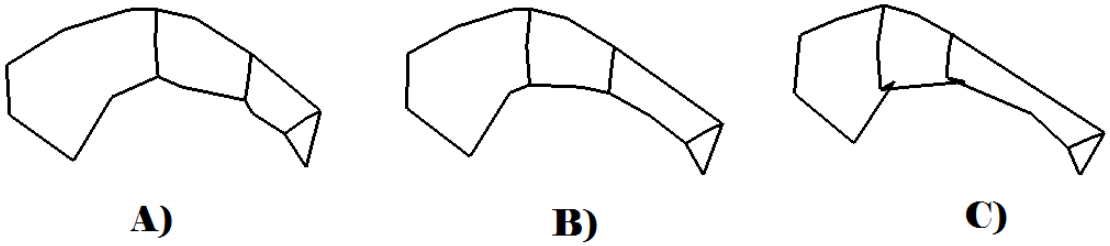

Figure I2. Variation in Supraorbital Landmarks along RW1 for the male subsample: A) Lower extreme of variation, B) Consensus form, C) Upper extreme of variation.

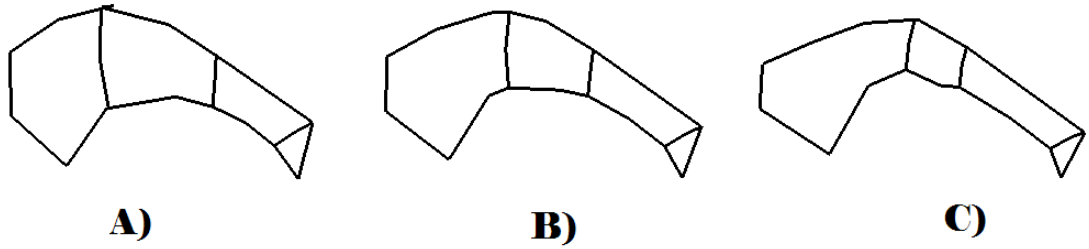

Figure I3. Variation in Supraorbital Landmarks along RW2 for the male subsample: A) Lower extreme of variation, B) Consensus form, C) Upper extreme of variation.

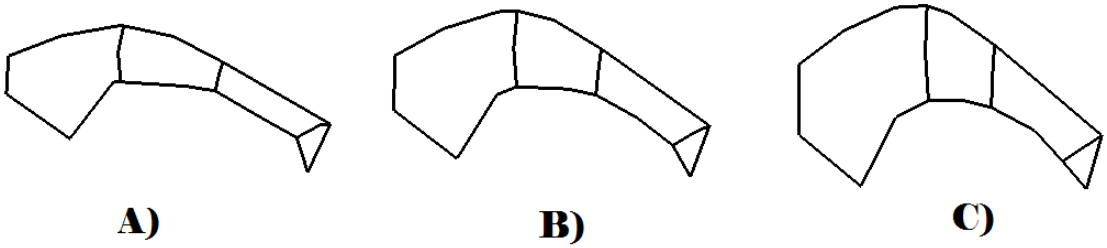

Figure I4. Variation in Supraorbital Landmarks along RW3 for the male subsample: A) Lower extreme of variation, B) Consensus form, C) Upper extreme of variation.

APPENDIX J. MORPHOLOGICAL VARIATION IN ZYGOMAXILLARY LANDMARK DATASET FOR MALE SUBSAMPLE

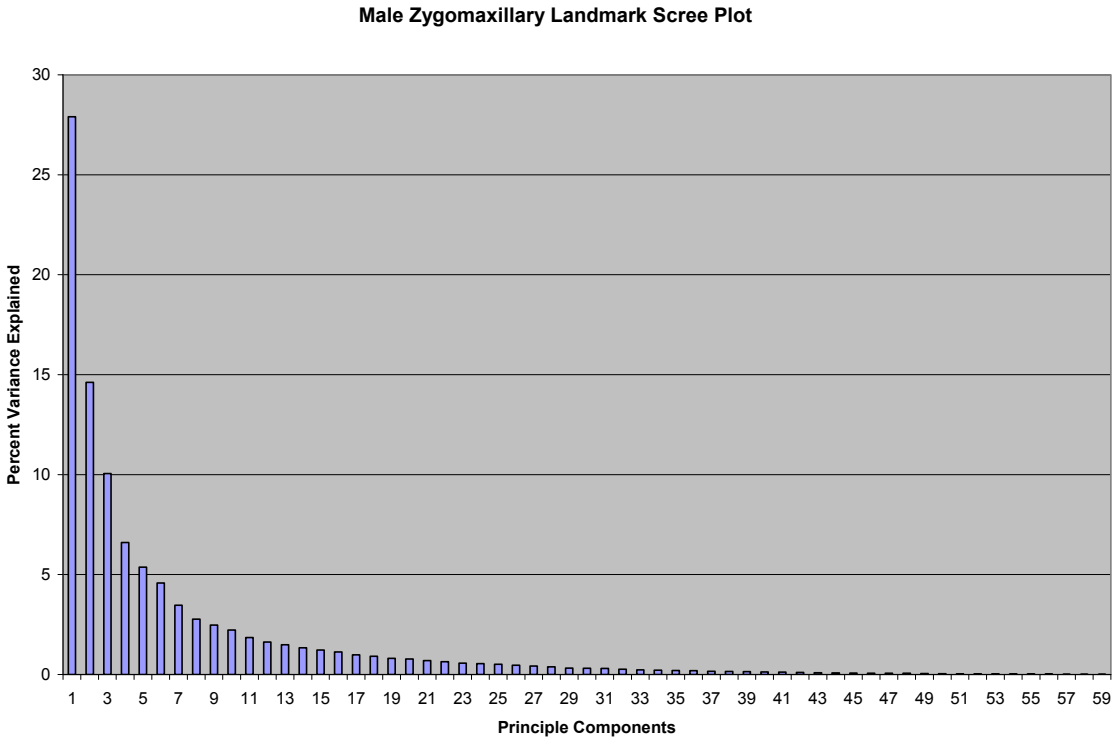

Figure J1. Scree plot of the 59 relative warps for the zygomaxillary region coordinate landmark dataset of the male subsample. Warps 1-3 were selected for subsequent analyses.

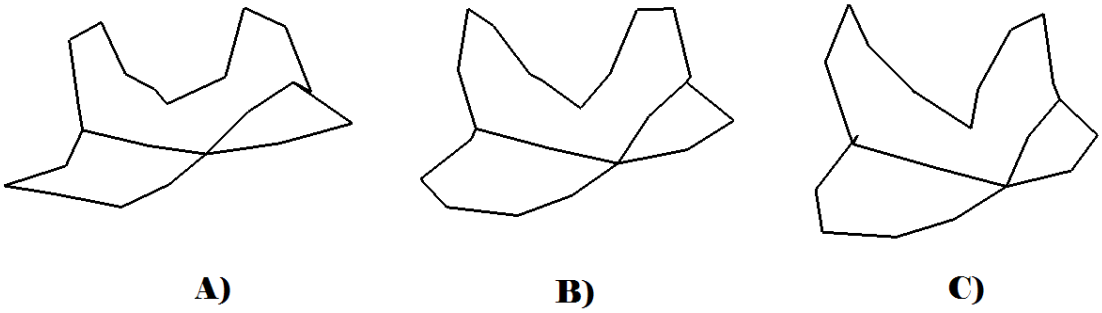

Figure J2. Variation in Zygomaxillary Landmarks along RW1 for the male subsample: A) Lower extreme of variation, B) Consensus form, C) Upper extreme of variation.

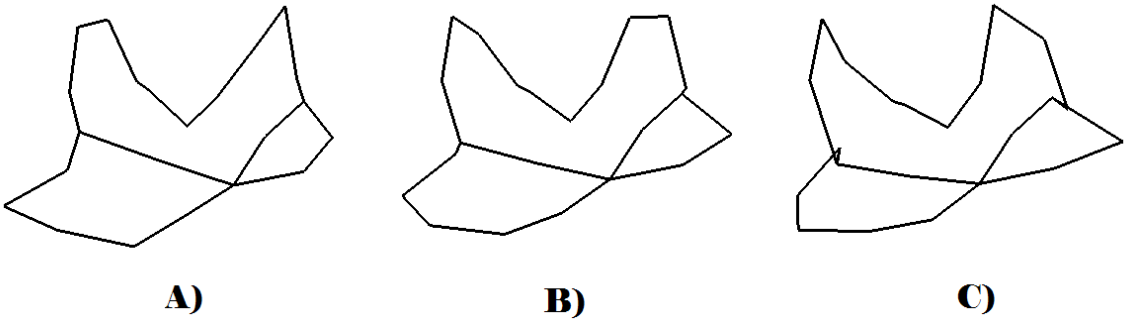

Figure J3. Variation in Zygomaxillary Landmarks along RW2 for the male subsample: A) Lower extreme of variation, B) Consensus form, C) Upper extreme of variation.

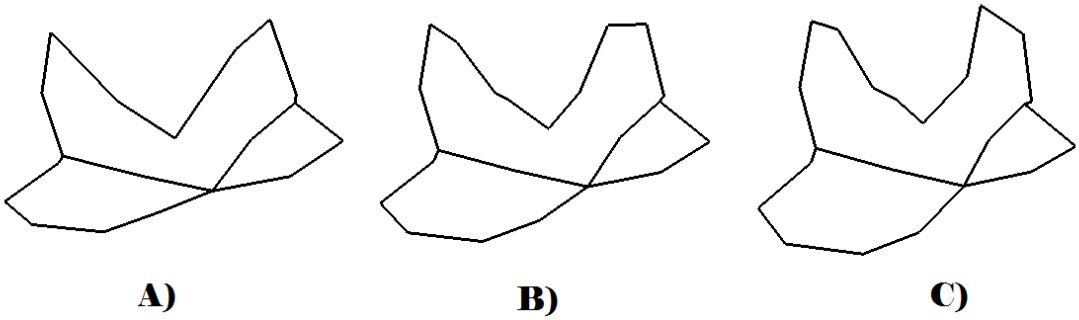

Figure J4. Variation in Zygomaxillary Landmarks along RW3 for the male subsample: A) Lower extreme of variation, B) Consensus form, C) Upper extreme of variation.

APPENDIX K. MORPHOLOGICAL VARIATION IN MASTOID LANDMARK DATASET FOR MALE SUBSAMPLE

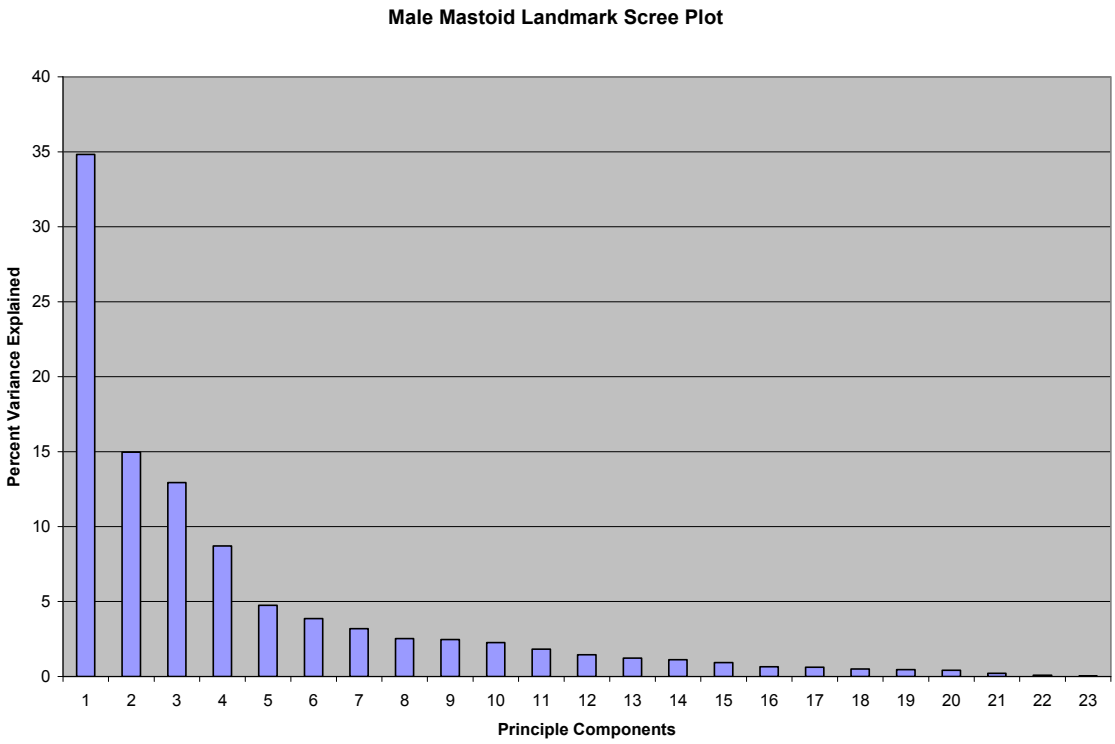

Figure K1. Scree plot of the 23 relative warps for the mastoid region coordinate landmark dataset of the male subsample. Warps 1-4 were selected for subsequent analyses.

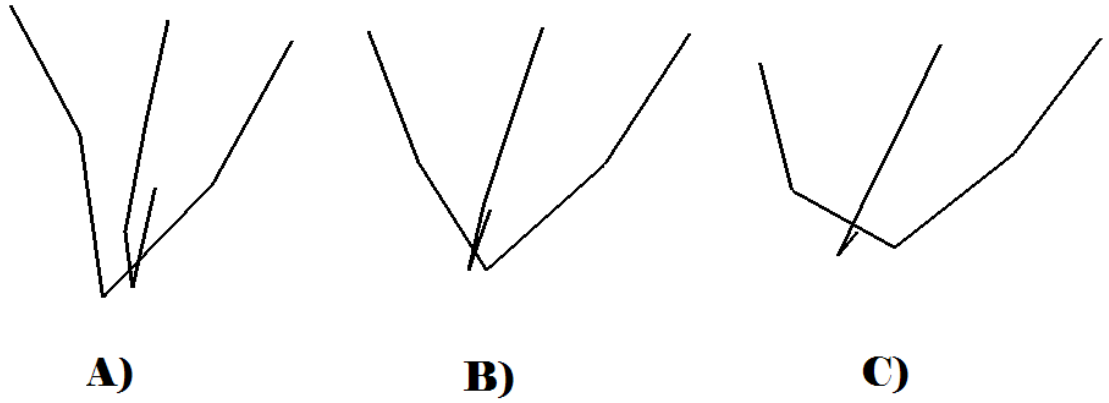

Figure K2. Variation in Mastoid Landmarks along RW1 for the male subsample: A) Lower extreme of variation, B) Consensus form, C) Upper extreme of variation.

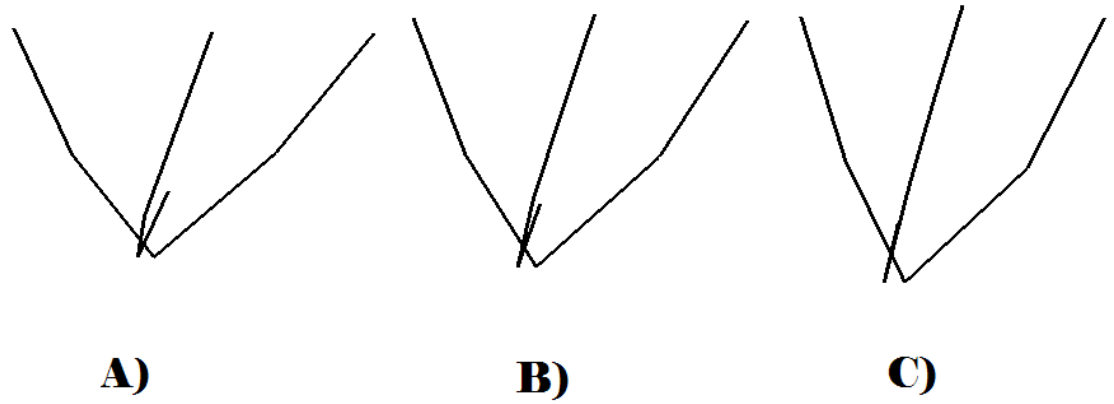

Figure K3. Variation in Mastoid Landmarks along RW2 for the male subsample: A) Lower extreme of variation, B) Consensus form, C) Upper extreme of variation.

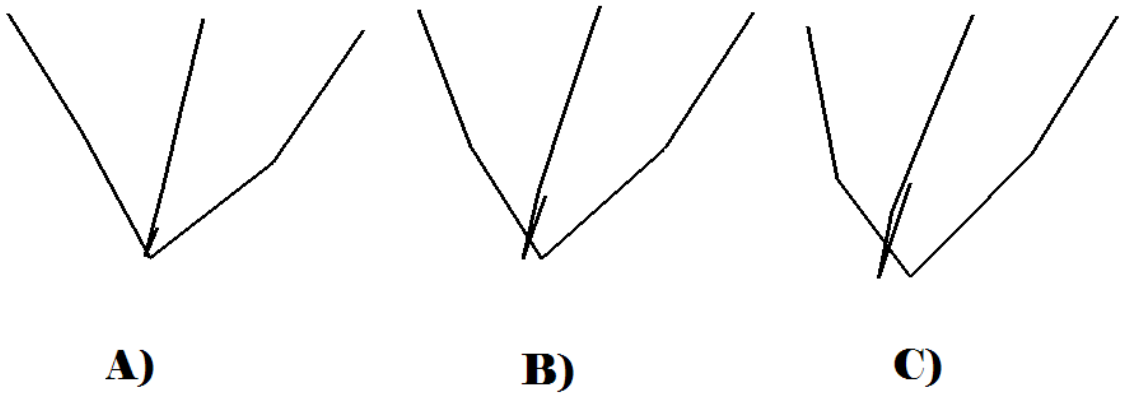

Figure K4. Variation in Mastoid Landmarks along RW3 for the male subsample: A) Lower extreme of variation, B) Consensus form, C) Upper extreme of variation.

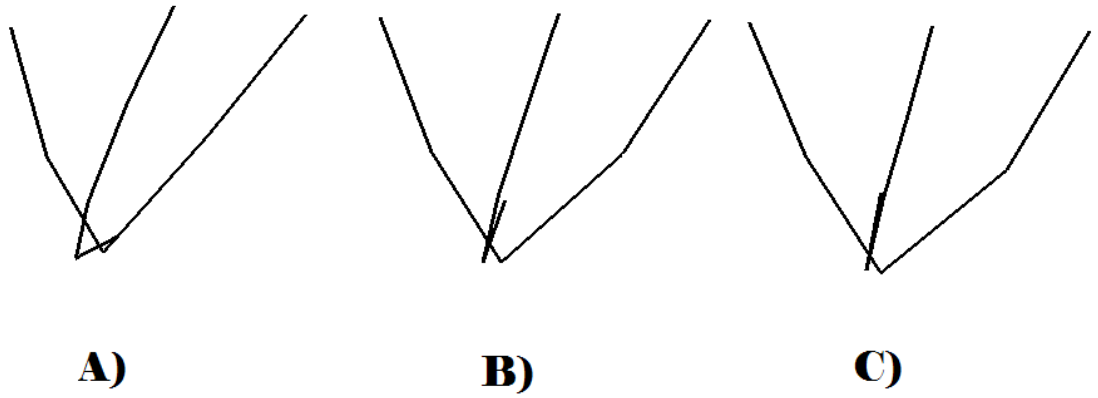

Figure K5. Variation in Mastoid Landmarks along RW4 for the male subsample: A) Lower extreme of variation, B) Consensus form, C) Upper extreme of variation.

APPENDIX L. MORPHOLOGICAL VARIATION IN OCCIPITAL LANDMARK DATASET FOR MALE SUBSAMPLE

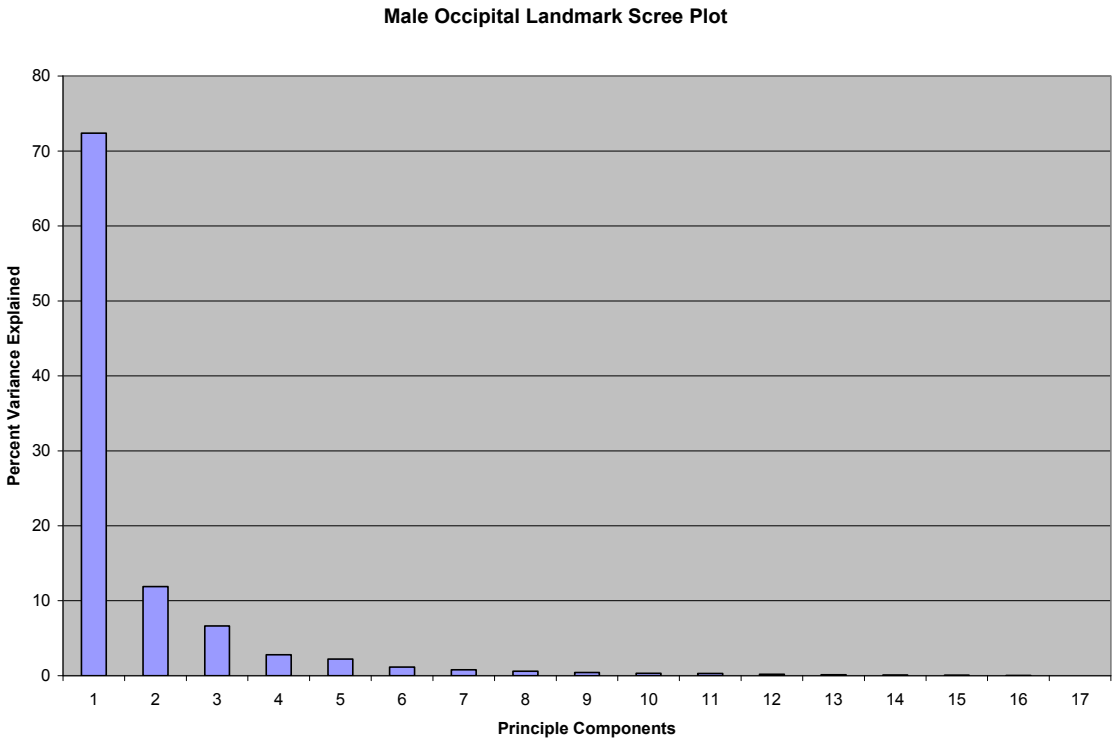

Figure L1. Scree plot of the 17 relative warps for the occipital region coordinate landmark dataset of the male subsample. Warps 1-3 were selected for subsequent analyses.

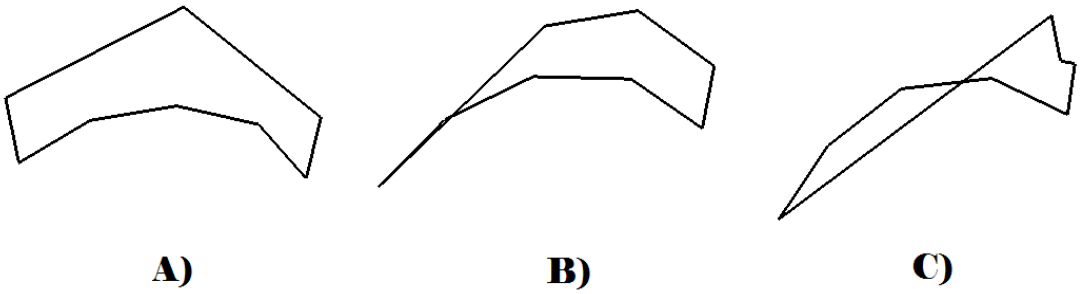

Figure L2. Variation in Occipital Landmarks along RW1 for the male subsample: A) Lower extreme of variation, B) Consensus form, C) Upper extreme of variation.

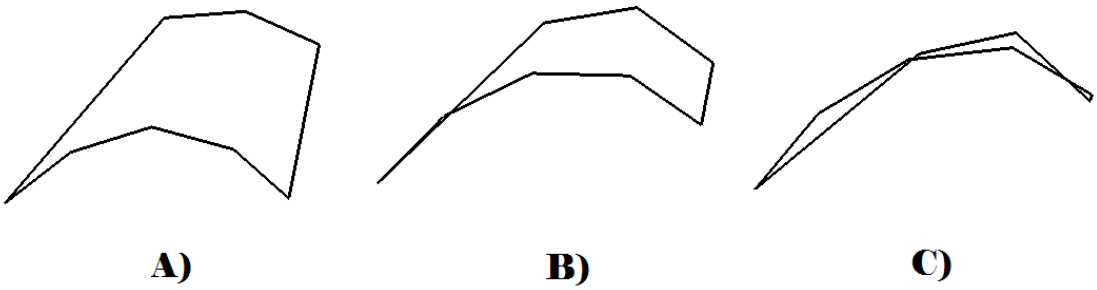

Figure L3. Variation in Occipital Landmarks along RW2 for the male subsample: A) Lower extreme of variation, B) Consensus form, C) Upper extreme of variation.

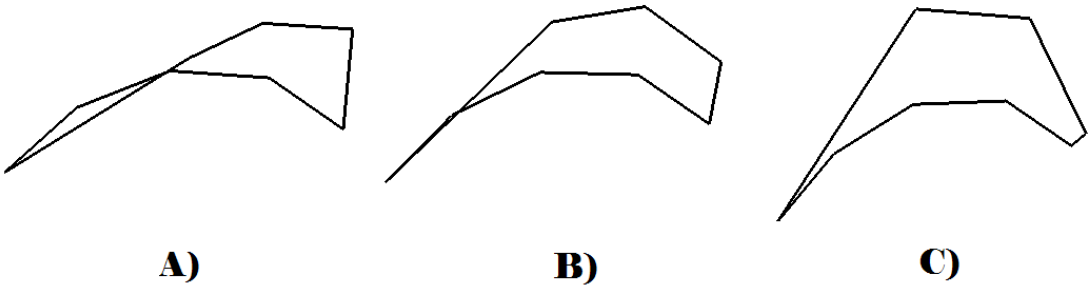

Figure L4. Variation in Occipital Landmarks along RW3 for the male subsample: A) Lower extreme of variation, B) Consensus form, C) Upper extreme of variation.

APPENDIX M. MORPHOLOGICAL VARIATION IN SUPRAORBITAL LANDMARK DATASET FOR FEMALE SUBSAMPLE

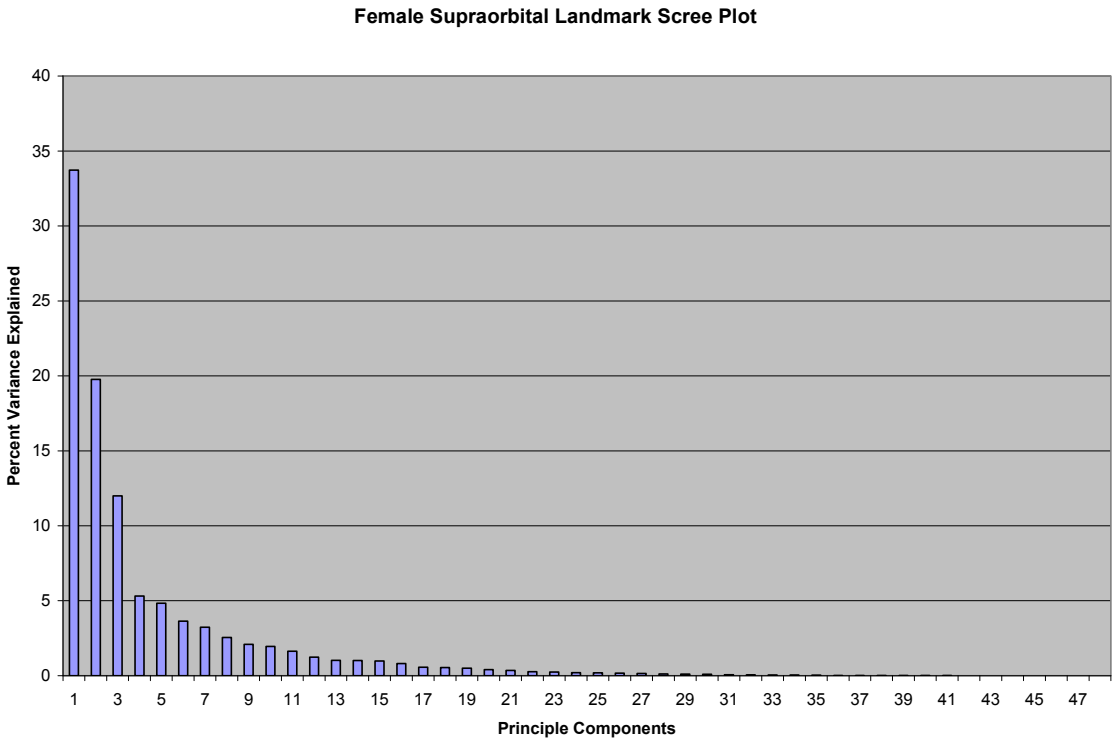

Figure M1. Scree plot of the 48 relative warps for the frontal region coordinate landmark dataset of the female subsample. Warps 1-3 were selected for subsequent analyses.

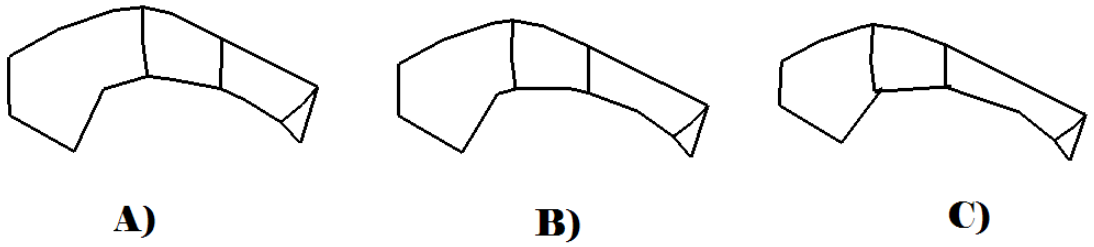

Figure M2. Variation in Supraorbital Landmarks along RW1 for the female subsample: A) Lower extreme of variation, B) Consensus form, C) Upper extreme of variation.

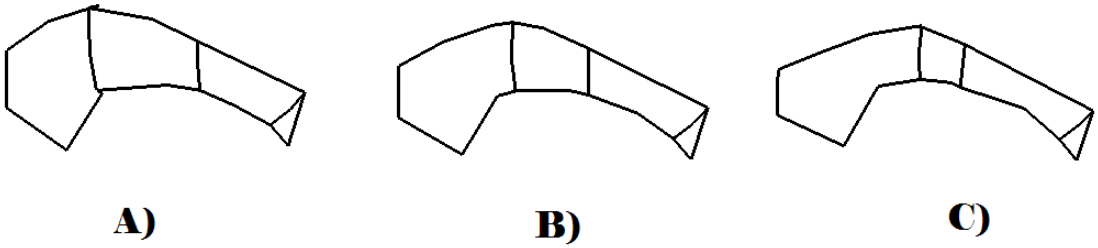

Figure M3. Variation in Supraorbital Landmarks along RW2 for the female subsample: A) Lower extreme of variation, B) Consensus form, C) Upper extreme of variation.

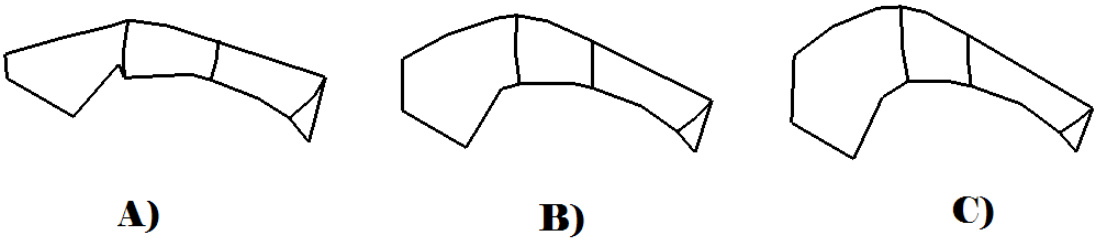

Figure M4. Variation in Supraorbital Landmarks along RW3 for the female subsample: A) Lower extreme of variation, B) Consensus form, C) Upper extreme of variation.

APPENDIX N. MORPHOLOGICAL VARIATION IN ZYGOMAXILLARY LANDMARK DATASET FOR FEMALE SUBSAMPLE

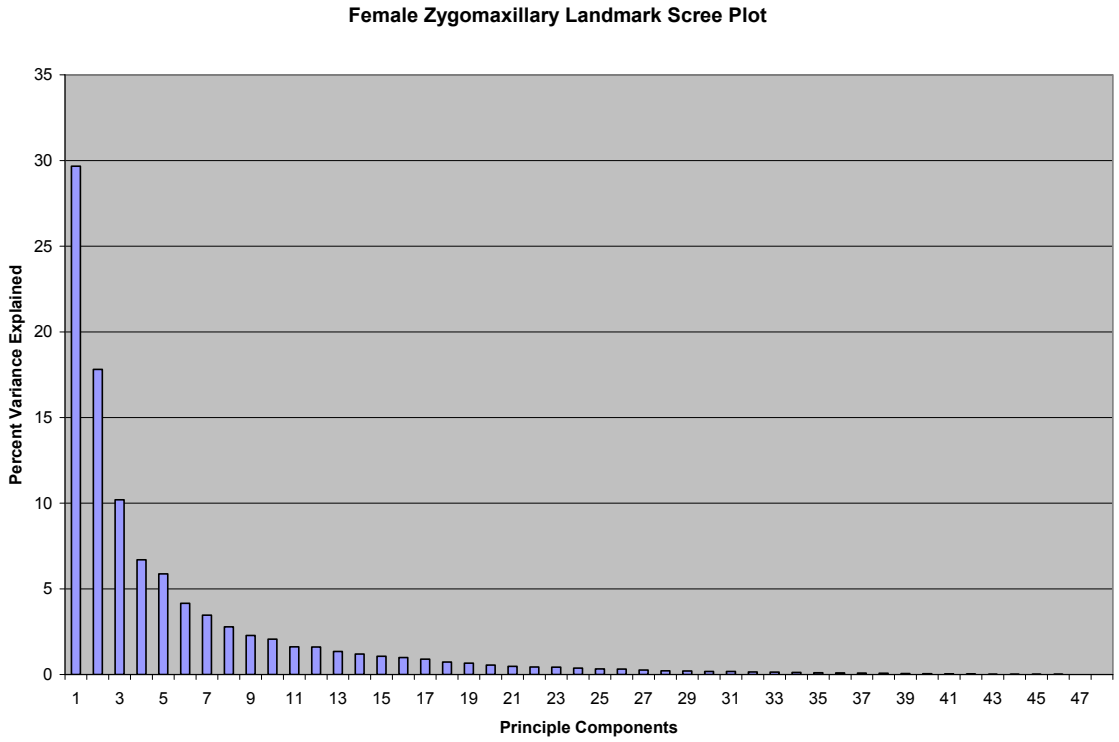

Figure N1. Scree plot of the 48 relative warps for the zygomaxillary region coordinate landmark dataset of the female subsample. Warps 1-3 were selected for subsequent analyses.

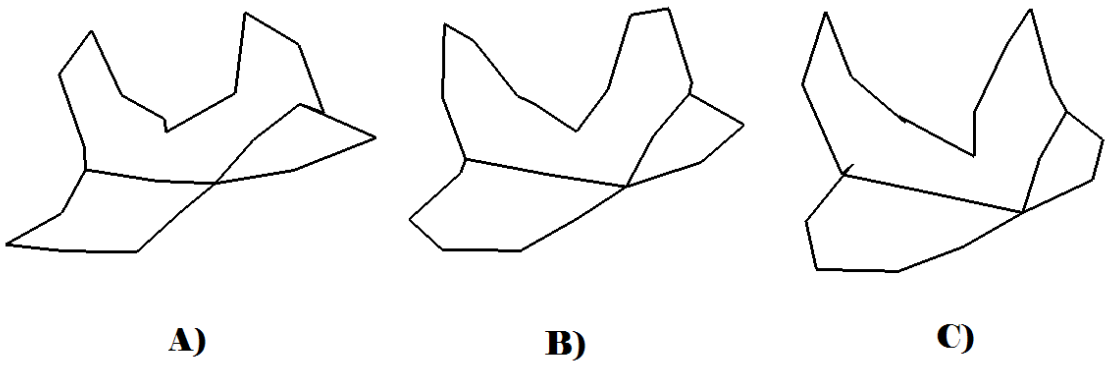

Figure N2. Variation in Zygomaxillary Landmarks along RW1 for the female subsample: A) Lower extreme of variation, B) Consensus form, C) Upper extreme of variation.

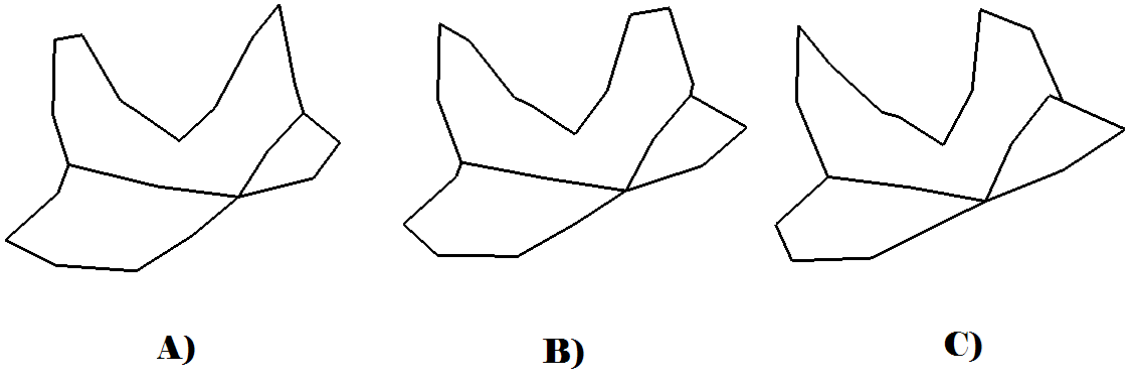

Figure N3. Variation in Zygomaxillary Landmarks along RW2 for the female subsample: A) Lower extreme of variation, B) Consensus form, C) Upper extreme of variation.

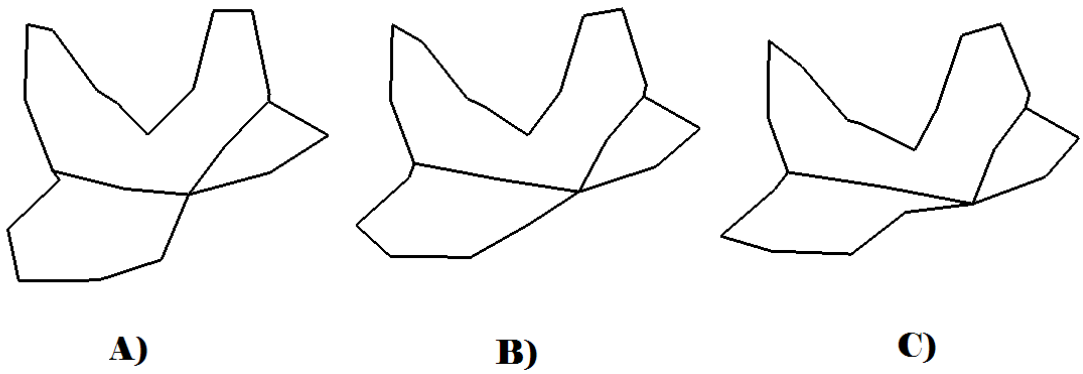

Figure N4. Variation in Zygomaxillary Landmarks along RW3 for the female subsample: A) Lower extreme of variation, B) Consensus form, C) Upper extreme of variation.

APPENDIX O. MORPHOLOGICAL VARIATION IN MASTOID LANDMARK DATASET FOR FEMALE SUBSAMPLE

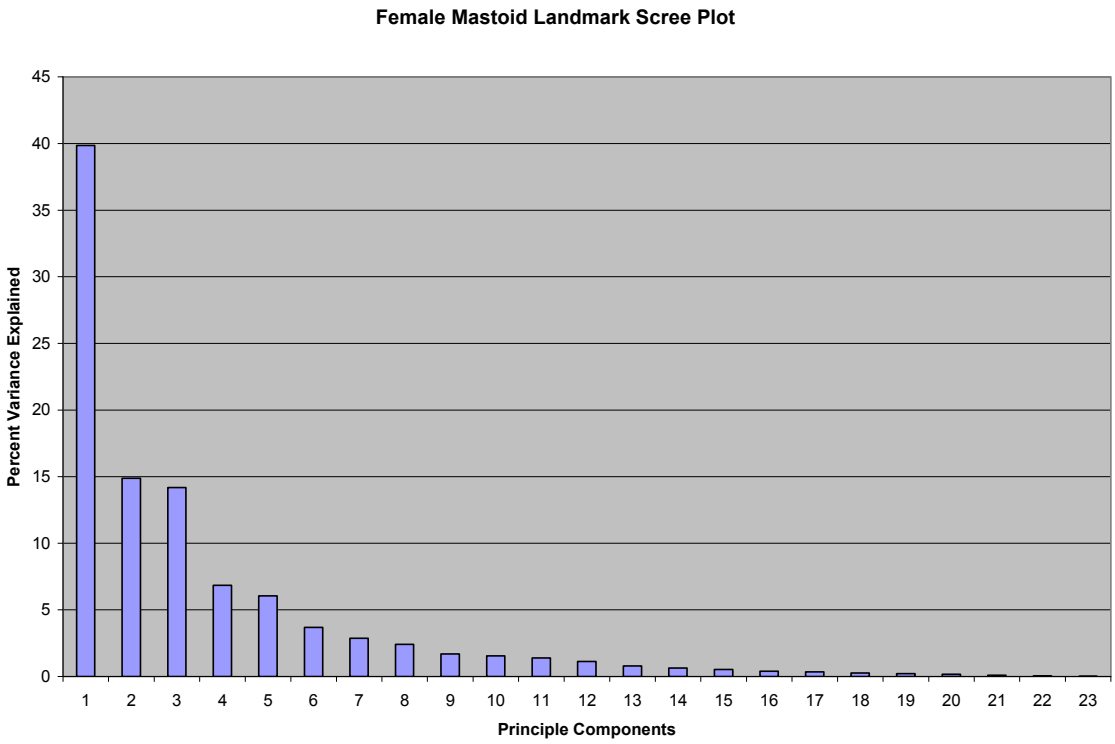

Figure O1. Scree plot of the 23 relative warps for the mastoid region coordinate landmark dataset of the female subsample. Warps 1-3 were selected for subsequent analyses.

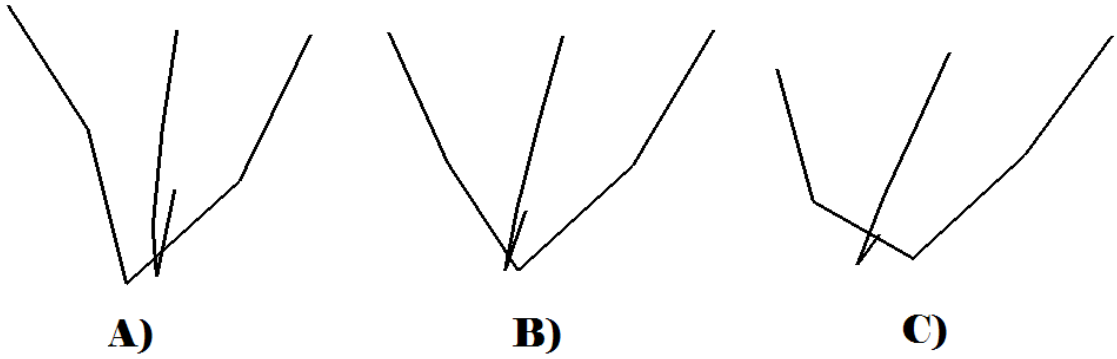

Figure O2. Variation in Mastoid Landmarks along RW1 for the female subsample: A) Lower extreme of variation, B) Consensus form, C) Upper extreme of variation.

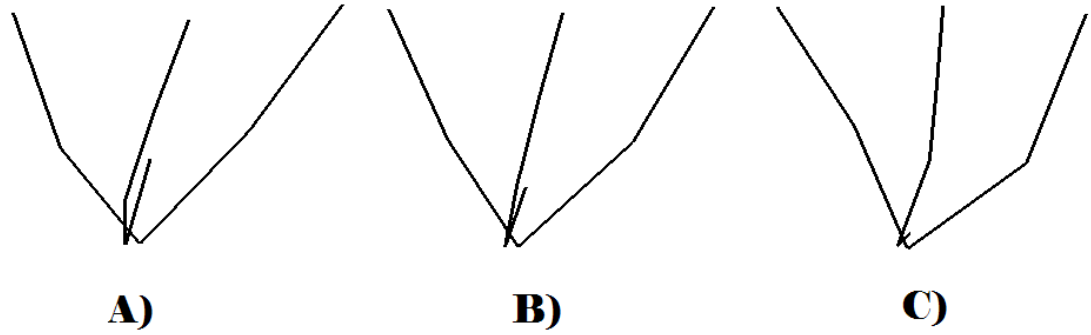

Figure O3. Variation in Mastoid Landmarks along RW2 for the female subsample: A) Lower extreme of variation, B) Consensus form, C) Upper extreme of variation.

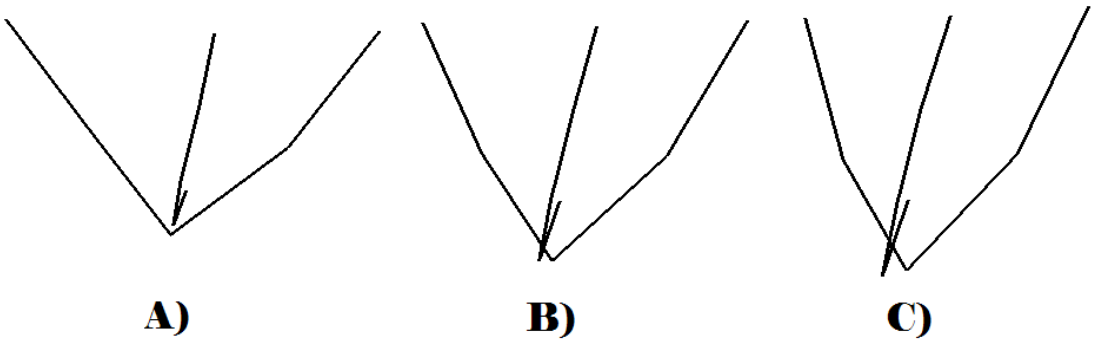

Figure O4. Variation in Mastoid Landmarks along RW3 for the female subsample: A) Lower extreme of variation, B) Consensus form, C) Upper extreme of variation.

APPENDIX P. MORPHOLOGICAL VARIATION IN OCCIPITAL LANDMARK DATASET FOR FEMALE SUBSAMPLE

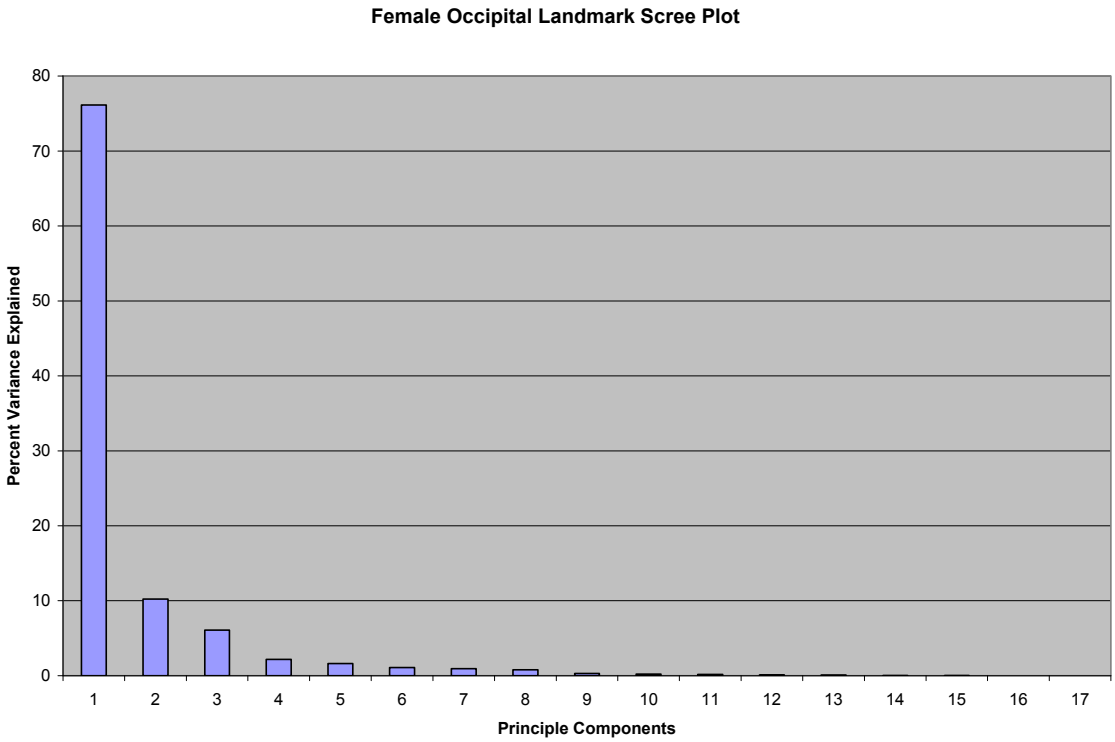

Figure P1. Scree plot of the 17 relative warps for the occipital region coordinate landmark dataset of the female subsample. Warps 1-3 were selected for subsequent analyses.

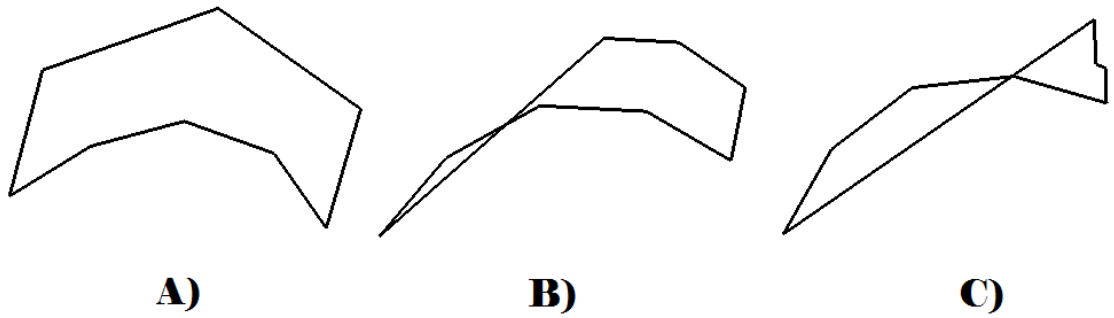

Figure P2. Variation in Occipital Landmarks along RW1 for the female subsample: A) Lower extreme of variation, B) Consensus form, C) Upper extreme of variation.

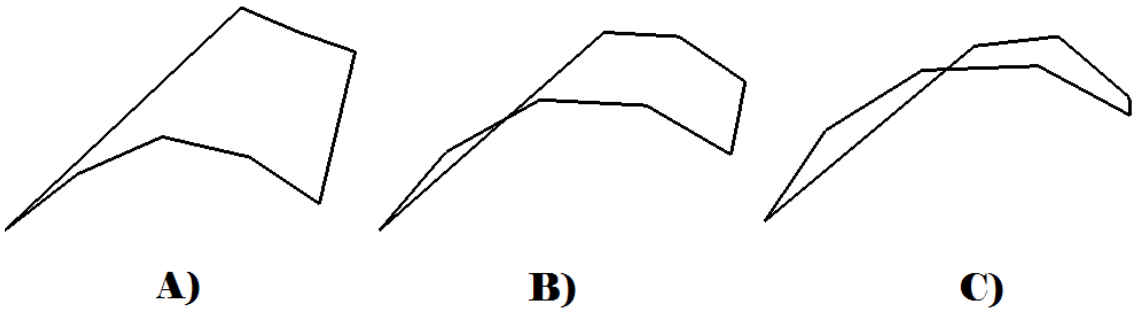

Figure P3. Variation in Occipital Landmarks along RW2 for the female subsample: A) Lower extreme of variation, B) Consensus form, C) Upper extreme of variation.

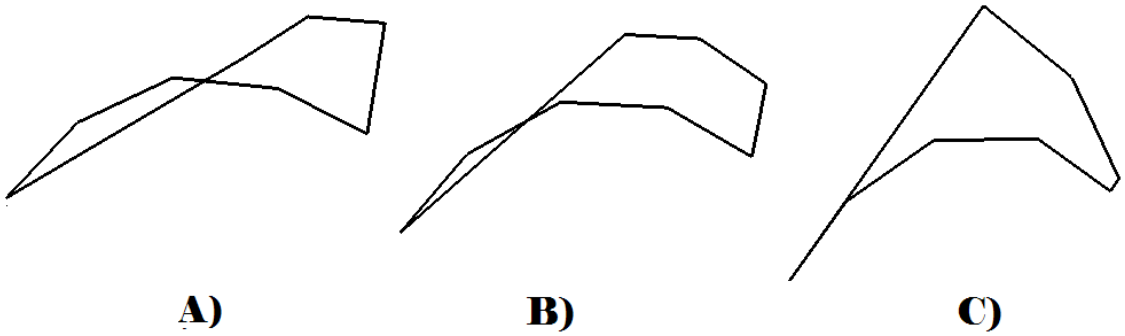

Figure P4. Variation in Occipital Landmarks along RW3 for the female subsample: A) Lower extreme of variation, B) Consensus form, C) Upper extreme of variation.

APPENDIX Q. GLOBAL SAMPLE PLS RESULTS

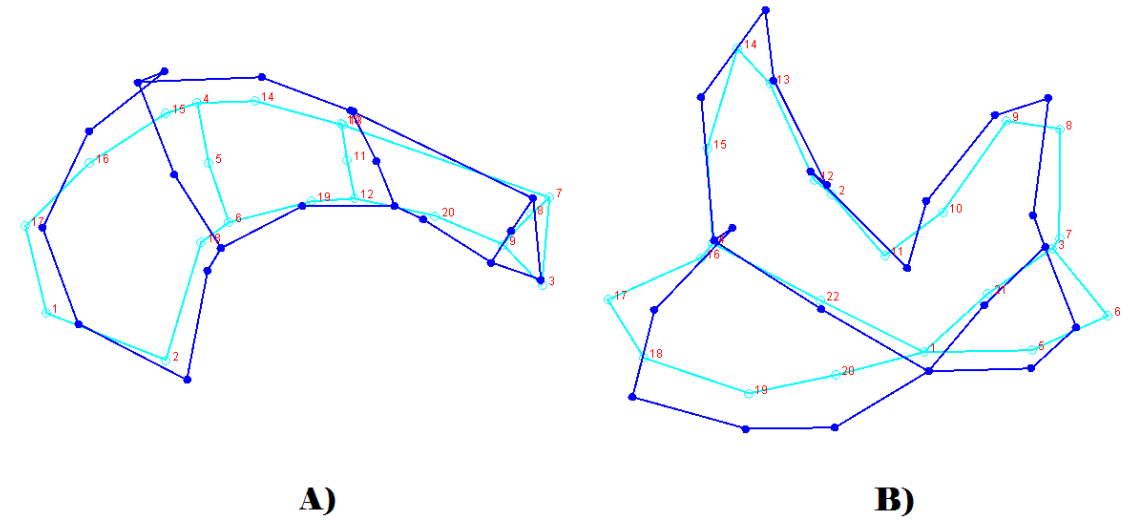

Figure Q1. PLS1 of the frontal and zygomaxillary data from the 2B-PLS analysis: A) Supraorbital Block, B) Zygomaxillary Block (Light Blue = consensus form, Dark Blue = shape variation).

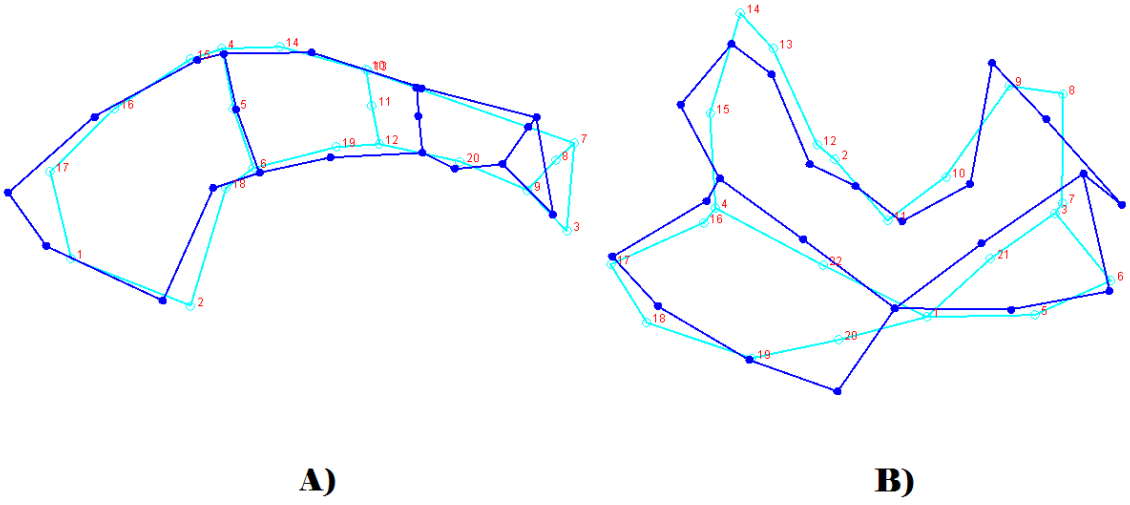

Figure Q2. PLS2 of the frontal and zygomaxillary data from the 2B-PLS analysis: A) Supraorbital Block, B) Zygomaxillary Block (Light Blue = consensus form, Dark Blue = shape variation).

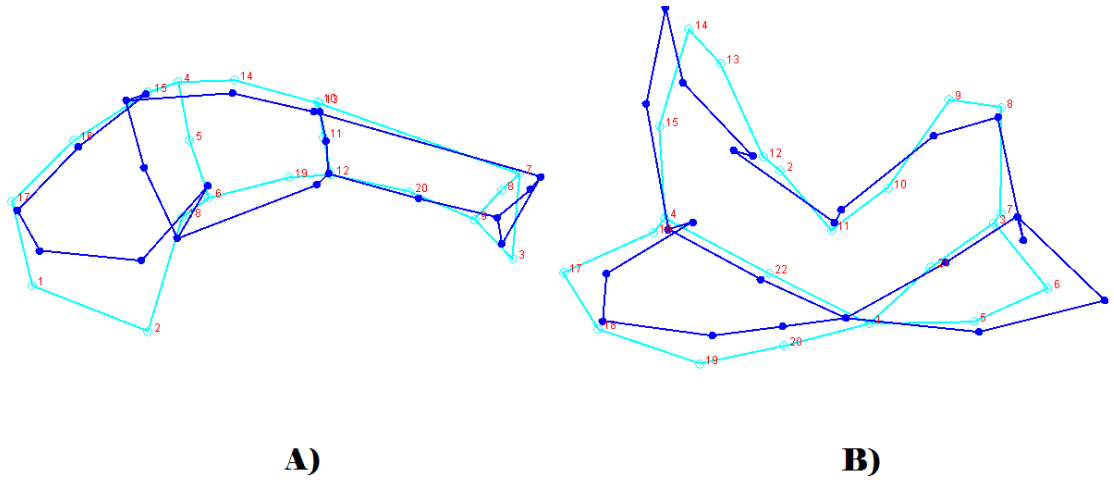

Figure Q3. PLS3 of the frontal and zygomaxillary data from the 2B-PLS analysis: A) Supraorbital Block, B) Zygomaxillary Block (Light Blue = consensus form, Dark Blue = shape variation).

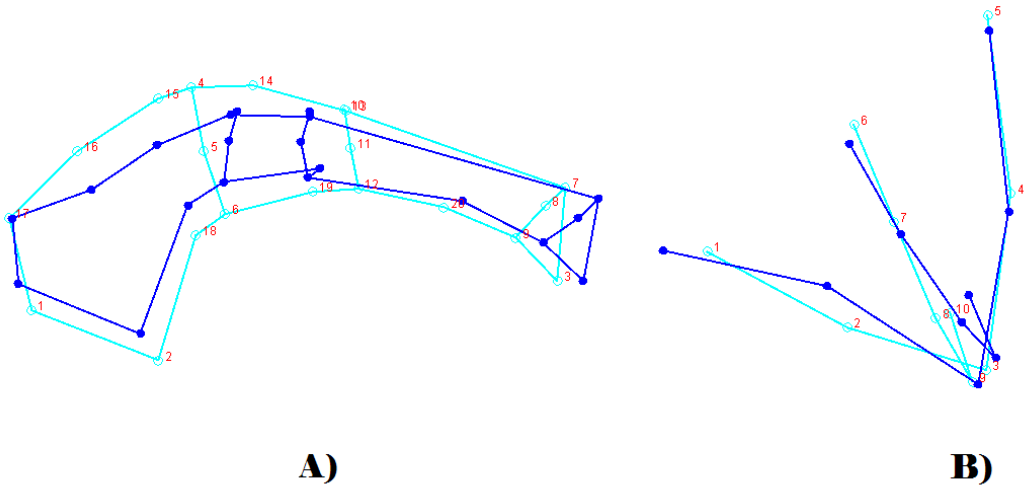

Figure Q4. PLS1 of the frontal and mastoid data from the 2B-PLS analysis: A) Supraorbital Block, B) Mastoid Block (Light Blue = consensus form, Dark Blue = shape variation).

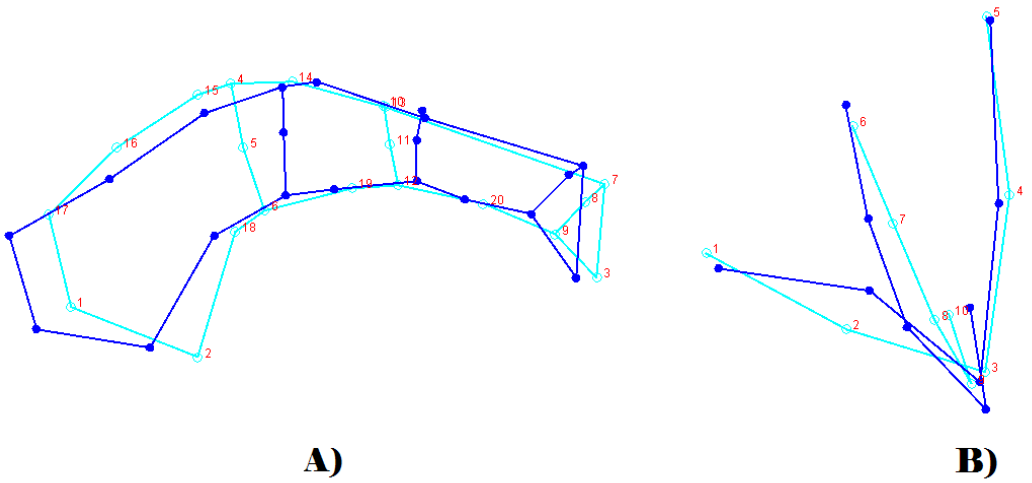

Figure Q5. PLS2 of the frontal and mastoid data from the 2B-PLS analysis: A) Supraorbital Block, B) Mastoid Block (Light Blue = consensus form, Dark Blue = shape variation).

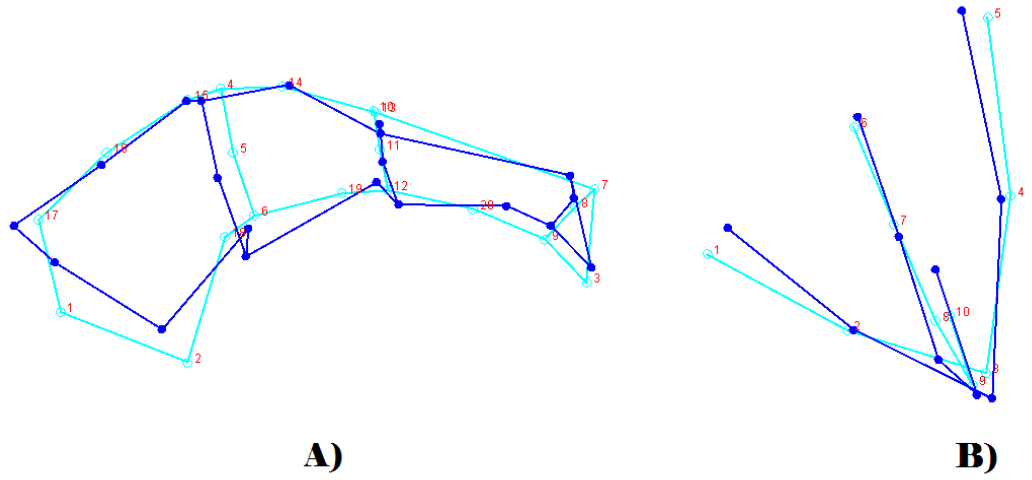

Figure Q6. PLS3 of the frontal and mastoid data from the 2B-PLS analysis: A) Supraorbital Block, B) Mastoid Block (Light Blue = consensus form, Dark Blue = shape variation).

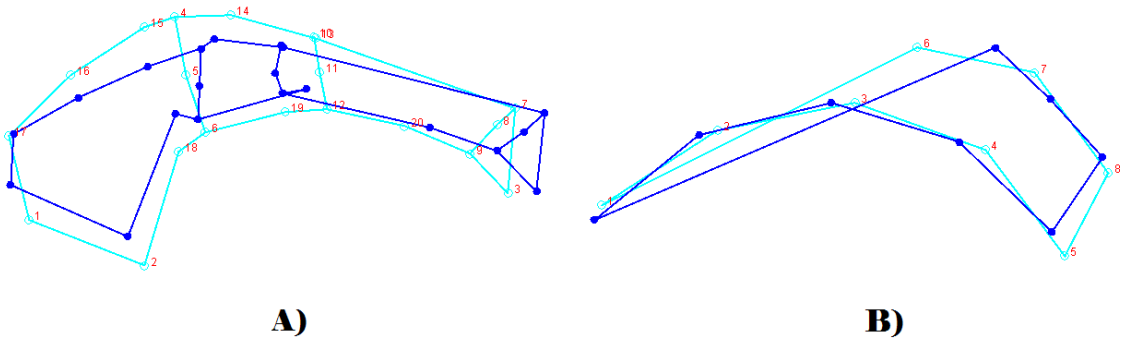

Figure Q7. PLS1 of the frontal and occipital data from the 2B-PLS analysis: A) Supraorbital Block, B) Nuchal Block (Light Blue = consensus form, Dark Blue = shape variation).

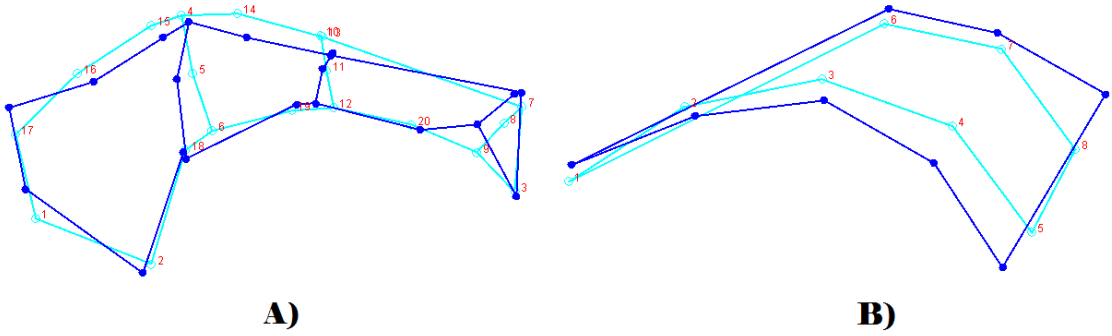

Figure Q8. PLS2 of the frontal and occipital data from the 2B-PLS analysis: A) Supraorbital Block, B) Nuchal Block (Light Blue = consensus form, Dark Blue = shape variation).

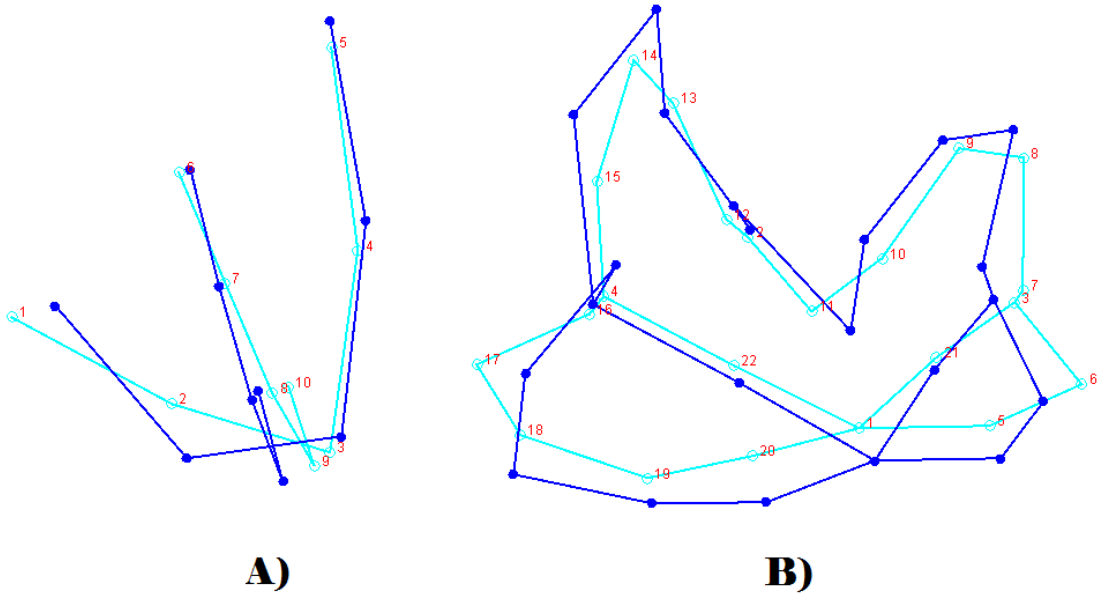

Figure Q9. PLS1 of the mastoid and zygomaxillary data from the 2B-PLS analysis: A) Mastoid Block, B) Zygomaxillary Block (Light Blue = consensus form, Dark Blue = shape variation).

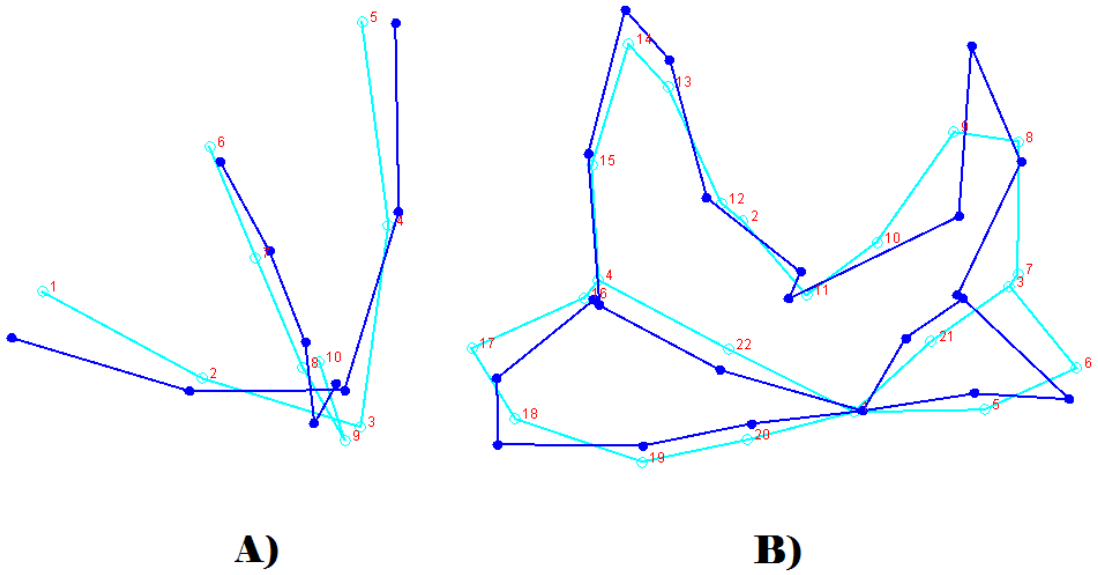

Figure Q10. PLS2 of the mastoid and zygomaxillary data from the 2B-PLS analysis: A) Mastoid Block, B) Zygomaxillary Block (Light Blue = consensus form, Dark Blue = shape variation).

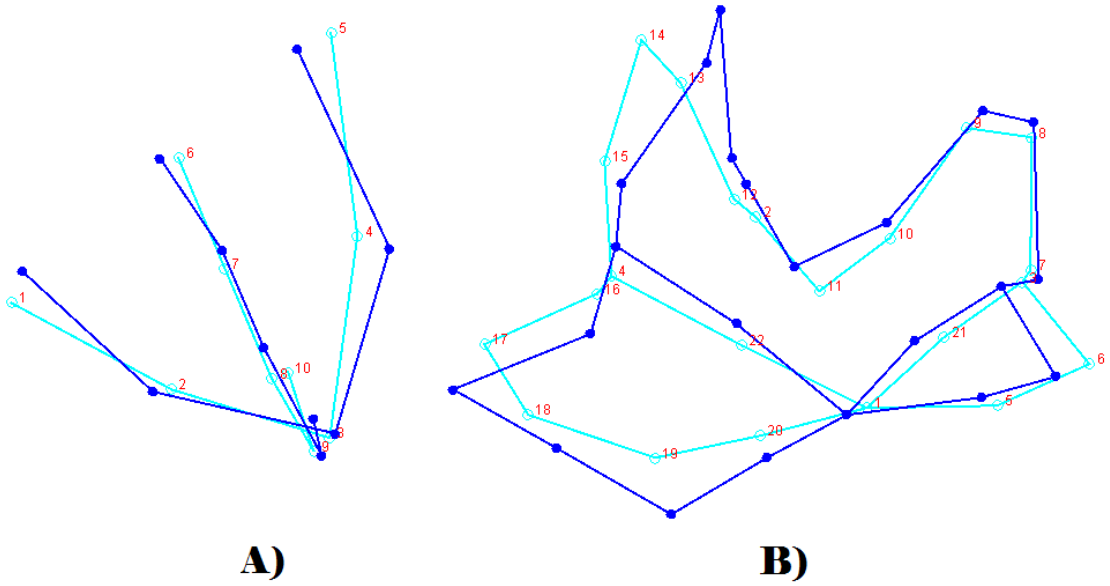

Figure Q11. PLS3 of the mastoid and zygomaxillary data from the 2B-PLS analysis: A) Mastoid Block, B) Zygomaxillary Block (Light Blue = consensus form, Dark Blue = shape variation).

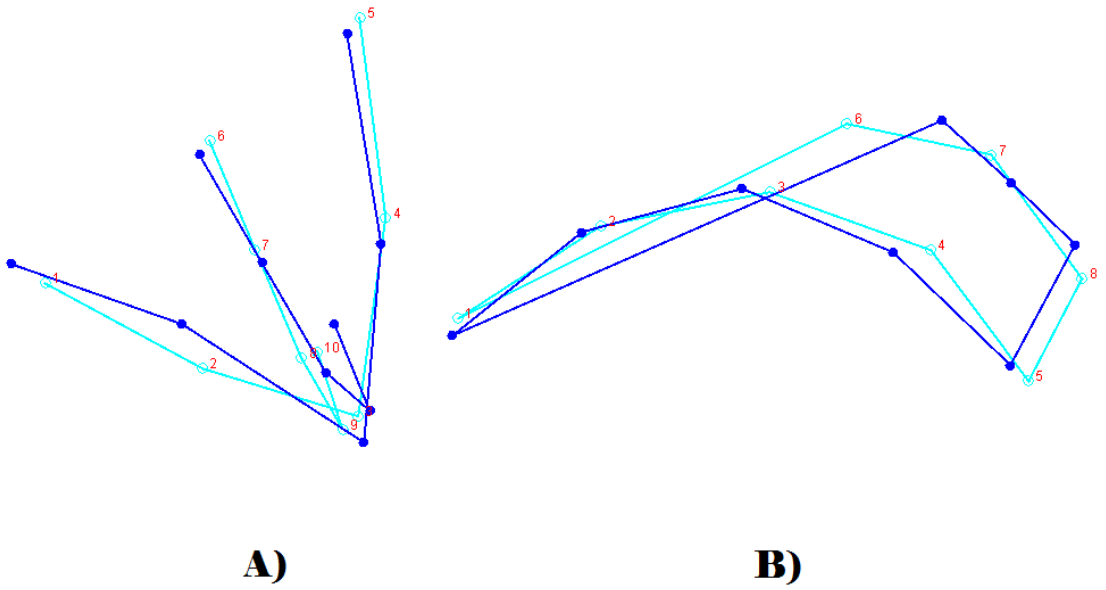

Figure Q12. PLS1 of the mastoid and occipital data from the 2B-PLS analysis: A) Mastoid Block, B) Nuchal Block (Light Blue = consensus form, Dark Blue = shape variation).

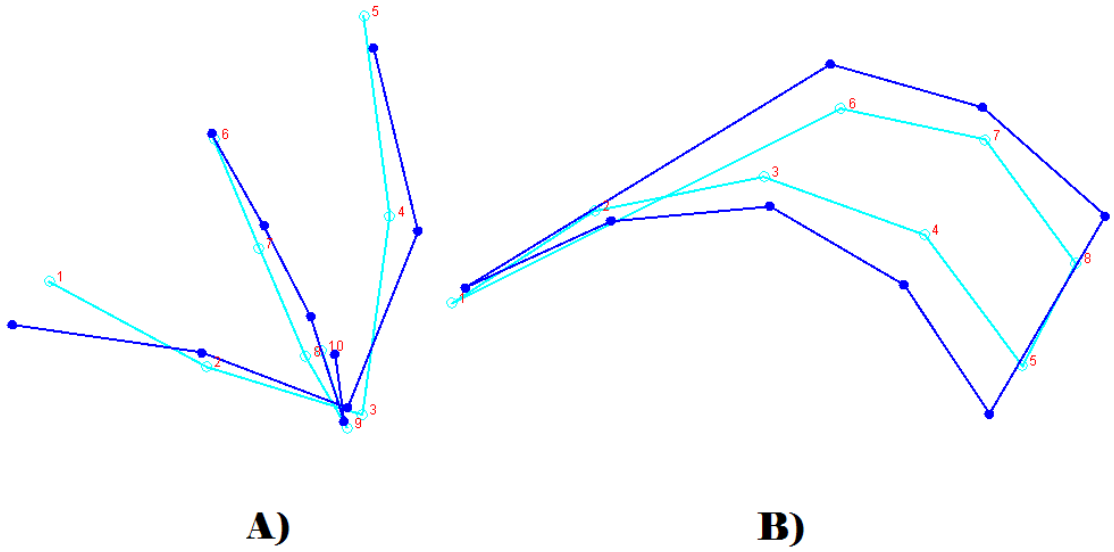

Figure Q13. PLS2 of the mastoid and occipital data from the 2B-PLS analysis: A) Mastoid Block, B) Nuchal Block (Light Blue = consensus form, Dark Blue = shape variation).

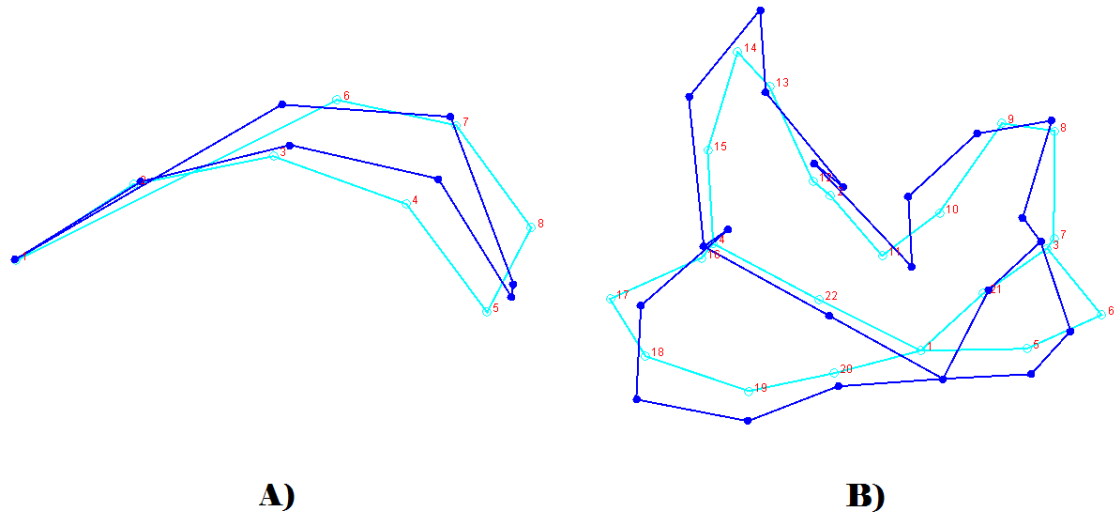

Figure Q14. PLS1 of the occipital and zygomaxillary data from the 2B-PLS analysis: A) Nuchal Block, B) Zygomaxillary Block (Light Blue = consensus form, Dark Blue = shape variation).

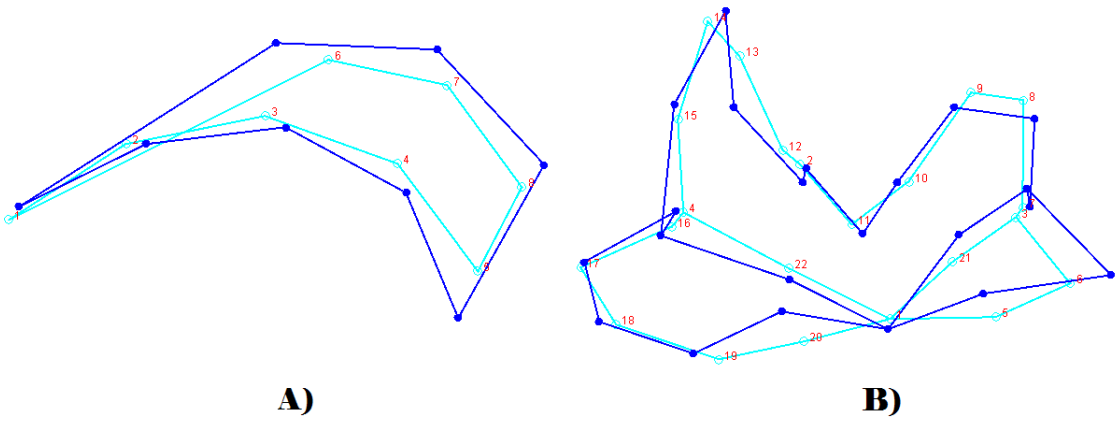

Figure Q15. PLS2 of the occipital and zygomaxillary data from the 2B-PLS analysis: A) Nuchal Block, B) Zygomaxillary Block (Light Blue = consensus form, Dark Blue = shape variation).

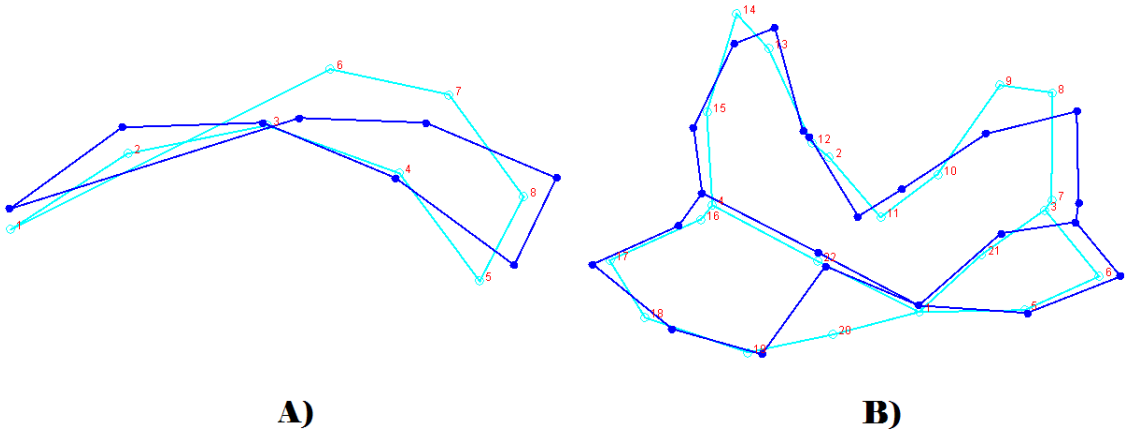

Figure Q16. PLS3 of the occipital and zygomaxillary data from the 2B-PLS analysis: A) Nuchal Block, B) Zygomaxillary Block (Light Blue = consensus form, Dark Blue = shape variation).

APPENDIX R. MALE/FEMALE SUBSAMPLE PLS RESULTS

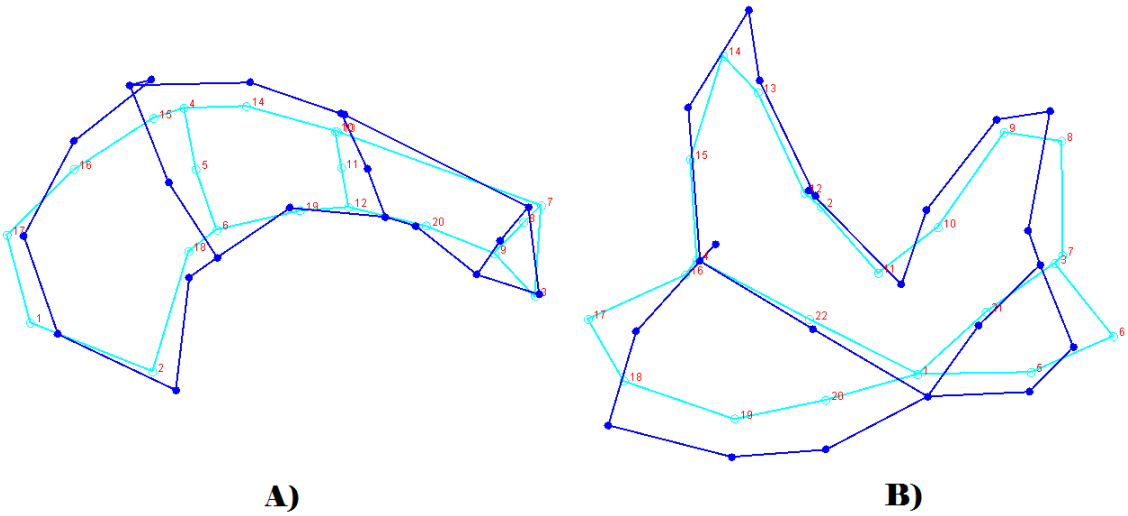

Figure R1. PLS1 of the frontal and zygomaxillary data (male subsample) from the 2B-PLS analysis: A) Supraorbital Block, B) Zygomaxillary Block (Light Blue = consensus form, Dark Blue = shape variation).

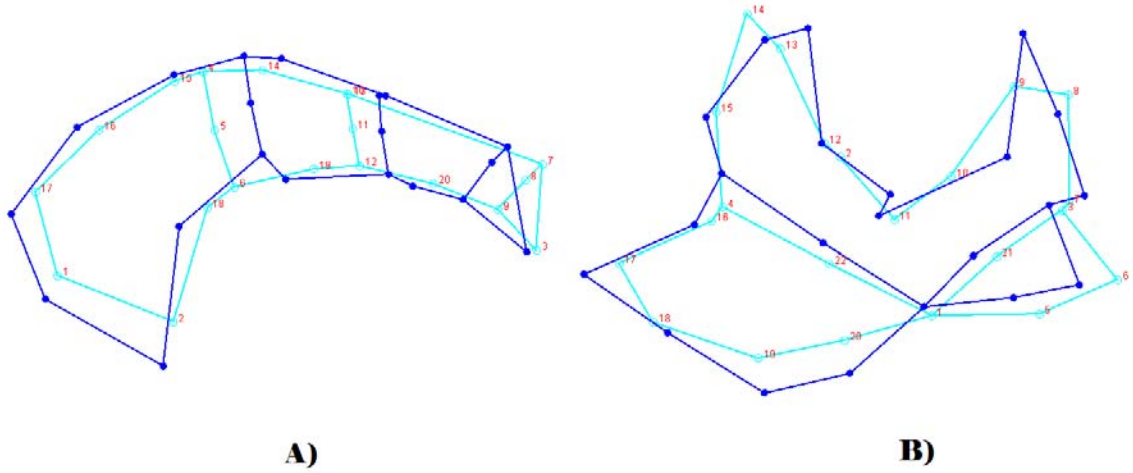

Figure R2. PLS2 of the frontal and zygomaxillary data (male subsample) from the 2B-PLS analysis: A) Supraorbital Block, B) Zygomaxillary Block (Light Blue = consensus form, Dark Blue = shape variation).

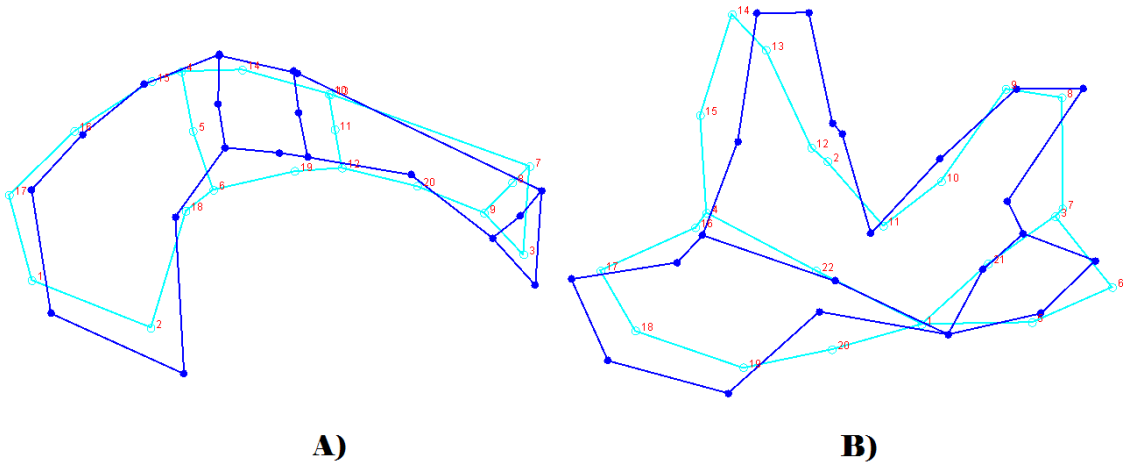

Figure R3. PLS3 of the frontal and zygomaxillary data (male subsample) from the 2B-PLS analysis: A) Supraorbital Block, B) Zygomaxillary Block (Light Blue = consensus form, Dark Blue = shape variation).

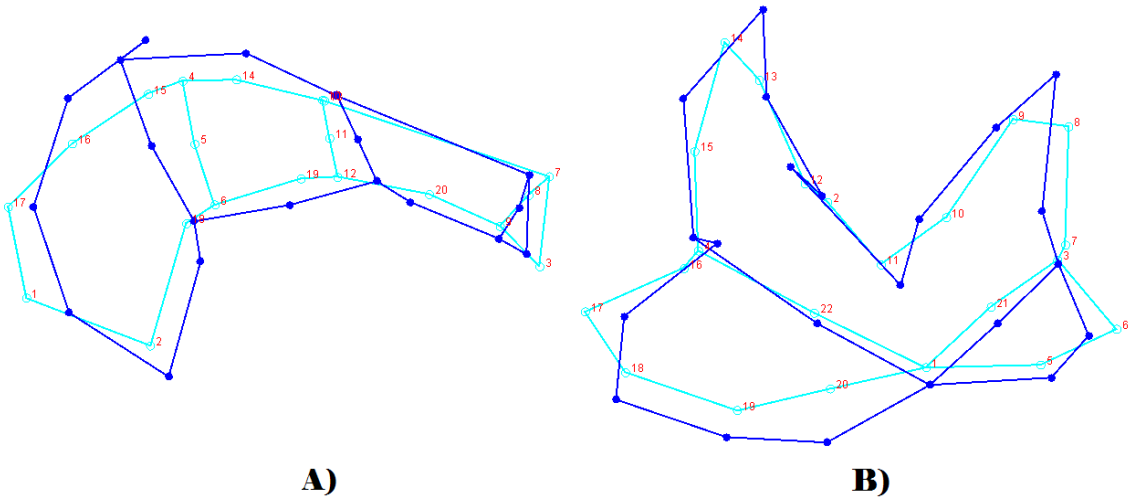

Figure R4. PLS1 of the frontal and zygomaxillary data (female subsample) from the 2B-PLS analysis: A) Supraorbital Block, B) Zygomaxillary Block (Light Blue = consensus form, Dark Blue = shape variation).

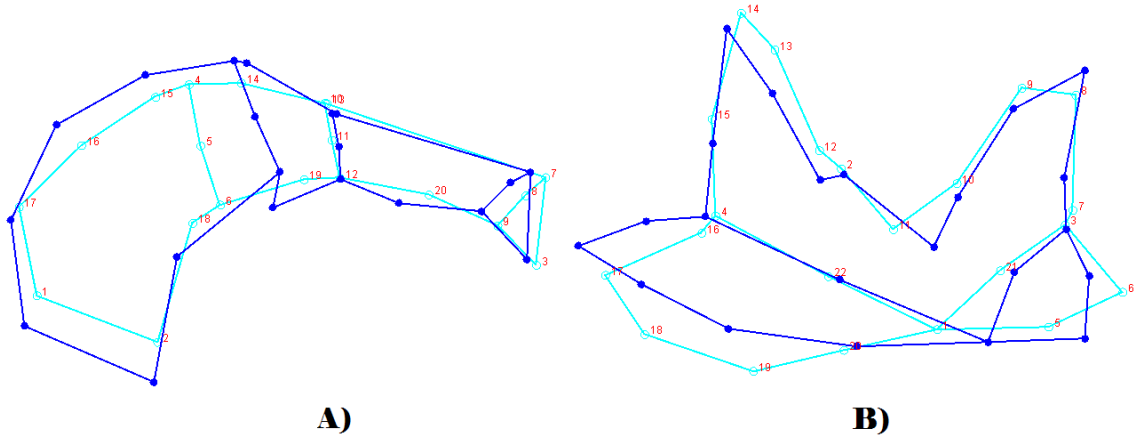

Figure R5. PLS2 of the frontal and zygomaxillary data (female subsample) from the 2B-PLS analysis: A) Supraorbital Block, B) Zygomaxillary Block (Light Blue = consensus form, Dark Blue = shape variation).

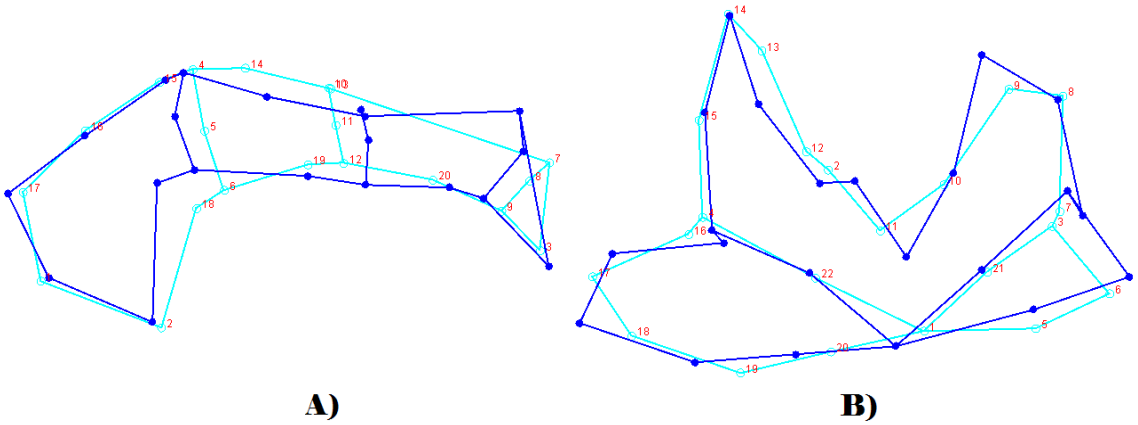

Figure R6. PLS3 of the frontal and zygomaxillary data (female subsample) from the 2B-PLS analysis: A) Supraorbital Block, B) Zygomaxillary Block (Light Blue = consensus form, Dark Blue = shape variation).

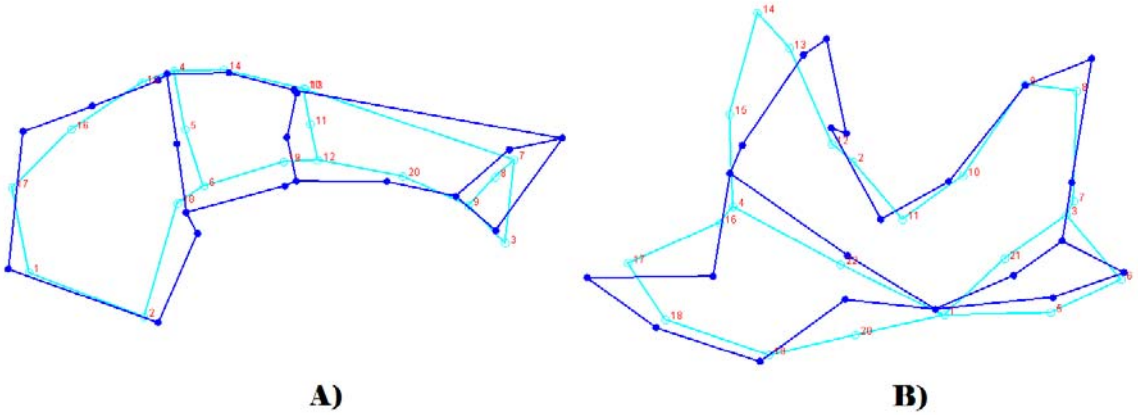

Figure R7. PLS4 of the frontal and zygomaxillary data (female subsample) from the 2B-PLS analysis: A) Supraorbital Block, B) Zygomaxillary Block (Light Blue = consensus form, Dark Blue = shape variation).

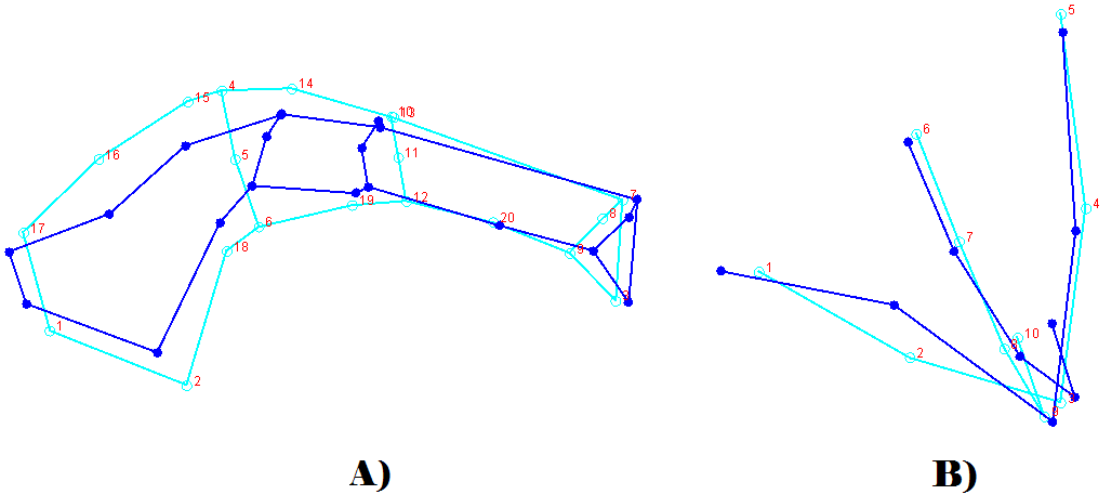

Figure R8. PLS1 of the frontal and mastoid data (male subsample) from the 2B-PLS analysis: A) Supraorbital Block, B) Mastoid Block (Light Blue = consensus form, Dark Blue = shape variation).

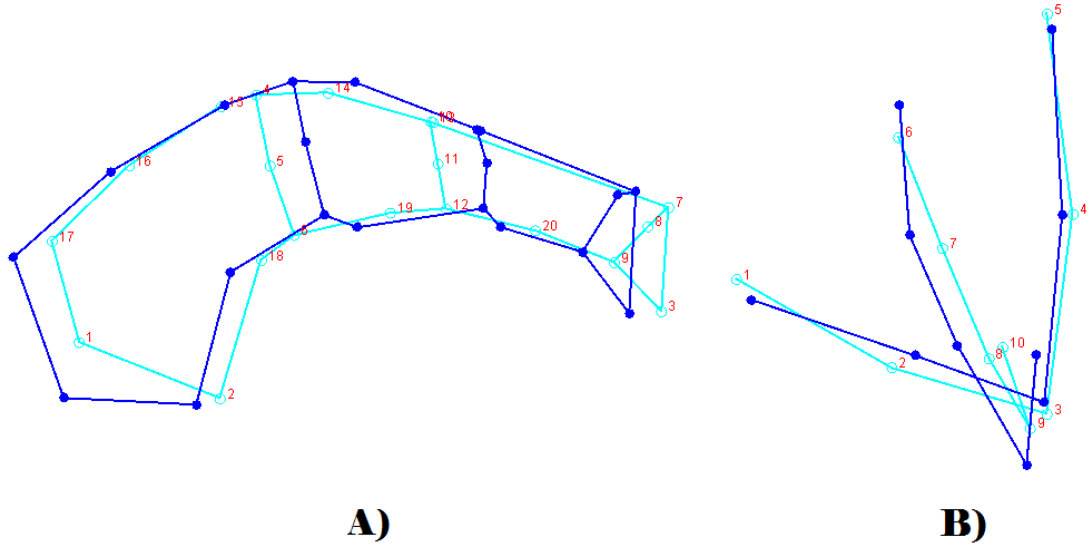

Figure R9. PLS2 of the frontal and mastoid data (male subsample) from the 2B-PLS analysis: A) Supraorbital Block, B) Mastoid Block (Light Blue = consensus form, Dark Blue = shape variation).

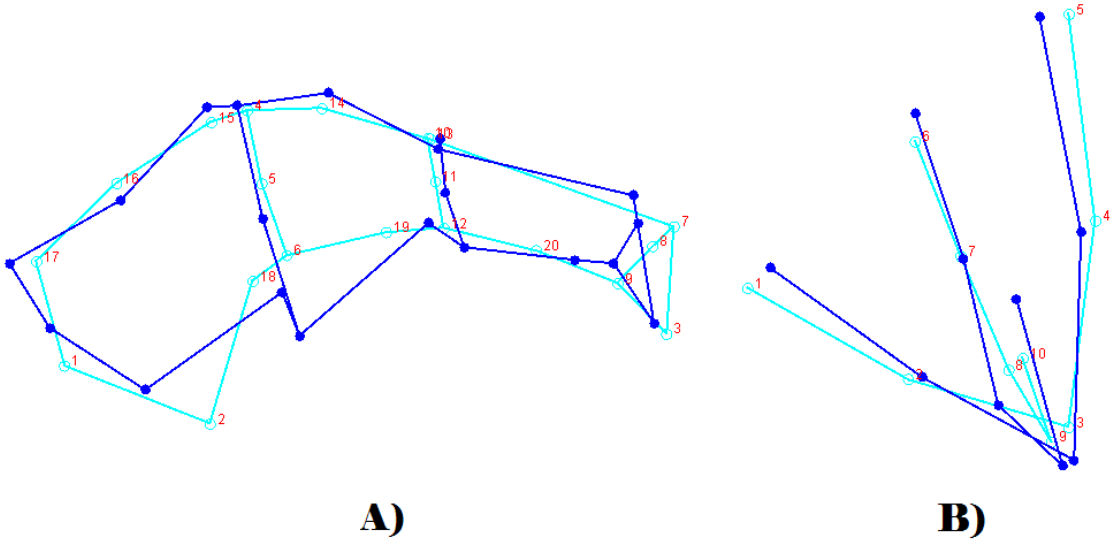

Figure R10. PLS3 of the frontal and mastoid data (male subsample) from the 2B-PLS analysis: A) Supraorbital Block, B) Mastoid Block (Light Blue = consensus form, Dark Blue = shape variation).

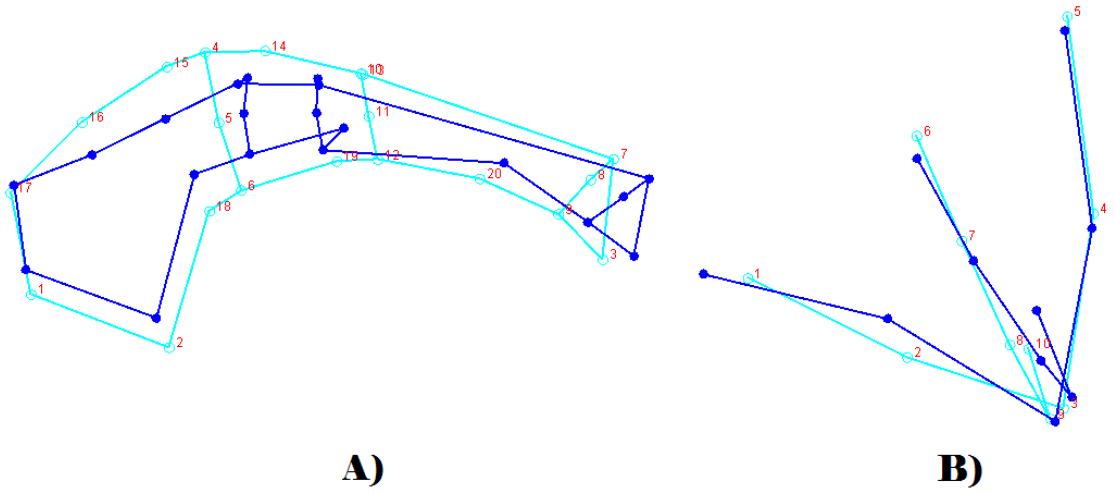

Figure R11. PLS1 of the frontal and mastoid data (female subsample) from the 2B-PLS analysis: A) Supraorbital Block, B) Mastoid Block (Light Blue = consensus form, Dark Blue = shape variation).

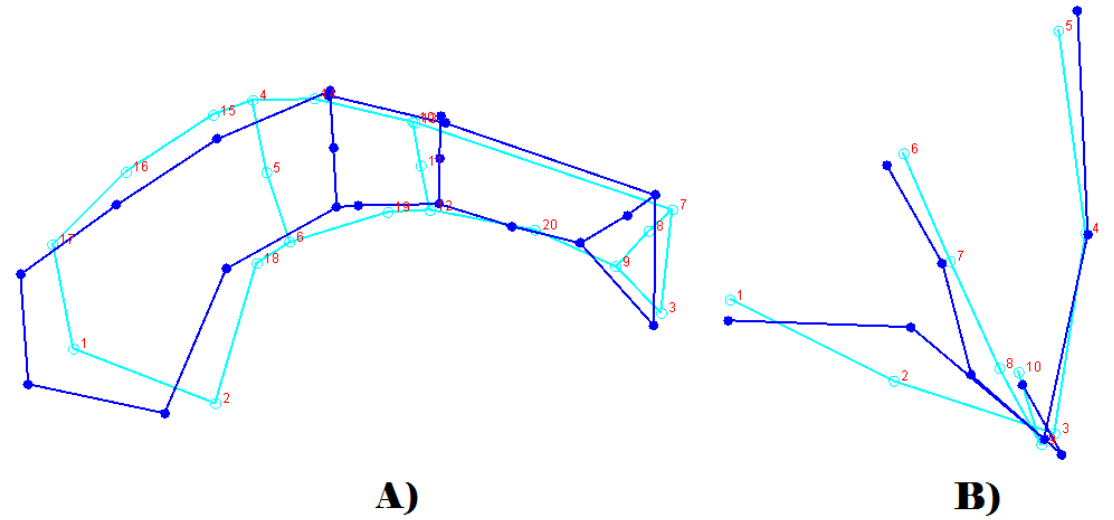

Figure R12. PLS2 of the frontal and mastoid data (female subsample) from the 2B-PLS analysis: A) Supraorbital Block, B) Mastoid Block (Light Blue = consensus form, Dark Blue = shape variation).

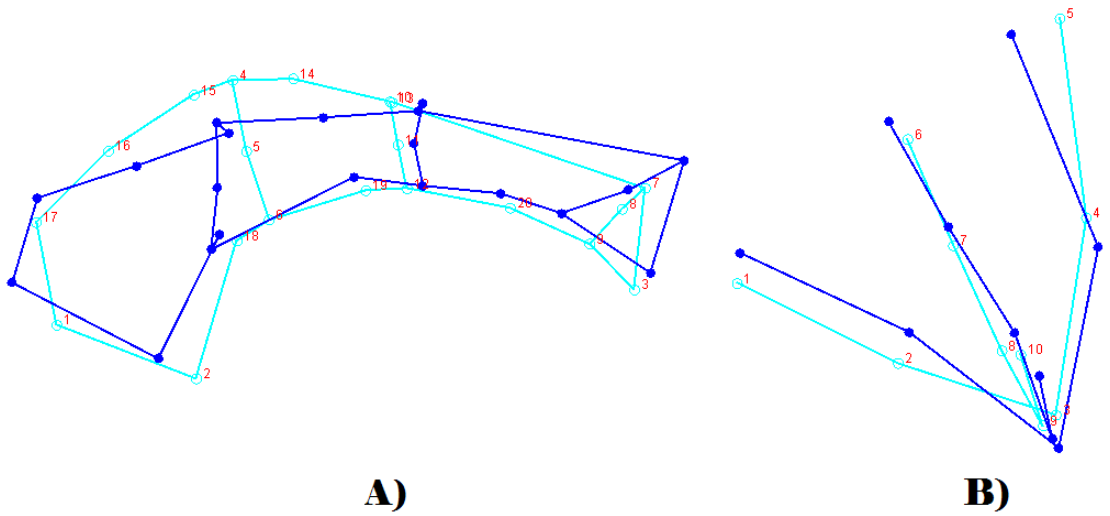

Figure R13. PLS3 of the frontal and mastoid data (female subsample) from the 2B-PLS analysis: A) Supraorbital Block, B) Mastoid Block (Light Blue = consensus form, Dark Blue = shape variation).

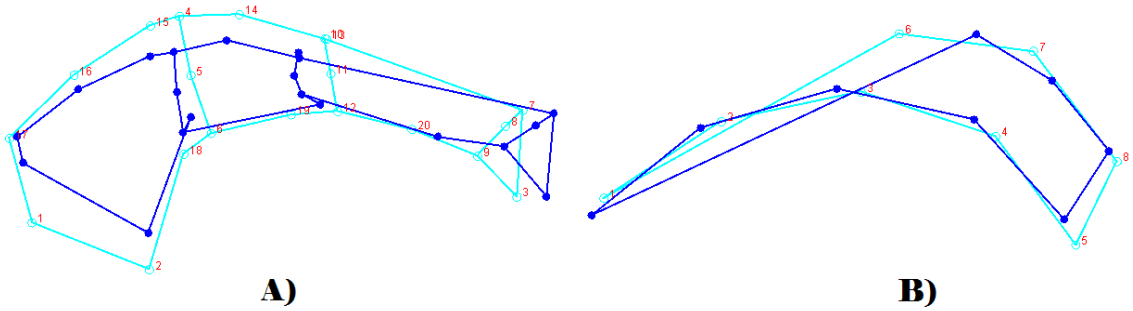

Figure R14. PLS1 of the frontal and occipital data (male subsample) from the 2B-PLS analysis: A) Supraorbital Block, B) Nuchal Block (Light Blue = consensus form, Dark Blue = shape variation).

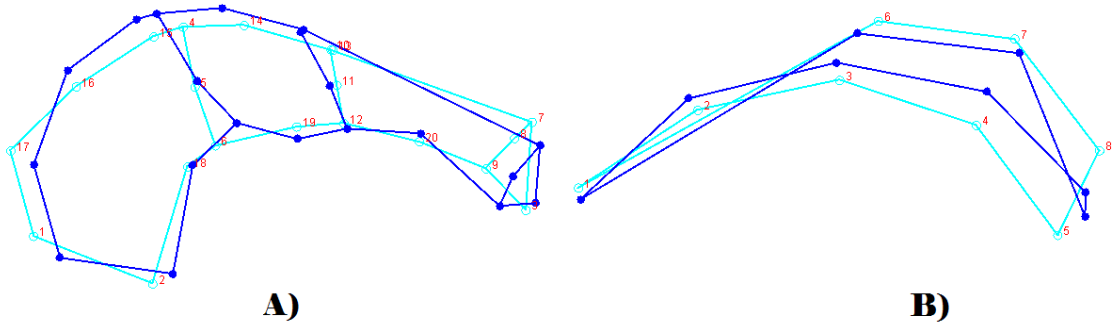

Figure R15. PLS2 of the frontal and occipital data (male subsample) from the 2B-PLS analysis: A) Supraorbital Block, B) Nuchal Block (Light Blue = consensus form, Dark Blue = shape variation).

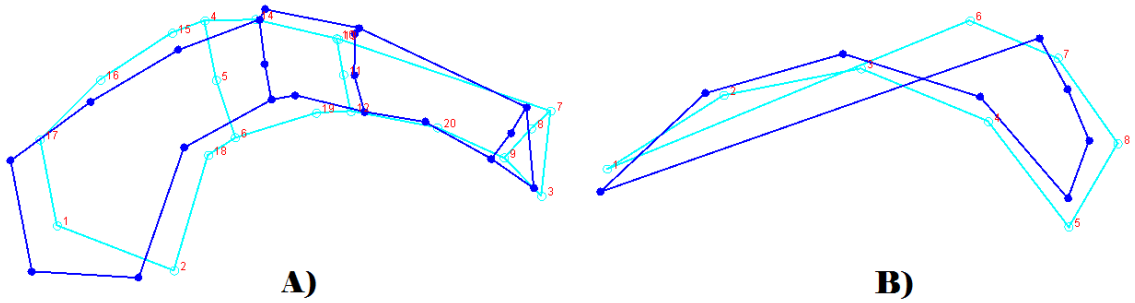

Figure R16. PLS1 of the frontal and occipital data (female subsample) from the 2B-PLS analysis: A) Supraorbital Block, B) Nuchal Block (Light Blue = consensus form, Dark Blue = shape variation).

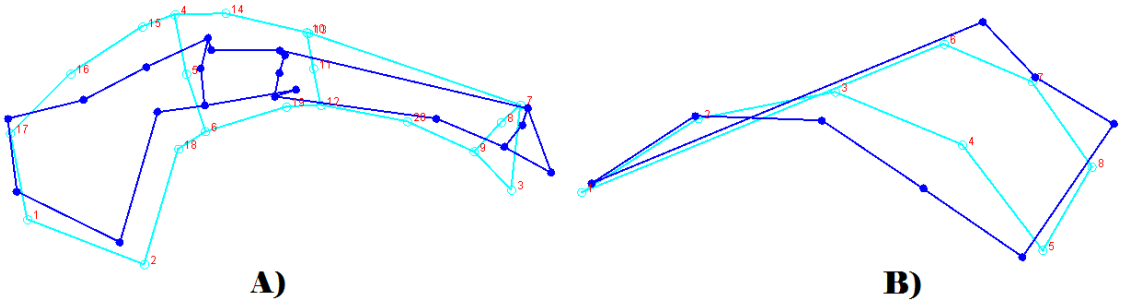

Figure R17. PLS2 of the frontal and occipital data (female subsample) from the 2B-PLS analysis: A) Supraorbital Block, B) Nuchal Block (Light Blue = consensus form, Dark Blue = shape variation).

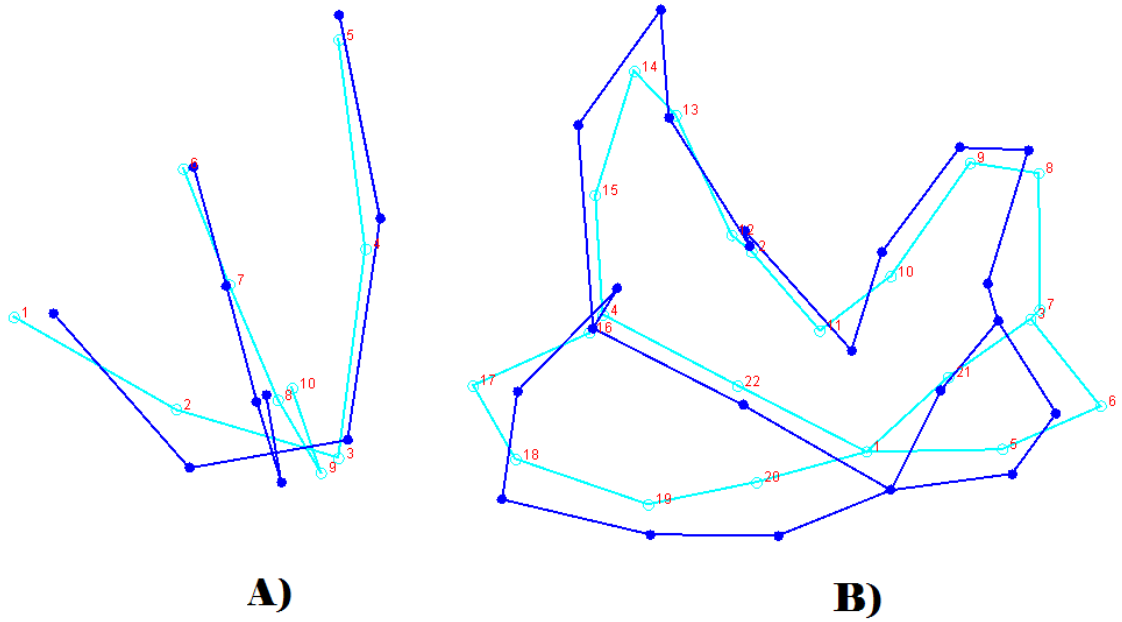

Figure R18. PLS1 of the mastoid and zygomaxillary data (male subsample) from the 2B-PLS analysis: A) Mastoid Block, B) Zygomaxillary Block (Light Blue = consensus form, Dark Blue = shape variation).

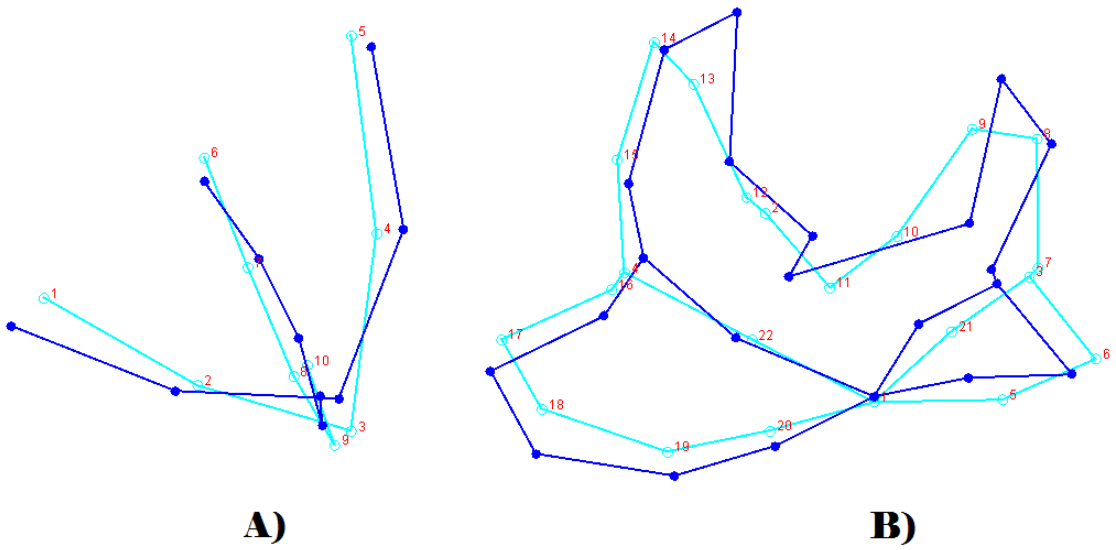

Figure R19. PLS2 of the mastoid and zygomaxillary data (male subsample) from the 2B-PLS analysis: A) Mastoid Block, B) Zygomaxillary Block (Light Blue = consensus form, Dark Blue = shape variation).

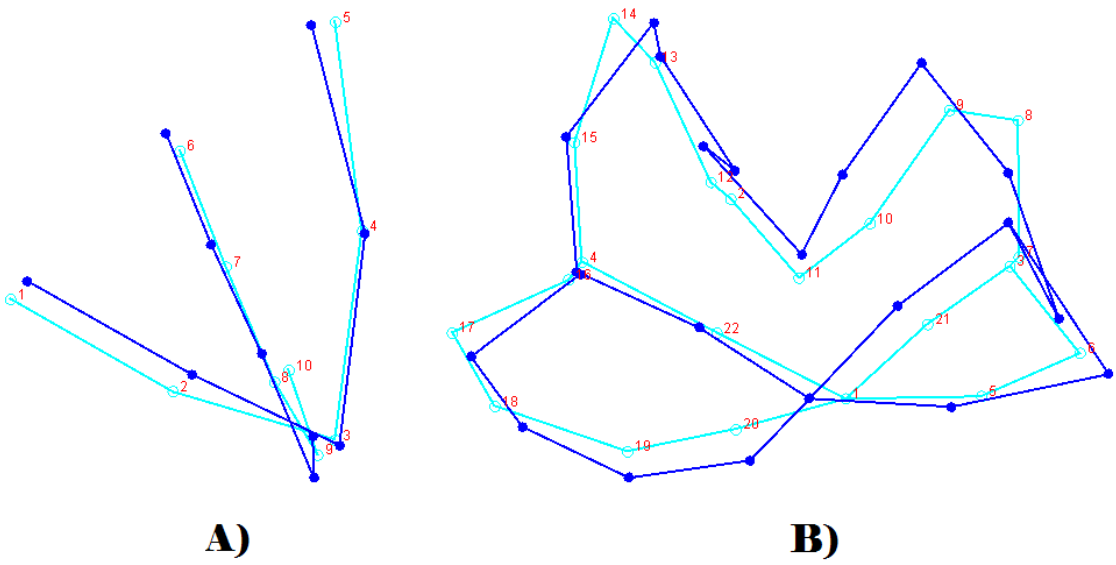

Figure R20. PLS3 of the mastoid and zygomaxillary data (male subsample) from the 2B-PLS analysis: A) Mastoid Block, B) Zygomaxillary Block (Light Blue = consensus form, Dark Blue = shape variation).

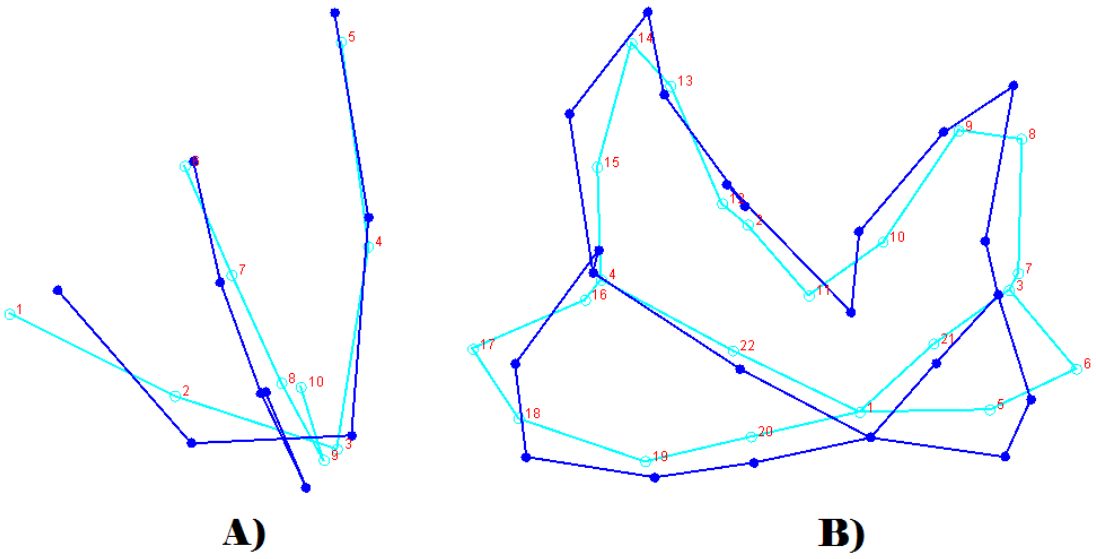

Figure R21. PLS1 of the mastoid and zygomaxillary data (female subsample) from the 2B-PLS analysis: A) Mastoid Block, B) Zygomaxillary Block (Light Blue = consensus form, Dark Blue = shape variation).

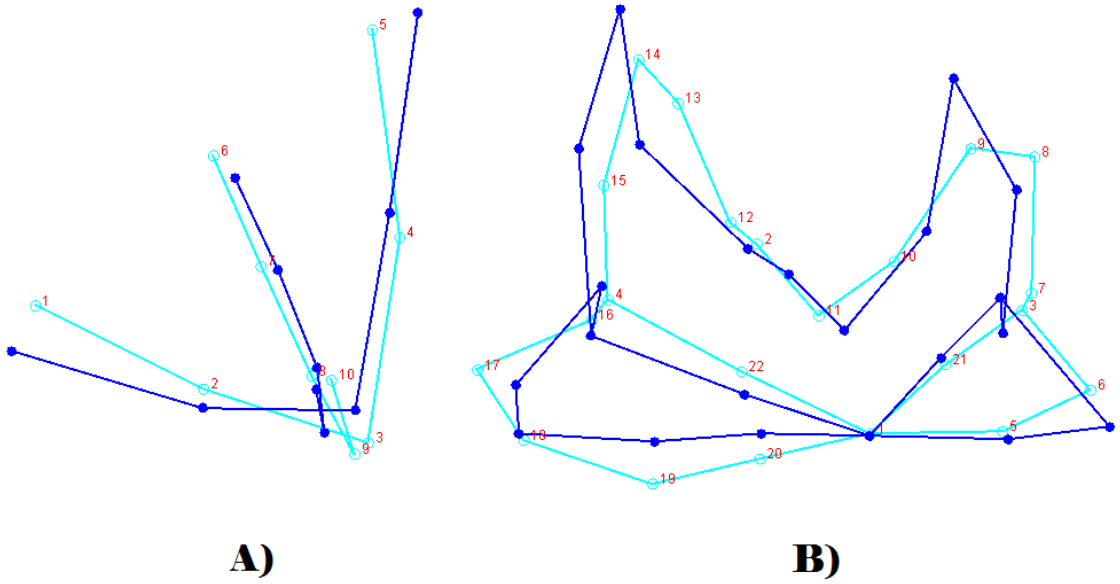

Figure R22. PLS2 of the mastoid and zygomaxillary data (female subsample) from the 2B-PLS analysis: A) Mastoid Block, B) Zygomaxillary Block (Light Blue = consensus form, Dark Blue = shape variation).

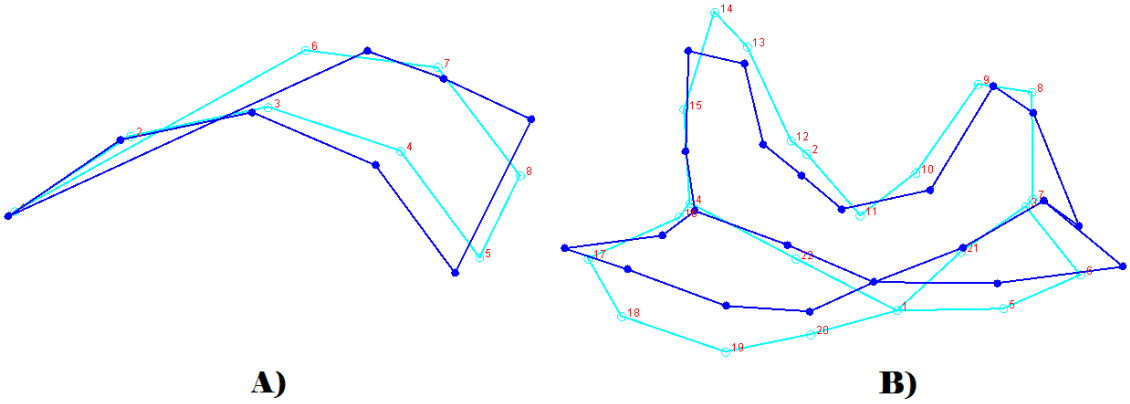

Figure R23. PLS1 of the occipital and zygomaxillary data (male subsample) from the 2B-PLS analysis: A) Nuchal Block, B) Zygomaxillary Block (Light Blue = consensus form, Dark Blue = shape variation).

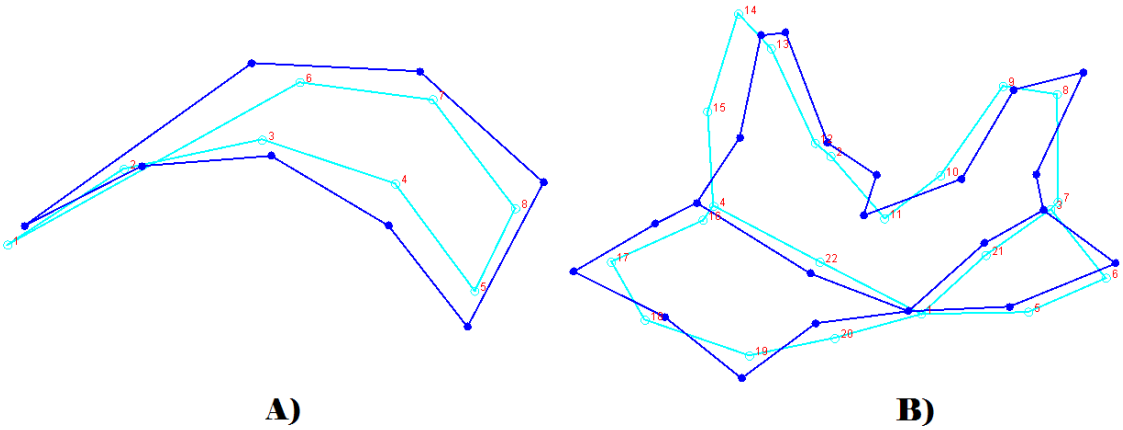

Figure R24. PLS2 of the occipital and zygomaxillary data (male subsample) from the 2B-PLS analysis: A) Nuchal Block, B) Zygomaxillary Block (Light Blue = consensus form, Dark Blue = shape variation).

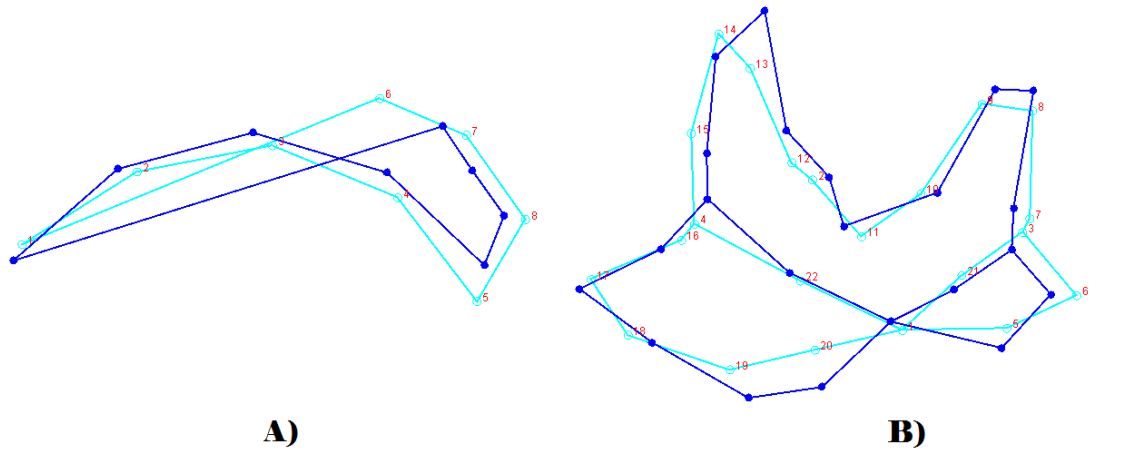

Figure R25. PLS1 of the occipital and zygomaxillary data (female subsample) from the 2B-PLS analysis: A) Nuchal Block, B) Zygomaxillary Block (Light Blue = consensus form, Dark Blue = shape variation).

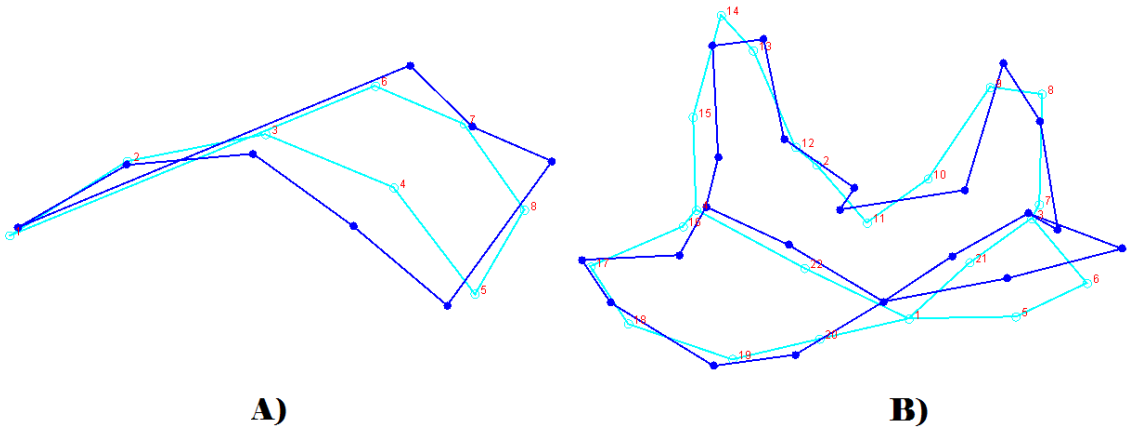

Figure R26. PLS2 of the occipital and zygomaxillary data (female subsample) from the 2B-PLS analysis: A) Nuchal Block, B) Zygomaxillary Block (Light Blue = consensus form, Dark Blue = shape variation).

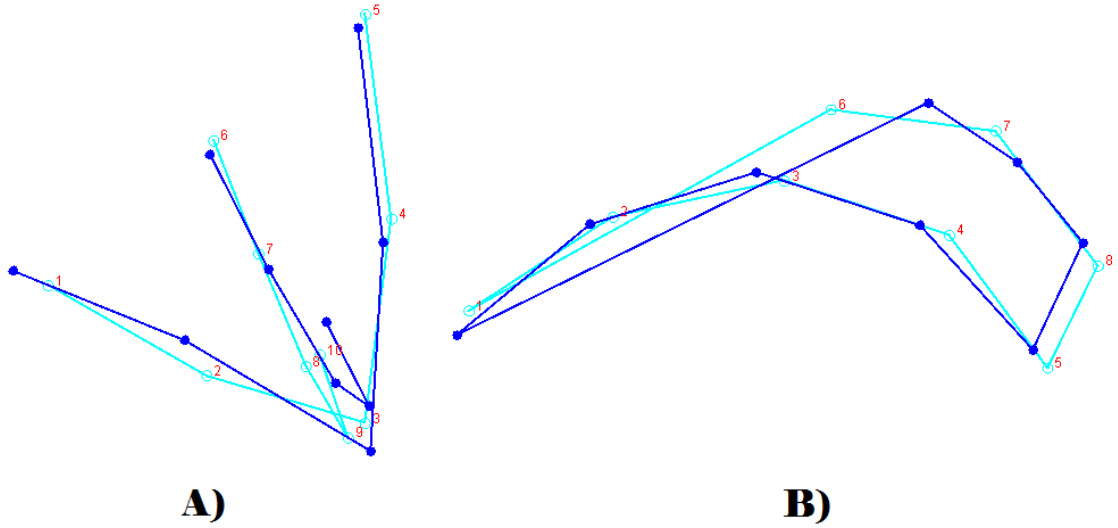

Figure R27. PLS1 of the mastoid and occipital data (male subsample) from the 2B-PLS analysis: A) Mastoid Block, B) Nuchal Block (Light Blue = consensus form, Dark Blue = shape variation).

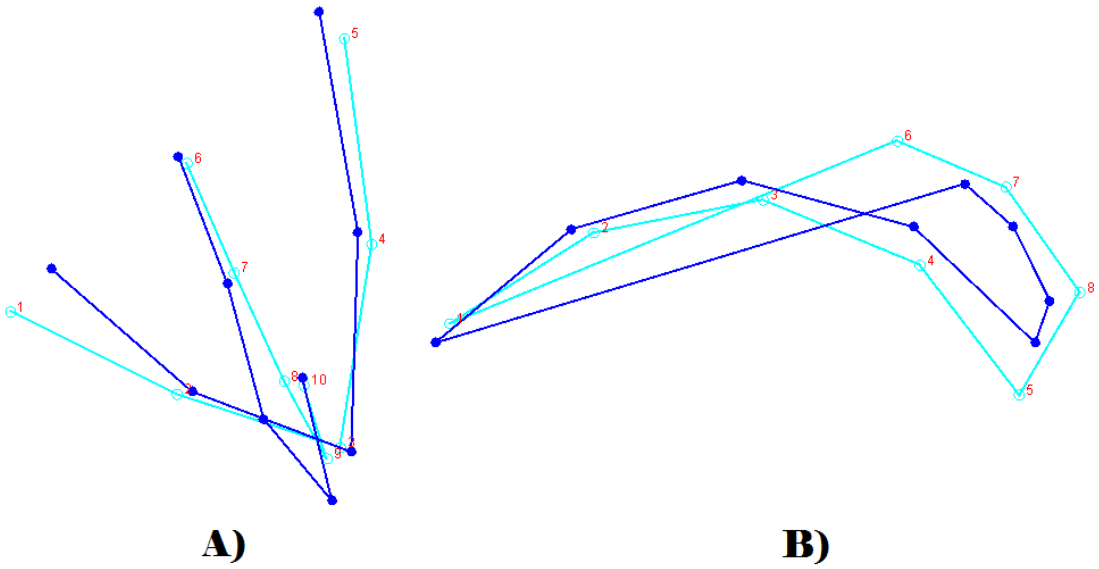

Figure R28. PLS1 of the mastoid and occipital data (female subsample) from the 2B-PLS analysis: A) Mastoid Block, B) Nuchal Block (Light Blue = consensus form, Dark Blue = shape variation).

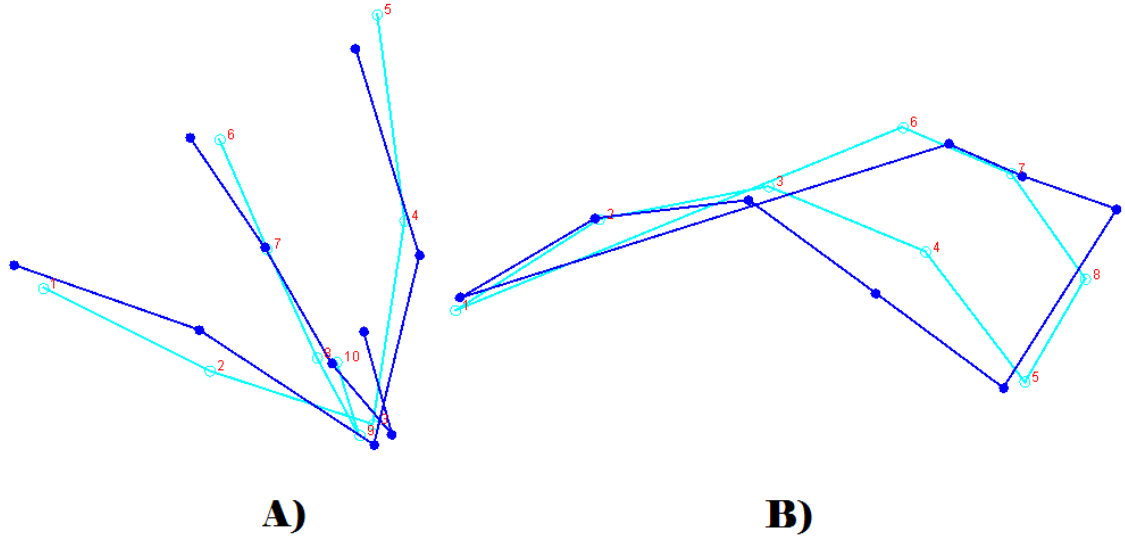

Figure R29. PLS2 of the mastoid and occipital data (female subsample) from the 2B-PLS analysis: A) Mastoid Block, B) Nuchal Block (Light Blue = consensus form, Dark Blue = shape variation).

APPENDIX S. MORPHOLOGICAL VARIATION IN COMPLETE LANDMARK DATASET BY REGIONAL SAMPLE

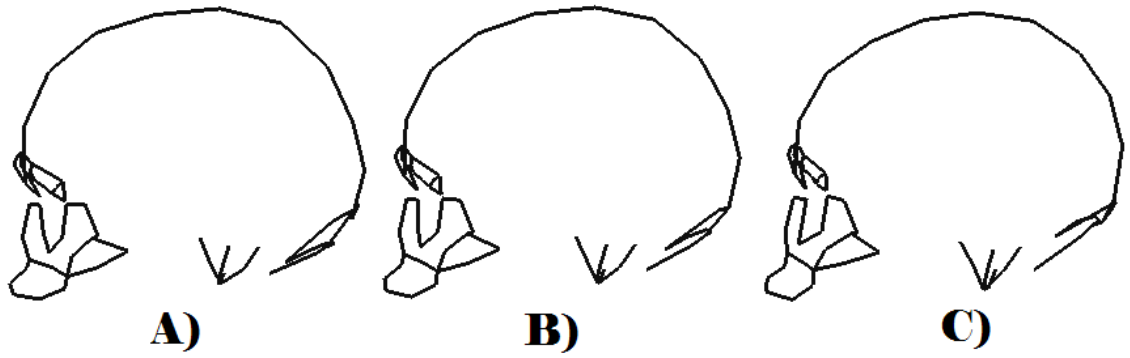

Figure S1. Morphological Variation along RW1 for the Australian Aborigine sub-sample: A) Lower extreme of variation, B) Consensus form, C) Upper extreme of variation.

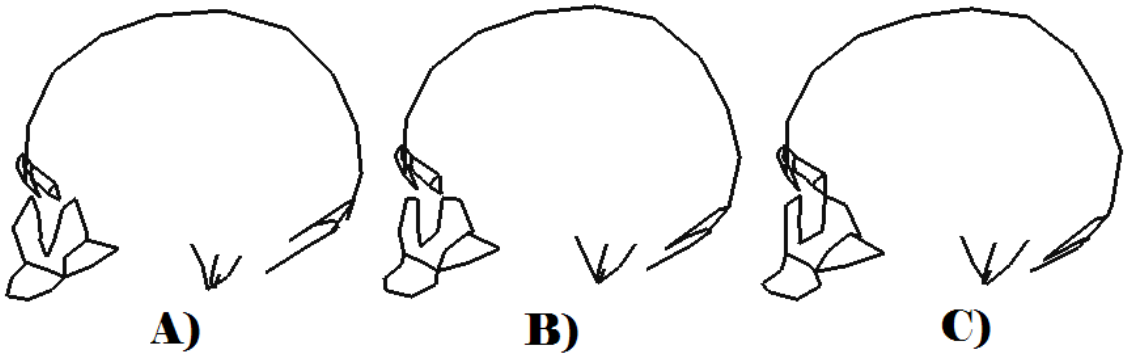

Figure S2. Morphological Variation along RW2 for the Australian Aborigine sub-sample: A) Lower extreme of variation, B) Consensus form, C) Upper extreme of variation.

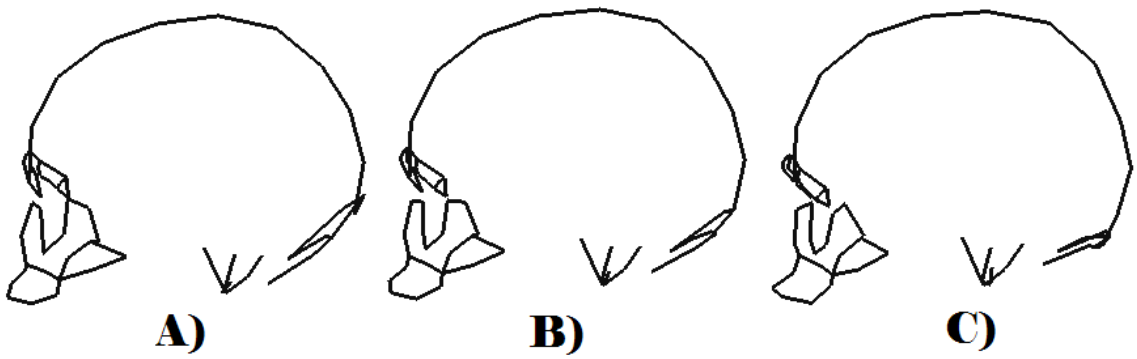

Figure S3. Morphological Variation along RW3 for the Australian Aborigine sub-sample: A) Lower extreme of variation, B) Consensus form, C) Upper extreme of variation.

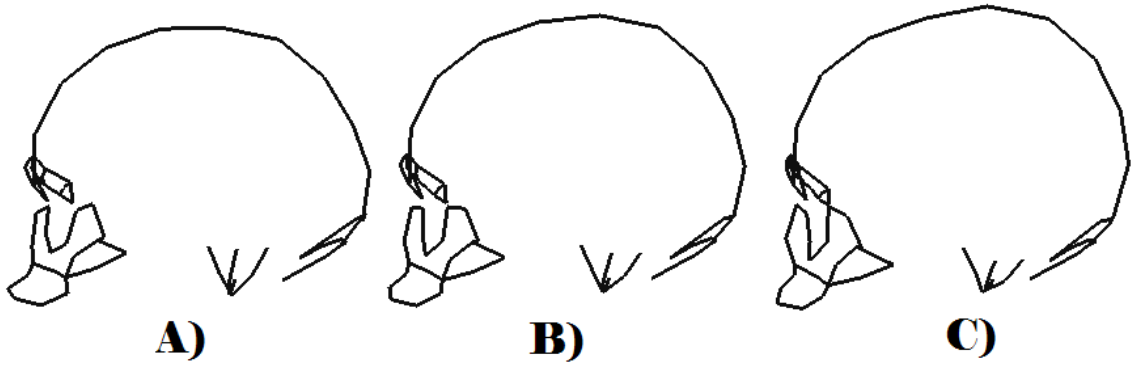

Figure S4. Morphological Variation along RW4 for the Australian Aborigine sub-sample: A) Lower extreme of variation, B) Consensus form, C) Upper extreme of variation.

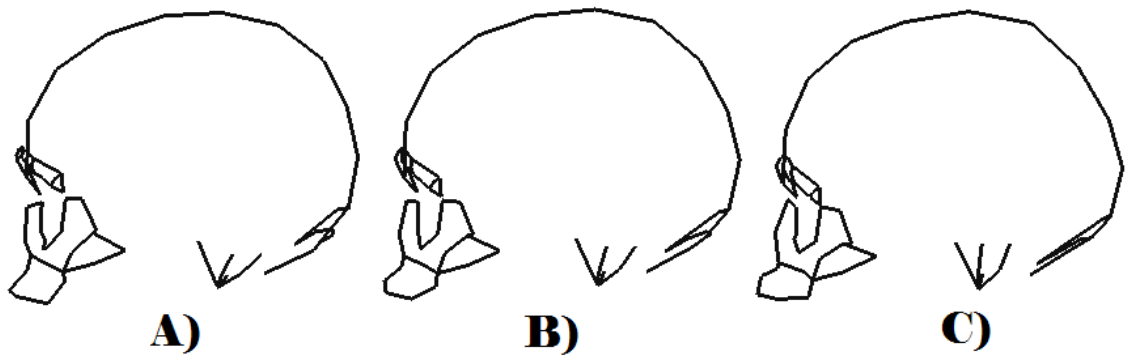

Figure S5. Morphological Variation along RW5 for the Australian Aborigine sub-sample: A) Lower extreme of variation, B) Consensus form, C) Upper extreme of variation.

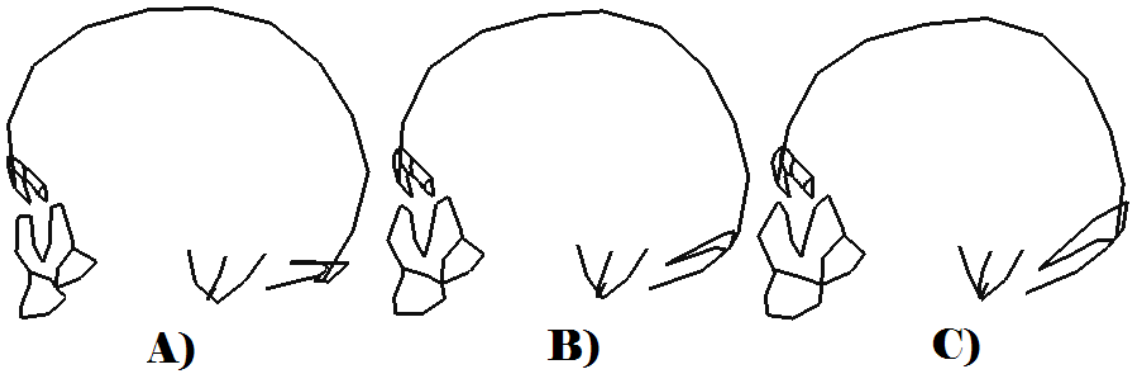

Figure S6. Morphological Variation along RW1 for the Central European sub-sample: A) Lower extreme of variation, B) Consensus form, C) Upper extreme of variation.

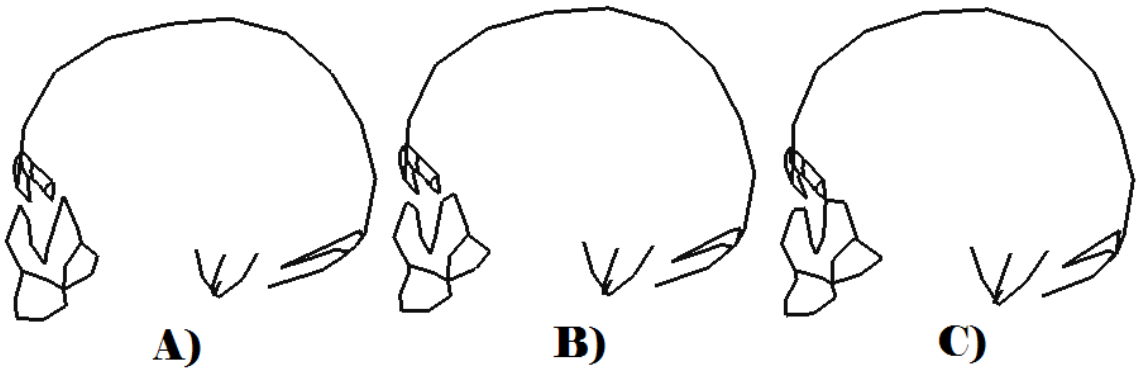

Figure S7. Morphological Variation along RW2 for the Central European sub-sample: A) Lower extreme of variation, B) Consensus form, C) Upper extreme of variation.

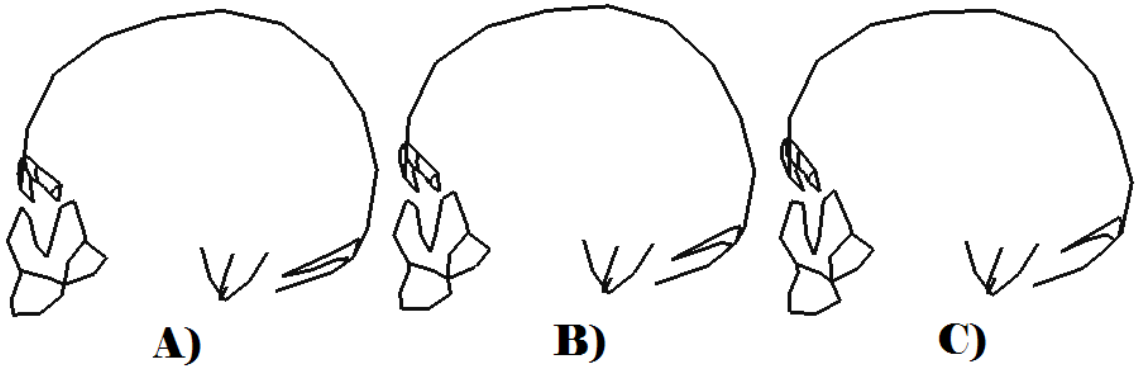

Figure S8. Morphological Variation along RW3 for the Central European sub-sample: A) Lower extreme of variation, B) Consensus form, C) Upper extreme of variation.

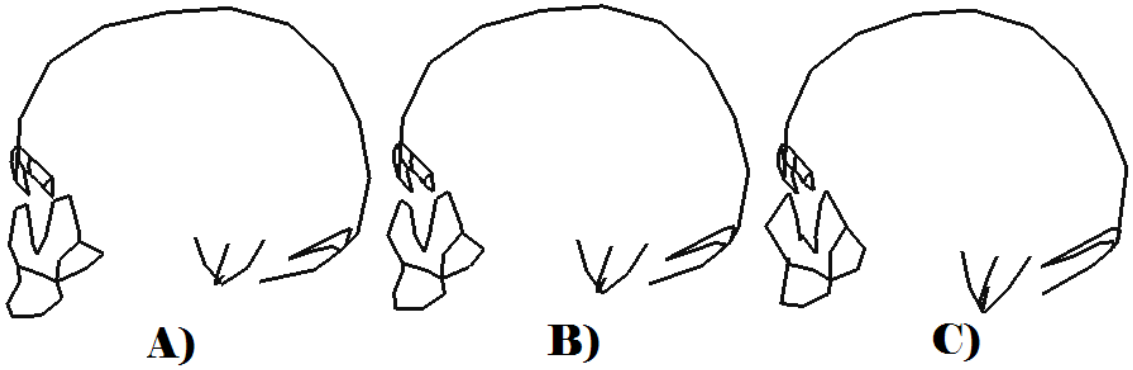

Figure S9. Morphological Variation along RW4 for the Central European sub-sample: A) Lower extreme of variation, B) Consensus form, C) Upper extreme of variation.

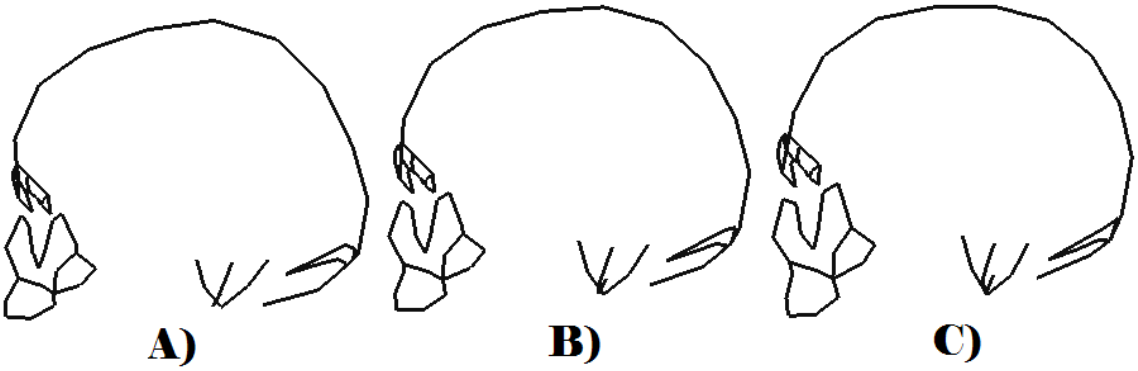

Figure S10. Morphological Variation along RW5 for the Central European sub-sample: A) Lower extreme of variation, B) Consensus form, C) Upper extreme of variation.

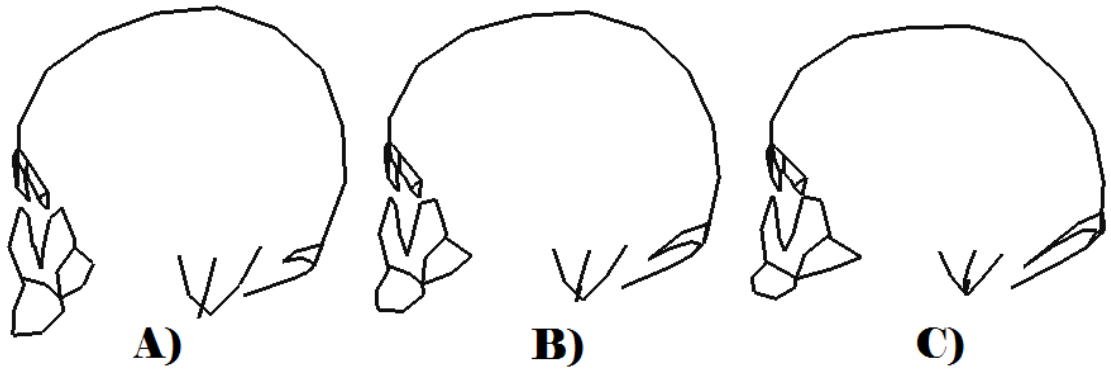

Figure S11. Morphological Variation along RW1 for the Chinese sub-sample: A) Lower extreme of variation, B) Consensus form, C) Upper extreme of variation.

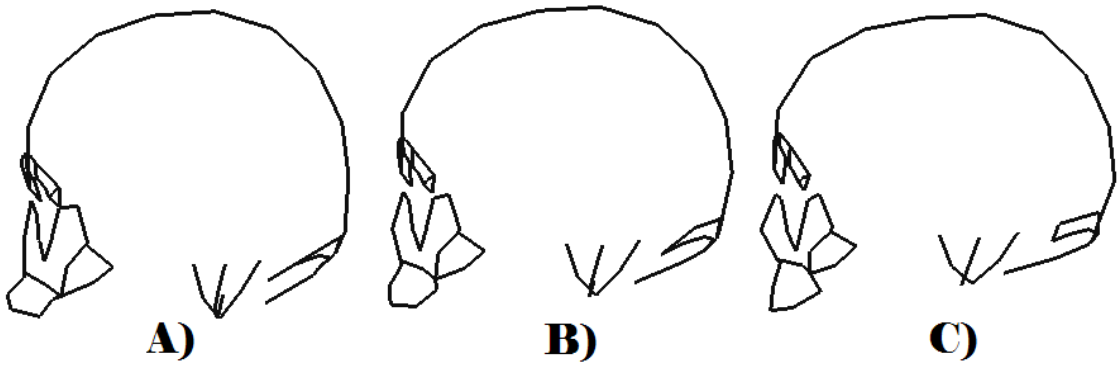

Figure S12. Morphological Variation along RW2 for the Chinese sub-sample: A) Lower extreme of variation, B) Consensus form, C) Upper extreme of variation.

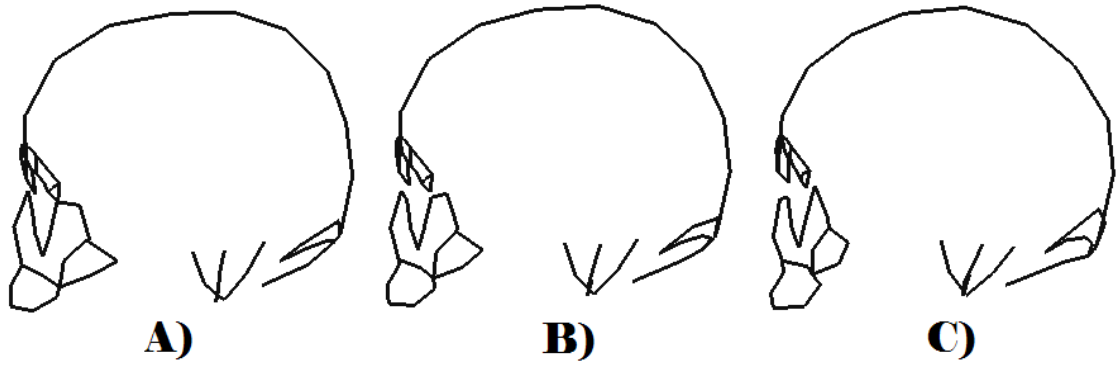

Figure S13. Morphological Variation along RW3 for the Chinese sub-sample: A) Lower extreme of variation, B) Consensus form, C) Upper extreme of variation.

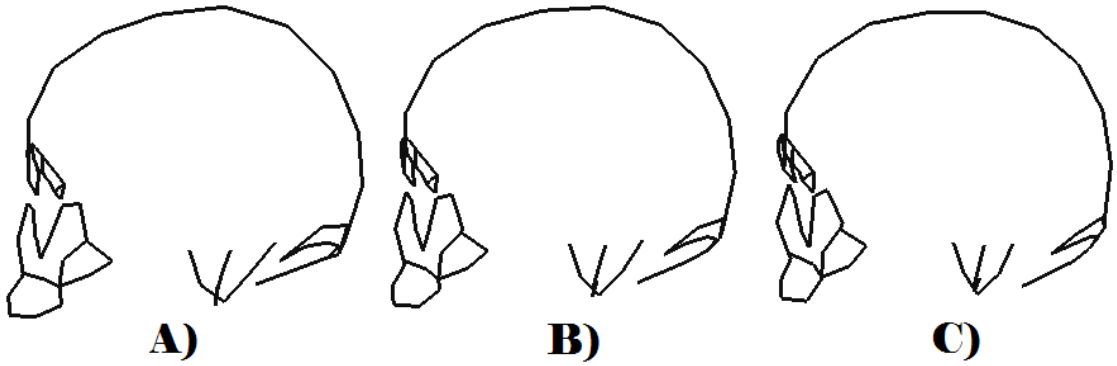

Figure S14. Morphological Variation along RW4 for the Chinese sub-sample: A) Lower extreme of variation, B) Consensus form, C) Upper extreme of variation.

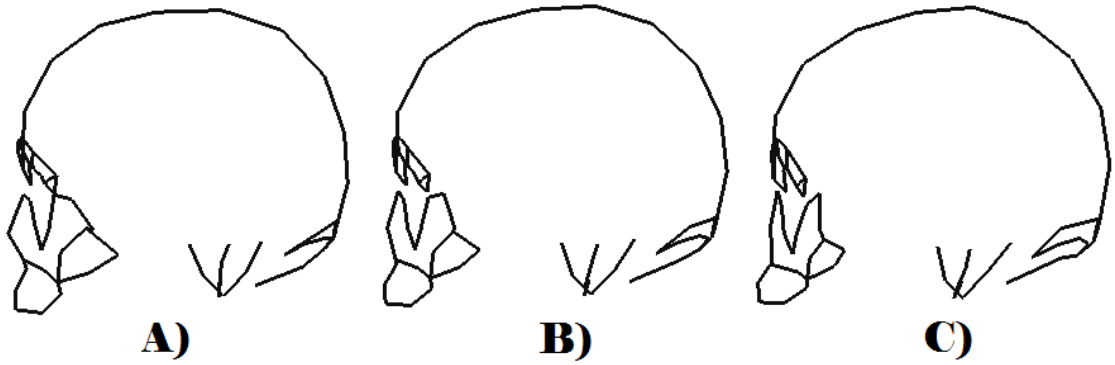

Figure S15. Morphological Variation along RW5 for the Chinese sub-sample: A) Lower extreme of variation, B) Consensus form, C) Upper extreme of variation.

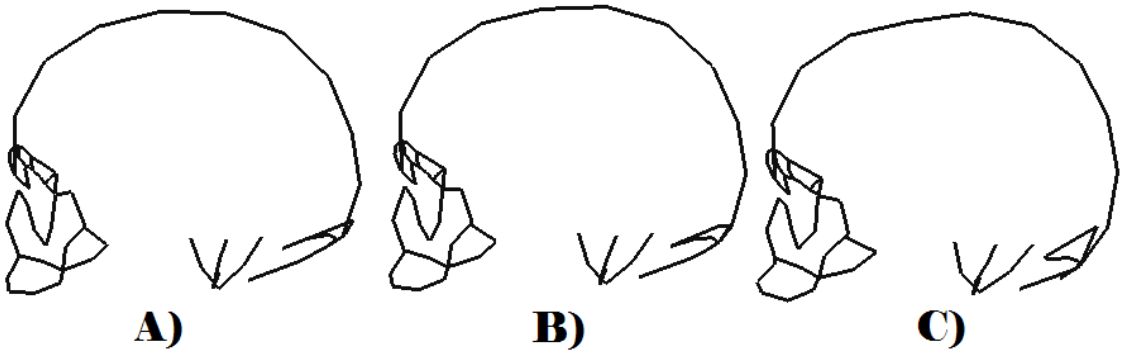

Figure S16. Morphological Variation along RW1 for the Indian sub-sample: A) Lower extreme of variation, B) Consensus form, C) Upper extreme of variation.

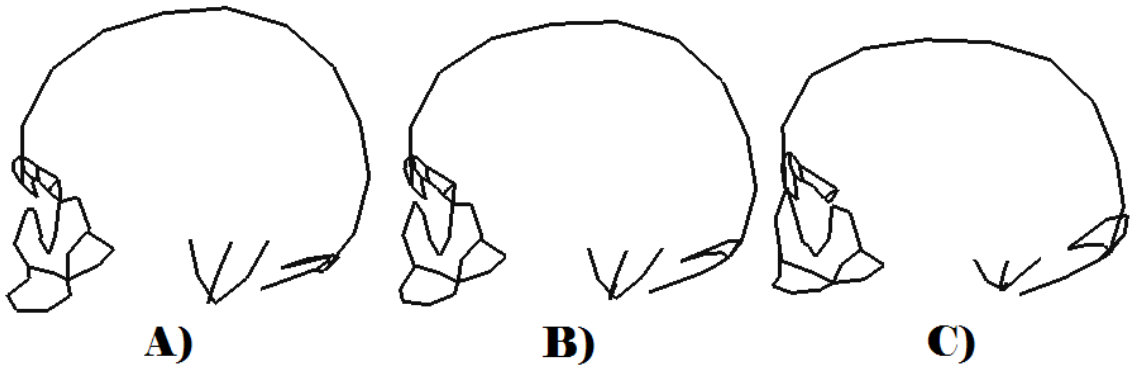

Figure S17. Morphological Variation along RW2 for the Indian sub-sample: A) Lower extreme of variation, B) Consensus form, C) Upper extreme of variation.

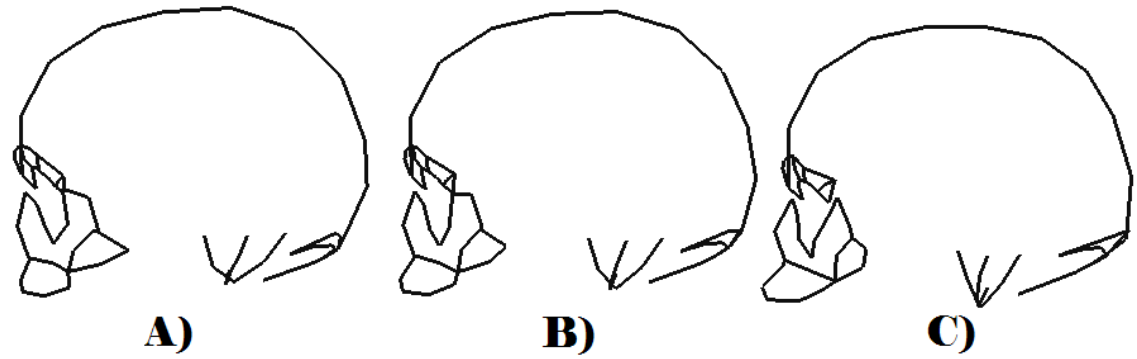

Figure S18. Morphological Variation along RW3 for the Indian sub-sample: A) Lower extreme of variation, B) Consensus form, C) Upper extreme of variation.

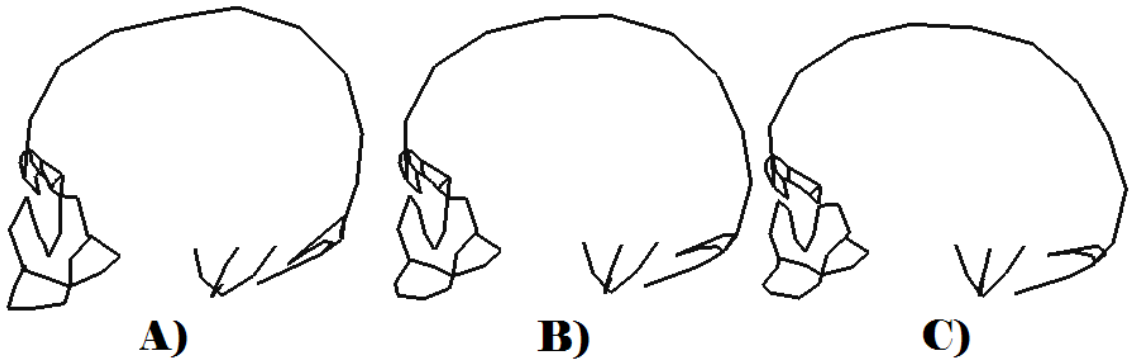

Figure S19. Morphological Variation along RW4 for the Indian sub-sample: A) Lower extreme of variation, B) Consensus form, C) Upper extreme of variation.

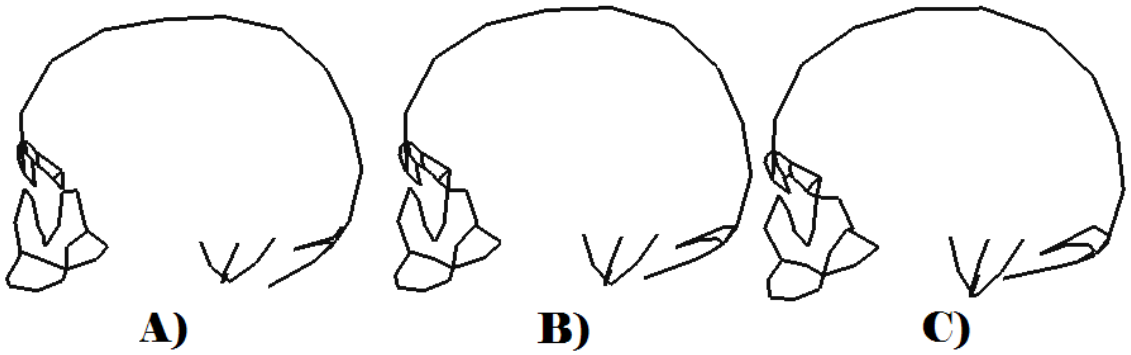

Figure S20. Morphological Variation along RW5 for the Indian sub-sample: A) Lower extreme of variation, B) Consensus form, C) Upper extreme of variation.

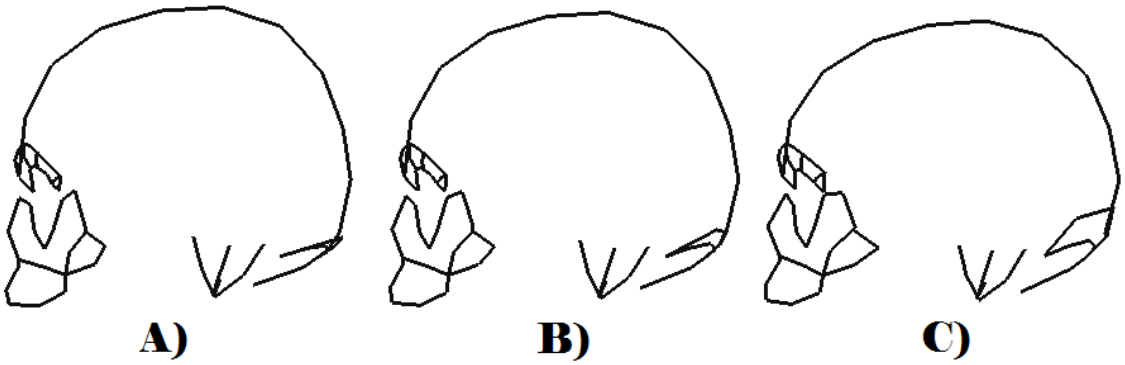

Figure S21. Morphological Variation along RW1 for the Medit/Near East sub-sample: A) Lower extreme of variation, B) Consensus form, C) Upper extreme of variation.

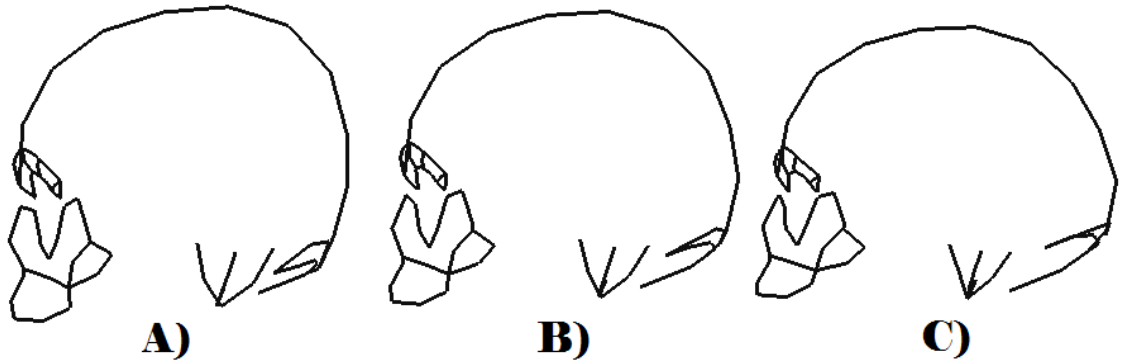

Figure S22. Morphological Variation along RW2 for the Medit/Near East sub-sample: A) Lower extreme of variation, B) Consensus form, C) Upper extreme of variation.

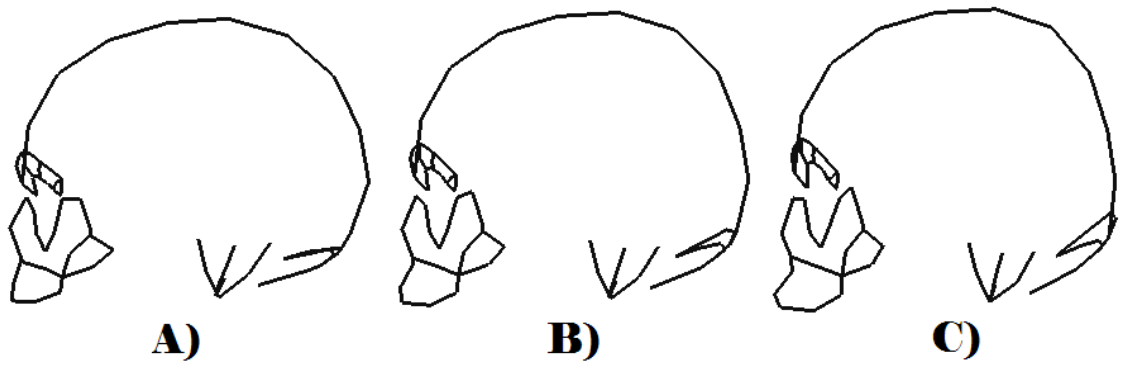

Figure S23. Morphological Variation along RW3 for the Medit/Near East sub-sample: A) Lower extreme of variation, B) Consensus form, C) Upper extreme of variation.

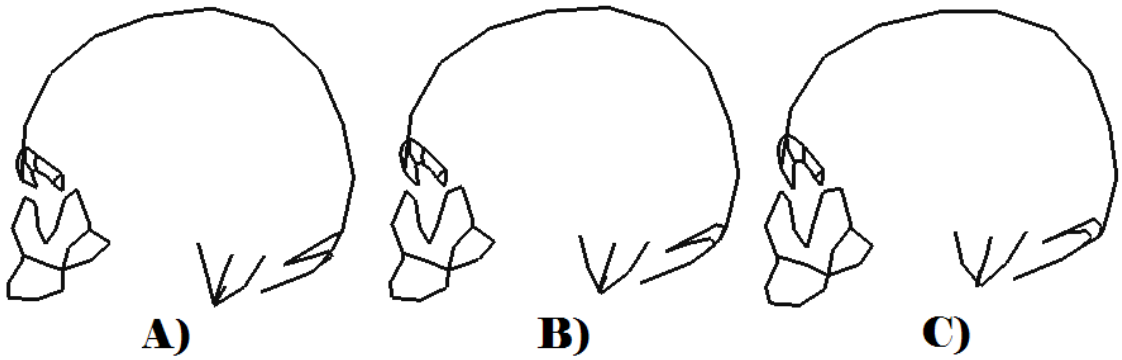

Figure S24. Morphological Variation along RW4 for the Medit/Near East sub-sample: A) Lower extreme of variation, B) Consensus form, C) Upper extreme of variation.

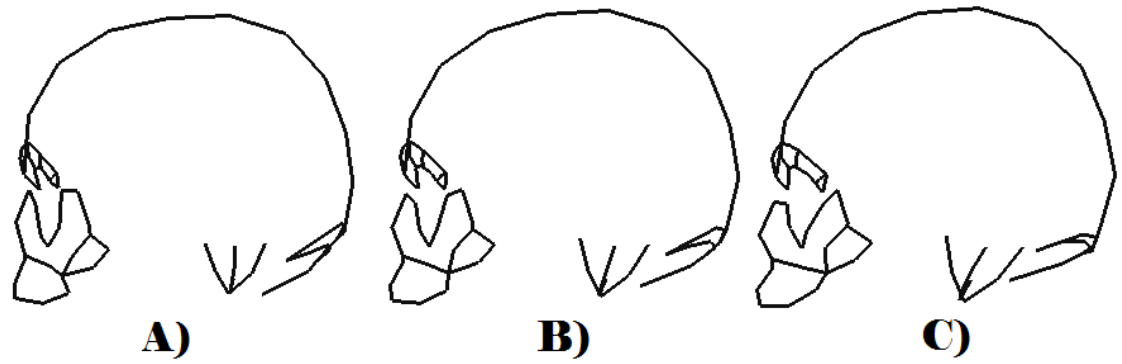

Figure S25. Morphological Variation along RW5 for the Medit/Near East sub-sample: A) Lower extreme of variation, B) Consensus form, C) Upper extreme of variation.

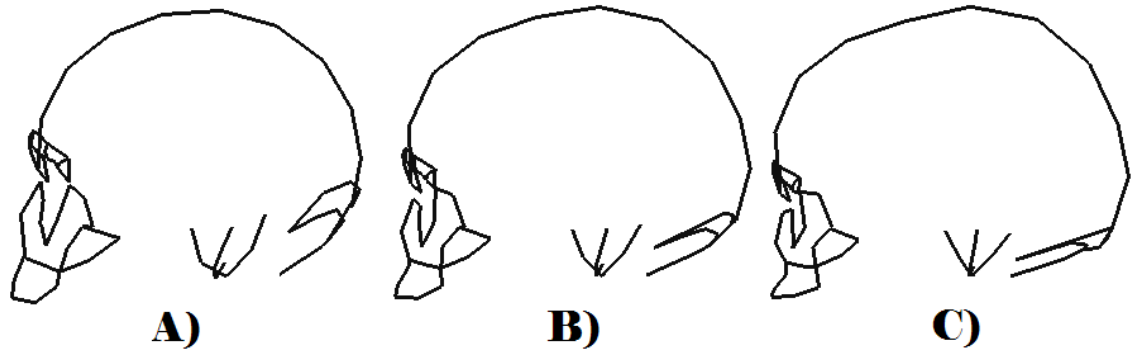

Figure S26. Morphological Variation along RW1 for the New Guinea sub-sample: A) Lower extreme of variation, B) Consensus form, C) Upper extreme of variation.

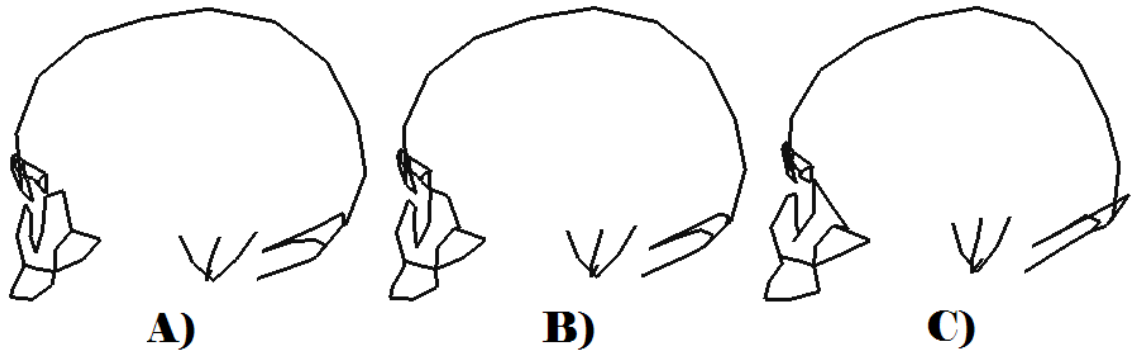

Figure S27. Morphological Variation along RW2 for the New Guinea sub-sample: A) Lower extreme of variation, B) Consensus form, C) Upper extreme of variation.

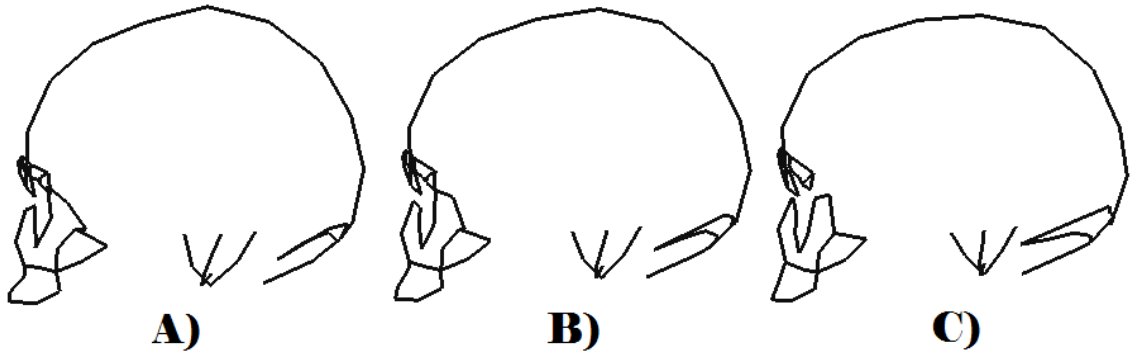

Figure S28. Morphological Variation along RW3 for the New Guinea sub-sample: A) Lower extreme of variation, B) Consensus form, C) Upper extreme of variation.

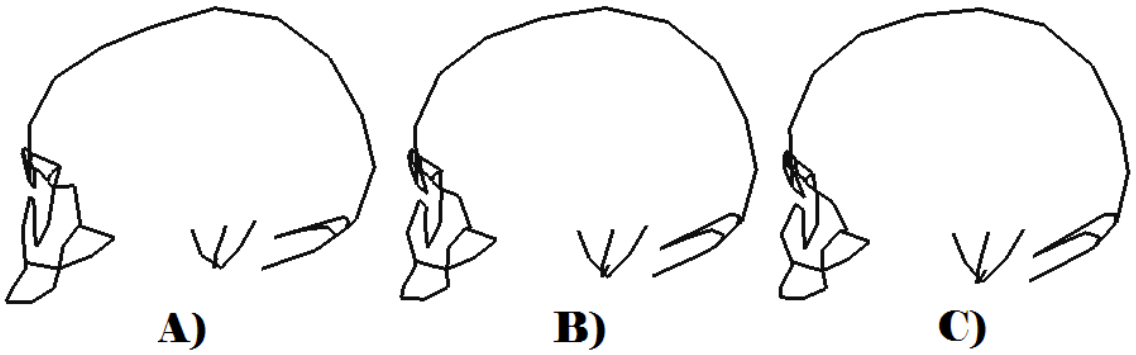

Figure S29. Morphological Variation along RW4 for the New Guinea sub-sample: A) Lower extreme of variation, B) Consensus form, C) Upper extreme of variation.

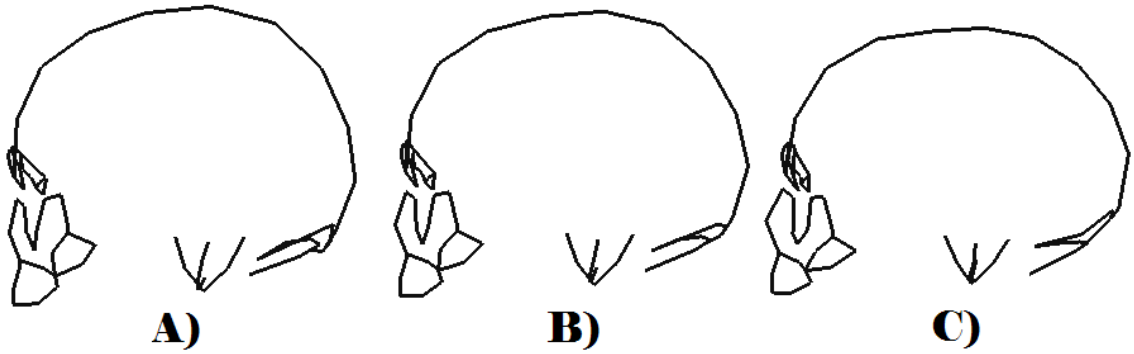

Figure S30. Morphological Variation along RW1 for the North African sub-sample: A) Lower extreme of variation, B) Consensus form, C) Upper extreme of variation.

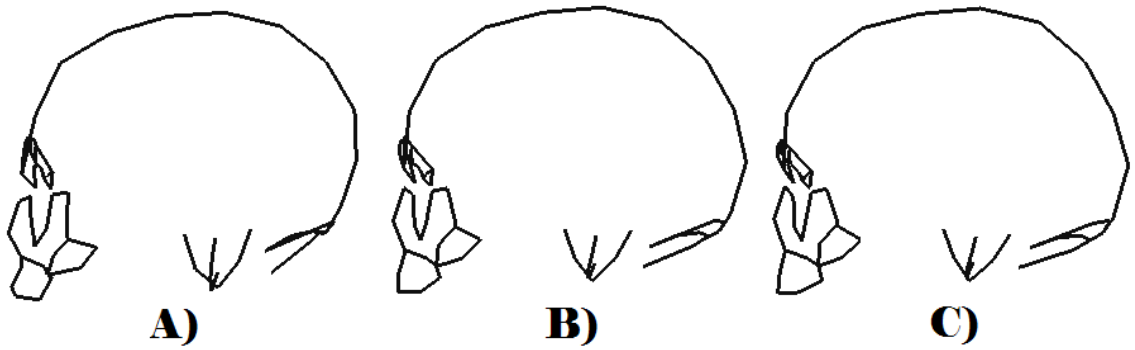

Figure S31. Morphological Variation along RW2 for the North African sub-sample: A) Lower extreme of variation, B) Consensus form, C) Upper extreme of variation.

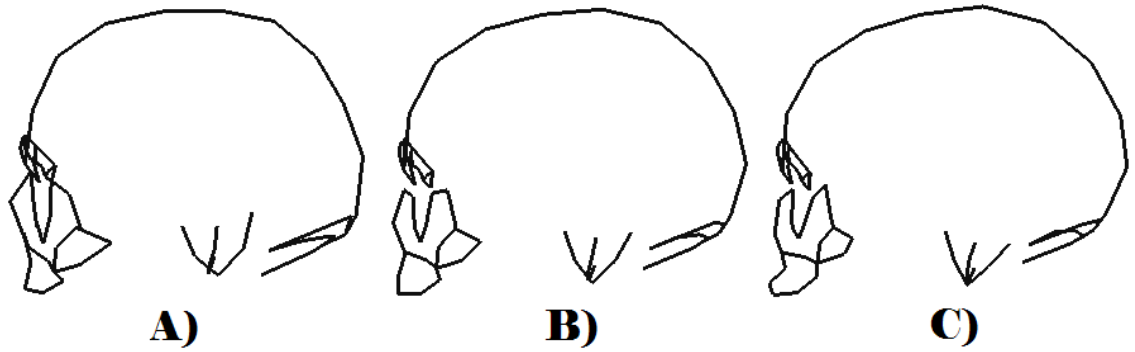

Figure S32. Morphological Variation along RW3 for the North African sub-sample: A) Lower extreme of variation, B) Consensus form, C) Upper extreme of variation.

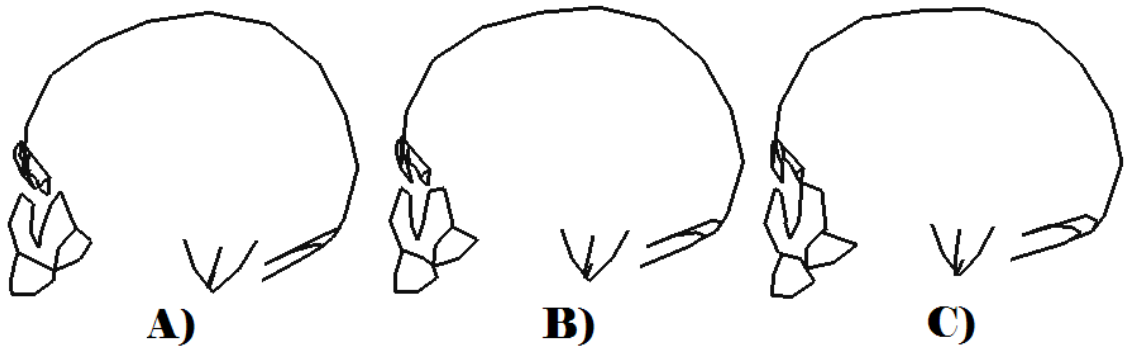

Figure S33. Morphological Variation along RW4 for the North African sub-sample: A) Lower extreme of variation, B) Consensus form, C) Upper extreme of variation.

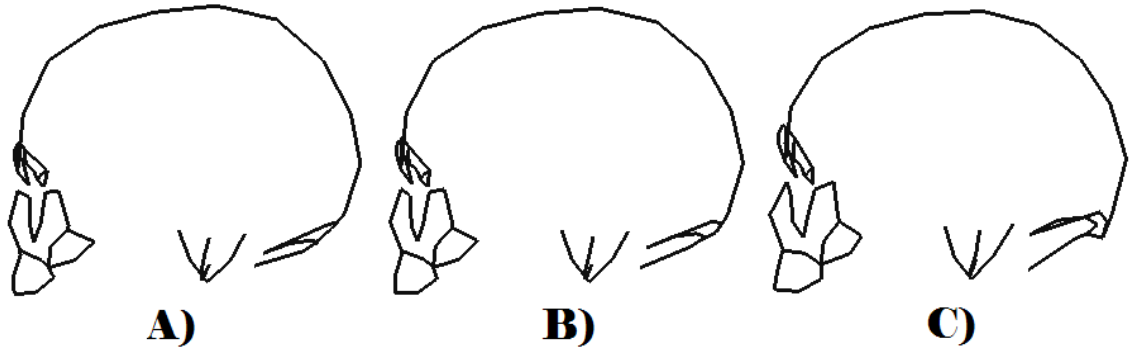

Figure S34. Morphological Variation along RW5 for the North African sub-sample: A) Lower extreme of variation, B) Consensus form, C) Upper extreme of variation.

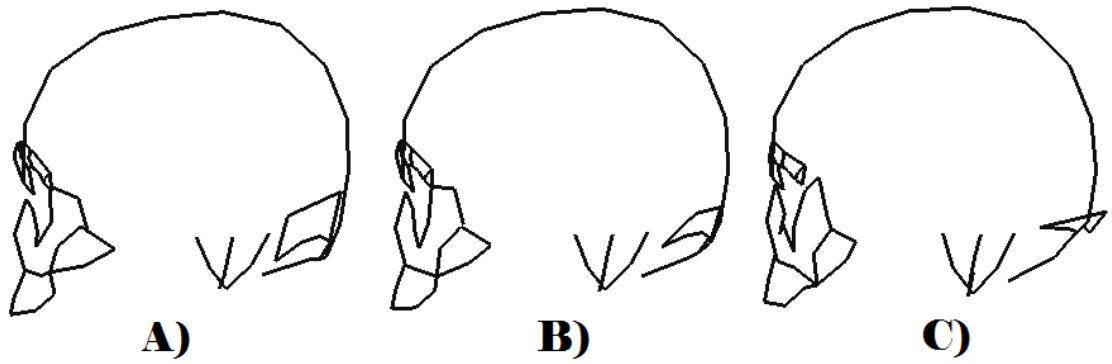

Figure S35. Morphological Variation along RW1 for the Singapore sub-sample: A) Lower extreme of variation, B) Consensus form, C) Upper extreme of variation.

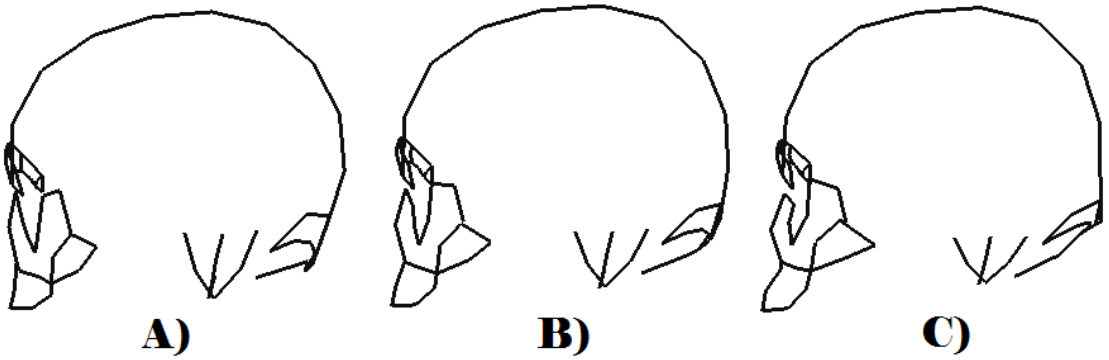

Figure S36. Morphological Variation along RW2 for the Singapore sub-sample: A) Lower extreme of variation, B) Consensus form, C) Upper extreme of variation.

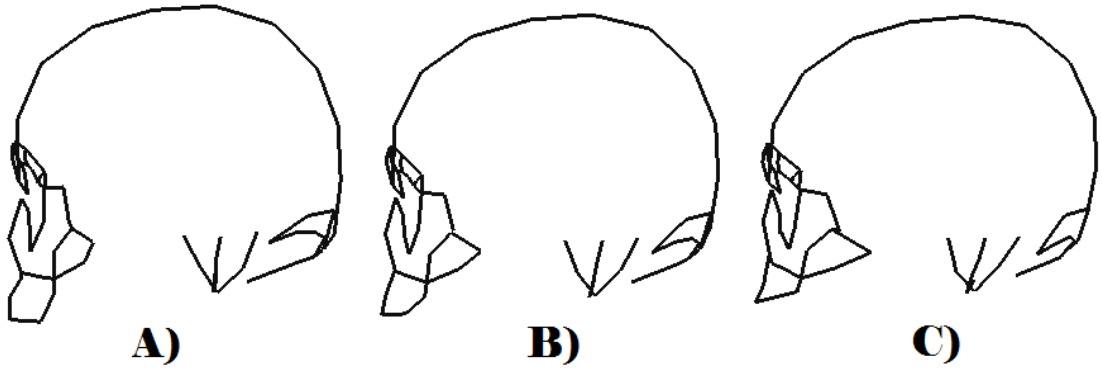

Figure S37. Morphological Variation along RW3 for the Singapore sub-sample: A) Lower extreme of variation, B) Consensus form, C) Upper extreme of variation.

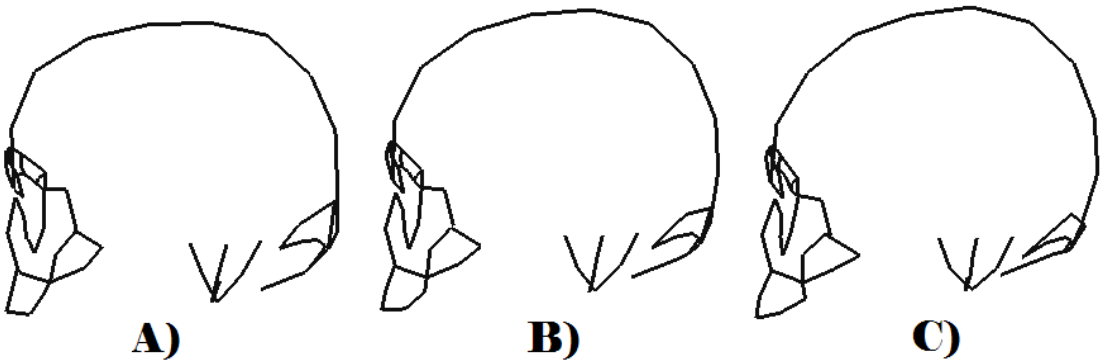

Figure S38. Morphological Variation along RW4 for the Singapore sub-sample: A) Lower extreme of variation, B) Consensus form, C) Upper extreme of variation.

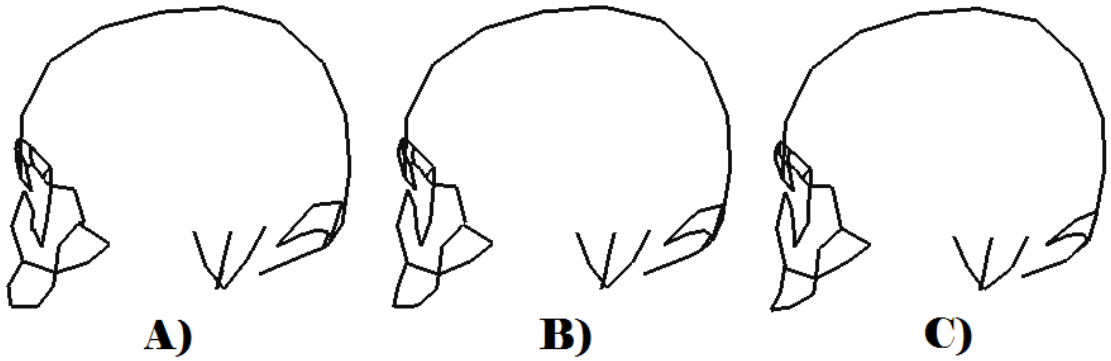

Figure S39. Morphological Variation along RW5 for the Singapore sub-sample: A) Lower extreme of variation, B) Consensus form, C) Upper extreme of variation.

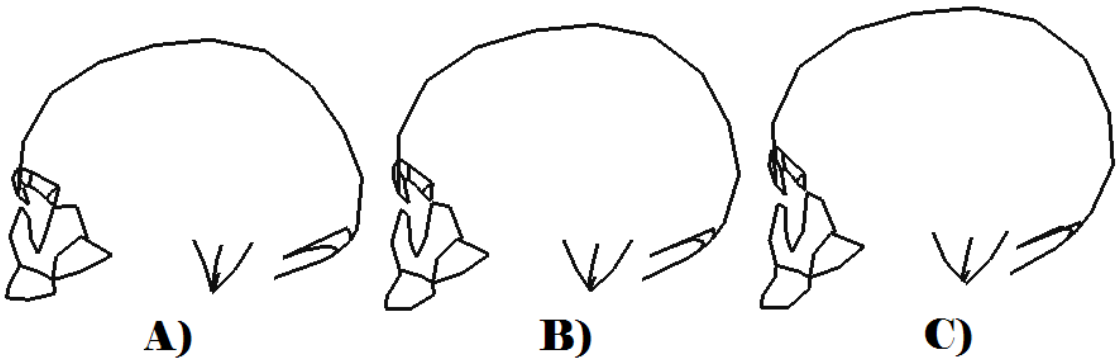

Figure S40. Morphological Variation along RW1 for the Bantu sub-sample: A) Lower extreme of variation, B) Consensus form, C) Upper extreme of variation.

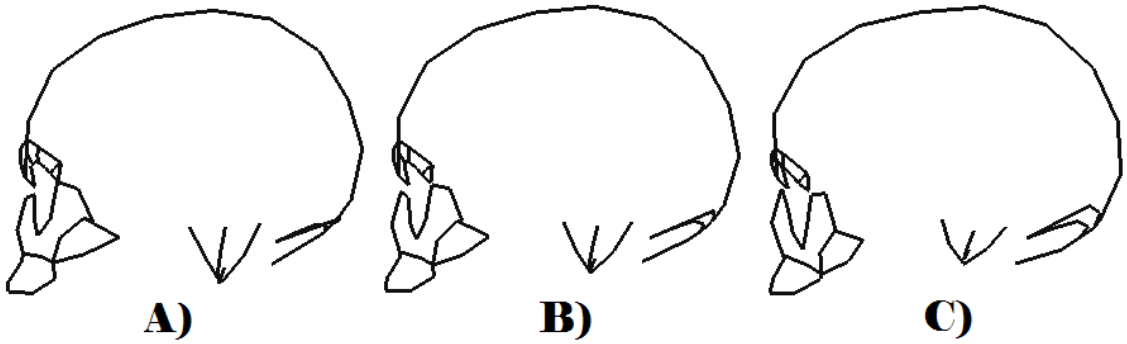

Figure S41. Morphological Variation along RW2 for the Bantu sub-sample: A) Lower extreme of variation, B) Consensus form, C) Upper extreme of variation.

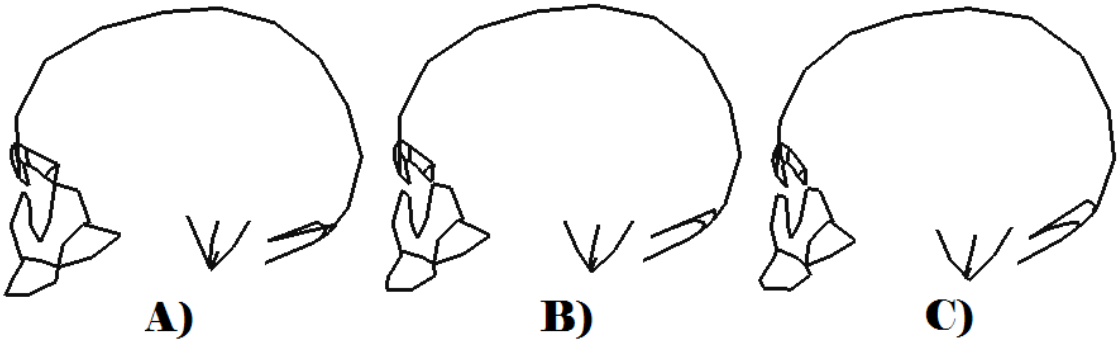

Figure S42. Morphological Variation along RW3 for the Bantu sub-sample: A) Lower extreme of variation, B) Consensus form, C) Upper extreme of variation.

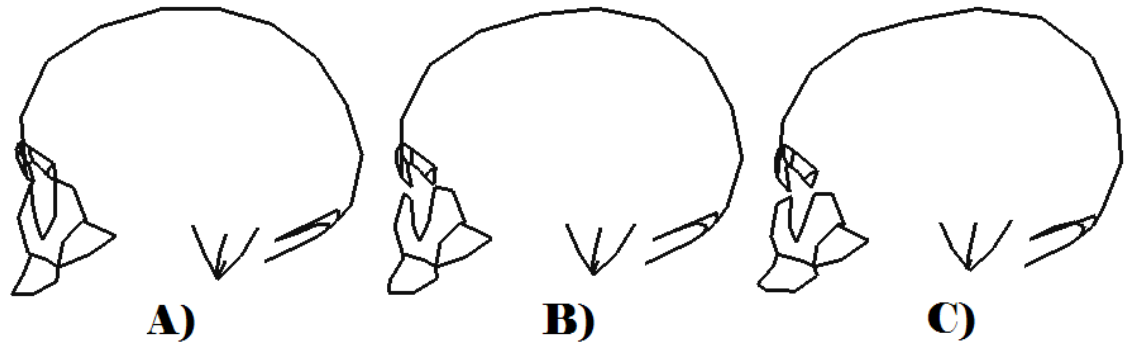

Figure S43. Morphological Variation along RW4 for the Bantu sub-sample: A) Lower extreme of variation, B) Consensus form, C) Upper extreme of variation.

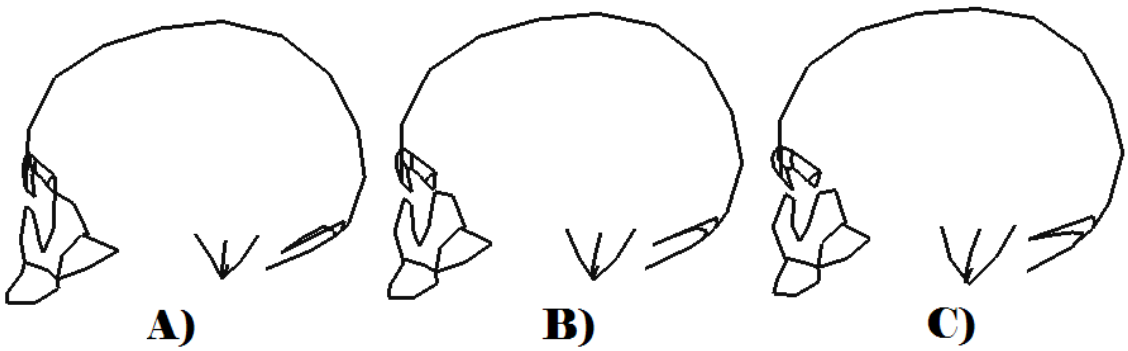

Figure S44. Morphological Variation along RW5 for the Bantu sub-sample: A) Lower extreme of variation, B) Consensus form, C) Upper extreme of variation.

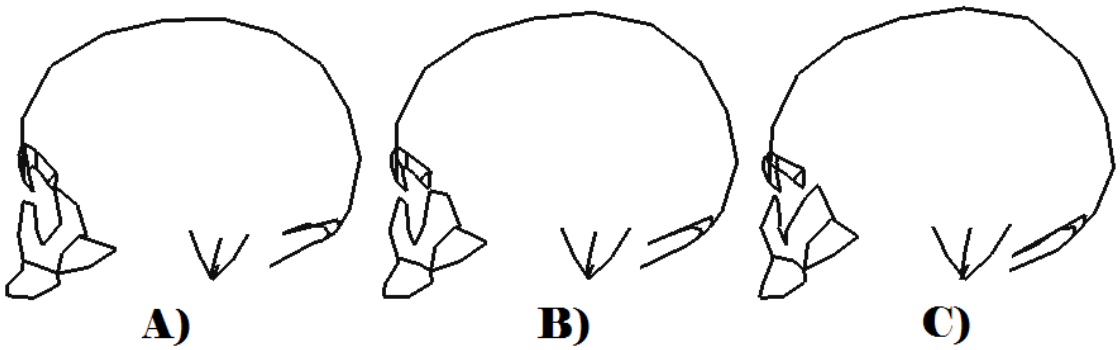

Figure S45. Morphological Variation along RW6 for the Bantu sub-sample: A) Lower extreme of variation, B) Consensus form, C) Upper extreme of variation.

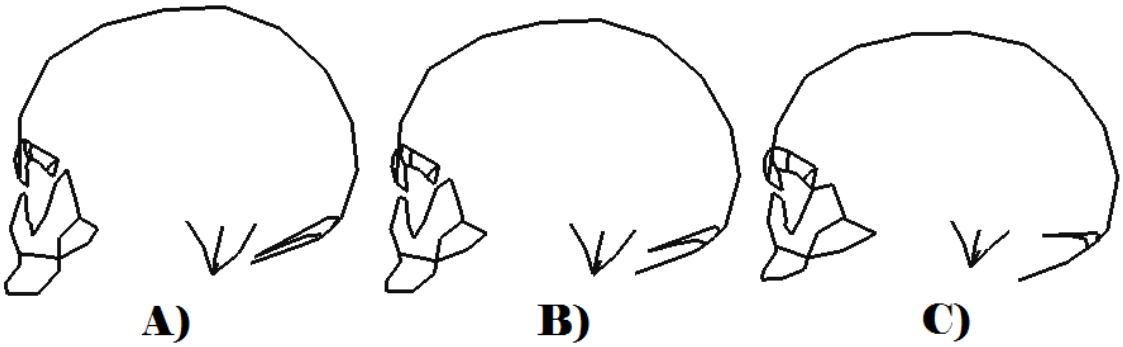

Figure S46. Morphological Variation along RW1 for the Khoisan sub-sample: A) Lower extreme of variation, B) Consensus form, C) Upper extreme of variation.

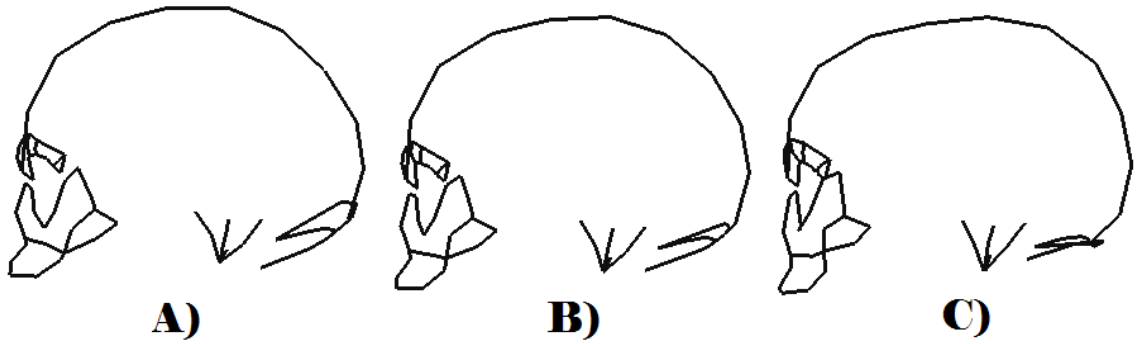

Figure S47. Morphological Variation along RW2 for the Khoisan sub-sample: A) Lower extreme of variation, B) Consensus form, C) Upper extreme of variation.

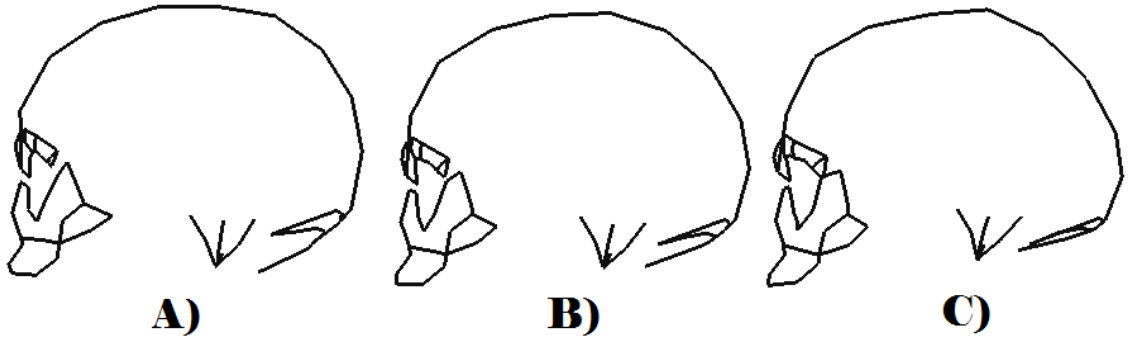

Figure S48. Morphological Variation along RW3 for the Khoisan sub-sample: A) Lower extreme of variation, B) Consensus form, C) Upper extreme of variation.

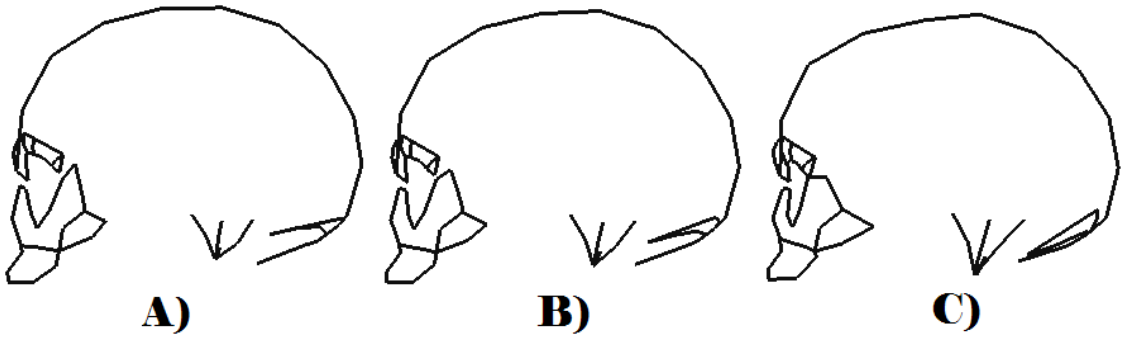

Figure S49. Morphological Variation along RW4 for the Khoisan sub-sample: A) Lower extreme of variation, B) Consensus form, C) Upper extreme of variation.

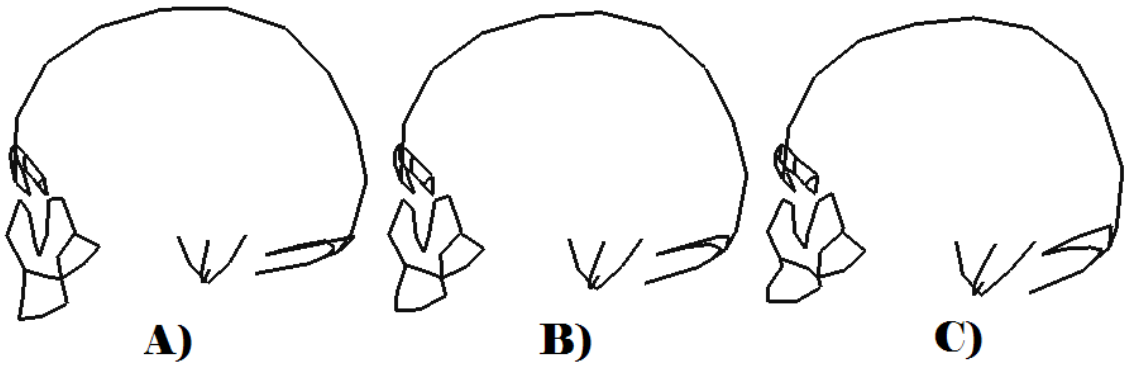

Figure S50. Morphological Variation along RW1 for the Western Europe sub-sample: A) Lower extreme of variation, B) Consensus form, C) Upper extreme of variation.

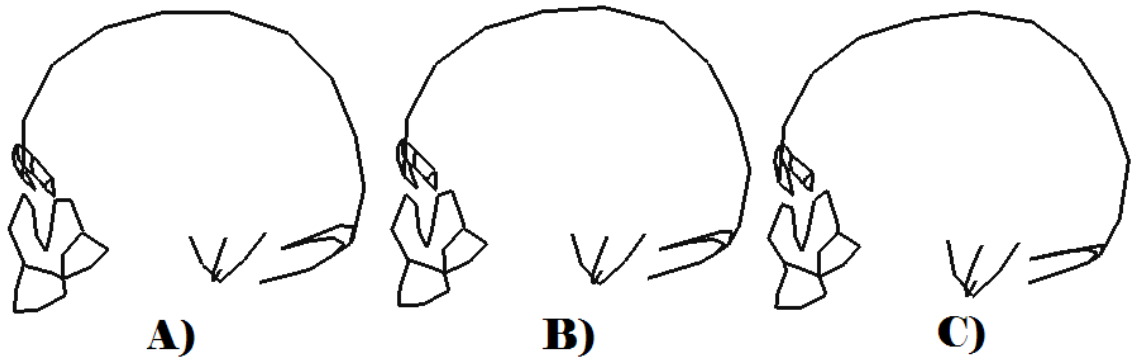

Figure S51. Morphological Variation along RW2 for the Western Europe sub-sample: A) Lower extreme of variation, B) Consensus form, C) Upper extreme of variation.

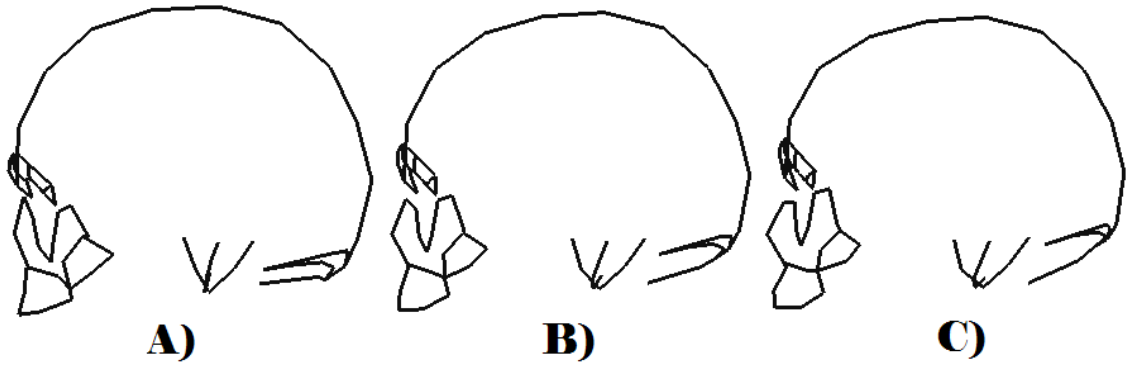

Figure S52. Morphological Variation along RW3 for the Western Europe sub-sample: A) Lower extreme of variation, B) Consensus form, C) Upper extreme of variation.

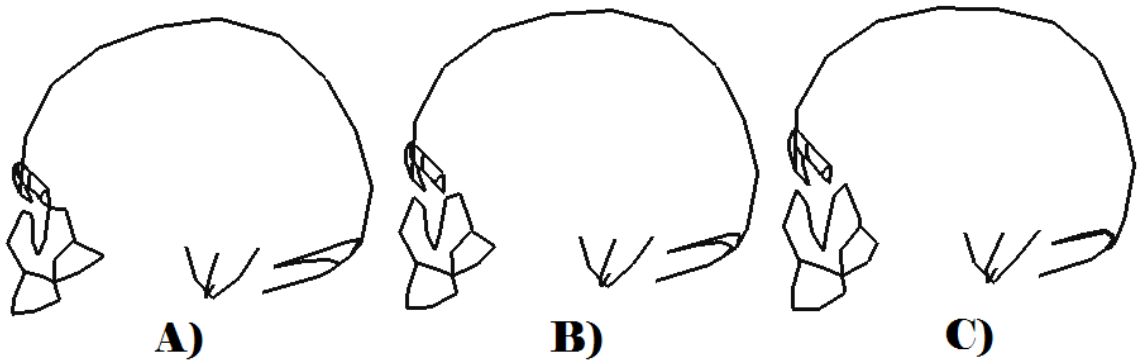

Figure S53. Morphological Variation along RW4 for the Western Europe sub-sample: A) Lower extreme of variation, B) Consensus form, C) Upper extreme of variation.

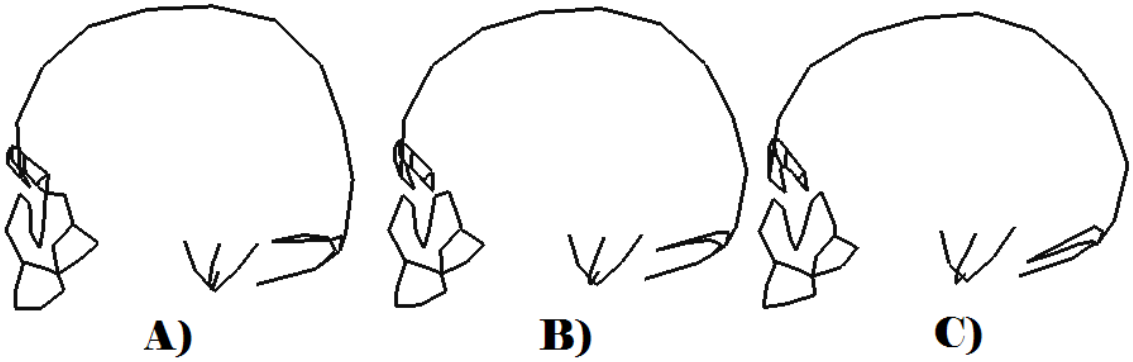

Figure S54. Morphological Variation along RW5 for the Western Europe sub-sample: A) Lower extreme of variation, B) Consensus form, C) Upper extreme of variation.

APPENDIX T. MORPHOLOGICAL VARIATION IN ROBUSTICITY LANDMARK SUBSET BY REGIONAL SAMPLE

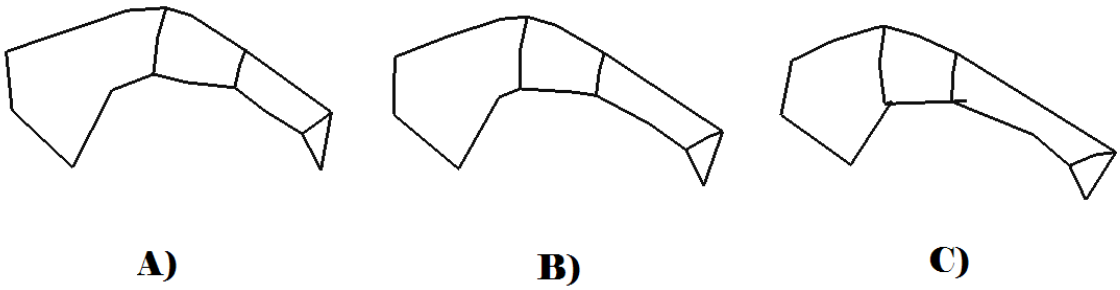

Figure T1. Variation of Supraorbital Landmarks along RW1 for the Australian Sample: A) Lower extreme of variation, B) Consensus form, C) Upper extreme of variation.

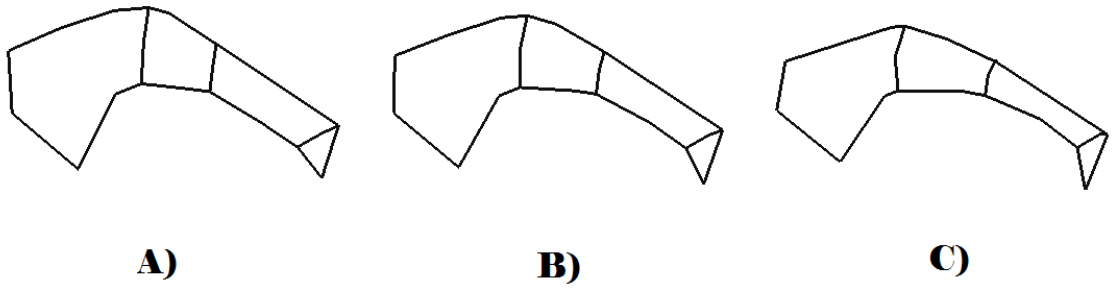

Figure T2. Variation of Supraorbital Landmarks along RW2 for the Australian Sample: A) Lower extreme of variation, B) Consensus form, C) Upper extreme of variation.

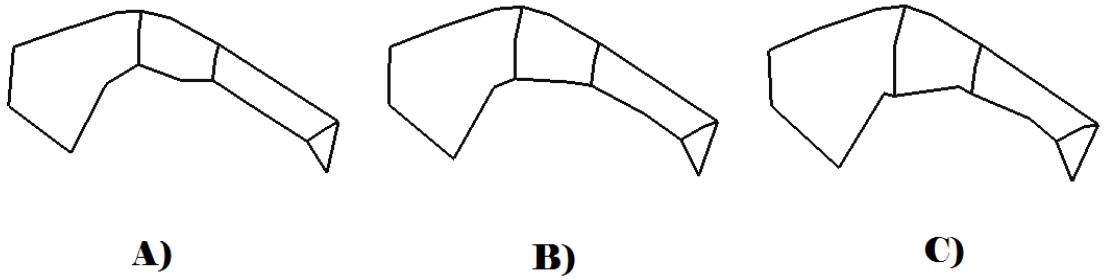

Figure T3. Variation of Supraorbital Landmarks along RW3 for the Australian Sample: A) Lower extreme of variation, B) Consensus form, C) Upper extreme of variation.

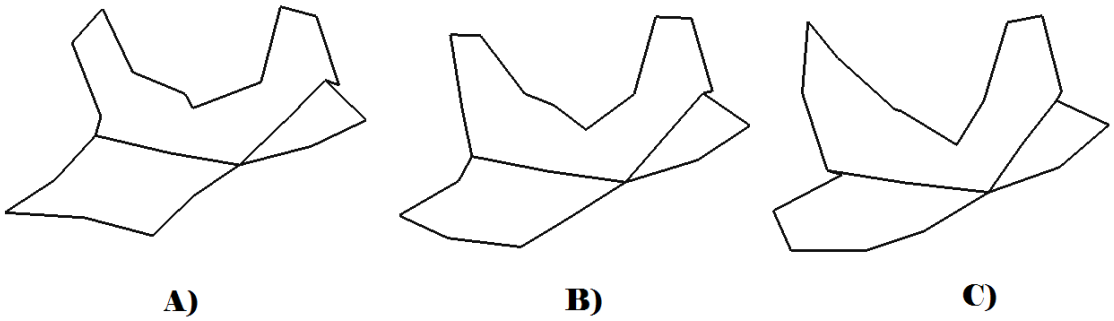

Figure T4. Variation of Zygomaxillary Landmarks along RW1 for the Australian Sample: A) Lower extreme of variation, B) Consensus form, C) Upper extreme of variation.

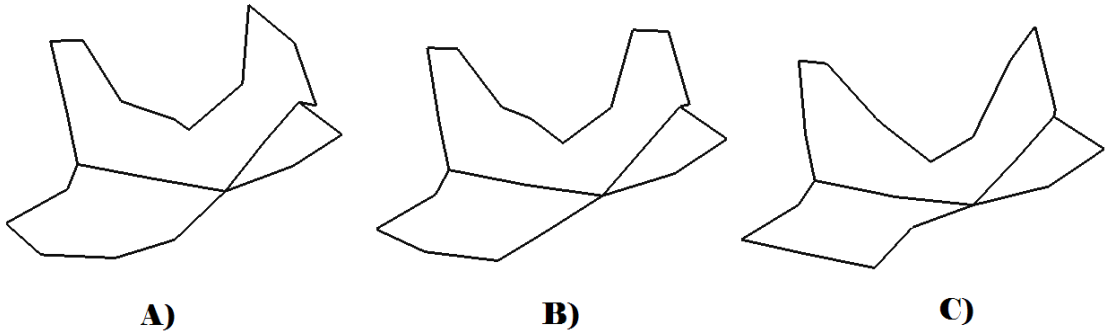

Figure T5. Variation of Zygomaxillary Landmarks along RW2 for the Australian Sample: A) Lower extreme of variation, B) Consensus form, C) Upper extreme of variation.

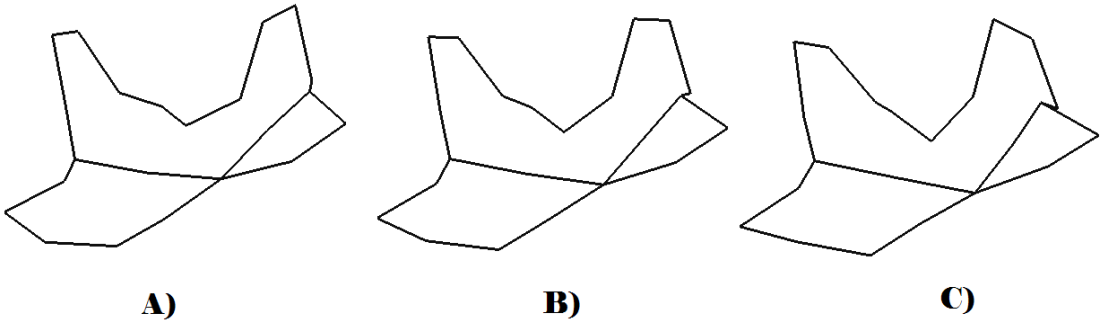

Figure T6. Variation of Zygomaxillary Landmarks along RW3 for the Australian Sample: A) Lower extreme of variation, B) Consensus form, C) Upper extreme of variation.

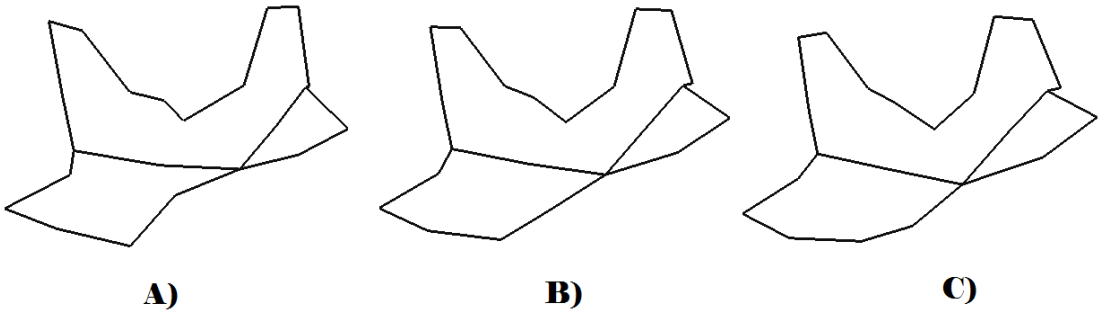

Figure T7. Variation of Zygomaxillary Landmarks along RW4 for the Australian Sample: A) Lower extreme of variation, B) Consensus form, C) Upper extreme of variation.

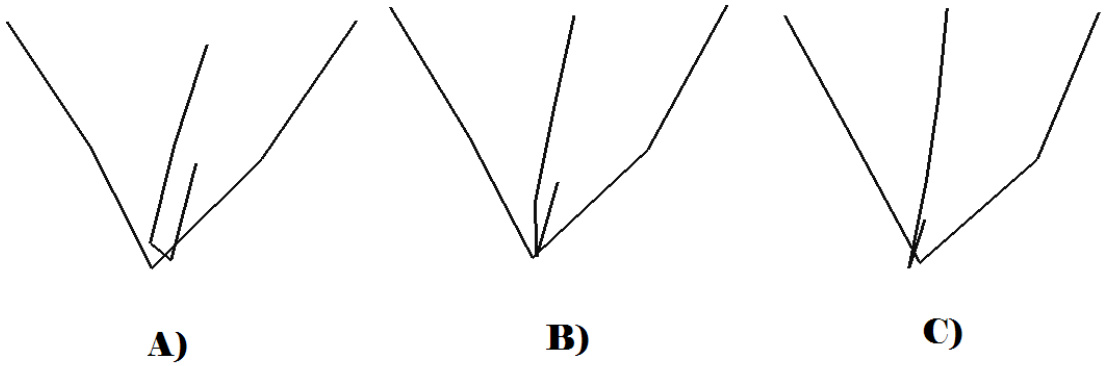

Figure T8. Variation of Mastoid Landmarks along RW1 for the Australian Sample: A) Lower extreme of variation, B) Consensus form, C) Upper extreme of variation.

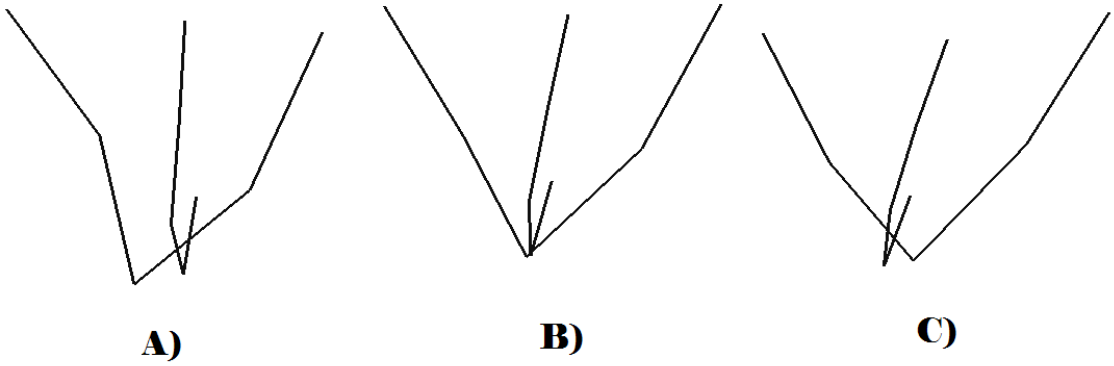

Figure T9. Variation of Mastoid Landmarks along RW2 for the Australian Sample: A) Lower extreme of variation, B) Consensus form, C) Upper extreme of variation.

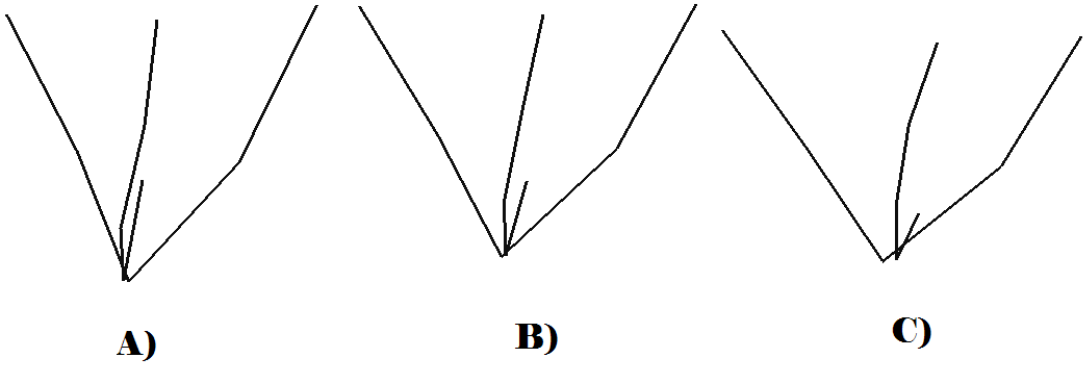

Figure T10. Variation of Mastoid Landmarks along RW3 for the Australian Sample: A) Lower extreme of variation, B) Consensus form, C) Upper extreme of variation.

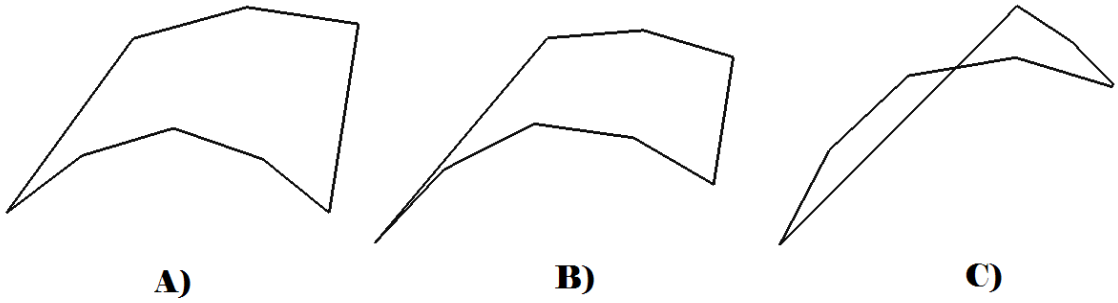

Figure T11. Variation of Occipital Landmarks along RW1 for the Australian Sample: A) Lower extreme of variation, B) Consensus form, C) Upper extreme of variation.

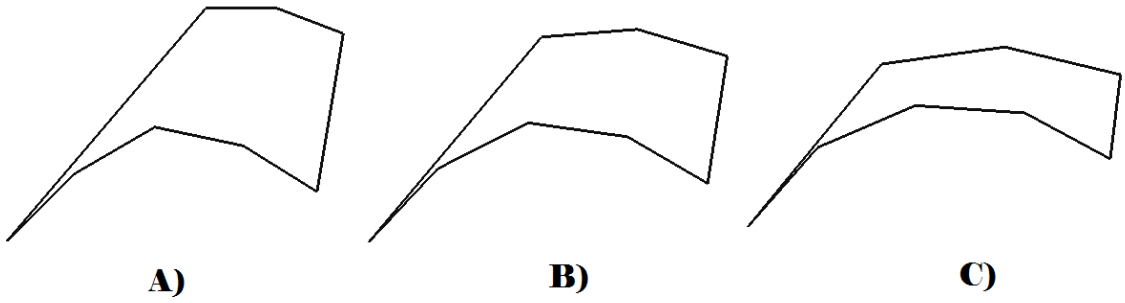

Figure T12. Variation of Occipital Landmarks along RW2 for the Australian Sample: A) Lower extreme of variation, B) Consensus form, C) Upper extreme of variation.

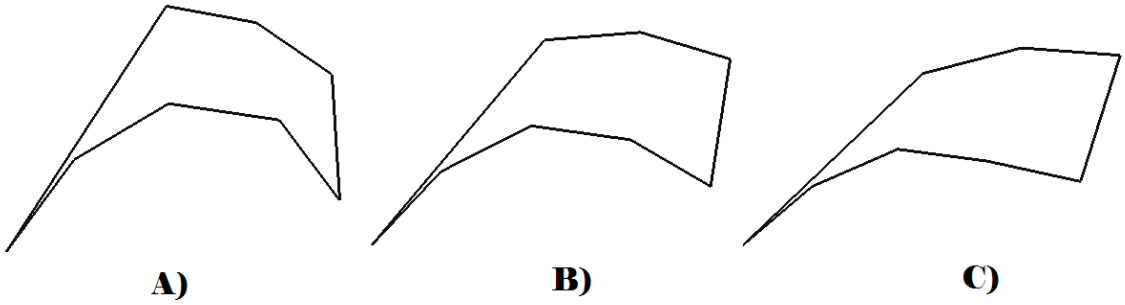

Figure T13. Variation of Occipital Landmarks along RW3 for the Australian Sample: A) Lower extreme of variation, B) Consensus form, C) Upper extreme of variation.

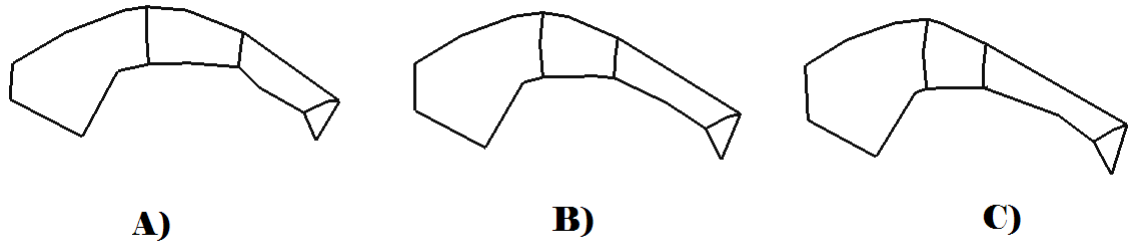

Figure T14. Variation of Supraorbital Landmarks along RW1 for the Bantu Sample: A) Lower extreme of variation, B) Consensus form, C) Upper extreme of variation.

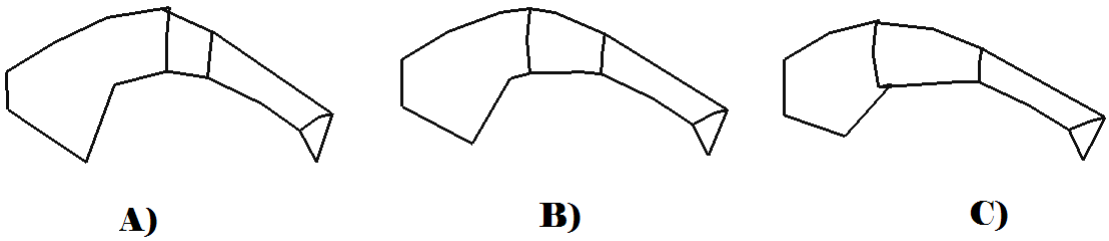

Figure T15. Variation of Supraorbital Landmarks along RW2 for the Bantu Sample: A) Lower extreme of variation, B) Consensus form, C) Upper extreme of variation.

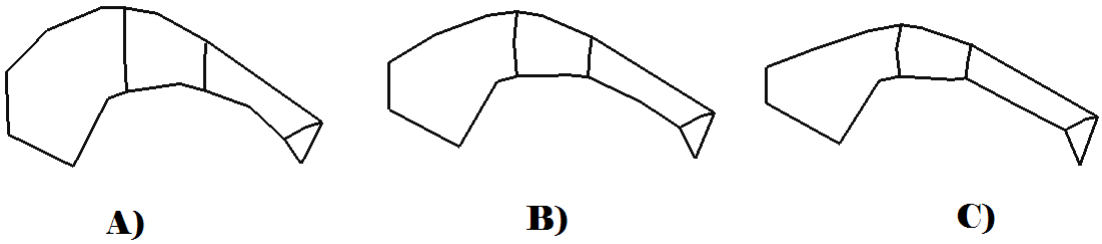

Figure T16. Variation of Supraorbital Landmarks along RW3 for the Bantu Sample: A) Lower extreme of variation, B) Consensus form, C) Upper extreme of variation.

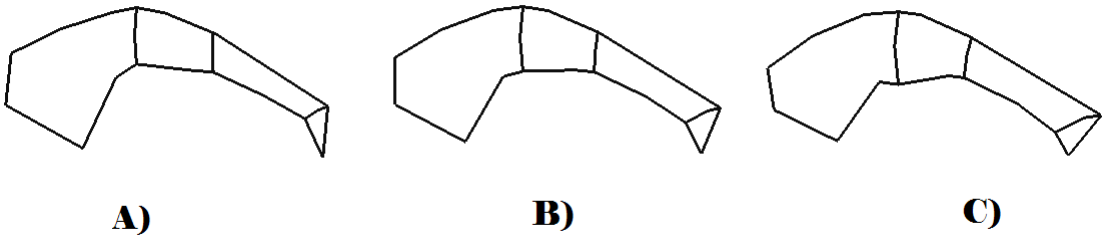

Figure T17. Variation of Supraorbital Landmarks along RW4 for the Bantu Sample: A) Lower extreme of variation, B) Consensus form, C) Upper extreme of variation.

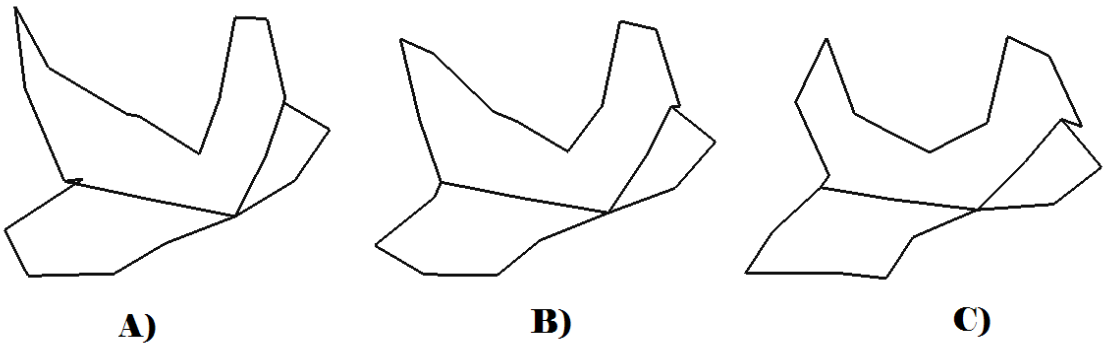

Figure T18. Variation of Zygomaxillary Landmarks along RW1 for the Bantu Sample: A) Lower extreme of variation, B) Consensus form, C) Upper extreme of variation.

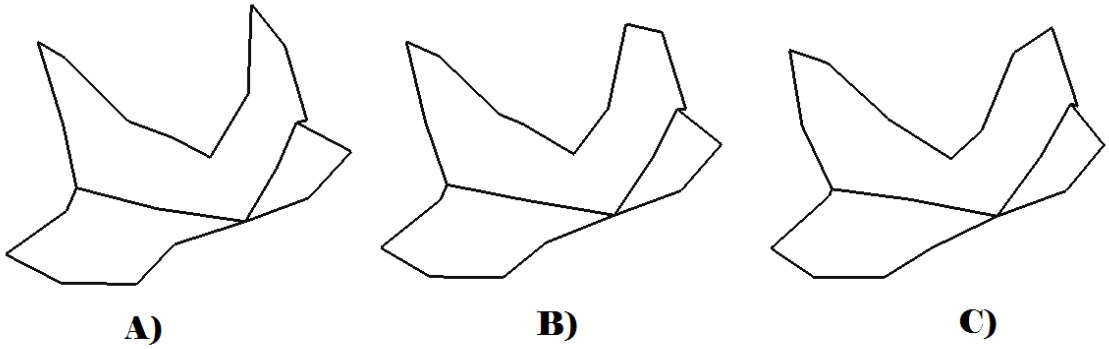

Figure T19. Variation of Zygomaxillary Landmarks along RW2 for the Bantu Sample: A) Lower extreme of variation, B) Consensus form, C) Upper extreme of variation.

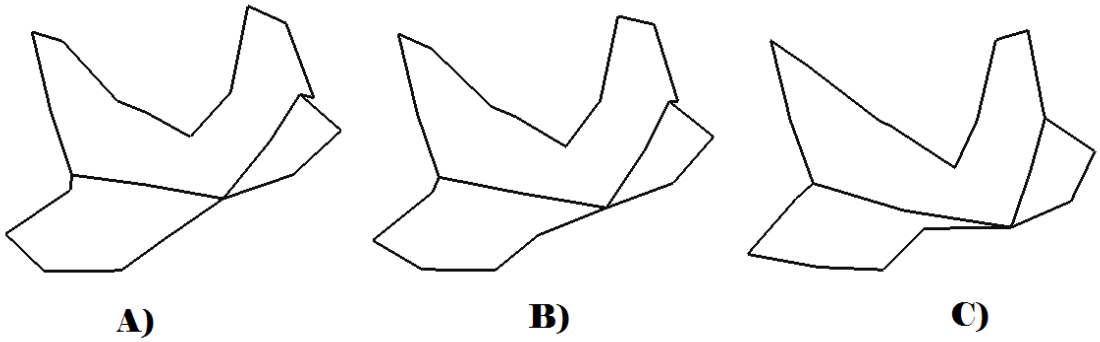

Figure T20. Variation of Zygomaxillary Landmarks along RW3 for the Bantu Sample: A) Lower extreme of variation, B) Consensus form, C) Upper extreme of variation.

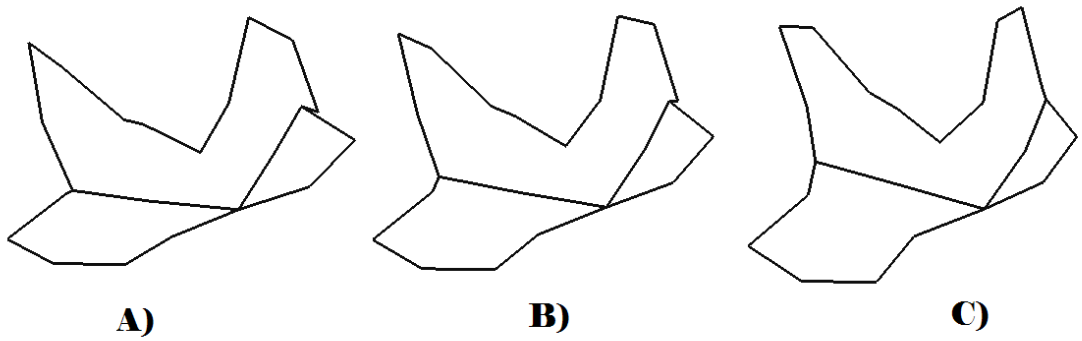

Figure T21. Variation of Zygomaxillary Landmarks along RW4 for the Bantu Sample: A) Lower extreme of variation, B) Consensus form, C) Upper extreme of variation.

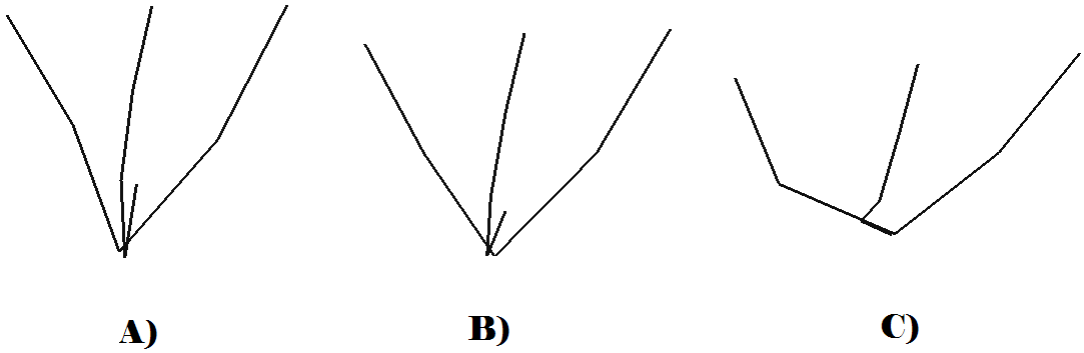

Figure T22. Variation of Mastoid Landmarks along RW1 for the Bantu Sample: A) Lower extreme of variation, B) Consensus form, C) Upper extreme of variation.

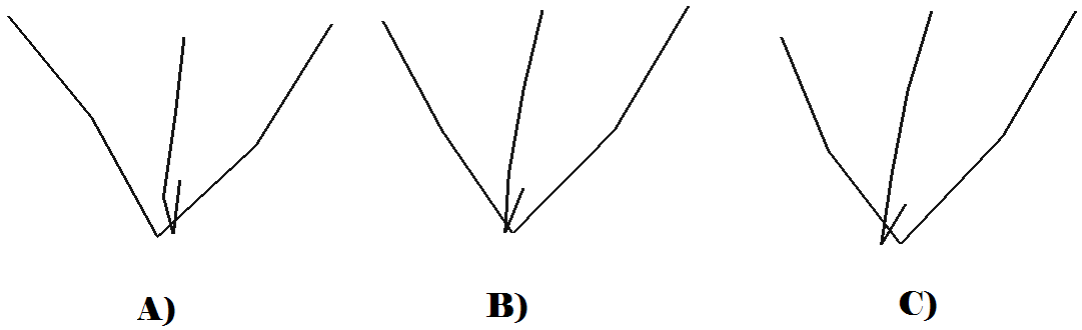

Figure T23. Variation of Mastoid Landmarks along RW2 for the Bantu Sample: A) Lower extreme of variation, B) Consensus form, C) Upper extreme of variation.

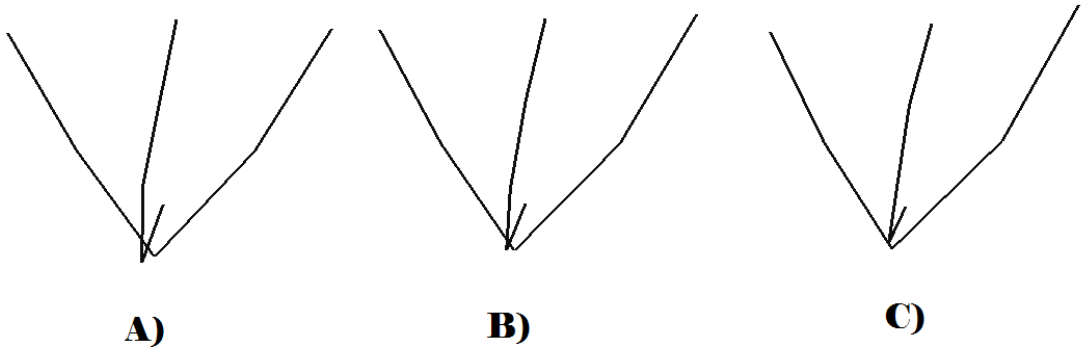

Figure T24. Variation of Mastoid Landmarks along RW3 for the Bantu Sample: A) Lower extreme of variation, B) Consensus form, C) Upper extreme of variation.

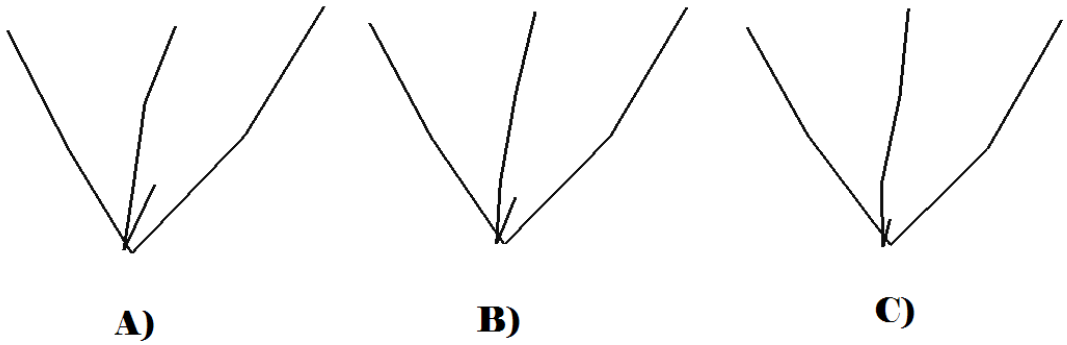

Figure T25. Variation of Mastoid Landmarks along RW4 for the Bantu Sample: A) Lower extreme of variation, B) Consensus form, C) Upper extreme of variation.

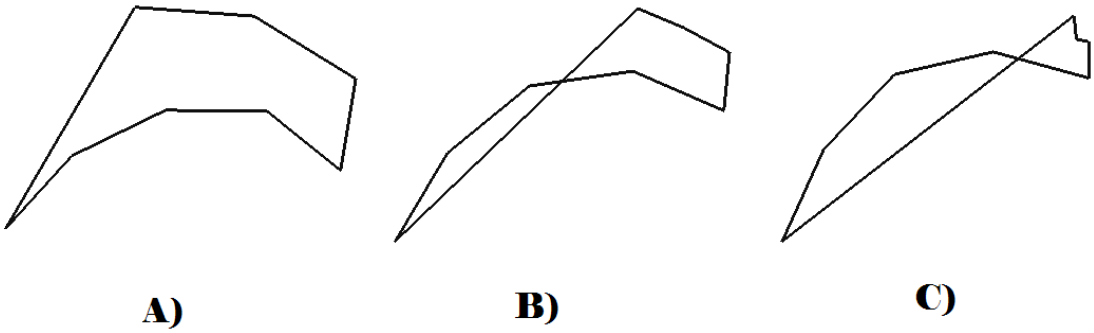

Figure T26. Variation of Occipital Landmarks along RW1 for the Bantu Sample: A) Lower extreme of variation, B) Consensus form, C) Upper extreme of variation.

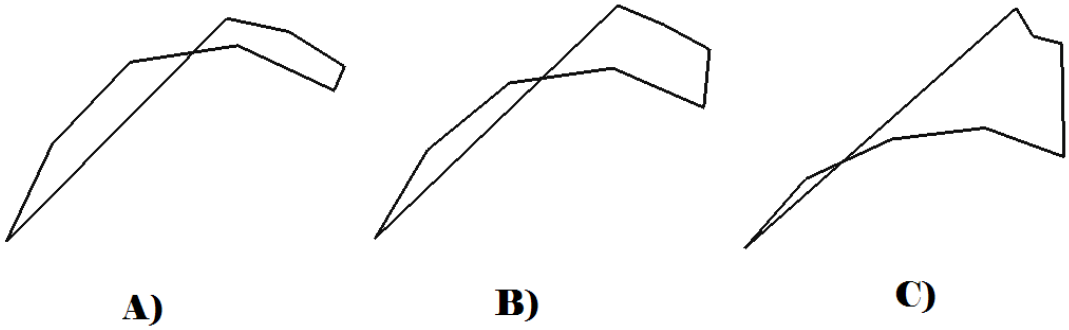

Figure T27. Variation of Occipital Landmarks along RW2 for the Bantu Sample: A) Lower extreme of variation, B) Consensus form, C) Upper extreme of variation.

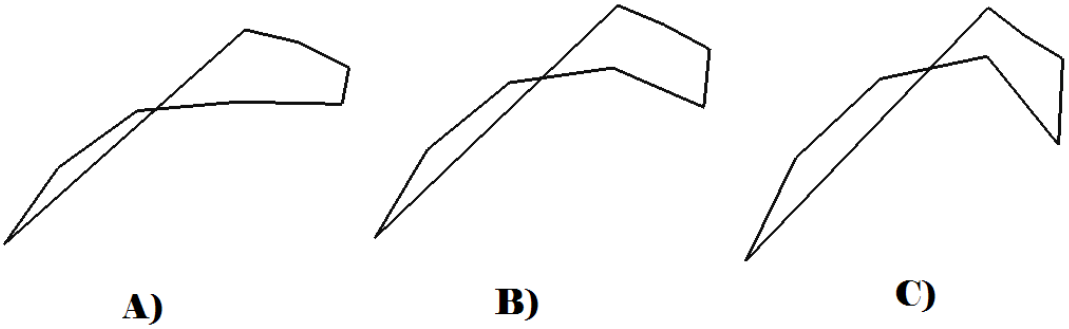

Figure T28. Variation of Occipital Landmarks along RW3 for the Bantu Sample: A) Lower extreme of variation, B) Consensus form, C) Upper extreme of variation.

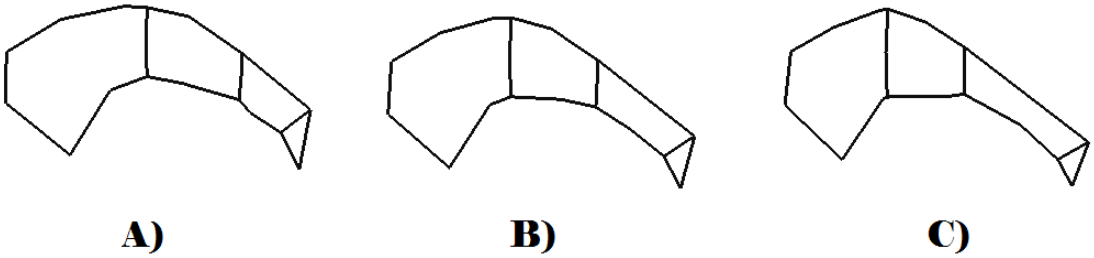

Figure T29. Variation of Supraorbital Landmarks along RW1 for the Central European Sample: A) Lower extreme of variation, B) Consensus form, C) Upper extreme of variation.

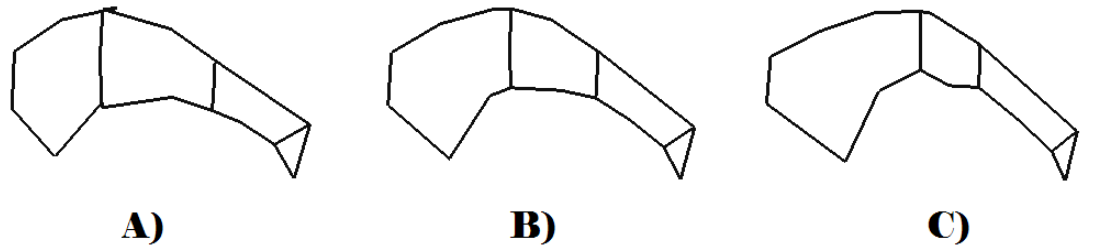

Figure T30. Variation of Supraorbital Landmarks along RW2 for the Central European Sample: A) Lower extreme of variation, B) Consensus form, C) Upper extreme of variation.

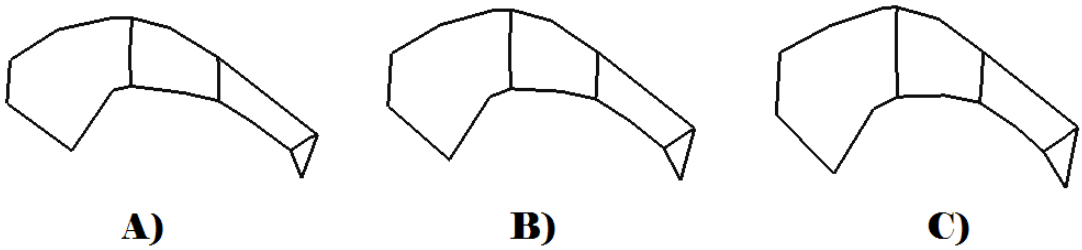

Figure T31. Variation of Supraorbital Landmarks along RW3 for the Central European Sample: A) Lower extreme of variation, B) Consensus form, C) Upper extreme of variation.

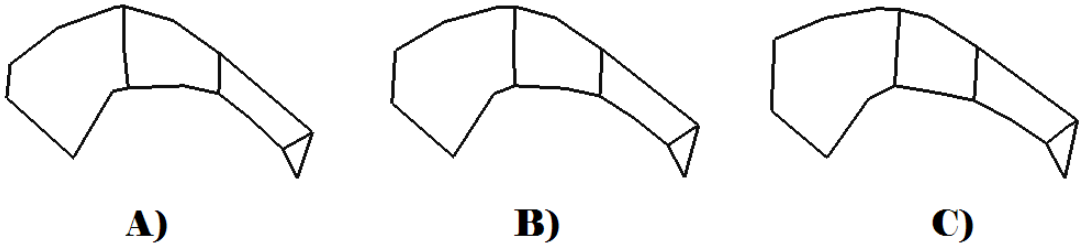

Figure T32. Variation of Supraorbital Landmarks along RW4 for the Central European Sample: A) Lower extreme of variation, B) Consensus form, C) Upper extreme of variation.

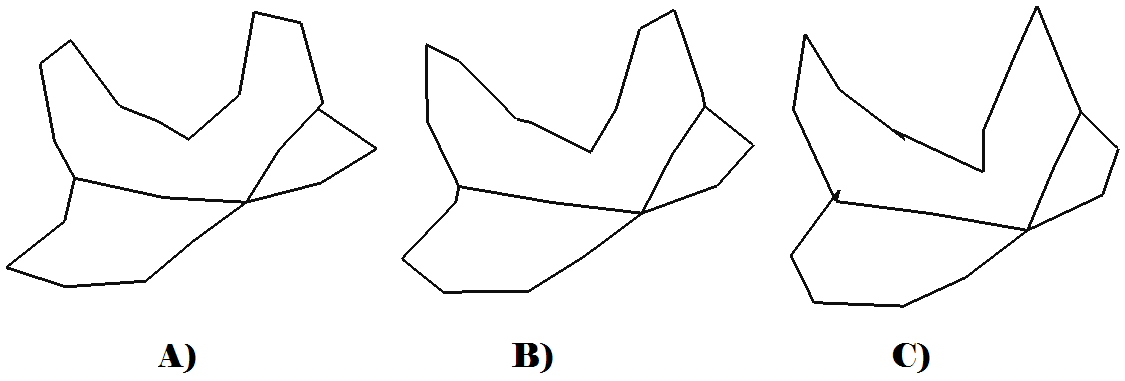

Figure T33. Variation of Zygomaxillary Landmarks along RW1 for the Central European Sample: A) Lower extreme of variation, B) Consensus form, C) Upper extreme of variation.

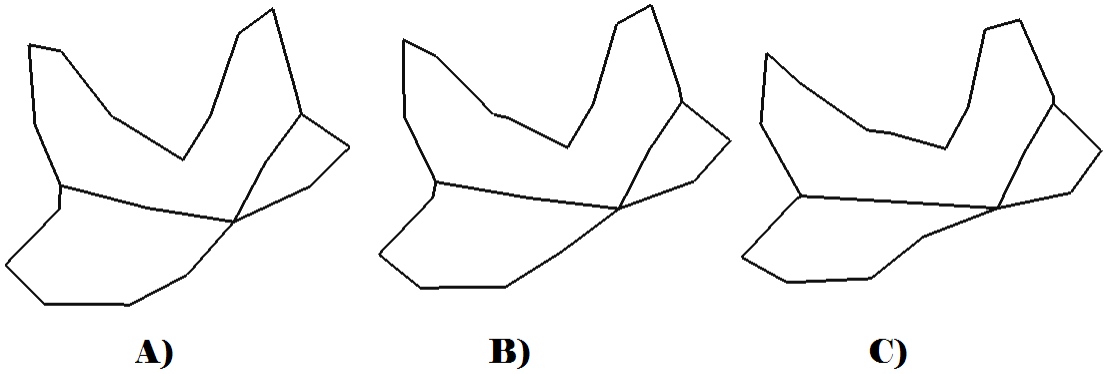

Figure T34. Variation of Zygomaxillary Landmarks along RW2 for the Central European Sample: A) Lower extreme of variation, B) Consensus form, C) Upper extreme of variation.

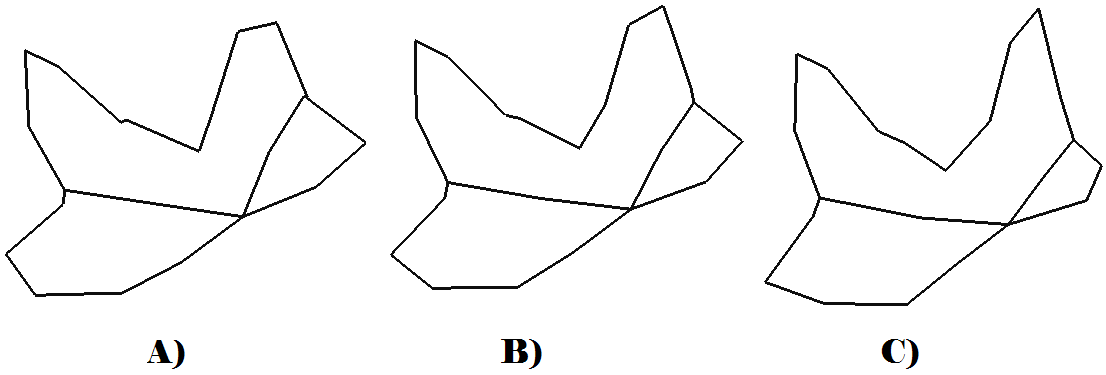

Figure T35. Variation of Zygomaxillary Landmarks along RW3 for the Central European Sample: A) Lower extreme of variation, B) Consensus form, C) Upper extreme of variation.

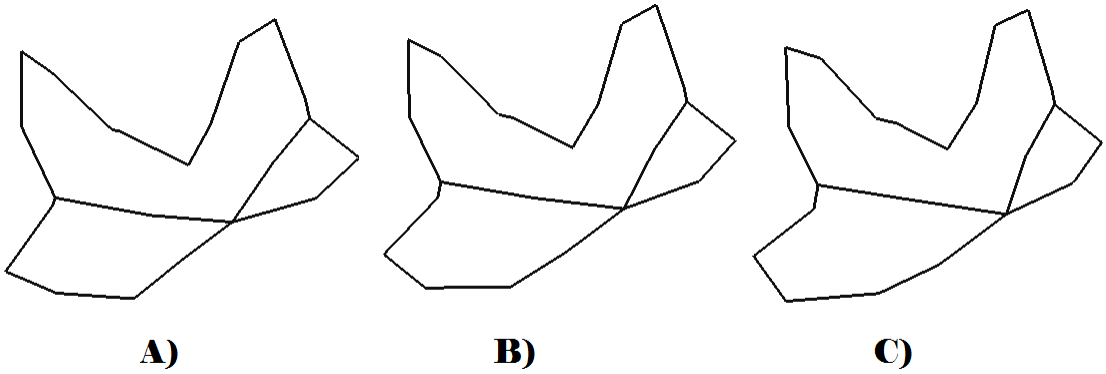

Figure T36. Variation of Zygomaxillary Landmarks along RW4 for the Central European Sample: A) Lower extreme of variation, B) Consensus form, C) Upper extreme of variation.

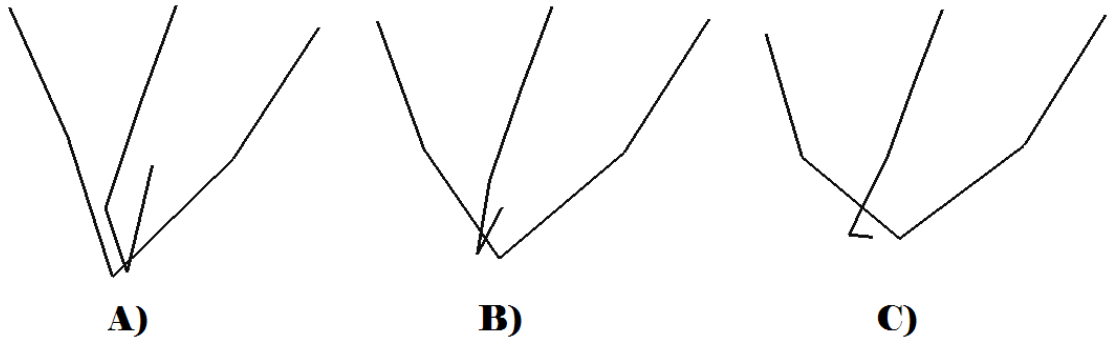

Figure T37. Variation of Mastoid Landmarks along RW1 for the Central European Sample: A) Lower extreme of variation, B) Consensus form, C) Upper extreme of variation.

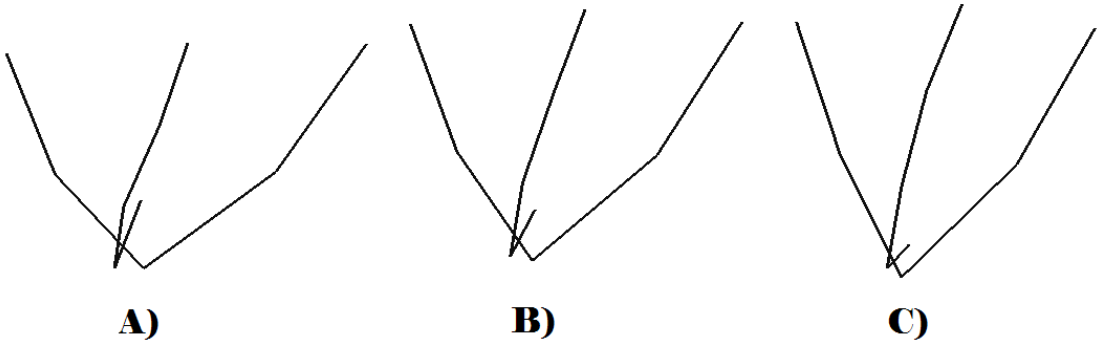

Figure T38. Variation of Mastoid Landmarks along RW2 for the Central European Sample: A) Lower extreme of variation, B) Consensus form, C) Upper extreme of variation.

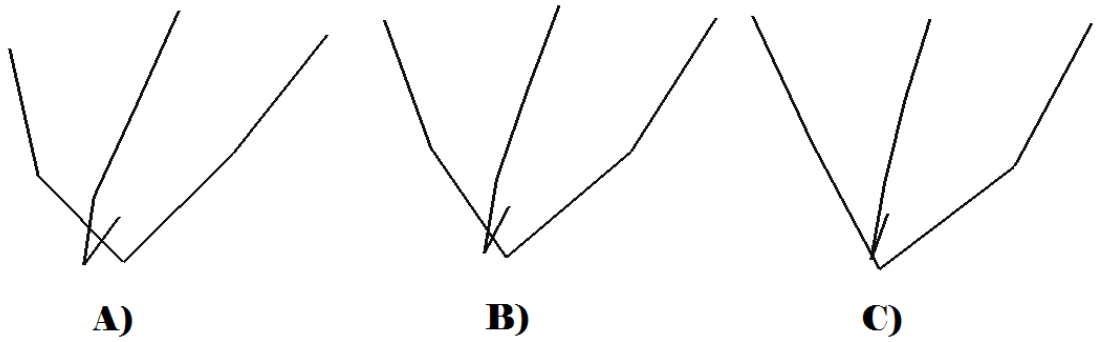

Figure T39. Variation of Mastoid Landmarks along RW3 for the Central European Sample: A) Lower extreme of variation, B) Consensus form, C) Upper extreme of variation.

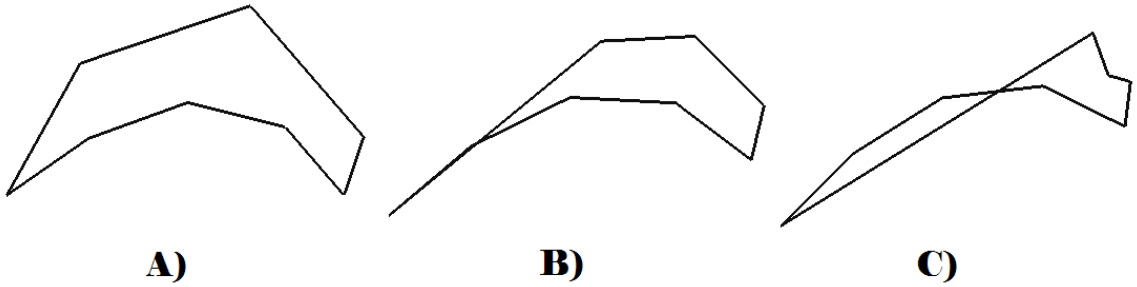

Figure T40. Variation of Occipital Landmarks along RW1 for the Central European Sample: A) Lower extreme of variation, B) Consensus form, C) Upper extreme of variation.

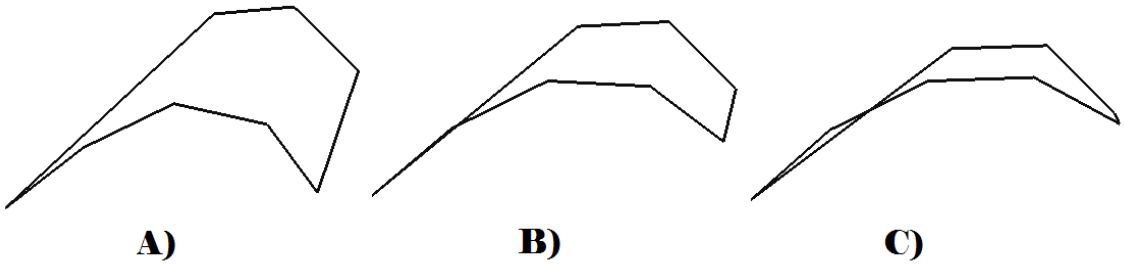

Figure T41. Variation of Occipital Landmarks along RW2 for the Central European Sample: A) Lower extreme of variation, B) Consensus form, C) Upper extreme of variation.

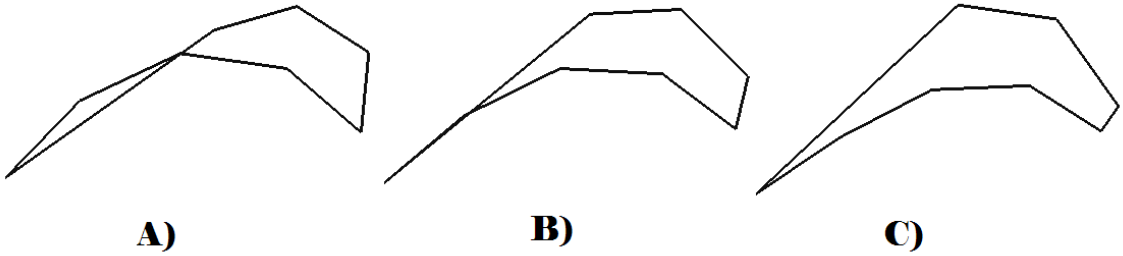

Figure T42. Variation of Occipital Landmarks along RW3 for the Central European Sample: A) Lower extreme of variation, B) Consensus form, C) Upper extreme of variation.

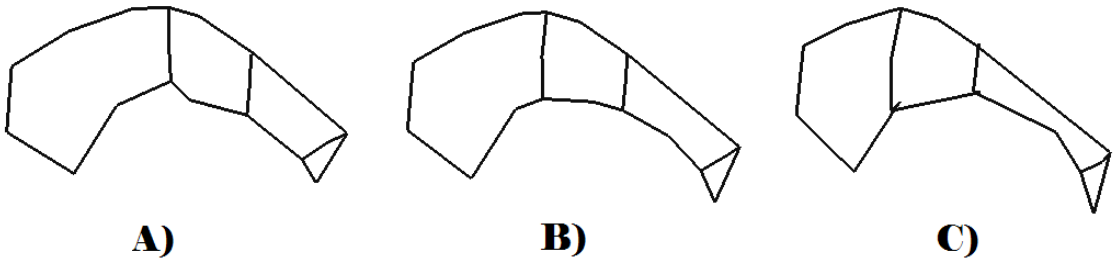

Figure T43. Variation of Supraorbital Landmarks along RW1 for the China Sample: A) Lower extreme of variation, B) Consensus form, C) Upper extreme of variation.

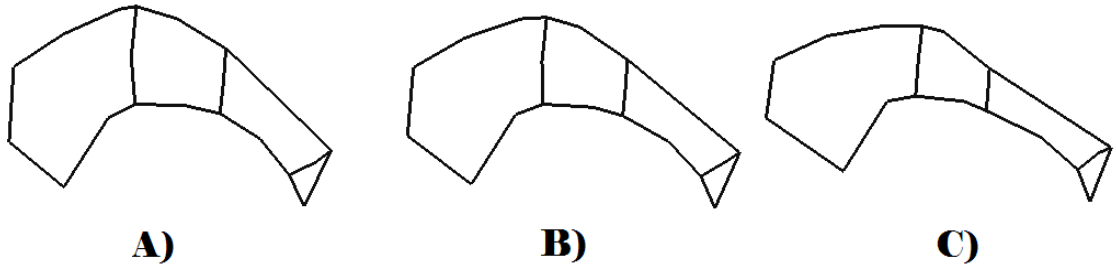

Figure T44. Variation of Supraorbital Landmarks along RW2 for the China Sample: A) Lower extreme of variation, B) Consensus form, C) Upper extreme of variation.

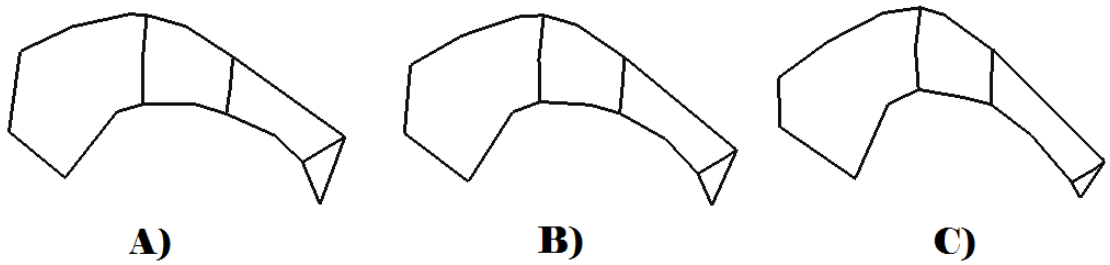

Figure T45. Variation of Supraorbital Landmarks along RW3 for the China Sample: A) Lower extreme of variation, B) Consensus form, C) Upper extreme of variation.

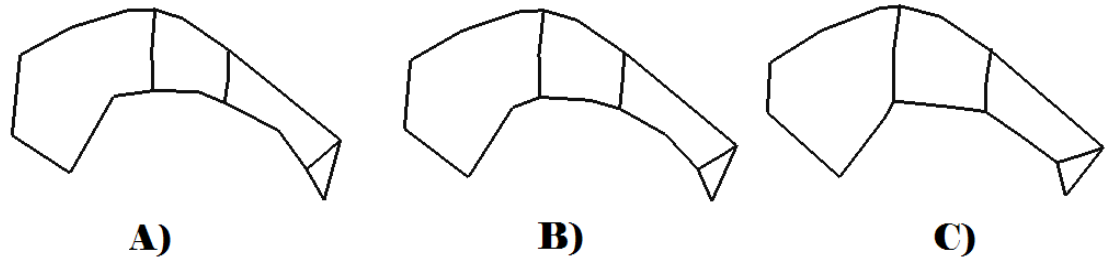

Figure T46. Variation of Supraorbital Landmarks along RW4 for the China Sample: A) Lower extreme of variation, B) Consensus form, C) Upper extreme of variation.

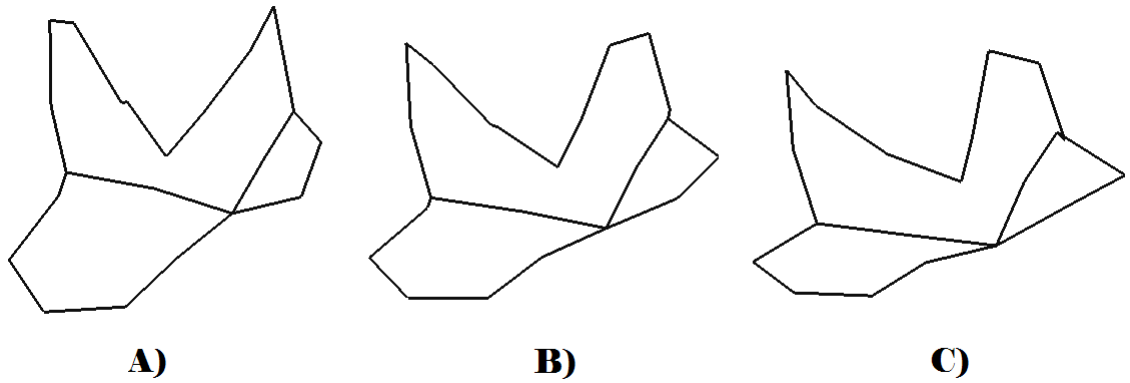

Figure T47. Variation of Zygomaxillary Landmarks along RW1 for the China Sample: A) Lower extreme of variation, B) Consensus form, C) Upper extreme of variation.

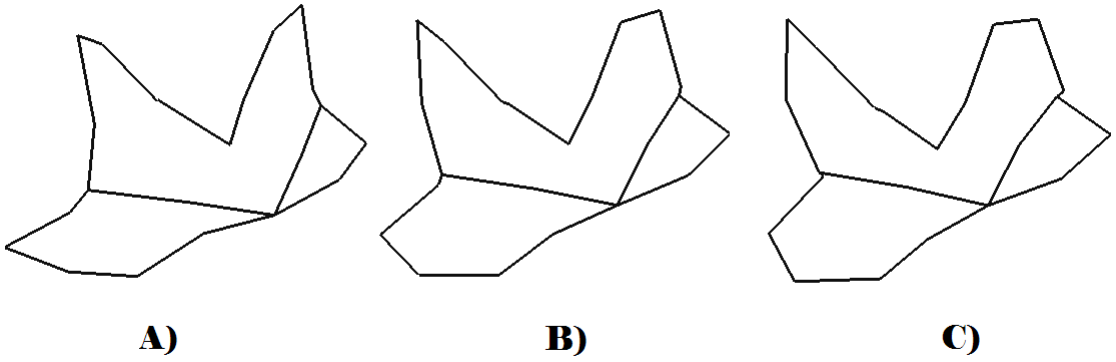

Figure T48. Variation of Zygomaxillary Landmarks along RW2 for the China Sample: A) Lower extreme of variation, B) Consensus form, C) Upper extreme of variation.

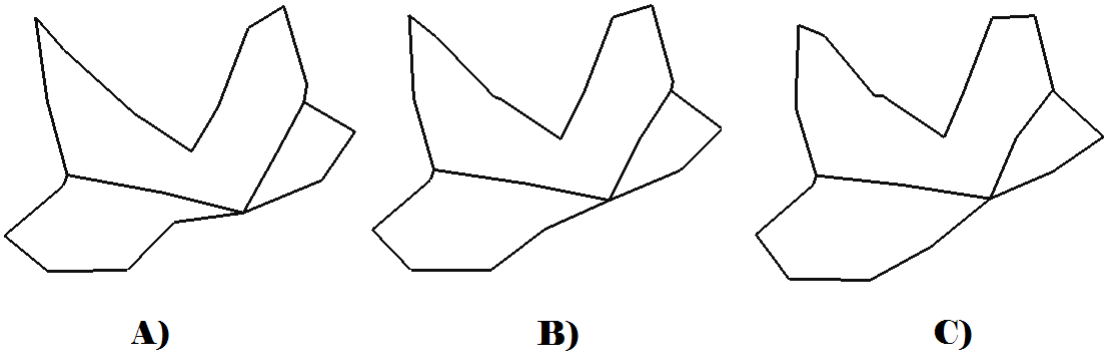

Figure T49. Variation of Zygomaxillary Landmarks along RW3 for the China Sample: A) Lower extreme of variation, B) Consensus form, C) Upper extreme of variation.

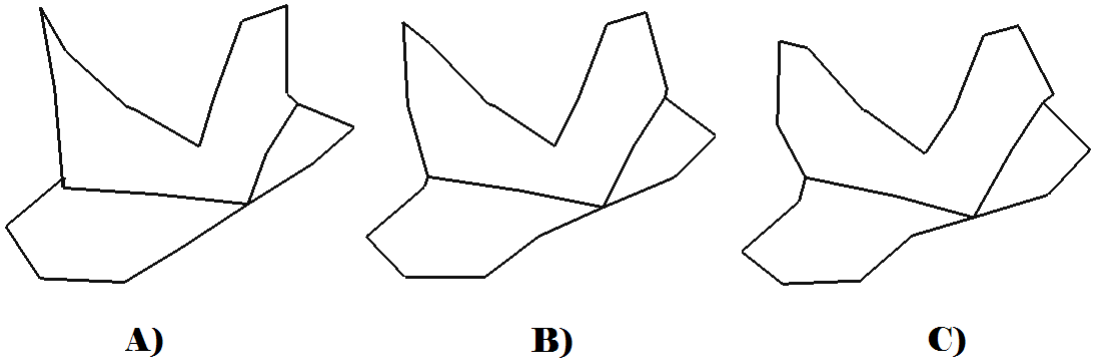

Figure T50. Variation of Zygomaxillary Landmarks along RW4 for the China Sample: A) Lower extreme of variation, B) Consensus form, C) Upper extreme of variation.

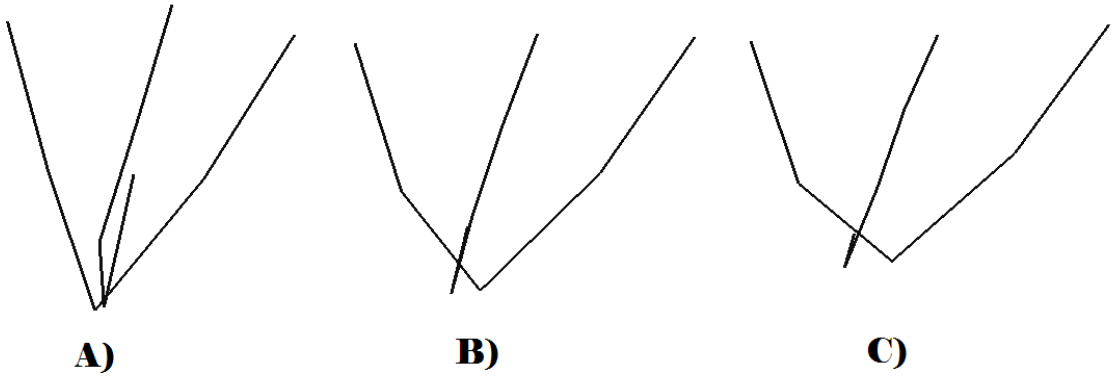

Figure T51. Variation of Mastoid Landmarks along RW1 for the China Sample: A) Lower extreme of variation, B) Consensus form, C) Upper extreme of variation.

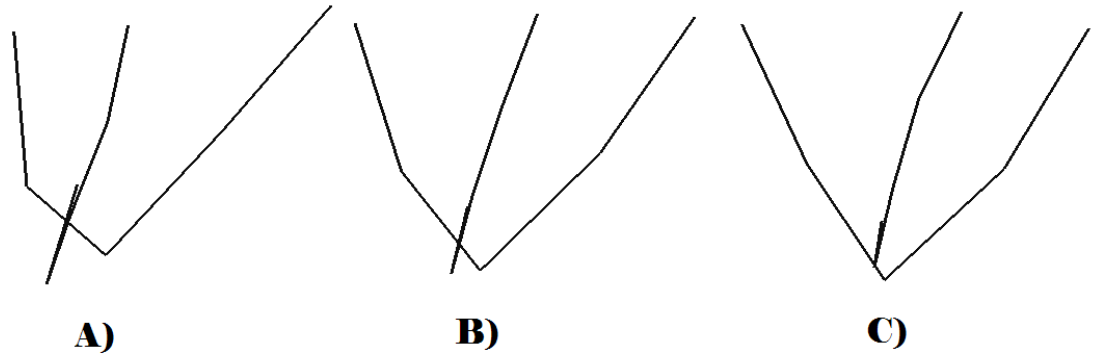

Figure T52. Variation of Mastoid Landmarks along RW2 for the China Sample: A) Lower extreme of variation, B) Consensus form, C) Upper extreme of variation.

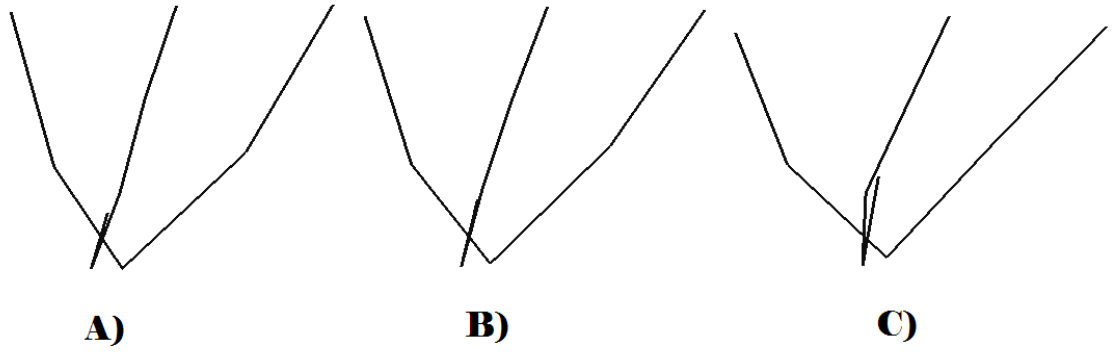

Figure T53. Variation of Mastoid Landmarks along RW3 for the China Sample: A) Lower extreme of variation, B) Consensus form, C) Upper extreme of variation.

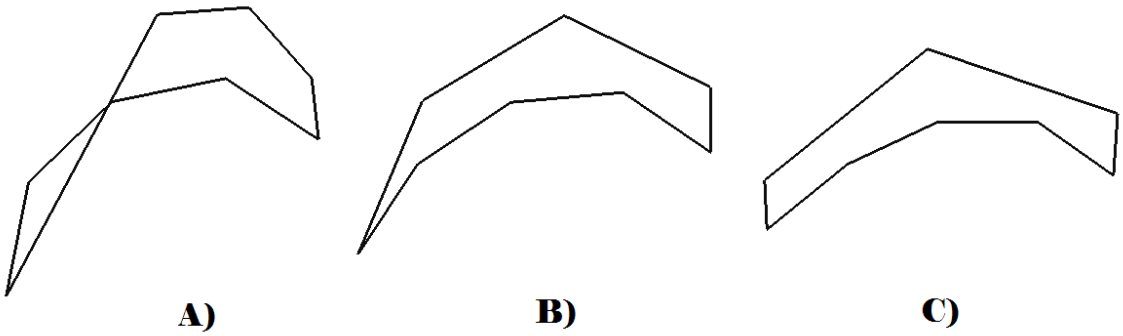

Figure T54. Variation of Occipital Landmarks along RW1 for the China Sample: A) Lower extreme of variation, B) Consensus form, C) Upper extreme of variation.

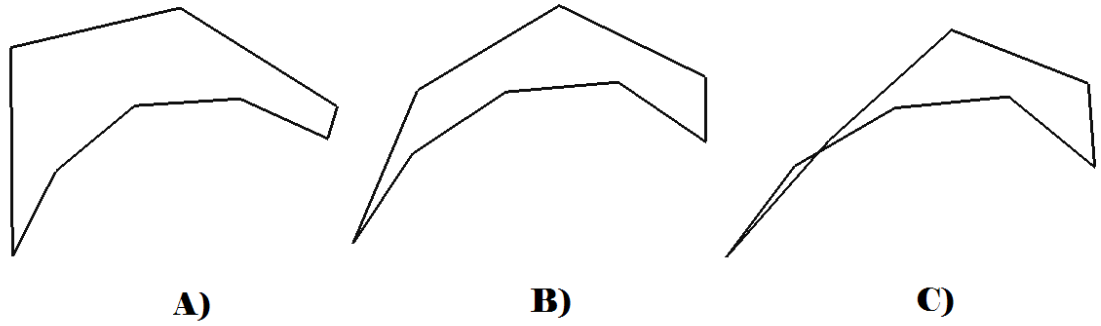

Figure T55. Variation of Occipital Landmarks along RW2 for the China Sample: A) Lower extreme of variation, B) Consensus form, C) Upper extreme of variation.

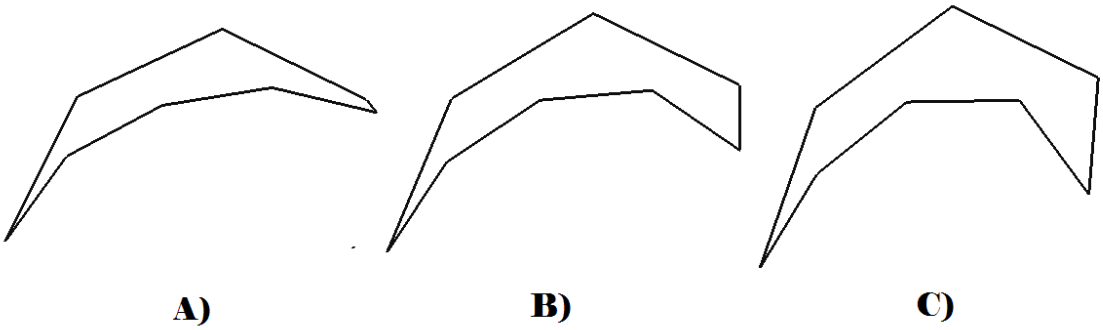

Figure T56. Variation of Occipital Landmarks along RW3 for the China Sample: A) Lower extreme of variation, B) Consensus form, C) Upper extreme of variation.

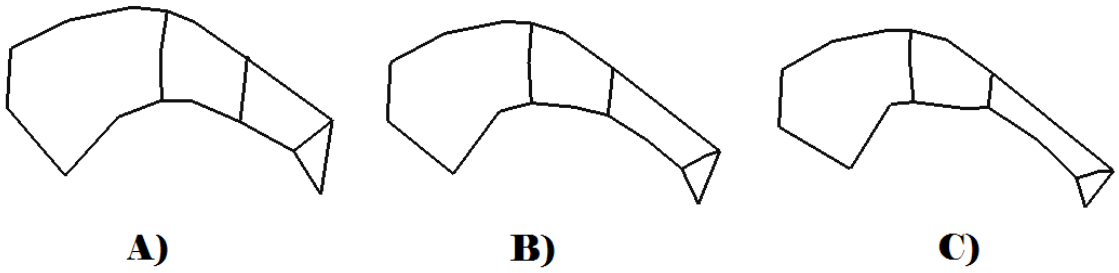

Figure T57. Variation of Supraorbital Landmarks along RW1 for the India Sample: A) Lower extreme of variation, B) Consensus form, C) Upper extreme of variation.

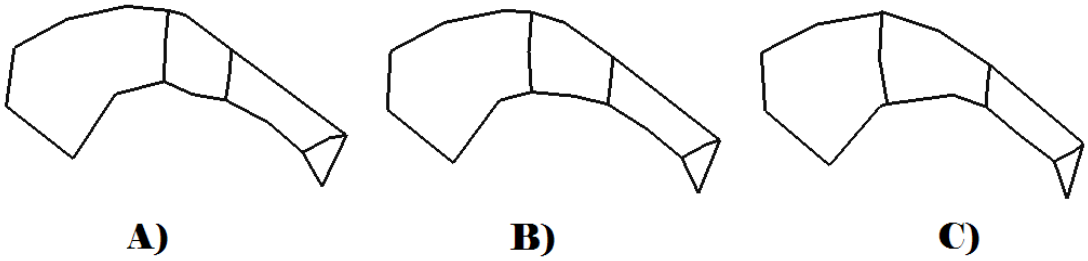

Figure T58. Variation of Supraorbital Landmarks along RW2 for the India Sample: A) Lower extreme of variation, B) Consensus form, C) Upper extreme of variation.

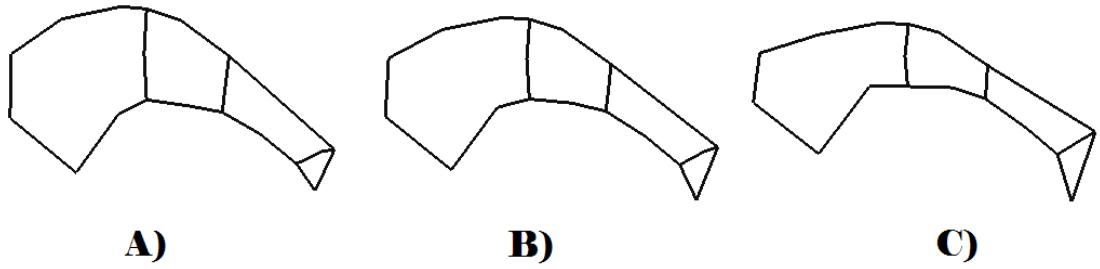

Figure T59. Variation of Supraorbital Landmarks along RW3 for the India Sample: A) Lower extreme of variation, B) Consensus form, C) Upper extreme of variation.

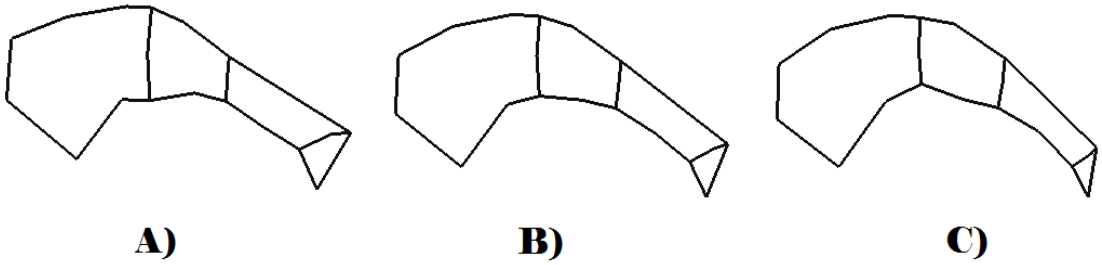

Figure T60. Variation of Supraorbital Landmarks along RW4 for the India Sample: A) Lower extreme of variation, B) Consensus form, C) Upper extreme of variation.

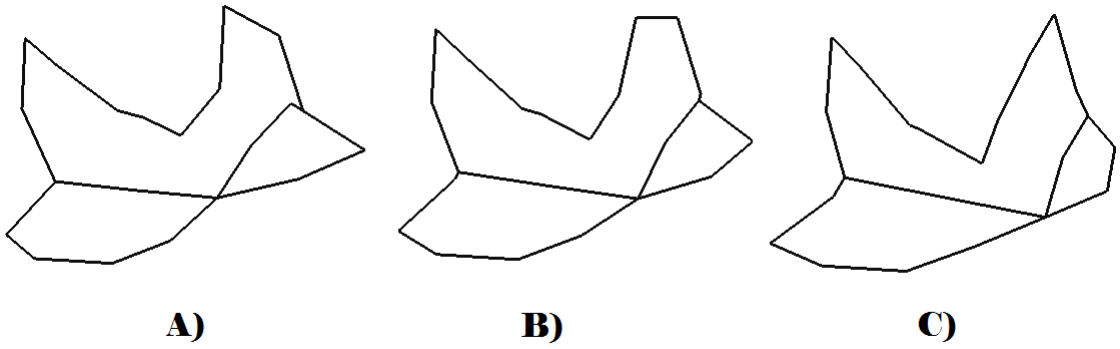

Figure T61. Variation of Zygomaxillary Landmarks along RW1 for the India Sample: A) Lower extreme of variation, B) Consensus form, C) Upper extreme of variation.

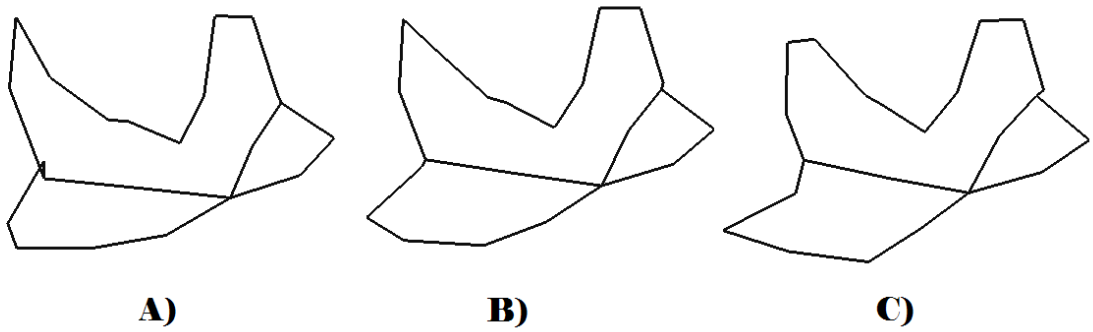

Figure T62. Variation of Zygomaxillary Landmarks along RW2 for the India Sample: A) Lower extreme of variation, B) Consensus form, C) Upper extreme of variation.

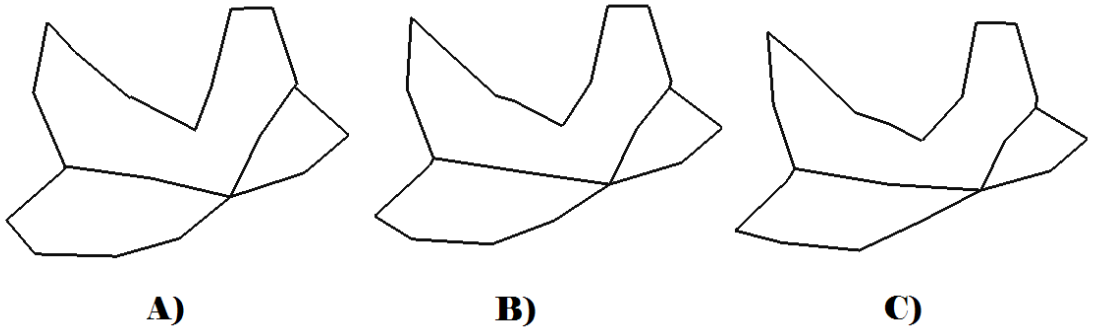

Figure T63. Variation of Zygomaxillary Landmarks along RW3 for the India Sample: A) Lower extreme of variation, B) Consensus form, C) Upper extreme of variation.

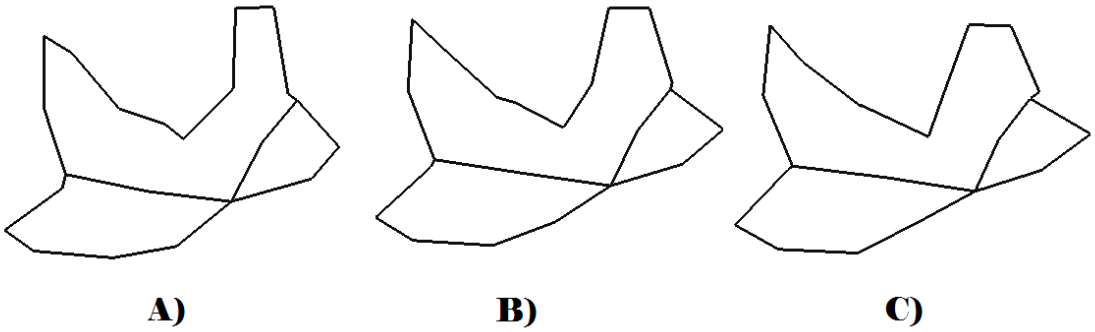

Figure T64. Variation of Zygomaxillary Landmarks along RW4 for the India Sample: A) Lower extreme of variation, B) Consensus form, C) Upper extreme of variation.

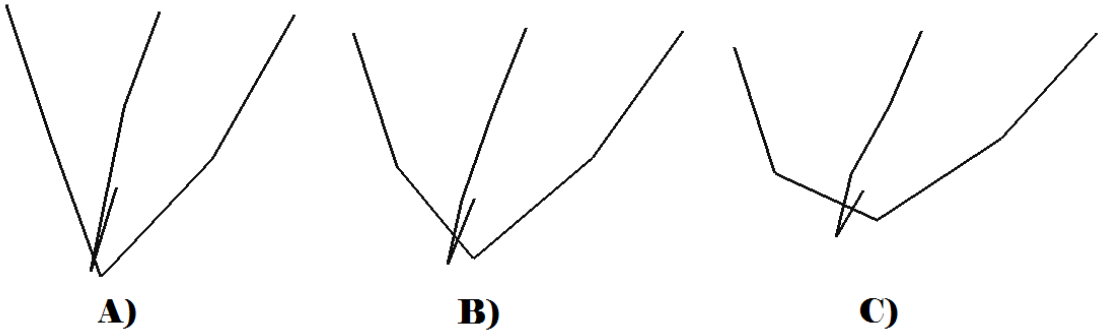

Figure T65. Variation of Mastoid Landmarks along RW1 for the India Sample: A) Lower extreme of variation, B) Consensus form, C) Upper extreme of variation.

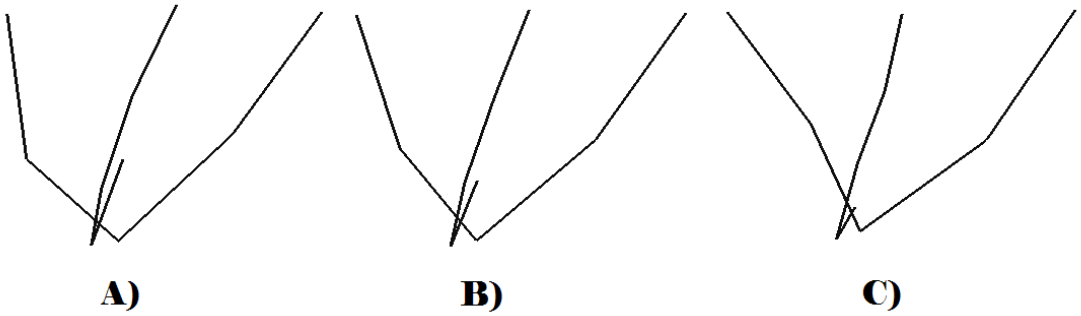

Figure T66. Variation of Mastoid Landmarks along RW2 for the India Sample: A) Lower extreme of variation, B) Consensus form, C) Upper extreme of variation.

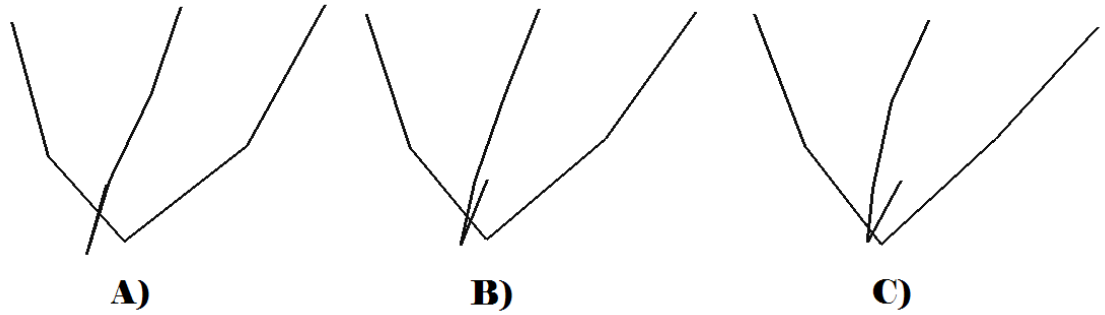

Figure T67. Variation of Mastoid Landmarks along RW3 for the India Sample: A) Lower extreme of variation, B) Consensus form, C) Upper extreme of variation.

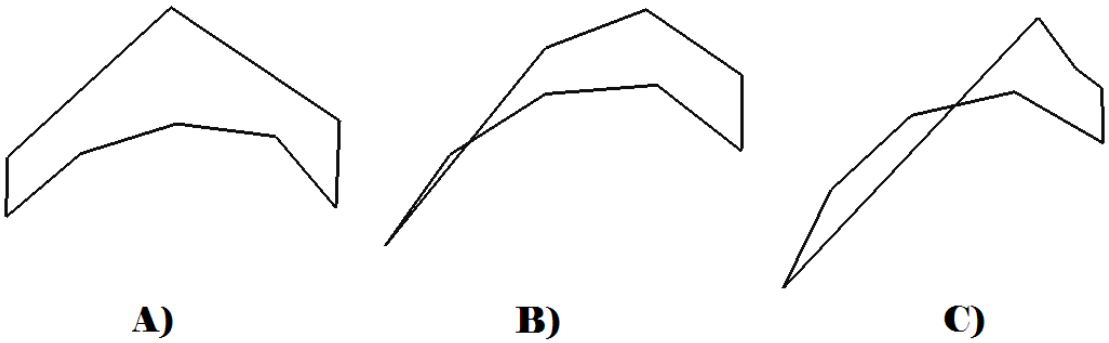

Figure T68. Variation of Occipital Landmarks along RW1 for the India Sample: A) Lower extreme of variation, B) Consensus form, C) Upper extreme of variation.

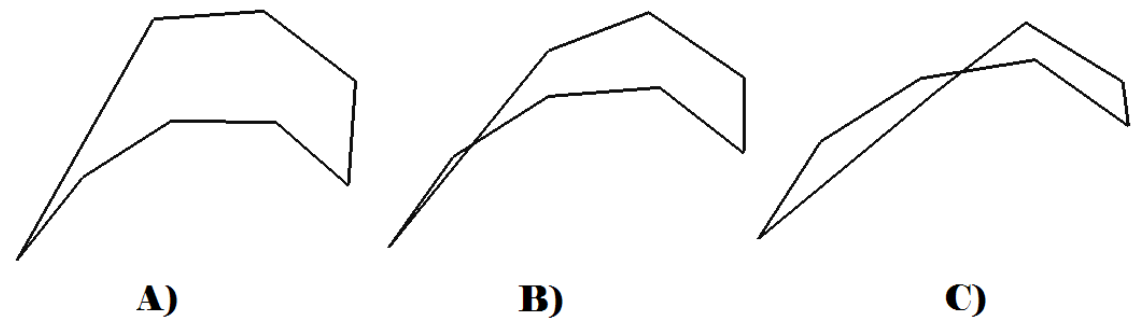

Figure T69. Variation of Occipital Landmarks along RW2 for the India Sample: A) Lower extreme of variation, B) Consensus form, C) Upper extreme of variation.

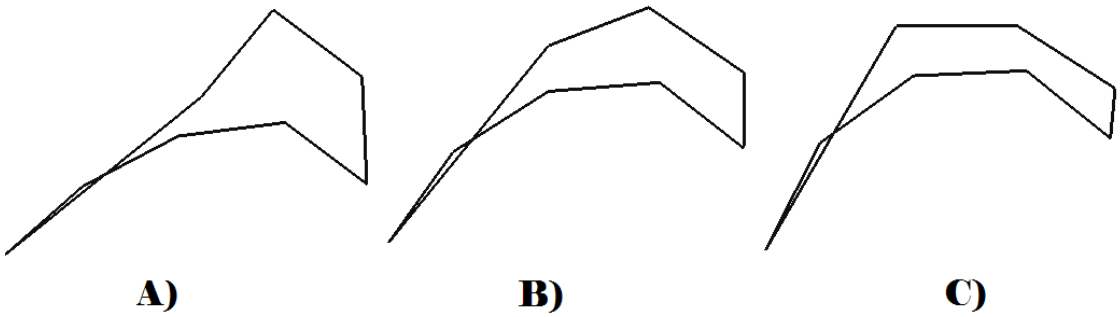

Figure T70. Variation of Occipital Landmarks along RW3 for the India Sample: A) Lower extreme of variation, B) Consensus form, C) Upper extreme of variation.

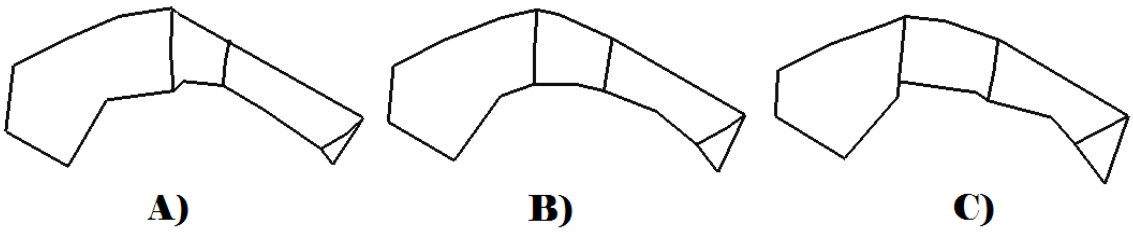

Figure T71. Variation of Supraorbital Landmarks along RW1 for the Khoisan Sample: A) Lower extreme of variation, B) Consensus form, C) Upper extreme of variation.

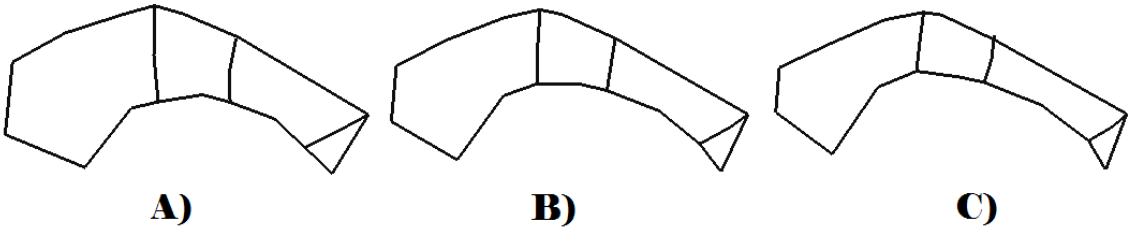

Figure T72. Variation of Supraorbital Landmarks along RW2 for the Khoisan Sample: A) Lower extreme of variation, B) Consensus form, C) Upper extreme of variation.

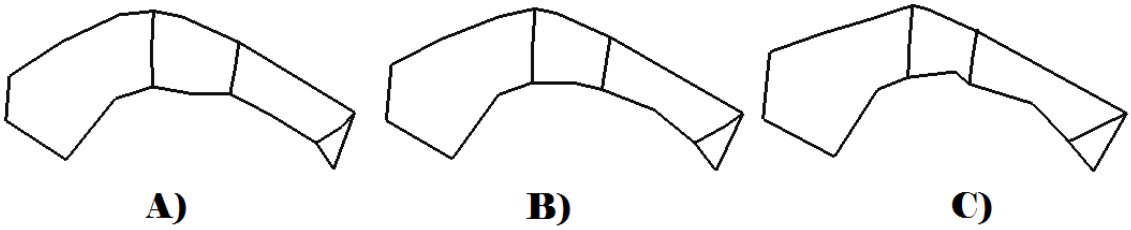

Figure T73. Variation of Supraorbital Landmarks along RW3 for the Khoisan Sample: A) Lower extreme of variation, B) Consensus form, C) Upper extreme of variation.

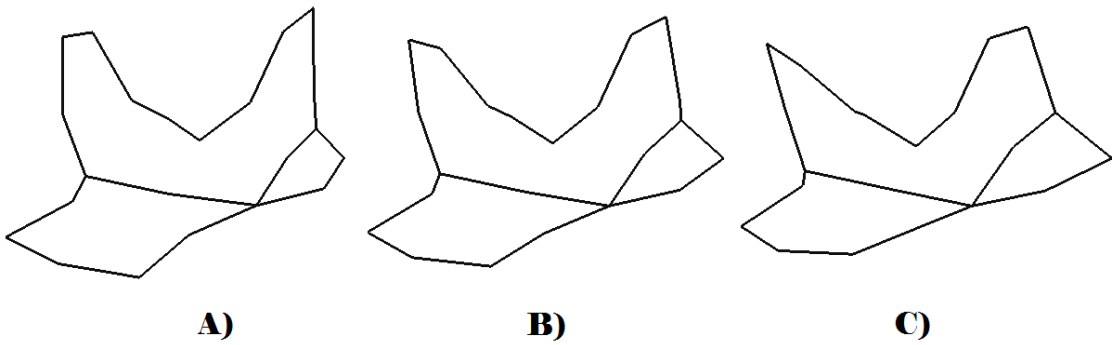

Figure T74. Variation of Zygomaxillary Landmarks along RW1 for the Khoisan Sample: A) Lower extreme of variation, B) Consensus form, C) Upper extreme of variation.

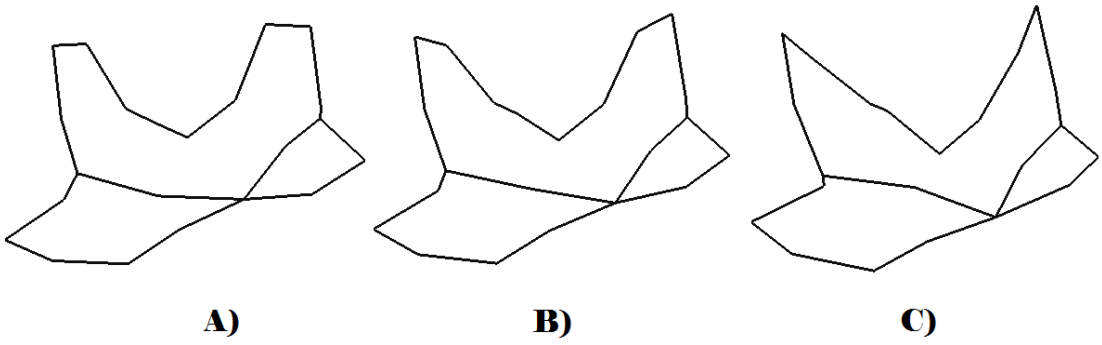

Figure T75. Variation of Zygomaxillary Landmarks along RW2 for the Khoisan Sample: A) Lower extreme of variation, B) Consensus form, C) Upper extreme of variation.

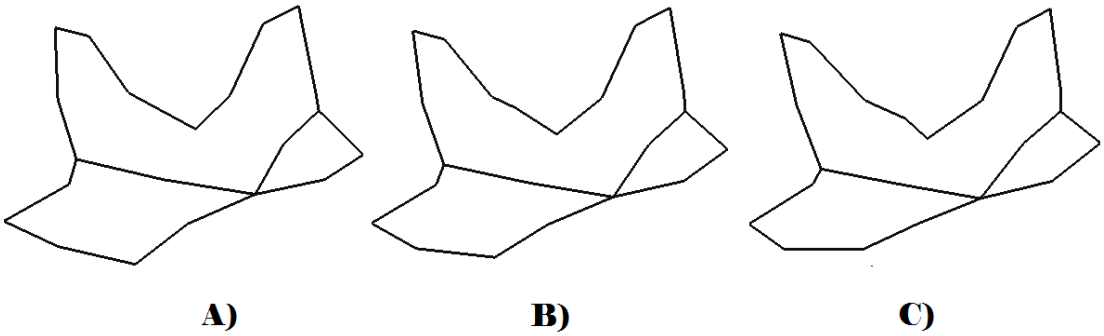

Figure T76. Variation of Zygomaxillary Landmarks along RW3 for the Khoisan Sample: A) Lower extreme of variation, B) Consensus form, C) Upper extreme of variation.

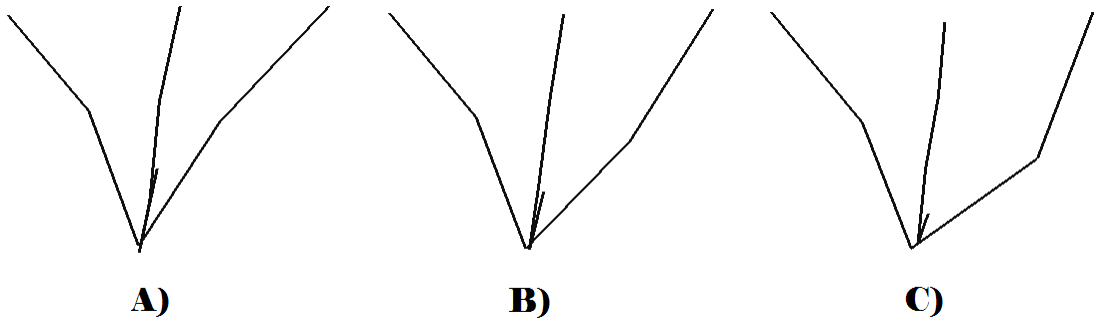

Figure T77. Variation of Mastoid Landmarks along RW1 for the Khoisan Sample: A) Lower extreme of variation, B) Consensus form, C) Upper extreme of variation.

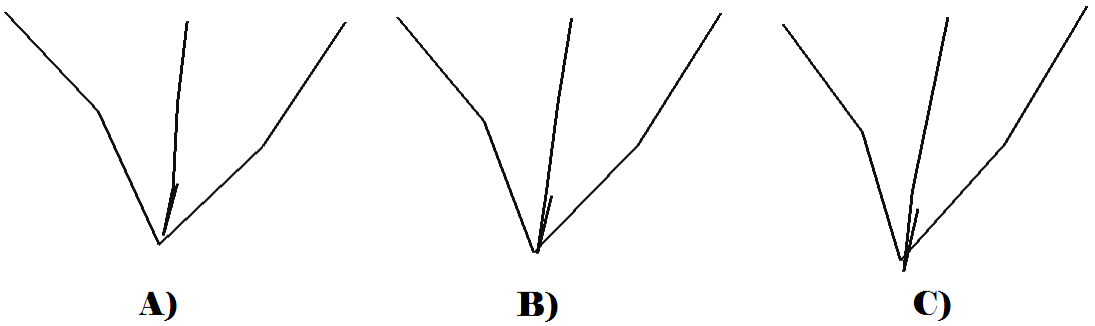

Figure T78. Variation of Mastoid Landmarks along RW2 for the Khoisan Sample: A) Lower extreme of variation, B) Consensus form, C) Upper extreme of variation.

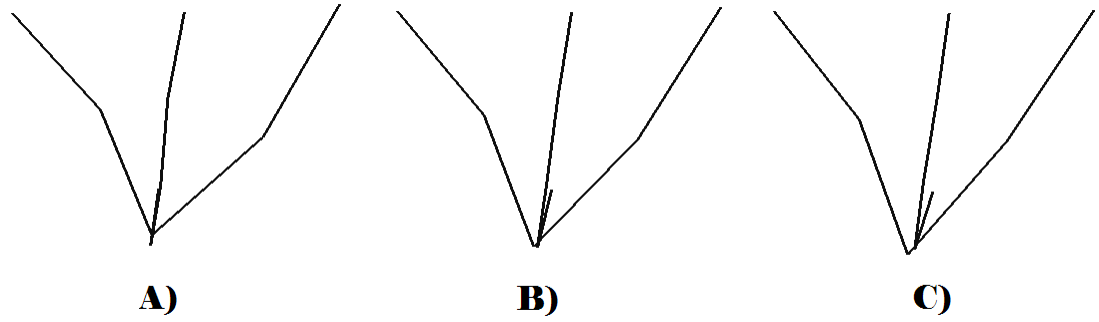

Figure T79. Variation of Mastoid Landmarks along RW3 for the Khoisan Sample: A) Lower extreme of variation, B) Consensus form, C) Upper extreme of variation.

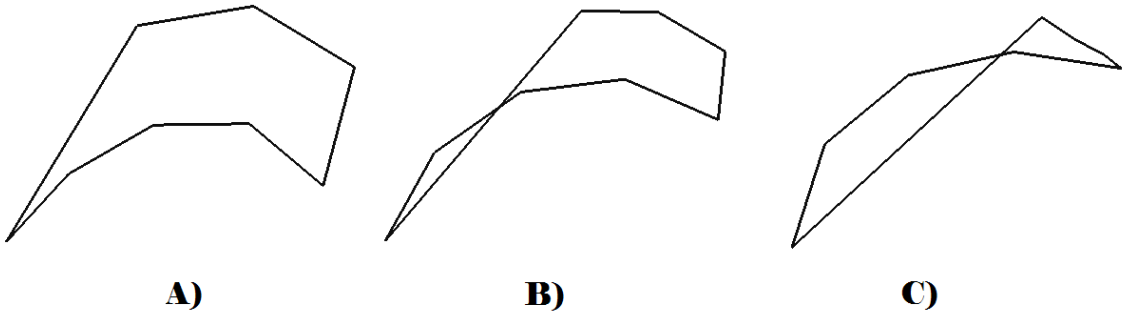

Figure T80. Variation of Occipital Landmarks along RW1 for the Khoisan Sample: A) Lower extreme of variation, B) Consensus form, C) Upper extreme of variation.

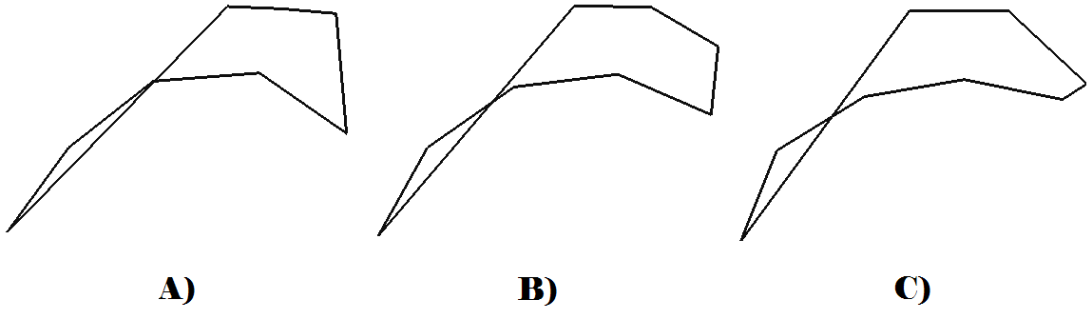

Figure T81. Variation of Occipital Landmarks along RW2 for the Khoisan Sample: A) Lower extreme of variation, B) Consensus form, C) Upper extreme of variation.

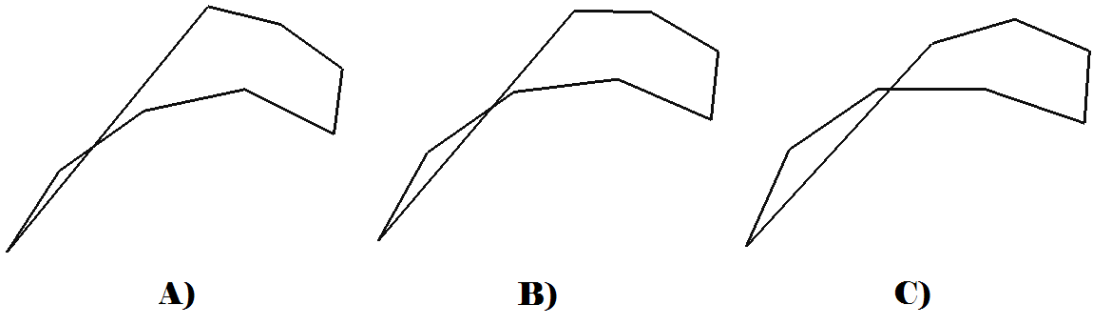

Figure T82. Variation of Occipital Landmarks along RW3 for the Khoisan Sample: A) Lower extreme of variation, B) Consensus form, C) Upper extreme of variation.

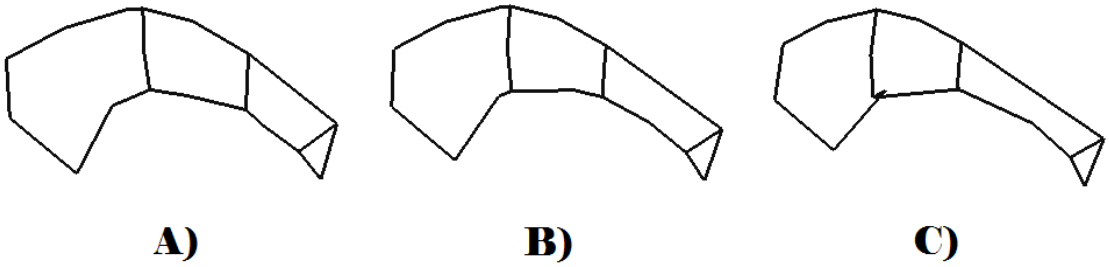

Figure T83. Variation of Supraorbital Landmarks along RW1 for the Medit-Near East Sample: A) Lower extreme of variation, B) Consensus form, C) Upper extreme of variation.

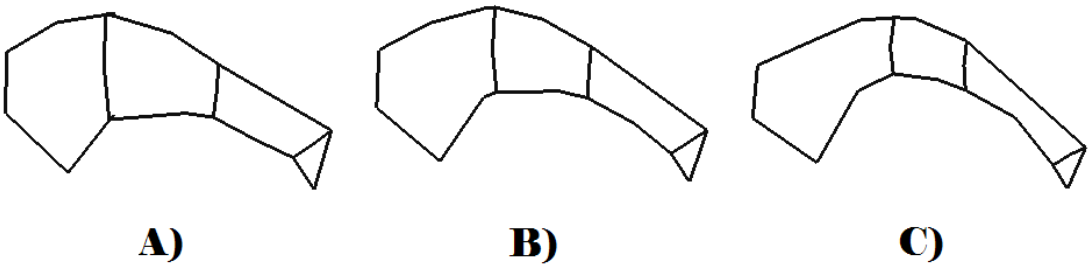

Figure T84. Variation of Supraorbital Landmarks along RW2 for the Medit-Near East Sample: A) Lower extreme of variation, B) Consensus form, C) Upper extreme of variation.

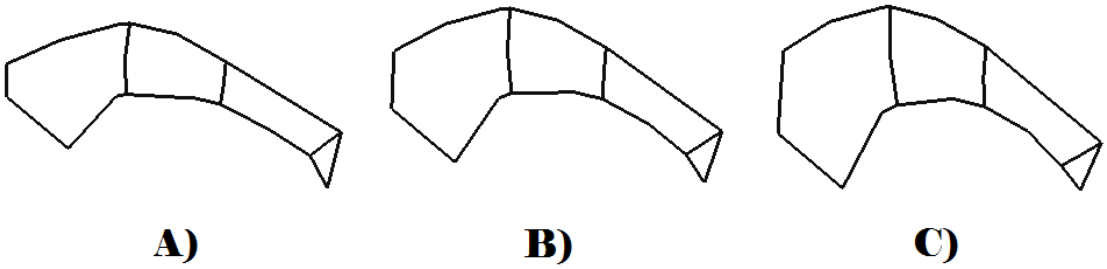

Figure T85. Variation of Supraorbital Landmarks along RW3 for the Medit-Near East Sample: A) Lower extreme of variation, B) Consensus form, C) Upper extreme of variation.

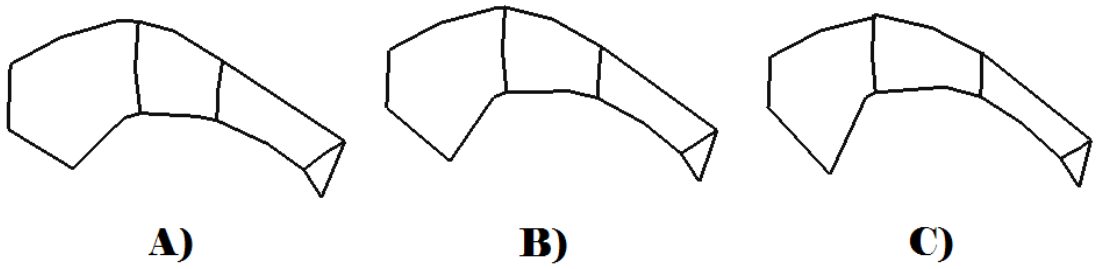

Figure T86. Variation of Supraorbital Landmarks along RW4 for the Medit-Near East Sample: A) Lower extreme of variation, B) Consensus form, C) Upper extreme of variation.

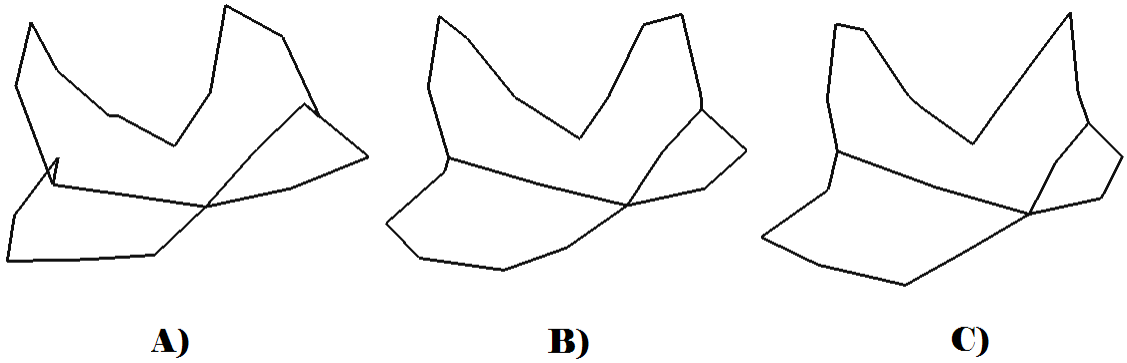

Figure T87. Variation of Zygomaxillary Landmarks along RW1 for the Medit-Near East Sample: A) Lower extreme of variation, B) Consensus form, C) Upper extreme of variation.

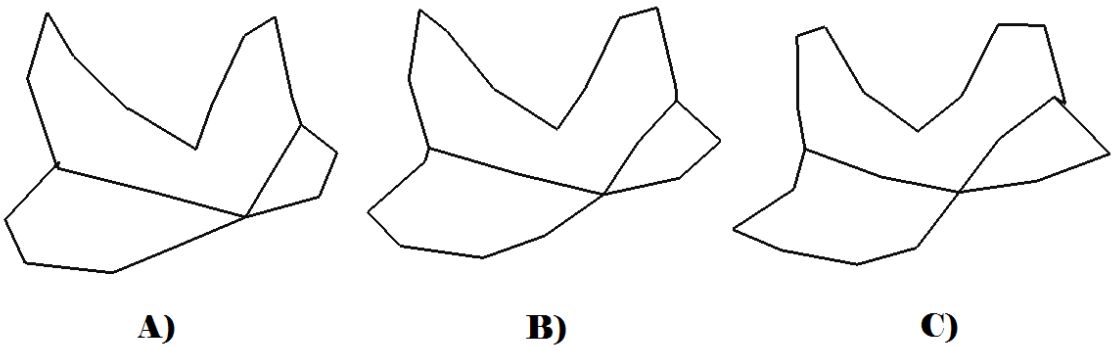

Figure T88. Variation of Zygomaxillary Landmarks along RW2 for the Medit-Near East Sample: A) Lower extreme of variation, B) Consensus form, C) Upper extreme of variation.

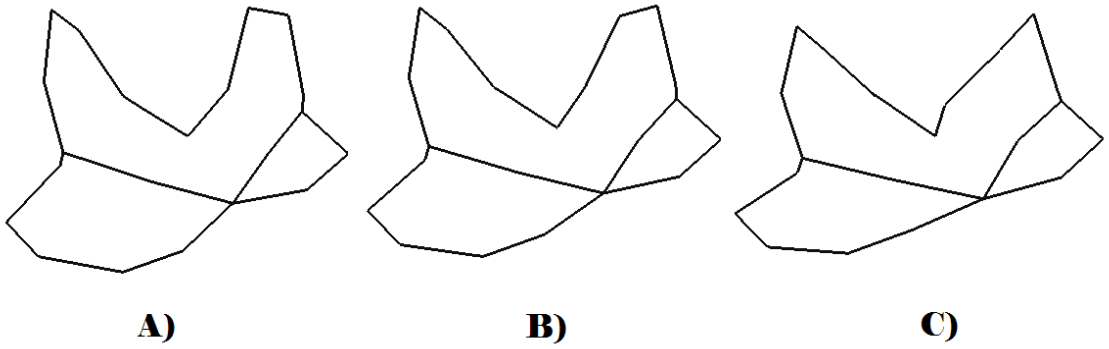

Figure T89. Variation of Zygomaxillary Landmarks along RW3 for the Medit-Near East Sample: A) Lower extreme of variation, B) Consensus form, C) Upper extreme of variation.

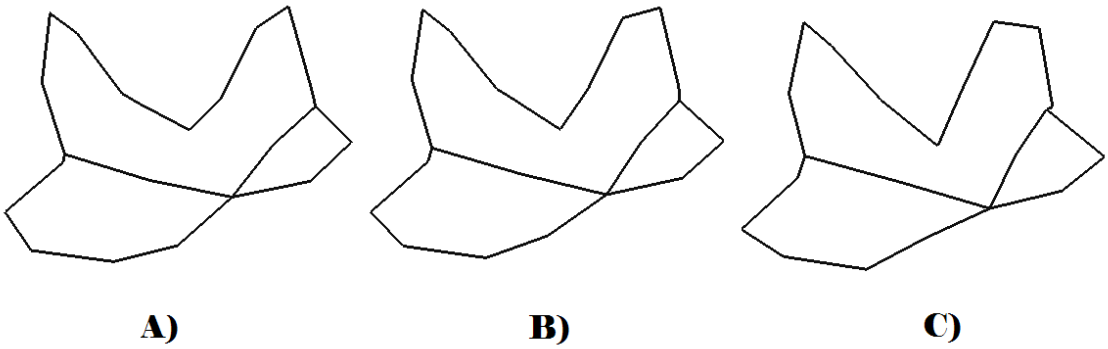

Figure T90. Variation of Zygomaxillary Landmarks along RW4 for the Medit-Near East Sample: A) Lower extreme of variation, B) Consensus form, C) Upper extreme of variation.

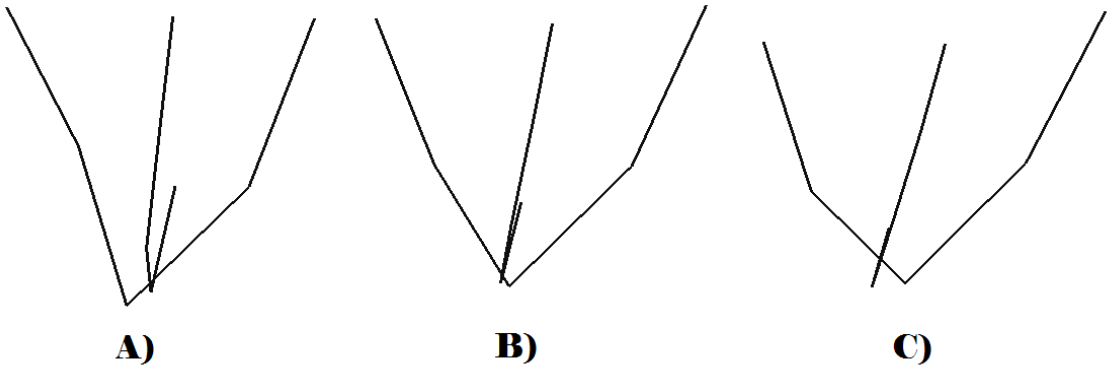

Figure T91. Variation of Mastoid Landmarks along RW1 for the Medit-Near East Sample: A) Lower extreme of variation, B) Consensus form, C) Upper extreme of variation.

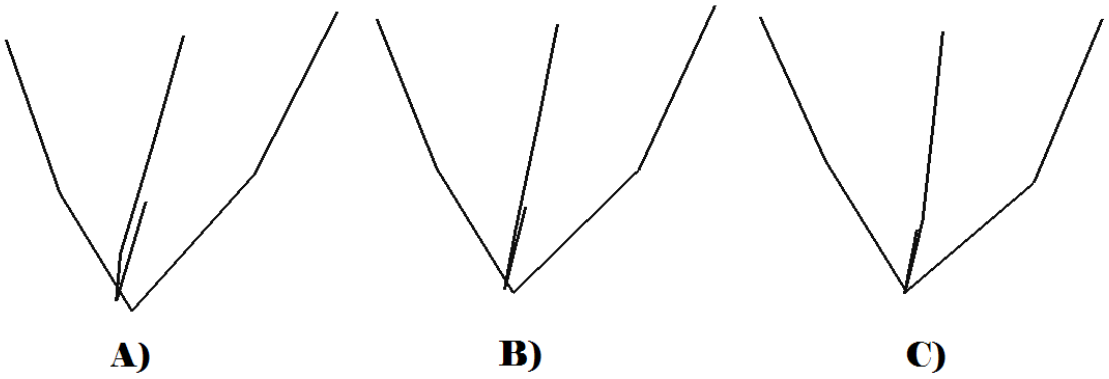

Figure T92. Variation of Mastoid Landmarks along RW2 for the Medit-Near East Sample: A) Lower extreme of variation, B) Consensus form, C) Upper extreme of variation.

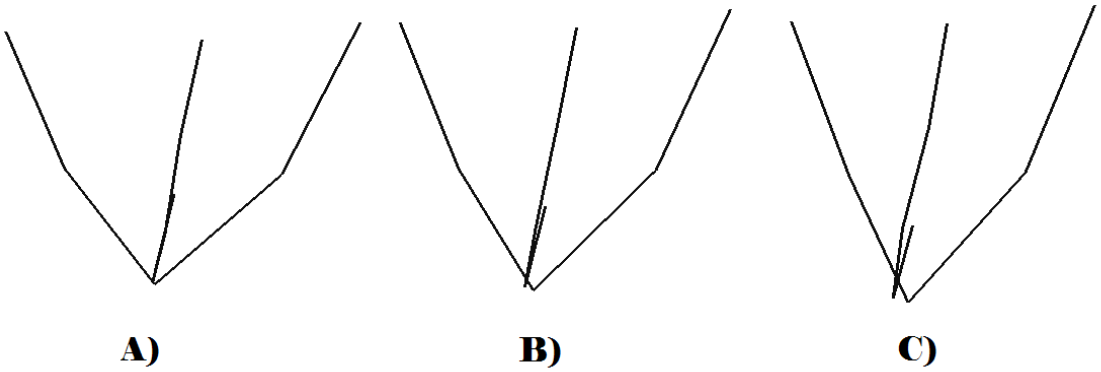

Figure T93. Variation of Mastoid Landmarks along RW3 for the Medit-Near East Sample: A) Lower extreme of variation, B) Consensus form, C) Upper extreme of variation.

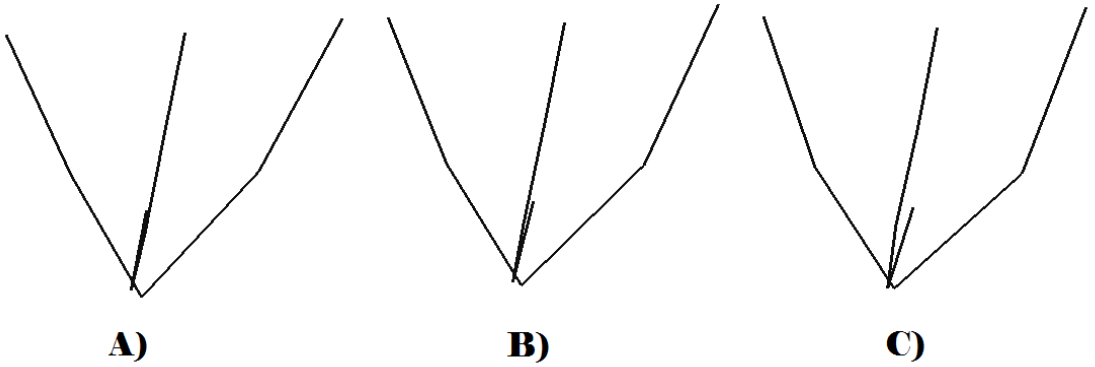

Figure T94. Variation of Mastoid Landmarks along RW4 for the Medit-Near East Sample: A) Lower extreme of variation, B) Consensus form, C) Upper extreme of variation.

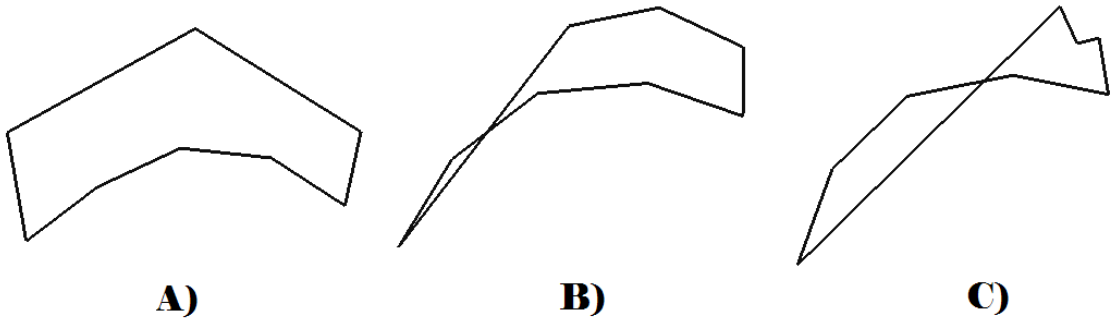

Figure T95. Variation of Occipital Landmarks along RW1 for the Medit-Near East Sample: A) Lower extreme of variation, B) Consensus form, C) Upper extreme of variation.

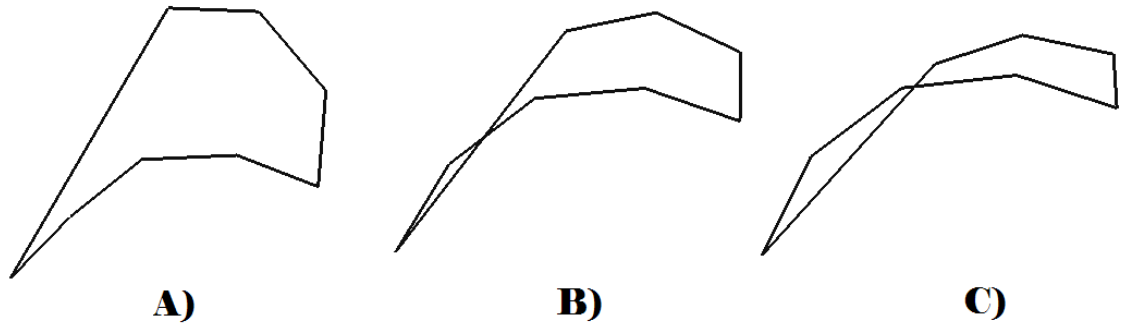

Figure T96. Variation of Occipital Landmarks along RW2 for the Medit-Near East Sample: A) Lower extreme of variation, B) Consensus form, C) Upper extreme of variation.

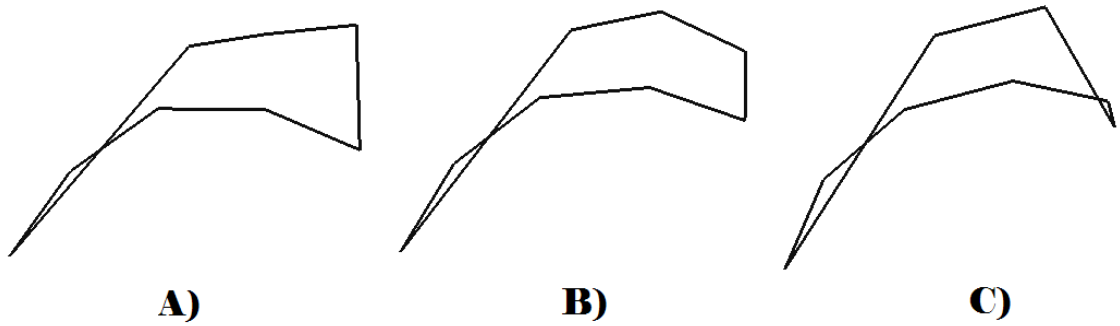

Figure T97. Variation of Occipital Landmarks along RW3 for the Medit-Near East Sample: A) Lower extreme of variation, B) Consensus form, C) Upper extreme of variation.

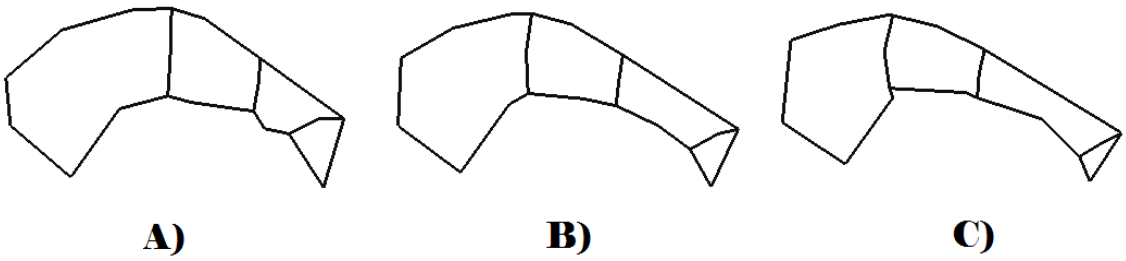

Figure T98. Variation of Supraorbital Landmarks along RW1 for the New Guinea Sample: A) Lower extreme of variation, B) Consensus form, C) Upper extreme of variation.

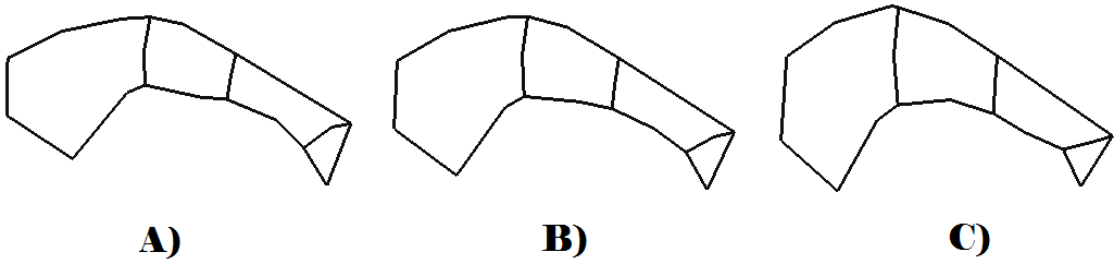

Figure T99. Variation of Supraorbital Landmarks along RW2 for the New Guinea Sample: A) Lower extreme of variation, B) Consensus form, C) Upper extreme of variation.

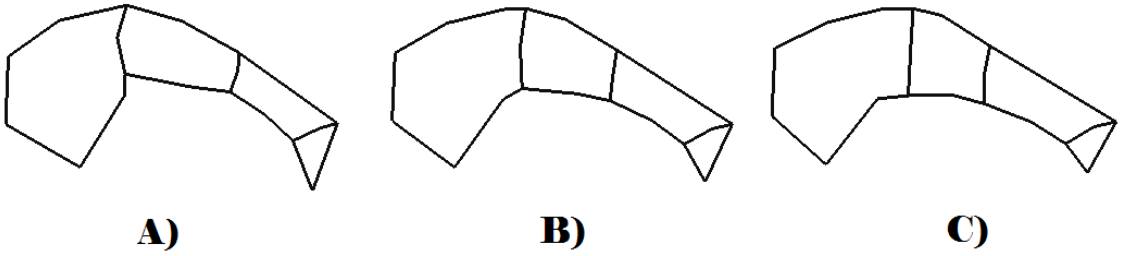

Figure T100. Variation of Supraorbital Landmarks along RW3 for the New Guinea Sample: A) Lower extreme of variation, B) Consensus form, C) Upper extreme of variation.

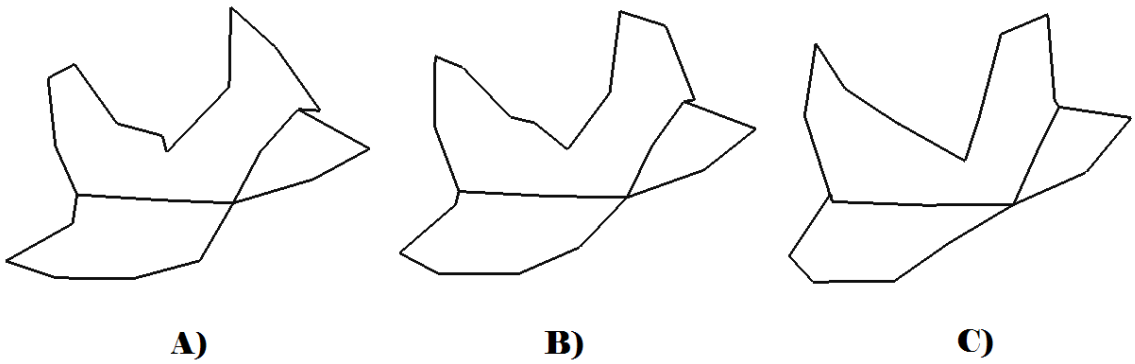

Figure T101. Variation of Zygomaxillary Landmarks along RW1 for the New Guinea Sample: A) Lower extreme of variation, B) Consensus form, C) Upper extreme of variation.

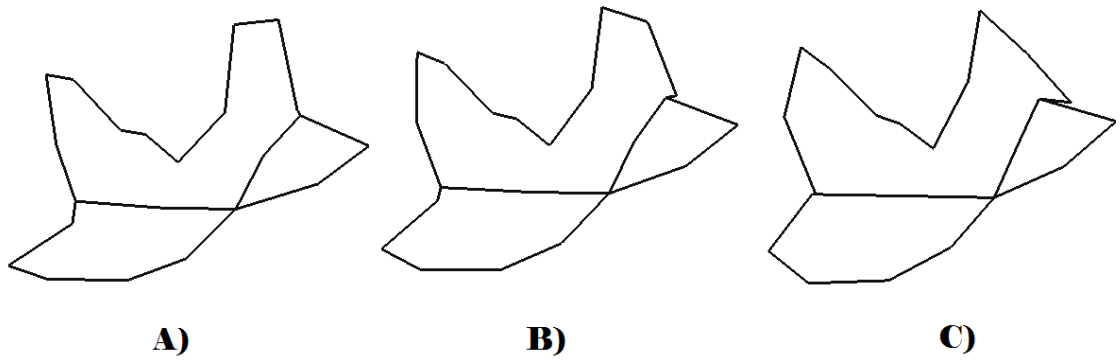

Figure T102. Variation of Zygomaxillary Landmarks along RW2 for the New Guinea Sample: A) Lower extreme of variation, B) Consensus form, C) Upper extreme of variation.

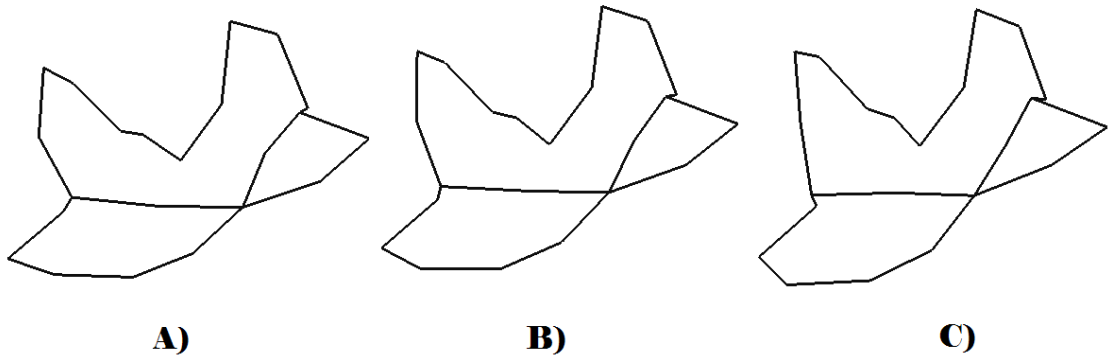

Figure T103. Variation of Zygomaxillary Landmarks along RW3 for the New Guinea Sample: A) Lower extreme of variation, B) Consensus form, C) Upper extreme of variation.

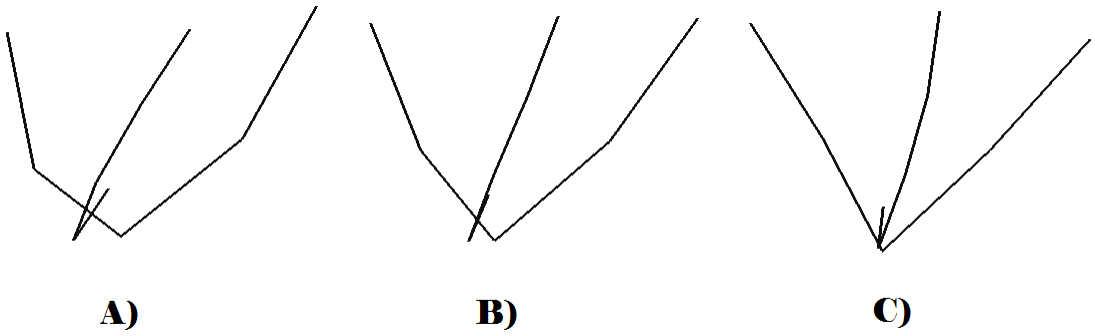

Figure T104. Variation of Mastoid Landmarks along RW1 for the New Guinea Sample: A) Lower extreme of variation, B) Consensus form, C) Upper extreme of variation.

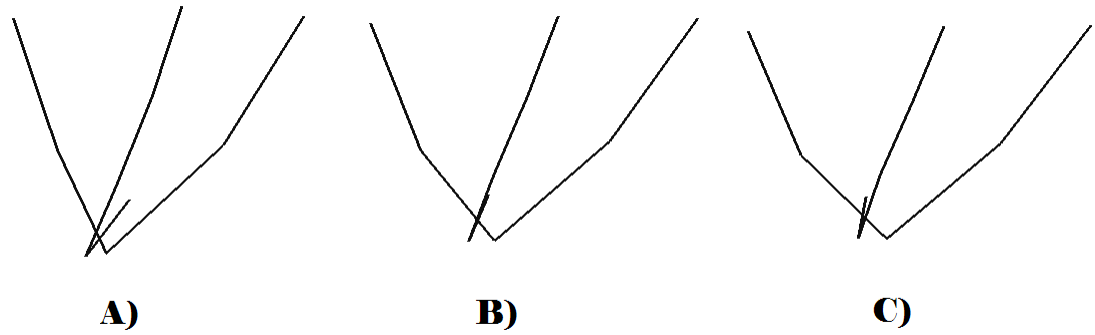

Figure T105. Variation of Mastoid Landmarks along RW2 for the New Guinea Sample: A) Lower extreme of variation, B) Consensus form, C) Upper extreme of variation.

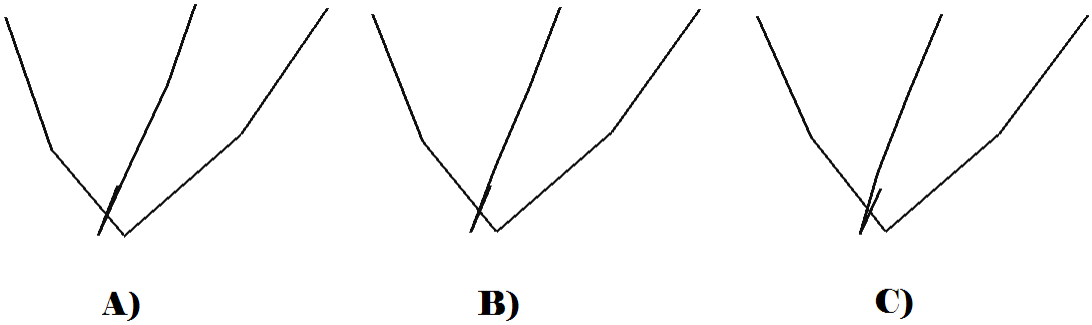

Figure T106. Variation of Mastoid Landmarks along RW3 for the New Guinea Sample: A) Lower extreme of variation, B) Consensus form, C) Upper extreme of variation.

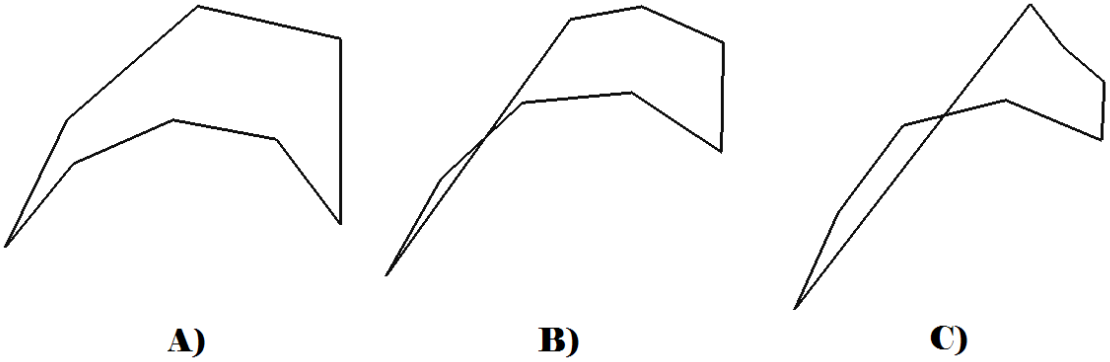

Figure T107. Variation of Occipital Landmarks along RW1 for the New Guinea Sample: A) Lower extreme of variation, B) Consensus form, C) Upper extreme of variation.

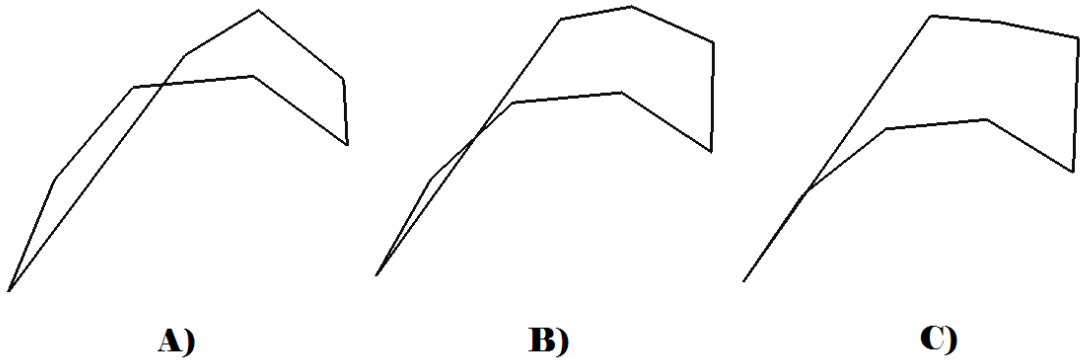

Figure T108. Variation of Occipital Landmarks along RW2 for the New Guinea Sample: A) Lower extreme of variation, B) Consensus form, C) Upper extreme of variation.

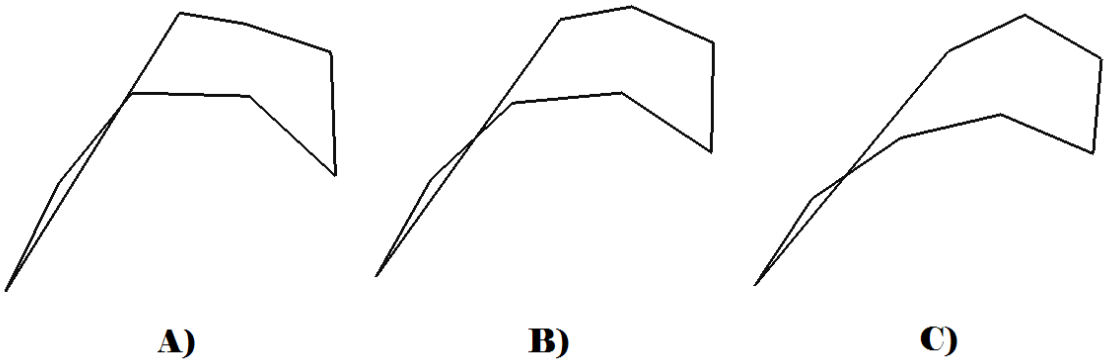

Figure T109. Variation of Occipital Landmarks along RW3 for the New Guinea Sample: A) Lower extreme of variation, B) Consensus form, C) Upper extreme of variation.

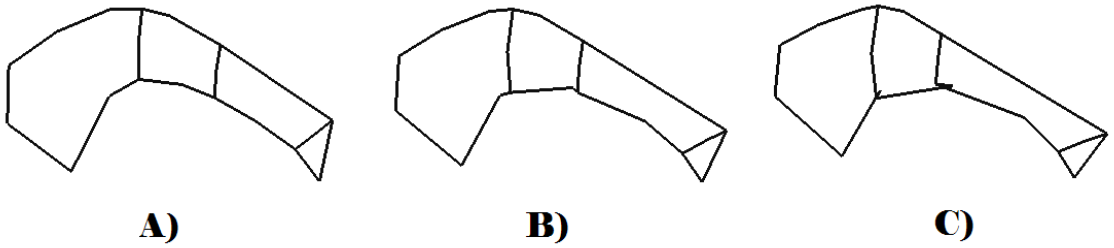

Figure T110. Variation of Supraorbital Landmarks along RW1 for the North Africa Sample: A) Lower extreme of variation, B) Consensus form, C) Upper extreme of variation.

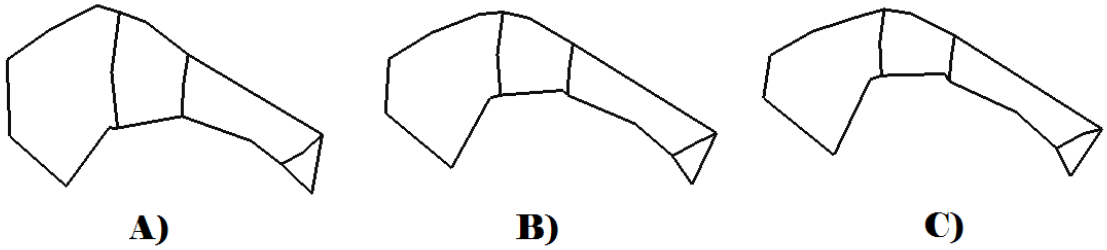

Figure T111. Variation of Supraorbital Landmarks along RW2 for the North Africa Sample: A) Lower extreme of variation, B) Consensus form, C) Upper extreme of variation.

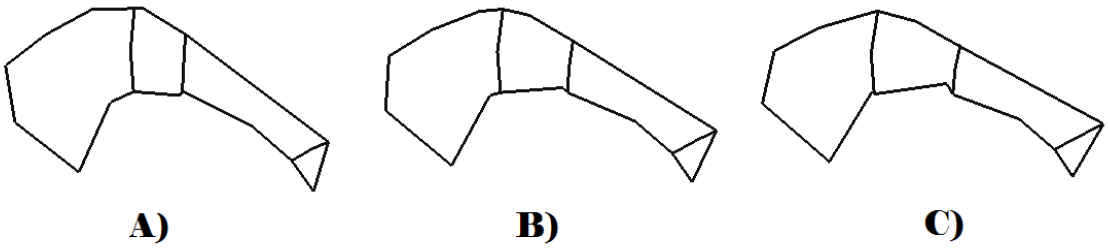

Figure T112. Variation of Supraorbital Landmarks along RW3 for the North Africa Sample: A) Lower extreme of variation, B) Consensus form, C) Upper extreme of variation.

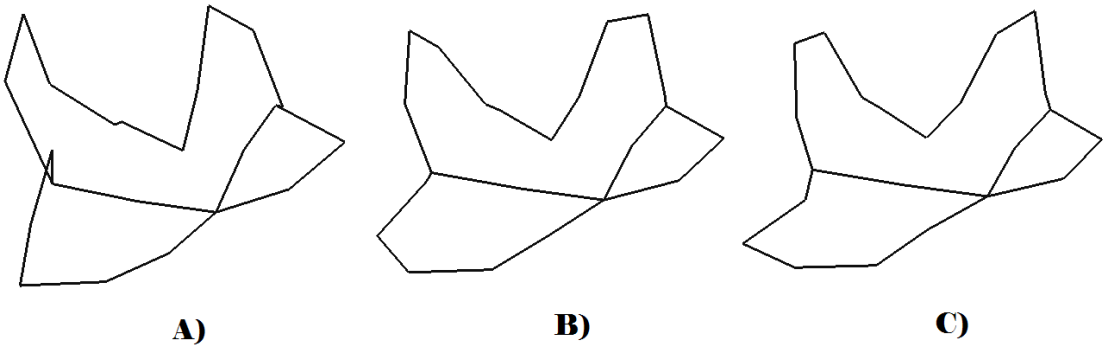

Figure T113. Variation of Zygomaxillary Landmarks along RW1 for the North African Sample: A) Lower extreme of variation, B) Consensus form, C) Upper extreme of variation.

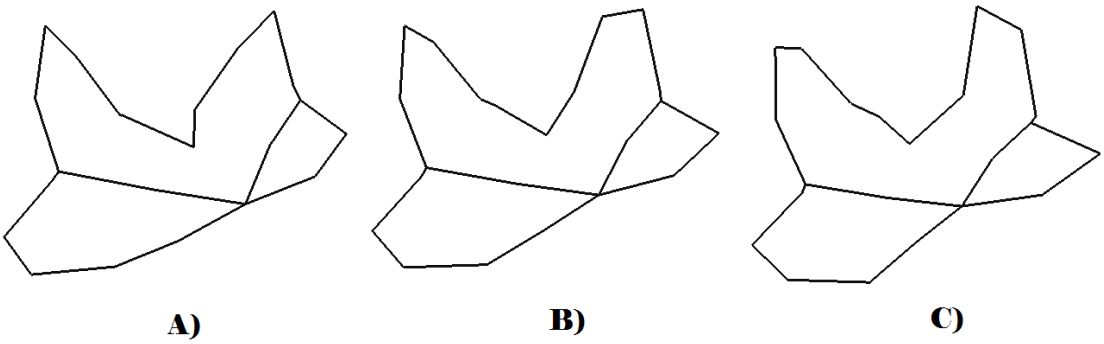

Figure T114. Variation of Zygomaxillary Landmarks along RW2 for the North African Sample: A) Lower extreme of variation, B) Consensus form, C) Upper extreme of variation.

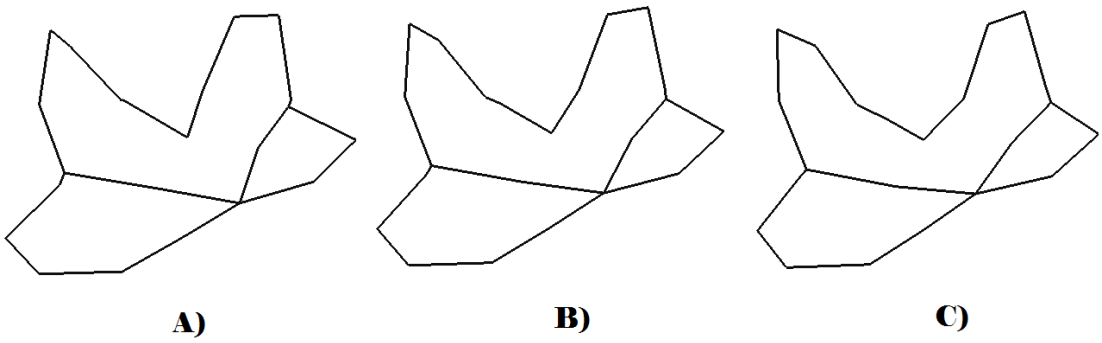

Figure T115. Variation of Zygomaxillary Landmarks along RW3 for the North African Sample: A) Lower extreme of variation, B) Consensus form, C) Upper extreme of variation.

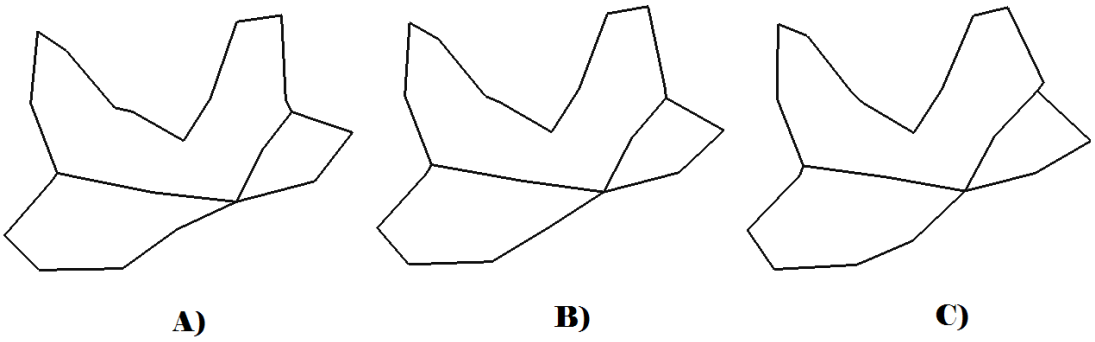

Figure T116. Variation of Zygomaxillary Landmarks along RW4 for the North African Sample: A) Lower extreme of variation, B) Consensus form, C) Upper extreme of variation.

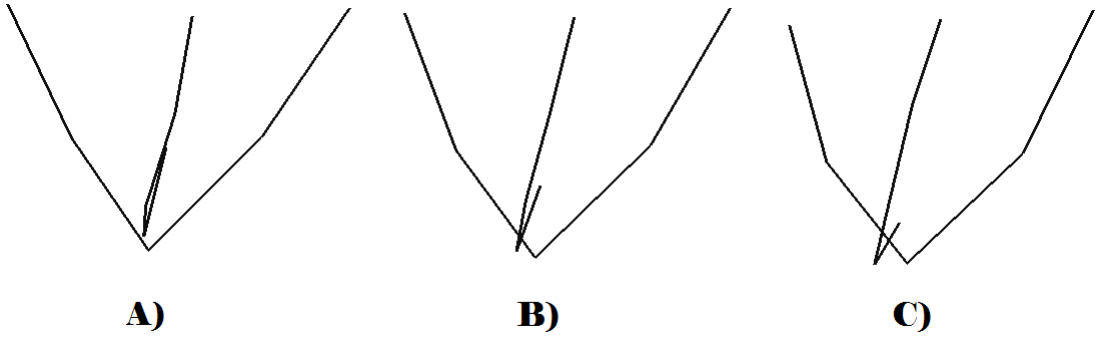

Figure T117. Variation of Mastoid Landmarks along RW1 for the North African Sample: A) Lower extreme of variation, B) Consensus form, C) Upper extreme of variation.

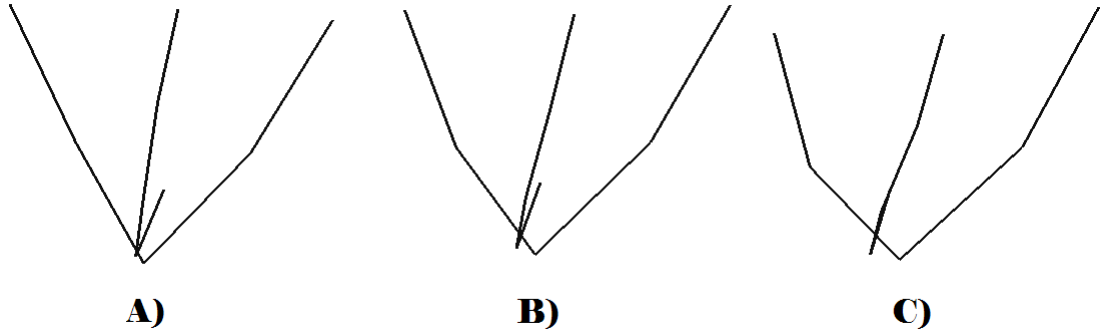

Figure T118. Variation of Mastoid Landmarks along RW2 for the North African Sample: A) Lower extreme of variation, B) Consensus form, C) Upper extreme of variation.

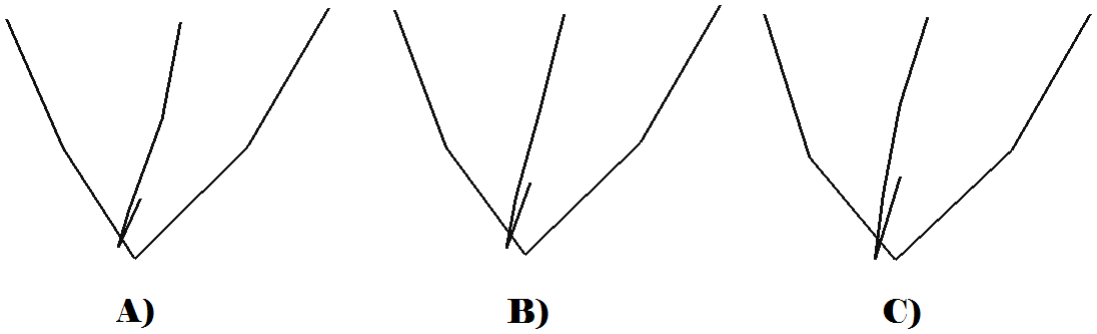

Figure T119. Variation of Mastoid Landmarks along RW3 for the North African Sample: A) Lower extreme of variation, B) Consensus form, C) Upper extreme of variation.

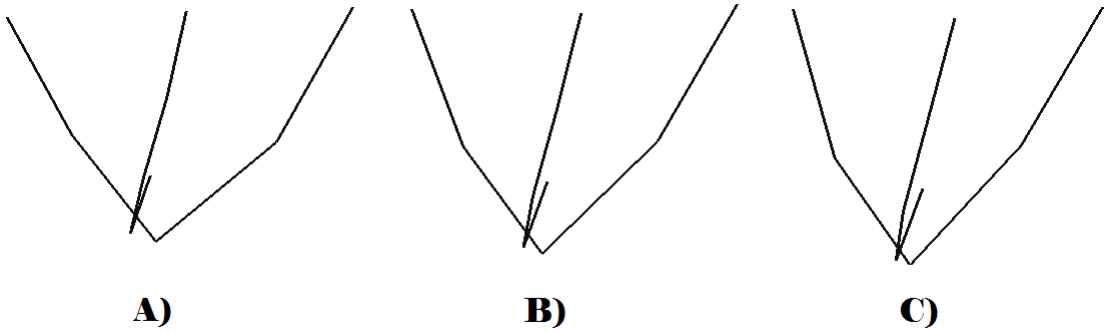

Figure T120. Variation of Mastoid Landmarks along RW4 for the North African Sample: A) Lower extreme of variation, B) Consensus form, C) Upper extreme of variation.

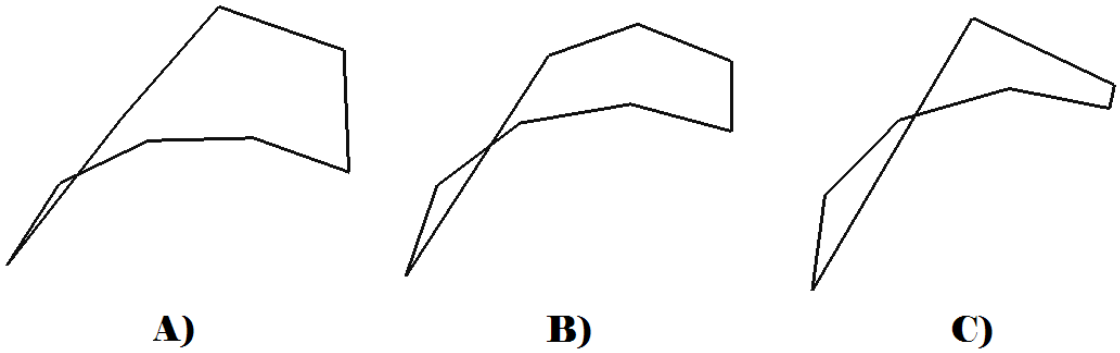

Figure T121. Variation of Occipital Landmarks along RW1 for the North African Sample: A) Lower extreme of variation, B) Consensus form, C) Upper extreme of variation.

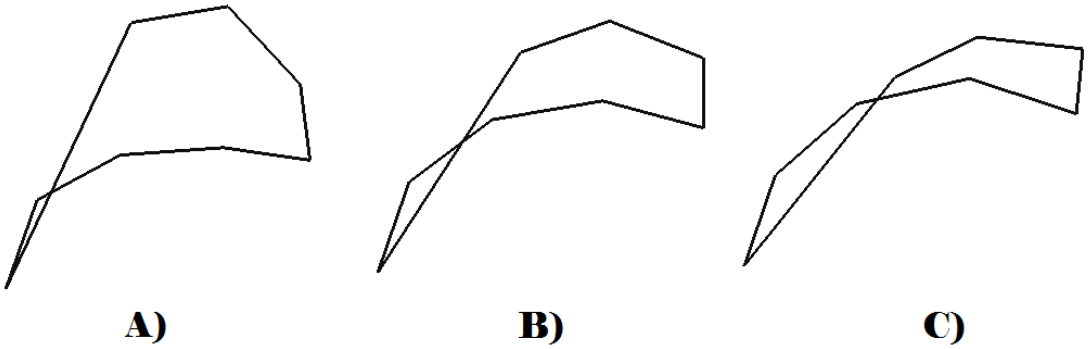

Figure T122. Variation of Occipital Landmarks along RW2 for the North African Sample: A) Lower extreme of variation, B) Consensus form, C) Upper extreme of variation.

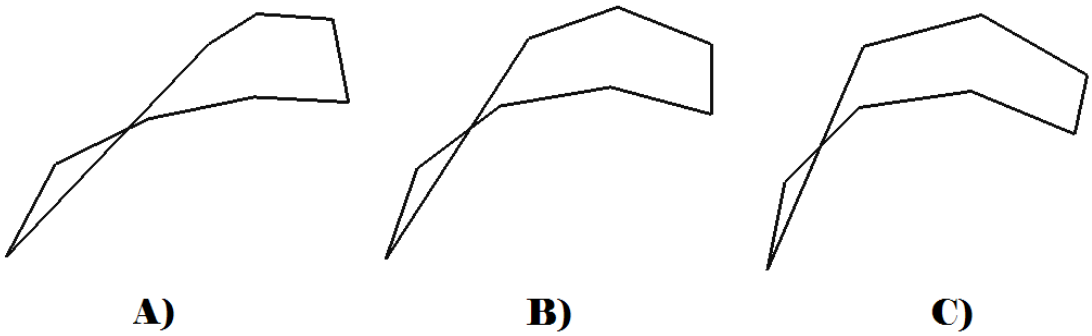

Figure T123. Variation of Occipital Landmarks along RW3 for the North African Sample: A) Lower extreme of variation, B) Consensus form, C) Upper extreme of variation.

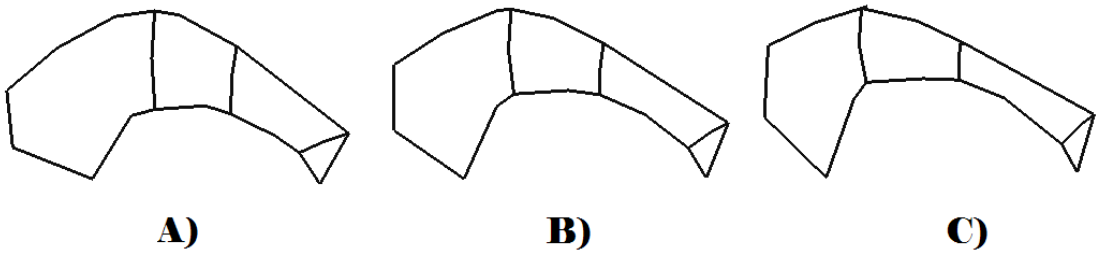

Figure T124. Variation of Supraorbital Landmarks along RW1 for the Singapore Sample: A) Lower extreme of variation, B) Consensus form, C) Upper extreme of variation.

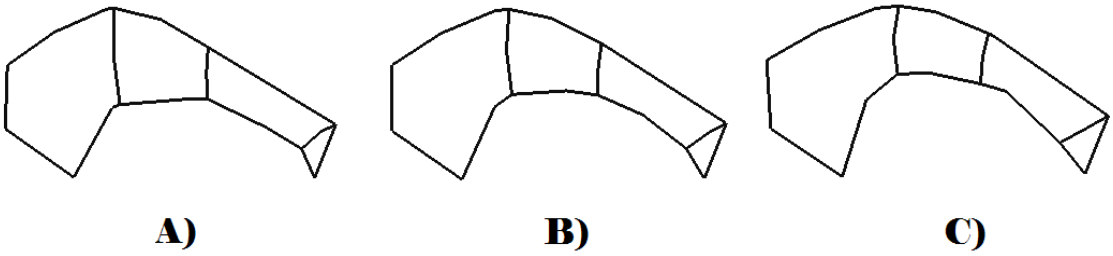

Figure T125. Variation of Supraorbital Landmarks along RW2 for the Singapore Sample: A) Lower extreme of variation, B) Consensus form, C) Upper extreme of variation.

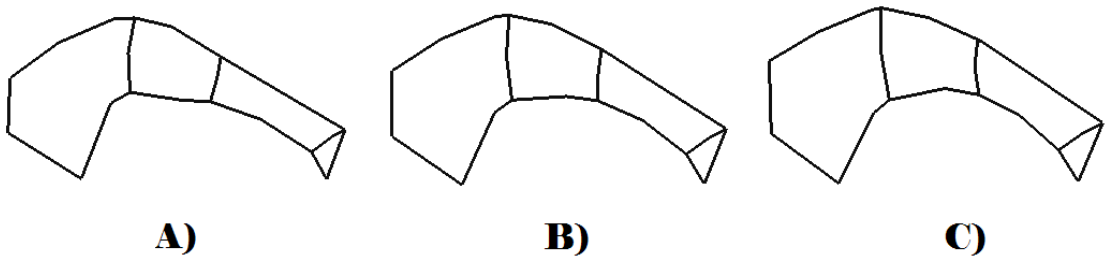

Figure T126. Variation of Supraorbital Landmarks along RW3 for the Singapore Sample: A) Lower extreme of variation, B) Consensus form, C) Upper extreme of variation.

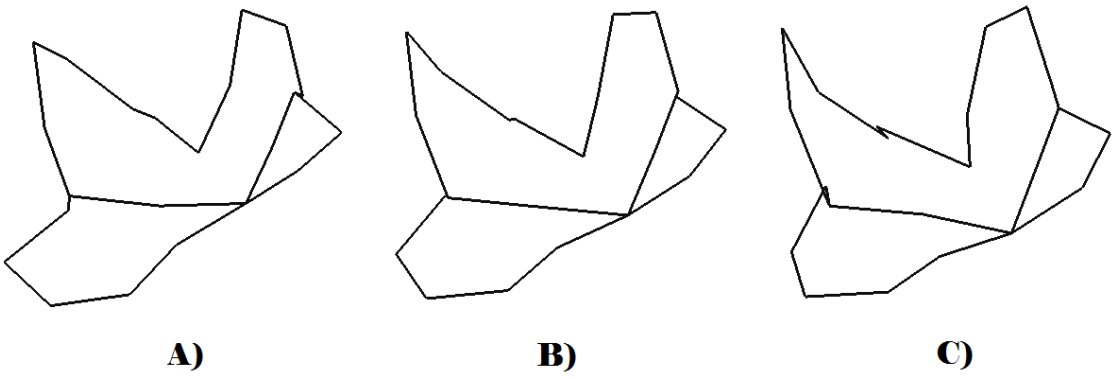

Figure T127. Variation of Zygomaxillary Landmarks along RW1 for the Singapore Sample: A) Lower extreme of variation, B) Consensus form, C) Upper extreme of variation.

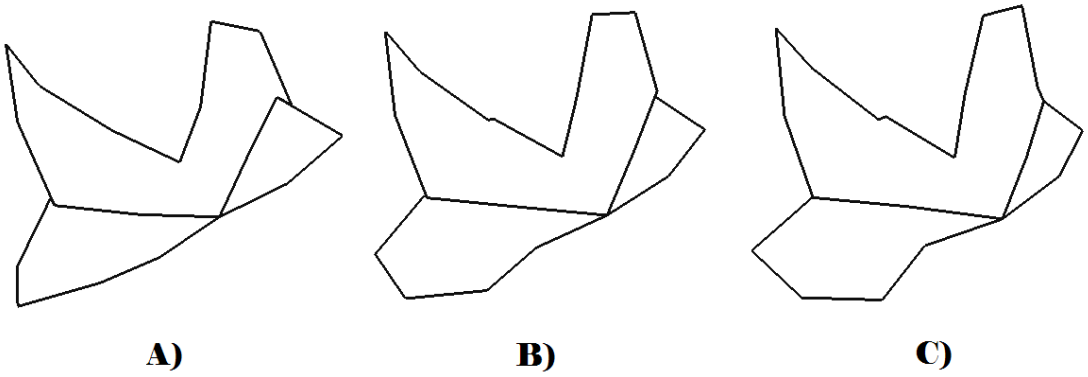

Figure T128. Variation of Zygomaxillary Landmarks along RW2 for the Singapore Sample: A) Lower extreme of variation, B) Consensus form, C) Upper extreme of variation.

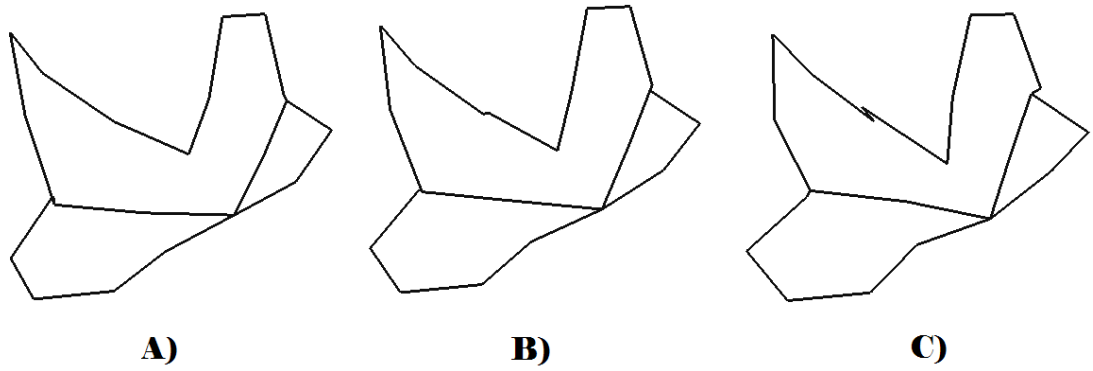

Figure T129. Variation of Zygomaxillary Landmarks along RW3 for the Singapore Sample: A) Lower extreme of variation, B) Consensus form, C) Upper extreme of variation.

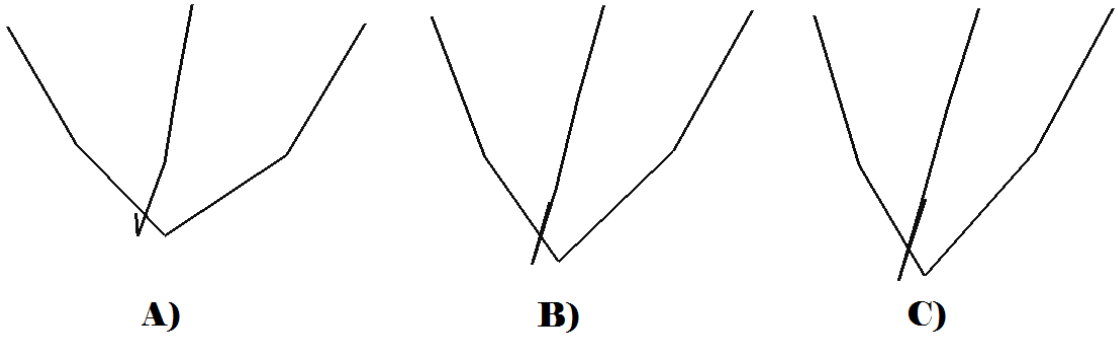

Figure T130. Variation of Mastoid Landmarks along RW1 for the Singapore Sample: A) Lower extreme of variation, B) Consensus form, C) Upper extreme of variation.

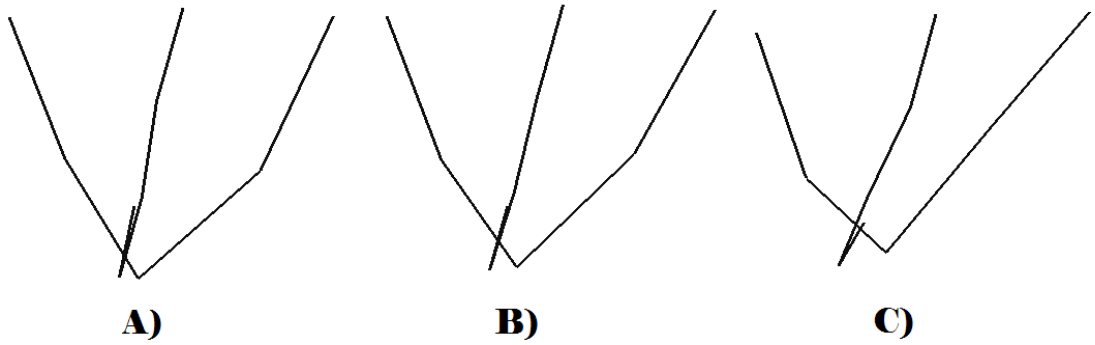

Figure T131. Variation of Mastoid Landmarks along RW2 for the Singapore Sample: A) Lower extreme of variation, B) Consensus form, C) Upper extreme of variation.

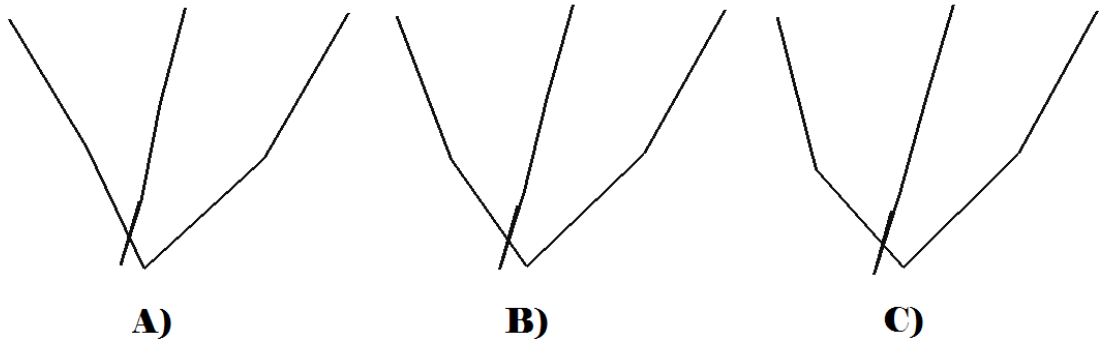

Figure T132. Variation of Mastoid Landmarks along RW3 for the Singapore Sample: A) Lower extreme of variation, B) Consensus form, C) Upper extreme of variation.

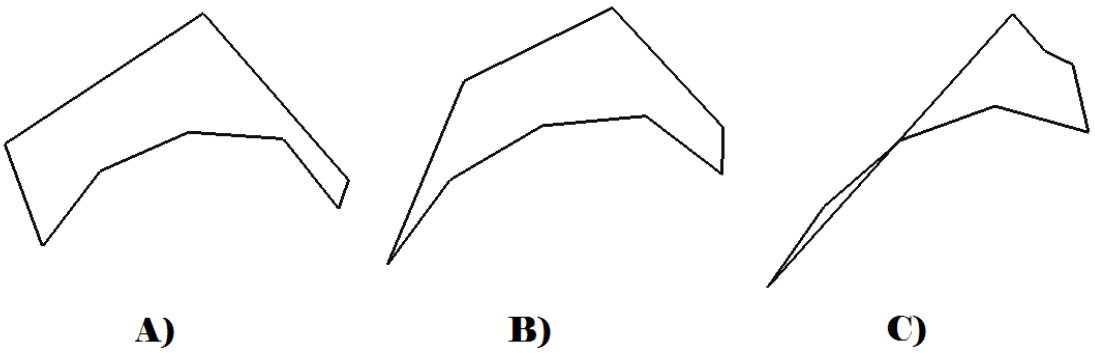

Figure T133. Variation of Occipital Landmarks along RW1 for the Singapore Sample: A) Lower extreme of variation, B) Consensus form, C) Upper extreme of variation.

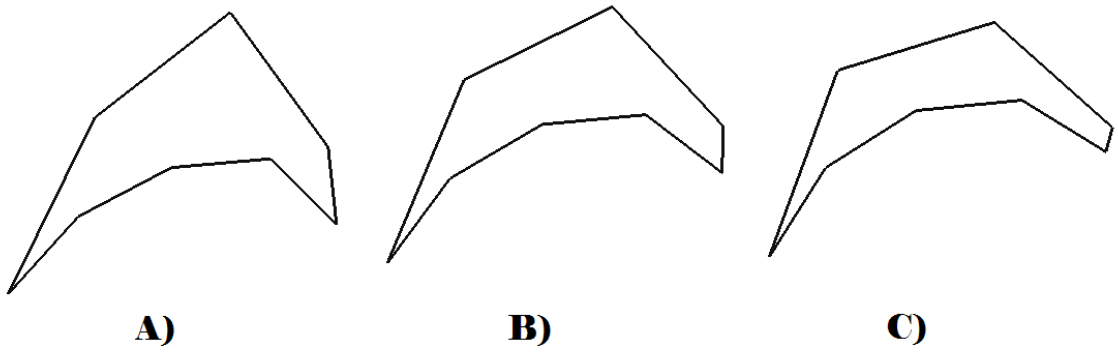

Figure T134. Variation of Occipital Landmarks along RW2 for the Singapore Sample: A) Lower extreme of variation, B) Consensus form, C) Upper extreme of variation.

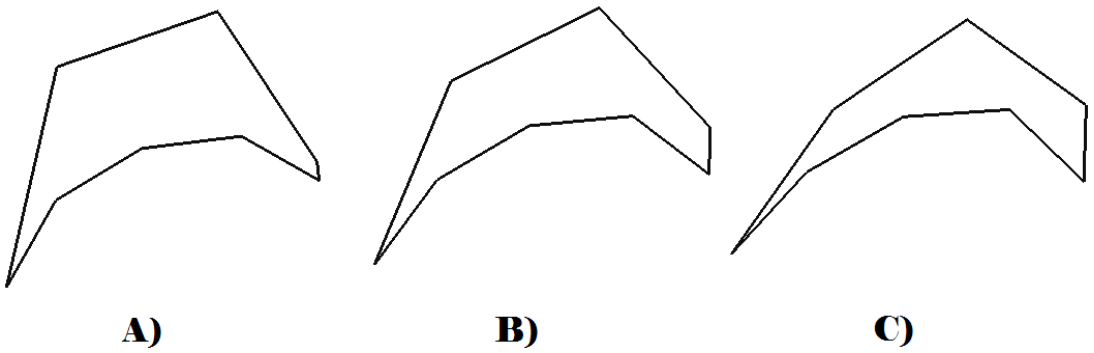

Figure T135. Variation of Occipital Landmarks along RW3 for the Singapore Sample: A) Lower extreme of variation, B) Consensus form, C) Upper extreme of variation.

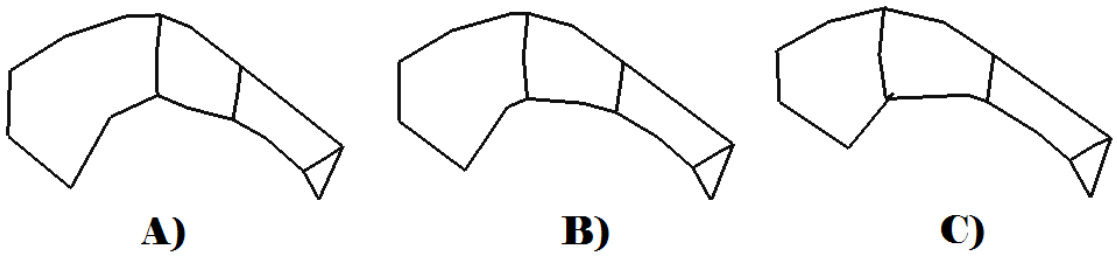

Figure T136. Variation of Supraorbital Landmarks along RW1 for the Western Europe Sample: A) Lower extreme of variation, B) Consensus form, C) Upper extreme of variation.

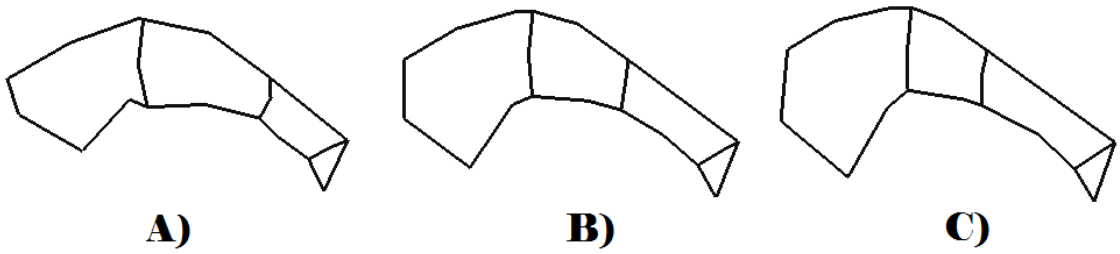

Figure T137. Variation of Supraorbital Landmarks along RW2 for the Western Europe Sample: A) Lower extreme of variation, B) Consensus form, C) Upper extreme of variation.

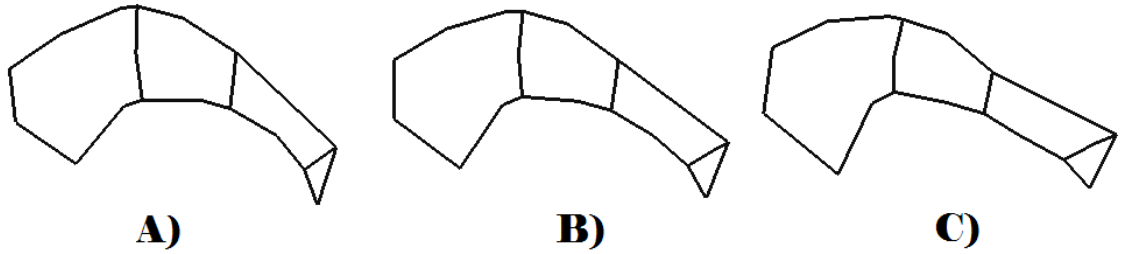

Figure T138. Variation of Supraorbital Landmarks along RW3 for the Western Europe Sample: A) Lower extreme of variation, B) Consensus form, C) Upper extreme of variation.

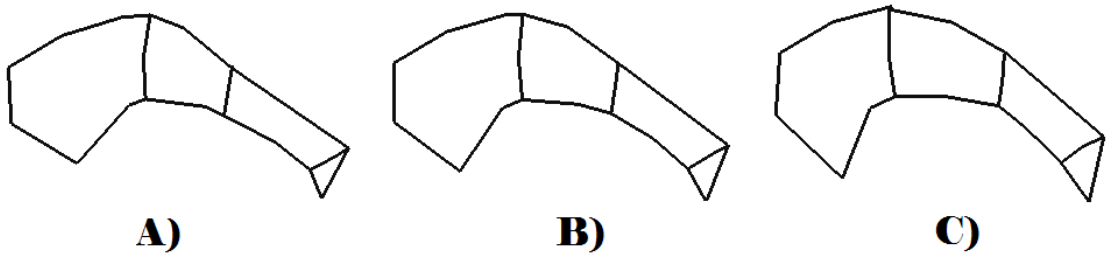

Figure T139. Variation of Supraorbital Landmarks along RW4 for the Western Europe Sample: A) Lower extreme of variation, B) Consensus form, C) Upper extreme of variation.

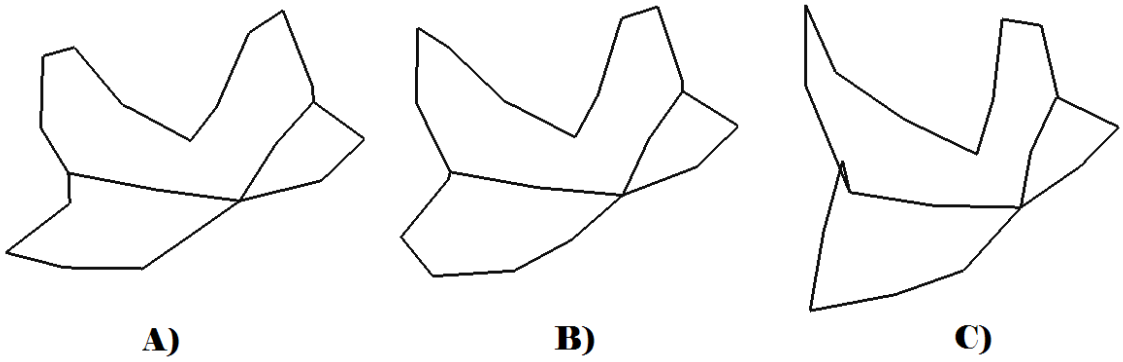

Figure T140. Variation of Zygomaxillary Landmarks along RW1 for the Western Europe Sample: A) Lower extreme of variation, B) Consensus form, C) Upper extreme of variation.

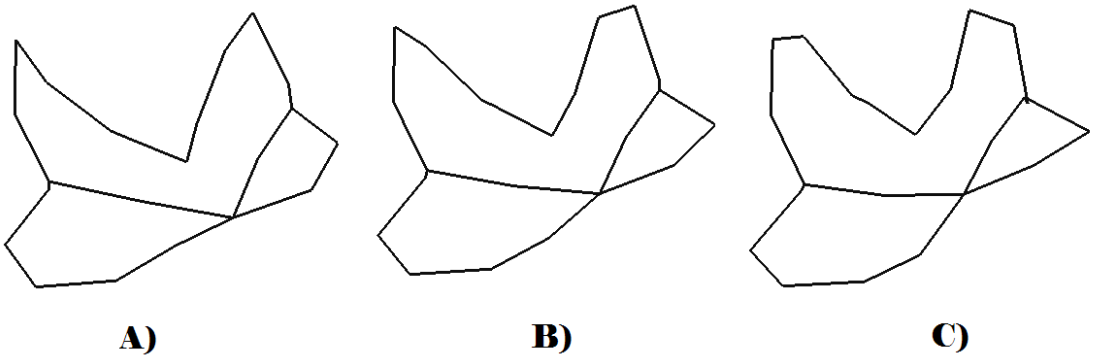

Figure T141. Variation of Zygomaxillary Landmarks along RW2 for the Western Europe Sample: A) Lower extreme of variation, B) Consensus form, C) Upper extreme of variation.

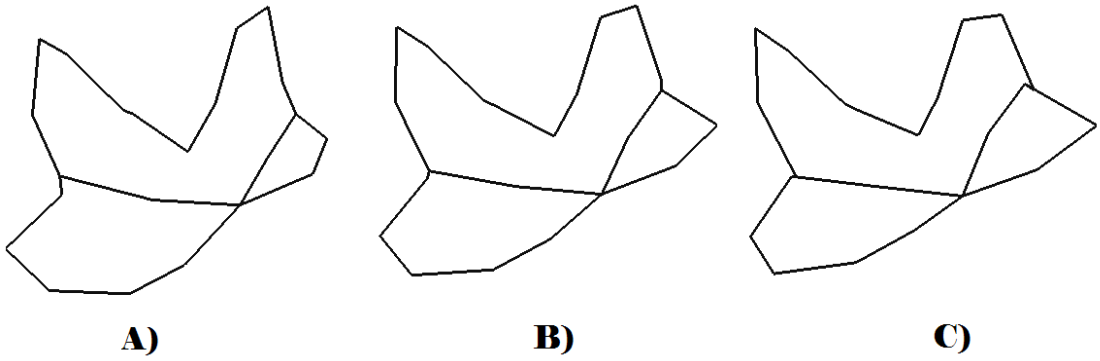

Figure T142. Variation of Zygomaxillary Landmarks along RW3 for the Western Europe Sample: A) Lower extreme of variation, B) Consensus form, C) Upper extreme of variation.

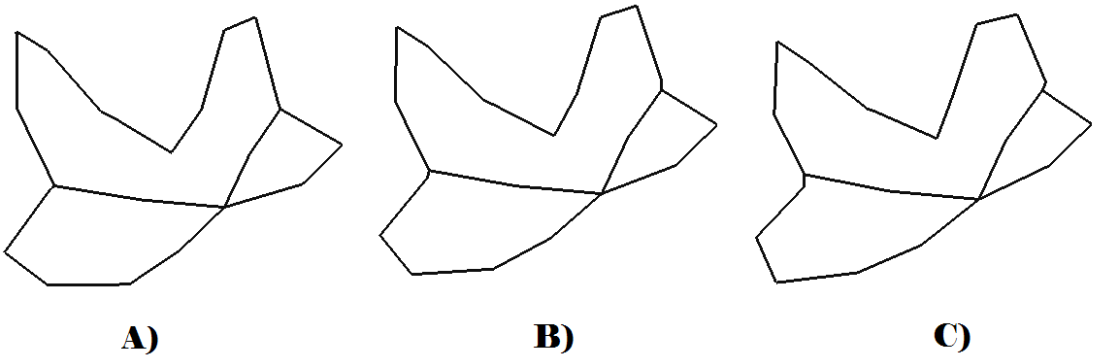

Figure T143. Variation of Zygomaxillary Landmarks along RW4 for the Western Europe Sample: A) Lower extreme of variation, B) Consensus form, C) Upper extreme of variation.

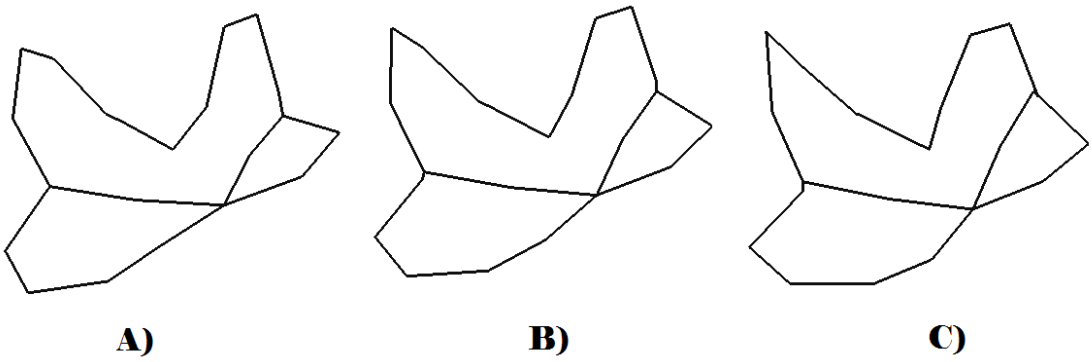

Figure T144. Variation of Zygomaxillary Landmarks along RW5 for the Western Europe Sample: A) Lower extreme of variation, B) Consensus form, C) Upper extreme of variation.

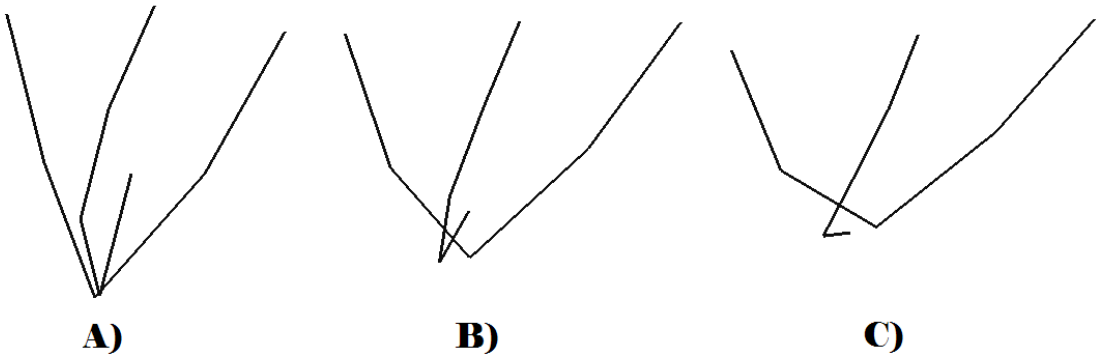

Figure T145. Variation of Mastoid Landmarks along RW1 for the Western Europe Sample: A) Lower extreme of variation, B) Consensus form, C) Upper extreme of variation.

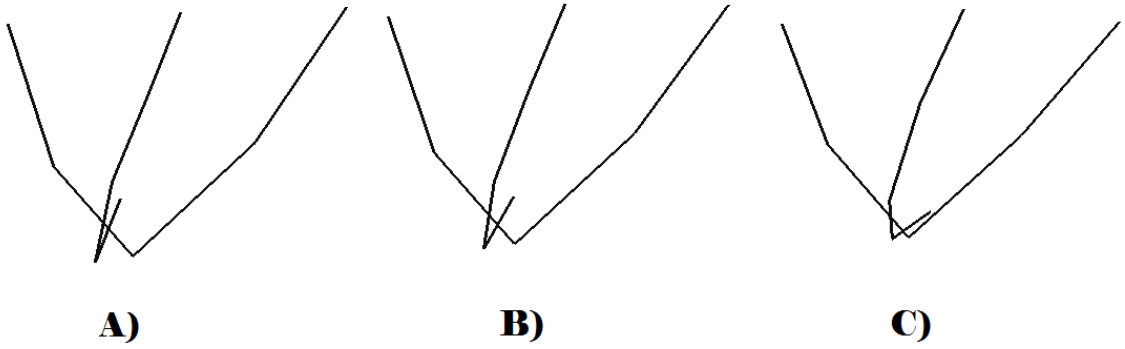

Figure T146. Variation of Mastoid Landmarks along RW2 for the Western Europe Sample: A) Lower extreme of variation, B) Consensus form, C) Upper extreme of variation.

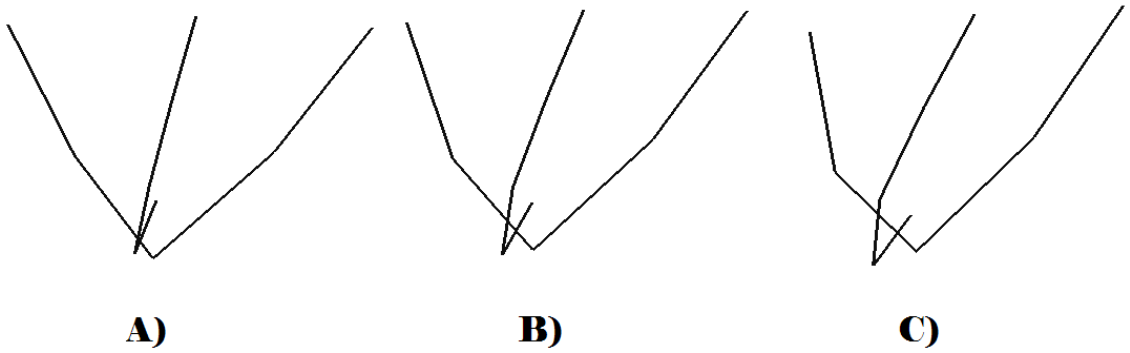

Figure T147. Variation of Mastoid Landmarks along RW3 for the Western Europe Sample: A) Lower extreme of variation, B) Consensus form, C) Upper extreme of variation.

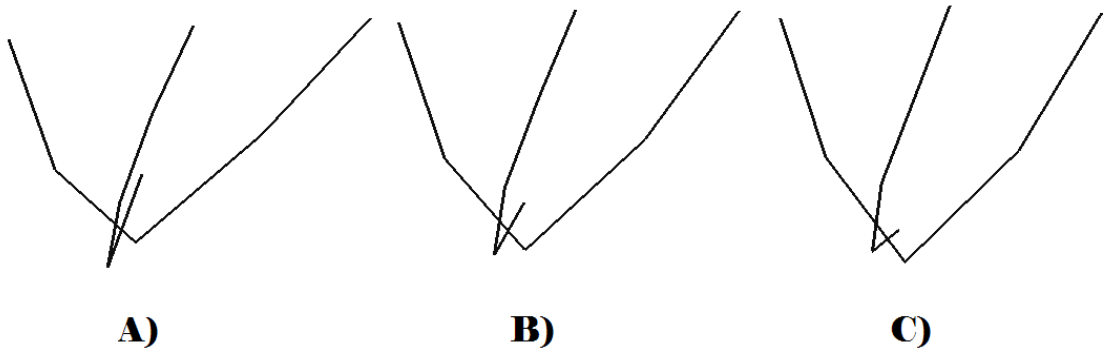

Figure T148. Variation of Mastoid Landmarks along RW4 for the Western Europe Sample: A) Lower extreme of variation, B) Consensus form, C) Upper extreme of variation.

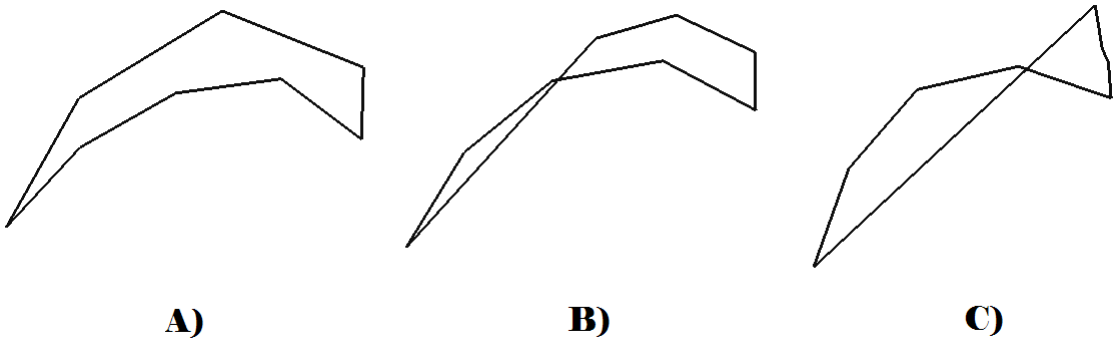

Figure T149. Variation of Occipital Landmarks along RW1 for the Western Europe Sample: A) Lower extreme of variation, B) Consensus form, C) Upper extreme of variation.

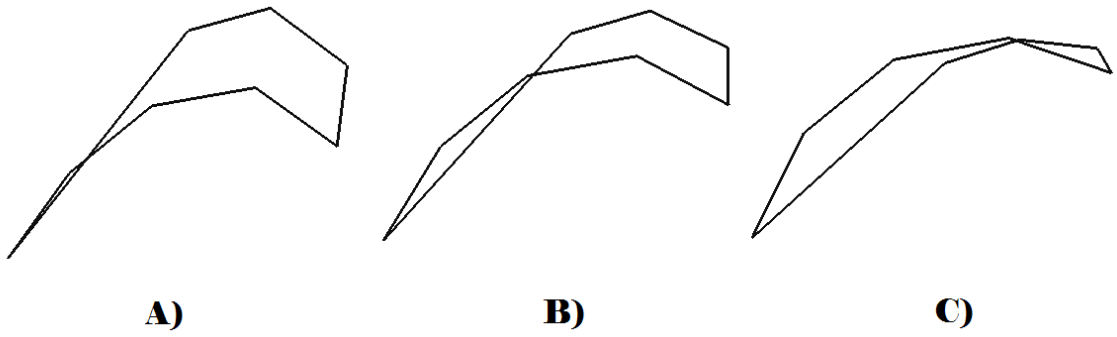

Figure T150. Variation of Occipital Landmarks along RW2 for the Western Europe Sample: A) Lower extreme of variation, B) Consensus form, C) Upper extreme of variation.

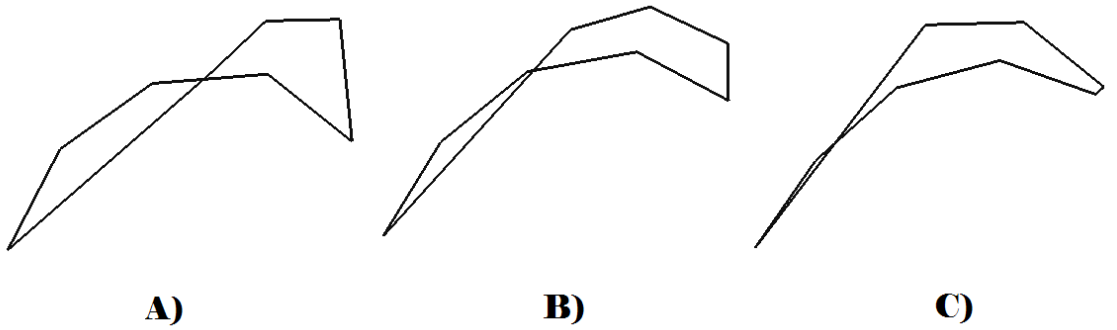

Figure T151. Variation of Occipital Landmarks along RW3 for the Western Europe Sample: A) Lower extreme of variation, B) Consensus form, C) Upper extreme of variation.

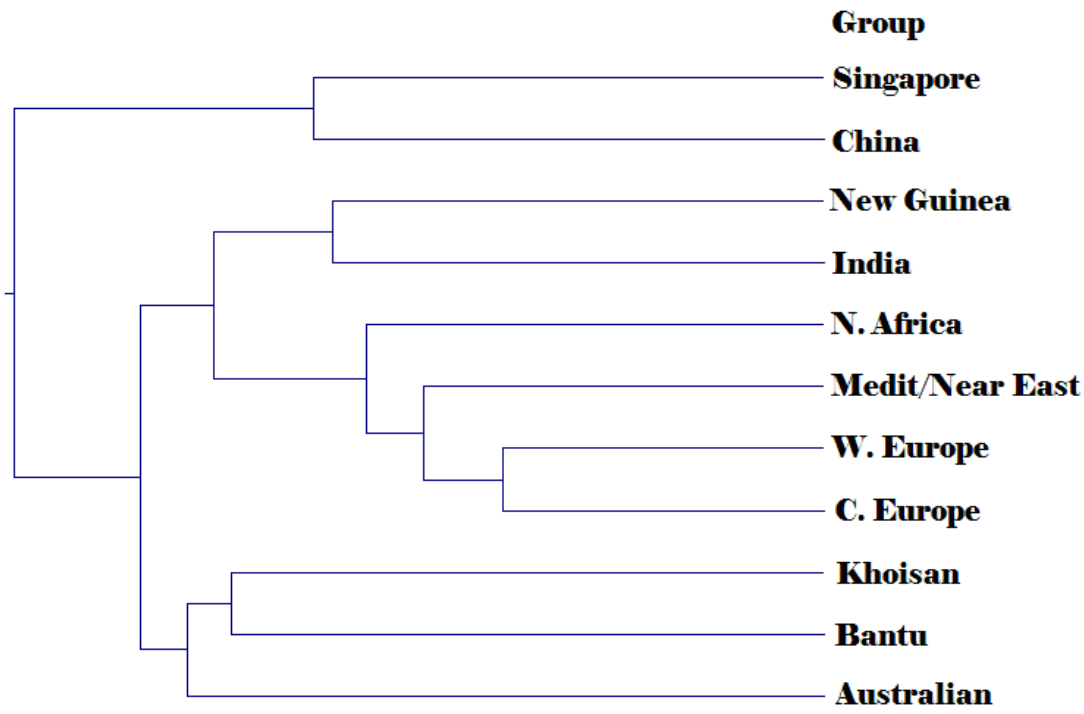

Figure T152. Dendrogram based on the relative warp scores for the full 72 landmark coordinate dataset across the entire global sample.

REFERENCES

Ackermann RR, Cheverud JM. 2000. Phenotypic Covariance Structure in Tamarins (Genus Saguinus): A Comparison of Variation Patterns Using Matrix Correlation and Common Principal Component Analysis. Am J Phys Anthropol 111:489-501.

Ackermann RR, Cheverud JM. 2002. Discerning Evolutionary Processes in Patterns of Tamarin (Genus *Saguinus*) Craniofacial Variation. Am J Phys Anthropol 117:260-271.

Ackermann RR. 2002. Patterns of covariation in the hominoid craniofacial skeleton: implications for paleoanthropological models. J Hum Evol 42:167-187.

Ackermann RR. 2003. Using extant morphological variation to understand fossil relationships: a cautionary tale. S Afr J Sci 99:255-258.

Ackermann RR. 2005. Variation in Neandertals: a response to Harvati (2003). J Hum Evol 48:643-646.

Adams DC, Rohlf JF, Slice DE. 2004. Geometric morphometrics: ten years of progress following the 'revolution'. Ital J Zool 71:5-16.

Ahern JCM, Hawks JD, Lee S. 2005. Neandertal taxonomy reconsidered…again: a response to Harvati et al. (2004). J Hum Evol 48:647-652.

Ahn DG, Kourakis MJ, Rohde LA, Silver LM, Ho RK. 2002. T-box gene tbx5 is essential for formation of the pectoral limb bud. Nature 417:754-758.

Aiello LC, Wheeler P. 1995. The Expensive-Tissue Hypothesis: The Brain and the Digestive System in Human and Primate Evolution. Curr Anthropol 36 (2):199-221.

Alberch P, Gould SJ, Oster GF, Wake DB. 1979. Size and shape in ontogeny and phylogeny. Paleobiology 5:296-317.

Amzallag GN. 2000. Canalization as a non-genetic source of adaptiveness during morphogenesis: experimental evidence from analysis of reproductive development in Sorghum bicolor. BioSystems 57:95-107.

Anapol F, Lee S. 1994. Morphological adaptation to diet in Platyrrhine primates. Am J Phys Anthropol 94:239-261.

Ancel LW, Fontana W. 2000. Plasticity, Evolvability, and Modularity in RNA. J Exp Zool 288:242-283.

Anklin M, et al. 1993. Climate instability during the last interglacial period recorded in the GRIP ice core. Nature 364:203-207.

Antón SC, Franzen JL. 1997. The occipital torus and developmental age of Sangiran-3. J Hum Evol 33:599-610.

Antón SC. 1994. Mechanical and Other Perspectives on Neandertal Craniofacial Morphology. Integrative Paths to the Past: Paleoanthropological advances in honor of F. Clark Howell (Edited by Corruccini RS and Ciochon RL) Englewood Cliffs, NJ: Prentice Hall. pp. 677-695.

Antón SC. 1996. Tendon-associated bone features of the masticatory system in Neandertals. J Hum Evol 31:391-408.

Antón SC. 1997. Endocranial hyperostosis in Sangiran 2, Gibraltar 1, and Shanidar 5. Am J Phys Anthropol 102:111-122.

Antón SC. 1999. Cranial growth in Homo erectus: how credible are the Ngandong juveniles? Am J Phys Anthropol 108:223-236.

Antón SC. 2002. Evolutionary Significance of Cranial Variation in Asian *Homo erectus*. Am J Phys Anthropol 118:301-323.

Arjan J. de Visser GM, Hermisson J, Wagner GP, Meyers LA, Bagheri-Chaichian H, Blanchard JL, Chao L, Cheverud JM, Elena SF, Fontana W, Gibson G, Hansen TF, Krakauer D, Lewontin RC, Ofria C, Rice SH, von Dassow G, Wagner A, Whitlock MC. 2003. Perspective: Evolution and Detection of Genetic Robustness. Evolution 57:1959-1972.

Armelagos GJ, Van Gerven DP. 1980. Sexual dimorphism and human evolution: an overview. J Hum Evol 9:437-446.

Baab KL, Freidline SE, Wang SL. 2006. An Investigation of Robusticity in Modern Human Crania: Implications for *Homo erectus*. PaleoAnthropology A50.

Baab KL, Freidline SE, Wang SL, Hanson T. 2010. Relationship of Cranial Robusticity to Cranial Form, Geography and Climate in *Homo sapiens*. Am J Phys Anthropol 141:97-115.

Baab KL. 2008a. The taxonomic implications of cranial shape variation in *Homo erectus*. J Hum Evol 54:827-847.

Baab KL. 2008b. A re-evaluation of the taxonomic affinities of the early *Homo* cranium KNM-ER 42700. J Hum Evol 55:741-746.

Balzeau A, Grimauld-Herve D. 2006. Cranial base morphology and temporal bone pneumatization in Asian *Homo erectus*. J Hum Evol 51:350-359.

Balzeau A, Radovcic J. 2008. Variation and modalities of growth and development of the temporal bone pneumatization in Neandertals. J Hum Evol 54:546-567.

Barni T, Fantoni G, Gloria L, Maggi M, Peri A, Balsi E, Grappone C, Vannelli GB. 1998. Role of endothelin in the human craniofacial morphogenesis. J Craniofac Genet Dev Biol 18:183-194.

Bastir M, Rosas A. 2005. Hierarchical Nature of Morphological Integration and Modularity in the Human Posterior Face. Am J Phys Anthropol 128:26-34.

Bastir M, Rosas A, Garcia Tabernero A, Pena-Melian A, Estalrrich A, de la Rasilla M, Fortea J. 2010. Comparative morphology and morphometric assessment of the Neandertal occipital remains from the El Sidro´n site (Asturias, Spain: years 2000–2008). J Hum Evol 58:68-78.

Baughan B, Demirjian A. 1978. Sexual Dimorphism in the Growth of the Cranium. Am J Phys Anthropol 49:383-390.

Beals KL, Smith CL, Dodd SM. 1984. Brain Size, Cranial Morphology, Climate, and Time Machines. Curr Anthropol 25:301-330.

Beldade P, Brakefield PM. 2003. Concerted evolution and developmental integration in modular butterfly wing patterns. Evolution & Development 5 (2):169-179.

Beldade P, Koops K, Brakefield PM. 2002. Modularity, individuality and evo-devo in butterfly wing patterns. Proc Natl Acad Sci USA 99:14262-14267.

Berge C, Penin X. 2004. Ontogenetic allometry, heterochrony, and interspecific differences in the skull of African apes, using tridimensional Procrustes analysis. Am J Phys Anthropol.

Bernal V, Perez SI, Gonzalez PN. 2006. Variation and causal factors of craniofacial robusticity in Patagonian hunter-gatherers from Late Holocene. Am J Hum Biol 18:748-765.

Birch JM, 1999. Skull Allometry in the Marine Toad, Bufo marinus. J Morph. 241:115 126.

Bolker JA. 2000. Modularity in Development and Why It Matters to Evo-Devo. Amer Zool 40:770-776.

Bookstein F, Schäfer K, Prossinger H, Seidler H, Fieder M, Stringer C, Weber GW, Arsuaga J, Slice DE, Rohlf FJ, Recheis W, Mariam AJ, Marcus LF. 1999. Comparing Frontal Cranial Profiles in Archaic and Modern Homo by Morphometric Analysis. The Anatomical Record 257:217-224.

Bookstein FL, Gunz P, Mitterœcker P, Prossinger H, Schæfer K, Seidler H. 2003. Cranial integration in Homo: singular warps analysis of the midsagittal plane in ontogeny and evolution. J Hum Evol 44:167-187.

Bookstein FL. 1989. "Size and shape": a comment on semantics. Syst Zool 38:173-183.

Bookstein FL. 1991. Morphometric tools for landmark data. Geometry and biology. Cambridge University Press, Cambridge.

Bookstein FL. 1997. Landmark methods for forms without landmarks: localizing group differences in outline shape. Med Image Anal 1:225-243.

Brace CL. 1963. Structural Reduction in Evolution. The American Naturalist 97:39-49.

Brace CL. 1967. Environment, tooth form, and size in the Pleistocene. J Dent Res 46:809-816

Brace CL. 1995. Biocultural Interaction and the Mechanism of Mosaic Evolution in the Emergence of "Modern" Morphology. American Anthropologist 97:711-721.

Brakefield PM. 1984. The ecological genetics of quantitative characters of *Maniola jurtina* and other butterflies. In: Vane-Wright RI, Ackery PR, editors. The biology of butterflies. London: Academic Press. P 167-190.

Brakefield PM. 2001. Structure of a Character and the Evolution of Butterfly Eyespot Patterns. Mol Dev Evol 291:93-104.

Brose DS, Wolpoff MH. 1971. Early Upper Paleolithic Man and Late Middle Paleolithic Tools. American Anthropologist 73:1156-1194.

Brothwell D. 1975. Adaptive Growth Rate Changes as a Possible Explanation for the Distinctiveness of the Neanderthalers. J Archaeol Sci 2:161-163.

Bruner E, Manzi G. 2007. Landmark-Based Shape Analysis of the Archaic *Homo* Calvarium from Ceprano (Italy). Am J Phys Anthropol 132:355-366.

Brůžek J, Franciscus RG, Novotný V, Trinkaus E. 2006. The assessment of sex. In: Trinkaus E, Svoboda J. (Eds.), Early Modern Human Evolution in Central Europe: The People of Dolni Vestonice and Pavlov. Oxford University Press, London, pp. 46–62.

Buikstra JE, Ubelaker DH. 1994. Standards for Data Collection from Human Skeletal Remains. Research Series No. 44. Arkansas Archaeological Survey, Fayetteville.

Cachel S. 1997. Dietary shifts and the European Upper Paleolithic transition. Curr Anthropol 38:579-603.

Capdevila J, Izpisua Belmonte JC. 2000. Perspectives on the Evolutionary Origin of Tetrapod Limbs. Mol Dev Evol 288:287-303.

Capdevila J, Izpisua Belmonte JC. 2001. Patterning mechanisms controlling vertebrate limb development. Annu Rev Cell Dev Biol 17:87-132.

Carlson DS, Van Gerven DP. 1977. Masticatory Function and Post-Pleistocene Evolution in Nubia. Am J Phys Anthropol 46:495-506.

Carlson KJ, Grine FR, Pearson OM. 2007. Robusticity and Sexual Dimorphism in the Postcranium of Modern Hunter-Gatherers From Australia. Am J Phys Anthropol 134:9-23.

Carlsson GE. 1974. Bite force and chewing efficiency. Frontiers of Oral Physiology, Vol. 1 (Edited by Kawamura Y), Karger, Basel. pp. 265-292.

Carroll SB. 2001. Chance and necessity: the evolution of morphological complexity and diversity. Nature 409:1102-1109.

Caspari R. 1991. The evolution of the posterior cranial vault in the Central European Upper Pleistocene. PhD thesis. Univ. Michigan.

Caspari R, Radovcic J. 2006. New Reconstruction of Krapina 5, a Male Neandertal Cranial Vault from Krapina, Croatia. Am J Phys Anthropol 130:294-307.

Cerney MM, Adams DC, Vance JM. 2003. Image Warping of Three-Dimensional Body Scan Data. Proceedings of the SAE Digital Human Modeling Conference. Montreal, Canada. 2003-01-2231.

Chen X, Chen H. 1998. The influence of alveolar structures on the torsional strain field in a gorilla corporeal cross-section. J Hum Evol 35:611-633.

Cheverud JM, Routman EJ, Irschick DK. 1997. Pleiotropic effects of individual gene loci on mandibular morphology. Evolution 51:2004-2014.

Cheverud JM. 1982. Phenotypic, genetic, and environmental integration in the cranium. Evolution 36:499-516.

Cheverud JM. 1984. Quantitative genetics and developmental constraints on evolution by selection. J Theor Biol 110:155-171.

Cheverud JM. 1995. Morphological integration in the saddle-back tamarin (Saguinus fuscicollis) cranium. Am Nat 145:63-89.

Cheverud JM. 1996. Quantitative genetic analysis of cranial morphology in the cotton-top (Saguinus Oedipus) and saddle-back (S. fuscicollis) tamarins. J Evol Biol 9:5-42.

Chui C, Hamrick MW. 2002. Evolution and Development of the Primate Limb Skeleton. Evol Anthropol 11:94-107.

Churchill SE, Brink JS, Gruss LT. 2000. Middle Pleistocene to Holocene postcranial gracilization in black wildebeest, Connochaetes gnou, and its implications for understanding diachronic changes in robusticity in the genus Homo. Am J Phys Anthropol 30(suppl):124-125.

Churchill SE, Smith FH. 2000. Makers of the Early Aurignacian of Europe. Yrbk Phys Anthropol 43:61-115.

Churchill SE. 1996. Particulate Versus Integrated Evolution of the Upper Body in Late Pleistocene Humans: A Test of Two Models. Am J Phys Anthropol 100:559-583.

Churchill SE. 1997. Endocrine models of skeletal robusticity and the origins of gracility. Am J Phys Anthropol 24(suppl):92.

Churchill SE. 1998. Cold Adaptation, Heterochrony, and Neandertals. Evol Anthropol 7:46-61.

Churchill SE. 2006. Bioenergetic perspectives on Neanderthal thermoregulatory and activity budgets. In: K. Harvati and T. Harrison (eds.) Neanderthals Revisited: New Approaches and Perspectives. Springer, Dordrecht, pp. 113-133.

Cole III TM, Richtsmeier JT. 1998. A Simple Method for Visualization of Influential Landmarks When Using Euclidean Distance Matrix Analysis. Am J Phys Anthropol 107:273-283.

Collard M, Wood B. 2007. Hominin homoiology: An assessment of the impact of phenotypic plasticity on phylogenetic analyses of humans and their fossil relatives. J Hum Evol 52:573-584.

Constantino P, Wood BA. 2007. The evolution of *Zinjanthropus boisei*. Evol Anthropol 16: 49–62.

Copes LE. 2009. How and why do humans grow thin skulls? A test of the systemic robusticity hypothesis. Am J Phys Anthropol 138(S48):109.

Cowgill LW, Hager LD. 2007. Variation in the Development of Postcranial Robusticity: An Example from Catalhoyuk, Turkey. Int J Osteoarchaeol 17:235-252.

Cowgill LW, Warrener A, Pontzer H, Ocobock C. 2010. Waddling and Toddling: The Biomechanical Effects of an Immature Gait. Am J Phys Anthropol (in press).

Cowgill LW. 2010. The Ontogeny of Holocene and Late Pleistocene Human Postcranial Strength. Am J Phys Anthropol 141:16-37.

Cramon-Taubadel N. 2009. Revisiting the homoiology hypothesis: the impact of phenotypic plasticity on the reconstruction of human population history from craniometric data. J Hum Evol 57:179-190.

Daegling DJ, Hylander WL. 1998. Biomechanics of torsion in the human mandible. Am J Phys Anthropol 105:73-87.

Daegling DJ, Highlander WL. 2000. Experimental Observation, Theoretical Models, and Biomechanical Inference in the Study of Mandibular Form. Am J Phys Anthropol 112:541-551.

Daegling DJ, McGraw SW. 2007. Functional Morphology of the Mangabey Mandibular Corpus: Relationship to Dental Specializations and Feeding Behavior. Am J Phys Anthropol 134:50-62.

Daegling DJ. 1989. Biomechanics of cross-sectional size and shape in the hominoid mandibular corpus. Am J Phys Anthropol 80: 91–106.

Daegling DJ. 1992. Mandibular morphology and diet in the genus Cebus. Int J Primatol 13:545-570.

Daegling DJ. 2007. Morphometric Estimation of Torsional Stiffness and Strength in Primate Mandibles. Am J Phys Anthropol 132:261-266.

Dahlstrom L, Tzakis M, Haraldson T. 1988. Endurance tests of the masticatory system on different bite force levels. Scand J Dent Res 96:137-142.

Dansgaard W, Johnsen SJ, Clausen HB, Dahl-Jensen D, Gundestrup NS, Hammer CU, Hvidberg CS, Steffensen JP, Sveinbjornsdottir AE, Jouzel J, Bond G. 1993. Evidence for general instability of past climate from a 250-kyr ice-core record. Nature 364:218-220.

Dechow PC, Wang Q, Peterson J. 2010. Edentulation Alters Material Properties of Cortical Bone in the Human Craniofacial Skeleton: Functional Implications for Craniofacial Structure in Primate Evolution. The Anatomical Record 293:618-629.

Demes B, Creel N. 1988. Bite force, diet, and cranial morphology of fossil hominins. J Hum Evol 17:657-670.

Demes B. 1987. Another look at an old face: biomechanics of the neandertal facial skeleton reconsidered. J Hum Evol 16:287-303.

Duarte C, Maurício J, Pettitt PB, Souto P, Trinkaus E, van der Plicht H, Zilhão J. 1999. The early Upper Paleolithic human skeleton from the Abrigo do Lagar Velho (Portugal) and modern human emergence in Iberia. PNAS 96:7604-7609.

Đuric M, Zoran Rakoćević Z, Đonić D. 2005. The reliability of sex determination of skeletons from forensic context in the Balkans. Forensic Sci Int 147:159-164.

Ebner M, Shackleton M, Shipman R. 2002. How Neutral Networks Influence Evolvability. Complexity 7:19-33.

Ehrich TH, Vaughn TT, Koreishi SF, Linsey RB, Pletscher LS, Cheverud JM. 2003. Pleiotropic effects on Mandibular Morphology I. Developmental Morphological Integration and Differential Dominance. J Exp Zool 296B:58-79.

Endo B. 1966. Experimental studies on the mechanical significance of the form of the human facial skeleton. Journal of the Faculty of Science University of Tokyo, Section V, Anthropology 3:1-106.

Fink WL, Zelditch ML. 1995. Phylogenetic Analysis of Ontogenetic Shape Transformations: A Reassessment of the Piranha genus Pygocentrus (Teleostei). Syst Biol 44:343-360.

Frayer DW. 1984. Biological and Cultural Change in the European Late Pleistocene and Early Holocene. The Origins of Modern Humans: A World Survey of the Fossil Evidence. Smith FH and Spencer F (eds.). New York: Liss pp. 211-250.

Frayer DW, Wolpoff MH, Thorne AG, Smith FH, Pope GG. 1993. Theories of Modern Human Origins: The Paleontological Test. American Anthropologist 95:14-50.

Frost SR, Marcus LF, Bookstein FL, Reddy DP, Delson E. 2003. Cranial Allometry, Phylogeography, and Systematics of Large-Bodied Papionins (Primates: Cercopithecinae) Inferred From Geometric Morphometric Analysis of Landmark Data. The Anatomical Record 275A:1048-1072.

Gardner A, Zuidema W. 2003. Is Evolvability Involved in the Origin of Modular Variation? Evolution 57:1448-1450.

Gauld SC. 1996. Allometric patters of cranial bone thickness in fossil hominins. Am J Phys Anthropol 100:411-426.

Genovés S. 1954. The problem of the sex of certain fossil hominids, with special reference to the Neandertal skeletons from Spy. J R Anthropol Inst 84:131-144.

Gilligan I, Bulbeck D. 2007. Environment and Morphology in Australian Aborigines: A Re-analysis of the Birdsell Database. Am J Phys Anthropol 124:75-91.

Gison G, Wagner G. 2000. Canalization in evolutionary genetics: a stabilizing theory? BioEssays 22:372-380.

Godfrey LR, Sutherland MR. 1995. What's growth got to do with it? Process and product in the evolution of ontogeny. J Human Evol 29:405-431.

Gould SJ. 1977. Ontogeny and Phylogeny. Cambridge, MA: Harvard University Press.

Green M, Smith FH. 1990. Neandertal craniofacial growth. Am J Phys Anthropol 81:232-232.

Grine FE, Judex S, Daegling DJ, Ozcivici E, Ungar PS, Teaford MF, Sponheimer M, Scott J, Scott RS, Walker A. 2010. Craniofacial biomechanics and functional and dietary inferences in hominin paleontology. J Hum Evol 58:293-308.

Gunz P, Mitteroecker P, Bookstein FL, Weber GW. 2003. Completing fossil *Homo* crania by statistical and geometrical estimation methods. Am J Phys Anthropol 36 (suppl):106.

Gunz P, Harvati K. 2007. The Neanderthal ''chignon'': Variation, integration, and homology. J Hum Evol. 52:262-274.

Guy F, Brunet M, Schmittbuhl M, Viriot L. 2003. New Approaches in Hominoid Taxonomy: Morphometrics. Am J Phys Anthropol 121:198-218.

Hagberg C, Agerberg G, Harberg M. 1985. Regression analysis of electromyographic activity of masticatory muscles versus bite force. Scand J Dent Res 93:396-402.

Hallgimsson B, Willmore K, Hall BK. 2002. Canalization, Developmental Stability, and Morphological Integration in Primate Limbs. Yrbk Phys Anthropol 45:131-158.

Hanken J, Carl TF, Richardson MK, Olsson L, Schlosser G, Osabutey CK, Klymkowsky MW. 2001. Limb Development in a "Nonmodel" Vertebrate, the Direct-Developing Frog *Eleutherodactylus coqui*. Mol Dev Evol 291: 375-388.

Hansen TF, Armbruster WS, Carlson ML, Pélabon C. 2003. Evolvability and Genetic Constraint in Dalechampia Blossoms: Genetic Correlations and Conditional Evolvability. J Exp Zool 296B:23-39.

Hansen TF. 2003. Is modularity necessary for evolvability? Remarks on the relationship between pleiotropy and evolvability. BioSystems 69:83-94.

Harvati K, Frost SR, McNulty KP. 2005. Neandertal variation and taxonomy–a reply to Ackermann (2005) and Ahern et al. (2005). J Hum Evol 48:653-660.

Harvati K. 2002. Models of Shape Variation Between And Within Species And The Neandertal Taxonomic Position: A 3D Geometric Morphometrics Approach Based On Temporal Bone Morphology. Three-Dimensional Imaging in Paleoanthropology and Prehistoric Archaeology Mafart B and Delingette H (eds.) BAR International Series 1049. pp 25-30.

Harvati K. 2003a. The Neandertal taxonomic position: models of intra- and inter-specific craniofacial variation. J Hum Evol 107-132.

Harvati K. 2003b. Quantitative Analysis of Neanderthal Temporal Bone Morphology Using Three-Dimensional Geometric Morphometrics. Am J Phys Anthropol 120:323-338.

Hennessy RJ, Stringer CB. 2002. Geometric Morphometric Study of the Regional Variation of Modern Human Craniofacial Form. Am J Phys Anthropol 117:37-48.

Hintze JL. 2000. NCSS Statistical Software. Version i.o. 329 N. 1000 East, Kaysville, UT 84037.

Holliday TW. 2002. Body size and postcranial robusticity of European Upper Paleolithic hominins. J Hum Evol 43:513-528.

Holt BM, Formicola V. 2008. Hunters of the Ice Age: The Biology of Upper Paleolithic People. Yrbk Phys Anthropol 51:70-99.

Houghton P. 1990. The adaptive significance of Polynesian body form. Annals of Human Biology 17:19-32.

Howells WW. 1973. Cranial Variation in Man: A study by Multivariate Analysis of Patterns of Difference Among Recent Populations. Peabody Museum of Archaeology and Ethnology, Cambridge, MA: Harvard University Press.

Howells WW. 1989. Skull Shapes and the Map. Craniometric Analyses in the Dispersion of Modern Homo. Papers of the Peabody Museum of Archaeology and Ethnology vol 79. Cambridge, MA: Peabody Museum.

Hublin JJ. 1992. *Homo erectus*: are the “autapomorphies” reversible? Am J Phys Anthropol 14(suppl):92.

Hylander WL, Picq PG, Johnson KR. 1991. Masticatory-Stress Hypotheses and the Supraorbital Region of Primates. Am J Phys Anthropol 86:1-36.

Hylander WL, Johnson KR. 1997. In vivo bone strain patterns in the zygomatic arch of macaques and the significance of these patterns for functional interpretations of craniofacial form. Am J Phys Anthropol 102:203-232.

Hylander WL. 1977. The adaptive significance of Eskimo craniofacial morphology. Orofacial Growth and Development. Dahlberg AA, Graber TM (eds.). Mouton Publishers: The Hague. pp. 129-170.

Hylander WL. 1988. Implications of *in vivo* experiments for interpreting the functional significance of "robust" australopithecine jaws. In: Grine FE, editor. Evolutionary history of the "robust" australopithecines. Chicago: Aldine. p 55–80.

Kawecki TJ. 2000. The Evolution of Genetic Canalization under Fluctuating Selection. Evolution 54:1-12.

Kelley J. 1995. Sexual dimorphism in canine shape among extant great apes. Am J Phys Anthropol 96:365-389.

Kendall DG. 1984. Shape manifolds, procrustean metrics, and complex projective spaces. Bull London Math Soc 16:81-121.

Kirschner M, Gerhart J. 1998. Evolvability. PNAS 95 (15):8420-8427.

Kjellstrom A. 2004. Evaluations of Sex Assessment using Weighted Traits on Incomplete Skeletal Remains. Int J Osteoarchaeol 14:360-373.

Klingenberg CP, Badyaev AV, Sowry SM, Beckwith NJ. 2001. Inferring Developmental Modularity from Morphological Integration: Analysis of Individual Variation and Asymmetry in Bumblebee Wings. Am Nat 157:11-23.

Klingenberg CP, Zaklan ST. 2000. Morphological Integration Between Developmental Compartments In The Drosophila Wing. Evolution 54:1273-1285.

Klingenberg CP. 2002. Morphometrics and the role of the phenotype in studies of the evolution of developmental mechanisms. Gene 287:3-10.

Klingenberg CP. 2009. Morphometric integration and modularity in configurations of landmarks: Tools for evaluating a-priori hypotheses. Evol Dev 11:in press.

Klingenberg CP. 2011. MorphoJ: an integrated software package for geometric morphometrics. Molecular Ecology Resources, advance online publication. doi: 10.1111/j.1755-0998.2010.02924.x

Konigsberg LW, Hens SM. 1998. Use of Ordinal Categorical Variables in Skeletal Assessment of Sex From the Cranium. Am J Phys Anthropol 107:97-112.

Korioth TWP, Romilly DP, Hannam AG. 1992. Three-Dimensional Finite Element Stress Analysis of the Dentate Human Mandible. Am J Phys Anthropol 88:69-96.

Korioth TWP, Versluis A. 1997. Modeling the Mechanical Behavior of the Jaws and Their Related Structures By Finite Element (Fe) Analysis. Crit. Rev. Oral Biol. Med. 8:90-104.

Koyabu DB, Endo H. 2009. Craniofacial variation and dietary adaptations of African colobines. J Hum Evol 56:525-536.

Kupczik K, Dobson CA, Crompton RH, Phillips R, Oxnard CE, Fagan MJ, O'Higgins P. 2009. Masticatory Loading and Bone Adaptation in the Supraorbital Torus of Developing Macaques. Am J Phys Anthropol 139:193-203.

Lahr MM, Wright RVS. 1996. The question of robusticity and the relationship between cranial size and shape in Homo sapiens. J Hum Evol 31: 157-191.

Lahr MM. 1994. The Multiregional Model of modern human origins: a reassessment of its morphological basis. J Hum Evol 23:23-56.

Lahr MM. 1995. Comments on "Testing Hypotheses about Recent Human Evolution from Skulls". Curr Anthropol 36 (2):180-181.

Lahr MM. 1996. The evolution of modern human diversity: A study of cranial variation. New York: Cambridge University Press.

Larson PM. 2002. Chondrocranial Development in Larval Rana sylvatica (Anura: Ranidae): Morphometric Analysis of Cranial Allometry and Ontogenetic Shape Change. J Morph 252:131-144.

Lele S, Richtsmeier JT. 1991. Euclidean distance matrix analysis: a coordinate free approach to comparing biological shapes using landmark data. Am J Phys Anthropol 98:73-86.

Lele S. 1993. Euclidean distance matrix analysis (EDMA) of landmarks data: estimation of mean form and mean form difference. Math Geol 25:573-602.

Lieberman DE, Pearson OM, Mowbray KM. 2000a. Basicranial influence on overall cranial shape. J Hum Evol 38:291-315.

Lieberman DE, Callum RF, Ravosa MJ. 2000b. The Primate Cranial Base: Ontogeny, Function, and Integration. Yrbk Phys Anthropol 43:117-169.

Lieberman DE, Devlin MJ, Pearson OM. 2001. Articular Area Responses to Mechanical Loading: Effects of Exercise, Age, and Skeletal Location. Am J Phys Anthropol 116:266-277.

Lieberman DE, McBratney BM, Krovitz G. 2002. The evolution and development of cranial form in Homo sapiens. PNAS 99 (3):1134-1139.

Lieberman DE, Krovitz GE, Yatesa FW, Devlina M, St. Claire M. 2004. Effects of food processing on masticatory strain and craniofacial growth in a retrognathic face. J Hum Evol 46:655-677.

Lieberman DE. 1995. Testing Hypotheses about Recent Human Evolution from Skulls. Current Anthropology 36:159-197.

Lieberman DE. 1996. How and Why Humans Grow Thin Skulls: Experimental Evidence for Systemic Cortical Robusticity. Am J Phys Anthropol 101:217-236.

Lieberman DE. 1999. Homology and Hominin Phylogeny: Problems and Potential Solutions. Evol Anthropol 7:142-151.

Lieberman DE. 2008. Speculations About the Selective Basis for Modern Human Craniofacial Form. Evol Anthropol 17:55-68.

Lipson H, Pollack JB, Suh NP. 2002. On the Origin of Modular Variation. Evolution 56:1549-1556.

Logan M, Tabin CJ. 1999. Role of Pitx1 upstream of Tbx4 in specification of hind limb identity. Science 283:1736-1739.

Loy A, Mariani L, Bertelletti M, Tunesi L. 1998. Visualizing Allometry: Geometric Morphometrics in the Study of Shape Changes in the Early Stages of the Two-Banded Sea Bream, Diplodus vulgaris(Perciformes, Sparidae). J Morph 237:137-146.

Mabee PM, Crotwell PL, Bird NC, Burke AC. 2002. Evolution of Median Fin Modules in the Axial Skeleton of Fishes. J Exp Zool 294:77-90.

MacLeod N. 2002. Phylogenetic signals in morphometrics data. Morphology, shape and phylogeny. MacLeod N and Forey PL (eds.) London: Taylor & Francis pp. 100-138.

Maddux SD, Franciscus RG. 2009. Allometric scaling of infraorbital surface topography in *Homo*. J Hum Evol 56:161-174.

Maggiano IS, Schultz M, Kierdorf H, Sierra Sosa T, Maggiano CM, Tiesler Blos V. 2008. Cross-Sectional Analysis of Long Bones, Occupational Activities and Long-Distance Trade of the Classic Maya From Xcambo – Archaeological and Osteological Evidence. Am J Phys Anthropol 136:470-477.

Marroig G, Cheverud JM. 2001. A Comparison of Phenotypic Variation and Covariation Patterns and the Role of Phylogeny, Ecology, and Ontogeny During Cranial Evolution of New World Monkeys. Evolution 55:2576-2600.

Martin GR. 1998. The role of FGFs in the early development of vertebrate limbs. Genes Dev 12:1571-1586.

Martin G. 2001. Making a vertebrate limb: new players enter from the wings. Bioessays 23:865-868.

McAdams HH, Arkin A. 1997. Stochastic mechanisms in gene expression. Proc Natl Acad Sci USA 94:814-819.

McAdams HH, Arkin A. 1999. It's a noisy business! Genetic regulation at the nanomolar scale. Trends Genet 15:65-69.

McKinney ML, McNamara KJ. 1991. Heterochrony: the Evolution of Ontogeny. Plenum Press, New York.

McShea D. 2000. Functional Complexity in Organisms: Parts as Proxies. Biology and Philosophy 15:641-668.

Menegaz RA, Sublett SV, Figueroa SD, Hoffman TJ, Ravosa MJ. 2009. Phenotypic plasticity and function of the hard palate in growing rabbits. Anat Rec 292: 277–284.

Menegaz RA, Sublett SV, Figueroa SD, Hoffman TJ, Ravosa MJ, Aldridge K. 2010. Evidence for the Influence of Diet on Cranial Form and Robusticity. The Anatomical Record 293:630-641.

Monteiro LR, Abe AS. 1999. Functional and Historical Determinants of Shape in the Scapula of Xenarthran Mammals: Evolution of a Complex Morphological Structure. J Morph 241:251-263.

Monteiro AF, Brakefield PM, French V. 1994. The evolutionary genetics and developmental basis of wing pattern variation in the butterfly *Bicyclus anynana*. Evolution 48:1147-1157.

Moss ML, Young RW. 1960. A functional approach to craniology. Am J Phys Anthropol 18:281-292.

Nijhout HF. 1991. The Development and Evolution of Butterfly Wing Patterns. Washington, DC: Smithsonian Institute Press.

Nijhout HF. 2001. Elements of butterfly wing patterns. J Exp Zool 291:213-295.

O'Connor CF, Franciscus RG, Holton N. 2005. Bite force production capability and efficiency in Neandertals and modern humans. Am J Phys Anthropol 127:129-151.

O'Higgins P, Dryden IL. 1993. Sexual dimorphism in hominoids: further studies of craniofacial shape differences in *Pan*, *Gorilla* and *Pongo*. J Hum Evol 24:183-205.

O'Higgins P, Jones N. 1998. Facial growth in Cercocebus torquatus: An application of three dimensional geometric morphometric techniques to the study of morphological variation. J Anat 193:251-272.

O'Higgins P, Jones N. 2006. Morphologika v2.5: Tools for statistical shape analysis. Hull York Medical School. http://hyms.fme.googlepages.com/resources.

O'Higgins P. 2000. The study of morphological variation in the hominin fossil record: biology, landmarks and geometry. J Anat 197:103-120.

Olson EC, Miller RL. 1951. A mathematical model applied to a study of the evolution of species. Evolution 5:256-338.

Olson EC, Miller RA. 1958. Morphological integration. Chicago: University of Chicago Press.

Osborn JW, Mao J. 1993. A thin bite force transducer with three-dimensional capabilities reveals a change in bite-force direction during jaw muscle fatigue. Archs Oral Biol 38:139-144.

Osborn JW. 1996. Features of human jaw design which maximize the bite force. J Biomech 29:589-595.

Ozbudak EM, Thattai M, Kurtser I, Grossman AD, Van Oudenaarden A. 2002. Regulation of noise in the expression of a single gene. Nat Genet 31:69-73.

Pan R, Wei F, Li M. 2003. Craniofacial Variation of the Chinese Macaques Explored With Morphologika. J Morph 256:342-348.

Patton MQ. 1990. Qualitative Evaluation and Research Methods. Sage, Newbury Park, CA.

Paulsen SM, Nijhout HF. 1993. Phenotypic correlation structure among elements of the color pattern in *Precis coenia* (Lepidoptera, Nymphalidae). Evolution 47:593-618.

Paulsen SM. 1994. Quantitative genetics of butterfly wing color patterns. Dev Genet 15:79-91.

Pearson OM, Lieberman DE. 2004. The Aging of Wolff's "Law": Ontogeny and Responses to Mechanical Loading in Cortical Bone. Yrbk Phys Anthropol 47:63-99.

Pearson OM. 2000. Activity, Climate, and Postcranial Robusticity: Implications for Modern Human Origins and Scenarios of Adaptive Change. Curr Anthropol 41:569-607.

Pearson OM. 2008. Statistical and Biological Definitions of ''Anatomically Modern'' Humans: Suggestions for a Unified Approach to Modern Morphology. Evol Anthropol 17:38-48.

Penin X, Berge C, Baylac M. 2002. Ontogenetic Study of the Skull in Modern Humans and the Common Chimpanzees: Neotenic Hypothesis Reconsidered With a Tridimensional Procrustes Analysis. Am J Phys Anthropol 118:50-62.

Pepper JW. 2003. The evolution of evolvability in genetic linkage patterns. BioSystems 69:115-126.

Perez SI, Bernal V, Gonzalez PN. 2007. Morphological differentiation of aboriginal human populations from Tierra del Fuego (Patagonia): implications for South American peopling. Am J Phys Anthropol 133:1067–1079.

Peterson J, Dechow PC. 2002. Material Properties of the Inner and Outer Cortical Tables of the Human Parietal Bone. The Anatomical Record 268:7-15.

Peterson J, Dechow PC. 2003. Material Properties of the Human Cranial Vault and Zygoma. The Anatomical Record Part A 274A:785-797.

Platt JR. 1964. Strong Inference. Science 146 (3642):347-353.

Polanski JM, Franciscus RG. 2006. Patterns of Craniofacial Integration in Extant *Homo*, *Pan*, and *Gorilla*. Am J Phys Anthropol 131:38-49.

Polly PD. 2001. On morphological clocks and paleophylogeography: towards a timescale for Sorex hybrid zones. Genetica 112–113:339–357.

Ponce de Leon MS, Zollikofer CPE. 2001. Neanderthal cranial ontogeny and its implications for late hominin diversity. Nature 412:534-538.

Ponce de Leon MS, Zollikofer CPE. 2006. Neanderthals and modern humans – chimps and bonobos: similarities and differences in developmental evolution. In: K. Harvati and T. Harrison (eds.) Neanderthals Revisited: New Approaches and Perspectives. Springer, Dordrecht, pp. 71-88.

Rae TC, Koppe T. 2008. Independence of Biomechanical Forces and Craniofacial Pneumatization in *Cebus*. The Anatomical Record 291:1414-1419.

Raff EC, Raff RA. 2000. Dissociability, modularity, evolvability. Evolution & Development 2 (5):235-237.

Rak Y. 1983. The Australopithecine face. New York: Academic Press.

Rak Y. 1986. The Neandertal face: A new look at an old face. J Hum Evol 15:151-164.

Ravosa MJ, Johnson KR, Hylander WL. 2000. Strain in the Galago facial skull. J Morphol 245:51-66.

Ravosa MJ, Vinyard CJ, Hylander WL. 2000. Stressed out: Masticatory forces and primate circumorbital form. The Anatomical Record 261:173-175.

Ravosa MJ. 1991. Ontogenetic perspective on mechanical and nonmechanical models of primate circumorbital morphology. Am J Phys Anthropol 85:95-112.

Ravosa MJ. 2000. Size and scaling in the mandible of living and extinct apes. Folia Primatol 71:305-322.

Redies C, Peulles L. 2001. Modularity in vertebrate brain development and evolution. BioEssays 23:1100-1111.

Richmond BG, Jungers WL. 1995. Size variation and sexual dimorphism in Australopithecus afarensis and living hominoids. J Hum Evol 29:229-245.

Richtsmeier JT, Walker A. 1993. Morphometric analysis of facial growth in Homo erectus. In The Nariokotome Homo erectus skeleton, RE Leakey and A Walker, eds., Harvard University Press. Pp. 391-410.

Richtsmeier JT, Cheverud JM, Lele S. 1992. Advances in anthropological morphometrics. Annu Rev Anthropol 21:231-253.

Richtsmeier JT, Burke Deleon V, Lele SR. 2002. The Promise of Geometric Morphometrics. Yrbk Phys Anthropol 45:63-91.

Ricklan DE, Tobias PV. 1986. Unusually Low Sexual Dimorphism of Endocranial Capacity in a Zulu Cranial Series. Am J Phys Anthropol 71:285-293.

Rightmire GP. 1995. Comments on "Testing Hypotheses about Recent Human Evolution from Skulls". Curr Anthropol 36 (2):182-183.

Robert P, Escoufier Y. 1976. A Unifying Tool for Linear Multivariate Statistical Methods: The RV-Coefficient. Appl Statist 25:257-265.

Rodriguez-Esteban C, Tsukui T, Yonei S, Magallon J, Tamura K, Izpisua Belmonte JC. 1999. The T-box genes Tbx4 and Ybx5 regulate limb outgrowth and identity. Nature 398:814-818.

Rohlf FJ, Marcus LF. 1993. A revolution in morphometrics. Trends Ecol Evol 8:129-132.

Rohlf FJ. 1998. On Applications of Geometric Morphometrics to Studies of Ontogeny and Phylogeny. Syst Biol 47:147-158.

Rohlf FJ. 1999. Shape Statistics: Procrustes Superimpositions and Tangent Spaces. J Class 16:197-223.

Rohlf FJ. 2000. Statistical Power Comparisons Among Alternative Morphometric Methods. Am J Phys Anthropol 111:463-478.

Rohlf FJ. 2003. Bias and error in estimates of mean shape in geometric morphometrics. J Hum Evol 44:665-683.

Rosas A, Bastir M. 2002. Thin-Plate Spline Analysis of Allometry and Sexual Dimorphism in the Human Craniofacial Complex. Am J Phys Anthropol 117:236-245.

Rosas A, Bastir M, Martinez-Maza C, Garcia-Tabernero A, Lalueza-Fox C. 2006. Inquiries into Neanderthal craniofacial development and evolution: "accretion" versus "organismic" models. In: K. Harvati and T. Harrison (eds.) Neanderthals Revisited: New Approaches and Perspectives. Springer, Dordrecht, pp. 37-69.

Ruff CB, Trinkaus E, Walker A, Larsen CS. 1993. Postcranial robusticity in *Homo*: Temporal trends and mechanical interpretation. Am J Phys Anthropol 91: 21-53.

Ruff CB, Walker A, Trinkaus E. 1994. Postcranial Robusticity in *Homo* III: Ontogeny. Am J Phys Anthropol 93:35-54.

Ruff CB, Trinkaus E, Holliday TW. 1997. Body mass and encephalization in Pleistocene Homo. Nature 387:173-176.

Ruff CB, Holt B, Trinkaus E. 2006. Who's Afraid of the Big Bad Wolff?: ''Wolff's Law'' and Bone Functional Adaptation. Am J Phys Anthropol 129:484-498.

Ruff CB. 2000. Body size, body shape, and long bone strength in modern humans. J Hum Evol 38:269-290.

Ruff CB. 2002. Long Bone Articular and Diaphyseal Structure in Old World Monkeys and Apes I: Locomotor Effects. Am J Phys Anthropol 119:305-342.

Ruff CB. 2003. Long Bone Articular and Diaphyseal Structure in Old World Monkeys and Apes II: Estimation of Body Mass. Am J Phys Anthropol 120:16-37.

Russell MD. 1985. The Supraorbital Torus: "A Most Remarkable Peculiarity". Curr Anthropol 26:337-360.

Santa Luca AP. 1978. A re-examination of presumed Neandertal-like fossils. J Hum Evol 7:169-636.

Schmalhausen II. 1949. Factors of evolution. Chicago: University of Chicago Press.

Schumacher GH. 1999. Regulative and adaptive factors in craniofacial growth. Ann Anatomy 181:9-13.

Shackelford LL. 2007. Regional Variation in the Postcranial Robusticity of Late Upper Paleolithic Humans. Am J Phys Anthropol 133:655-668.

Shaw CN, Stock JT. 2009a. Intensity, Repetitiveness, and Directionality of Habitual Adolescent Mobility Patterns Influence the Tibial Diaphysis Morphology of Athletes. Am J Phys Anthropol 140:149-159.

Shaw CN, Stock JT. 2009b. Habitual Throwing and Swimming Correspond With Upper Limb Diaphyseal Strength and Shape in Modern Human Athletes. Am J Phys Anthropol 140:160-172.

Shea BT. 1985. The ontogeny of sexual dimorphism in the African apes. American Journal of Primatology 8:183-188.

Shea JJ. 2003a. The Middle Paleolithic of the East Mediterranean Levant. Journal of World Prehistory 17:313-394.

Shea JJ. 2003b. Neandertals, Competition, and the Origin of Modern Human Behavior in the Levant. Evol Anthropol 12:173-187.

Shea JJ. 2007. Behavioral Differences Between Middle and Upper Paleolithic *Homo sapiens* in the East Mediterranean Levant: The Roles of Intraspecific Competition and Dispersal from Africa. Journal of Anthropological Research 63:449-488.

Shea JJ. 2008. Transitions or turnovers? Climatically-forced extinctions of *Homo sapiens* and Neanderthals in the east Mediterranean Levant. Quaternary Science Reviews 27:2253-2270.

Shubin N, Tabin C, Carroll S. 1997. Fossils, genes and the evolution of animal limbs. Nature 388:639-648.

Simmons T, Falsetti AB, Smith FH. 1991. Frontal bone morphometrics of southwest Asian Pleistocene hominins. J Human Evol 20:249-269.

Singleton M. 2002. Patterns of cranial shape variation in the Papionini (Primates: Cercopithecinae). J Hum Evol 42:547-578.

Sládek V, Šefčáková A, Brůžek J. 2001. Sex dimorphism among the early Upper Paleolithic hominids from Central Europe: cranial and pelvic metric variation. J Hum Evol 43:A23.

Slavkin H. 2000. Toward understanding the molecular basis of craniofacial growth and development. Am J Orthodont Dent Orthop 117:538-539.

Slice DE, Bookstein FL, Marcus LF, Rohlf FJ. 1996. A glossary for geometric morphometrics. Pages 531–551 in Advances in morphometrics (L. F. Marcus, M. Corti, A. Loy, G. J. P. Naylor, and D. E. Slice, eds.) Plenum, New York.

Slice DE. 2001. Landmark Coordinates Aligned by Procrustes Analysis Do Not Lie in Kendall's Shape Space. Syst Biol 50:141-149.

Smith FH, Green M. 1991. Heterochrony, life history, and Neandertal morphology. Am J Phys Anthropol 12(suppl):164.

Smith FH, Ranyard GC. 1980. Evolution of the Supraorbital Region in Upper Pleistocene Fossil Hominins From South-Central Europe. Am J Phys Anthropol 53:589-610.

Smith FH. 1983. Behavioral interpretation of changes in craniofacial morphology across the archaic/modern Homo sapiens transition. The Mousterian Legacy: Human Biocultural Change in the Upper Pleistocene. Trinkaus E. (ed.). British Archaeological Reports, International Series 164:141-163.

Smith FH. 1984. Fossil Hominins From the Upper Pleistocene of Central Europe and the Origin of Modern Europeans. The Origins of Modern Humans: A World Survey of the Fossil Evidence. Smith FH and Spencer F (eds.). New York: Liss pp. 137-209.

Smith HF, Grine FE. 2008. Cladistic analysis of early *Homo* crania from Swartkrans and Sterkfontein, South Africa. J Hum Evol 54:684-704.

Spears LR, Crompton RH. 1996. The mechanical significance of the occlusal geometry of great ape molars in food breakdown. J Hum Evol 31:517-535.

Spencer MA, Demes B. 1993. Biomechanical analysis of masticatory system configuration in Neandertals and Inuits. Am J Phys Anthropol 91:1-20.

Spencer MA. 1998. Force production in the primate masticatory system: electromyographic tests of biomechanical hypotheses. J Hum Evol 34:25-54.

Spoor F, Leakey MG, Anton, SC, Leakey LN. 2008. The taxonomic status of KNM-ER 42700: A reply to Baab (2008a). J Hum Evol 55:747-750.

Sterns SC. 1982. The role of development in the evolution of life histories. Evolution and Development. Bonner JT (ed). Berlin: Springer Verlag. pp. 237-258.

Stock JT, Shaw CN. 2007. Which Measures of Diaphyseal Robusticity Are Robust? A Comparison of External Methods of Quantifying the Strength of Long Bone Diaphyses to Cross-Sectional Geometric Properties. Am J Phys Anthropol 134:412-423.

Strait DS, Richmond BG, Spencer MA, Ross CF, Dechow PC, Wood BA. 2007. Masticatory biomechanics and its relevance to early hominid phylogeny: An examination of palatal thickness using finite-element analysis. J Hum Evol 52:585-599.

Strait DS. 2001. Integration, Phylogeny, and the Hominin Cranial Base. Am J Phys Anthropol 114:273-297.

Tarricone FC. 2000. The role of body mass in browridge evolution. Masters Thesis: Binghamton University.

Taylor K, Lamorey G, Doyle G, Alley R, Grootes P, Mayewsi P, White J, Barlow L. 1993. The “flickering switch” of the late Pleistocene climate change. Nature 361:432-436.

Taylor AB. 2002. Masticatory Form and Function in the African Apes. Am J Phys Anthropol 117:133-156.

Taylor AB. 2006. Diet and Mandibular Morphology in African Apes. International Journal of Primatology 27:181-201.

Thompson JL, Nelson AJ. 2000. The place of Neandertals in the evolution of hominin patterns of growth and development. J Hum Evol 38:475-495.

Tobias PV. 2006. Longevity, death and encephalisation among Plio-Pleistocene hominins. International Congress Series 1296:1-15.

Trinkaus E, Churchill SE, Villemeur I, Riley KG, Heller JA, Ruff CB. 1991. Robusticity versus shape – The functional interpretation of Neandertal appendicular morphology. J Anthropol Soc Nippon 99:257-278.

Trinkaus E, Churchill SE, Ruff CB. 1994. Postcranial Robusticity in *Homo* II: Humeral Bilateral Asymmetry and Bone Plasticity. Am J Phys Anthropol 93:1-34.

Trinkaus E, LeMay M. 1982. Occipital Bunning Among Later Pleistocene Hominins. Am J Phys Anthropol 57:27-35.

Trinkaus E. 1983. Neandertal postcrania and the adaptive shift to modern humans. The Mousterian Legacy. Trinkaus E (ed). Oxford: British Archaeological Reports. pp. 165-200.

Trinkaus E. 1984. Western Asia. The Origins of Modern Humans. Smith FH and Spencer F (eds). New York: Alan R. Liss. pp. 251-293.

Trinkaus E. 1986. The Neandertals and modern human origins. Annu. Rev. Anthropol. 15:193-218.

Trinkaus E. 1987. The Neandertal face: evolutionary and functional perspectives on a recent hominin face. J Hum Evol 16:429-433.

Trinkaus E. 1995. Comments on "Testing Hypotheses about Recent Human Evolution from Skulls". Curr Anthropol 36 (2):185-186.

Trinkaus E. 1997. Appendicular robusticity and the paleobiology of modern human emergence. PNAS 94:13367-13373.

Trinkaus E. 2000a. The "Robusticity Transition" Revisited. Neanderthals on the Edge. Stringer CB, Barton RNE and Finlayson JC (eds.). Oxbow Books.

Trinkaus E. 2000b. Human patellar articular proportions: recent and Pleistocene patterns. J Anat 196:473-483.

Trinkaus E. 2005. Early Modern Humans. Annu Rev Anthropol 34:207-230.

Tsunori M, Mashita M, Kasai K. 1998. Relationship between facial types and tooth and bone characteristics of the mandible obtained by CT scanning. Angle Orthodont 68:557-562.

Van Valen LM. 1962. A study of fluctuating asymmetry. Evolution 16:125-142.

Van Valen L. 1965. The study of morphological integratoin. Evolution 19:347-349.

Vieille-Grosjean I, Hunt P, Gulisano M, Boncinelli E, Thorogood P. 1997. Branchial HOX gene expression and human craniofacial development. Develop Biol 183:49-60.

Vinyard CJ, Smith FH. 1997. Morphometric relationships between the supraorbital region and frontal sinus in Melanesian crania. Homo 48 (1):1-21.

Vinyard CJ, Smith FH. 2001. Morphometric Testing of Structural Hypotheses of the Supraorbital Region in Modern Humans. Z Morph Anthrop 83:23-41.

Vinyard CJ. 1994. A quantitative assessment of the supraorbital region in modern Melanesian crania. Masters Thesis: Northern Illinois University.

von Dassow G, Munro E. 1999. Modularity in Animal Development and Evolution: Elements of a Conceptual Framework for EvoDevo. Journal of Experimental Zoology 285:307-325.

Waddington CH. 1942. The canalization of development and the inheritance of acquired characters. Nature 150:563.

Waddington CH. 1957. The Strategy of the Genes. New York: Macmillan Co.

Wagner GP, Altenberg L. 1996. Perspective: Complex Adaptations and the Evolution of Evolvability. Evolution 50:967-976.

Wagner GP, Gauthier JA. 1999. 1,2,3 = 2,3,4: a solution to the problem of the homology of the digits in the avian hand. PNAS 96:5111-5116.

Wagner GP, Booth G, Bagheri-Chaichian H. 1997. A Population Genetic Theory of Canalization. Evolution 51:329-347.

Wagner GP. 1996. Homologues, natural kinds and the evolution of modularity. Am Zool 36:36-43.

Wang Q, Dechow PC. 2006. Elastic Properties of External Cortical Bone in the Craniofacial Skeleton of the Rhesus Monkey. Am J Phys Anthropol 131:402-415.

Wang Q, Strait DS, Dechow PC. 2006. A comparison of cortical elastic properties in the craniofacial skeletons of three primate species and its relevance to the study of human evolution. J Hum Evol 51:375-382.

Wang Q, Ashley DW, Dechow PC. 2010. Regional, Ontogenetic, and Sex-Related Variations in Elastic Properties of Cortical Bone in Baboon Mandibles. Am J Phys Anthropol 141:526-549.

Weaver ME, Ingram DL. 1969. Morphological changes in swine associated with environmental temperature. Ecology 50:710-713.

White TD. 2000. Human Osteology 2nd Ed. New York: Academic Press.

Williams FL, Krovitz GE. 2004. Ontogenetic migration of the mental foramen in Neandertals and modern humans. J Hum Evol 47:199-219.

Williams FL, Orban R. 2007. Ontogeny and Phylogeny of the Pelvis in *Gorilla*, *Pongo*, *Pan*, *Australopithecus* and *Homo*. Folia Primatol 78:99-117.

Williams PL, Bannister LH, Berry MM, Collins P, Dyson M, Dussek JE, Ferguson MWJ. 1999. Gray's Anatomy. New York: Churchill Livingstone.

Williams TA, Nagy LM. 2001. Developmental Modularity and the Evolutionary Diversification of Arthropod Limbs. J Exp Zool 291:241-257.

Winther RG. 2001. Varieties of Modules: Kinds, Levels, Origins, and Behaviors. Journal of Experimental Zoology 291:116-129.

Wolpoff MH, Crummett TL. 1995. Comments on "Testing Hypotheses about Recent Human Evolution from Skulls". Curr Anthropol 36 (2):186-188.

Wolpoff MH, Frayer DW, Oliva M, Jelinek J. 2000. The male Aurignacian crania from Mladec caves, Moravia. Am J Phys Anthropol S30:325-326.

Wolpoff MH. 1999. Paleoanthropology. 2nd ed. New York: McGraw-Hill.

Wood B. 1991. Taxonomy and evolutionary relationships of *Homo erectus*. Courier Forsch Inst Senckenberg 171:159-165.

Wrangham RW, Conklin-Brittain N. 2003. Cooking as a biological trait. Comp Biochem Physiol A 136:35-46.

Wrangham RW, Jones JH, Laden G, Pilbeam D, Conklin-Brittain N. 1999. The Raw and the Stolen: Cooking and the Ecology of Human Origins. Curr Anthropol 40:567-594.

Wrangham RW. 2009. Catching Fire: How Cooking Made Us Human. Basic Books, New York, NY.

Wright BW. 2005. Craniodental biomechanics and dietary toughness in the genus *Cebus*. J Hum Evol 48:473-492.

Yang AS. 2001. Modularity, evolvability, and adaptive radiations: a comparison of the hemi- and holometabolous insects. Evolution & Development 3 (2):59-72.

Yaroch LA. 1996. Shape Analysis Using the Thin-Plate Spline: Neanderthal Cranial Shape as an Example. Yearbook of Physical Anthropology 29:43-89.

Zelditch ML, Bookstein FL, Lundrigan BL. 1992. Ontogeny of Integrated Skull Growth in the Cotton Rat Sigmodon fulviventer. Evolution 46:1164-1180.

Zelditch ML, Carmichael AC. 1989. Ontogenetic Variation in Patterns of Developmental and Functional Integration in Skulls of Sigmodon fulviventer. Evolution 43:814-824.

Zelditch ML, Fink WL, Swiderski DL, Lundrigan BL. 1998. On Applications of Geometric Morphometrics to Studies of Ontogeny and Phylogeny: A Reply to Rohlf. Syst Biol 47:159-167.

Zelditch ML, Swiderski DL, Sheets HD, Fink WL. 2004. Geometric Morphometrics for Biologists: A Primer. New York: Elsevier Academic Press.

Zhang LQ, Attie-Bitach T, Korshunova Y, Cai J, Messina D, Auge J, Vekemans M, Jabs EW, Lovett M. 2000. Gene expression profiles form early stages of human craniofacial development. Am J Hum Genet 67(suppl):915-915.

Zollikofer CPE, Ponce de Leon MS. 2006. Cranial Growth Models: heterochrony, heterotropy, and the kinematics of ontogeny. In: K. Harvati and T. Harrison (eds.) Neanderthals Revisited: New Approaches and Perspectives. Springer, Dordrecht, pp. 89-111.